Handbook of instrumental techniques for materials, chemical and biosciences research

Centres Científics i Tecnològics

Universitat de Barcelona

Edited by: José Ramón Seoane
Xavier Llovet

Design: Centres Científics i Tecnològics UB (CCiTUB)

ISBN: 978-84-615-5373-0

Dipòsit Legal: B-41606-2011

Handbook of instrumental techniques for materials, chemical and biosciences research

edited by

José Ramón Seoane

and

Xavier Llovet

Centres Científics i Tecnològics
Universitat de Barcelona

Foreword by the Rector of the University of Barcelona

The University of Barcelona (UB) is one of Spain's leading research-intensive universities. Our University combines the values of tradition with its position as an institution whose various missions are dedicated to excellence and innovation: a modern University that is urban, outward-looking and builds on more than 560 years of history.

At the UB, we believe that teaching excellence must be linked with excellence in research. And indeed, our university's work in this area has been recognized with two campuses of international excellence: the Barcelona Knowledge Campus, and the Health Universitat de Barcelona campus.

The UB conducts multidisciplinary research through a total of 243 research groups recognized by the Generalitat de Catalunya (Catalan Government)and more than 6,500 professionals in R&D, including lecturers and professors, post- and pre-doctoral researchers, and technicians and research assistants in a variety of disciplines, from humanities and social sciences to experimental sciences and health. These research groups collaborate with the leading research institutions and networks in Spain and abroad.

Through the creation of its Science and Technology Centres (CCiT), our university has pioneered scientific development at the level of higher education. In recent years and as the means by which the UB's different technological facilities could be brought together, the CCiT has allowed us to optimize our resources and improve the quality of our research and currently provides an important concentration of research infrastructure in Spain.

This handbook is a clear example of the quality of the research carried out at the UB.

Dídac Ramírez
Rector of the University of Barcelona

Foreword by the Vice-rector for Research of the University of Barcelona

The Scientific and Technological Centers of the University of Barcelona (CCiTUB) are a group of advanced facilities whose major mission is to support both research and innovation of researchers from the University of Barcelona, other public organizations and industry. In order to achieve this goal, the CCiTUB provide state-of-the-art instrumentation and expertise for use in R+D and Innovation projects and they also carry out methodological developments in order to improve both the capabilities and infrastructure of the centers.

One of the strengths of the CCiTUB is their wide technological offer, which is grouped into three key areas, namely Chemical, Materials, and Biosciences technologies. The strategic coordination and leveraging of resources at the CCiTUB allows successful completion of multidisciplinary projects, which often require both a coordinated and integrated approach.

The CCiTUB were set up in 1987 as the Scientific and Technical Services in order to house together all the high-technology instrumentation available at the UB, coordinated under unified technical management. Over the years, the analytical capabilities of the center have substantially increased to accommodate the latest technologies required by the research community. The center was renamed as the Scientific and Technological Centers in 2010.

The CCiTUB have both implemented and maintained a Quality Management System that fulfills the ISO 9001:2008 standard and are an acknowledged laboratory of the Register of Food and Agriculture Laboratories of Catalonia. The CCiTUB belong to the TECNIO network, promoted by the ACC10 agency of the Catalan Government.

The CCiTUB facilities are housed on different campuses at the UB and, as a result, enjoy the benefits of continuous interaction with the research community at our university.

Jordi Alberch
Vice-Rector for Research
University of Barcelona

Foreword by the Director of the CCiTUB

Belonging to the University of Barcelona, the Scientific and Technological Centers are a group of infrastructure facilities with the main goal to support research and innovation in the areas of chemistry, materials sciences and biosciences. In order to accomplish this goal, we provide state-of-the-art characterization technologies and specializing technological advice to both the research community and industry. An important part of our attention is devoted to methodological research in the above mentioned areas, aimed to improve both the capabilities and infrastructure of our centers. We also aim to enforce the university-industry relationship and promote innovation and technological transfer by participating in agreements and R+D+i projects with industry. Finally, we offer training courses and workshops regularly and are involved as partners in different European and International Infrastructure Networks.

We are one of the largest mid-size infrastructure facilities in Spain, with highly-qualified staff specialists, and the broadest range of characterization technologies. The latter are grouped in technological units which include microscopy and advanced characterization techniques, nuclear magnetic resonance, mass spectrometry, chemical spectroscopy, high-performance biotechnology, radiological protection, and animal facilities. Over the years we have built a solid reputation for quality and timely service, as our yearly customer satisfaction survey indicate. Our capabilities are used by well over thousand users in a typical year; these researchers originate from both university departments and public research institutes, as well as from industry. Our industrial customers represent sectors of economy that include pharmaceutical, cosmetics, chemical, environmental, health services, food, automotive and energy.

José Ramón Seoane
Director of the CCiTUB

Preface

This Handbook contains a collection of articles describing instrumental techniques used for Materials, Chemical and Biosciences research that are available at the Scientific and Technological Centers of the University of Barcelona (CCiTUB). The CCiTUB are a group of facilities of the UB that provide both the research community and industry with ready access to a wide range of major instrumentation. Together with the latest equipment and technology, the CCiTUB provide expertise in addressing the methodological research needs of the user community and they also collaborate in R+D+i Projects with industry. CCiTUB specialists include technical and Ph.D.-level professional staff members who are actively engaged in methodological research. Detailed information on the centers' resources and activities can be found at the CCiTUB website www.ccit.ub.edu.

The Handbook is intended to provide the reader with updated information on various technologies available at the CCiTUB. Each contribution summarizes the basic principles of a particular technique and gives examples of applications that illustrate capabilities of the technique. In addition, a wide selection of references give the reader ready access to more detailed information should it be required. The content and style of each contribution is intended to be suited to readers who are not familiar with the different techniques.

The CCiTUB are essentially organized into 3 main areas, namely Materials, Chemical and Biosciences technologies. The different techniques presented in this Handbook have been grouped under the umbrella of the corresponding area. It should be emphasized that this Handbook does not provide an overview of every instrumental technology available at the CCiTUB, but is focused only on a selection of the techniques available.

The Handbook is divided into 3 parts. Part 1 presents techniques that are used for materials characterization. These include x-ray photoelectron spectroscopy, electron energy loss spectroscopy, precession electron diffraction, electron probe microanalysis, advanced scanning electron microscopy, advanced optical microscopies, atomic force microscopy, x-ray single crystal and powder diffraction and paleomagnetism. In Part 2, characterization techniques relevant for chemical research are presented, which include crystal engineering, Fourier transform infrared spectroscopy, Raman spectroscopy, nuclear magnetic resonance, mass spectrometry and hyphenated techniques in gas chromatography mass spectroscopy, liquid chromatography mass spectrometry and isotope ratio mass spectrometry. In Part 3, the techniques used in biosciences research are discussed, including tri-dimensional (cryo) electron microscopy, advanced light microscopies, bioinformatics, proteomics, flow citometry, genomics, next-generation sequencing technology, surface plasmon resonance, and biological and biomedical applications of transmission and scanning electron microscopy. In Part 3, three contributions that are devoted to radiation protection issues are included, namely liquid and solid scintillation technologies, x-ray systems and radiation protection education.

It goes without saying that this Handbook could not have been written without the time and effort of so many contributors. Each contribution represents a distillation of the expertise and experience gained by the contributor(s) over the years working at the CCiTUB. We wish to thank them all for their efforts. We also wish to thank all the CCiTUB staff who have helped during the writing of this Handbook.

We hope the present Handbook will become a convenient source of information for researchers using characterization techniques at the CCiTUB.

José Ramón Seoane
Xavier Llovet

Contents

Part I. Materials technologies (MT)

Part II. Chemical technologies (ChT)

Part III. Biosciences technologies (BT)

Handbook of instrumental techniques from CCiTUB

Photoelectron spectroscopy for surface analysis: X-ray and UV excitation

Lorenzo Calvo-Barrio and Gardenia Vargas

Unitat d'Anàlisi de Superfícies, CCiTUB, Universitat de Barcelona. Lluís Solé i Sabarís, 1-3, 08028 Barcelona, Spain.

email: *lorenzo@ccit.ub.edu*

Abstract. This article summarizes the basic principles of photoelectron spectroscopy for surface analysis, with examples of applications in material science that illustrate the capabilities of the related techniques.

1. Introduction

Photoelectron Spectroscopy (PES) is a general term used to describe the characterization techniques that study the surface of a material by using either X-rays or ultraviolet (UV) light as an excitation source to promote an electronic emission. In both cases, the physical effect upon which these techniques are based is the same, the photoelectric effect, which can be traced back to its first documented observation by Hertz in 1887. During the first decades of the last century, the theory underlying this effect was quickly established together with the quantum theory, being Rutherford and Einstein [1] two of the well-known scientists who worked on its development. But it was not until the second half of the century that other researchers could develop some experimental devices that used the photoelectric effect to characterize the surface properties of materials. Those initial works culminated with a publication in 1967 by Kai Siegbahn [2], who explained how to obtain a spectrum by using X-rays as excitation source. At the same time, David W. Turner started to study free molecules in a gas phase by exciting them with ultraviolet light and collecting the emitted electrons. Since then, PES equipments have been built, their commercialization is in constant evolution and the technological parts, such as vacuum pumps, excitation sources, analyzers and electronics, are in continuous improvement. Nowadays, hundreds of PES spectrometers are being used in cutting edge technology research centres. Instruments combining both X-ray and UV excitation are not uncommon since, besides the excitation source, the remaining parts of the equipment are practically identical.

When X-ray excitation is used in PES, the technique is called XPS. It is also known as Electron Spectroscopy for Chemical Analysis (ESCA), given the use made of the emitted electrons. In short terms, XPS involves the irradiation with soft monochromatic X-rays of a solid in vacuum, and the subsequent emission and study of the electrons produced by photoelectric effect. The collected electrons can be represented in a plot where the number of electrons versus their kinetic or binding energy is drawn. The information obtained concerns only the surface of the material, because the mean free path of electrons in solids is so small that the detected electrons originate from a few top atomic layers. The achievement of quantitative measurements of the elemental composition and the identification of the different chemical states of the elements present at any surface are some of the main utilities of this technique.

On the other hand, the technique is called UPS when UV excitation is used in PES. Principles are essentially the same as those of XPS, but such a low-energy radiation (below 50 eV) is only capable of ionizing electrons from the outermost levels of atoms, the valence band (VB). Since these levels are directly involved in molecular bonding features, this technique is also known as molecular photoelectron spectroscopy. The study of the lower energy region of the spectra gives information about the density of occupied states (DOS) in the VB. Among other applications, this technique can be used to calculate the electronic band structure of a material and some relevant parameters concerning the interaction between interfaces.

2. Methodology

2.1. Basic Principles

Electrons are arranged in orbital levels around the nucleus and are bound to it by electrostatic attraction. Each orbital level has discrete energy levels that differ in value from the same orbital level in atoms of different elements, due to the different electrostatic attraction to the nuclei with different number of protons. The amount of energy required to remove one electron from the atom (the energy of its orbital level) is directly the binding energy of the electron. Therefore, a short wavelength photon from a specific X-ray source can be used to irradiate and thus to ionize an atom, producing an ejected free electron which characterizes the atom, as shown in Figure 1.

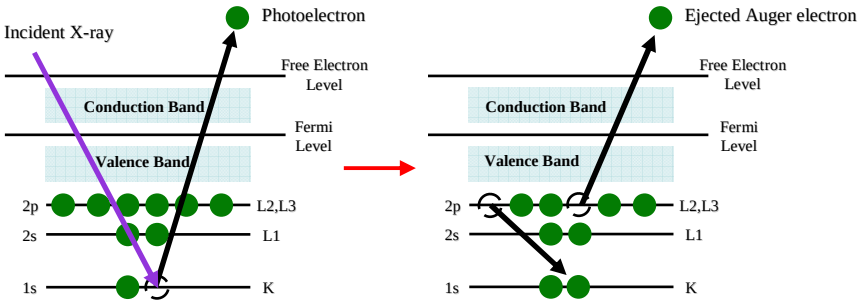

Figure 1. Schematic plot of the photoelectric effect (left) and the subsequent Auger effect (right).

The kinetic energy of the emitted electron depends on the energy of the photon, which is given by Einstein's photoelectric law

$$KE = h\nu - BE,$$

where *BE* is the binding energy of the atomic orbital from which the electron originates, *hν* is the energy of the incident X-ray (photon), and *KE* is the kinetic energy of the ejected electron (photoelectron).

Just after this process (at about 10^{-14} s), the resultant excited ion relaxes by moving a second electron from an outer orbital level into the inner hole left by the photolectron. This transition produces a quantity of energy that the ion can use in two ways, either by releasing an X-ray or by emitting an electron. This third electron is called Auger electron, and its energy is given by

$$KE_{auger} = BE_1 - BE_2 - BE_3,$$

where BE_i is the binding energy of the *i*-atomic orbital from which the photoelectron originates, and KE_{auger} is the kinetic energy of the last emitted electron. The main difference between the two emitted electrons is that the photoelectron is dependent on the irradiation energy while the Auger electron is only dependent on the energy difference between the orbital levels, which is characteristic of each chemical element.

It should be noticed that, when making realistic measurements, a new term, the work function of the spectrometer Φ_{spec}, has to be subtracted from the right hand side of these two equations. This constant value is related to the fact that a small portion of energy is needed to capture the electron from the free electron level (or vacuum level) and bring it to the entrance of the analyzer to be counted. Furthermore, if the BE is referred to the Fermi level of the ion (E_F, is the energy of the least tightly bound electrons within the solid) rather than to the free electron level, another small correction to the equations has to be done in order to account for the work function of the material Φ.

The photoelectric process occurs in the whole electronic structure from inner levels (also called core levels) to the less-bounded electrons of the VB. Moreover, the photoelectric process occurs all over the material that has been excited by the irradiation source, not only at the surface but typically some microns in depth. However, the surface sensitivity is an inherent characteristic of PES measurements due to the small inelastic electron mean free path (λ). This parameter is dependent on the kinetic energy of the electron, and also on the substrate that has to cross. It varies from 1 to 10 nm for the majority of substrates and for kinetic energies below 2 keV. In addition, because of these low values, the path from the surface to the analyzer has to be controlled in order to avoid the loss of too many electrons due to scattering by air molecules. Therefore, ultra-high-vacuum chambers (UHV, less than 10^{-7} Pa) are highly recommended for acquiring reliable PES spectra.

2.2. XPS spectra

By collecting the emitted photoelectrons with an appropriate electron analyzer, counting them and studying the spectrum of the number of electrons versus its distribution of kinetic or binding energy

(using the former equation), it is possible to recognize the material they come from. The analysis of a wide range of BEs will provide unique signatures of the elements as a function of their atomic number, thus providing elemental analysis. Moreover, if a mixture of elements is present, BE information will be related to all the elements and to their concentration ratio (the spectrum of a mixture of elements is approximately the sum of the spectra of the individual components). In this case a new problem arises: to determine the element from which a specific electron belongs, because overlapping of orbital levels from different elements could appear. This difficulty can be solved by looking for all the other orbital levels to know if the element is present or not.

The main features of a XPS spectrum of elemental uranium excited by a 1486.6 eV AlKα monochromatic X-ray line are shown in Figure 2. First of all, primary peaks resulting from the photoelectron process (*a*) can be seen. Some of them are in groups of two peaks as a consequence of the spin-orbit splitting (degeneration) that takes place in all orbital levels except in the *s* one. The intensity ratio between the two peaks depends only on the angular momentum *1* of the orbital level, but the distance between them depends also on the atomic number Z. The width of every primary peak depends quadratically on three contributions, one related to the physical nature of the atoms, another one concerning the analyzer characteristics, and a final one produced by the excitation source. The physical contribution cannot be modified because it originates from Heisenberg's uncertainty principle [3], but the two others can be reduced by improving the technique methodology.

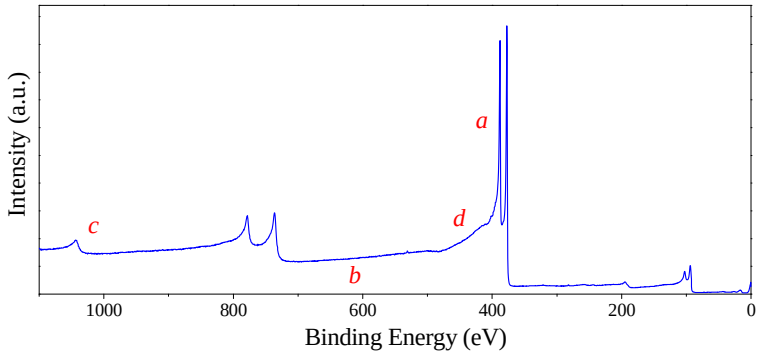

Figure 2. XPS spectrum of elemental uranium.

The characteristic background (*b*) of the XPS spectrum is mainly due to the inelastically scattered electrons. The electrons excited by the X-ray source at a certain depth not too far from surface cannot leave the surface without losing kinetic energy by inelastic scattering with atoms of the solid. This random energy loss appears in the spectrum as an increase of the background for binding energies greater than each primary peak.

The Auger electrons (*c*) can also be detected in the spectrum. Some Auger transitions can be seen, but the energy position is not relevant because the transitions do not dependent on the irradiation energy. They appear as a broad band because they are the result of the different combinations of energy losses from electrons of two or three different orbital levels.

Second order features of the XPS spectra (*d*) worth pointing out are: peaks due to the X-ray satellites of the excitation sources, shake-up and shake-off satellites, multiple splitting and asymmetric metal levels (all them related to the reorganization in different ways of the VB when the photoelectron leaves the surface), and bulk and surface plasmons (related to excitation of the modes of collective oscillation in the sea of conduction electrons). All these features can change dramatically the aspect of a high resolution (HR) spectrum for a selected BE window.

Finally, it is known that the interactions between atoms which form the different types of chemical bonds in molecules and compounds depend only on the VB levels, while the core levels are not directly involved in the bonding process. However, according to Koopmans' theorem, if the energy of the initial state of the atom changes by the formation of a chemical bond, the BE of the core electrons will change in a fixed quantity equal to the difference in the two atom states

$$\Delta BE = \Delta(E_{initial}(n) - E_{final}(n-1)),$$

being *n* the number of electrons that remains in the atom or ion. The fact that one type of bound or another is formed will affect slightly enough the electron bounded to the core level so as to observe changes when studying its energy at high enough resolution. Thus, chemical information can be extracted from XPS spectra by a HR spectrum fitting for determining the amount of each type of bond present in the elements of the surface. The level of accuracy when determining the zero of energy is of vital importance and this is a particularly difficult parameter to fix. Sometimes it is possible to measure where electrons start to be counted and equal this energy level to zero, but usually it is better to use an internal calibration, such as the position of one peak not affected by chemical bonding at the surface. For this purpose adventitious carbon (C) present by atmospheric contamination is very useful, and 284.8 eV can be fixed as an energy reference [4].

2.3. UPS spectra

UPS measurements deal with the structure of the VB and the less bounded electrons. Obtaining a UPS spectrum is similar to measuring a XPS spectrum, being UPS also a very surface sensitive technique. The same equipment can be used with the only difference of the excitation source. The great advantages of using UV radiation over X-rays, which also excite the low-energy bound electrons, are the very narrow line width of the radiation and the high flux of photons available from simple discharge sources, and as a result, the quick and better answer in terms of intensity and energy resolution of that low-energy part of the spectrum. To understand a UPS spectrum it is necessary to clarify some basic concepts from solid state physics and molecular chemistry, such as vacuum level (at surface and infinity), lowest unoccupied molecular orbital (LUMO), highest occupied molecular orbital (HOMO) and ionization potential (also called ionization energy, IE). All of them are outlined in Figure 3, together with an example of UPS spectrum of gold (Au) excited by a HeI line (Au is a standard material for UPS measurements, due to its total metallic behaviour).

It is worth mentioning that UPS measurements are more complicated than XPS measurements from the experimental point of view, because they can be affected by artefacts such as different charging and sputtering effects or damage produced by irradiation which are difficult to avoid or even to detect.

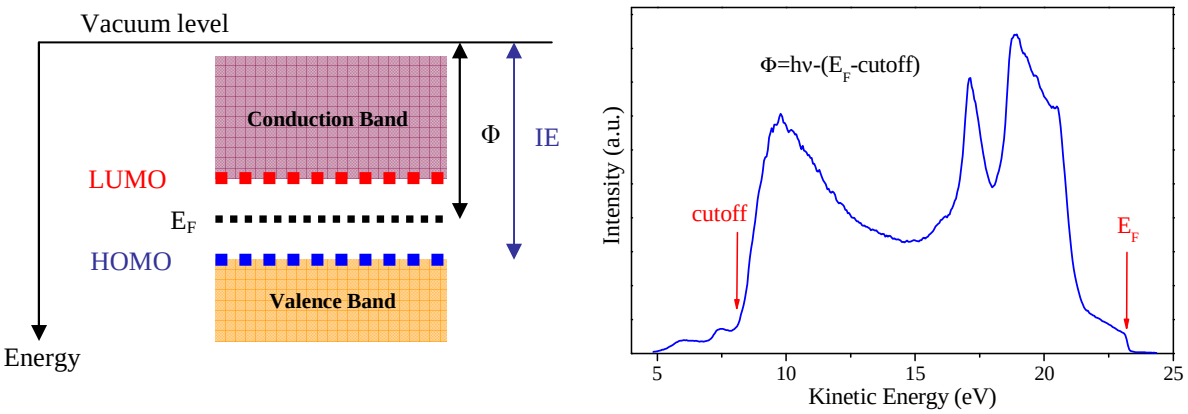

Figure 3. Sketch plot of atom outer energy levels (left) and UPS spectrum of Au (right).

The bands present in a UPS spectrum are very complex, since they are the result of a combination of the molecular orbital (MO) levels present at the surface (each MO is constructed by combining atomic orbital levels from each atom). For this reason, UPS is not as well established as XPS, but it can provide some very useful parameters such as the shape and peaks at the VB, the energy gap or band gap (distance between HOMO and LUMO), the fine structure due to vibrational levels of the molecular ion (bonding and antibonding MO levels), and the Φ of the surface. This latter parameter can be determined by measuring the full width of the spectrum, from the highest

kinetic energy (E_F) to the lowest kinetic energy cutoff, and then by subtracting the photon energy of the exciting radiation. For this purpose, it is necessary to measure accurately the energy cutoff (also called the onset of secondary electrons or onset of photoemission), defined as the minimum kinetic energy for which electrons are detected [5].

2.4. Analysis capabilities: Quantification, angle resolved and in-depth (profile) analysis

MT.1

2.4.1. Quantification. XPS can be considered as a quantitative technique, because the relative atomic concentration of the different constituents can be determined in elemental percentage. The number of electrons produced by photoelectric effect depends not only on the quantity of chemical elements present, but also on the ionization cross section of the orbital level (the probability that an ionization is produced) and other geometrical and analyzer parameters. The most common method used for quantification is the relative sensitivity factor (RSF) method, which supposes that

$$I=n\cdot F_s \qquad \text{and} \qquad F_s=f\cdot\sigma\cdot\theta y\cdot\lambda\cdot A\cdot T,$$

where I is the intensity (or the area) of a photoelectric peak of a given element, n is the number of atoms per cm^3 of the element in the sample and F_s is a constant value called sensitivity factor. F_s depends on the X-ray flux in photons/$cm^2\cdot$sec f, the photoelectric cross section for the atomic orbital of interest in cm^2 σ, the angular efficiency factor for the instrumental arrangement based on the angle between the photon path and detected electron θ, the efficiency in the photoelectric process for formation of photoelectrons of the normal photoelectron energy y, the λ, the area of the sample from which photoelectrons are detected A, and the detection efficiency for electrons emitted from the sample T. Thus, if all elements present at the surface are detected and one peak of each element with its well known F_s can be chosen, the following equation can be established

$$C_x = \frac{N_x}{\Sigma n_i} = \frac{I_x/F_s}{\Sigma I_i/F_i} \quad ,$$

where C_x is the concentration of one element in percentage present at the surface.

This method is currently used and software programs and databases are available [6]. Nevertheless, it has also some drawbacks namely it does not work for inhomogeneous structures in the nanometric scale, or some F_s values are not well established (they are far from being constant or simply do not exist for some photoelectric peaks of several elements). Another approach less used for quantification is to simulate theoretical spectra and then to compare them with the experimental results, paying special attention to the background [7].

2.4.2. Angle resolved XPS (ARXPS). ARXPS measurements define the sample tilting with respect to the analyzer. Changes in the design source-sample-analyzer will affect the escape depth of the electrons. Tilting the sample towards the analyzer will improve the relative signal from the outer part of the surface (from 1 to 2 nm) in front of the inner part, but will decrease in global terms the total amount of collected intensity. Moreover, the thickness of very thin overlayers of the surface (less than 5 nm) can be determined by assuming knowledge of some parameters. For this reason, the technique is sometimes called non-destructive depth profiling. The simplest approach to this calculation is to assume that the intensity of the collected electrons that come specifically from the substrate material below the overlayer I_s can be expressed by the following equation

$$I_s=I_o\cdot e^{-d/(\lambda\cos\theta)},$$

where I_o is the measured intensity if there was no overlayer on the substrate, d is the thickness of the overlayer and θ is the angle between the normal to the surface and the analyzer (take off angle). More complex attempts can be done to increase accuracy in these calculations, and to study either a heterogeneous layer or a multilayer on a substrate [8].

2.4.3. In-depth XPS. The erosion of the surface under UHV conditions allows to perform in-depth measurements. For this purpose an ion gun of a noble gas such as argon (Ar) is sputtered over the surface. Measurements alternate with the sputtering and, as a consequence, a new surface is present for the analysis every time. Thus, an elemental profile can be drawn. By controlling both intensity

and energy from the ions, the damage produced by the sputtering and the chemical interaction of the implanted ions can be minimized. In very specific cases it is even possible to measure in depth some elements with enough resolution to obtain a chemical state profile [9].

2.5. Instrumentation

PES equipment at the CCiTUB includes two systems, a XPS PHI-5500 from Physical Electronics (1991) and a XPS plus UPS SAGE-HR from Specs (2004). The following explanations of the instrument characteristics will refer to these systems [10].

In XPS measurements, a soft monochromatic X-ray source obtained by high-voltage excitation (10 to 15 kV) under UHV conditions is used as excitation source. Usually Al kα or Mg kα lines, with energies of 1486.6 eV and 1256.6 eV respectively, are used because they have enough energy to excite orbital levels of all stable atoms and are thin enough to be used in HR measurements. To decrease the energy width that these sources introduce, the use of a monochromator is advisable, which also reduces satellites, Bremsstralhlung irradiation and other minor artefacts. The irradiated surface is normally a large area of about 0.5 cm^2. In UPS measurements the radiation source is a helium (He) discharge lamp that emits two lines of radiation, HeI at 21.22 eV and HeII at 40.82 eV. The energetic difference between these two lines is a constant value that allows checking the good electric behaviour of the spectrometer (if the analyzer and the sample holder are grounded). The irradiated surface is a large area of about $1cm^2$.

The spectrometer part of PES equipments consists of electromagnetic lenses, an analyzer and a detector or electronic counting system. The lenses usually operate in a mode called constant analysis energy (CAE), which retards the electrons to specific energies (called pass energies) and allows to have constant energy resolution along all the range of kinetic energies. The lenses also drive the electrons to the entrance of the concentric hemispherical analyzer (CHA). A CHA consists of two charged concentric metal hemispheres that create an electric field between them. The electrons going across it are captured by the outer or inner sphere depending on their kinetic energy. Only electrons in a narrow energy region (close to the pass energy) succeed in getting all the way round from the hemispheres to the detector. The detector is often a multi channel electronic device that can collect several groups of electrons with different kinetic energies. Spectrometers define the effective area of measurement, typically a circle of about 0.8 mm in diameter. A tricky feature of them is that the intensity is inversely proportional to the energy resolution of any mode of working.

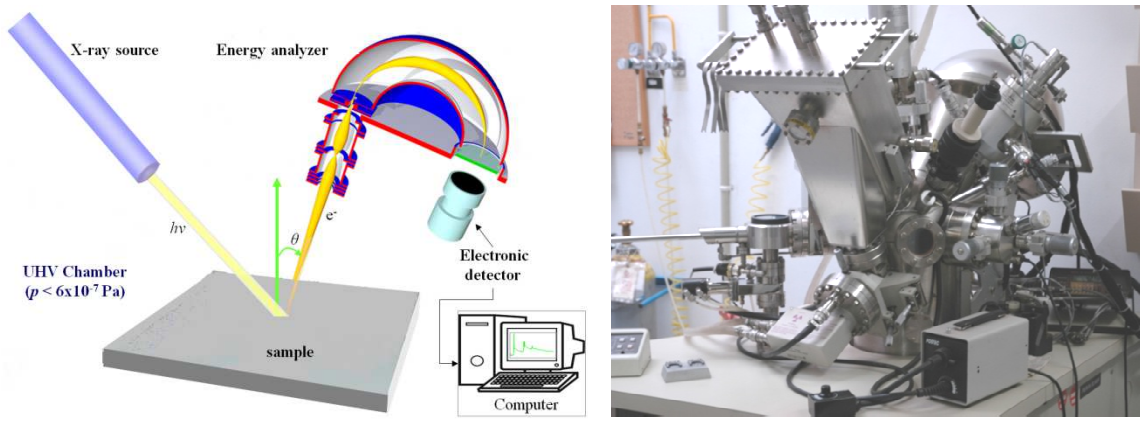

Figure 4. Basic drawing of PES instrument (left) and picture of our PHI-5500 XPS system (right)

In order to achieve UHV (10^{-7} Pa), PES equipments use three different types of vacuum pumps namely rotary, turbomolecular and ion pumps, each one useful to reach a different level of vacuum, from atmospheric to UHV. When pumps are joined, very accurately pressure control systems and filaments that help to improve vacuum are also necessary.

Moreover, two indispensable systems are the ion gun and the electron gun. An ion gun of a noble gas (usually Ar) helps not only to perform an in-depth profile (as explained before) but also to clean under UHV conditions the contamination on surfaces. Slight sputters (1 or 2 nm) at low energies (typically 3.5 KeV) and low fluxes allow to remove the absorber contaminants, such as adventitious C. On the other hand, a low-energy electron gun helps to keep non-conductive samples free from electrical charging. As electrons go out from the surface by photoelectric process, non conductive samples increase the BE of its remaining electrons. One effective way to prevent this fact is to inject low-energy electrons (less than 10 eV), which will be captured and start a dynamical reincorporation of them on the surface. This solution cannot be used in UPS, where sometimes a bias voltage is applied to the sample holder to discriminate the energy cutoff.

A specific sample preparation is not required for PES measurements. Theoretically, a flat surface is needed, but powders can also be measured by sticking them on bi-adhesive C tapes that work well in UHV conditions. Sample characteristics are often limited by vacuum and electrical behaviour.

3. Applications and Practical Examples

XPS and UPS can be used in very different types of surfaces, ranging from the homogeneous to the most heterogeneous surfaces, such as powders, fibers, or particles in suspension (dried at the surface before measurement). A list of the fields where these techniques are applied includes metal alloys, ceramic materials, polymers and plastics, coatings, implants, composite materials, semiconductors, inorganic and organic compounds, surface contaminant identification, interfacial chemistry, catalysis and corrosion. Moreover, new fields such as biological surfaces or nanostructured materials, previously forbidden to UHV and X-ray related techniques, start to be trendy due to the latest possibilities in terms of technology [11]. In the following, some examples of PES applications will be presented in order to show the enormous capabilities of these techniques.

3.1. Elemental identification, quantification and chemical bonding in Cr-doped TiO_2 samples

Titanium dioxide (TiO_2 or Titania) is a technological excellent material widely used for many applications, such as sensors, optical coatings, pigments, solar cells or photocatalysis. Its good and varied properties (strong oxidation power, chemical and mechanical stability, high refractive index, photostability or environmental friendly nature) can be improved as desired with doping, especially with transition metal atoms like chromium (Cr). TiO_2 doped thin films, inorganic nanotubes and nanoribbons can be prepared with many methods, for instance CVD, sol–gel, reactive sputtering or pyrolysis, allowing the use of this material in very small devices. But the resultant chemical characteristics and especially the band gap can be very different depending on the preparation method and doping characteristics, and only a surface sensitive technique such as XPS can control them [12].

Spectra from a TiO_2 thin film doped with Cr are shown in figure 5. A wide XPS low resolution spectrum reveals peaks related to four chemical elements, oxygen (O), titanium (Ti), Cr and C. By choosing the main peaks of each element and using the RSF method, their atomic concentration percentage is calculated, resulting in 14.7% of C, 56.4% of O, 22.4% of Ti and 6.5% of Cr.

Assuming that C comes from atmospheric contamination (adventitious C), a previous accurate calibration of the binding energy is done. The HR spectrum of Ti and Cr can be fitted to identify its chemical bonding. The Ti2p orbital level fits well with a doublet from only one chemical specimen assumed to be TiO_2 by shape and energy position. Instead, Cr2p shows clearly that each peak of the doublet has to be fitted with two chemical specimens, which correlate with Cr^{3+} and Cr^{6+} by shape and energy position. All important data fits, such as BE, full width at half maximum (FWHM) and area percentage, are reported in Table 1.

The proposed chemical bonds not only have to agree with the energy position, but also the total O content. Assuming TiO_2, Cr_2O_3 and CrO_3 to be the present oxides, the total amount of O calculated taking into account its ratios to the metals should be 44.8% in TiO_2 plus 6.1% in Cr_2O_3

and 4.4% in CrO_3, making a total of 55.3%. This number approaches the total amount of O (56.3%). The small difference could be explained by either experimental error or some C=O bonds related to atmospheric contamination. These numbers evidence the good agreement in both energy position and fit for the proposed chemical specimens and validate the chemical bonding identifications. Unfortunately, the HR spectrum of O (not shown here) cannot be used to trace back these chemical bonding identifications, due to the almost inexistent difference in energy for the different bonds (all of them at about 530 eV).

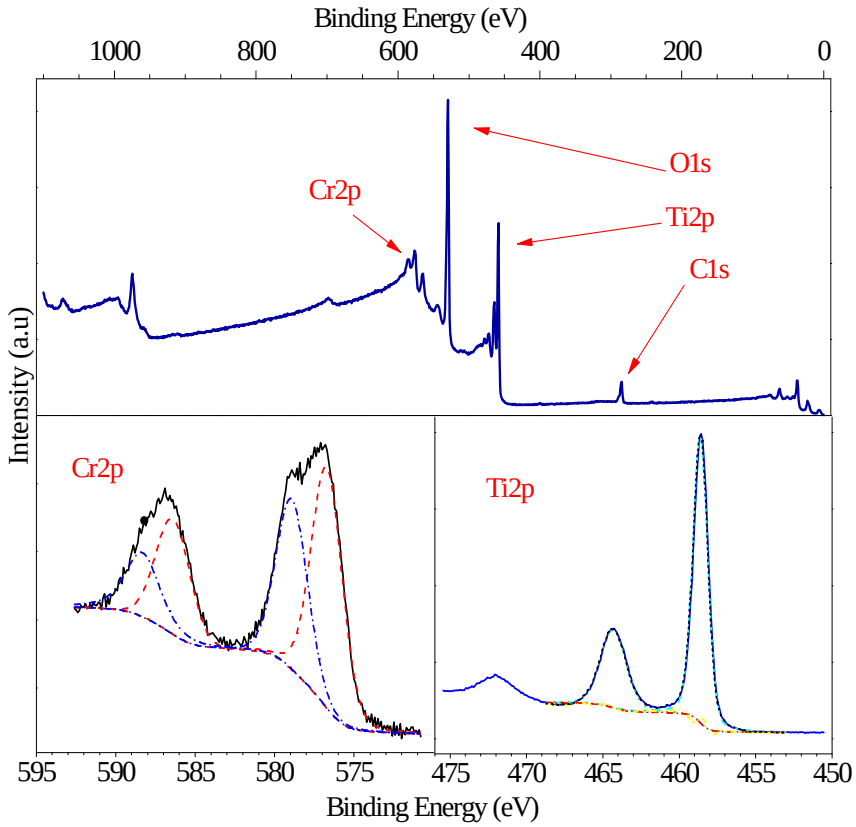

Figure 5. At the top: a wide low resolution XPS spectrum. The bottom figures are HR XPS spectra of Cr2p and Ti2p orbital levels and their fits.

Table 1. XPS parameters corresponding to a Cr-doped TiO_2 sample

Cr2p					Ti2p				
Line	BE (eV)	FWHM (eV)	Area (%)	Suggested bond	Line	BE (eV)	FWHM (eV)	Area (%)	Suggested bond
2p3/2	576.76	2.31	38.97	Cr_2O_3	2p3/2	458.62	1.14	66.67	TiO_2
	578.96	2.33	27.69	CrO_3	2p1/2	464.31	2.01	33.33	TiO_2
2p1/2	586.45	2.53	19.49	Cr_2O_3					
	588.35	2.55	13.85	CrO_3					

3.2. ARXPS in polymers absorbed on metal surfaces

The deposit and bonding of organic molecules and polymers in inorganic surfaces is being considered as one of the most outstanding fields in surface science, since this is the way to reach biocompatible devices. Synthesis methods as well as quality of initial surfaces play an extremely important role for obtaining the best features in the final material. The analysis of chemical structure and morphology, and the determination of physical properties in relation to compositional and structural parameters of self assembled monolayers (SAMs) of organic molecules on metals can be done by ARXPS. This technique allows to discriminate the actual element that is bound to the metal surface [13].

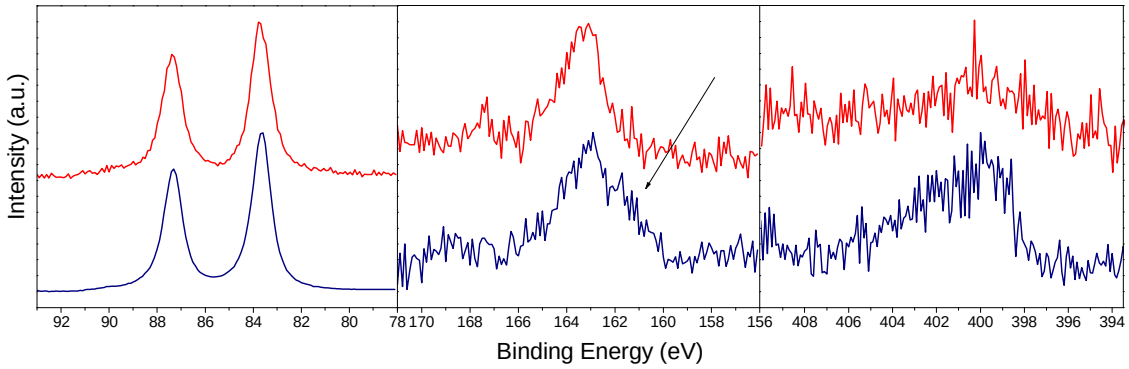

Figure 6. HR XPS spectrum at 5º (top) and 45º (bottom) of take off angle. From left to right: Au4f, S2p and N1s.

Figure 6 shows an overlaid plot of Au, sulphur (S) and nitrogen (N) HR spectra at two different take-off angles observed in SAMs of 4-thiolphencyphos and dodecanothiol on polycrystalline gold over glass. By changing the take off angle from 45º to 5º, data coming from the top surface is improved. These data reveal no differences in Au (as expected), but changes in both S and N. The S spectrum at 5º is composed by a single peak, while the spectrum at 45º has a shoulder at low energies (marked by the arrow) that indicates an additional chemical state that would be responsible for the bound with the metal. Moreover, the N spectra do not show a clear peak at 5º but a peak formed by two o three chemical states appears at 45º revealing that N is not on top, and maybe is also involved in the bound with Au.

3.3. Chemical characterization of new chalcogenide absorbers for next generation photovoltaic technologies (PV): in-depth XPS concentration profiles

Cu_2ZnSnS_4 and $Cu_2ZnSnSe_4$ (CZT(S,Se)) compounds are receiving an increasing interest for the replacement of chalcopyrite absorbers used in $Cu(In,Ga)(S,Se)_2$ (CIS) solar cells [14,15]. In relation to CIS based PV technologies, CZT(S,Se) materials are formed by abundant and non-toxic materials, which make them more suited for their massive deployment in the next years to compete in a more efficient way with traditional non-renewable energy sources. However, efficiencies achieved with these absorbers are still lower than 10%. One of the reasons for low efficiency values in these devices is the potential presence of secondary phases, probably at the grain boundary regions, which deteriorate the optoelectronic properties of the layers. Full identification and characterization of phase inhomogeneities is crucial for further optimization of these technologies In-depth XPS analysis provides both the atomic concentration profile and the chemical information of the layers when minimizing the damage produced by the Ar^+ sputtering.

On the left of Figure 7, all the spectra of $Zn2p_{3/2}$ orbital level from the surface to the bulk are shown. A plot like this one can be obtained from one orbital level of each element present at the sample. Using the RSF method, the atomic concentration percentage versus sputter time is calculated (on the right). The percentages of the different elements do not agree with the theoretical assumptions of composition of the material. The Cu signal is large enough all along the layer which indicates that some Cu-rich secondary phases (like Cu_3SnS_4) are also formed. This phase will certainly alter the electric behaviour of the solar cell. The comparison of XPS in-depth data with X-ray diffraction (XRD) and Raman scattering spectroscopy data will help in clarifying this point [16].

3.4. Study of VB and molecular bonds: determination of HOMO levels in pentacene deposited on nanostructured substrates

Organics electronics, i.e. the conjunction between organic surfaces and inorganic materials, is one of the most outstanding fields in material science. Correct understanding of these systems requires knowledge of the physics and chemistry of its surfaces and interfaces. The complex structures created by the chemical reactions between organic adsorbed molecules and metal surfaces can be

studied by looking at the molecular orbital levels by UPS. Nowadays, metal substrates are nanostructured (in order to create nanodevices) which leads to greater complexity on the subject [17, 18].

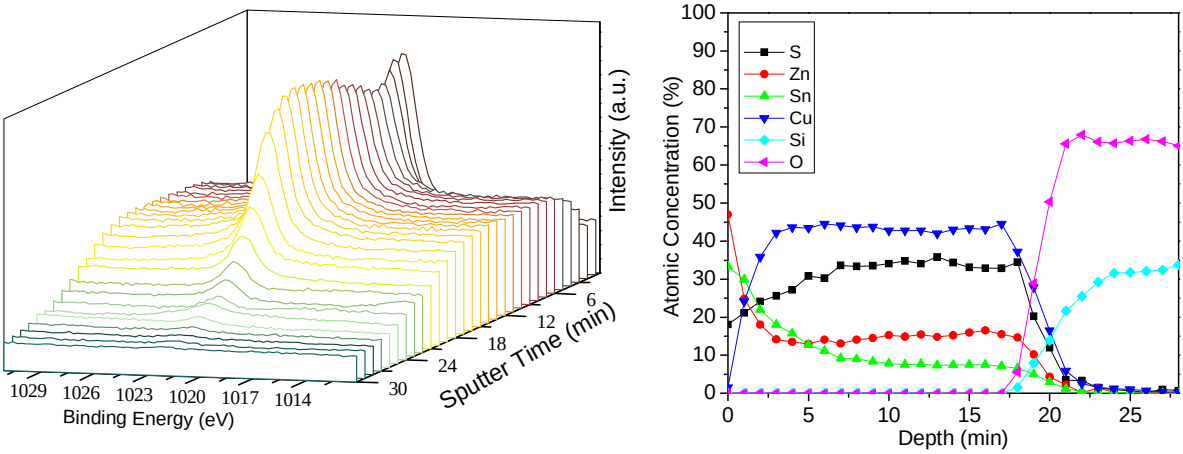

Figure 7. XPS depth profile of CZTS on silicon oxide. In-depth spectra from $Zn2p_{3/2}$ (left) and elemental atomic concentration in % (right).

In Figure 8, UPS spectra of pentacene absorbed on inorganic surfaces used in nanoelectronics, such as Au or silicon carbide (SiC), are presented. These materials are very useful for new generations of organic light-emitting diodes (OLEDs) and organic field-effect transistors (OFETs). The objective is to know the nature of the interaction between the organic material and the different metals, and a point of starting is to look at parameters such as the variation of HOMO levels, IE, Φ, and the hole injection barrier (HIB, the difference between E_F and HOMO). The spectra show the main characteristics of a UPS measurement, a peak at high binding energy from secondary electrons, and several bands that appear from medium BEs to near the E_F value. Reference measurement in Au presents E_F at -0.07 eV, and a Φ value of 6.14 eV, higher than the expected. This trend will help to compare the relevant data from samples covered by pentacene (presented in Table 2) with the values from the literature.

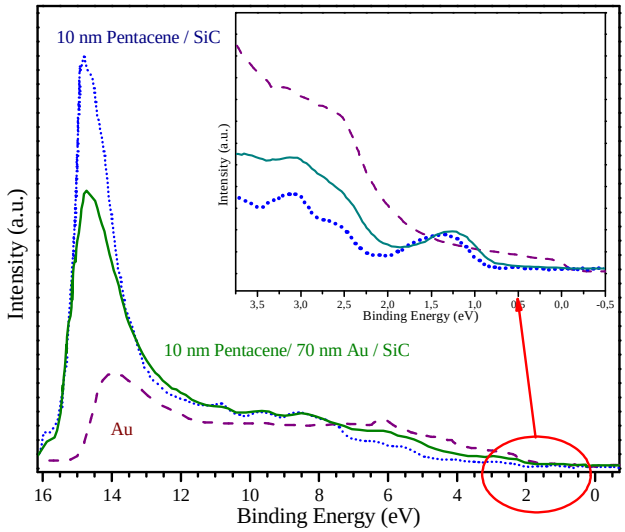

Table 2. UPS parameters

Sample	Pentacene on SiC	Pentacene on Au
HOMO (eV)	0.95	0.83
IE (eV)	6.62	6.33
Φ (%)	5.59	5.42
HIB (eV)	1.02	0.87

Figure 8. UPS spectra (HeI excited) of Au, 10-nm-thick pentacene on SiC and 10-nm-thick pentacene on 70 nm of Au over SiC.

Acknowledgments

The authors would like to thank Dr. David Amabilino and Angela Bejarano for allowing to use unpublished results of ARXPS, and Johanna Fuks for the work done in UPS with us in the past.

References

MT.1

[1] A. Einstein was awarded the Nobel in 1921 for his developments on the photoelectric theory.
[2] K. M. Siegbahn was awarded the Nobel in 1981 for his achievements in XPS.
[3] W. Heisenberg was awarded the Nobel in 1932 for his contributions in quantum mechanics.
[4] M. P. Seah, D. Briggs 1992 *Practical Surface Analysis by Auger and X-ray Photoelectron Spectroscopy*, Wiley & Sons Chichester, UK.
[5] D. Cahen, A. Kahn 2003 *Advanced Materials* **15** 271.
[6] Multipak V8.2B, 2006 ULVAC-PHI Inc. and CasaXPS V2.3.15, 2009 Casa Software Ltd.
[7] S. Tougaard 1998 *Surface and Interface Analysis* **26** 249.
[8] P. J. Cumpson 1995 *Journal of Electron Spectroscopy and Related Phenomena* **73** 25.
[9] C. Serre, L. Calvo−Barrio, A. Perez-Rodriguez et al 1996 *Journal of Applied Physics* **79** 6907.
[10] Detailed information about these instruments in www.phi.com and www.specs.com.
[11] D. R. Baer, M. H. Engelhard 2010 *Journal of Electron Spectroscopy and Related Phenomena* **178-179** 415.
[12] R. López, R. Gómez, S. Oros-Ruiz 2011 *Catalysis Today*, article in press.
[13] J.J. Dubowski, O. Voznyy, G. M. Marshall 2010 *Applied Surface Science* **256** 5714.
[14] L. Calvo-Barrio, A. Perez-Rodriguez et al 2001 *Vacuum* **63** 315.
[15] X. Fontane, V. Izquierdo-Roca, L. Calvo-Barrio et al 2009 *Applied Physics Letters* **95** 261912.
[16] X. Fontane, L. Calvo-Barrio et al 2011 *Applied Physics Letters* **98** 181905.
[17] N. Kock 2008 *Journal of Physics: Condensed Matter* **20** 184008.
[18] F. Amy, C.Chan, A.Kahn 2005 *Organic Electronics* **6** 85.

Handbook of instrumental techniques from CCiTUB

Electron Energy Loss Spectroscopy: physical principles, state of the art and applications to the nanosciences

Sònia Estradé

Unitat Microscòpia Electrònica de Transmissió aplicada als Materials, CCiTUB, Universitat de Barcelona. Lluís Solé i Sabarís, 1-3. 08028 Barcelona. Spain.

email: *sestrade@ccit.ub.edu*

Abstract. In the present work we review the way in which the electron-matter interaction allows us to perform electron energy loss spectroscopy (EELS), as well as the latest developments in the technique and some of the most relevant results of EELS as a characterization tool in nanoscience and nanotechnology.

MT.2

1. Introduction: EELS in a nutshell

In the Transmission Electron Microscope (TEM), an incident electron suffers both elastic and inelastic scattering by the solid state thin sample that is being characterised. In the event of inelastic scattering, the incident electron gives a part of its energy to the electrons in the sample. The amount of lost energy can then be measured by a magnetic filter at the end of the column, and a plot displaying how many electrons have lost what amount of energy will give us an Electron Energy Loss (EEL) Spectrum. Thus, in an EEL Spectrum the ordinate axis corresponds to the number of electrons, or counts, and the abscise corresponds to the Energy Loss.

Notice that most electrons shall not suffer any inelastic scattering whatsoever. As a consequence, the greatest contribution to the spectrum is due to these electrons having lost zero energy, giving rise to the so-called zero-loss peak (ZLP). As for those electrons having lost a certain amount of energy, they may lose it to give rise to a ionization of specimen electrons, transitions from occupied core states to unoccupied core states or to conduction band states, to interband transitions or excitations of collective vibrations of conduction band electrons.

Incident electrons carry a given momentum, and it is worth keeping in mind that in an elastic scattering event not only energy, but also momentum, may be transferred. In fact, this is the reason why it is not straightforward to compare EELS results with those obtained by means of optical spectroscopies.

EELS detectors can provide an energy resolution down to the order of the 0.1 eV. In addition, incident electrons can be tuned by TEM optics, making it possible to obtain spectroscopic information from an extremely constrained area, and to combine EEL Spectroscopy with TEM imaging.

2. Understanding inelastic scattering

Whenever an incident beam interacts with a solid state specimen in the TEM, a number of signals are generated, as schematically displayed in figure 1.

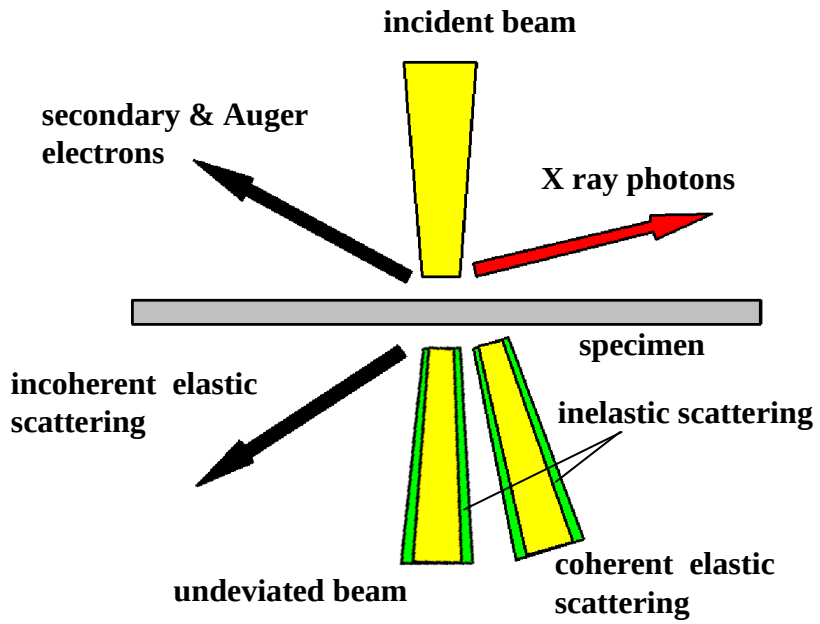

Figure 1: Signals generated from the beam/specimen interaction in the TEM.

A scattering event is inelastic if the incident fast electron suffers a detectable energy loss. Elastic scattering can be viewed as being billiard-ball-like, with very little energy loss implied. Yet,

Rutherford scattering may cause appreciable displacement damage to the sample, with an energy interchange in the order of the tens of eV.

Single scattering refers to one single scattering event; plural scattering, to a string of several (countable) scattering events suffered by the incident electron; finally, multiple scattering refers to a string of scattering events which are too numerous to keep track of them, and, thus, to implement accurate calculations.

The probability for a scattering event to take place is described by its cross section. The cross section is the apparent area each atom makes available in relation to the event. In order to understand this definition, it is important to keep in mind that, if the number of atoms per unit volume in the solid state sample is n_a, then, the probability that a scattering event X, described by a cross section σ_X, takes place in a differential thickness dy is: Probability (X) = $n_a\sigma_X dy$. Alternatively, we can define the mean free path (mfp) λ as the average distance travelled before the event takes place, thus $\lambda = 1/n_a\sigma_X$.

The cross section may be a function of angle, and of the energy lost by the incident electron in the case of an inelastic event, and, in this sense, the differential cross section per unit solid angle

$$\frac{d\sigma_X}{d\Omega}$$

and the double differential cross section

$$\frac{d^2\sigma_X}{d\Omega dE}$$

are usually referred to.

A simplistic description of **elastic scattering** is given by assuming Rutherford scattering from the whole atom. In this case,

$$\frac{d\sigma}{d\Omega} = \frac{4\gamma^2 Z^2}{a_0^2 q^4}$$

where Z is the atomic number,

$$\gamma = \left(1 - \frac{v^2}{c^2}\right)^{-1/2}$$

$a_0 = 0.529\text{x}10^{-10}$ m is the Bohr radius and q is the scattering vector $q = 2k_0\sin(\theta/2)$, with $\vec{q}$ being the momentum transferred to the nucleus in $\hbar$ units. Notice that the above formula implies a strongly forward peaked scattering.

Rutherford scattering does not take into account the screening of the nucleus potential by localized electrons, overestimates scattering at low angles and, if integrated over all angles, yields an infinite cross section.

In order to take the screening into account, a Yukawa potential with a screening radius r_0 can be considered:

$$V(r) = \frac{Ze}{4\pi\varepsilon_0 r}\exp(-r/r_0)$$

Then, the obtained differential cross section is of the form:

$$\frac{d\sigma}{d\Omega} = \frac{4\gamma^2 Z r_0^4}{a_0^2}\left(\frac{Z}{q^2 r_0^2 + 1}\right)^2$$

We will later discuss the physics of **inelastic scattering** in detail. Inelastic scattering can promote a number of excitations in the specimen. Phonons are the lowest form of life in the de-excitation chain, as everything else dies by exciting a phonon. Their energy is yet too low (less than 0.1 eV) to be detected in the EELS spectrum.

Collective oscillations of the free electrons, ejections of a single valence electron (single electron excitation) and ejections of a single atom core electron (core-loss) will be present in the EELS spectrum.

2.1. Lentz formalism of atomic inelastic scattering

Let us consider the inelastic scattering of an electron by a single atom. This event is described by a differential cross section $d\sigma_i/d\Omega$.

Lentz modification of Morse's theory of elastic scattering gives an expression for the inelastic differential cross section of the form:

$$\frac{d\sigma_i}{d\Omega} = \frac{4\gamma^2 Z}{a_0^2 q^4}\left[1 - \frac{1}{(1+(qr_0)^2)^2}\right]$$

where again the electrons in the atom are described by a screening radius r_0 (in a Thomas-Fermi model, r_0 can be assumed to be $r_0 = a_0 Z^{-1/3}$). $\vec{q}$ is the scattering vector $\vec{q} = \vec{k}_f - \vec{k}_0$, where $\vec{k}_f, \vec{k}_0$ are the final and initial momentum of the incident electron respectively (see figure 2). q^2 can be written as

$$q^2 = k_0^2\left(2 - 2\sqrt{1-2\theta_E}\cos\theta - 2\theta_E\right)$$

where θ is the scattering angle (i. e.: the angle between $\vec{k}_f$ and $\vec{k}_0$, as shown in figure 2), and θ_E is the characteristic scattering angle

$$\theta_E = \frac{E}{2E_0}$$

with E_0 being the initial energy, and E, the energy loss.

Using a Taylor expansion for $\sqrt{1-2\theta_E}$ and $\cos\theta$ up to second order in θ_E and θ, we obtain

$$q^2 \approx k_0^2\left(\theta^2 + \theta_E^2\right)$$

Substituting in the differential inelastic cross section expression, we obtain:

$$\frac{d\sigma_i}{d\Omega} \approx \frac{4\gamma^2 Z}{a_0^2 k_0^4}\frac{1}{(\theta^2+\theta_E^2)^2}\left[1 - \frac{\theta_0^4}{(\theta^2+\theta_E^2+\theta_0^2)^2}\right]$$

where

$$\theta_0 = \frac{1}{k_0 r_0}$$

The above equation contains the information relative to the angular distribution of the scattered electrons. Notice that the largest part of the scattering falls between θ_E and θ_0, where the differential inelastic cross section is roughly proportional to θ^{-2}.

One can be interested in the total cross section integrated up to a certain angle β. In this case,

$$\sigma_i(\beta) \approx \frac{8\pi\gamma^2 Z}{k_0^2}\ln\left[\frac{(\beta^2+\theta_E^2)(\theta_0^2+\theta_E^2)}{\theta_E^2(\beta^2+\theta_0^2+\theta_E^2)}\right]$$

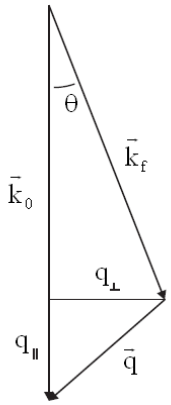

Figure 2: Geometric construction of the scattering vector.

2.2. The quantum mechanical approach: Bethe Theory

Let us now consider a sample, consisting of one atom for simplicity (we will later see how accurate this simplification is), as being described before and after the inelastic scattering event by its wavefunctions, Ψ_0 and Ψ_n. Ψ_0 will then be the ground state of the atom and Ψ_n a certain excited state.

If we can regard the interaction with the atom as a perturbation for the fast electron, which we can reasonably do in any practical EELS experiment, we can use the first order Born approximation to obtain a differential cross section of the form

$$\frac{d\sigma_n}{d\Omega} = \left(\frac{m_0}{2\pi\hbar^2}\right)\frac{k_f}{k_0}\left|\int V(\vec{r})\psi_0\psi_n^* e^{i\vec{q}\vec{r}}d\tau\right|^2$$

Again, $\vec{q}$ is the scattering vector, and, thus, $\hbar\vec{q} = \hbar(\vec{k}_0 - \vec{k}_f)$ is the moment transferred to the atom. $\vec{r}$ is the coordinate of the fast electron, $V(\vec{r})$ is the interaction potential and, finally, $d\tau$ is a differential volume element within the atom.

The explicit form for $V(\vec{r})$ is given by

$$V(\vec{r}) = \frac{Ze^2}{4\pi\varepsilon_0 r} - \frac{1}{4\pi\varepsilon_0 r}\sum_{j=1}^{Z}\frac{e^2}{\left|\vec{r} - \vec{r}_j\right|}$$

where $\vec{r}_j$ is the position of the j-th electron in the atom. Notice that the interaction potential is not a proper potential. In fact, it is related to the electrostatic potential ϕ as $V = e\phi = -U$, where U is the potential energy of the fast electron.

Also notice that the atomic nucleus contribution to V amounts to zero when integrated, because of its symmetry. In physical terms, we could say that the nucleus mass is by no means comparable to the mass of the incident electron, and thus no inelastic scattering is allowed. Inelastic scattering is an electron-electron event. Integrating, we obtain

$$\frac{d\sigma_n}{d\Omega} = \left(\frac{4\gamma^2}{a_0 q^4}\right)^{(a)}\frac{k_f}{k_0}\left|\varepsilon_n(q)\right|^2$$

where the term (a) is the Rutherford cross section for a single electron, and ε_n is the dynamical structure factor

$$\varepsilon_n = \left\langle \psi_n \left| \sum_j \exp(i\vec{q}\vec{r}_j) \right| \psi_n \right\rangle = \int \psi_n^* \sum_j \exp(i\vec{q}\vec{r}_j)\psi_n d\tau$$

It is then convenient to define the generalized oscillator strength (GOS) as

$$f_n(q) = \frac{E_n}{R}\frac{|\varepsilon_n(q)|^2}{(qa_0^2)}$$

where E_n is the energy lost in the transition (finally appearing in an explicit form) and R is the Rydberg energy

$$R = \frac{m_0 e^4/2}{(4\pi\varepsilon_0\hbar)^2} = 13.6\text{eV}$$

Substituting, we obtain

$$\frac{d\sigma_n}{d\Omega} = \frac{4\gamma^2 R}{E_n q^2}\frac{k_f}{k_0} f_n(q)$$

It is worth noticing that in the $q\rightarrow 0$ limit, $f_n(q) = f_n$, with f_n being the dipole oscillation strength –optical absorption is governed by the dipole oscillation strength.

As we are interested in the E dependence of the differential cross section, we can now define

$$\frac{d^2\sigma}{d\Omega dE} = \frac{4\gamma^2 R}{Eq^2}\frac{k_f}{k_0}\frac{df}{dE}(q,E)$$

As

$$\frac{k_1}{k_0} = \sqrt{\frac{E_0 - E}{E_0}}$$

and $E_0 >> E$, then we can assume

$$\frac{k_1}{k_0} \approx 1$$

We then obtain

$$\frac{d^2\sigma}{d\Omega dE} \approx \frac{4\gamma^2 R}{Ek_0^2}\left(\frac{1}{\theta^2 + \theta_E^2}\right)\frac{df}{dE}$$

This formalism applies to single atoms or gas specimens, but TEM experiments are supposed to deal with solid state samples. Is this the wrong approach? Not really. The formalism still applies to the inner atomic shells of atoms in a solid, and, even if solid state effects modify df/dE, it can be treated as a perturbation. A scheme of an inelastic scattering event in a crystal is given in figure 3.

As for outer shell electrons, their wavefunctions are modified by chemical bonding, and collective effects cannot be ruled out.

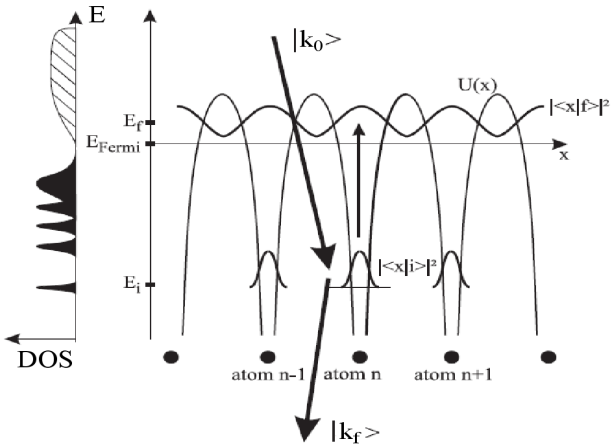

Figure 3: Schematic diagram of an inelastic scattering event in a crystal.

3. EELS as a tool for materials science

Some twenty years ago, scientists interested in EELS had to overcome the impression that "EELS [was] a playground for physicists and of little help for solving materials science problems"[7]. Nowadays, given the eventual reduction in scale of the problems at hand and the progressive instrumental advances that have taken place in microscopy in general and in EELS in particular, it seems clear that EELS has become a most crucial tool in materials science and even the life sciences[8,9].

As EELS is performed in the Transmission Electron Microscope (TEM), it benefits from the very high spatial resolution that can be achieved with electron optics, which can focus the electron beam to form a subnanometric probe. In particular, if a field-emission gun (FEG) is used, sufficient current can be obtained for a 1 nm probe. Within aberration corrected instruments, this figure can be reduced to 0.1 nm. In addition, EELS can be easily combined with structural information as obtained from the TEM imaging and diffraction modes, and even with complementary X-ray energy-dispersive spectroscopy (EDXS) if needed.

There is a fundamental limit to the minimum lateral resolution that can be achieved by EELS, irrespective of the electron optics. As commented in chapter 1.1, this limit is given by the delocalisation produced in inelastic scattering, and depends on the energy loss (the lower the loss, the greater the delocalisation)[10]. Yet, fortunately, this limit does not prevent from getting EELS signal from single atom columns at core-loss[11] or subnanometric resolution in low-loss experiments[12].

4. Recent developments

With the recent advances in instrumentation (spherical aberration correctors, electron monochromators, new energy filters and CCD detectors) EELS experiments can now be performed with a spatial resolution well below 0.1 nm and an energy resolution better than 0.2 eV.

One of the instrumental highlights in the history of TEM is the recent introduction of systems to compensate for spherical and even chromatic aberrations[13,14,15]. One way of achieving spherical aberration (C_s) correction is based upon the use of two hexapoles where the second order aberrations from the first hexapole are compensated by the second hexapole element. As the two hexapoles additionally induce a third-order spherical aberration which is rotationally symmetric and proportional to the square of the hexapole strength, and is of the opposite sign to that of the objective lens, the spherical aberration of the entire system can be compensated by appropriately controlling the strength of the hexapoles[13]. Alternatively, spherical aberration correction can be achieved through quadrupole-octupole (QO) corrector[14,15]. The QO corrector uses a quadrupole to put a line focus along the negative spherical aberration axis of an octupole, a further two

quadrupoles to produce a line focus in the perpendicular direction in a second octupole, and a fourth quadrupole to reform a round beam. The two octupoles add a negative spherical aberration in x and y, but also cause some four-fold distortion of the beam. A third octupole, acting on a round beam, is used to correct that distortion. A potential advantage of a QO corrector over a hexapole corrector is the possibility of also correcting the first-order chromatic aberration[15]. Spherical aberration, parasitic second-order axial aberrations, coma and threefold astigmatism, and the non-spherical axial third-order aberrations, star aberration and fourfold astigmatism need to be compensated at the same time by adequately changing the intensity of all the involved lenses. This is achieved by software assisted recursive measuring and compensation of the aberrations. All kinds of instabilities must be suppressed for the corrector to perform adequately[13,14,15]. Using aberration corrected microscopy, an electron probe smaller than 1 Å can be achieved, which allows imaging of single atoms, clusters of a few atoms, and atomic columns.

A multipole corrector built into the illumination system of a STEM increases the image resolution and allows more current to be focused in a given probe. This is of great importance for spectroscopy, as both lateral resolution and signal-to-noise ratio are enhanced.

If EELS presents a lower energy resolution when compared to other spectroscopies as X-ray absorption spectroscopy (XAS), the limitation does not lye in the capabilities of the spectrometers, but in the energy width of the electron source. This energy dispersion is typically 1–2 eV for a thermionic source and 0.5–1 eV for a Schottky or field-emission tip. For a cold FEG, this figure can go down to 0.3 eV. For comparison, synchrotron X-ray sources and beam-line spectrometers commonly provide a resolution below 0.1 eV for absorption spectroscopy, and even below 1 meV in certain cases[16].

In order to reduce the source energy spread, monochromators have been recently introduced. There are two main approaches: the electromagnetic Wien filter and the electrostatic Omega filter. Both types improve the energy width to about 0.2 eV. Yet, they both produce an energy spectrum of the electron source at a dispersion plane, where a narrow energy-selecting slit selects a small fraction of the electron distribution. As a result, many electrons are absorbed by the slit -the beam current at the specimen is reduced by a factor at least equal to the fractional improvement in energy resolution[12]. Nowadays, the monocromators yield a beam current in the order of several 100 pA[16].

The single Wien filter limits the probe size to about 2 nm, whereas there is no such limitation in the case of the Omega filter[17]. In some Wien filter designs[18], the dispersion is compensated and the beam reduced to its original size by using second monochromator section which produces an achromatic image of the electron source (double Wien filter).

5. Solving problems with EELS

5.1. Low-loss applications

Bulk plasmon peak position can be used as an indirect compositional measure, and has been extensively used as a local chemical characterization tool, especially in the case of semiconductors. It can be primarily used as an identification tag for determining which compound is there at a given region of the studied specimen[19, 20]. As the plasmon peak position depends on the lattice parameter (as well as the bandgap energy and the dielectric constant) it can also give an indirect measure of structural properties[21, 22].

The need for characterization techniques that provide precise information regarding the bandgap and general optical properties at high spatial resolution seems to be out of question, given the scaling down that has taken place in the field of materials science and the rapidly widening use of nanostructures. In this sense, standard optical techniques such as vacuum ultra-violet spectroscopy do not provide the spatial resolution required to probe a material on the nanometer scale. Low-loss EELS seems to be a most fitting technique for the local characterization of optoelectronic properties at the nanoscale.

For insulators or semiconductors with a sufficiently wide bandgap (that can be less than 1 eV using a monochromated Scanning Transmission Electron Microscope (STEM)[23]), interband transitions can be observed in the EELS spectrum. It is possible to identify through EELS the

bandgap energy of given nanostructures[24,25,26]. It is also possible to assess the existence of localized states within the bandpgap, which may be due to the presence of dislocations or other kinds of defects, for instance[27, 28], which create new energy levels in the local density of states (DOS).

A most promising EELS capability is in characterizing the local optical properties of semiconductors through Kramers-Kronig analysis of low-loss data. In 1999, experiments carried in a cold FEG VG 501 STEM demonstrated the possibility to access the local dielectric function of several semiconducting nitrides at the nanoscale through EELS[29]. The reliability of the result directly depends on the quality of the EELS data, mostly concerning the accuracy of the EELS intensity measurement at very low energy. Surface modes of excitation of small particles and nanotubes (in the range of 12-18 eV) have also been studied through EELS in a cold FEG VG 501 STEM. They have been shown to highly depend on the anisotropy of the nanostructure[30]. Yet, surface plasmons of nanostructures often occur at energy losses below 10 eV and are often poorly resolved, even for very thin specimens. A low energy spread (and hence the use of a monochromator) can greatly benefit the characterization of such surface modes, which mostly describe their optical properties. In this sense, a very recent work by Schaffer et al.[31], demonstrated high resolution Energy Filtered Transmission Electron Microscopy (EFTEM) mapping of gold nanoparticles surface plasmons using a monochromator. On the other hand, Nelayah et al[32]. showed that optical properties can be analyzed in the near-infrared/visible/ultraviolet domain (energy loss under 3 eV) without a monochromator. A statistical technique and customized acquisition process were used to enable the observation of very low energy surface plasmon peaks. This method was applied to an equilateral Ag nanoprism with 78-nm-long sides and allowed the observation of three plasmon resonance modes centered at 1.75, 2.70 and 3.20 eV, corresponding respectively to wavelengths of 709, 459 and 387 nm.

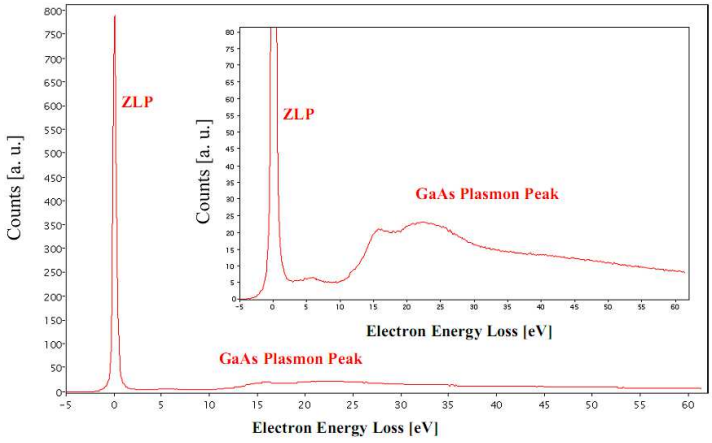

Figure 4: Low-loss EELS spectrum of a GaAs nanowire, including the ZLP. Inset: detail of the low-loss spectrum

5.2. Core-Loss EELS elemental identification and quantification. Single atom detection Maybe the most common question that is addressed using EELS as a characterization tool is which elements, and in what proportion, are found, locally, in a given specimen. Problems such as interdiffusions at interfaces, or elemental distributions in nanostructures, sometimes specifically require EELS because the involved scales exceed the spatial resolution otherwise available.

Elemental identification is straightforward, but quantification is problematic. EELS quantification of a spectrum involves background removal and intensity conversion to chemical concentration through the appropriate, energy dependent, experimental geometry dependent, single-atom cross-section. Quite a lot of discussion has been centered on the optimal way of extracting the background[33,34,35], and a great deal of effort has been devoted to the calculations of EELS cross-sections[36,37,38]. Nowadays, both background fitting and extraction and cross-section calculations are generally carried out using the EELS quantification tools in the Gatan Digital Micrograph software. Although this is a robust and reliable tool, it is also extremely user-dependent, and may give rise to biased or plain nonsensical results depending on their level of

expertise (no matter how badly the quantification is made, the software will always produce a number). In order to avoid the problems associated with this usual quantification procedure, Verbeeck and coworkers[38,39,40] proposed the use of a C based software package (EELSmodel) to carry out a model based quantification of EELS spectra. The EELSmodel program works starting from a series of parameters which are introduced by user, and through a choice of different possible statistical tools, tunes these parameters to finally reach the model which better matches the experimental spectrum. A python model-based quantification program (EELSlab) is currently being implemented by de la Peña and coworkers in STEM Group in Orsay.

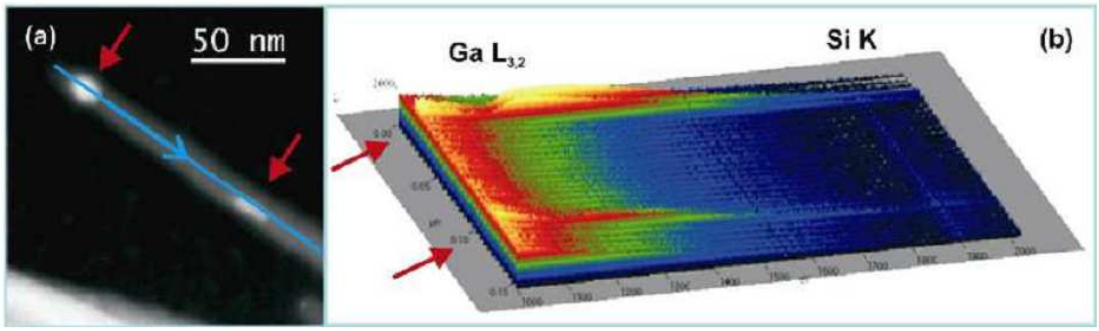

Figure 5: (a) High Angular Annular Dark Field image of a Si nanowire. (b) EEL spectra obtained in the nanowire along the line indicated in (a), which demonstrate the presence of gallium segregation along the nanowire.

Recent applications of EELS elemental quantification include the characterization of semiconducting nanostructures[41,42], thin films with applications in spintronics[43,44], or shape memory alloys[45].

As it has been previously stated, the incorporation of monochromators and aberration correctors for TEM has much helped improve the spatial and energetic resolution of EELS. Yet, best energy and best spatial resolution are not found in the same experimental configurations[46]. Best energy resolution (about 0.1 eV), achieved with monochromators, and most useful for low-loss EELS, comes with a spatial resolution in the order of the 1 nm. In an aberration corrected STEM, where energy resolution is about 0.4eV can achieve a spatial resolution in the order of the Armstrong. Such configuration is best for the core-loss chemical analysis of atomic columns and the localisation of individual atoms in nanostructures.

In this sense, Kimoto and coworkers[47] demonstrated atomic-column imaging of a crystal using core-loss EELS. In particular, the atomic columns of La, Mn and O in manganite $La_{1.2}Sr_{1.8}Mn_2O_7$ were visualized as two-dimensional images, using the La $N_{4,5}$, O K, Mn $L_{3,2}$ and La $M_{5,4}$ edges signal.

Muller and coworkers succeeded in quantifying the vacancy concentrations in $SrTiO_3$ (STO) at atomic scale through core-loss EELS[48]. Varela and coworkers detected a single La dopant atom in $CaTiO_3$, through High Angular Annular Dark Field (HAADF) intensity and La $M_{5,4}$ edge signal[49]. Recently, single Au atoms were observed in Si nanowires grown using Au as a catalyst[50].

5.3. Core-Loss EELS atomic coordination and oxidation state determination

In compounds where there is a coordinate bonding, information of the kind of bonding which is present is of the utmost importance to gain insight into the compound structure. The energy loss near edge structure (ELNES) of an EELS edge is given by the local DOS of the atom suffering the inelastic scattering, and, thus, contains information on its bonding. Coordination determination from ELNES fingerprinting is a standard technique from as soon as the mid 1980s[51]. As energy resolution is improved, so is the level of detail in ELNES of EELS edges. In this sense, many efforts have been recently devoted to theoretical calculations of ELNES, which allow the use of theoretical references to compare to actual EELS spectra, and further comprehension of the individual features in the ELNES[52,53].

The shift of the threshold energy of a given edge is a measure of charge transfer but also of coordination number[4]. Chemical shift can thus be used as a fingerprint to determine to which compound belongs the atom giving rise to the observed transition. A thoroughly studied classic case is that of the chemical shift of Si $L_{2,3}$ edge, that has been correlated to the electronegativity of nearest neighbour atoms for Si alloys[54], or to the mean Si-O bond lengths in Si oxides[55], for instance.

White lines ($L_{2,3}$ edges of transition metals and $M_{4,5}$ edges of rare earths) appear in the shape of two sharp peaks, with an energy separation given by the spin-orbit splitting of the initial states. The relative intensity of those peaks, yet, does not correspond to the number of electrons in the initial state, as it would be intuitive. This is so because of a spin selection rule. The final white-line intensity ratio depends on Z number and on the oxidation state[1].

References

[1] Egerton, R. F., "Electron Energy Loss in the Electron Microscope" (2nd ed.) Plenum Press (1996)

[2] Williams, D. B. and Carter, C.B., "Transmission Electron Microscopy: A Textbook for Materials Science Basics", Plenum Press (1996)

[3] Goodhew, P. J., Humphreys, J., Beanland, R., Electron Microscopy and Analysis (3rd ed.), Taylor & Francis (2000)

[4] Bransden, B. H. ; Joachain, C. J., "Quantum mechanics" (2nd ed.), Pearson Education, (2000)

[5] Kittel, C., "Introducción a la física del estado sólido" (3a ed.), Reverté (1993)

[6] Verbeek, J., Thesis, Antwerp University (2002)

[7] Colliex, C., Microsc. Microanal. Microstruct., 2, 403 (1991)

[8] Pan, Y., Sader, K., Powell, J. J., Bleloch, A., Gass, M., Trinick, J., Warley, A. , Li, A., Brydson, R., Brown, A., Journal of Structural Biology 166, 22 (2009)

[9] Calvert, C. C., Brown, A., Brydson, R., Journal of Electron Spectroscopy and Related Phenomena, 143, 173 (2005)

[10] Egerton, R. F. and Malac, M., Journal of Electron Spectroscopy and Related Phenomena, 143, 43 (2005)

[11] Hofer, F. and Kothleitner, G., Microsc. Microanal. Microstruct., 4, 539 (1993)

[12] Haider, M., Uhlemann, S., Schwan, E., Rose, H., Kabius, B. Urban, K., Nature 392, 768 (1998)

[13] Batson, P. E., Dellby, N., Krivanek, O. L., Nature 418, 617 (2002)

[14] Bleloch, A., Lupini, A., Materials Today 7, 42 (2004)

[15] Egerton, R. F., Micron 34, 127 (2003)

[16] Sigle, W., Annual Review of Materials Research, 35, 239 (2005)

[17] Tsuno, K., Microsc. Microanal. 6, 142 (2000)

[18] Topuria, T., Browning, N. D., Ma, Z., Applied Physics Letters, 83, 4432 (2003)

[19] Irrera, A., Iacona, F., Franzò, G., Boninelli, S., Pacifici, D., Miritello, M., Spinella, C., Sanfilippo, D., Di Stefano, G., Fallica P. G., Priolo, F., Optical Materials 27, 1031 (2005)

[20] Shen, Y. G., Mai, Y. W., McKenzie, D. R. , Zhang, Q. C., McFall, W. D., McBride, W. E., Journal of Applied Physics, 88, 1380 (2000)

[21] Sanchez, A. M., Beanland, R., Papworth, A. J., Goodhew, P. J., Gass, M. H., Applied Physics Letters, 88, 051917 (2006)

[22] Erni, R. and Browning, N. D., Ultramicroscopy, 104, 176 (2005)

[23] Kuykendall, T., Ulrich, P., Aloni, S., Yang, P., Nature Materials 6, 951 (2007)

[24] Iakoubovskii, K., Mitsuishi, K., Furuya, K., Nanotechnology 19, 155705 (2008)

[25] Arenal, R., Stéphan, O., Kociak, M., Taverna, D., Loiseau, A., Colliex, C., Microscopy and Microanalysis, 14, 274 (2008)

[26] Batson, P. E., Kavanah, K. L., Woodall, J. M., Mayer, J. M., Phys. Rev. Lett. 57, 2719 (1986)

[27] Xin, Y., James, E. M., Arslan, I., Sivananthan, S., Browninga, N. D., Pennycook, S. J., Omnes, F., Beaumont, B., Faurie, J., Gibart, P., Applied Physics Letters, 76, 466 (2000)
[28] Lakner, H,, Raferty, B., Brockt, G., Journal of Microscopy, 194, 79 (1999)
[29] Kociak, M., L. Henrard, L., Stéphan, O., Suenaga, K., Colliex, C., Physical Review B, 61, 13936 (2000)
[30] Schaffer, B., Hohenester, U., Trügler, A., Hofer, F., Physical Review B, 79, 041401 (2009)
[31] Nelayah, J., Kociak, M., Stéphan, O., de Abajo, F. J. G., Tencé, M., Henrard, L., Taverna, D., Pastoriza-Santos, I., Liz-Marzán, L. M., Colliex, C., Nature Physics 3, 348 (2007)
[32] Su, D. S. and Zeitler, E., Physical Review B, 47, 14734 (1993)
[33] Liu, D. R. and Brown, L. M., Journal of Microscopy, 147, 37 (1987)
[34] Pun, T., Ellis, J. R., Eden, M., Journal of Microscopy, 137, 93 (1985)
[35] A. Weickenmeier; H. Kohl, Philosophical Magazine Part B, 60, 1463 (1989)
[36] Hofer, F., Microsc. Microanal. Microstruct., 2, 215 (1991)
[37] Potapov, P.L., Jorissen, K., Schryvers, D., Lamoen, D., Physical Review B, 70, 045106 (2004)
[38] Verbeeck, J. and Van Aert, S., Ultamicroscopy, 101, 207 (2004)
[39] Verbeeck, J, Van Aert, S., Bertoni, G., Ultamicroscopy, 106, 976 (2006)
[40] Schade, M., Heyroth, F. Syrowatka, F., Leipner, H.S., Boeck, T., Hanke, M., Applied Physics Letters 90, 263101 (2007)
[41] Lari, L., Murray, R.T., Bullough, T.J., Chalker, P.R., Gass, M., Chezec, C., Geelhaar, L., Riechert, H., Physica E 40 2457 (2008)
[42] Samet, L., Imhoff, D., Maurice, J.-L., Contour, J.-P. Gloter, A., Manoubi, T., Fert, A., Colliex, C., European Physical Journal B 34, 179 (2003)
[43] Simon, J., Walther, T., Mader, W., Klein, J., Reisinger, D., Alff, L., Gross, R., Applied Physics Letters 84, 19 (2004)
[44] Yang, Z.Q., Schryvers, D., Materials Science and Engineering A 481, 214 (2008)
[45] Browning, N. D., , Arslan, I., Erni, R., Idrobo, J. C., Ziegler, A., Bradley, J., Dai, Z., Stach, E. A., Bleloch, A., Journal of Physics: Conference Series 26, 59 (2006)
[46] Kimoto, K., Asaka, T., Nagai, T., Saito, M., Matsui, Y., Ishizuka, K., Nature, 450, 702 (2007)
[47] Muller D. A., Nakagawa, N., Ohtomo, A., Grazul, J. L., Hwang, H. Y., Nature 430, 657 (2004)
[48] Varela, M., Findlay, S. D., Lupini, A. R,, Christen, H. M., Borisevich, A. Y., Dellby, N., Krivanek, O. L., Nellist, P. D., Oxley, M. P., Allen, L. J., Pennycook, S. J. Physical Review Letters, 92, 095502 (2004)
[49] Allen, J. E., Hemesath, E. R., Perea, D. E., Lensch-Falk, J. E., Li Z. Y., Yin, F., Gass, M. H., Wang, P., Bleloch, A. L., Palmer, R. E., Lauhon, L. J., ature Nanotechnology 3, 168 (2008)
[50] Garvie, L. A., Craven, A. J., Brydson, R., American Mineralogist, 79, 411 (1984)
[51] Eustace, D. A., McComb, D. W., Docherty, F. T., Craven, A. J., Microscopy and Microanalysis,13, 1276 (2007)
[52] Mauchamp, V., Boucher, F., Ouvrard, G., Moreau, P., Physical Review B, 74, 115106 (2006)
[53] Auchterlonie, G. J., McKenzie, D. R., Cockayne, D. J. H., Ultramicroscopy, 31, 217 (1989)
[54] Garvie, L. A. J., and Buseck, P. R., American Mineralogist, 84, 946 (1999)
[55] Wang, Z. L., Yin, J. S., Mo, W. D., Zhang, Z. J., Journal of Physical Chemistry B, 101, 6794 (1997)
[56] Estradé, S., Thesis, Universitat de Barcelona (2009)

Handbook of instrumental techniques from CCiTUB

Precession Electron Diffraction in the Transmission Electron Microscope: electron crystallography and orientational mapping

Joaquim Portillo

Unitat Microscòpia Electrònica de Transmissió aplicada als Materials, CCiTUB, Universitat de Barcelona. Lluís Solé i Sabarís, 1-3. 08028 Barcelona. Spain.

email: *quim@ccit.ub.edu*

Abstract. Precession electron diffraction (PED) is a hollow cone non-stationary illumination technique for electron diffraction pattern collection under quasi-kinematical conditions (as in X-ray Diffraction), which enables “ab-initio” solving of crystalline structures of nanocrystals. The PED technique is recently used in TEM instruments of voltages 100 to 300 kV to turn them into true electron diffractometers, thus enabling electron crystallography. The PED technique, when combined with fast electron diffraction acquisition and pattern matching software techniques, may also be used for the high magnification ultra-fast mapping of variable crystal orientations and phases, similarly to what is achieved with the Electron Backscatter Diffraction (EBSD) technique in Scanning Electron Microscopes (SEM) at lower magnifications and longer acquisition times.

1. Introduction

Precession electron diffraction (PED) is an inverted hollow cone illumination technique for electron diffraction pattern collection under quasi-kinematical conditions (as in X-ray Diffraction), which allows solving "ab-initio" crystal structures of nanocrystals. Diffraction patterns are collected while the TEM electron beam is precessing on an inverted cone surface; in this way, only a few reflections are simultaneously excited and, therefore, dynamical effects are strongly reduced.

In comparison with normal selected area electron diffraction, PED has the following advantages:

- Oriented electron diffraction (ED) patterns may be obtained even if the crystal is not perfectly aligned to a particular zone axis. Thus, reliable ED patterns may be collected very quickly without the need to accurately align the observed crystal along a particular zone axis, which is very useful when dealing with beam sensitive materials (zeolites, pharmaceuticals, proteins, etc.)
- Geometry of PED patterns, when including first-order Laue zone excitation, show all symmetry elements necessary to determine the space and point group of the nanocrystal under investigation, without the need of applying further special techniques, such as Convergent Beam Electron Diffraction.
- PED intensities are quasi-kinematical, likewise to X-rays , up to a thickness of 100 nm and may be used to solve the structure of nanocrystals

PED has recently gained large recognition in TEM and X-Ray community and several new nanocrystalline structures have been solved with this technique [1,2]. On the other hand, a new field of precession diffraction has recently been developed, the orientational/phase mapping through rapid precessed electron diffraction data collection, which may be regarded as the equivalent in the TEM to the Scanning Electron Microscopy (SEM) based EBSD technique (Electron Backscatter Diffraction)[3].

2. Precession Electron Diffraction and Electron Crystallography

The principle of precessed illumination consists in scanning the electron beam over the surface of an inverted cone with its vertex at the specific location in the sample from which a structure determination is desired. The scanning is achieved by feeding AC signal from an external generator to the beam tilt and beam deflection coils, which are depicted as four groups of three red dots over the specimen plane in figure 1. The scanning frequency is variable and may be adjusted from 1 to 100 Hz. The AC signal is also fed in phase opposition to the image deflection coils -depicted as two groups of three red dots bellow the specimen plane in figure 1- in order to form a pseudo-stationary electron diffraction pattern, the so-called precession pattern. This pattern contains diffracted amplitudes with intensities which may largely differ from those obtained in conventional non-precessed, stationary electron diffraction pattern as the inset in figure 1 shows for a complex oxide structure investigated by C.Own et al in 2004[4].

The reason why the technique may be successfully applied -in a number of cases- to structural elucidation lies in the fact that at each specific point in time, only a limited number of crystal lattice planes satisfy the exact or near-exact Bragg diffracting condition. This fact implies that the possibility of multiple scattering or "cross talk" between diffracted amplitudes at a frozen moment of the scanned illumination is largely reduced in comparison to conventional static zone axis illumination of the sample. The partial diffraction pattern thus obtained is then completed by adding up in time over the number of turns described by the electron beam (this is frequency dependent) over the usual diffraction pattern acquisition time. For instance, for a total recording time of 4 seconds, working at 100Hz, the electron beam would have turned 400 times over the surface of the inverted illumination cone giving rise to 400 partial diffraction patterns, the total sum of which would be shown as in the lower right-hand side of figure 1. It is important to note that each reflection in the pattern, when looked in real time through the TEM binocular, shows a titillating intensity, just as spinning stars do in astronomical observation.

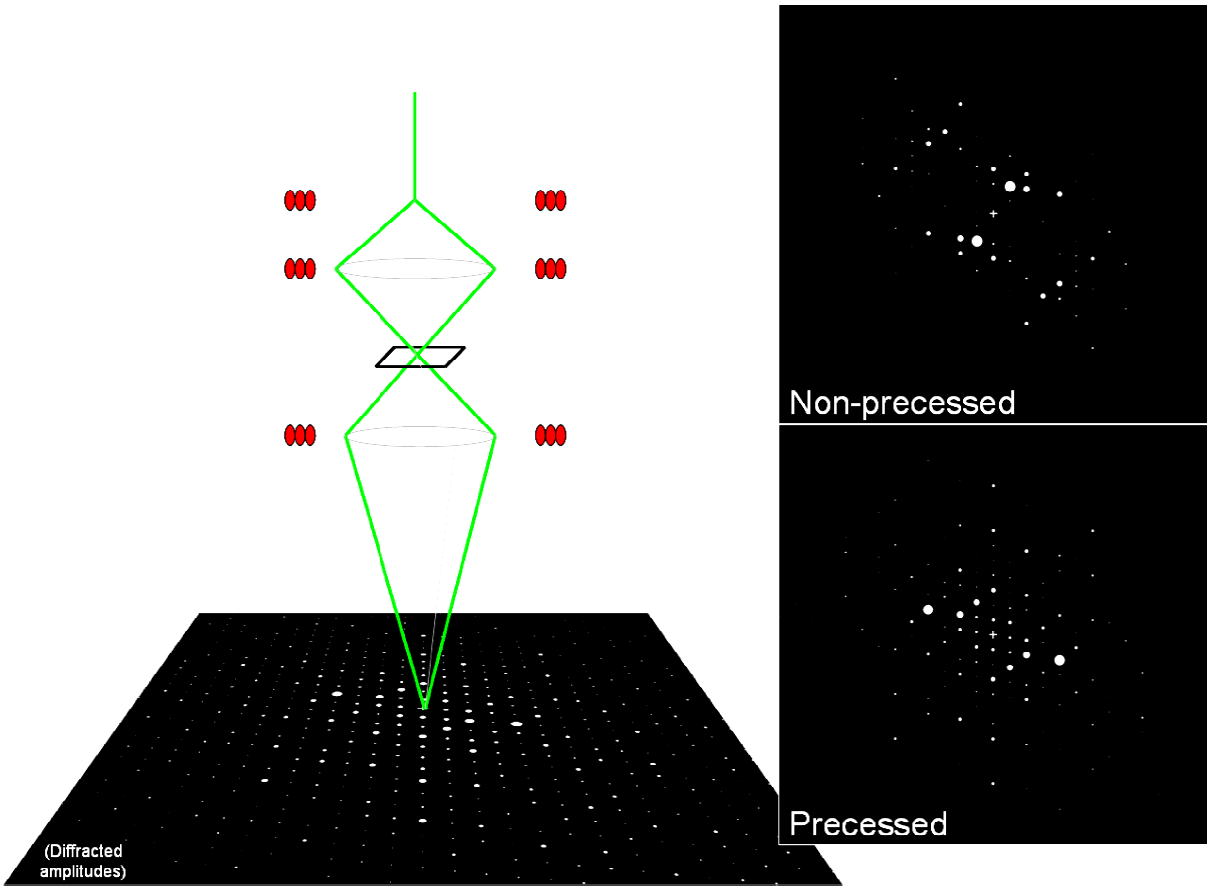

Figure 1: Electron ray-path in precessed (or inverted hollow cone scanned) illumination of the sample, together with de-scan to produce pseudo-stationary diffracted amplitudes.

Applying this technique, a number of structures have been solved, with the same methodology used for single crystal X-ray diffraction patterns, that is, diffraction pattern indexing, intensity extraction, re-scaling of projected symmetry related intensities and phase assignation based on direct methods using programs such as SIR2008 or similar. The final output is a list of proposed atomic structures (number of atoms and their positions in the unit cell) with different residual values, which are taken as a reliability factor to validate the most plausible one. The residual is defined as the sum over all reflections of the relative differences between experimental diffracted amplitudes and calculated diffracted amplitudes for the proposed atomic structure, see image 2 for an overview of the described process in the particular case of the mayenite mineral.

It is interesting to note in the mayenite case that a huge difference exists between the unprecessed and precessed electron diffraction patterns, as seen in figure 3. Therefore, the above described procedure would have rendered a totally wrong atomic model when applied to the conventional electron diffraction pattern.

MT.3

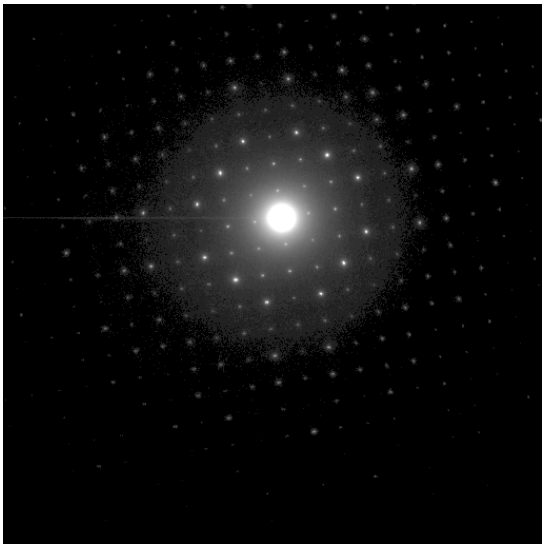

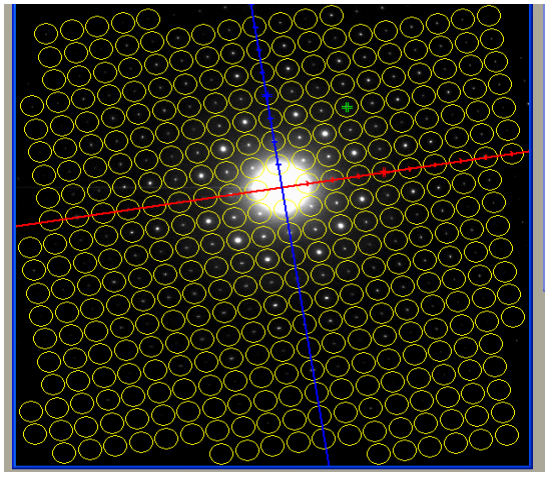

```
;
; a= 8.398Å, b= 8.455Å, gamma=89.358
;
Format: h k l d s a
; h   k   l  d-val  Aobs   Aest
;-------------------------------------
  1  -1   0  8.455  22.1   21.91
 -1   1   0  8.455  28.6   25.40
 -1  -1   0  8.398  22.1   22.27
  1   1   0  8.398  21.0   21.03
 -2   0   0  5.992  20.2   15.11
  2   0   0  5.992  15.9   12.47
  0  -2   0  5.925  18.8   17.66
  0   2   0  5.925  17.6   16.45
  2  -2   0  4.227  26.1   26.07
 -2   2   0  4.227  30.8   30.78
 -2  -2   0  4.199  29.5   28.61
  2   2   0  4.199  29.1   28.12
 -3   1   0  3.793  25.0   25.03
  3  -1   0  3.793  17.8   17.09
 -3  -1   0  3.778  23.3   23.34
  3   1   0  3.778  21.9   21.89
  1  -3   0  3.759  23.8   24.30
 -1   3   0  3.759  24.6   24.65
 -1  -3   0  3.744  22.2   20.54
  1   3   0  3.744  22.9   22.90
 -4   0   0  2.996  60.8   60.82
  4   0   0  2.996  52.7   52.75
```

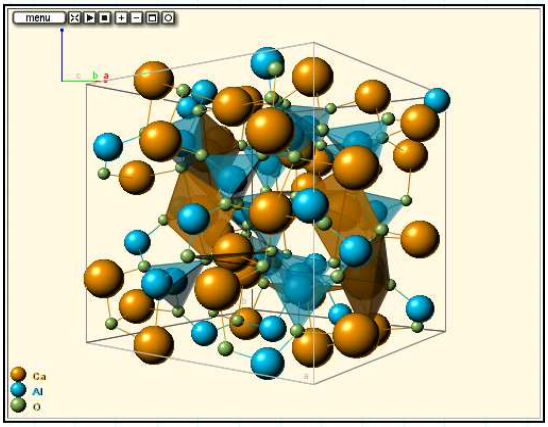

Figure 2: PED pattern for cubic mayenite <001> , a=11.96A with corresponding spot intensity localization and list of indexed intensities. The file is used as input for SIR2008 program which generates proposed atomic model, provided a rough estimate of present atomic species is given. In this case, Ca_6 Al_7 O_{16}.

A digital precession instrument has been developed (called DigiSTAR) that can be exchanged among several TEM instruments, since it allows stocking in computer memory different TEM-dependent alignment values for driving the beam and image coils simultaneously at different frequencies and precession angles. It is possible with this instrument to increase precession angle continuously from minimum to maximum with no need to re-align pivot points or readjust descan values, as it is the case with the analogue versions of precession instrumentation.

Effectively, the most severe limitation imposed on the precession technique is the focused beam deformation and broadening due to several TEM aberrations, namely, spherical and three-fold astigmatism [4]. Thus, the beam spot size diameter is broadened by a factor of at least 3 times when the precession angle increases to 60% of the maximum available on each particular TEM instrument, and at angles of > 2º the spot shape is no longer circular, but highly deformed. The software driving the digital version of the precession instrument enables accurate correction of beam shape and dimension (Fig. 4) even at high precession angles and, therefore, precessed electron diffraction patterns formed on nanocrystals may now be effectively studied under high precession angles.

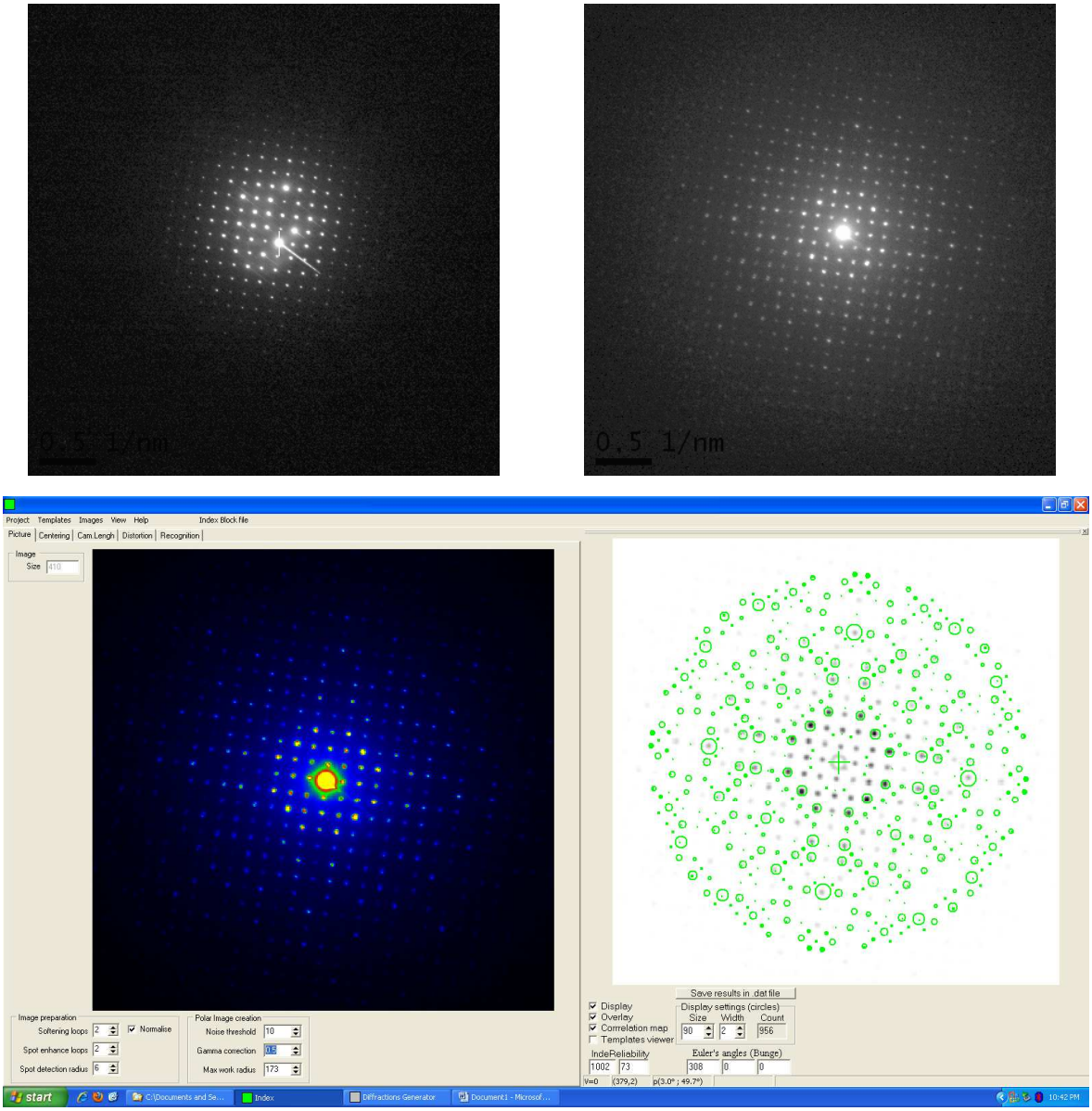

Figure 3: ED pattern for mayenite along Zone Axis <001>: conventional static illumination (top left); PED 2.4º (top right); comparison with simulated pure kinematical pattern in green (bottom)

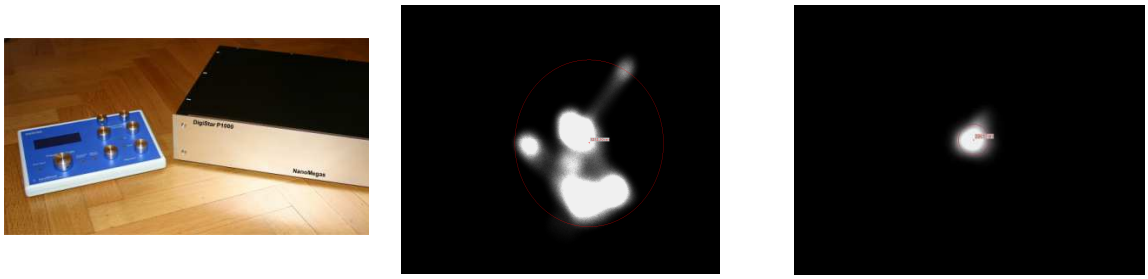

Figure 4. Digital precession unit "DigiSTAR", shown with manual interface and control electronics (left); Deformed beam spot size at precession angle of 2º on a TEM Jeol 2000FX at 8K times magnification, diameter size 1212 nm before software correction (center); same image after on-line software correction (x8000 magnification, beam diameter 226nm); note a 6-fold reduction of the beam size (right)

3. Precession Electron Diffraction and Orientational Mapping

Structural information from crystalline materials is present in their electron diffraction patterns, which consist of Kikuchi lines and/or individual diffraction spots. In the Precession Electron Diffraction assisted Orientational and Phase Mapping technique, collected patterns consist exclusively in spots, since Kikuchi lines are smeared out by the high frequency of the precession illumination.

Electron Backscatter Diffraction in the Scanning Electron Microscope has gained popularity over the last decade as it provides an effective tool for the characterization of bulk crystalline materials, provided lateral resolution demanded on the sample is not smaller than 500 nm [5].If a field emission gun is used in the Scanning Electron Microscope, lateral resolution may be improved down to some 50 nm, and a number of applications have been reported mainly on metals and alloys [6]. The EBSD-SEM technique is based on precise measurements of backscattered Kikuchi line diffraction patterns. However, these lines only appear after incident electron backscattering and double interaction (first inelastic scatter, then elastic diffraction) on surfaces of samples polished to mirror condition, which is a severe limitation on deformed crystalline materials. Moreover, acquisition times, although continuously improved, are still on the hour scale.

It is now possible to apply an analogue of the SEM-EBSD analysis in the TEM, by ultra-fast collection of precessed electron diffraction patterns obtained on a user-selectable area of the TEM with a point spread resolution well within the nanometer range (typically 10 nm) and without the need of additional surface sample preparation [7].

ED spot patterns are collected sequentially with an ultra-fast optical CCD camera while an area on the sample is simultaneously being scanned by the TEM focused electron beam, which is at the same time being precessed around the direction of incidence at each point. Beam scanning and precessing is controlled by a dedicated external device, which also allows control of beam pivot points and descan pivot points, called “Digistar” and manufactured by the NanoMEGAS company [8]. This device is connected to the beam and image deflector coil control boards present in the TEM. Thus, a TEM retrofitted with this precession device need not necessarily include a scanning option itself. An external ultrafast optical CCD camera, with only 8 bit dynamical range and 250 x 250 pixel image size, mounted in front of the TEM screen is used for the diffraction pattern image collection. This camera records the rapidly changing patterns appearing on the fluorescent screen of the TEM and is the key to a high collection speed since it may work as fast as 180frames/sec, although fluorescent screen reminiscence slightly slows down this performance. During the scanning and precessing of the primary electron beam, thousands of ED spot patterns are recorded and stored in memory of a dedicated computer. In order to proceed with nanocrystal orientation and/or phase identification, each one of the experimental ED spot patterns is compared to one or several sets of thousands of computer generated ED spot patterns, the so-called templates. The software technique for the comparison is based on optimal template matching using cross-correlation (Fig.4) [9].

For a typical map of 500 x 300 pixels, it may typically take only 15 minutes to scan (while precessing) over the sample area and record the associated 150.000 PED patterns. Comparison with simulated templates can be done off-line and takes about 5 minutes for highly symmetric cubic materials and 2 to 24 times longer for unit cells with lower symmetry, because more templates must be generated and compared with experimental ED spot patterns for the same angular resolution (typically 0.5 to 1º). The scanning step chosen for the rastering is about half the size of the primary electron beam size, that is 12 nm for a 25 nm spot size on a TEM with LaB_6 electron gun, and the resulting lateral resolution of the obtained map will be of the order of the latter value. Template generation is done on the basis of unit cell dimensions and geometry as well as inherent atomic positions, for each of the known phases present in the examined sample. Using these data, a complete spatial set of ED spot patterns is generated under purely kinematical conditions. The comparison of these templates with experimental ED spot patterns is run, searching a maximum match for spot positions and their relative intensities, and the parameter quantifying the match is called the correlation index.

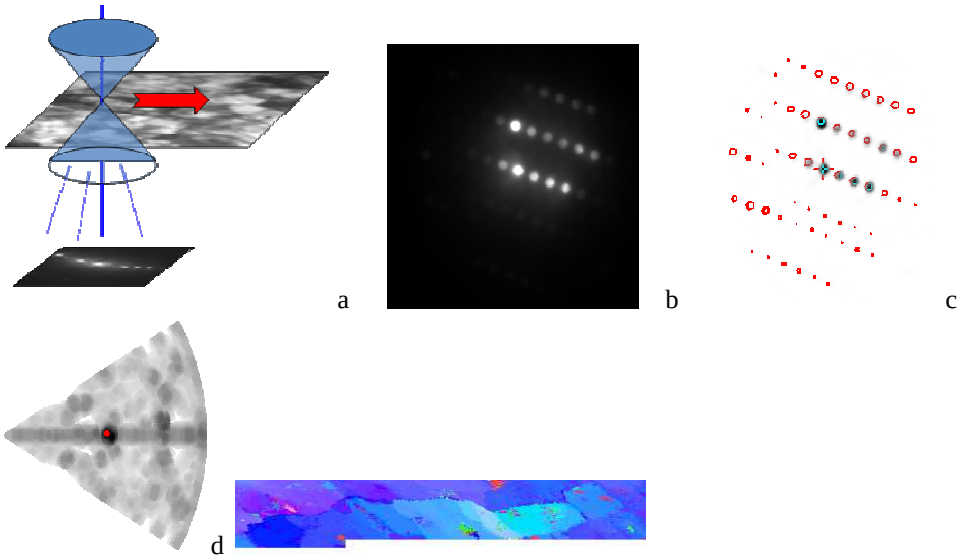

Figure 4: Schematics of PED assisted Orientational Mapping: (a) beam scanning over a user-defined sample area combined with precession, (b) experimental spot PED pattern serial recording in computer memory, (c) superposition of individual ED template (red dot pattern) which best matches the experimental PED pattern (grey dot pattern), and (d) orientation directional map with grey intensity plot of matching index for the experimental spot PED pattern.

The software developed specifically for the technique allows production of crystal orientation maps, virtual bright field maps, correlation index maps and reliability index maps. The latter are related to the statistical significance of the orientational assignation chosen for each point of the map.

Essentially, the virtual bright field map is obtained by plotting the intensity fluctuations of the central spot in the PED pattern. Such maps are often more helpful for comparison with the final orientation map of the scanned area than real bright-field TEM images of the same area, since these are usually suffering from diffraction contrast and curvature contrast (which fades significantly under precessed illumination). Correlation index maps are mainly used to emphasize structural details such as crystals having different orientations. The reliability index, which is analogous to the SEM-EBSD confidence index, is defined in such a way that it has a minimum when more than one solution is proposed. Such reliability maps clearly reveal grain boundaries and textures (Fig. 5).

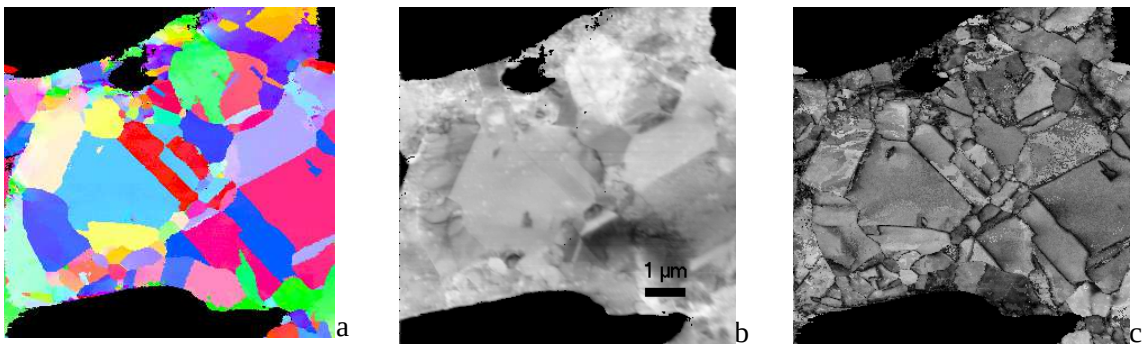

Fig. 5 a) Orientation map revealing nanotwins in a Cu thin foil sample (Jeol 3010 LaB6 TEM, 300KV, spot size 12 nm, step 5nm); b) Pseudo-bright field area of the same sample; (c) Reliability map showing clearly grain boundaries.

Although orientation and phase mapping coupled with template matching works satisfactorily for a number of materials without using precession of the primary electron beam, some limitations

are present in the form of ambiguous orientation/phase maps due to the poor quality of experimentally acquired ED spot patterns. This is the case for thick crystals where ED patterns show a combination of a strong diffuse inelastic scattering background with Kikuchi lines and a reduced number of faint diffraction spots. For such thick crystals and in general, precessed ED patterns exhibit a higher number of ED spots with specific intensity distribution and do not show Kikuchi lines. Consequently, the template matching software routine will produce higher values of the correlation index when using PED patterns and orientation maps will exhibit less ambiguity [10].

A specific experiment was designed in order to outline the influence of beam precession on template matching/indexing for local orientation determination. A series of ED patterns were acquired on a single nanocrystal of mayenite, starting from an initial electron beam incidence parallel to the <100> and then tilting the TEM sample holder along its axis away from <100> in steps of 0.05º until a final off-axis incidence direction of 18º was attained. The series of experimental ED patterns were recorded twice, first without and then with a precession angle of 0.35º, while keeping the beam stationary on the same crystal. Over 400 diffraction patterns were collected for each tilt series and then analyzed with the template matching software. The results are shown in figure 6.

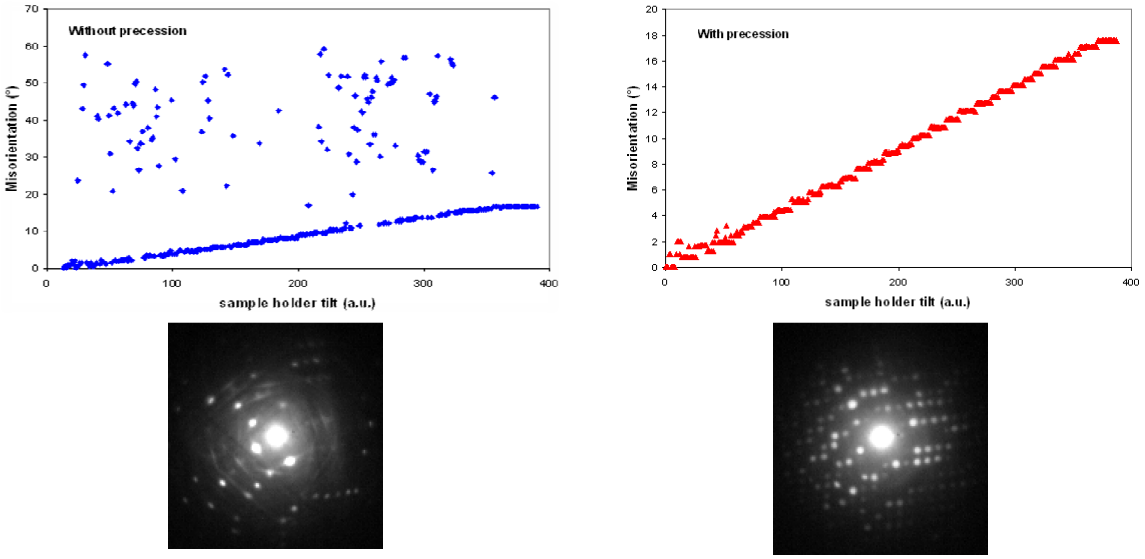

Fig. 6 Orientation values for mayenite <100> nanocrystal obtained after tilting it off-axis from 0 to18º (step 0.05º) along sample holder direction (top left) and the same experiment with 0.25º precession angle applied (top right); bellow each, experimental spot ED patterns from which the curves are derived. Note absence of Kikuchi lines and increased number of spots at lower right ED.

The misorientation values of figure 6 were calculated for every experimental pattern with respect to the initial orientation. The origin of both graphs starts in 0º misorientation for the first data point and should extend towards 18º for the last measured data point (number 400).

The blue unprecessed data show significant ambiguous orientation assignation, while the red precessed data nicely scale along a constant slope. The stepwise shape of the red curve is due to the fact that the database is generated in orientation steps of half a degree. When comparing the experimental spot ED patterns shown in figure 6, it is worth remarking the absence of Kikuchi lines and the increased number of spots present in the precessed pattern compared to the unprecessed pattern, which explains the cause of the orientation assignation ambiguity in the blue curve.

This demonstrates that even at small precession small angles, a substantial quality improvement is obtained in orientation maps obtained in the TEM when activating precession illumination.

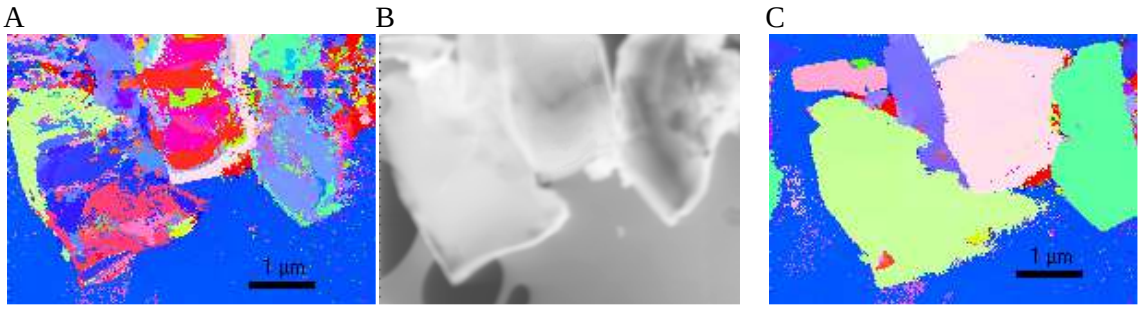

Fig. 7 (a) Orientation mapping of mayenite crystals without precession; (b) Virtual bright field; (c) Orientation map obtained with precession angle of 0.35º

This clear improvement of orientation determination can also be shown in the maps of Fig. 7 where an area that contains randomly oriented mayenite crystals was scanned twice (with and without precession). The orientation map in Fig. 7a shows color fluctuations indicating frequent misassigned patterns because of their low quality when compared with simulated templates. The map in Fig. 7c was obtained under the same conditions as in Fig.7a but using precession at 0.35º angle during beam scanning. As it can be observed, orientation map quality increases with precession, since each color domain corresponds to a single crystal grain with a definite orientation and should not show color fluctuations, as it is the case.

Acknowledgments

Samples for Figure 5 were supplied by Prof. Nuria Llorca of the University of Barcelona. The author is also indebted to Dr. Francesca Peiró of the University of Barcelona for fruitful discussions, encouragement and willing collaboration on Precession related topics.

References

[1] T.E.Weirich, J.Portillo, G.Cox, H.Hibst, S.Nicolopoulos, “Ab initio determination of framework structure of CsNbWO from 100KV precession data”, Ultramicroscopy **106** (2007), 164-175

[2] A.Avilov, K.Kuligin, S.Nicolopoulos, M.Nickolsky, K.Boulahya, J.Portillo, G.Lepeshov, B.Sobolev, J.P.Collette, N.Martin, A.C.Robins, P.Fischione, “Precession technique and electron diffractometry as new tools for crystal structure and chemical bonding”, Ultramicroscopy **107** (2007), 431-444

[3] E.F.Rauch, M.Veron, J.Portillo, D.Bultreys, Y.Maniette, S.Nicolopoulos, “Automatic crystal orientation and phase mapping in TEM by precession diffraction”, Microsc. Anal. **93** (2008), 5-8

[4] C. Own, PhD dissertation, Northwestern University, Chicago, December 2004, http://www.numis.northwestern.edu/Research/Current/precession

[5] V.Randle, O.Engler, “Introduction to texture Analysis: Macrotexture, Microtexture and Orientation Mapping”, CRC Press, 2000

[6] D.P.Field, S.I.Wright, D.J.Dingley, Proc. 11th International Conference on Textures of Materials (ICOTOM11), Ed. Z. Liang et al, International Academic Publishers, China, 1994

[7] E.F.Rauch, M.Veron, “Coupled microstructural observations of local texture measurements with an automated crystallographic orientation mapping tool attached to a TEM”, J.Mater.Sci. Eng. Tech. **36** (2005), 552-556

[8] http://www.nanomegas.com, NanoMEGAS-CNRS Patent pending technique

[9] E.F. Rauch, L. Dupuy, “Rapid spot diffraction pattern identification through template matching”, Arch. Metall. Mater **50** (2005), 87-99.

[10] J.Portillo, E.F.Rauch, S.Nicolopoulos, M.Gemmi, D.Bultreys, “Precession Electron Diffraction assisted Orientation Mapping in the Transmission Electron Microscope”, Mat. Sci. Forum **644** (2010), 1-7

Handbook of instrumental techniques from CCiTUB

Electron probe microanalysis: principles and applications

Xavier Llovet

Unitat Microsonda Electrònica, CCiTUB, Universitat de Barcelona. Lluís Solé i Sabarís, 1-3. 08028 Barcelona. Spain.

email: *xavier@ccit.ub.edu*

Abstract. This article summarizes the basic principles of electron probe microanalysis, with examples of applications in materials science and geology that illustrate the capabilities of the technique.

Introduction

Electron probe microanalysis (EPMA) is a nondestructive analytical technique widely used for determining the local composition of solid samples [1, 2, 3]. The technique is based on the measurement of characteristic x-ray intensities emitted by the elements present in the sample when the latter is bombarded with a focused electron beam. For each element, the ratio of the characteristic x-ray intensity emitted from the sample to that emitted from a standard of known composition is measured. This ratio is usually referred to as k-ratio. The transformation from measured k-ratios to concentrations is performed by means of relatively simple, analytical algorithms, which assume that the sample region from which x rays emerge has a homogeneous composition. For keV electron beams, this region is typically about 1 μm, depending on the density of the material and the analytical conditions. Accordingly, EPMA is suitable for the analysis of samples that are homogeneous on the micron scale.

Using wavelength-dispersive (WD) spectrometers, elements from Be to U can be analyzed by EPMA with detection limits for most elements down to 100 ppm or lower, accuracy of 2% for major element concentrations and a spatial resolution of few microns. EPMA also couples quantitative analytical capabilities with the imaging capabilities of a scanning electron microscope (SEM), allowing detailed x-ray mapping of composition contrast. Moreover, EPMA can also be used to determine the thickness and composition of thin films and multilayers with thickness in the sub-micron range, providing information on the lateral variation in thickness and composition at the micrometer scale. EPMA is extensively used in many fields and has been central for the microanalysis of ceramic, metallurgical, geological, biological, and other materials.

The first electron microprobe was developed by Raimond Castaing in 1950 by fitting a crystal spectrometer to a modified electron microscope. Using the developed instrument, Castaing established the basic principles of quantitative EPMA [4]. A few years later, in 1958, the French company CAMECA manufactured the first commercial electron microprobe. Since then, many improvements in the probe-forming system, as well as in the x-ray spectrometers have been performed, which have advanced electron microprobes, in terms of stability, reproducibility and detection limits. Recently, the incorporation of field-emission electron sources in EPMA equipment has opened the possibility of obtaining x-ray maps of chemical contrast and point analyses with sub-micron spatial resolution.

This article summarizes the basic principles of EPMA, with examples of applications that illustrate the capabilities of the technique.

1. Methodology

1.1. Physical principles

When an electron beam impinges on a sample, electrons interact repeatedly with the sample atoms until they come to rest or emerge from the surface. In the keV energy range, the possible interactions of electrons with atoms are elastic scattering, inelastic collisions and bremsstrahlung emission [5, 6]. Elastic interactions are those in which the initial and final states of the atom are the same, normally the ground state. These interactions change the direction of movement of the electrons. Inelastic collisions are those in which the atom is brought to an excited state, i.e. a part of the electron's kinetic energy is taken up by the atomic electrons. Inelastic collisions include excitation of electrons in the conduction or valence bands, plasmon excitations and inner-shell ionization, i.e. the production of a vacancy in an inner-electron shell (see Fig. 1). After inner-shell ionization, the atom de-excites by migration of the vacancy to outer shells through a cascade of electron transitions and energy is released as characteristic x rays or Auger electrons. Inner-shell ionization is thus responsible for the emission of characteristic x rays. Emission of bremsstrahlung takes place when the electron is decelerated in the electrostatic field of the target atom. Bremsstrahlung emission has almost no effect on the electron trajectories but it is the source of the continuous background in an x-ray spectrum.

Emitted photons (either as characteristic x rays or bremsstrahlung) originate at sample depths extending from the surface to some maximum depth, which depends on the material and on the energy of incident electrons. Before emerging from the surface, generated x rays may interact with the sample atoms through different mechanisms, mainly photoelectric absorption, and as a result, fluorescent x rays may be emitted.

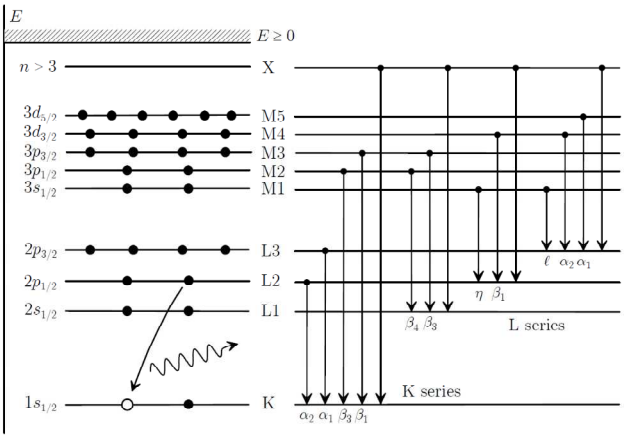

Figure 1. Schematic diagram of the different atomic inner atomic shells and main possible transitions to these shells that release characteristic x rays.

1.2. Instrumentation

The electron microprobe essentially consists of an electron column and several x-ray spectrometers, which can be WD and/or energy-dispersive (ED) spectrometers.

The electron column consists of an electron gun and an electromagnetic lens system (see Fig.2). The electron gun acts as a source of electrons. It is commonly a thermoionic gun, usually made of W or LaB_6 which is heated to liberate electrons by thermionic emission. The filament is held at a negative potential by a power supply, which accelerates the electrons escaping from the filament through an aperture. Typical accelerating voltages range from 1 kV up to 40 kV. The electromagnetic lenses are used to focus the electron beam onto the target, with a final diameter of about 0.1-1 μm. They are also used to control the electron current, i.e. the number of incoming electrons per unit time, with values typically of 1-300 nA. The electron current is measured with a Faraday cup and stabilized by means of a beam regulator device. The sample is connected to ground to ensure electron conductivity.

Conventional high vacuum technology is generally used in order to prevent oxidation of the filament, breakdown of the accelerating voltage and scattering of the electrons in the beam by the residual gas. In order to minimize carbon contamination at the point of electron impact due to the cracking of hydrocarbons present in the chamber, the electron microprobe is equipped with a liquid nitrogen “cold finger”, placed close to the specimen, and an air jet directed towards the point of electron impact.

An optical microscope co-axial to the electron beam is commonly used to locate the areas of interest in the sample. For the same purpose, the beam can be scanned as in conventional SEMs. Images can then be generated by using the signal from an electron detector, which usually records secondary (SE) and/or backscattered electrons (BSE) from the target.

The WD spectrometer consists of a crystal monochromator and an x-ray detector, usually a gas proportional counter, arranged in such a way that x rays impinging on the crystal are diffracted according to Bragg’s law and some of them reach the detector and are recorded. The Bragg law reads $n\lambda=2d\sin\theta$, where λ is the x ray wavelength, n is the diffraction order, d is the spacing between atomic planes of the monochromator crystal and θ is the angle of incidence of the x rays.

With flat crystals and point x-ray sources, Bragg reflection occurs only on a small portion of the crystal surface. Improved reflection is obtained by placing the target, the crystal and the detector on a focal circle of radius R (the Rowland circle) and bending the atomic planes of the crystal to a radius $2R$. This focussing geometry is known as the “Johann” type. Much improved reflection is obtained if the crystal surface is bent to the radius R (“Johansson” type). With this arrangement, the

angle of incidence of x rays is constant over the line defined by the intersection of the Rowland circle plane and the crystal surface. Coordinated mechanical rotation of the crystal and the detector allows us to record the x-ray spectrum as a function of wavelength. In the focussing geometries, the source-crystal distance is proportional to sinθ and thus proportional to the wavelength. Therefore, the crystal is simultaneously rotated and moved along a straight line by means of mechanical linkage. This allows calibration of the wavelength by just measuring the source-crystal distance and moreover, the take-off angle is kept constant for all wavelengths.

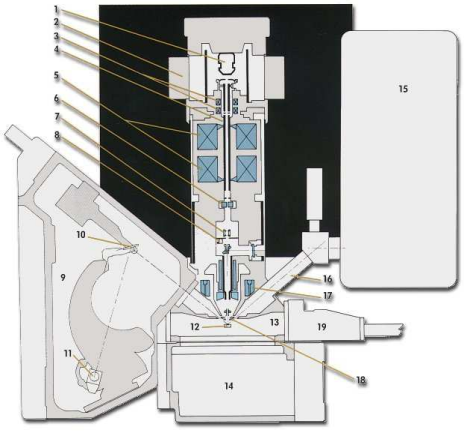

Figure 2: Cross section of an electron microprobe.

Figure 3: Electron microprobe CAMECA SX-50 at the CCiTUB (4 WD spectrometers + 1 EDS).

Besides mechanical limitations of the crystal driver, the range of reflected wavelengths is only limited by the crystal inter-atomic spacing *d* and, therefore, crystals with different spacings are required to cover a wide wavelength range. Crystals commonly used for microanalysis are Lithium Fluoride (LiF), Pentaerythritol (PET), and Thallium Acid Phthalate (TAP). The wavelength range covered by using these three crystals is $\lambda \sim$ 1-24 Å. For longer wavelengths, layered synthetic multistructures (LSM) consisting of many alternating layers of high- and low-*Z* materials, such as W/Si, Ni/C and Mo/BC can be employed. In these cases, *d* is equal to the sum of the thickness of one layer pair of the high-*Z* and low-*Z* materials.

The gas proportional counter consists of a gas-filled tube with a coaxial wire held at a potential of 1-2 kV with respect to the outer wall of the tube. X rays enter the counter through a window; they are absorbed by the gas molecules through photoelectric effect and generate free photoelectrons, which are accelerated by the electric field and produce a cascade of secondary electrons. As a result, each incoming x ray produces a pulse whose height is proportional to the energy of the x ray. The output pulses are sent to a pulse-height analyzer (PHA) that counts pulses with selected heights –usually contained within a certain voltage window–. Visualization of the PHA display helps us to properly select the values of the counter high voltage, the gain and the discriminatory settings (baseline and window). Proportional counters can be of flow type, in which case the gas escapes through the window and therefore must be supplied continuously, or of the sealed type. Since WD spectrometers only allow the recording of one wavelength at a time, electron microprobes are usually equipped with several (up to 5) spectrometers (Fig. 3), each with several interchangeable crystals.

The ED spectrometer uses a solid-state x-ray detector, usually a crystal semiconductor such as Si or Ge, which discriminates x rays based on their energy. In Fig. 3, x-ray spectra of InSb recorded with WD and ED spectrometers are compared. In the ED spectrum, the overlap between adjacent lines makes it difficult to obtain the corresponding x-ray intensities, while for the WD spectrum, the majority of x-ray lines are clearly resolved. Because of its better resolution, WD spectrometers have better (lower) detection limits than ED spectrometers (typically ten times).

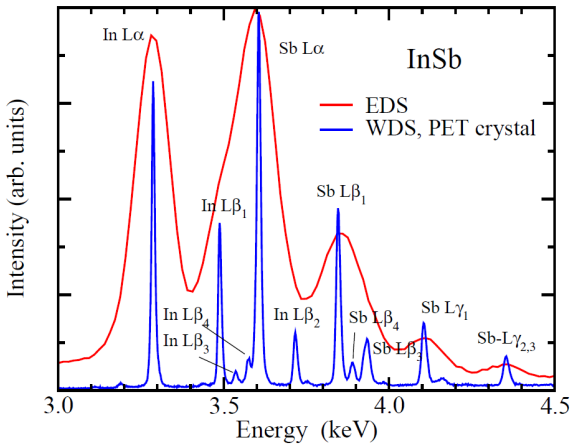

Figure 3: Experimental x-ray spectra of InSb.

The standard procedure to obtain the net peak intensity is to record the counting rate at the channel corresponding to the maximum of the peak, and at two background positions at both sides of the peak. Background intensity is then obtained by simple linear interpolation and subtracted from the measured counting rate. This procedures gives, in general, accurate results because of the high peak-to-background ratio of WD x-ray spectra. Higher order reflections, i.e. n=2,3,4.. in Bragg's law, must not be ignored since they are a source of spectral interference. In general, it is possible to suppress the influence of high-order diffraction peaks by properly setting a narrow window in the PHA.

1.3. Quantitative analysis

The starting point of quantitative analysis methods is to establish a relation between the concentration c_i of element i and the intensity of characteristic x rays, I_i, mesured in the direction of the take-off angle θ. This relation can be written as

$$I_i = \mathcal{C}\, c_i \left[\int_0^\infty \Phi_i(\rho z)\, \exp\left(-\chi_i\, \rho z\right)\, \mathrm{d}(\rho z)\right] \left(1 + \sum_j f_j + f_c\right), \qquad (1)$$

with $\chi_i=(\mu_i/\rho)\ \csc\theta$, where (μ_i/ρ) is the mass attenuation coefficient for the considered x-ray line, $(1+\Sigma f_j + f_c)$ is the fluorescence contribution, i.e. the x-ray intensity resulting from the absorption of characteristic x rays (f_i) or bremsstrahlung (f_c), and $\Phi(\rho z)$ is the depth-distribution of x-ray production. The factor C in Eq. (1) includes instrumental and atomic parameters that are generally not well known. To minimize the effect of the uncertainties in these parameters, the x-ray intensity is normalized to that emitted from a reference standard that contains the element of interest. By doing so, the factor C cancels out. The k-ratio is given by

$$k_i = \frac{I_i}{I_i^*} = \frac{c_i}{c_i^*} \left[\frac{\int_0^\infty \Phi_i(\rho z)\, \exp\left(-\chi_i\, \rho z\right)\, \mathrm{d}(\rho z)}{\int_0^\infty \Phi_i^*(\rho z)\, \exp\left(-\chi_i^*\, \rho z\right)\, \mathrm{d}(\rho z)}\right] \left[\frac{\left(1 + \sum f_j + f_c\right)}{\left(1 + \sum f_j^* + f_c^*\right)}\right], \qquad (2)$$

where superscript "*" indicates that the corresponding quantity is evaluated on the standard (notice that c_i* is known). Eq. (2) can be written in a compact form as

$$k_i = \frac{I_i}{I_i^*} = \frac{c_i}{c_i^*} [\mathcal{ZA}]\, \mathcal{F}, \qquad (3)$$

where [ZA] and F represent the expressions in brackets in Eq. (2), respectively. [ZA] is usually referred to as the atomic number and absorption correction factor, while F is the fluorescence correction factor. Notice that by choosing suitable standards, the uncertainties in the calculation of [ZA] and F can be reduced.

A number of analytical expressions have been proposed to parameterize the $\Phi(\rho z)$ function, which makes it possible to obtain c_i from I_i (see Eq. (1)) by using relatively simple algorithms [7].

Examples of such parameterizations are the widely used PAP [8] or X-PHI [9] models. In practice, *k*-ratios are measured for all elements present in the sample (except for those estimated by stoichiometry or by other means) and the resulting system of equations is solved by using an iterative procedure. This is so because the factors [*ZA*] and *F* that occur in Eq. (3) depend themselves on sample composition. In general, convergence is quickly achieved using simple iterative procedures.

As mentioned in the introduction, EPMA can also be used to determine the thickness and composition of thin films and multilayers. Correction procedures that allow the analysis of thin films and multilayers are known as thin-film programs [10]. Examples of available thin-film programs are the widely used STRATAGEM [11] or X-FILM [12]. For the analysis of heterogeneous samples such as sub-micron particles, embedded inclusions or lamellae structures, the simplifications underlying correction procedures are not firmly established and there is a need for more realistic procedures. In this context, the Monte Carlo simulation method [13] is a valuable tool as a basis of quantitative procedures.

2. Examples of applications

EPMA capabilities include point analysis, line profiles and x-ray mappings, both qualitative and quantitative, as well as the determination of the composition and thickness of thin films and multilayers. Applications of EPMA in the earth and environmental sciences include the description and classification of rocks (mineral chemistry); identification of minerals; determination of temperatures and pressures of rock formation (geothermobarometry); chemical zoning within mineral crystals on the micron-scale for petrological, crystal growth and diffusion studies (e.g. for the determination of time scales of magmatic and volcanic processes); study of mineral indicators in mineral exploration; analysis of minerals of economic and strategic importance (e.g. ore deposits, carbon sequestration); study of fossil materials, limestones and corals; determination of rock ages via U-Pb radioactive decays.

In materials science and physical metallurgy, EPMA is extensively used for the determination of the chemical composition and microstructure of alloys, steel, metals, glass, ceramics, composite and advanced materials; determination of phase diagrams; analysis of inclusions and precipitates; analysis of elemental distributions, e.g. diffusion profiles, depletion zones, nitrided and carburized surfaces, corrosion and oxidation phenomena; analysis of thin films and coatings.

EPMA can also be used as a scattering chamber to determine physical quantities related to the production of x rays (e.g. [14]) which are needed in medical and industrial applications.

In this section, we show some of our own examples of applications of EPMA which briefly illustrate the capabilities of the technique.

2.1. Characterization of duplex stainless steel

Duplex stainless steels (DSS) are a family of steel grades that have a two-phase microstructure consisting of grains of ferritic (α) and austenitic (γ) stainless steel, with diameters of several micrometers. These steels are valuable for applications where good mechanical and anti-corrosion properties are required simultaneously, such as refinery pipes or off-shore platforms. The use of DSS at high temperatures requires knowledge of the phase transformations that they undergo after heat treatment. The most important phases that occur during heat treatment are the so-called σ and χ phases, which form between 650 ^{o}C and 1000 ^{o}C mainly at the α/γ interface, and are associated with a reduction of anticorrosion and toughness properties. Other phases that can occur in the same range of temperatures are secondary austenite (γ_2), and several nitrides and carbides. EPMA is a valuable tool for the characterization of DSS as it combines micrometer spatial resolution with low detection limits.

Figure 3 shows the microstructure of a DSS sample after heat treatment (8h, 850^{o}C) [15]. The following phases can be observed: ferrite (α), austenite (γ), secondary austenite (γ_2), and the σ and χ phases. Figure 4 displays a portion of the x-ray spectrum near the N Kα line emitted from an austenite grain. Nitrogen plays an important role on the properties of DSS as it can partially replace

Ni, which is of economic interest. Accurate measurement of N is difficult mainly because of its low peak-to-background ratio and the curved background under the peak (see Fig. 4). One way of overcoming this difficulty is to use a calibration curve, which can be obtained from (mono-phase) steel reference samples [16]. Typical EPMA analyses of the observed phases are shown in Table 1. In this example, the detection limit (DL) of N is ~ 0.025 wt.%; the precision of the N determination is ~ 15-20 % for the α and σ phases and ~ 5% for the γ and χ phases [15].

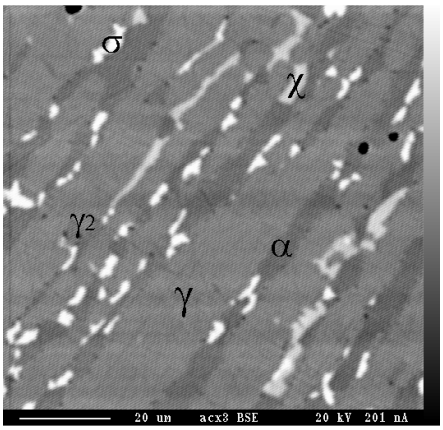

Figure 3: BSE image showing the microstructure of a DSS after heat treatment.

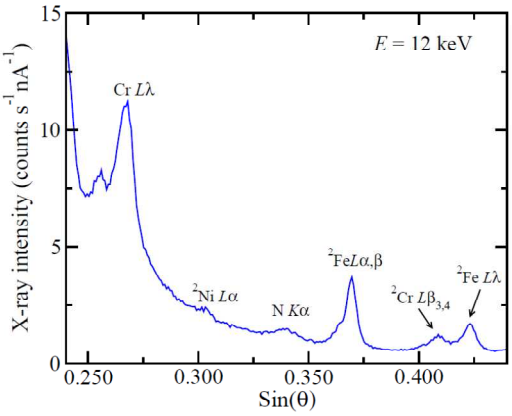

Figure 4: X-ray spectra around the position of N measured on an austenite grain (γ).

Table 1*:* Phase composition of a duplex stainless steel after heat treatment (8h, 850 °C)

	Phase type				
wt.%	Austenite (γ)	Sec. aust. (γ_2)	Ferrite (α)	Phase σ	Phase χ
N	0.40	<DL	0.05	0.07	0.14
Si	0.21	0.56	0.25	0.38	0.38
Cr	20.28	18.39	22.84	27.65	23.27
Mn	4.48	4.73	3.47	4.25	4.56
Fe	68.81	69.96	68.97	59.01	58.61
Ni	2.97	3.25	1.47	1.40	1.22
Cu	1.14	1.29	0.73	0.31	0.27
Mo	2.30	1.81	2.71	7.92	15.01
Total	100. 59	99.99	100.49	101.09	103.46

2.2. Analysis of chemical segregation in ferritic steel

Applications of ferritic stainless steels are commonly related to conformation, usually stretching and deep drawing, of house-hold appliances. These applications require knowledge of the deformation mechanisms of these steels and the effect of microstructure and microsegregation on their behaviour during deformation. A convenient method to analyze microsegregation is by means of x-ray mapping, which allows to record the distribution of elements over an area of the sample. Depending on the area, x-ray mappings can be obtained by scanning the beam across the sample or, alternatively, by moving the sample back and forth under a fixed electron beam. Mappings can display x-ray intensity in each pixel (qualitative) or concentration (quantitative). The mappings of Fig. 5 show the quantitative distribution of Fe, Cr and V in ferritic stainless steel after bi-axial tension deformation [17]. The colormap at the righ-hand side of each map displays the equivalence between color and concentration (in wt. %). In this example, x-ray mapping allowed to correlate the effect of tension deformation with the intensity and width of microsegregation [17].

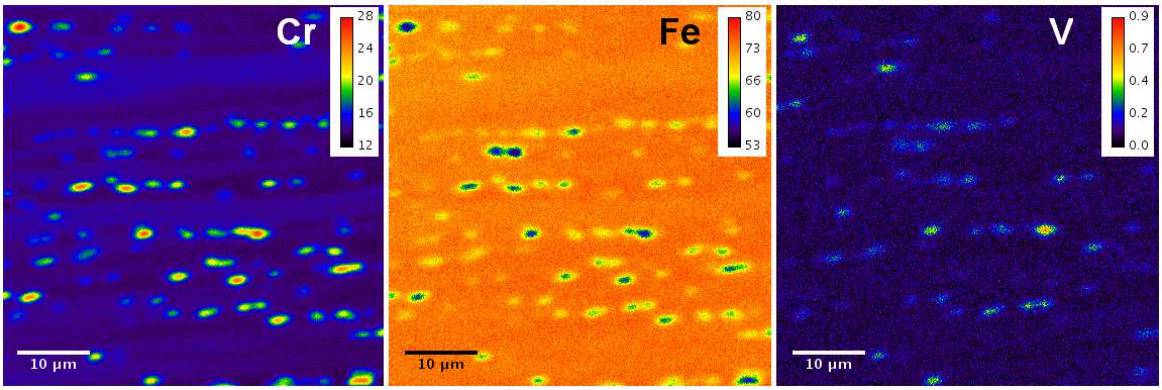

Figure 5: Quantitative x-ray mappings showing the distribution of Cr, Fe, Cr and V in a ferritic steel after bi-axial tension deformation. Concentration is given in wt.%.

2.3. Determination of the pressure and temperature of formation of rocks

The temperature and pressure of formation of minerals within rocks can be estimated from the composition of selected mineral pairs coexisting in the rock. These mineral pairs display a partition of chemical constituents as a function of temperature or pressure, and are referred to as geo-thermometers (if they depend on temperature) or geo-barometers (if they depend on pressure). In this example, the pressure-temperature path of a mantle xenolith hosted by basaltic rocks from the Canet d'Adri volcano (Girona, NE Spain) was derived [18]. Figure 6 shows an optical microscope image of the studied sample, showing the different minerals that occur (spl= spinel; opx = orthopyroxene; cpx = clinopyroxene; ol = olivine). Representative EPMA analyses of such minerals are shown in Table 2. Together with the EPMA analyses, thermodinamic and calibration data are required in order to apply a particular geothermometer or geobarometer. In this example, temperatures were determined from the composition of coexisting clinopyroxene and orthopyroxene crystals. The Ca content in olivine coexisting with clinopyroxene, previously corrected for the effect of secondary fluorescence, was used to estimate pressures (see Ref. [18] for details). The results indicated an adiabatic decompressional path for this sample, with earlier pressure-temperature conditions of 20.9 ± 0.18 kbar, 1160 ± 4^{o}C, respectively, followed by 17.0 ± 0.4 kbar and similar temperature, down to 12.4 ± 0.9 kbar, 1044 ± 4^{o}C. It was deduced that this rock had been extracted from ~ 80 km depth, indicating a minimum lithosphere thickness in the area at the time of the volcanic activity.

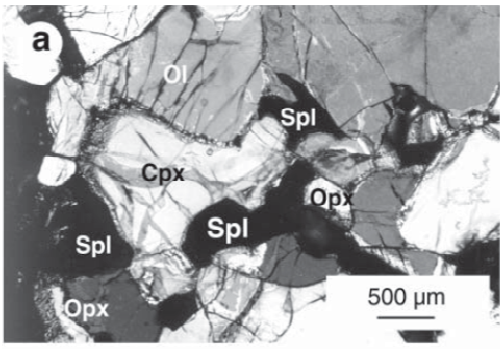

Figure 6: Optical microscopy image of a basaltic sample. The observed minerals are clinopyroxene (cpx), olivine (ol), ortopyroxene (opx) and spinel (spl)

Table 2: Representative analyses of olivine, clinopyroxene, ortopyroxene and spinel (in Ox.%).

	Mineral phases							
Ox.%	Ol1	Ol2	Cpx1	Cpx2	Opx1	Opx2	Spl1	Spl2
SiO	40.48	40.14	51.29	51.35	54.05	54.83	0.12	0.14
AlO	0.04	0.03	6.84	5.43	5.34	5.44	0.25	0.20
TiO	0.00	0.04	0.38	0.45	0.12	0.13	51.59	51.14
CrO	0.07	0.03	1.02	1.26	0.55	0.57	13.87	13.95
FeO	9.78	9.46	3.77	3.34	6.21	6.04	8.84	8.32
FeO							4.38	4.32
MnO	0.08	0.12	0.15	0.07	0.14	0.13	0.10	0.10
MgO	49.24	49.28	16.43	16.94	32.24	32.30	20.07	20.12
NiO	0.40	0.36	0.03	0.03	0.10	0.11	0.36	0.42
CaO	0.12	0.13	17.96	20.90	1.19	1.15		
NaO	1.43	1.52	0.16	0.14				
Total	100.09	99.46	99.39	100.16	100.10	100.84	99.58	98.71

2.4. Analisis of rare/complex minerals

Zirconolite is a rare oxide mineral described from a few locations on Earth which is used for storage of high-level radioactive waste. The composition of zirconolite can be summarized as ABCO where A = (Ca, Y, REE, Th, U, Fe, Mg, Mn) in 8-fold coordination, B = Zr in 7-fold coordination with minor substitution by REE, Hf, U, Ca, and Ti, and C = (Ti, Nb, Fe, Fe, Zr, Mg, Ta) in 5- or 6-fold coordination (REE = rare earth element).

The analysis of zirconolite by x-ray spectrometry methods faces several difficulties associated with the complex character of their x-ray spectra, which include a number of multiple interferences. Indeed, for each REE element at least ten lines are detectable. Examples of peak interferences include the following lines: Ho Lα–Gd Lβ, Hf Lα–Er Lα, La Lα–Nd L*l* and Lu Lα–Dy Lα. Figure 7 shows a BSE image of a zirconolite phase, in contact with ilmenite, from Mina Potosí (Cuba), as well as the corresponding qualitative x-ray maps of Ti and Y [19]. The results of our EPMA analyses, including the analytical error and detection limits, are given in Table **3**. As shown in the table, this particular zirconolite sample has a relatively high Y content, which is among the largest described in Earth and only comparable with lunar samples.

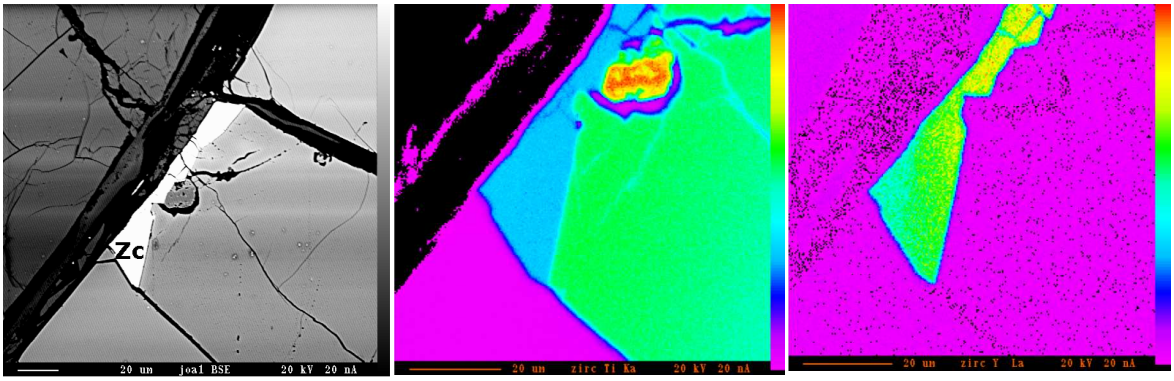

Figure 7. BSE image and x-ray maps (Ti and Y) of a zirconolite (Zc) mineral.

Table 3: Average composition (C), analytical error and detection limits (DL) of a zirconolite

	C(wt.%)	Error (%)	DL (wt.%)		C(wt%)	Error (%)	DL (wt.%)
Mg	0.32	3.1	0.007	Al	0.25	4.0	0.007
Si	0.073	9.8	0.034	Ca	3.95	1.2	0.030
Ti	19.13	0.5	0.086	Cr	0.32	2.4	0.008
Mn	0.04	36.2	0.236	Fe	5.05	0.07	0.035
Y	8.57	1.2	0.025	Zr	23.86	0.8	0.050
Nb	0.06	87.1	0.054	La	0.02	66.7	0.023
Ce	0.59	3.6	0.024	Pr	0.15	14.8	0.027
Nd	1.18	6.4	0.056	Sm	0.92	3.5	0.031
Eu	0.21	21.7	0.055	Gd	1.20	6.7	0.053
Tb	0.27	17.0	0.056	Dy	1.84	3.6	0.047
Ho	0.41	4.8	0.044	Er	0.99	4.8	0.047
Tm	0.18	17.8	0.042	Yb	0.64	8.7	0.001
Lu	0.10	10	0.020	O	28.68		
Hf	0.80	9.9	0.020	Total	99.89		

2.5. Thickness and composition of thin films and multilayers

The last example illustrates the analysis of thin films by variable-voltage EPMA. The technique consists of measuring the x-ray intensities (*k*-ratios) emitted by the film and substrate atoms at different electron incident energies. Measured intensities are then analyzed with the help of a thin-film program, which calculates the thickness and composition of the film by least squares fitting of an x-ray emission model to the measured intensities [12]. EPMA allows to measure the thickness and composition of thin films and multilayers with thickness from few nanometers [20] up to ~ 1 micron. Figure 7 shows the variation of the measured x-ray intensity against electron beam energy, together with the best fit obtained using the thin-film program STRATAGEM [11], for a C-coated P-doped glass film deposited on Si [12]. These glasses are typically used as inter-metal dielectrics in microelectronic devices. For P, O and Si, the *k*-ratios increase with beam energy until they reach a flat region (approximately from 4-12 keV) from which the Si intensity starts increasing again, while that of P and O decreases. It is therefore likely that at 12 keV the beam starts penetrating the Si substrate. The fit resulting from STRATAGEM yielded the following result: C 26 nm / P-SiO_2 1234 nm / Si (assuming ρ= 2.2 g/cm for C and ρ= 2.6 g/cm for the P-doped glass), with a P concentration of 5.2 wt.% and agreed reasonably well with the measured *k*-ratios.

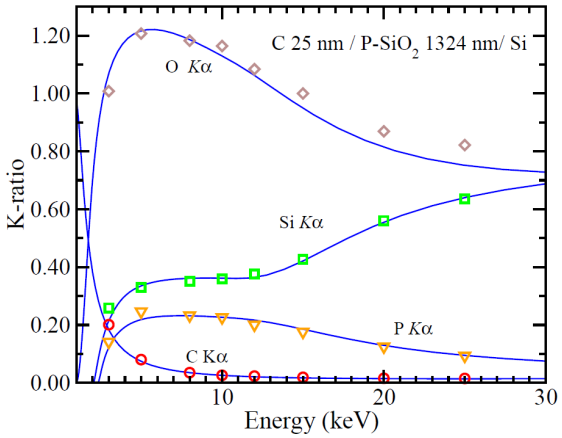

Figure 8: Comparison between calculated and measured k-ratios for a C-coated, P-doped glass film deposited on Si. Symbols represent experimental data. Continuous lines are results from STRATAGEM.

Acknowledgments

The author would like to thank Joaquin Proenza for allowing to use unpublished results. Fruitful discussions with Juan Almagro, Andrés Núñez, Gumer Galán and Claude Merlet are also acknowledged.

References

[1] Reed S J B 1993 *Electron Microprobe Analysis*, Cambridge Univ. Press, Cambridge
[2] Mackenzie A P 1993 *Rep. Prog. Phys.* **56** 557
[3] Scott V D, Love G, Reed S J B, 1995 *Quantitative Electron-Probe Microanalysis*. Chichester, Ellis Horwood
[4] R. Castaing 1951 *Ph. Thesis*, University of Paris, Publication ONERA No. 55
[5] Salvat F, Llovet X, and Fernández-Varea J M 2004 *Microchim. Acta* **145** 193
[6] Llovet X, Salvat F, Fernández-Varea J M 2004 *Microchim. Acta* **145** 111
[7] Lavrent'ev L G, Korolyuk V N, and Usova L V 2004 *J. Anal. Chem.* **59** 600
[8] Pouchou J L and Pichoir F 1984 *Rech. Aerosp.* **3** 167
[9] Merlet C. 1992 *Mikrochim. Acta Suppl.* **12** 107
[10] Pouchou J L and Pichoir F 1993 *Scanning Microsc. Supl.* **7** 167
[11] Pouchou J L 2002 *Mikrochim. Acta* **138** 133
[12] Llovet X and Merlet C 2010 *Micros. Microanal.* **16** 21
[13] Llovet X, Sorbier L, Campos C S, Acosta E and Salvat F 2003 *J. Appl. Phys.* **93** 3844
[14] Merlet C, Llovet X and Fernández–Varea J.M 2006 *Phys. Rev.* **A 73** 062719
[15] Corrales A, Luna C, Almagro J F and Llovet X 2005 *9th European Workshop on Modern Developments and Applications in Microbeam Analysis (EMAS),* Florence (Italy), 263.
[16] Moreno I, Almagro J F and Llovet X 2002 *Microchim. Acta* **139** 105
[17] Núnez A, Almagro J F and Llovet X 2011 *IOP Conf. Ser.: Mater. Sci. Eng.* (accepted)
[18] Llovet X and Galán G 2003 *Am. Mineral.* **88** 121
[19] Melgarejo J C, Proenza J A, Gervilla F and Llovet X 2002 *18th General Meeting of the International Mineralogical Association,* Edinburgh (UK)
[20] Campos C S,Vasconzellos M A Z, Llovet X and Salvat F 2004 *Microchim. Acta* **145** 13

Handbook of instrumental techniques from CCiTUB

Advanced applications of Scanning Electron Microscopy in Geology

Javier García-Veigas, Eva Prats, Anna Domínguez, and Aranzazu Villuendas

Unitat de Microscòpia de Rastreig, CCiTUB, Universitat de Barcelona. Lluís Solé i Sabarís, 1-3. 08028 Barcelona. Spain.

email: *sem@ccit.ub.edu*

Abstract. Nowadays Scanning Electron Microscopy (SEM) is a basic and fundamental tool in the study of geologic samples. The collision of a highly-accelerated electron beam with the atoms of a solid sample results in the production of several radiation types than can be detected and analysed by specific detectors, providing information of the chemistry and crystallography of the studied material. From this point of view, the chamber of a SEM can be considered as a laboratory where different experiments can be carried out. The application of SEM to geology, especially in the fields of mineralogy and petrology has been summarised by Reed (1996).The aim of this paper is to show some recent applications in the characterization of geologic materials.

1. Principle of the SEM

The SEM consists mainly of a column, a specimen chamber, a display and an operating device. The interior of the column is kept under high vacuum, and the electron beam produced by the electron gun is converged into a fine beam via electromagnetic lenses (condenser and objective lenses). By applying a scan signal to the deflection coils, the electron bean is scanned along the sample surface. The specimen chamber can be kept under high vacuum (conventional SEM) or under poor vacuum ("environmental" ESEM/"low vacuum" LV-SEM) conditions. As a result of electron-matter interaction, some signals are generated: secondary electrons, backscattered electrons, characteristic X-rays, cathodoluminescent light and others. The SEM utilizes these signals to form images.

Secondary electrons are produced near the sample surface and reflect the fine topographical structure of the sample. Backscattered electrons are those reflected upon striking the atoms composing the sample, and the number of these electrons is dependent on the composition (average atomic number, crystal orientation, etc.) of the sample. The primary (exciting) electrons may also be scattered inelastically by the sample's atoms, ejecting electrons of the inner-atomic shells and originating characteristic X-rays. In some types of samples, electron bombardment may raise bound electrons to higher energy levels, from which they return to their original states stimulating the emission of light by the process known as cathodoluminiscence (CL).

2. High resolution SEM (Field Emission Scanning Electron Microscope FESEM)

Secondary electrons are emitted from an extremely narrow area and carry information of the specimen surface. The spatial resolution of a SEM image is governed by the beam diameter which it depends on the emission source. In a Field Emission SEM (FESEM), the electron source consists of an extremely fine tungsten point from which electrons are drawn by a strong electric field. Nanometre resolution required for clay and whiskers crystals can be achieved by FESEMs. An example of a secondary electrons image obtained with a FESEM is given in Fig. 1.

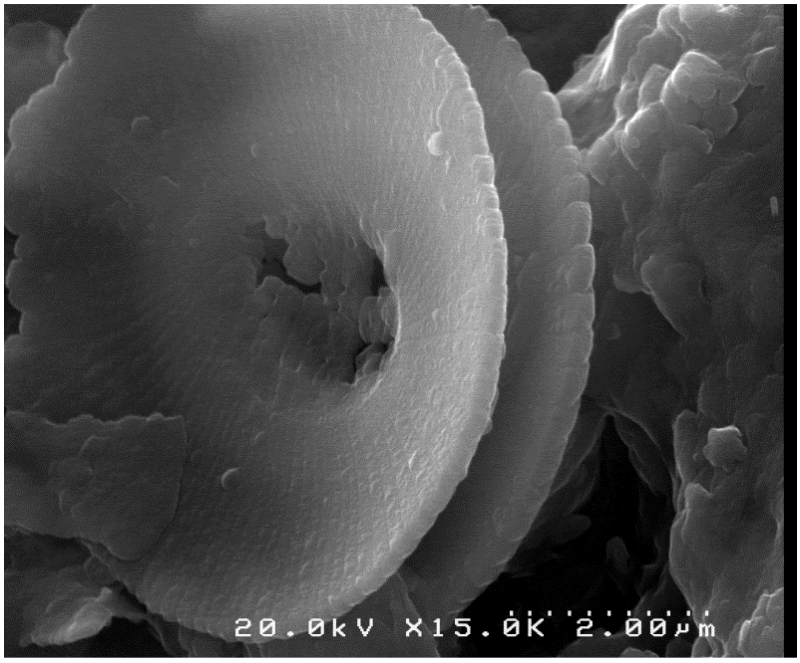

Figure 1: SEM micrograph of a calcareous nannoplankton (coccolithophore) in marine Miocene sediments of the Granada Basin obtained with a FESEM.

3. Chemical-contrast mineral identification (Backscattered electron images BSE)

The elastically scattered electrons having approximately the same energy as the incident electrons are collectively called as backscattered electrons (BSE) or reflected electrons. The probability that a primary electron is scattered elastically becomes larger as the mean atomic number (or electron density) of the specimen increases. Thus, backscattered electron signals provide rapid information about the compositional distribution of the specimen surface. BSE imaging in geological materials gives valuable information of petrographic textures and chemical zonation. Figure 2 shows a BSE micrograph of a zoned garnet crystal.

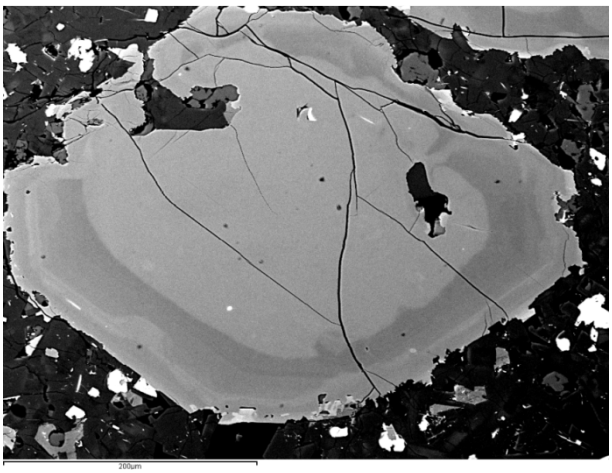

Figure 2: Chemical contrast with backscattered electrons of a garnet crystal.

4. Cathodoluminiscence images (CL-SEM)

Some minerals are inherently cathodoluminescent, but the intensity and colour of the light are often strongly influenced by defects in the crystal structure and by impurity atoms which behave as "activators" because they give rise to additional energy levels (Mn in calcite is a common example). Much geological CL work is done with an electron beam from a cold-cathode source coupled to an optical microscope. The use of a CL detector in a scanning electron microscope (CL-SEM) permits the generation CLimages of higher spatial resolution (Fig. 3).

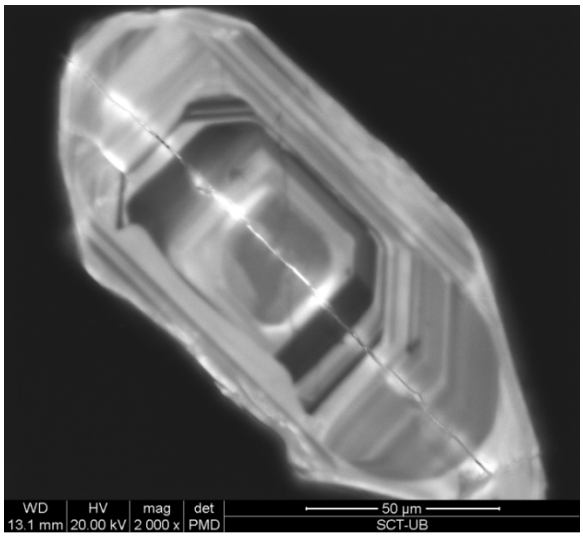

Figure 3: SEM-CL image of a zircon crystal.

5. X-ray analysis of fluid inclusions in salt (Cryo-SEM-EDS)

Direct access to brines trapped in old halite is possible by freezing and breaking halite crystals on a cooling stage inside a SEM (Fig. 4). Quantitative Energy Dispersive X-ray Spectroscopy (EDS) analyses of major solutes (Na, Mg, K, Ca, Cl and SO_4) in fluid inclusions can be obtained by comparing measured X-ray intensities with those obtained from liquid standard solutions with known composition (Ayora et al., 1994).

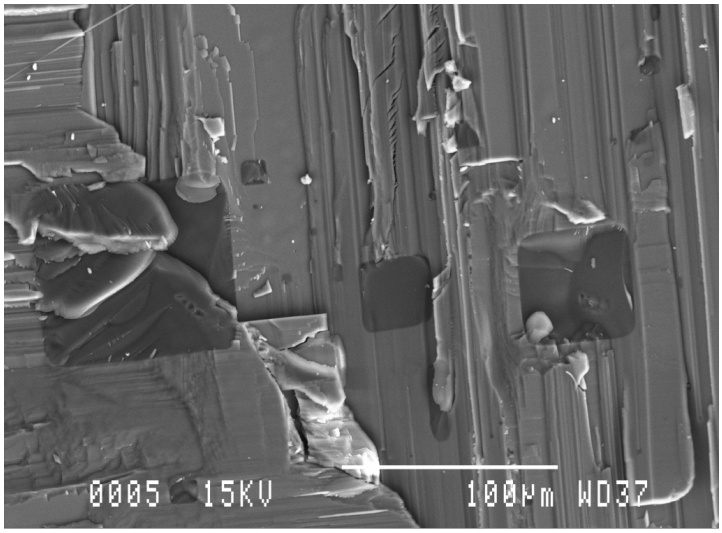

Figure 4: Secondary electron image of frozen fluid inclusions in a halite crystal.

The major ion composition of seawater varied through the geological time (Fig. 5). Fluid inclusion composition data obtained by Cryo-SEM-EDS from primary halite crystals in old marine evaporite deposits (Lowenstein et al., 2003) indicate that seawater had high Mg/Ca molar ratios (>2) and relatively elevated magnesium and sulphate concentrations during the Late Neoproterozoic, Permian, Triassic and the last 40 Ma. During Cambrian, Silurian, Devonian, Jurassic, and Cretaceous, seawater had relatively low Mg/ca ratios (<2) and Ca>SO_4. K concentrations have remained stable throughout Phanerozoic time.

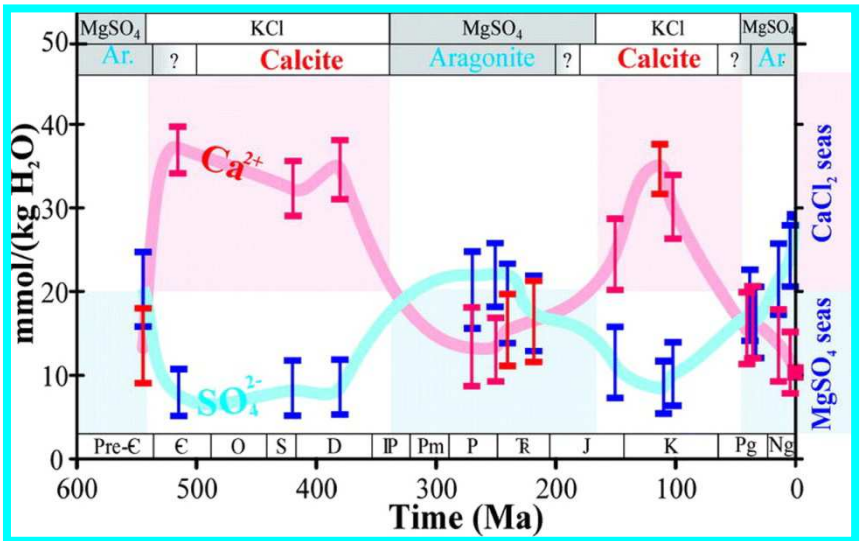

Figure 5: Secular variation in the Ca and SO_4 concentrations (in mmol/kg water) of seawater during Phanerozoic estimated from fluid inclusions in marine halites (Lowenstein et al., 2003).

6. Electron Backscatter Diffraction – *EBSD*

Electron backscatter diffraction (EBSD) is a SEM-based technique used for microstructure research, phase identification and also strain measurement. This technique relies on the interaction of the electron beam with the surface specimen. As a result of that, part of the primary electrons will be scattered within the sample in all directions. High-energy electrons which exit the specimen after one or more scattering events are named backscatter electrons (BSE) . Of these, the most useful for an EBSD analysis are the BSE which satisfy the Bragg equation for diffraction ($n\lambda = 2d\sin\Theta$; Θ being the angle of incidence of the incident beam, d the interplanar spacing, λ the wavelength of the incident electron beam and n an integer) Under these conditions, they describe conical trajectories for each lattice plane and may be imaged on a phosphor screen as a diffraction lines called bands. A set of diffraction lines forms an electron backscatter diffraction pattern (EBSP) or Kikuchi pattern (Fig. 6).

Intersecting bands result in bright spots on the EBSP which correspond to zone axes, i.e. crystallographic directions. Thus elements of geometry can be recognized in EBSPs. In addition many electrons are inelastically scattered and contribute to the formation of a diffuse background in the pattern.

The resolution of EBSD is a function of the acceleration voltage, which controls the depth of penetration of the electrons in the specimen (interaction volume). The smaller the interaction volume is, the higher the resolution. Also, an angle of incidence of 70º between the electron beam and the specimen enhances the proportion of BSE able to be diffracted and escape from few tens of nanometers of these sample surface.

The quality of EBSPs is controlled by the beam current (or spot size). In order to obtain sharp EBSPs, a larger spot size will be required.

In non-conductive materials such as rocks and minerals, problems with the quality of the patterns and their resolution due to charging effects often appear. Next section explains how these problems can be solved.

6.1. Specimen preparation

Samples that are to be analysed by EBSD have to be crystalline. All minerals can be analysed although several minerals are challenging because of complex crystallography. Whole rock or minerals embedded in epoxy can also be investigated. If the aim of the study is the absolute orientation of crystals or structures, the sample should be orientated in space according to important directions such as lineation, foliation plane, etc.

The surface of interest must be smooth to avoid shadowing caused by topography. This can be achieved by mechanical polishing. During this polishing, an amorphous layer can be produced. This layer may be removed using chemo-mechanical polishing (colloid silica polishing). A large number of rock forming minerals can be chemo-mechanical polished successfully.

As we mentioned, insulating specimens will experience charge build-up under an electron beam. Coating the specimen with a conductive material such as carbon or gold removes that problem, but also reduces the quality of EBSP and orientation contrast images. EBSP quality can be increased by raising beam current, that is to say, increasing the spot size.

6.2. Applications of EBSD in mineralogy and geology.

Figure 7 shows some examples of typical analysis for a geological sample. From all the data obtained, one can examine the distributions of individual orientation measurements related to the microstructure (microtexture), the statistical distributions of orientations (the average texture of a bulk sample: macrotexture), and the misorientations between individual measurements (mesotexture).

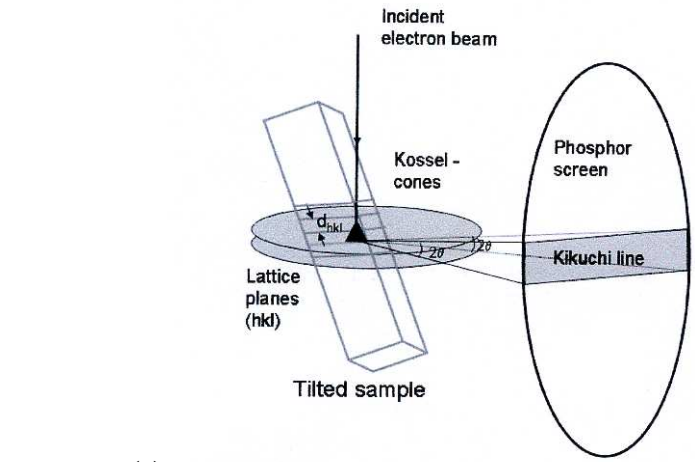

(a)

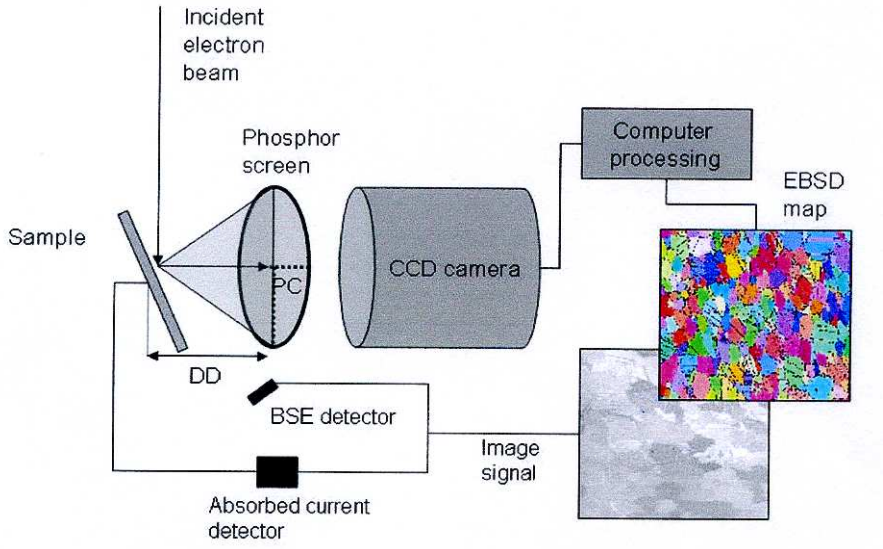

(b)

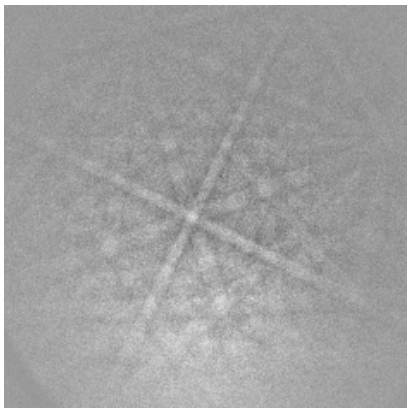

(c)

Figure 6: (a) Origin of Kikuchi lines from EBSD (adapted from Schwartz et al, 2000) (b) Typical EBSD hardware setup inside the SEM. (PC is pattern centre, DD is detector distance). (c) Example of a Kikuchi pattern for sphalerite. Acceleration voltage: 20kV.

All the measurements presented in this chapter have been made on a sphalerite (ZnS) sample from the Pyrenees region, specifically the Liat Mine. At each image point, we have calculated a value for the image quality (IQ) of the EBSPs (Fig. 7a). Inside grains, the IQ brightness depends on crystal orientation and is displayed in fairly bright grey levels, while along grain boundaries the IQ is low.

Misorientation distribution depends on mineral symmetry, which in this example is cubic, and it is plotted, most commonly, by means of inverse pole figures (Fig. 7b), as all the symmetrical equivalents will be plotted in the same place.

Pole figures (PF) are used to represent the texture of the analysed region. These kind of plots are useful to show when a sample is deformed following one direction, as we can see in Fig. 9, where a sharp texture (110) direction is represented.

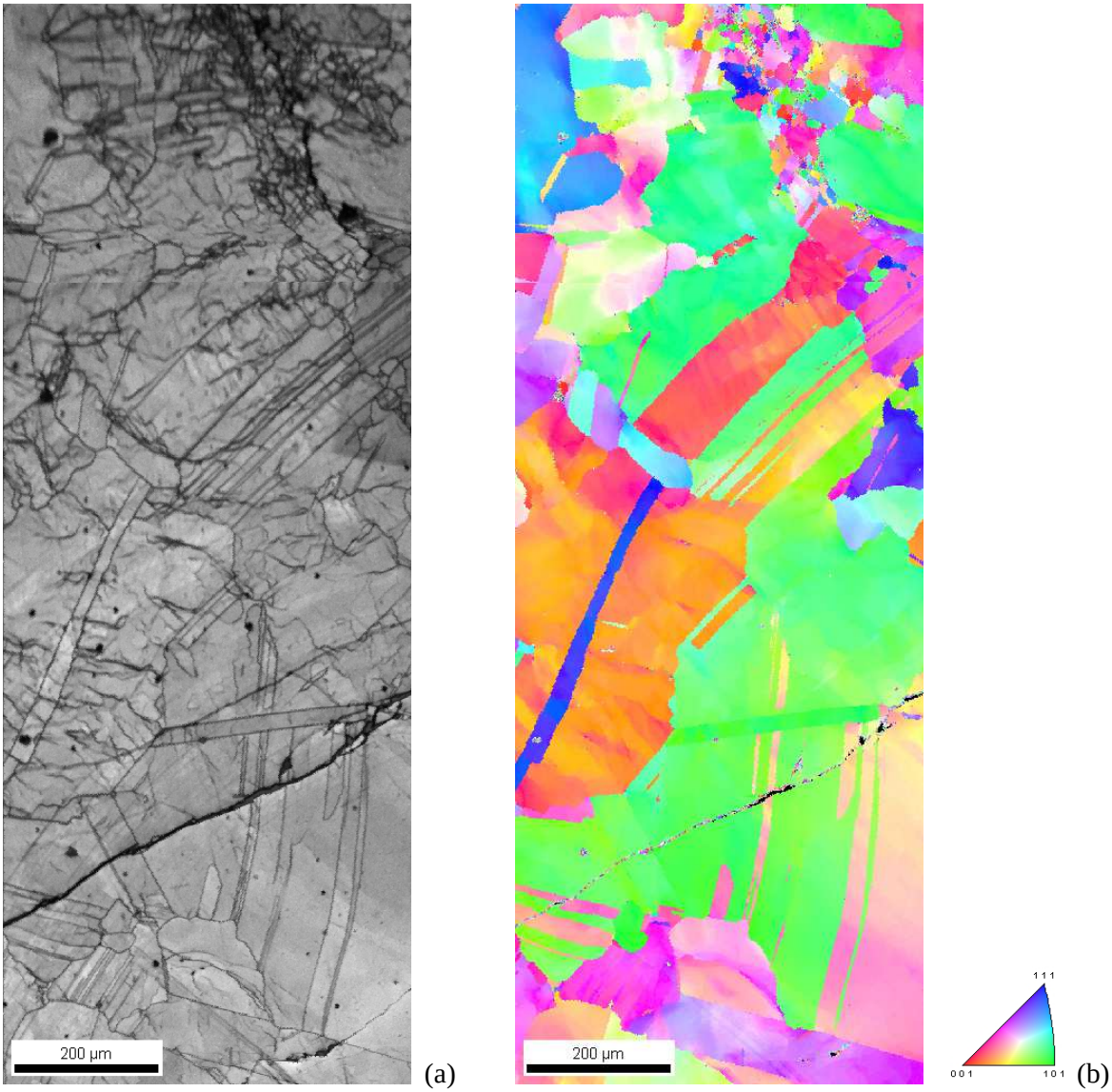

Figure 7: Examples of results from EBSD. The analyzed mineral was a sphalerite (ZnS) from the Liat Mine at the Pyrenees. (a) Image Quality map. (b) Inverse Pole Figure (IPF) map. General boundaries between grains could be defined (Fig. 8). In this figure, high-angle boundaries are shown in blue, whereas low angle boundaries (2 – 5º) are shown in red. These misorientation angles can also be represented in a chart.

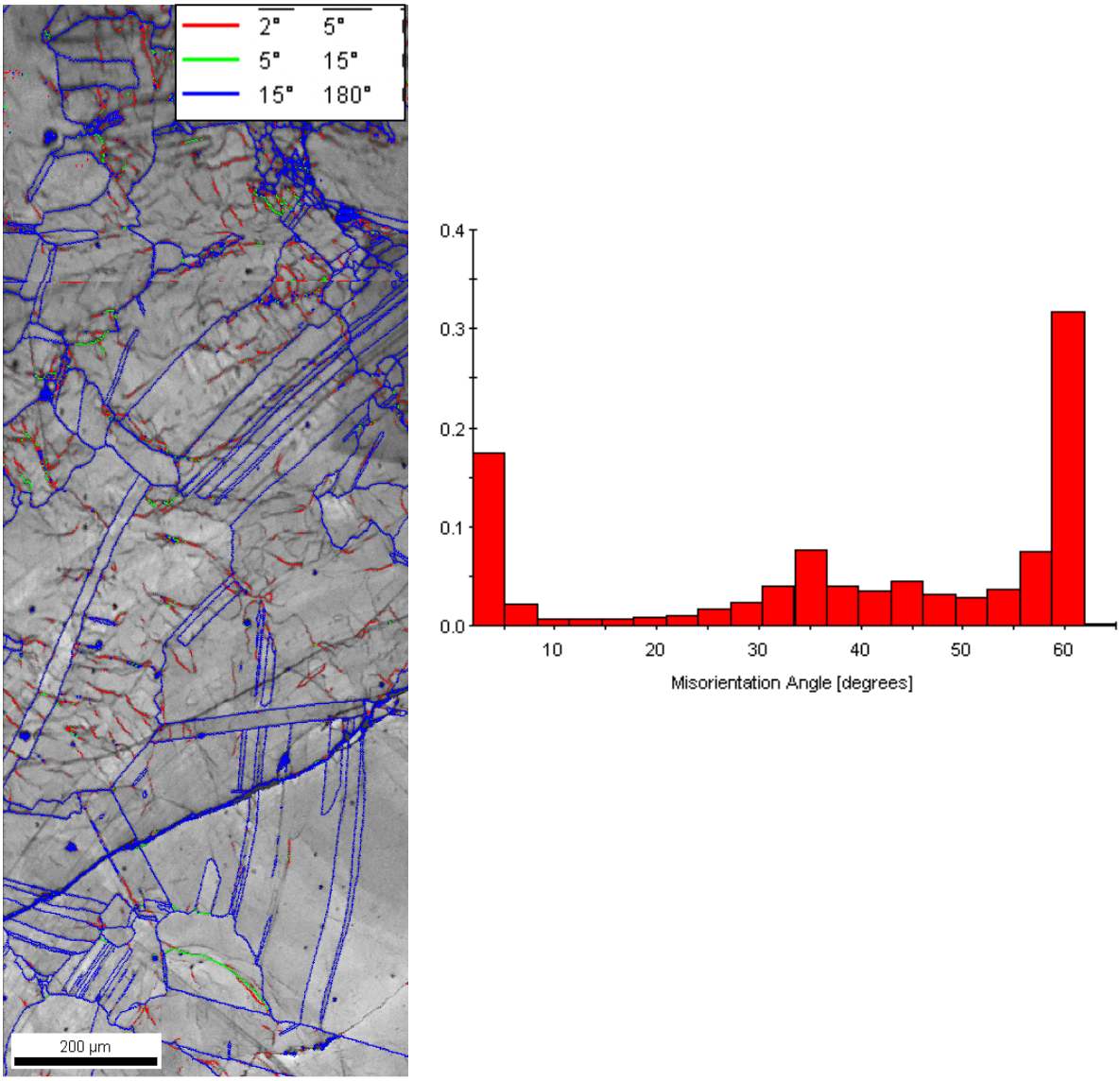

Figure 8: Grain Boundary map and misorientation chart corresponding to a sphalerite sample (ZnS) from the Liat Mine (Pyrenees)

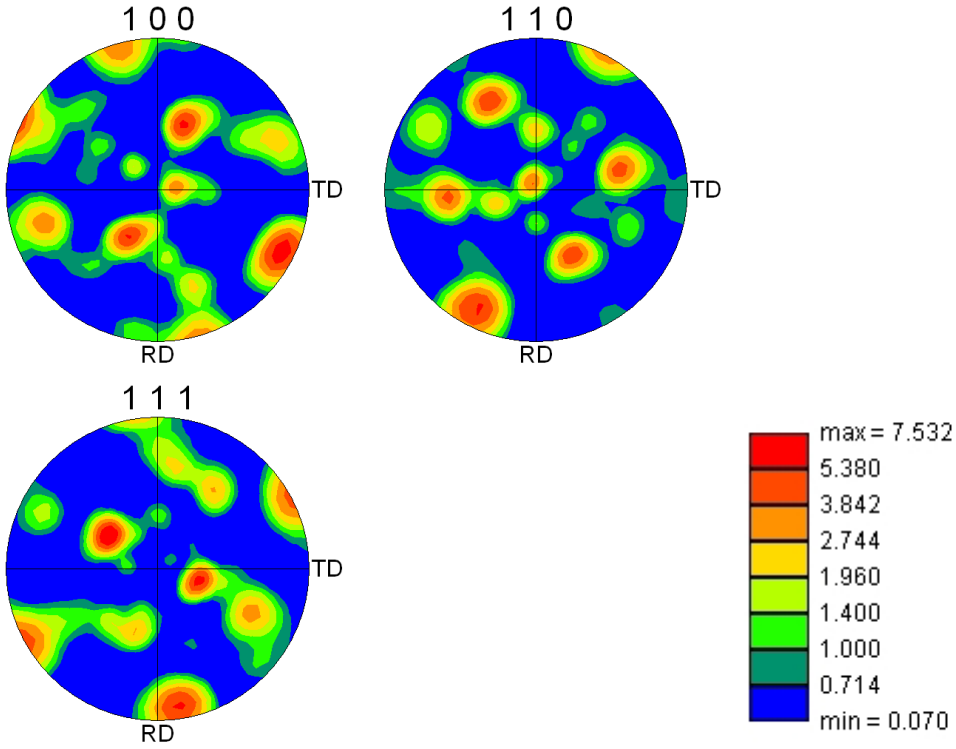

Figure 9: Pole figure for selected poles (100), (110) and (111) corresponding to a sphalerite sample (ZnS) from the Liat Mine (Pyrenees)

References

Ayora, C., García-Veigas, J., Pueyo, J.J., 1994. X-ray microanalysis of fluid inclusions and its aplication to the geochemical modeling of evaporite basins.

Lowenstein, T., Hardie L.A., Timofeeff, M.N., Demicco, R.V., 2003. Secular variation in seawater chemistry and the origin of calcium chloride basinal brines. Geology 31, 857-860.

Prior, D. J., Boyle, A.P. et al., 1999. The application of electron backscatter diffraction and orientation contrast imaging in the SEM to textural problems in rocks. Amer. Mineral., 84, 1741-1759.

Randle, V.,2002. Microtexture determination and its applications. London, The Institute of Materials.

Reed, S. J. B., 1996, Electron Microprobe Analysis and Scanning Electron Microscopy in Geology, Cambridge University Press

Schwartz, A. J., Kumar, M., and Adams, B. L., 2000. Electron backscatter diffraction in materials science : New York, Klumer Academic/Plenum Publishers.

Handbook of instrumental techniques from CCiTUB

Advanced Optical Microscopies for Materials: New trends

Jordi Diaz-Marcos, Francesca Pinna, and Gerard Oncins

Unitat de Tècniques Nanomètriques, CCiTUB, Universitat de Barcelona. Lluís Solé i Sabarís, 1-3. 08028 Barcelona. Spain.

email: *jdiaz@ccit.ub.edu*

Abstract. This article summarizes the new trends of Optical Microscopy applied to Materials, with examples of applications that illustrate the capabilities of the technique.

1. Introduction

Optical microscopy is in a state of explosive development. This is partly due to new technical advances, such as the combination of different optical microscopes set up, i.e. of Confocal Scanning, Phase Shift Interferometry, Vertical Scanning Interferometry and Spectroscopic Reflectometry [1], new objectives (i.e. in oil), new light sources (i.e. laser diodes), …

Optical techniques are becoming of increasing importance in the engineering and measurement of surface finish and form. The principal motivations for the growing use of such techniques are that they are non-contact, non-destructive/non-invasive and surface and volume-average particle. There are many optical techniques both for on-line and for off-line surface-roughness measurement [2].

Confocal microscopy and white-light interferometry microscopy are the two major metrological technologies used in the optical reconstruction. Both the confocal technique and the interferometric technique are able to measure surface topography precisely and reliably on the micrometric and nanometric scales. The measurement principles involved in the confocal technique and the interferometric technique are very different, and consequently the capacities of the two techniques are more complementary than coincident.

1.1. Confocal Profilometry

Confocal profilometers allow height measurement of surfaces with a wide range of textures (from very rough surfaces to very smooth ones) by scanning the sample vertically in steps so that each point on the surface passes through the focus. The height of the surface at each point is established by detecting the position of the maximum value of the axial response. Since only one or a very small number of points on the surface are illuminated simultaneously, an in-plane scan must be carried out in order to build up the axial response, i.e. the confocal image, in each vertical step for all the points falling within the field of view of the lens used (figure 1a).

The focus-detection instruments are gaining popularity due to their ability to carry out non-contact measurement over a wide measurement range with high resolution. Confocal scanning optical microscopes (CSOMs) use this focus detection technique. They were earlier used to measure the tomography of cells and tissues and two-dimensional profiles [3]. Since the early 1980s various three-dimensional measurement systems using this technique have been introduced [4].

In the confocal mode, the profilometer can carry out measurements with an extraordinary lateral resolution. This makes it possible to reduce spatial sampling to values of 0.15 μm for a conventional 150× lens, making it ideal for measurement of critical dimensions on the nanometric scale. In this mode, lenses with a large numerical aperture (NA) may be used, allowing measurement of polished surfaces with very high slopes (up to 70°). It is also possible to use lenses with super-large working distances (SLWD), allowing measurement of surfaces with high aspect ratio. In all cases, structured samples containing dissimilar materials can also be measured.

1.2. Interferometric Profilometry

The last few decades have witnessed major advances in interferometry [5]. We can look forward with confidence to an exciting future for this technique. The father of optical interferometry was undoubtedly Michelson. He was awarded the Nobel Prize in 1907 for ‘his precision optical instruments and the spectroscopic and metrological investigations conducted therewith’.

Optical interferometry (figure 1b) uses interference between light waves to make extremely accurate measurements. The two main working modes are phase shift interferometry (PSI), which allows measurement of the topography of very smooth surfaces with subnanometric resolution, and vertical scanning interferometry (VSI) with white light to measure the topography of smooth or moderately rough surfaces (figure 1c). The above mentioned PSI and VSI interferometers can carry out very fast measurements on the micrometric and nanometric scales. In addition, there is no intrinsic limitation in the vertical measurement range with the VSI technique. Nevertheless, both

techniques have the drawback that they cannot easily deal with highly inclined smooth surfaces or with structured samples containing dissimilar materials.

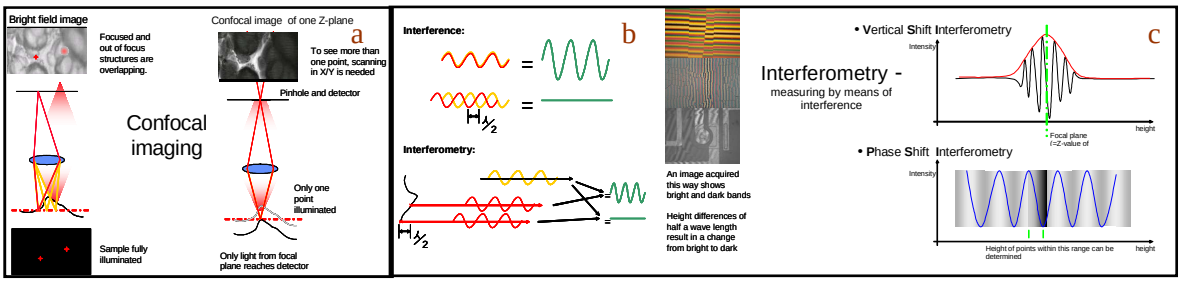

Figure 1. (a) Confocal imaging composition, (b) Interferometry imaging composition and (c) PSI and VSI interference formation.

2. Methodology

2.1. System

Dual (confocal and interferometric) technology optical profilometry (figure 2) provides a new optical surface metrology device for non-physical contact surface measurements that combines in one device the advantages of both techniques.

The system which is available at the Scientific and Technological Centers of the University of Barcelona (CCiTUB) comprises a light source including a light-emitting diode, beam splitters, a CCD (charge coupled device) and a number of interchangeable microscope lenses. These interchangeable microscope lenses comprise conventional lenses that may be used to obtain confocal images and interferometric lenses that may be used to obtain interferometric images. All this lenses are mounted on a rotating element that allows them to be changed easily, depending on the desired type of profilometer function.

The profilometer is provided with an illumination liquid crystal on silicon (LCOS) micro-display that allows the generation of a sequence of illumination patterns that provides, by means of application of the mentioned algorithms, confocal images, or allows total opening of all the illumination pixels to obtain interferometric images. The profilometer is completed with a polarising beam splitter associated with said micro-display.

Lastly, the profilometer includes a system to carry out the required vertical scanning of the sample so that all the points on the surface pass through the focus. This scanning is required for both PSI and VSI modes. The vertical scanning for measurement of the surface topography of the sample is carried out by means of a motor-driven vertical scanning system. The optical profilometer is completed with a system for positioning samples, comprising a motor-driven X-Y movement in the plane perpendicular to the optical axis of the profilometer. The profilometer software allows positioning of the area of the sample to be measured within the field of view of the lens in use by means of joysticks and also allows automatic topographic measurement of profiles or topographies extending beyond the field of view of the lens by means of the field stitching technique.

In the confocal mode, only one or a small number of points on the surface of the sample are illuminated simultaneously by the illumination pattern represented on the LCOS micro-display and the axial response for each of these points is calculated using the appropriate algorithm. In order to cover all the points on the surface to be measured, a series of illumination patterns must be projected onto that surface to obtain the value of the axial response for all the points falling within the field of view. In this way, the confocal image is obtained for a specific vertical position, where the corresponding value of the axial response for each point will be higher the closer it is to the position of the focus. Thus, confocal images provide very high contrast, since light is only perceived in the areas near the focus, while the areas at a distance from the focus appear as dark.

Measurement of the topography of a surface requires a sequence of confocal images in different planes of the sample located at different heights

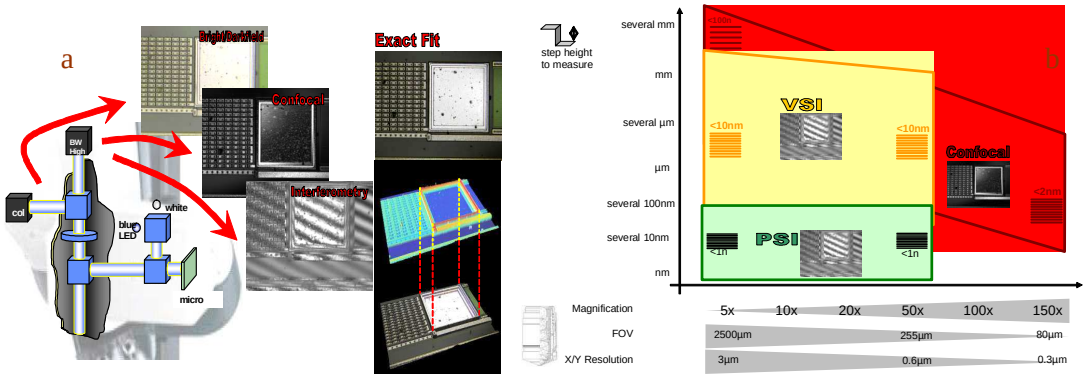

Figure 2. (a) Dual (confocal and interferometric) scheme. Same optical path for all methods and (b) comparison of technologies

In contrast with the confocal mode, the interferometric mode illuminates the whole surface to be analysed at once by means of a micro-display. In other words, in the interferometric mode, illumination patterns are not projected, but instead the whole surface is illuminated to obtain interferometric images for each plane of analysis. The beam emitted is passed through the splitter, which sends all the light to the surface of the sample and the image of the surface is projected onto the CCD device. The series of interferometric images resulting from the vertical scanning of the sample provides, by means of the appropriate algorithm, the surface topography of the sample being analysed. In this case a beam of light passes through a beam splitter. One part of the beam is sent to the surface of the sample and the other part is sent to a reference mirror. The light reflected from these surfaces is recombined and forms a pattern of interference fringes.

In this mode, the PSI technique may be used to measure continuous and very smooth surfaces with subnanometric vertical repeatability, regardless of the interferometric lens used, that is, for all values of numerical aperture. PSI devices allow users to carry out measurements of shape and texture even at scales lower than 0.1 nm. Nevertheless, they have the drawback of an extremely limited vertical measurement range. Likewise, the VSI technique may be used to measure either polished surfaces or rough surfaces with nanometric vertical repeatability for all values of numerical aperture. In addition, with the VSI technique the vertical measurement range is intrinsically unlimited and very high scanning speeds (up to 100 µm/s) may be used.

2.2. The performance of the system

2.2.1. The focus-spot dimension

The focus-spot dimension is an important factor, since it determines the spatial resolution (i.e. the smallest wavelengths which can be determined in the profile). The smallest spot which can be obtained is the so-called diffraction-limited spot, the size of which is determined by diffraction.

2.2.2. The depth response.

In a CSOM with point detection, the microscope image details are exactly at the focal plane. Thus, if a sample is vertically scanned through the focal plane, the photodetector receives the maximum amount of light when the surface is in focus. If the surface is in a lower or a higher position than the focus, the intensity of light gradually reduces to the background intensity. This response curve is referred to as the depth–response curve which is useful for optical sectioning of transparent samples and also during surface characterization using the intensity method. The depth response is dependent on the type of surface and the microscope objective. For determining the depth response, the microscope is initially aligned and the object surface is brought within the focusing range.

2.2.3. The range resolution

The distance dz between half-power points (A and B) of the detector response (figure 3) is called the range resolution. For a reflection-type CSOM it is given by [6]

$$dz = \frac{0.45\lambda}{1 - \cos\theta}$$

where θ is the half cone angle of the objective and it is equal to the numerical aperture of the objective.

The lateral resolution is determined by the size of the diffraction-limited focus spot.

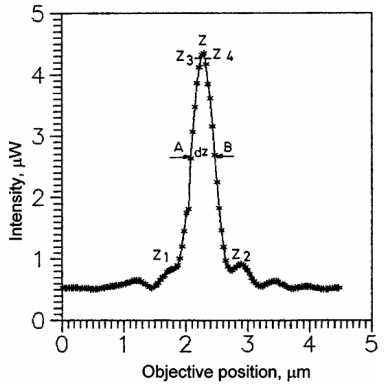

Figure 3. The depth–response curve for a mirror surface

2.2.4. The selection of the objective

Many parameters influence the measurement results obtained with optical measuring systems. Factors such as the nature of the sensor, optical system, illumination, object and mechanical system influence the results [7].

2.2.5. Maximum allowable slope

The maximum allowable slope of the surface is determined as the angle at which the reflected light misses the microscope objective.

2.3. Components of surface topography

There are different components of surface topography generated by most common machining processes [8]. Surface roughness has two main attributes: roughness heights (or depths) and lateral dimensions. Figure 4 shows three types of surface features: (a) thin films, (b) polishing marks, grain structure and scratches and (c) waviness or orange peel.

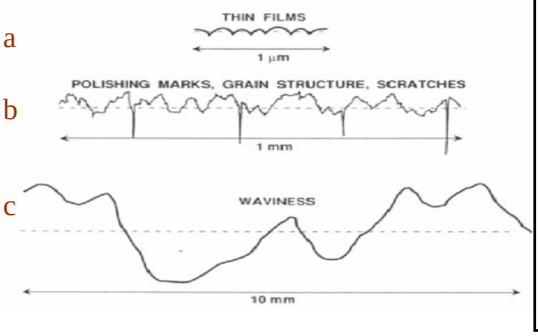

(a) Roughness: the irregularities in the surface which are inherent in the production process, left by the actual machining agent (e.g. a cutting tool, grit or a spark), but excluding waviness and error of form;
(b) Waviness: that component of the texture upon which roughness is superimposed, which may result from such factors as machine or workpiece deflection, vibrations, chatter or heat treatment, various causes of strain in the material and extraneous influences
(c) Form: the general shape of the surface, reflecting variations due to roughness & waviness (normally deviations from ideal form are referred to as 'errors of form').

Figure 4. Dimension of various types of surface features.

Surface structure can be divided into three general groups according to the lateral dimensions. Surface microroughness (often called roughness) has lengths up to approximately one millimeter and includes thin films, polishing marks, scratches and grain structure. Surface waviness, or mid-spatial-frequency roughness, has lengths from a few millimetres to perhaps one centimetre.

Chemically-polished surfaces such as silicon wafers exhibit mid-spatial-frequency roughness, commonly called Orange peel. The overall surface shape often called the optical figure (departure from a perfect surface of the desired shape) or form in the machining industry, has lengths from the centimetre range to the size of the piece.

Although roughness values can be measured by a variety of techniques (figure 5) [9, 10], care should be taken when comparing measurements made with different instruments since the surface spatial wavelength ranges may be different. For example, Scanning Probe Microscopy (SPM) techniques are mainly used to better understand surface roughness on an atomic scale with a much better resolution than that of light microscopes. Therefore, SPM are the most long-scan profilers that have better lateral resolution and can measure surface heights in the waviness regime [11].

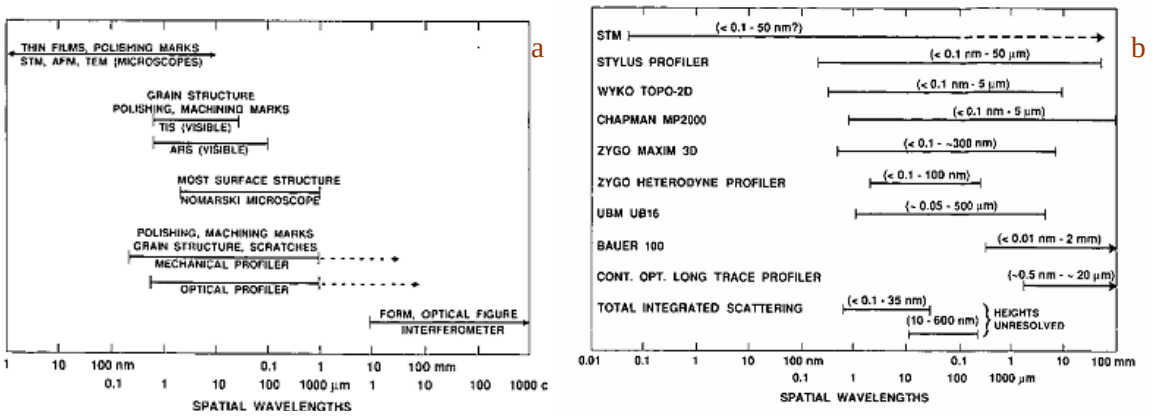

Figure 5. (a) Techniques for measuring surface roughness in various spatial wavelength regions and (b) Schematic diagram of the characteristics of surface profilers and light-scatter measuring instruments. The horizontal bars give surface spatial wavelength ranges, and numbers in parentheses are the range of Rq heights that can be measured with each instrument (adapted from [12]).

The surface data can then be analyzed to study the importance of surface texture in its relation to the surface performance. But the question is what features of the texture are important. Some features that appear as roughness in one application of a surface may well constitute waviness in another. Surface measurement is also limited by the resolution of the instrument used, as the real surface topography may be misrepresented owing to finite dimension of the stylus tip in stylus-based instruments [13-16].

Roughness of the structure is frequently measured and reported as a root-mean-square roughness (R_q) or, in precision machining, as an average roughness (R_z). For a three-dimensional surface, Rq is calculated by including all surface heights from the reference plane. For an isotropic, Gaussian surface, it can be shown that R_q values given by a two-dimensional profile are the same as given by a three-dimensional profile [17]. Typical units can be as small as angstroms or nanometers for the smoother surfaces and micrometers for rougher surfaces or lateral dimensions, called surface spatial wavelengths. Other roughness parameters are peak-to-valley distance (P-V) that is given by the distance between maximum peak or summit to minimum valley, peak-to-mean distance (R_p) that is the distance between maximum peak or summit and mean line (for a two-dimensional profile, the peak is defined as a point higher than its two adjacent points; for a three-dimensional profile, the summit is defined as a point higher than its four adjacent points and a valley is defined in the same way as a peak or a summit but in a reversed order) and correlation length (β) is a spatial parameter giving information about how surface heights are oriented in space.

2.3.1. Effect of scan size

It is commonly observed that the roughness parameters of engineered surfaces change with scan size. In particular, Rq and β generally increase with scan size. It is due to longer and longer wavelength features included in the image as the scan size is increased [18-19].

2.3.2. Selection of scan size

The selection of scan size and sampling interval can change the roughness parameters Rq, Rp, P-V and β. The question is: which is the suitable scan size and sampling interval?

In practice, the scan size should be related to the bandwidth covered by the nominal contact width of the physical problem involved. If a surface contains a broad bandwidth of wavelengths up to or longer than the contact width, then the scan size should be chosen as the contact width. On the other hand, if a surface contains a long-wavelength limit smaller than the contact width, then the scan size can be set equal to the long- wavelength limit.

2.3.3. The selection of the objective.

Also the roughness measurements are affected by the use of a low-NA objective because of an increase in the spot size which determines the spatial resolution. It can also be seen that the depth–response curve broadens as the surface roughness increases. Hence the response curve can give information about the surface roughness. The full-width-at-half-maximum characteristic of the response curve can be correlated to the surface roughness. The shape of this curve also indicates the glossy nature of the surface.

3. Applications

There are countless applications (figure 7) that require knowledge of the topography of the surface of an object and thus determination of its microscopic shape. Such analysis may, for example, form part of a quality control process. Functional characterization was carried out for some industrial applications [20]. Several researchers have also worked on the characterization of surfaces in three-dimensions using various instruments and techniques [21–23].

The optical profilometer is extremely versatile for carrying out accurate measurements of the shape and texture of all types of surfaces on the micrometric and nanometric scales, including structured or stratified samples containing dissimilar materials.

Optics in general played an important role in measurement and, with the advent of opto-mechatronics; it is once again at the forefront of measurement [24]. There are many applications in which the optical profiler may be used. By way of example, the profiler may be used for the measurement of high-aspect ratio surfaces such as those containing grooves, holes or indentations (figure 7g-h), the steeply sloped polished surfaces present in micro-optical structures as micro-lenses and micro-prisms or on-Si micro-finished surfaces, noticeably rough and not very reflective surfaces such as paper (figure 7o-p) or also surfaces of very low roughness containing dissimilar materials such as optical or electronic microdevices (figure 7i-j), surfaces exhibiting different textures and relatively large sized surfaces such as a mould, a coin or a wafer, which can be measured with the option of field stitching (figure 7k-l), etc.

Surface topography plays an important role in understanding the nature of sliding surfaces. No matter how finely finished, most machinery rubbing surfaces are rough from a microscopic viewpoint. As a result, the microtopography of a single surface and the nature of a contact between two surfaces form an essential background for developing a fundamental concept of the nature of two sliding surfaces.

On the other hand, roughness and form must be studied to determine the functional performance of engineering parts. The measurement and understanding of surface topography is rapidly attracting the attention of physicists, biologists and chemists as well as engineers.

The main emphasis in surface-related research is on the determination of parameters that characterize surface properties, mainly those which are correlated to surface-formation mechanisms and surface behaviour in a fundamental way [12]. Monitoring the texture has been a simple way of

controlling the manufacturing process. Measurement of surface topography falls within the field of quality control and product optimization. As we previously remarked, the surface-topographical aspects which influence product performances are roughness, waviness, form, lay, laps, tears and micro-cracks (figure 7a-b). The surface irregularities are broadly classified into micro and macro as shown in figure 6. Surface topography is important from the point of view of such fundamental problems as tribology (figure 7e-f), friction, contact, lubrication, wear, fatigue strength, tightness of joints, conduction of heat and electrical current, cleanliness, reflectivity, sealing, positional accuracy, load-carrying capacity, resistance to corrosion and adhesion of paint and coatings [24]

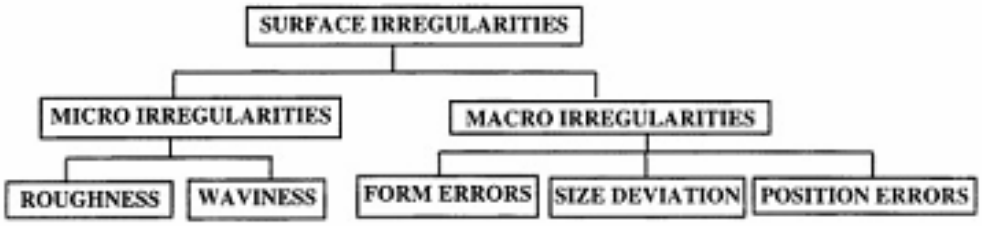

Figure 6. Types of surface irregularities

Some of the current applications of optical interferometry include measurements of distances (figure 7c-d), displacements and vibrations, tests of optical components and systems, studies of surface structure, studies of fluid flows, measurements of temperature, pressure, electrical and magnetic fields, rotation sensing and high-resolution stellar imaging.

Surface roughness [25] is becoming increasingly important for applications in many fields. In optics, low scatter lenses, mirrors, filters, beam splitters and other optical components. In the field of microelectronics, as line widths and circuit elements become smaller and shorter wavelengths are used to produce higher density microcircuits on silicon wafers, the wafer surfaces have to be smoother and less wavy. Disks require surfaces whose roughness properties are carefully controlled and finally, the characterization of stratified media such as semiconductors, flat panel displays, optical coatings (figure 7m-n) and medical devices involves measuring the thickness and optical constants of thin layers with high lateral and vertical resolutions.

In conclusion, the obvious advantage of any optical profiler is that, since it is non- contact, it cannot damage the surface. Also, optical profilers are user friendly, measurements can be carried out easily and rapidly, and data reduction is rapid. The main disadvantages of optical profilers are (a) their lateral resolutions are limited by the properties of the optical systems and by the light beams illuminating the surfaces, (b) they cannot distinguish between changes in topography and changes in optical constants on the surface since they are sensitive to the phase of the light reflected from the surface, (c) the maximum step height that can be measured is less than half of the incident wavelength.

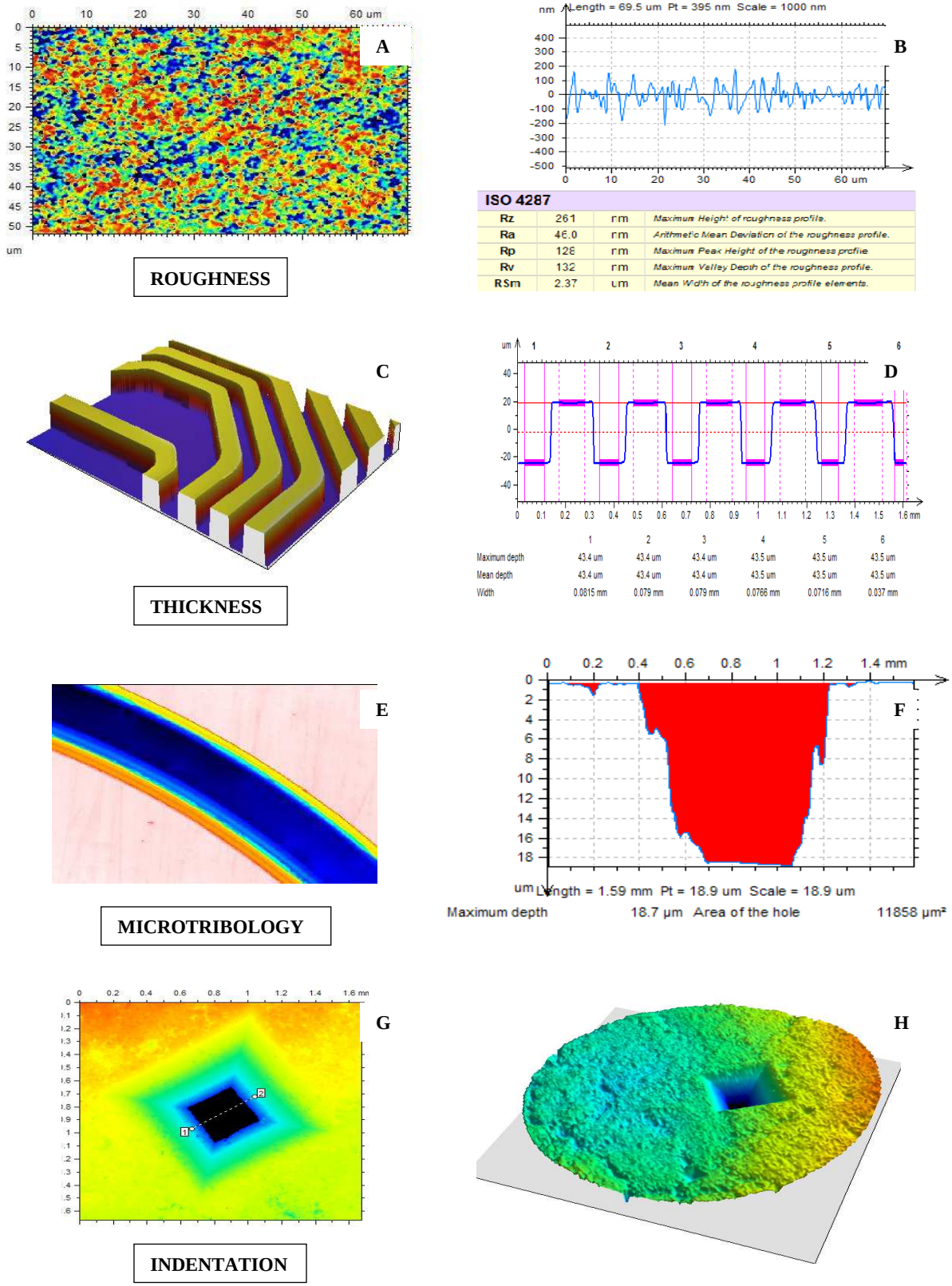

Figure 7a. Images of different applications of Optical Profilometers (a-b) roughness, (c-d) thickness, (e-f) microtribology, (g-h) indentation.

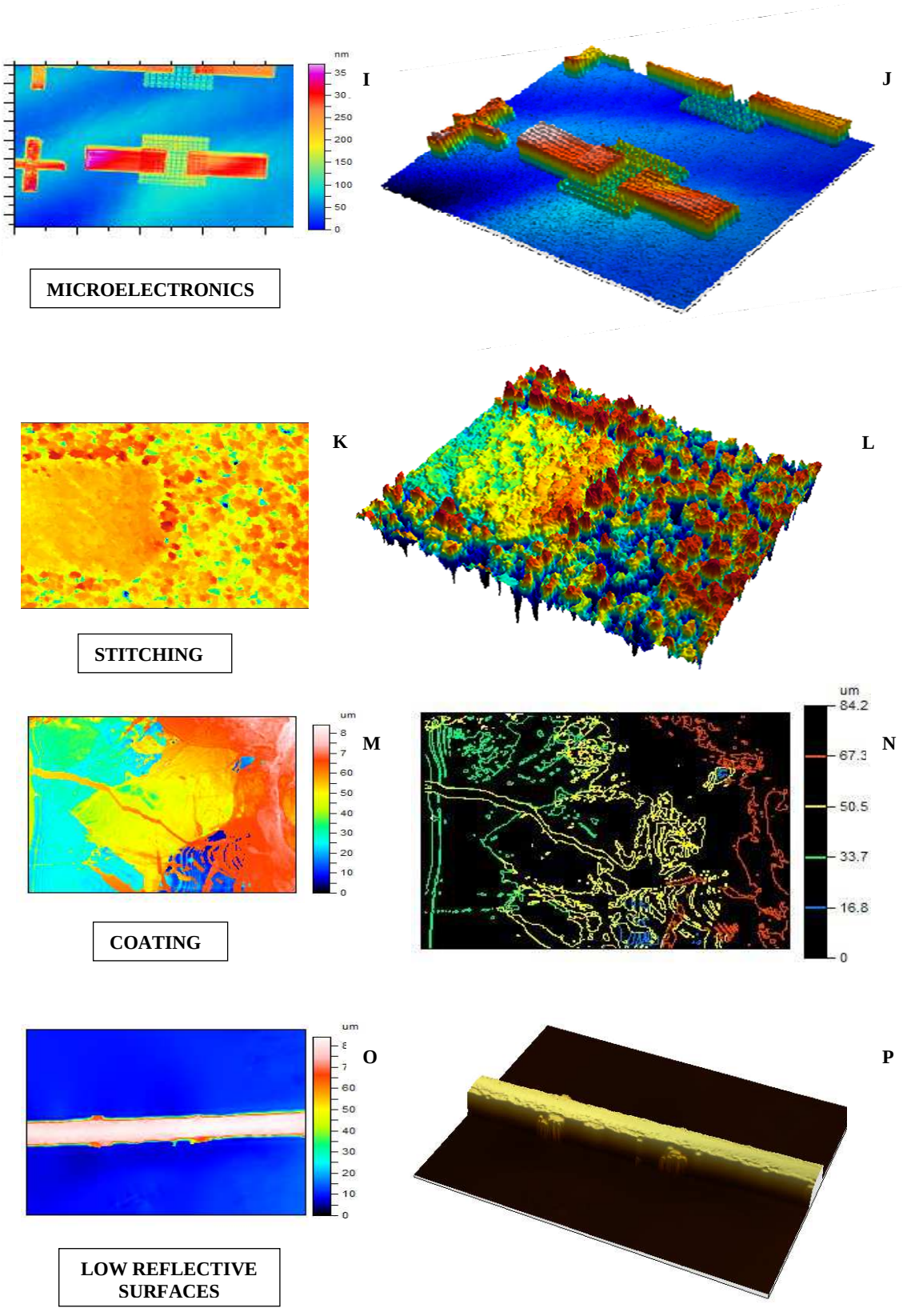

Figure 7b. Images of different applications of Optical Profilometers (i-j) microelectronics, (k-l) stitching, (m-n) coatings and (o-p) low reflective surfaces.

Acknowledgments

The authors would like to thank Dr. J.J. Jaramillo, Dra. Monica Martínez, Dr. Albert Romano, Dra. Núria Cinca and Adriana Velásquez for the reproduction of unpublished results.

References

[1] Patent US7636167 B2
[2] Sherrington I and Smith E H 1988 Modern measurement techniques in surface metrology: part II—optical instruments Wear 125 289–308
[3] Gordon S K and Timothy R C 1989 Confocal scanning optical microscopy Phys. Today September 55–62
[4] Migot J and Gorecki C 1983 Measurement of surface roughness: comparison between a defect-of-focus optical technique and the classical stylus technique Wear 87, 39–49.
[5] P Hariharan .Rep. Prog. Phys. 54 (1990) 339-390.
[6] Gordon S K and Timothy R C 1989 Confocal scanning optical microscopy Phys. Today September 55–62.
[7] De Chiffre L and Hansen H N 1995 Metrological limitations of optical probing techniques for dimensional measurements Ann. CIRP 44 501–4.
[8] Dagnall H 1986 Exploring Surface Texture (Leicester: Rank Taylor Hobson)
[9] De Chiffre L and Nielsen H S 1987 A digital system for surface roughness analysis of plane and cylindrical parts Prec. Engng 9 59–64.
[10] Carneiro K, Jensen C P, Jorgensen J F and Garnoes J 1995 Roughness parameters of surfaces by atomic force microscopy Ann. CIRP 44 517–20.
[11] ref. Handbook SPM
[12] Stout K J (ed) 1994 Three dimensional surface topography. Measurement Interpretations and Applications.
[13] D.J. Whitehouse, Handbook of Su$ace Metrology, Institute of Physics Bristol, 1994.
[14] T.R. Thomas (ed.), Rough Surfaces, Longman, London, 1982.
[15] D.J. Whitehouse and J.F. Archard, The properties of random surfaces of significance in their contact, Proc. R. Sot. London, Ser. A, 316 (1970). 97-121.
[16] D.J. Whitehouse, Theoretical analysis of stylus integration, Ann. CIRP, 23 (1974) 181-182.
[17] R.D. Gibson, The surface as a random process, in T.R. Thomas (ed.), Rough Swjaces, Longman, London, 1982.
[18] R. Sayles and T.R. Thomas, Surface topography as a nonstationary random process, Nafure (London), 271 (1978) 431-434.
[19] Chin Y. Poon, Bharat Bhushan Wear 190 1995) 76-88
[20] De Chiffre L, Christiansen S and Skade S 1994 Advantages and industrial applications of three dimensional surface roughness analysis Ann. CIRP 43 473–8.
[21] Boudreau B D and Raja J 1992 Analysis of lay characteristics of three-dimensional surface maps Int. J. Machine Tools Manufact. 32 171–7.
[22] Ganesha Udupa, M Singaperumal, R S Sirohi andM P Kothiyal. Meas. Sci. Technol. 11 (2000) 305–314
[23] Bennett J M and Mattson L 1989 Introduction 10 Surface Roughness and Scattering (Washington. DC: Optical Society of America)
[24] Bennett J M 1992 Surface Finish and Its Measurement (Washington, DC Optical Society of America)
[25] Jean M Bennett. Meas. Sci. Technol. 3 (1992) 1119-1127.

Handbook of instrumental techniques from CCiTUB

Atomic Force Microscopy: probing the Nanoworld

Gerard Oncins and Jordi Díaz-Marcos

Unitat de Tècniques Nanomètriques, CCiTUB, Universitat de Barcelona. Lluís Solé i Sabarís, 1-3. 08028 Barcelona. Spain.

email: *goncins@ccit.ub.edu*

Abstract. Atomic Force Microscope and related techniques have played a key role in the development of the nanotechnology revolution that is taking place in science. This paper reviews the basic principles behind the technique and its different operation modes and applications, pointing out research works performed in the Nanometric Techniques Unit of the CCiTUB in order to exemplify the vast array of capabilities of these instruments.

1. Introduction

Since Richard Feynman sentenced that "there is plenty of room at the bottom" in the 50's, nanoscience and nanotechnology have become two of the cornerstones of modern science. Nanotechnology, thanks to its interdisciplinary nature, is spreading fast in a variety of disciplines comprising, among others, engineering, physics, chemistry and life sciences. Although we usually assume that nano keeps on being a matter of theorists, there are plenty of daily life products that benefit from this new and revolutionary approach. Microelectronics is the most obvious field, as microprocessors and microfabricated parts are becoming smaller and more powerful. Nevertheless, life sciences, medicine and cosmetics are increasingly introducing nanoparticles in common products as solar filters and anti-ageing treatments [1]. These sorts of products have become controversial because they have not been intensively tested in human beings and long-term effects remain unknown [1]. The nanometric diameter of nanoparticles enables them to cross the skin-barrier and entering the blood stream, thus being possibly involved in a variety of cancers. In this uncertain scenario, nanotechnology related industries struggle to show the obvious benefits of their nano-products and to include them in the mainstream market, fact that will change the world we live in forever.

The study of nature in the nanometric range was boosted by the development of the Scanning Probe Microscopes (*SPM*s). The first member of this nowadays prolific family was the Scanning Tunnelling Microscope (*STM*), released in the 80's in the IBM headquarters [2] and famous for producing the first image of surfaces with atomic resolution (Binnig and Rohrer, the fathers of *STM*, won the Nobel prize in 1986). This technique proved to be a cornerstone in the study of catalysis and surface science thanks to its unmatched topographic resolution. Nevertheless, its use was restricted to conductive samples, limitation that soon disappeared with the development of the Atomic Force Microscope (*AFM*) [3], where all kind of samples could be investigated. Despite featuring lower resolution than the *STM*, it was still able to obtain subnanometric resolution in the vertical axis and its obvious versatility spread the number of applications to all kind of scientific fields. Now it was possible to image samples with minimal preparation, both in air and vacuum and also in all kinds of aqueous solutions. Today, it is also possible to perform topographic measurements in a range of temperatures going from 4K (Ultra High Vacuum, *UHV*, operation) up to 250ºC. Nevertheless, *AFM* is more than a way to obtain surface images of matter; it should be considered as a platform to manipulate the nanoworld with unprecedented resolution. In the field of Materials Science, *AFM* can be used as a classic indenter, now with the ability to control the applied vertical force (F_v) down to the tens of picoNewtons level. This is extremely important, for example, to characterize the mechanical properties of thin films and advanced coatings used in the development of Micro- and NanoElectroMechanical systems (*MEM*s and *NEM*s). Of course, this force control represents a breakthrough in biophysics, as now the mechanical properties of cells, proteins and membranes can be experimentally assessed [4]. *AFM* is also able to modify the sample surface by scratching or locally oxidizing it, to probe electric [5] and magnetic properties of samples and to release nanodroplets of molecules in surfaces in order to create selectively functionalized patterns.

Because of this, AFM should be considered as a platform to explore the nanoworld, the core of a system which is being constantly complemented with new operation modes the use of which is step by step demolishing the classic boundaries that still keep Chemistry, Physics, Biology and Engineering apart.

2. Methodology and applications

2.1. AFM basic operation principle

AFM is based on the contact between a microfabricated tip and the sample surface (Fig. 1). As it is a scanning technique, the tip rasters the sample resolving its fine details down to the nanometric level thanks to a tip apex radius ca. 5nm. In a sense, it is the same principle used in a record player, where the needle rides on the grooves of the vinyl record. As the piezo stage proceeds with the

scanning in the XY axis, the cantilever bends up or down (Z axis) and this deflection is detected by means of a laser that finally reflects on a photodetector which tracks the AFM probe response. Usually, the piezo is under the sample, although there are different AFM geometries where the tip is scanned while the sample remains still. Modern AFM piezos cover scanning ranges in the XY plane that goes from hundreds of nanometers to 200 micrometers.

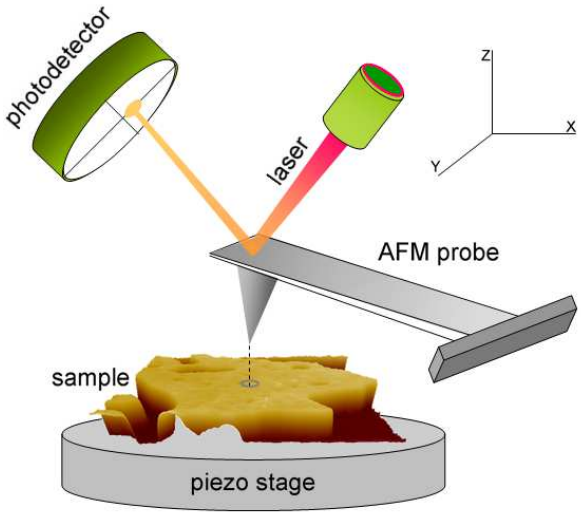

Figure 1. *AFM* schematics. The *AFM* probe tracks the sample surface, which is precisely moved in the XY axis by means of a piezo stage. The deflection of the AFM probe is tracked by a laser that reflects on a photodetector which can detect probe movements in the subnanometric range

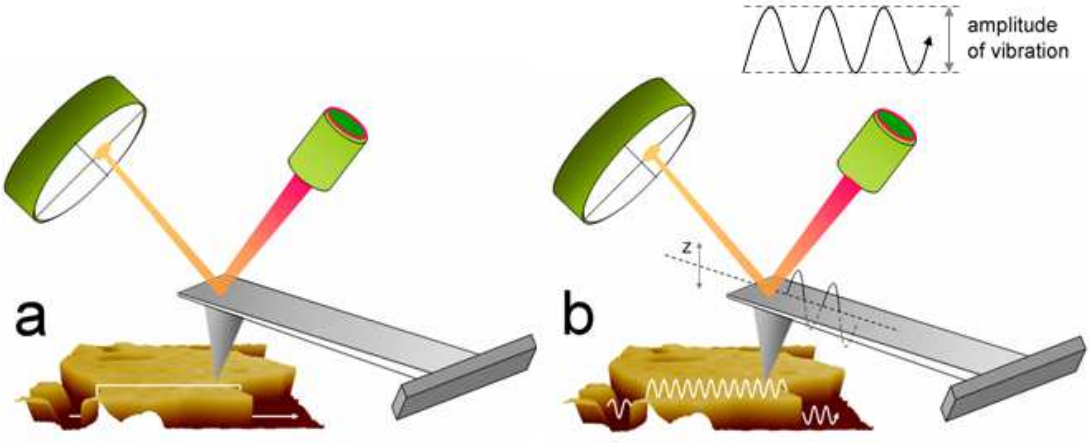

Figure 2. Two basic *AFM* topographic modes. a) In contact mode the *AFM* probe tracks the sample surface in close contact while the feedback loop keeps cantilever deflection constant. b) In intermittent contact mode, the *AFM* probe moves in a sinusoidal way in the Z axis so the contact with the sample is intermittent. In this case, the feedback does not try to keep control on the cantilever deflection but on the amplitude of vibration.

2.2. Topographic modes

2.2.1. Contact mode

In contact mode, the AFM probe is brought into contact with the sample up to a desired cantilever deflection, which results in the application of a certain F_v value. Then, feedback electronics keep the deflection constant as the tip scans the sample in the XY plane by moving the piezo in the Z axis. In fact, this movement corresponds with the sample topography.

This operation mode obtains images with the highest AFM resolution but, due to the direct contact with the sample, it can be aggressive and deform the surface by dragging material away. Besides, the probe radius wears fast due to friction forces and the quality of images can degrade in

a few scans. For all this, contact mode is recommended for atomic resolution topographic images of hard materials (polymers, metals, oxides) [6] or biological samples where structural resolution is mandatory [7] (protein crystals or ion channels on cell membranes).

2.2.2. Intermittent contact mode

Intermittent contact is the most commonly used of all *AFM* topographic modes because it is gentle with the sample surface and also with the *AFM* probe apex, producing consistent data of samples while inducing minimum deformation (Fig. 3e, f). In this mode, the *AFM* probe oscillates at its resonance frequency in the Z axis at a constant amplitude of vibration, which is kept constant by a feedback electronics, while lightly tapping the sample surface. The consequent contact intermittency is enough for the probe to track the sample topography and obtain accurate surface images. Because of this, it is used for imaging all kind of samples, especially biological material [8] both in air and in liquid environment [9]. Some efforts have been performed to improve this mode by combining it with techniques as Infrared spectroscopy (*IR*), *Raman* or *Scanning Near Field Ellipsometer Microscopy* (*SNEM*) [10].

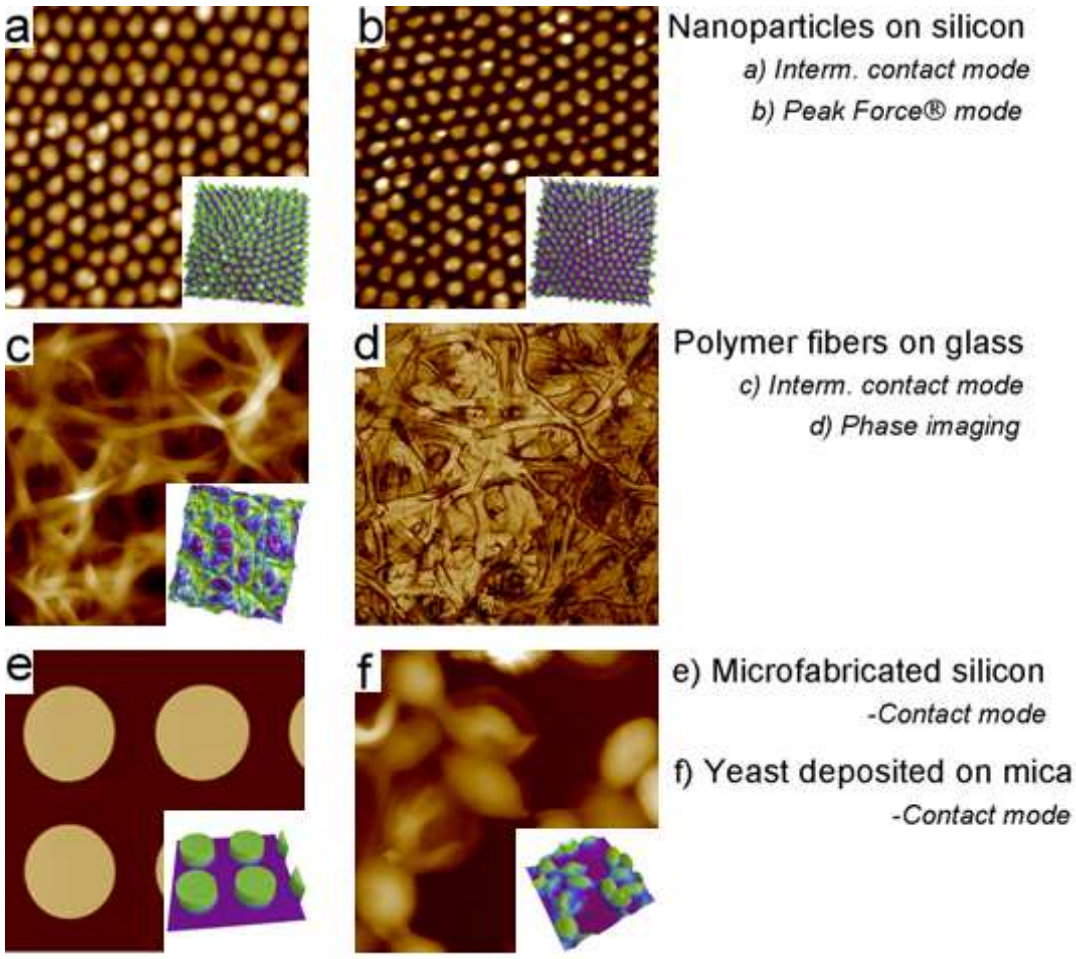

Figure 3. Topographic images obtained by *AFM* in the fields of nanostructures, polymer science, microelectronics and biology. Image sizes: a) and b) 500x500nm^2; c), d) 30x30μm^2; e) 50x50 μm^2; f) 12x12 μm^2. a) and b) correspond to the same sample, demonstrating that Peak Force® is less influenced by *AFM* probe radius, which results in particles with a diameter much closer to reality. c) and d) were obtained simultaneously; d) Phase image shows a compositional contrast which is impossible to detect in topographic image c).

One of the main drawbacks of *AFM* is its lack of compositional sample information. Nevertheless, Phase Imaging (a secondary mode in intermittent contact, Fig. 3d) can provide qualitative data in this direction. This mode is based on the different quantity of energy dissipated by the sample as the tip taps its surface in every vibration cycle. According to this, soft materials will absorb more energy than hard materials, resulting in a phase change of the vibration.

2.2.3. Peak Force® mode

In this mode, the *AFM* probe engages the sample and retracts with a frequency of several kHz. In each cycle, the F_v value is carefully controlled to maximize probe life and reduce sample damage. As this control is fully automatic while the probe scans the sample, Peak Force® is extremely interesting for users, both basic and advanced, that need accurate topographic images. Furthermore, the unprecedented quality of the images due to the low *AFM* probe wear makes it useful when resolution is paramount. An enlightening example can be seen in Fig. 3a) and b), where 10nm diameter nanoparticles deposited on silicon are imaged. a) corresponds to an Intermittent Contact image and b) was obtained in Peak Force® mode. In b) image, particles look much smaller than in a), despite the fact it is the same sample; this is because lateral resolution of images in *AFM* depends on the probe radius. Initially, both topographic modes use the same sort of probes (same final radius) but Intermittent Contact is more aggressive and wears down the radius from the initial 2nm to ca. 5nm to 10nm in a few scan lines. Peak Force® mode is gentler and keeps the initial radius for much longer. As a result, sharper and more accurate lateral resolution is obtained and the measured diameter of nanoparticles is much closer to reality.

2.3. Nanotribology and Nanomechanics

2.3.1 Force Spectroscopy

The *AFM* probe can be used as a nanoindenter to test the mechanical response of samples [11, 12, 13]. Its main advantage is that the measurements can be performed with nanometric spatial resolution and that the F_v values applied on the sample can be as small as tens of picoNewtons ($1pN=10^{-12}N$). Consider a polymeric matrix with embedded nanoparticles; a classic indenter would be able to obtain the Young modulus (*E*) of the whole sample but the *AFM* would be able to perform local nanoindentations both in the matrix and in the nanoparticles independently. These capabilities are especially interesting for biological samples, which have thicknesses usually below 1 micron and where it is extremely difficult to obtain quantitative nanomechanical information by other techniques (Fig. 4). At the CCiTUB, the *E* value of protein aggregates deposited on mica was quantitatively assessed [14] but our expertise has been mainly focused on the nanocharacterization of biological phospholipid membranes and nanometarials. In this field, we have quantitatively measured the F_v value necessary to puncture membranes in different buffer conditions, probing the effect of electrolytes concentration [15] or pH [16] in their stiffness and the influence of the phospholipids structure on their mechanical response [17, 18, 19, 20]. In the field of monolayers, fatty acid and thiols proved to deform under the pressure of the *AFM* probe in a sequential way (step-by-step mechanism), shedding light on the packing structure of these 2D structures [21, 22]. In the field of hard materials, the exploration of obtained *E* values both by traditional methods and AFM nanoindentation are leading to the comprehension of the differences between mechanical properties of surfaces and bulk materials [11, 12, 13]. Other parameters that can be extracted from the so-called force curves, that is, the nanoindentation experiment itself shown in Fig. 4a, are adhesion forces, dissipation energy, the vertical breakthrough force of nanostructures and the force where elastoplastic transitions take place.

Thanks to the Quantitative Nanomechanical Property Mapping Mode (*QNM*) derived from the Peak Force® technology developed by Bruker, all the mechanical parameters can be obtained in real time while capturing a topographic image (Fig. 5). The operation range of this technique goes from tens of MPa (soft biological samples, monolayers, proteins) up to 100GPa (metals, oxides, hard coatings).

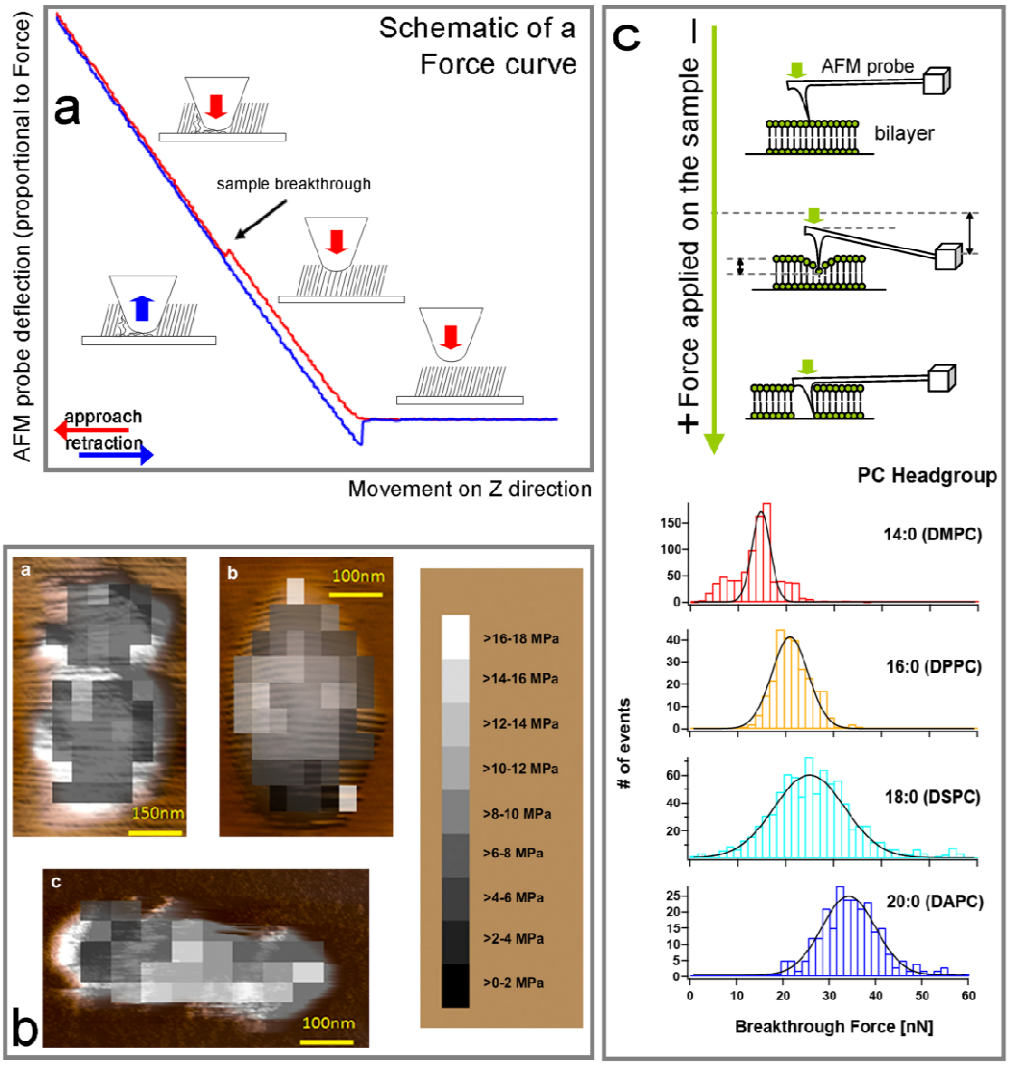

Figure 4. Nanomechanics by *AFM*. a) When a sample is compressed with an *AFM* probe, a force curve is obtained. In the case of mono/multilayered materials, it is possible to quantitatively measure the F_v value necessary to break the sample (shown as a discontinuity in the approach curve in Fig. 4a. b) Different globular proteins imaged by *AFM* where force curves have been performed. A map of Young modulus is over imposed on the topographic images. c) The mechanics of phospholipid membranes can be quantitatively assessed and the breakthrough force measured as a function of the length of the hydrocarbon chains of the phospholipids (in this case, from 14 to 20 carbons).

2.3.2 Friction Force Microscopy (FFM)

FFM is able to quantify the nanotribological properties of a huge variety of samples [23]. These measurements are of great interest when it comes to study materials science-related samples and it is especially useful to characterize the performance of thin films and advanced coatings [24]. In the last years, *FFM* has also been applied to organic films, both in air and in liquid, tapping into phenomena that had never been accessible by other techniques [25, 26, 27]. The operation principle is as follows: the sample is scanned by the *AFM* tip in a direction that is perpendicular to the long cantilever axis (figure 6a). In this way, a cantilever torque momentum is created which can be experimentally measured by following the path of the laser in the lateral quadrants of a four-segment photodetector. The lateral laser deviation is proportional to the friction force (F_f) between the tip and the sample, which in turn is proportional to the F_v value applied by the tip (measured by

the vertical displacement of the laser in the photodetector). F_f value can be measured in a quantitative way in the range that goes from the tens of picoNewtons to hundreds of nanoNewtons. Figure 6b) shows a front view of the cantilever and the tip and how the scanning movement creates a cantilever torsion which in turn is detected as a lateral laser deviation in the photodetector.

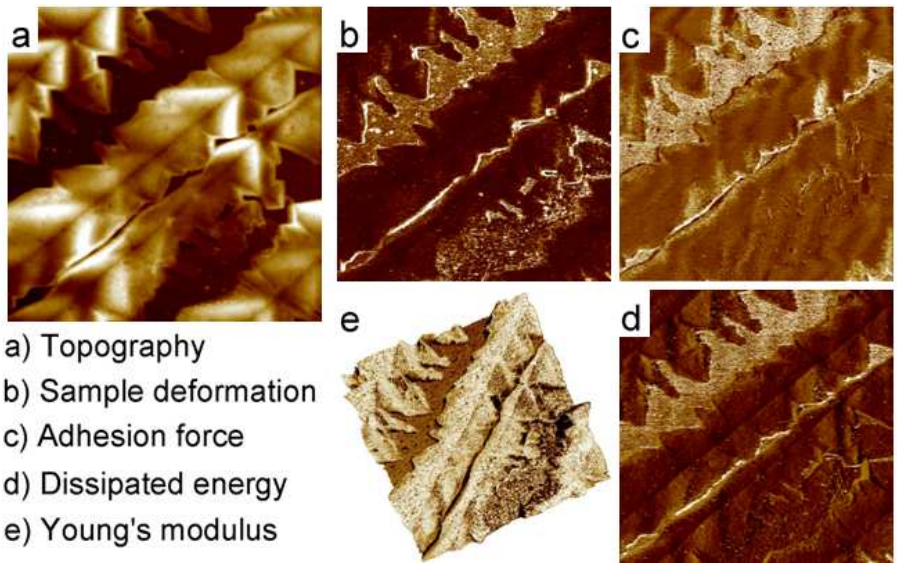

Figure 5. Salt crystals on a mica surface imaged by *QNM*. This mode enables to obtain important quantitative nanomechanical parameters that give information about the physicochemical properties of the sample surface. Image size: 20x20μm^2.

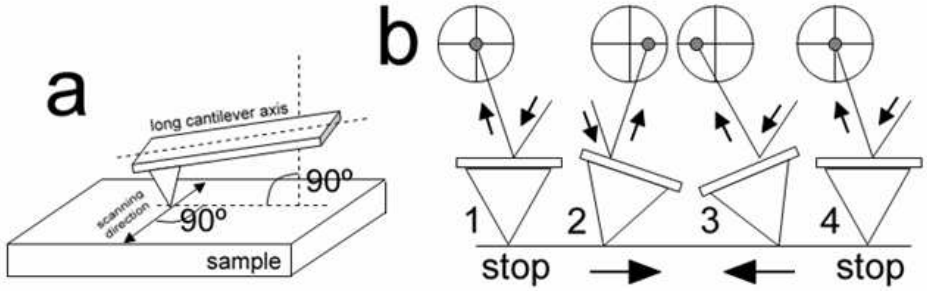

Figure 6. *FFM* operation principle. a) The scanning direction creates a torque on the cantilever which is proportional to the F_f value between the tip apex and the sample. b) The friction response can be measured as a function of the F_v value in order to acquire important nanomechanical parameters as friction coefficient and dissipated energy.

2.4. Electric and magnetic characterization

2.4.1 Conductive AFM (C-AFM)

C-AFM is a secondary imaging mode derived from contact *AFM* that characterizes conductivity variations across medium- to low-conducting and semiconducting materials. The operation principle is simple: a potential is applied between a metal-coated *AFM* tip and the sample; when both surfaces are in contact, an electric current (intensity, *I*) flows across the interface. Thanks to low-noise preamplifiers, *I* values as small as tens of femtoAmpers can be detected. In fact, what we obtain is a map of *I* value besides a topographic image [28]. This is of important relevance for the microlectronics and photovoltaics industry but also for the development of new nanometarials as carbon nanotubes [29] and graphene [30], where conductivity of extremely small parts of integrated circuits has to be measured. The variations in *I* map indicate the presence of defects in the

semiconductor materials, the control of which are mandatory in fabrication processes. Besides, the ability to control the position of the AFM tip in the nanometric range enables the user to stop the tip on a certain point of the sample surface, apply a desired F_v value and ramp the potential in order to obtain an extremely local *IV* curve.

2.4.2 Magnetic Force Microscopy (MFM)

Magnetic Force Microscopy (*MFM*) is a secondary imaging mode derived from Intermittent Contact topographic mode that maps magnetic force gradients above the sample surface. Thanks to a tip coated with a magnetic alloy, the topographic and magnetic images of the sample can be simultaneously obtained. The extremely high resolution of this technique enables the study of molecular magnets, as well as magnetic thin films [31] (Fig. 7).

MFM probes tip is coated with a ferromagnetic thin film. While scanning, it is the magnetic field's dependence on tip-sample separation that induces changes in the cantilever's resonance frequency or phase. *MFM* can be used to image both naturally occurring and deliberately written domain structures in magnetic materials (Fig. 7a and b).

2.4.3 Surface Potential (SP), also known as Elestrostatic Force Microscopy (EFM)

SP is a secondary imaging mode derived from Intermittent Contact topographic mode that maps the electrostatic potential on the sample surface. As the *AFM* probe has to be sensitive to electric charges, it is necessary to coat it with a metal or conductive layer as doped-diamond (highly wear-resistant). It is interesting to note that the sample can be an insulating because the only charges that are detected are on the surface; no electrons flow across the interface, as no voltage difference is applied between the *AFM* probe and the sample. This technique can be applied to detect the very subtle charge differences that arise when an organic monolayer is being formed on a substrate or to identify different domains in mixed phospholipid bilayers. It is worth to note that a slightly refined mode called Surface Potential Force Microscopy (*SPFM*) [32] is able to scan the sample in real non-contact while obtaining images of liquid droplets, being of special interest for the study of 2D lubricants [33] and corrosion science [34].

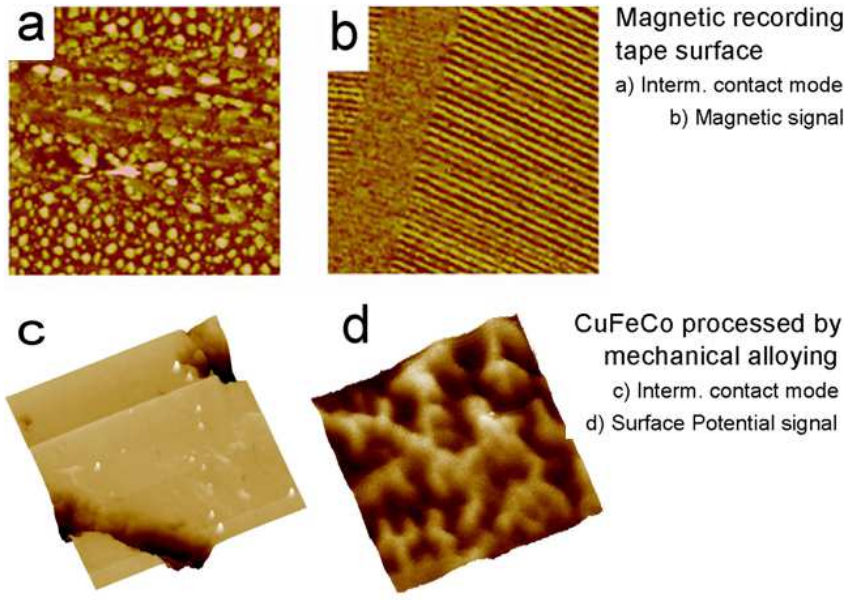

Figure 7. The ferrite grains present on the surface of a magnetic recording tape can be topographically resolved (a) and, at the same time, the magnetized domains are revealed by *MFM* (b). Notice that there is no cross-linking between the topography and the magnetic domains. c) and d) correspond to the topography and surface charge distribution signal (*SP*) on a metallic sample. Although topographic image reveals a smooth surface, *SP* signal is able to discern different charge domains which can be related to compositional gradients.

Acknowledgments

The authors would like to thank Dr. Paolo Pellegrini, Dr. Carmen García, Dr. Daniel Navarro, Dr. Núria Llorca and Rebeca Tudela for the reproduction of unpublished results.

Glossary

SPM. Scanning Probe Microscope
STM. Scanning Tunnelling Microscope
AFM. Atomic Force Microscope
UHV. Ultra High Vacuum
F_v. Vertical Force
*MEM*s. MicroElectroMechanical Systems
*NEM*s. NanoElectroMechanical Systems
SNEM. Scanning Near Field Ellipsometer Microscopy
E. Young's modulus
QNM. Quantitative Nanomechanical Property Mapping
F_f. Friction Force
FFM. Friction Force Microscopy
C-AFM. Conductive AFM
I. Current Intensity
V. Potential
SP. Surface Potential
SPFM. Surface Potential Force Microscopy
EFM. Electrostatic Force Microscopy

References

[1] Díaz-Marcos J., Velásquez A., Oncins G. 2001 *Revista de la sociedad Española de Químicos Cosméticos* **mayo-junio** 5
[2] Binnig G., Rohrer H., Gerber Ch., Weibel E. 1982 *Phys. Rev. Lett.* **49** 57
[3] Binnig G., Quate, C.F., Edward L., Gerber Ch. 1986 *Phys. Rev. Lett.* **56** 930
[4] Garcia-Manyes S., Sanz F. 2010 *BBA Biomembranes* **1798** 741
[5] Villares A., Lydon D.P, Low, P.J., Robinson, G.J., Ashwell G.J., Royo, F.M., Cea P. 2008 *Chem. Matter* **20** 258
[6] Palacios-Padrós, A. Caballero-Briones, F., Sanz F. 2010 *Electrochemistry Comm.* **12** 1025
[7] Valle-Delgado J.J., Alfonso-Prieto M., De Groot N., Ventura S., Samitier J., Rovira C., Fernández-Busquets X. *Faseb Journal* **24** 4250
[8] Basas M., Díaz J., Prieto M.J. Manresa A. 2008 *Microbiology and Biotechnology* **78** 587
[9] Haro M., Villares A., Martín I., Oriol L., Cea P. 2010 *Current Applied Physics* **10** 874
[10] Davide D., Tranchida D., Díaz J., Schön P., Schönherr H., Vancso J. 2011 *Nanoscale* **3** 233
[11] Roa J.J., Oncins G., Díaz J., Capdevila X.G., Sanz F., Segarra M. 2011 *J. European Ceramic Society* **31** 429
[12] Roa J.J. Jiménez-Piqué E., Capdevila X.G. Segarra M. 2010 *J. European Ceramic Society* **30** 1477
[13] Roa, J.J., Oncins G., Díaz J., Capdevila X.G. Segarra M. 2010 *Recent Patents in Nanotechnology* **5** 27
[14] Díez-Gil C., Krabbenborg S., Garcia-Fruitós E. 2010 *Biomaterials* **31** 5805
[15] Garcia-Manyes S., Oncins G., Sanz F. 2005 *Biophysical Journal* **89** 1812
[16] Garcia-Manyes S., Oncins G., Sanz F. 2005 *Electrochimica Acta* **51** 5029
[17] Garcia-Manyes S., Redondo-Morata L., Oncins G., Sanz F. *J. Am. Chem. Soc.* **132** 12874
[18] Nussio M.R., Oncins G., Ridelis I. 2009 *J. Phys. Chem. B* **113** 10339
[19] Oncins G., Picas L., Hernández-Borrell J. 2007 *Biophys. J.* **93** 2713

[20] Garcia-Manyes S., Oncins G., Sanz F. 2005 *Biophys. J.* **89** 4261
[21] Oncins G., Vericat C., Sanz F. 2008 *J. Chem. Phys.* **128** 044701
[22] Oncins G., Torrent-Burgués J., Sanz F. 2008 *J. Phys. Chem. C* **112** 1967
[23] Carpick R.W., Salmeron M. 1997 *Chemical Reviews* **97** 1163
[24] Corbella C., Vives M., Oncins G., Canal C., Andújar J.L., Bertran E. 2004 *Diamond and Related Materials* **13** 1494
[25] Oncins G., Garcia-Manyes S., Sanz F. 2005 *Langmuir* **21** 7373
[26] Gállego I., Oncins G., Sisquella X., Fernández-Busquets X., Daban J.R. 2010 *Biophysical Journal* **99** 3951
[27] Torrent-Burgués J., Oncins G., Garcia-Manyes S., Sanz F. 2010 *Biomimetics in Biophysics: Model Systems, Experimental Techniques and Computation.* Research Signpost, Trivandrum, India
[28] Gómez-Navarro C., dePablo P.J., Gómez-Herrero J., Biel B., García Vidal F.J., Rubio A., Flores F. 2005 *Nature Materials* **4** 534
[29] Sundqvist P., Garcia-Vidal F.J., Flores F., Moreno-Moreno M., Gomez-Navarro C., Bunch J.S., Gomez-Herrero J. 2007 *Nano Letters* **7** 2568
[30] Mativetsky J.M., Treossi E., Orgiu E., Melucci M., Veronese G.P., Samori P., Paermo V. 2010 *J. American Cehemical Society* **132** 14130
[31] Puntes V.F., Gorostiza P., Aruguete D.M., Bastus N.G., Alivisatos A.P. 2004 *Nature* 263
[32] Xu L., Salmeron, 1998 M. *J. Phys. Chem. B* **102** 7210
[33] Xu L., Ogletree D.F., Salmeron M., Tang H.A., Gui J., Marchon B. 2000. *J. Chem Phys.* **112** 2952
[34] Verdaguer A., Weis C., Oncins G., Ketteler G., Bluhm H., Salmeron M. 2007 *Langmuir* **23** 9699

Handbook of instrumental techniques from CCiTUB

Paleomagnetism: principles and applications

Elisabet Beamud

Laboratori de Paleomagnetisme, CCiTUB, Universitat de Barcelona. Institut de Ciencies de la Terra "Jaume Almera", Solé i Sabarés s/n. 08028 Barcelona. Spain.

email: *betbeamud@ccit.ub.edu*

Abstract. This article summarizes the basic principles of Paleomagnetism, with examples of applications in geology that illustrate the capabilities of the technique.

1. Introduction

Paleomagnetism is the study of the record of the Earth's magnetic field in rocks. The Earth's magnetic field has its origin in the convection of the iron rich material of the outer core of the Earth. At any point of the earth surface, the magnetic field (F) can be defined by two angles (Figure 1). Declination (Dec) is the angle between the horizontal component of F and the geographic north, ranging from 0 to 360 º and defined as positive clockwise; inclination (Inc) is the vertical angle or the angle between F and the horizontal, ranging from -90 to 90 º, positive downwards.

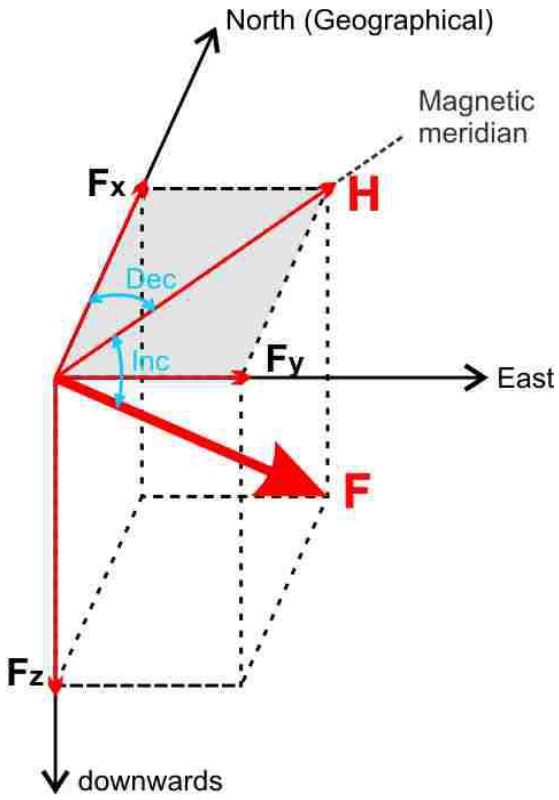

Figure 1 – Description of the direction of the magnetic field (F). Inclination (Inc) is the vertical angle (= dip) between the horizontal and F; declination (Dec), is the azimuthal angle between the horizontal component of F (H) and the geographic north.

At the Earth's surface, the geomagnetic field can be approximated to the field created by a geocentric axial dipole (GAD), a dipole placed at the center of the earth and aligned with the Earth's rotation axis (Figure 2). The GAD model only accounts for about the 90% of the Earth's surface field, the rest would be the sum of non geocentric dipolar fields, fields of non-dipolar origin and of external origin. In the Earth's surface, magnitude and direction of the geomagnetic field changes with time, ranging from milliseconds, hours, or days (pulsations or short-term fluctuations, daily magnetic variations, or magnetic storms) to centuries, thousands of years, or million of years (secular variations, magnetic excursions, and polarity reversals). Changes with periods between 1 year and 10^5 years constitute which is known as Geomagnetic Secular Variation. Among the longer term variations of the geomagnetic field the polarity reversals, with durations ranging from thousands of years to million years, are the switch of north and south magnetic poles. The present configuration of the dipole field with the north magnetic pole close to the north geographic pole is considered a normal polarity interval, while opposite configuration is considered a reversed polarity interval (Figure 2). Intervals of geological time having a constant geomagnetic field polarity delimitated by reversals are defined as polarity chrons. The magnetic reversals are long-period processes (longer than 10^5 years) which do not occur with a simple periodicity but instead appear to occur randomly in time. The duration of a polarity transition is imperfectly known but it is probably in the order of 10^3 to 10^4 years, fast enough to be considered globally synchronous on geologic time scales.

The pattern of polarity reversals providing a unique global "bar-code" recorded in Earth's rock of different ages constitutes the geomagnetic polarity time scale (GPTS) (Figure 2). For the construction of the GPTS geophysicists fundamentally rely on the marine magnetic anomaly record and also on the magnetostratigraphic record, both containing biostratigraphical constraints. Oceanic surveys carried out during the 1950's and 1960's and equipped with shipboard magnetometers found linear magnetic anomalies parallel to the mid-oceanic ridges. These anomalies resulted from the remanent magnetization of the oceanic crust, acquired during the process of seafloor spreading. The spreading process results in the magnetization of the crust in alternating normal and reverse polarity. The template of magnetic anomaly patterns from the ocean floor has remained essential for constructing the GPTS from Early Cretaceous onward (ca. 124.5 Ma to 0 Ma). The initial assumption of periodic behavior (Cox et al, 1963) was soon abandoned as new data became available. The first modern GPTS based on marine magnetic anomaly patterns was established by Heirtzler et al. (1968). Subsequent revisions by Labreque et al. (1977), Berggren et al. (1985), Cande and Kent (1992) showed improved age control and increased resolution. A major breakthrough came with the astronomical polarity time scale (APTS) in which every individual reversal is accurately dated (e. g. Hilgen et al., 1997). Because there is an excellent first-order reversal chronology for most of the Mesozoic and all of the Cenozoic and because these reversals occur randomly in time, sequences of reversals can be used for establishing the age of the rocks.

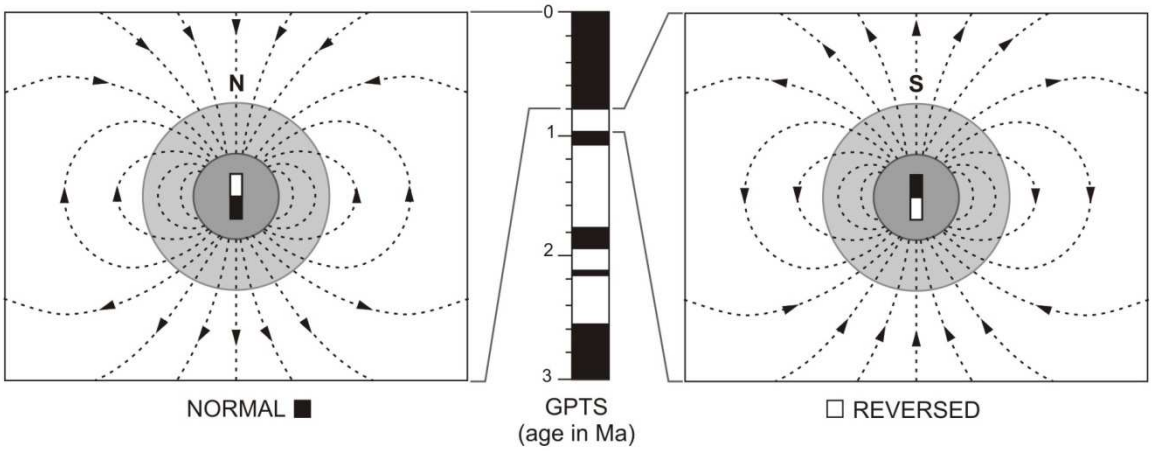

Figure 2 – Schematic representation of the geomagnetic field of a geocentric axial dipole. During normal polarity of the field the average magnetic north pole is at the geographic north pole, and a compass aligns along magnetic field lines. During normal polarity, the inclination is positive (downward directed) in the northern hemisphere and negative (upward directed) in the southern hemisphere. Conversely, during reversed polarity, the compass needle points south, and the inclination is negative in the northern and positive in the southern hemisphere. In the geomagnetic polarity time scale (column in the middle), periods of normal polarity are conventionally represented by black intervals, reversed intervals by white intervals. From Langereis et al (2010)

The study of the ancient Earth's magnetic field is possible because rocks contain ferromagnetic minerals in their internal structure. During the rock-forming processes these minerals statistically align with the ambient field, and are subsequently "locked in" the rock system, thus preserving the direction of the field as a natural remanent magnetization (NRM). Principal minerals contributing to the NRM are usually iron oxides such as magnetite, hematite, and maghemite, iron hydroxides (goethite), or iron sulphides including pyrrhotite and greigite. Other common minerals such as phyllosilicates (e.g., ilmenite), pyroxenes, and amphiboles can significantly contribute to the induced magnetization. However, they do not have the capability to carry a NRM.

As currently practiced, Paleomagnetism can be applied to age determination, stratigraphy, tectonics, polar wander, magnetic anomaly interpretation, paleoclimatology, as well as studies of the evolution and history of the Earth's magnetic field.

2. Methodology

2.1. Sampling

Samples are drilled in the field either with an electric or gasoline power drill cooled with water (Fig. 3). As the earth's magnetic field is a vector, samples need to be oriented in situ to get a geographic unambiguous position and orientation in order to provide a reference system to which refer the data obtained during the laboratory analyses. Therefore, samples are oriented in the field by a magnetic compass coupled to an orienting device with inclinometer (Fig. 4). The length of the cores is variable but it is desirable that 2 samples of 10 cm^3 can be obtained from each core. Sampling strategy may differ according to the main focus of the study. However, in any case, geological information such as bedding direction, presence of faults or fold axes orientations will be collected during the field work. For magnetostratigraphic purposes, 1 or 2 samples per level will be obtained at a certain stratigraphic spacing (depending on the total thickness of the stratigraphic section to be studied and the number of magnetozones expected to be identified within the section). Sampling focused on tectonic studies, such as identification of vertical-axis rotations within orogenic belts, will consist in the drilling of about 10 cores distributed along the site with an spacing enough to average the geomagnetic secular variation. Several sites distributed all along the study area will be drilled to get a regional pattern of tectonic rotations. In the case of archaeomagnetic studies, about 10-15 samples will be drilled in a random distribution within the archaeological structure and, whenever possible, they will be oriented with a sun compass in order to minimize the perturbation in the magnetic compass caused by the intense magnetization of the archaeological material.

Figure 3 – Paleomagnetic sampling

Figure 4 – I*n situ* orientation of drilled cores

2.2. Instrumentation and Measurement in the Laboratory

Paleomagnetism is mainly based on the measurement of the NRM of geological material, which is the fossil magnetism naturally present in a rock. The primary magnetization is the component of the NRM that was acquired when the rock was formed and may represent all, part, or none of the NRM. The primary magnetization may decay through time either partly or completely and additional components, referred to as secondary magnetizations, may be added by several processes. A major task in all paleomagnetic investigations is to identify and separate the magnetic components in the NRM, using a range of demagnetization and analysis procedures.

The main laboratory analysis consists in progressive demagnetization of the samples and the subsequent measurement of the NRM in order to identify and isolate the different paleomagnetic components recorded during the rock-geological history. Progressive demagnetization of the samples can be achieved by two different treatments, thermal (TH) or by alternating fields (AF). During demagnetization experiments, samples are subjected to stepwise increasing values of temperature or alternating field in a zero magnetic field (field-free) space. The residual magnetisation is measured after each demagnetization step and the resulting changes in direction

and intensity are displayed and analysed in order to reconstruct the complete component structure of the NRM. Measurements are made of components (Mx, My and Mz) of magnetic moment of the specimen (in sample coordinates). This usually entails multiple measurements of each component, allowing evaluation of homogeneity of NRM in the specimen and a measure of signal-to-noise ratio. Data are then fed into a computer containing orientation data for the sample and calculation of the best-fit direction of NRM in sample, geographic and stratigraphic coordinates is carried out.

2.3. Data analysis

Vector directions are described in terms of declination (D) and inclination (I). After the complete demagnetization of the samples, these directions are displayed with a projection that depicts three-dimension information on a two-dimension environment. Although projections on a sphere are commonly used, the most common representation of results of progressive demagnetization are vector end point or orthogonal projection diagrams, also known as Zijderveld diagrams (Zijderveld, 1967). The power of this display is the ability to display directional and intensity information on a single diagram by projecting the vector onto two orthogonal planes (Figure 5). Magnetic components are then extracted from the Zijderveld diagrams using least-square analysis (Kirschvink 1980), and the most stable and consistent component that can be isolated is referred to as the characteristic remanent magnetisation (ChRM). This ChRM is further investigated to establish if it represents a record of the geomagnetic field at, or close to, the time of rock formation, or a secondary magnetisation acquired later in geologic history by post-depositional processes. With this purpose, several stability tests can be performed on the obtained ChRM, being the most common ones:

- *Consistency test*: a ChRM is considered primary in origin when it defines a sequence of polarity reversals laterally traceable by independent means (e.g., lithostratigraphy) between distant sections from different parts of the basin.
- *Reversal test*: the observation of ChRM directions with different polarity and, in particular, the occurrence of antiparallel (within statistical error) directions is taken as a strong indication for the primary origin of that ChRM.
- *Fold test*: if the ChRM directions from differently tilted beds converge after correction for the dip of the strata, this remanence was acquired before tilting. Strictly speaking, this fold test does not directly prove a primary origin of this component, but only that it dates from before tilting.

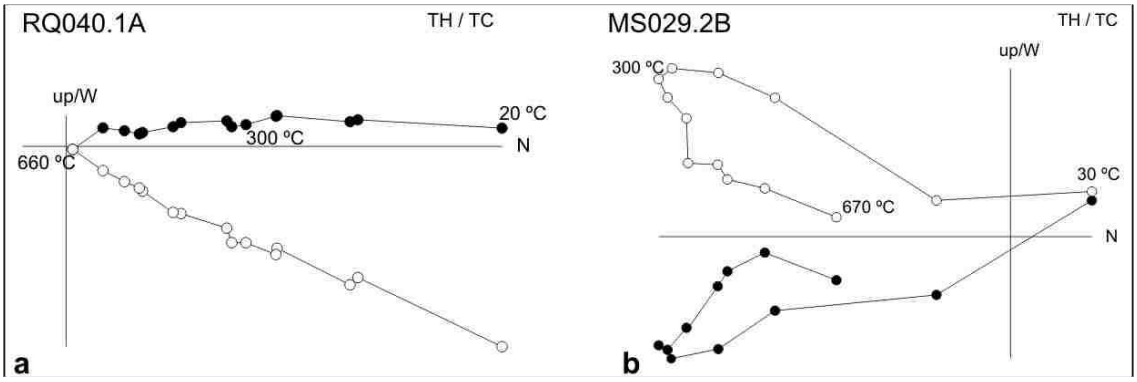

Figure 5 - Examples of Zijderveld diagrams. Solid (open) circles correspond to projection onto the horizontal (vertical) planes. a: sample of normal polarity (northward declination and positive inclination); b: sample with a low temperature normal polarity component, defined between 30º and 300 ºC, parallel to the present-day magnetic field and a ChRM of reversed polarity, defined from 300º to 670 ºC (southward declination and negative inclination)

3. Examples of applications

3.1. Magnetostratigraphy of Can Mata (Hostalets de Pierola, Vallès-Penedès Basin, NE Spain)

As mentioned above, magnetostratigraphy is based on the fact that the earth's magnetic field polarity changes through time at a non-constant frequency and on the fact that sediments have the capability to record and retain the magnetic field present at the moment of their formation. Therefore, if we study a sedimentary succession long and continuous enough we will be able to identify a reversals characteristic pattern which will allow us to establish a correlation to the Geomagnetic Polarity Time Scale (GPTS). The example presented corresponds to the magnetostratigraphic dating of the Middle Miocene sediments of Can Mata in the Hostalets de Pierola area, a sedimentary succession containing many fossil remains, being the main one among them the remnants of *Pierolapithecus catalanic*us and the hominoid *Dryopithecus fontani*. The magnetostratigraphic study was carried out in order to provide the mammal bearing sediments of Can Mata a robust absolute chronology. This paleomagnetic study was based on the analysis of 369 samples uniformly distributed along 460 m composite section. The correlation of the local magnetostratigraphy to the GPTS (Gradstein et al, 2004) (Figure 6) establishes the age of the sedimentary succession in Upper Aragonian-Vallesian (13 to around 10.5 Ma), and the estimated age of *Dryopithecus fontani* is established in 11.8 Ma (Moyà-Solà, et al, 2009).

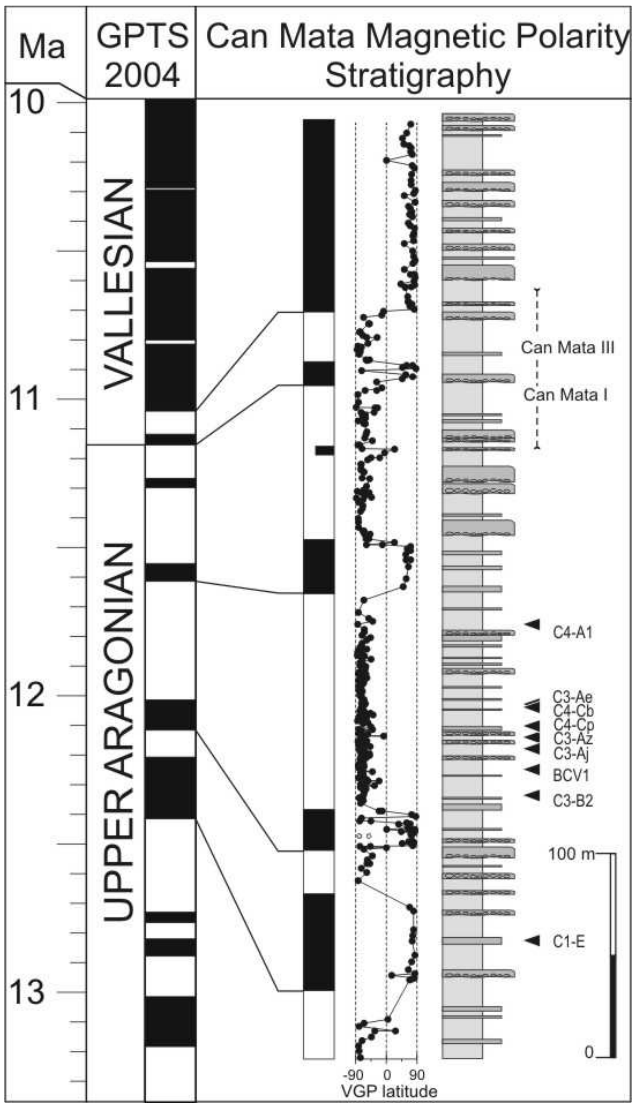

Figure 6 - Composite magnetic polarity stratigraphy of Can Mata and correlation with GPTS2004 (Gradstein et al, 2004).

3.2. Archaeomagnetic dating of combustion structures

Archaeomagnetic studies in Spain have undergone a significant progress during the last few years and a reference curve of the directional variation of the geomagnetic field over the past two millennia is now available for the Iberian Peninsula (Gómez-Paccard et al, 2006). These recent developments have made archaeomagnetism a straightforward dating tool for Spain and Portugal. In this example, we illustrate how this secular variation curve (SVC) can be used to date the last use of burnt structures from Spain. A kiln of the archaeological site of Can Xammar (Figure 7) (Mataró) of Mediaeval times has been studied and archaeomagnetically dated (Gómez-Paccard and Beamud, 2008). The directions of the characteristic remanent magnetization of the structure have been obtained from classical thermal and alternating field (AF) demagnetization procedures on the collected samples, and a mean direction for the combustion structure has been obtained (Figure 8). These directional results have been compared with the new reference curve for Iberia, providing archaeomagnetic dates for the last use of the kiln between 1492 and 1609, consistent with the archaeological evidences available (Figure 9).

Figure 7 - Combustion structure of the Can Xammar archaeological site and location of the samples. Modified from Gómez-Paccard and Beamud (2008)

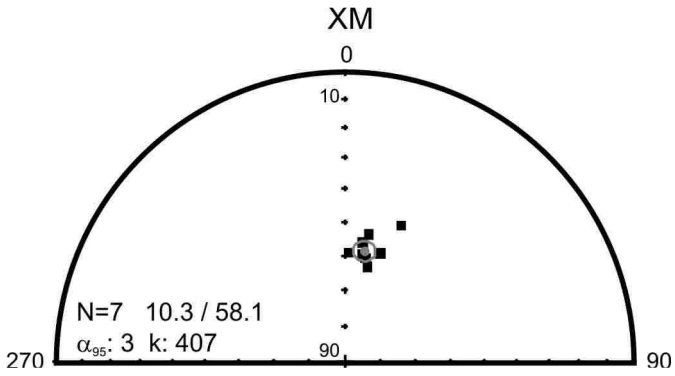

Figure 8 - Mean direction for the Can Xammar kiln. Modified from Gómez-Paccard and Beamud (2008)

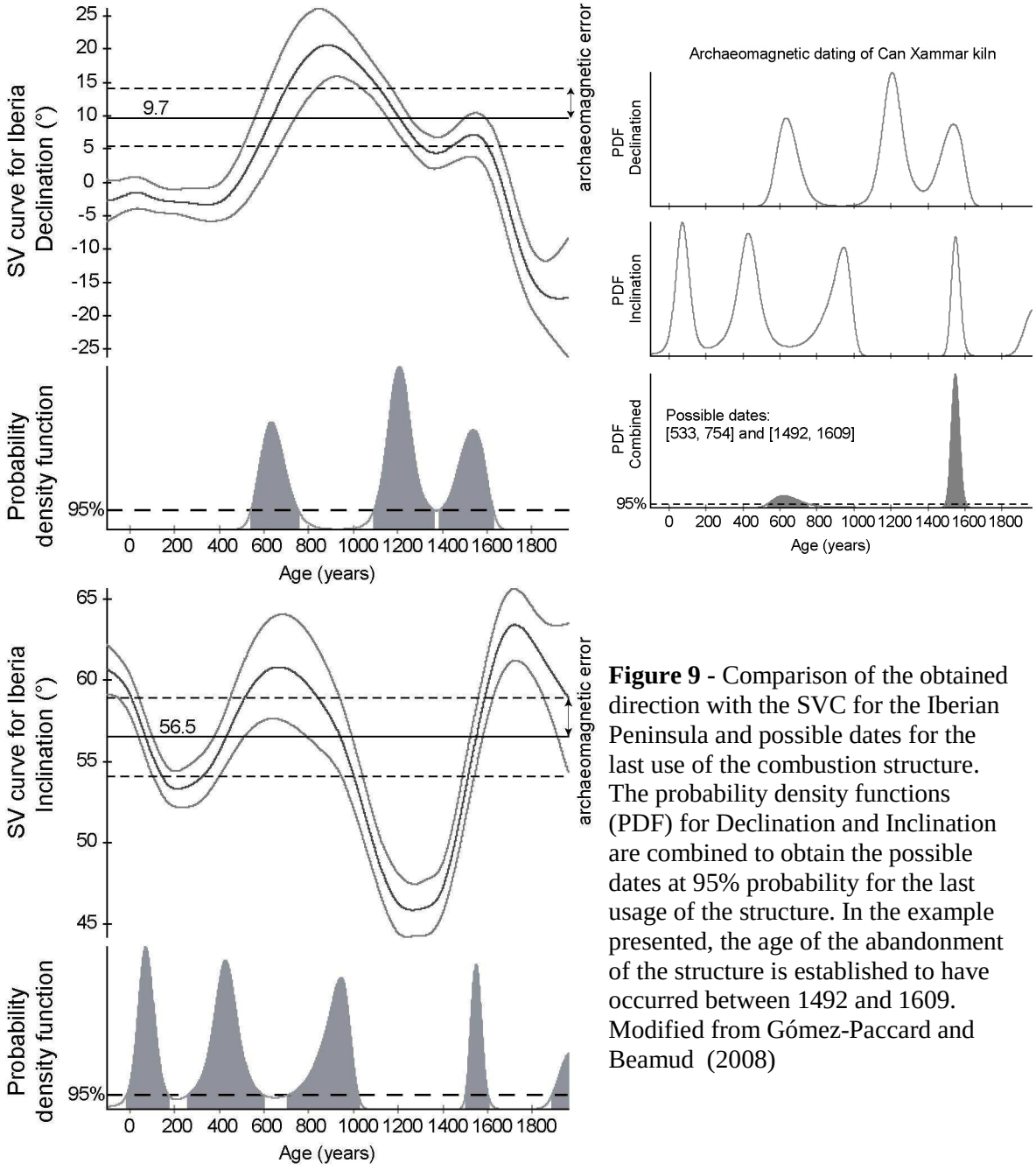

Figure 9 - Comparison of the obtained direction with the SVC for the Iberian Peninsula and possible dates for the last use of the combustion structure. The probability density functions (PDF) for Declination and Inclination are combined to obtain the possible dates at 95% probability for the last usage of the structure. In the example presented, the age of the abandonment of the structure is established to have occurred between 1492 and 1609. Modified from Gómez-Paccard and Beamud (2008)

3.3. Tectonic rotations in the south-central Pyrenees during theTertiary

The ability of rocks to record the direction of the ancient magnetic field provides the key quantitative information for unravelling tectonic deformation in orogenic belts. The orogenic environment, however, causes specific problems to the analysis of the magnetism in rocks due to the effects of strong deformation and temperature increase. Rocks in this environment are more likely to have their primary magnetism partially or completely overprinted by magnetizations linked to the deformation. Partially set against this disadvantage, the deformed nature of the rocks means that the paleomagnetic fold test is more readily applied to constrain the geological ages of the magnetizations than would be possible in less deformed settings. Paleomagnetic analysis assumes that the mean direction of magnetization recovered from the rock-unit is a record of the time averaged dipole field source at the time of magnetization. The cumulative deformation can then be resolved by comparing this direction with the predicted direction at the study location at the time of magnetization. Usually, the difference is the resultant of more than one episode of

deformation and in favourable circumstances it can be decomposed using geological evidence or from studying the paleomagnetism of rocks of different ages. The angular deformation is usually considered in terms of differences of declination and inclination with respect to the reference direction from the stable plate. The difference between the observed and expected directions is described in terms of rotation and flattening. A difference in declination implies rotation (R) of a crustal block about a quasi-vertical axis.

The Graus-Tremp piggy-back basin is an elongated trough formed during the emplacement of the allochtonous units of the South Central Pyrenean Units. Previous studies in both the Mesozoic basement and the Paleocene sediments of the Graus-Tremp basin have evidenced significant vertical axis clockwise rotations (Figure 10). These rock units are unconformable overlain by the syntectonic continental conglomerates of the Sierra de Sis and La Pobla de Segur, which were recently dated as Bartonian to Priabonian on basis of magnetostratigraphic correlation (Beamud et al, 2003). More recently, the syntectonic conglomerates of the Senterada basin have been dated as Oligocene also based on magnetostratigraphy (Beamud et al, 2011). Paleomagnetic data from these units provide constraints on the timing and spatial distribution of the tectonic rotations in the Graus-Tremp Basin. No significant rotations during the Tertiary are observed near the Noguera Pallaresa River. Further west, between the Esera and the Ribagorçana rivers, the lower Eocene materials record up to 30º of clockwise rotation. The lack of significant rotation in the overlying Bartonian sediments of the Sierra de Sis constrains this rotation to the Ypresian-Lutetian. In the Ainsa basin, about 30º of clockwise rotation is still recorded by Bartonian sediments. These data suggest an east-west trending of the vertical axis rotations magnitude and timing.

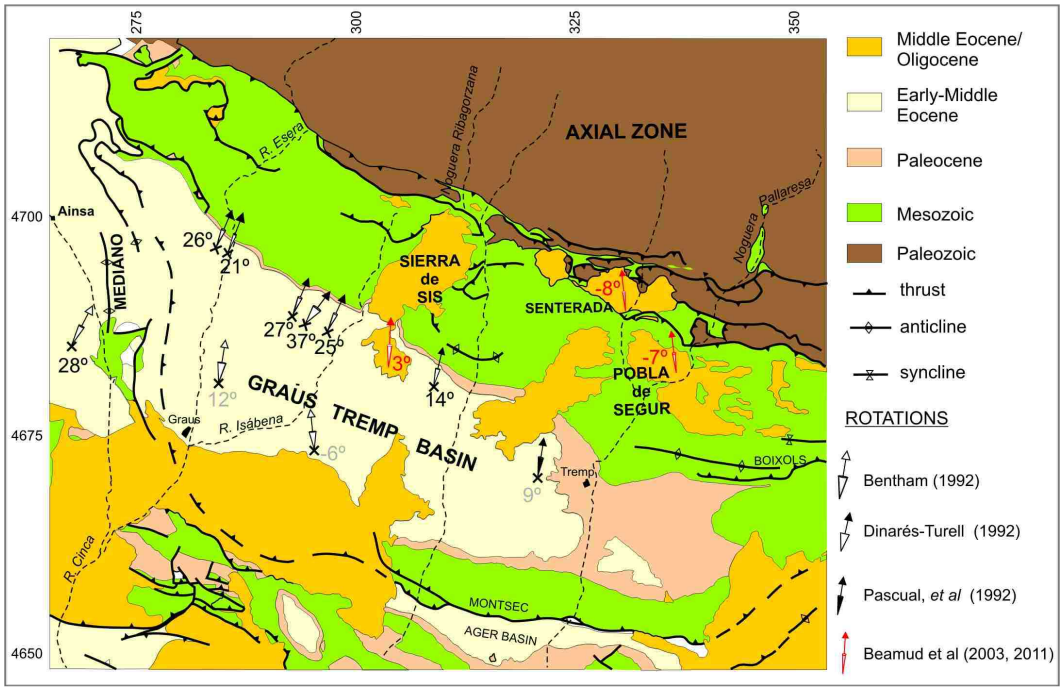

Figure 10 - Distribution of the vertical-axis rotations within the Graus-Tremp piggy-back basin during the Tertiary. Modified from Beamud et al (2004).

References

Beamud, E; Garcés, M; Cabrera, L; Muñoz, J.A; Almar, Y. (2003) A new Middle to Late Eocene continental chronostratigraphy from NE Spain. *Earth and Planetary Science Letters* 216 (4) 501-514

Beamud, E; Garcés, M; Muñoz, J.A; Cabrera, Ll; Almar, Y. (2004) Distribución de las

rotaciones paleomagnéticas en la cuenca de Graus-Tremp durante el Terciario. *Geotemas* 6 (4) 283-285

Beamud, E., Muñoz, J.A., Fitzgerald, P.G., Baldwin, S.L., Garcés, M., Cabrera, L., Metcalf, J.R. (2011) Magnetostratigraphy and detrital apatite fission track thermochronology in syntectonic conglomerates: constraints on the exhumation of the South-Central Pyrenees. *Basin Research* 23(3) 309-331

Berggren, W.A., Kent, D.V., Flynn, J.J., (1985) Cenozoic geochronology. *Geological Society of America Bulletin*, 96, 1407-1418

Bentham, P.A. (1992) *The tectono-stratigraphic development of the western oblique ramp of the South-Central Pyrenean thrust system, Northern Spain*. PhD Thesis, University of California, 252 pp.

Cande, S. C., Kent, D.V., 1992. A new geomagnetic polarity time-scale for the Late Cretaceous and Cenozoic. *Journal of Geophysical Research* 97, 13917–13951

Cox, A., Doell, R. R., Dalrymple, G. B., 1963. Geomagnetic polarity epochs and Pleistocene geochronometry, *Nature*198, 1049–1051

Dinarés-Turell, J. (1992) *Paleomagnetisme a les Unitats Sudpirinenques Superiors. Implicacions estructurals*. PhD Thesis, University of Barcelona

Gómez-Paccard, M., Chauvin, A., Lanos, P., McIntosh, G., Osete, M.L., Catanzariti, G., Ruiz-Martínez, V.C., Núñez, J.I., (2006). The first archaeomagnetic secular variation curve for the Iberian Peninsula. Comparison with other data from Western Europe and with global geomagnetic field models. *Geochem. Geophys. Geosyst*., 7, Q12001

Gómez-Paccard, M. & Beamud, E. (2008) Recent achievements in archaeomagnetic dating in the Iberian Peninsula: Application to Roman and Mediaeval Spanish structures. *Journal of Archaeological Science*, 35(5), 1389-1398

Gradstein, F.M., Ogg, J.G., Smith, A.G., (2004). *A Geologic Time Scale 2004*. Cambridge University Press, Cambridge. 589pp

Heirtzler, J.R., Dickson, G.O., Herron, E.M., Pitman Iii, W.C., Lepichon, X., (1968). Marine Magnetic Anomalies, Geomagnetic Field Reversals, and Motions of the Ocean Floor and Continents. *Journal of Geophysical Research*, 73, 2119-2136

Hilgen, F. J., Krijgsman, W., Langereis, C. G., Lourens, L. J. (1997) Breakthrough made in dating of the Geological Record, *EOS, Transactions of the AGU* 78, 285 & 288

Kirschvink, J.L., (1980). The least-squares line and plane and the analysis of paleomagnetic data. *Geophysical Journal of the Royal Astronomical Society*, 62, 699-718

LaBreque, J. L., Kent, D.V., Cande S. C., 1977. Revised magnetic polarity time scale for Late Cretaceous and Cenozoic time, *Geology* 5, 330–335.

Langereis, C.G., Krijgsman, W., Muttoni, G., Menning, M., (2010). Magnetostratigraphy - concepts, definitions, and applications. *Newsletter on Stratigraphy*, 43, 207-233

Moyà-Solà, S; Köhler, M; Albà, D; Casanovas-Vilar, I; Galindo, J; Robles, J.M; Cabrera, Ll; Garcés, M; Amécija, S; Beamud, E. - First partial face and upper dentition on the Middle Miocene hominoid Dryopithecus fontani from Abocador de Can Mata Vallès-Penedès Basin, Catalonia (Spain): taxonomic and phylogenetic implications. *American Journal of Physical Anthropology* 139 (2), 126-145

Pascual, J.O; Parés, J.M; Langereis, C.G; Zijderveld, J.D.A. (1992) – Magnetostratigraphy and rock magnetism of the Ilerdian stratotype at Tremp, Spain. *Physics of the Earth and Planetary Interiors*, 74, 139-157.

Soriano, C., Beamud, E., Garcés, M. (2008) Magma flow in dikes from rift zones of the basaltic shield of Tenerife, Canary Islands: implications for the emplacement of buoyant magma. *Journal of Volcanology and Geothermal Research*, 173(1-2), 55-68

Zijderveld, J.D.A. (1967) AC demagnetization of rocks: Analysis of results, In: *Methods in Paleomagnetism*, ed. D.W. Collinson, K.M. Creer and S.K. Runcorn, Elsevier, Amsterdam, pp.254-286

Handbook of instrumental techniques from CCiTUB

X-ray single crystal and powder diffraction: possibilities and applications

Mercè Font-Bardia and Xavier Alcobé

Unitat de Difracció de Raigs X, CCiTUB, Universitat de Barcelona. Lluís Solé i Sabarís, 1-3. 08028 Barcelona. Spain.

email: *mercef@ccit.ub.edu; alcobe@ccit.ub.edu*

Abstract. In this article the main possibilities of single crystal and powder diffraction analysis using conventional laboratory x-ray sources are introduced. Several examples of applications with different solid samples and in different fields of applications are shown illustrating the multidisciplinary capabilities of both techniques.

1. Introduction

Diffraction experiments using x-rays or particles in motion, such as neutrons and electrons, enable the study of the structural properties of materials. Diffraction using electron, neutron or brilliant synchrotron x-rays will not be considered. Only conventional laboratory x-ray sources produced by sealed x-ray tubes are taken into account. The wavelengths of the x-rays used in laboratory diffraction experiments (ranging from 0.5 to 2.5 Å) are of the same order than the shortest interatomic distances. When the material is irradiated with a controlled x-ray beam a diffraction pattern can be obtained. If the material is a crystal, the diffraction pattern is a transformation into reciprocal space of its ordered atomic structure. The direct image of the crystal, i.e. the three dimensional distribution of the atoms in the lattice, can be restored only after the diffraction pattern has been transformed back into direct space. The transformation is governed by the theory of diffraction. Comprehensive derivation of the theory of x-rays as well as detailed descriptions of the production and detection of x-rays and the processes of interaction of x-rays with matter can be found in several excellent books and reviews [1-4, for example].

In principle an x-ray diffraction (XRD) analysis can be performed in any kind of material. Nevertheless in most of the cases the materials are solid samples. Only in some quite specific applications the samples are liquid and in very special cases gases. Depending on the characteristics of the solid sample being analysed the possibilities and the kind of information that can be obtained from an XRD experiment change and are multiple and diverse. In a first level of distinction, and closely related to the kind of experimental devices, single-crystal samples in one side and polycrystalline samples on the other can be considered. A sample is a single crystal or monocrystalline if the lattice is continuous and unbroken on the entire sample and it is optically clear and with no grain boundaries. Furthermore in single crystal XRD, as an additional distinction, the size of the single crystal should be small, preferably in the range from 0.1 to 0.2 millimetres. Polycrystalline samples will include nearly all the other solid samples. Nevertheless there is no chance to characterize a no single crystal sample by XRD if the amount of crystallites constituting the sample is not large enough. Ideally an infinite number of crystallites of sizes no higher than some micrometers are needed. But practically the restrictions are no strictly exclusive and there are e.g. several applications carried out on samples with a finite, limited number of crystallites. Although other kind of polycrystalline samples should not be excluded, such as metallic or bulk ceramic or thin film samples, we will refer here to the analysis with samples other than single crystals as x-ray powder diffraction (XRPD) analysis.

From single-crystal XRD data it is possible to solve and refine the crystalline structure of a new material. It is a non destructive analysis and the possibilities of success are very high and have radically increased over the last 15 years with the improvement of the experimental devices and the continuous progress in crystal-structure solution and refinement methodologies [5, 6]. Knowledge of the crystal structure is of crucial relevance for a proper understanding of the material properties.

As it will be shown, XRPD analysis has a wide range of applications [7, 8]. From the basic distinction between amorphous and crystalline materials through phase analysis to full profile analysis (with possibilities of microstructural characterization and refinement and solution of crystalline structures), the analysis are always not destructive and cover a great variety of scientific disciplines.

In this article, possibilities and examples of applications of both single-crystal XRD and XRPD are presented.

2. Single crystal x-ray diffraction (single crystal XRD)

2.1. Samples, instrumentation and data collection

The samples are unfracturated and optically clear single crystals. Their size should be between 0.1 and 0.2 millimetres in the three directions of space. They are normally selected using an optical microscope (x40) equipped with a polarizing attachment and observing if light extinguishes regularly every 90º when turning the stage of the microscope.

A selected crystal is fixed on the tip of a thin glass fibre using epoxy or cement, or in a loop including specific oil, which fits into the goniometer head in the diffractometer. The crystal is then aligned along the beam direction.

It is necessary to know the stability properties of the crystals. Crystals can be sensitive to light, air or moisture, or susceptible to loss of crystallisation solvent. If so, a special treatment is required. For example, they can be mounted inside sealed glass capillaries or the data collection can be performed at low temperature.

Figure 1 depicts the x-ray single crystal diffractometer MAR345 at the CCiTUB. It works with the usual monochromatic Mo Kα radiation (λ=0.7108 Å) and it is equipped with a 2D Image Plate detector. Figure 2 shows a detail of the sample location, being visible the goniometer head and the low-temperature attachment.

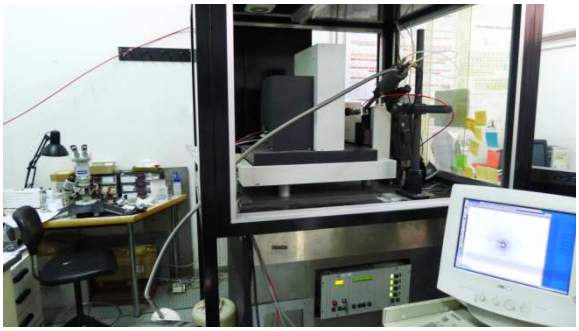

Figure 1: Single crystal x-ray diffractometer MAR345 at the CCiTUB.

Figure 2: Detail of the goniometer and low temperature system in the MAR345 single crystal diffractometer at the CCiTUB

Once the crystal is mounted on the diffractometer, the appropriate parameters for each measurement such as the distance to the detector and the space of the Ewald sphere are selected, and the intensity data is collected. Data are typically obtained between 3 º and 30 º2θ when using molybdenum radiation. Generally, a complete data collection may require between 3 to 12 hours, depending on the specimen and the diffractometer. Some of the measured intensities enable the calculation of the unit cell parameters. Then all the intensities are indexed and a list of observed hkl reflections is obtained (see below)

2.2. Structure determination methodology

The intensity of x-rays in a diffraction pattern depending only upon the crystal structure is referred to as called the structure factor:

$$F(hkl) = \sum_{j=1}^{N} f_j[\exp[2\pi i(hx_j + ky_j + lz_j)] \qquad (1)$$

where *h*, *k* and *l* are the indices of the diffraction planes (Bragg reflections), *N* is the number of atoms in the cell and (x_j ,y_j , z_j) are the fractional coordinates of the j^{th} atom with scattering factor f_j. Each structure factor represents a diffracted beam which has an amplitude $|F(hkl)|$ and a relative phase $\phi(hkl)$.

The crystal structure can be obtained from the diffraction pattern if the electron density function is calculated at every point in a single unit cell:

$$\rho(x,y,z) = \frac{1}{V}\sum_{h}\sum_{k}\sum_{l}|F(hkl)|\cos[\exp[2\pi(hx_j + ky_j + lz_j)] - \phi(hkl)] \qquad (2)$$

where the summation is over all values of *h*, *k* and *l* and *V* is the volume of the unit cell. Since x-rays are diffracted from the whole crystal, the calculation yields the contents of the unit cell averaged over the whole crystal. In practice, the calculation of the electron density produces maps. The maxima on these maps represent the position of the atoms in the cell.

The structure factors are reciprocal space vectors whereas the electron density is from the real space. The diffraction pattern is the Fourier transform of the electron density and the electron density is the inverse Fourier transform of the diffraction pattern. The measured intensities of a diffraction pattern enable the determination of only the structure factor amplitudes but not their phases. The calculation of the electron density is not then obtained directly from experimental measurements and the phases must be obtained by other methods. This is the so called phase problem. The most usual methods to overcome the phase problem are direct methods and methods based on the Patterson function. The former are the most important in chemical crystallography and the latter are currently applied when some heavy atoms are present. The phases are obtained approximately and have to be improved. With the calculated phases and structure factors amplitudes, a first electron density map is calculated, also approximate, from which the atomic positions will be obtained.

The next step is the completion of the structure by Fourier synthesis and refinement of the structural parameters to optimise the fitting between the observed and calculated intensities in the diffraction pattern. The refinement cycles include positional atomic parameters and anisotropic vibration parameters. Finally, the hydrogen atom positions, if present, are determined or calculated. The structural refinement is evaluated from the agreement between the calculated and the measured structure factors. The refinement is considered finished when the following essential conditions are fulfilled:

- The agreement factors are small enough.
- The structural model is chemically appropriate
- The estimated standard deviations of all geometrical parameters are as small as possible
- The peaks remaining in the electron density map are as small as possible.

Once the structure is determined and refined several geometrical parameters such as bond lengths, bond angles, torsion angles, π-stakings and hydrogen-bond are evaluated and appropriate tables and graphics representing the structure are prepared. A standard file (CIF: crystal information file) containing all the information of the structure is created and can be used to evaluate their quality and possible problems.

2.3 Examples of applications

The determination of the crystal structure is crucial in many different applications. The knowledge of the atomic, three dimensional distributions influences and enables to understand properties of molecules and materials. Three different fields of applications that include crystal structures solved at the CCiTUB are illustrated.

2.3.1. Magneto-structural correlations in molecular materials

Current trends in the research field of molecular magnetism mainly involve activities in three classes of molecular materials, namely, multifunctional magnetic materials, nanostructured magnetic materials, and molecular nanomagnets. As far as molecular nanomagnets are concerned, the past few years have witnessed an explosive growth in the interest in single-molecule magnets (SMMs) due to their potential interest as information storage materials, quantum-bits in quantum computation or bioinorganic/biomedical applications.

Magneto-structural correlations, often including discrete Fourier transform (DFT) calculations based on structural parameters are one of the main targets in molecular magnetism and the determination of the crystalline structures is the fundamental tool in this kind of research by two main reasons: it is the only technique able to give unambiguously the nuclearity and the intermetallic bridges which determine the magnetic properties and on the other hand, at molecular level the character of the magnetic interactions (ferro-, antiferro- or ferromagnetic response) and its magnitude, is strongly dependent on the overlap of molecular orbitals which are directly related to the magnitude of bond distances, angles or torsions.

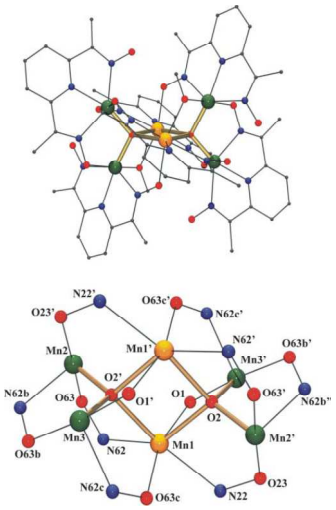

Figure 3: Molecular structure (top) and labelled core (bottom) of $[Mn_6O_2(OMe)_2(dapdoH)_4](NO_3)_2 \cdot 2(Et)_2 \cdot 2MeOH$

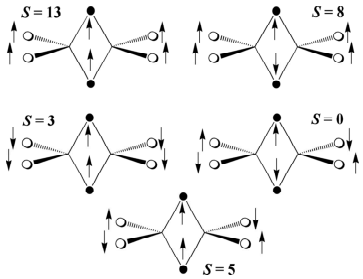

Figure 4: Possible spin arrangements for compounds of $[Mn_6O_2(OMe)_2(dapdoH)_4](NO_3)_2 \cdot 2(Et)_2 \cdot 2MeOH$

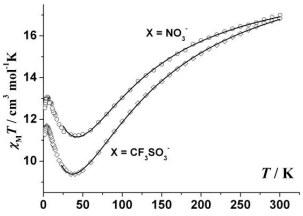

Figure 5: Plot of the $\chi_M T$ for compounds of $[Mn_6O_2(OMe)_2(dapdoH)_4](NO_3)_2 \cdot 2(Et)_2 \cdot 2MeOH$

The importance of the magneto-structural correlation is reflected for instance after the crystal structure solution of the compound $[Mn_6O_2(OMe)_2(dapdoH)_4](NO_3)_2 \cdot 2(Et)_2O \cdot 2MeOH$ [9]. The core of this compound consists of Mn_2^{II} Mn_4^{III} units arranged as two tetrahedral μ4-oxo bridged Mn_2^{II} Mn_4^{III} units, sharing the Mn_2^{II} edge. The coordination sphere of each manganese atom is occupied by three N atoms from each dioximato ligand whereas the remaining coordination sites link several O-donors from oxo, methoxo or oximato bridges: divalent Mn(1) atoms are heptacoordinated (N_3O_4 pentagonal bipyramid environment) and trivalent Mn(2) and Mn(3) ions are hexacoordinated (N_3O_3 distorted octahedral environment). Two dioximato ligands are bisdeprotonated and link three manganese atoms ($Mn^{II}...Mn^{II}...Mn^{III}$) in the coordination mode ηI: ηI: ηI:μ. The core of hexanuclear cluster is completed by means of two methoso bridge between $Mn^{II}....Mn^{III}$ atoms (Fig. 3). Magnetization measurements performed at 2K show magnetization plots that tend a quasi saturated value close to ten electrons (spin = 5). Low temperature $\chi_M T$ value, magnetization data and the analysis of the energy of the spin levels obtained in the fit of the experimental data strongly suggest an S = 5 ground state for this compound (Fig. 5). The topological analysis of the possible arrangement of the local spins, performed on the basis of the structural data, confirms the possibility of an S = 5 ground state and gives an univocal proposal of the spin arrangement of the paramagnetic centres (Fig. 4).

2.3.2. Absolute configuration determinations

Most biological molecules are chiral in the sense that they can, in principle, exist as two identical structures that are non-superimposable mirror images of one another. These two forms are referred to as enantiomers and are related to one another in the same sense as the left hand is related to the right hand. Although the molecules can exist in two forms, nature has evolved such that only single enantiomeric forms of chiral molecules exist in living organisms. This is of enormous consequence in the field of pharmaceuticals because it means that the two enantiomers of a chiral pharmaceutical, although they may have the same nominal structure, they do not interact with living organisms in the same manner. While one enantiomer of the drug may have therapeutic properties, the other can be toxic.

Heterogeneous catalytic synthesis of fine chemicals and complex chiral molecules is in its infancy.

The enantioselective synthesis of such molecules requires environments that are themselves chiral and of a single handedness. This has generated a great deal of interest in the preparation of chiral materials and surfaces for use as heterogeneous catalysts. The most widely pursued approach to the preparation of enantioselective heterogeneous catalysts has been the use of chiral organic templates which bind to the surface of a catalyst and create a chiral environment in which catalytic reactions can occur [10].

An example of chiral properties can be found in [11], where the synthesis and characterization of two new trans platinum complexes in the phosphane series was reported. In the mentioned study, the phosphane ligand is triphenylphosphine and the group in trans configuration is represented by chiral aliphatic amines. Unfortunately, the resolution of the structure was not of the expected quality for complex 1. But the structure of complex 2 (Fig. 6) consisted of discrete molecules in which PPh3 and $NH_2CH(CH_3)CH_2CH_3$ groups were σ bonded to the platinum atom in a trans configuration. Only two molecules were found in the unit cell, but in contrast to complex 1, the amines in both molecules were S enantiomers. Only slight differences were detected in the distances around the platinum atom for those molecules, in contrast to the trans phosphane complexes reported previously. Some hydrogen bonds were detected, and they are described as:N(2)–H(2B)·····Cl(12) = 3.262(8) and N(1)–H(1B)····Cl(21) = 3.199 Å (Fig. 7).

The anti-proliferative activity detected in tumor cells treated with the two new complexes is more pronounced when the aliphatic amine is racemic compared to the S-enantiomer. Moreover, for both compounds, the activity is fast after cell exposure and, unlike that of cisplatin, virtually independent of the duration of cell challenge.

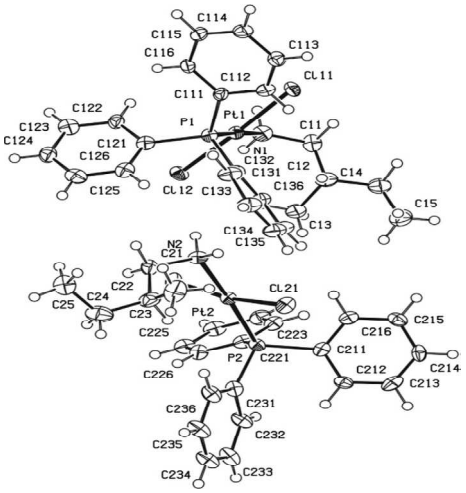

Figure 6: ORTEP view of complex trans-$[PtCl_2(S–NH_2CH_2CH(CH_3)CH_2CH_3)(PPh_3)]$

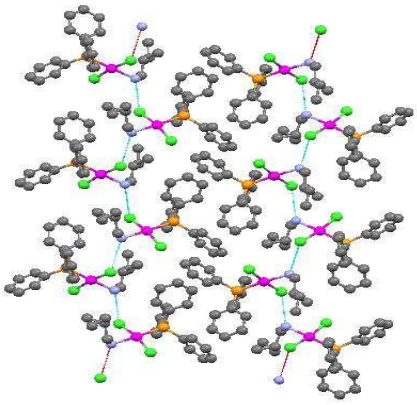

Figure 7: Schematic view of intermolecular NH—Cl between molecules of$[PtCl_2(S–NH_2CH_2\,CH\,(CH_3)CH_2CH_3)(PPh_3)]$

2.3.3. Molecular switches based on coordination complexes

Molecular switches can be converted from one state to another by an external stimulus such as light, electricity or a chemical reaction.

The design and development of molecular devices based on coordination or organometallic complexes is of great importance nowadays due to their applied interest in different fields. Among all types of molecular devices (i.e. clips, rotors, scissors, switches, twisters, etc.) with different architectures reported so far, molecular switches are targets of increasing interest for electronics and optical memory devices. In this type of devices, an external stimulus (e.g. light, electrons, pH, etc.) produces intra- or intermolecular changes that affect a characteristic physical or chemical property of the molecule. To allow their use in the development of sensors, information and storage materials, these transformations should be reversible, to permit the “switch on” and “switch off” of that property, and fast. On the other hand, and mainly promoted by the crucial role of platinum (II) in cancer therapy, several research groups have focused their attention on molecular switches based

on platinum (II) complexes. A few articles showing the utility of such compounds as sensors for amino acids and proteins have been published recently, but examples of acid/base-based molecular switches are scarce. In addition, ferrocene and its derivatives contain a redox-active centre, and this property, which is specially interesting in view of their applications in different areas including bio-organometallic chemistry, bio-technology and medicine, has also been used to prepare electrochemical devices for gene sensors and glucose detection as well as molecular switches for non-linear optical properties (NLO) or for the fluorescence of ferrocene derivatives.

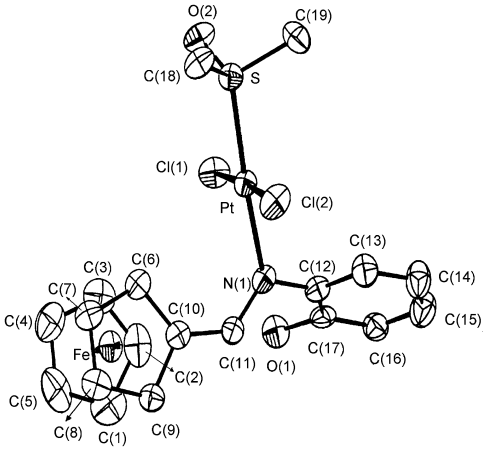

Figure 8: ORTEP plot of trans-[Pt(FeCH=N C_6H_4OH-2)Cl_2(dmso)]

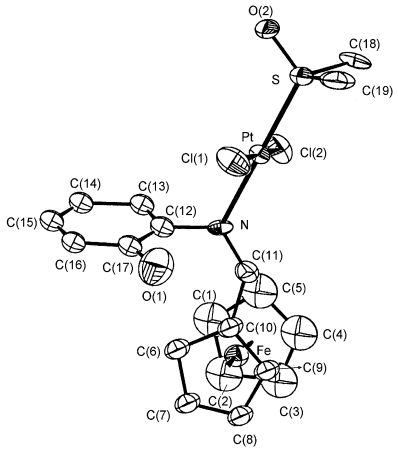

Figure 9: ORTEP plot of the isomer of trans-[Pt(FeCH=N C_6H_4OH-2)Cl_2(dmso)]

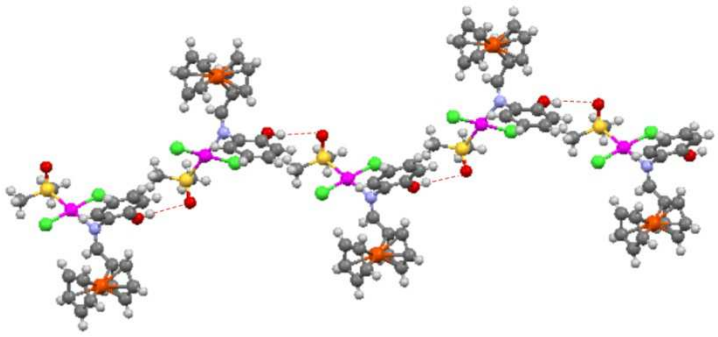

Figure 10: trans-[Pt(FcCH=NC6H4OH-2)Cl2(dmso)] in the isomer a through O(1)–H···O(2) forming a chain along the b-axis.

The crytal structures of two Platinum (II) complexes of formula [Pt(FeCH=NC_6H_4OH-2)Cl_2(dmso)], named 2b and 2c, and used as molecular switches [12] are briefly explained here [Fig. 8 and Fig. 9]. The platinum (II) atom is bound to the imine nitrogen atom, the sulfur atom of the dmso ligand and two chlorido ligands [Cl(1) and Cl(2)] in a trans arrangement, as reflected in the value of the bond angle Cl(1)–Pt–Cl(2) [176.18(5)°(2b), 175.59(13)° (2c)]. In the two complexes the bond lengths around the platinum (II) atom fall in the range reported for related complexes where the platinum (II) atom has a similar environment. The C(11)–N bond of 2b [1.285(6) Å] is longer than that in 2c [1.266(14) Å], and the imine group forms an angle of 15.5° (2b) and 13.9° (2c) with the C5H4 unit of the ferrocenyl moiety. The value of the torsion angles C(10)–C(11)–N(1)–C(12) of 2b (179.97°) and C(10)–C(11)–N– C(12) of 2c (3.86°) indicate that

the imine adopts the anti-(E) conformation in 2b and the syn-(Z) form in 2c, in good agreement with the results obtained from Nuclear Magnetic Resonance (NMR) experiments. The phenyl ring is planar, and its mean plane forms an angle of 72.1° (2b) and 69.6° (2c) with the coordination plane of the platinum atom. In the crystal of 2b, the separation between the O(1) atom of one of the molecules of [Pt(FcCH=NC6H4OH-2)-Cl2(dmso)] and the O(2) atom of a neighbouring molecule suggests the existence of an O(1)–H···O(2) interaction that connects the molecules forming a chain along the b-axis (Fig. 10).

3. X-ray powder diffraction (XRPD)

3.1. Samples and instrumentation

In an ideal XRPD experiment performed in a common Bragg-Brentano reflection geometry x-ray powder diffractometer, the sample should consist of powder particles of crystallite size between 0.1 and 1.0 micrometers. The sample should be packed in a cavity-type sample holder and genteelly pressed to avoid preferred orientations. The sample surface should be big enough to ensure that the incident beam impinges over the sample in the full angular measuring range. Furthermore, the sample should be thick enough to ensure that the whole incident x-ray beam interacts with the sample and does not pass through it. Nevertheless, in practice depending on the goals of the analysis and on the available instrumental devices, these requirements can be satisfied only partially:

- It is possible to work in transmission configurations with the samples introduced in glass capillaries or in flat sample holders sandwiched between slices of thin transparent films (of kapton or polyester or equivalent). The transmission geometry is advantageous to reduce preferred orientations and it is highly recommended in the case of analysis of transparent samples (samples consisting only of light elements, especially organic samples).
- Sometimes, since grinding and sieving the samples is usually complicated, it is difficult to obtain particle sizes down to the order of 1 micrometer. If only qualitative analysis is required (and no quantitative or profile analysis is needed), and assuming that orientation and particle size effects are negligible, it is possible to use powder samples with particle sizes of 30 micrometers or even higher. On the other side there is no limitation and it is possible to analyse samples with crystallite size below 0.1 micrometers.
- It is possible to analyse bulk samples, such as metallic or ceramic samples, pieces of rocks, or thin film samples. In these cases, the specific size and shape of the sample and the goal of the analysis will define the preparation and the experimental device. In most of these cases, it will be usual to work in diffractometers of parallel optics geometries.
- If a diffractometer with a programmable divergence slit is available, there will be more chance to control the incident beam so as to impinge over the sample in the full angular range and samples of small surfaces could be more properly analyzed. The intensities of the diffraction peaks should be then adequately corrected.
- Samples of finite thickness, such as thin films on substrates, can be analysed either in specific devices, e.g. in grazing-incident attachments, or in standard devices assuming possible corrections and limitations.

An x-ray powder diffractometer consists basically of a goniometer with a sample stage in its centre, the x-ray tube and the incident beam optics in its primary arm and the diffracted beam optics and a detector in its secondary arm. The goniometer is normally inside a shielded cabine in the upper part of a console. The x-ray generator and the measuring and control electronics are in the bottom part. Figure 11 shows a picture of a difractometer available at the x-ray diffraction department of the CCiTUB and Fig.12 shows a detail of its goniometer.

Nearly always XRPD experiments are performed using monochromatic radiation and in most cases using the Cu Kα spectral line. Although x-ray lines of shorter wavelength, such as the Kα lines of Mo or Ag, or longer wavelengths, such as the Kα lines of Co, Fe or Cr, are used for some specific applications and samples, the Cu Kα line offers good d-space and 2θ resolution and a suitable level of penetration in samples of many different compositions. When using incident beam

monochromators, normally the Cu $K\alpha_1$ line (λ =1.5406 Å) will be isolated. If the monochromatization system is by means of filters, single x-ray mirrors or diffracted beam monochromators, the doublet Cu $K\alpha_{1+2}$ will be used ($\lambda_{average}$=1.5418 Å). Since the x-ray beam emerging from the tube is divergent, the standard configuration (normally the Bragg-Brentano configuration) is of divergent optics type. However, it is also usual to work with parallel beam optics, in grazing-incidence experiments for example, or with convergent beam optics, in transmission configurations. Both beam optics systems can be available by using incident beam x-ray mirrors, parabolic for parallel beam optics an elliptic for convergent beam optics. The standard sample platforms are suitable for flat samples in reflection focalizing, Bragg-Brentano configurations. Other possible, less standard platforms are those for transmissions configurations, those for big and rough samples or those available in texture goniometers. The goniometer can be θ/2θ (the incident beam is stationary) or θ/θ. The latter offers some clear advantages, mainly related to the fact that the sample holder is stationary, and is more and more used. There are several different types of detectors: point (0D) detectors (proportional, scintillation or solid-state detectors); lD lineal (silicon strip or silicon pixel detectors) or curved-position sensitive detectors; and area 2D detectors (e.g. CCD or image plate detectors).

Figure 11: X-ray powder diffractometer PANalytical X'Pert PRO MPD alpha1 at the CCiTUB

Figure 12: θ/2θ goniometer, in Bragg-Brentano Cu $K\alpha_{1+2}$ configuration, of the X-ray powder diffractometer PANalytical X'Pert PRO MPD alpha1 at the CCiTUB.

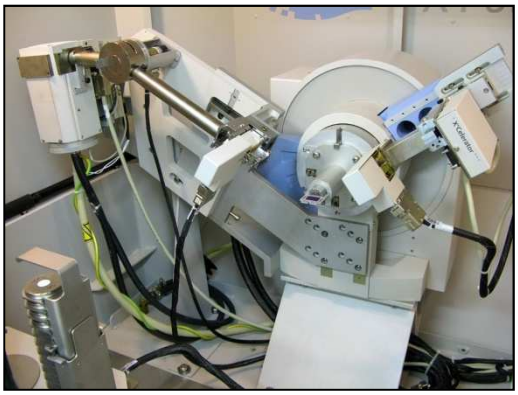

Figure 13: Cu Kα1 θ/2θ Bragg-Brentano configuration with X'Celerator detector in the X-ray powder diffractometer PANalytical X'Pert PRO MPD alpha1at the CCiTUB.

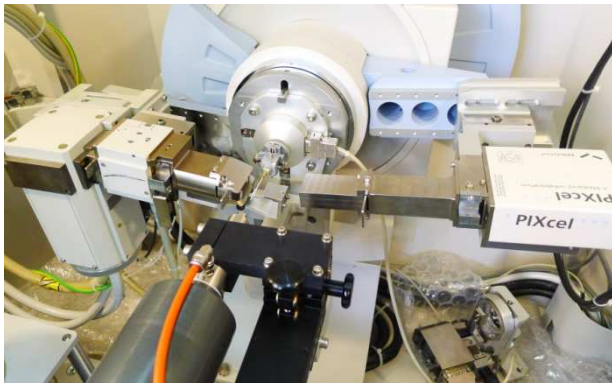

Figure 14: Cu $K\alpha_{1+2}$ configuration with focalizing mirror, capillary stage, low temperature attacment and PIXcel detector in an X-ray powder diffractometer PANalytical X'Pert PRO MPD θ/θ at the CCiTUB.

Every adequate combination of x-ray tube, incident and diffracted beam optics, sample platform and detector defines a configuration. Usually several configurations are possible in a single diffractometer. Figure 13 and Fig.14 depict two of the most used configurations in the x-ray diffraction department of the CCiTUB.

3.2. Possibilities and applications

After a fast and standard XRPD measurement, it is possible to distinguish if a solid material is crystalline or amorphous. This very basic capability can be applied to all kind of solid materials and it is of general interest. There is a second basic and general application, namely if the material or sample consists of a crystalline phase, its powder diffraction pattern is characteristic of its crystalline structure and it is a fingerprint of the phase. XRPD is a phase analysis technique. If the sample is a mixture of crystalline phases, in principle, all of them can be identified. Phase analysis is normally performed by comparing the experimental patterns with those tabulated in data bases patterns [13]. Although probably no other techniques or methodologies offer better possibilities in this field, several important limitations should be kept in mind: i) isostructurality, i.e. the fact that two chemically completely different phases can have the same crystalline structure and hence a very close powder diffraction pattern (this is much more possible if samples are simple phases, as single or binary compounds, and it is very usual e.g. in the case of metallic phases); ii) amorphous phases cannot be identified; iii) if the phase is not tabulated and its crystalline structure is not known, it will not be possible to identify it; iv) it is hard to identify minor phases (normally it is difficult if they are present in less than 1% in weight). Furthermore, in principle, crystalline phases can be quantified. Even if the sample is a mixture of crystalline and amorphous phases, the total amount of the amorphous phases can be determined. Nevertheless, frequently phase quantification cannot be applied straightaway and it is time consuming and difficult in most cases.

Other less standard applications of XRPD are:

- Isostructurality and isomorphism studies
- Solid state miscibility studies and solid solution characterization
- Polymorphism studies
- Temperature dependent XRPD analysis: phase transformations, solid state reactions, thermal expansion …
- Texture analysis. Determination and characterisation of the preferred crystallographic orientations
- Strain and residual stress analysis
- Microstructural characterization. Crystallite size and microstrain determination.
- Grazing-incidence analysis: phase analysis as a function of the penetration in film samples.
- Determination of strain - relaxed states and composition of semiconductor heteroepitaxial layers.
- Resolution and refinement of crystalline structures.

Full profile analysis of a powder pattern is necessary or highly recommended for some of the most important applications of the XRPD method. To carry out properly a full profile analysis on a powder pattern, it is necessary to know at least the cell parameters and the space group of the crystalline phase or phases observed. There is chance to index and thus to find the cell of an unknown phase. With this aim, nearly always the methods of automatic indexation, such as the successive dichotomy method [14], should be applied. Once the cell is known, from the systematic absences the diffraction symbol can be found and, from the latter, there is chance to determine the space group. Using the cell and the space group full profile pattern matching refinements by the Le Bail [15] or Pawley [16] methods can be performed and a set of integrated intensities is obtained. These integrated intensities can then be used to solve the crystal structure. If the crystalline structures are known, full profile analysis can be performed using the Rietveld method [17, 18]. The main applications of the full profile analysis by the Rietveld method are the quantitative phase analysis [19] and the refinement of crystalline structures. The potentiality and the reliability of the quantitative phase analysis have increased drastically with the possibility of using the Rietveld method. The refinement of crystalline structures starting from a known, similar structural model is

the first application of the Rietveld method. Furthermore, at present, the method is applied extensively to refine structures solved *ab initio* from XRPD data. In addition, full profile analysis either with the pattern matching or with the Rietveld method can be applied for microstructural characterization.

3.3. Examples of applications

In this section, four examples of different XRPD applications using four different kind of samples analysed at the CCiTUB are presented.

3.3.1. Phase identification of minerals of the group of asbestos

The industrial term asbestos includes a group of hydrated silicate minerals having in common its asbestiform habit: long (1:20), thin fibrous crystals. Their physical properties make them useful for many of industrial applications, but these materials produce important health problems. The inhalation of asbestos fibres can cause serious illnesses such as lung cancer, mesothelioma and asbestosis. Industrial materials containing asbestos are being eliminated from usage. Although the fibrous habit generates preferred orientation and sample preparation problems, XRPD is a powerful method to identify the type of asbestos possibly present in an industrial sample. Figure 15 and Fig. 16 depict the XRPD diagrams of two different samples containing asbestos analysed at the x-ray diffraction department of the CCiTUB. The sample of Fig. 15 is a fibre cement sample in which Chrysothile, serpentine asbestos, has been identified. Figure 16 corresponds to a sample of an acoustic ceiling in which the amphibole asbestos Crocidolite (blue asbestos), perhaps the most damaging variety, has been identified as a major phase.

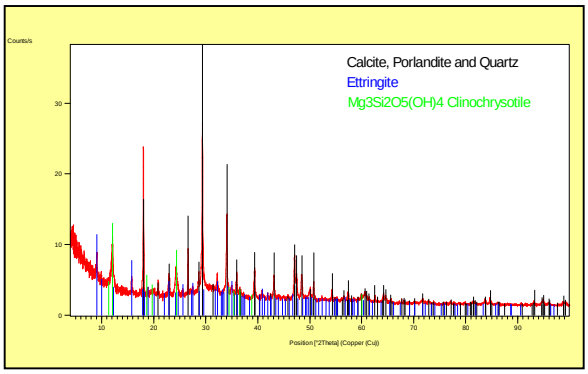

Figure 15: XRPD diagram of a fibre cement sample. The patterns of the identified phases are superimposed. Clinochrysotile is the serpentine asbestos phase.

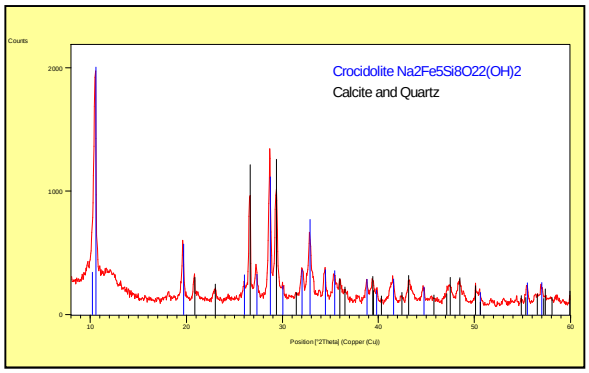

Figure 16: XRPD diagram of a sample from an acoustic ceiling. The patterns of the identified phases are superimposed. Crocidolite is the blue-amphibole-like asbestos phase.

3.3.2. Quantitative phase analyses of cements by the Rietveld method

Cement samples can be analysed by XRPD with the aim to identify and quantify the crystalline phases present. The complexity of the powder patterns of cement samples makes nearly mandatory to apply full profile analysis normally by means of the Rietveld method to properly quantify their crystalline phases. Figure 17 represents the Rietveld plot, result of the Rietveld refinement, of an XRPD pattern of a Portland sample corresponding to a Round-Robin study of Rietveld quantitative phase analysis of Portland cements [20]. Up to ten different phases were identified and quantified. The phases and the quantification results are reported in table 1.

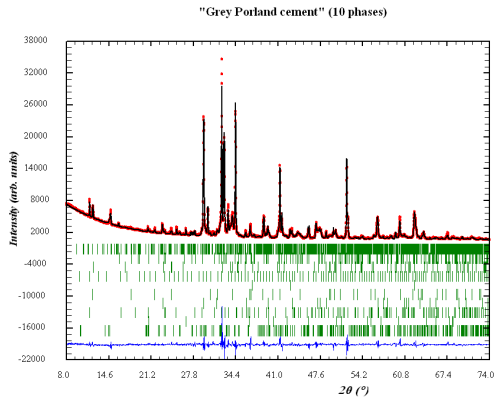

Figure 17: Rietveld plot of a grey Porland cement sample. Ten phases were considered and quantified

Table 1: Results of the quantification by the Rietveld method of a grey Porland cement sample.

Phase	Quantitative phase analysis results (weight fraction)
C3S, Ca_3SiO_5	61.9 (1.5) %
C2S, Ca_2SiO_4	10.9 (1.0) %
C4AF, Ca_2AlFeO_5	9.2 (0.5) %
$CaCO_3$ Calcite	5.3 (0.6) %
C3A, $Ca_3Al_2O_6$	4.4 (0.4) %
$CaSO_4 \cdot 0.5H_2O$ Bassanite	3.5 (0.6) %
Aphthitalite $K_3Na(SO_4)_2$	1.8 (0.3) %
MgO Periclase	1.3 (0.3) %
$CaSO_4 \cdot 2H_2O$ Gypsum	1.2 (0.4) %
SiO_2 Quartz	0.5 (0.2) %

3.3.3. Isotropic microstructural analysis of SnO_2 samples by the Rietveld method

The possible broadening of XRPD peaks due to sample effects can be treated by full profile analysis if the instrumental broadening is considered. The characteristics determining the sample broadening are usually referred to as microstructural effects. In many cases, the main microestructrual effects are the size of the diffracting domains (the crystallites) and the microstrain. Small crystallites of size below 0.1 micrometers broaden the XRPD peaks. On the other hand, if there is microstrain, there will be crystal lattice distortions that will also produce peak broadening. The size and microstrain contributions can be separated and determined by performing profile analysis. If the profile analysis is carried out over the full diffraction angle (2θ) range, these size and microstrain determinations will be more reliable and the possible anisotropy could be evaluated. Furthermore, if the full profile microstructural analysis is achieved by the Rietveld method, it will be consistent with the crystal structure of the analysed material.

Figure 18 represents the Rietveld plot of an isotropic microstructural analysis based on pseudo-Voigt profile fittings and using the methodology described in [21] of a Sb doped SnO_2 powder sample. Figure 19 compares the powder pattern of this Sb doped SnO_2 powder sample with that of the LaB_6 (NIST SRM-660a) sample used to determine the instrumental broadening (the instrumental resolution function). The huge difference between the widths of the peaks of the problem sample (Sb doped SnO_2) and those of the instrumental calibration standard (LaB_6) is consequence of the important microstructural effects affecting the problem sample. The values obtained for size and microstrain are reported in figure 18.

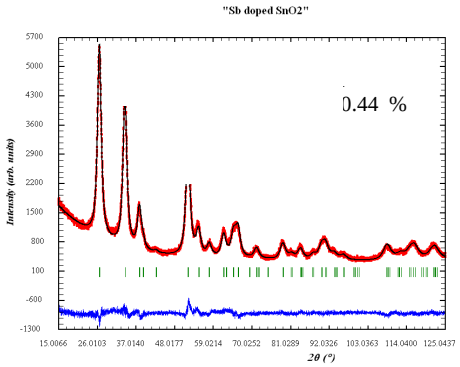

Figure 18: Rieveld plot and microstructural results of a Sb doped SnO_2 sample.

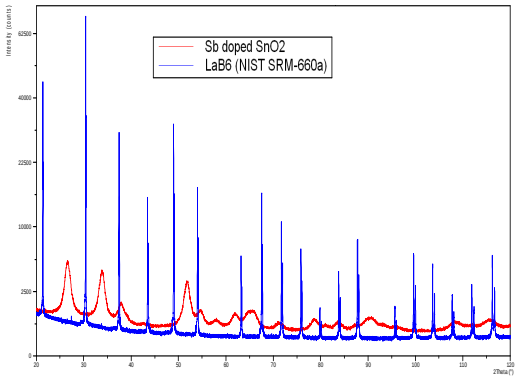

Figure 19: Comparison of the XRPD diagrams of the Sb doped SnO_2 and LaB_6 NIST SRM-660a samples.

3.3.4. Structure solution of an organic molecular compound from powder diffraction data

XRPD plays an important role in the crystal structure determination of new materials which are not available as single crystals. In the last 20 years, the number of structure determinations using powder diffraction has increased considerably. The methods used to solve crystal structures by powder diffraction can be divided in two groups. In the first group there are the reciprocal-space methods, generally direct methods in an analogous way than with single-crystal data, but with strong limitations mainly related to the difficulties of extracting the factor structure amplitudes from the peak intensities due to strong peak overlapping. These limitations are much stronger in the case of molecular compounds and only if x-ray synchrotron data are available, the possibilities of success increase. In the second group of methods, there are the direct-space methods. These methods do not require the extraction of the structure factors, and building units (molecules, polyhedra, …) are located in the unit cell using global optimization methods (such as Monte Carlo, simulated annealing or genetic algorithms). The calculated XRPD diagrams are compared with the observed diagrams in order to find the best agreement. The possibilities of success increase with respect to the reciprocal-space methods and it is possible and quite usual e.g. to solve a structure of a molecular compound with laboratory XRPD data.

Figure 20 shows the crystal structure of the α form of Vorinostat [22], a pharmaceutical molecular compound, solved by direct-space methods by means of the FOX software [23] and using laboratory XRPD data obtained with a PANalytical X`Pert MPD diffractometer in a capillary transmission geometry. Figure 21 depicts the Rietveld plot of the final refinement of this crystal structure performed with FullProf [24].

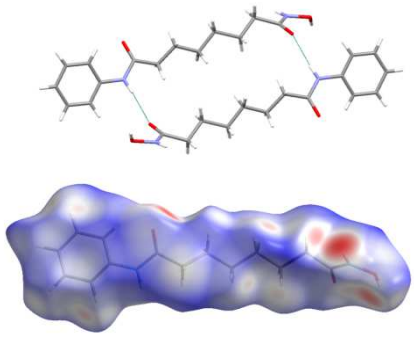

Figure 20: Crystal structure and Hirshfeld's surface of form α of Vorinostat solved by XRPD showing H-bonding contacts

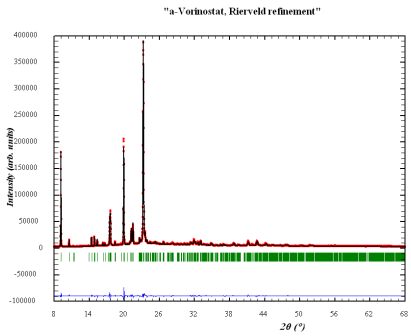

Figure 21: Rietveld plot of the final refinement of the crystal structure of form α of Vorinostat.

References

[1] Shmueli, U. Ed. 2001 *International Tables for Crystallography*, vol. B, Second Edition, Kluwer Academic Publishers, Boston/Dordrecht/London

[2] Wilson, A.J.C., Prince E., Ed. 1999 *International Tables for Crystallography*, vol. C, Second Edition, Kluwer Academic Publishers, Boston/Dordrecht/London

[3] Cullity, B.D. 1978 *Elements of X-ray Diffraction*, 2nd ed. Reading, Massachusetts, Addison-Wesley publishing company inc.

[4] Klug, H.P. Alexander, L.E.S 1974 *X-ray Diffraction Procedures. For Policrystalline and Amorphous Materials*, 2nd ed., New York, John Willey and Sons

[5] Clegg, W., Blake, A.J., Gould, R.O., Maint, P. 2001 *Crystal structure analysis. Principles and Practice*, Oxford University Press.

[6] Müller, P., Herbst-Irmer, R., Spek, A.L., T.R. Schneider, M. Sawaya 2005 *Crystal Structure Refinement*, Oxford University Press

[7] Bish, D.L., POST, J.E. 1989 *Modern Powder Diffraction*, Washington D.C., The Mineralogical Society of America (Reviews in Mineralogy)

[8] Pecharsky, V.K., Zavalij, P.Y. 2003 *Fundamentals of Powder Diffraction and Structural Characterization of Materials*. New York: Springer

[9] Escuer, A., Cordero, B., Font-Bardia, M., Calvet, T., Roubeau, O., Teat, S.J., Fedi, S., Fabrizzi de Biani, F. 2010, *Dalton Transactions* **39** 4817

[10] Gellman, A.J., Horvatha, J.D., Buelowa, M.T. 2001, *Journal of Molecular Catalysis A: Chemical* **167,** 1-2, 3

[11] A.G. Quiroga, A.G., Ramos-Lima, F.J., Alvarez-Valdés, A., Font-Bardia, M., Bergamo, A., Sava, G., Navarro-Ranninger, C. 2011 *Polyhedron* **30** 1646

[12] S. Pérez, S. López, C., Caubet, A., Solans, X, Font-Bardia, M. 2008, *Eur. J. Inorg. Chem.* 1599

[13] PDF-2; PDF-4 *Powder Diffraction File* 2010, *International Centre for Diffraction Data* (ICDD) 20, 12 Campus Boulevard., Newton Square, Pennsylvania 19073-3273, USA. <http://www.icdd.com>

[14] A. Boultif, A., Louër, D. 2004 *J. Appl. Cryst.*, **37**, 724

[15] Le Bail, A., Duroy, H., Fourquet, J.L. 1998, *Mat. Res. Bull.* **23**, 447-452.

[16] Pawley, G.S. 1981, *J. Appl. Cryst.* **14**, 357

[17] Rietveld, H.M. 1969, *J. Appl. Cryst*. **2** 65

[18] Young, R.A., ed. 1993, The Rietveld Method, Oxford: IUCr, Oxford University Press, (Monographs on Crystallography; number 5)

[19] Bish, D.L., Howard, S.A. 1988 *J. Appl. Cryst.* **21** 86

[20] Leon Reina, L, De la Torre, A.G, Porras-Vazques, J.M., Cruz M., Ordonez, L.M., Alcobé, X., Gispert-Guirado, F., Larrañaga-Varga, A., Paul, M., Fuellman, T, Schmidt, R., Aranda, M.A.G. 2009 *J. Appl. Cryst.* **42**, 906

[21] Rodríguez-Carvajal, J., Rosinel, T. 2004, *Materials Science Forum*, **443**, 123

[22] Puigjaner, C., Barbas, R., Portell, A., Alcobé, X., Font-Bardia, M., Prohens, R. 2011 (in press)

[23] Favre-Nicolin, V., Cerny, R. 2002 *J. Appl. Cryst.* **35**, 734-743

[24] Rodriguez-Carvajal, J., 1993 *Physica B*. **192**, 55

Handbook of instrumental techniques from CCiTUB

Secondary Ion Mass Spectrometry (SIMS): principles and applications

Francisco López

Unitat SIMS, CCiTUB, Universitat de Barcelona. Martí i Franquès, s/n. 08028 Barcelona. Spain.

email: *franlopez@ccit.ub.edu*

Abstract. This article outlines the basis of the technique and shows some examples of applications in order to exhibit the expectations of this technique in varied scientific fields.

1. Introduction

SIMS is an instrumental technique of microscopic surface analysis of composition and layer structure of solids [1-8]. It is based on the detection of emitted atomic and molecular charged particles when a material is bombarded by energetic particles.

The most important feature of SIMS is its high sensitivity for the detection of most elements of the periodic table including the lightest. Also important is the ability to distinguish isotopes, followed by a remarkable depth resolution and a large dynamic range for detection of most elements (more than 6 orders of magnitude). The combination of this set of features makes SIMS an attractive analytical method. However, as major drawback, one has to mention its difficulties for quantification because SIMS only detects the ionized fraction of the species being measured, which is difficult to evaluate in general.

The technique is of great significance in science of new materials in the fields of electronics, optics and mechanics. Within these fields it can be applied to thin layers of different materials, such as hard coatings for cutting tools, thin-film superconductors, amorphous semiconductors, thin layers of optical applications, etc. Its versatility also places it as an important analytical technique in other fields such as metallurgy, ceramics, geology, organic chemistry, biology, etc. Each of the applications of SIMS is preceded by some considerations regarding the most appropriate experimental parameters (vacuum, primary current and energy, mass resolution, sensitivity, etc.).

The different forms of embodiment of a SIMS with respect to the different types of instruments that form it create a variety of SIMS systems. Each system is optimized in a certain way that takes into account the applications that are intended.

2. Physical principles

2.1 Fundamentals

SIMS uses an energetic primary ions beam (several keV) to bombard the sample surface, resulting in the emission of ionized secondary particles (secondary ions) -the sputtering process- which are detected by a mass spectrometer. Figure 1 illustrates schematically the basic elements that make up a SIMS experiment. In Figure 2 the sputtering process is represented. The primary ions may be of various types. The available primary ions in our instrument are $O2^+$ and Ar^+.

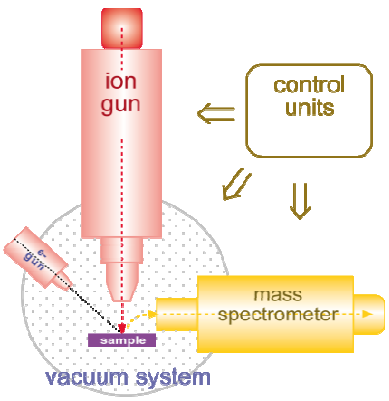

Figure 1: Basic blocks that make up a SIMS experiment.

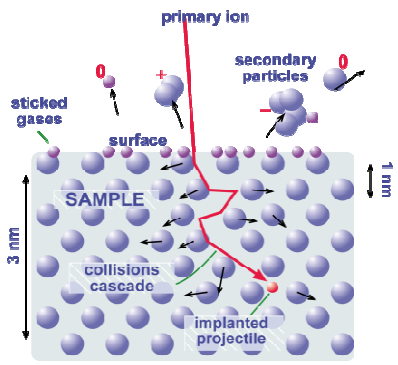

Figure 2: Illustration of the process of sputtering.

The sputtering consists in the implantation of the primary species into the sample, and the emission of surface atoms and molecules due to the energy lost by the primary species in the material [3, 6, 7, 9, 10]. The thickness of the area affected by the cascade of collisions is comparable to the primary ion path R which is given by

$$R = \int_0^E \frac{1}{dE/dx}\, dE$$

where E is the energy of primary ion, dE/dx the energy loss per unit length perpendicular to the surface. For 1 keV Ar^+ on copper, dE/dx= 100 eV/Å and R = 10 Å. A common estimate is R = 10 Å / 1 keV.

An important parameter related to the sputtering process is the atomic *sputter yield Y*, defined as the average number of atoms emitted per primary ion. The sputter yield is related to the energy transmitted by an incident ion on the target surface, or energy loss per unit length in the direction normal to the surface. For average-mass ions and 1 keV energies, Y takes values between 0.5 and 20.

SIMS is a destructive analytical technique, however, we should clarify that in most cases it requires only a small volume of material for analysis. A value of typical crater area in depth analysis is of the order of 1 mm^2. An analysis to reach 1 micron deep with an area of 1 mm^2, represent a material volume loss of 10^{-6} cm^3.

2.2 Secondary Species

As a result of the interaction of the primary beam with the sample, many new species are formed. For a given material, it is difficult to predict which secondary species will be formed and with which ionic proportions, due to the complexity of the mechanisms involved [3, 11]. In an analysis by SIMS, one can find any individual atoms that are present in the material and also any molecule that can be formed as a combination of these atoms, although many of them may have a low chance of formation or too low ionization to be detected.

Some molecules are formed inside the material before being issued as a result of the rearrangement of atoms caused by the energy deposited by primary ions, while others, may be formed out of the material near the surface by recombination of atoms and molecules once they have been emitted. Recombination is also possible with species from the residual gas molecules.

Another common problem in the detection of secondary species is mass interference, that is, different molecular aggregates with the same mass have coincident signals, and therefore, at that point the sum of all signals is measured. Some of these cases are resolved by taking as a representative signal of the element under study that corresponds to an aggregate of the atom instead of the mono-atomic ion (for example we measure $^{28}Si^{14}N(42)$, instead of ^{14}N, which interfere with $^{28}Si^{+2}$ in a matrix of Si [12]).

2.3 Energy distribution of secondary ions

Secondary ions leave the sample surface with different energies following a certain distribution which has a single maximum [3, 13, 14]. The maximum is usually located at relatively low energies of the order of ten eV and depends scarcely on primary ion energy. The energy distributions have tails that can reach several hundred volts; the more complex is the molecular aggregate, the narrower is the energy distribution. The overall energy distributions depend on the ionization mechanism, the nature and energy of the primary beam, and the chemical structure of the surface.

Typically, mass spectrometers apply an electrical potential to extract ions from the area where erosion occurs, which increases the atomic number of ions collected and therefore increases the sensitivity. However, it destroys the information about the initial direction of the ion.

In common with all methods of surface analysis involving either incoming or outgoing charged particles, surface charging of insulators can be a problem. The surface potential due to charging causes a large shift on the energy distribution of secondary ions, taking it outside the energy acceptance window of the mass spectrometer and making impossible its measurement.

The charging problem requires extra equipment in order to compensate charging effects. The most common being an electron gun that sprays the measuring surface with electrons, so neutralizing positive charges. A useful method, published by the author, has been incorporated to our instrument in routine analysis in order to improve measurements conditions in insulators [15].

2.4 Quantification

As in any other analytical technique for compositional analysis, SIMS seeks to establish a relationship between measured signals and the concentration of the corresponding elements in the

material; although in SIMS, this task is especially complicated. We may establish a general equation expressed as

$$I_x = Y\ \alpha_x^{\pm}\ \frac{I_p}{e}\ \beta\ C_x$$

where $\mathbf{I_X}$ = Intensity of secondary ions, **Y** = Sputter yield, $\alpha_x^{\pm}$ = Ionization factor, **β** = Transmission of the mass spectrometer, $\mathbf{C_X}$ = Concentration of element x and $\mathbf{I_P}$ = Intensity of primary ions.

The likelihood of positive ionization of the elements emitted from common matrix, exhibits a regular dependence of inverse exponential on ionization potential of the element pulled, and a similar dependence of the ionization probability of negative ions on electron affinity [6]. But there are many deviations from this behavior due to the influence of chemical and electronic states of the matrix and its interaction with the emitted ion, which makes the calculation of the probability of ionization a much more complicated problem. SIMS technique requires, therefore, carefully calibrations if quantitative results are required.

Quantification is an important issue for any analysis technique, which has led to enormous efforts to seek methods and models to convert the intensities of secondary ions into concentrations of elements present in the material [7, 16]. Today there is no single model or method of general application that allows good quantification in most SIMS analysis. Empirical or semi-empirical alternatives often give better results than theoretical models.

The use of patterns is one of such empirical methods used to obtain quantitative results in SIMS [17]. However, the diversity of possible matrices makes it a challenge to find patterns that have the same matrix effects as the sample of study. A widely used method to achieve an internal standard consists of implanting an isotope of the element of study, used as a standard in the depth profile [18].

2.5 Sensitivity

SIMS in general may be qualified as the most sensitive micro-analytical technique available nowadays. This is possible, on the one hand, because the amount of particles extracted from the material is large even in a small volume, and on the other hand, because of the high sensitivity of modern detectors that can detect the arrival of individual ions.

The sensitivity in an analysis depends on the sputter rate, Y, and the probability of ionization, $\alpha_x^{\pm}$, which will determine the minimum concentration of an element that can be detected by the spectrometer. SIMS sensitivity also depends on the transmission of the detection system, **β**. A typical value of the transmission in a quadrupole mass spectrometer type is 10^{-3}, while for a time-of-flight system is10^{-1}.

2.6 Detection Limit

The detection limit for a certain element is defined as the minimum concentration of this element that can be analyzed. A typical detection limit of SIMS is of the order of 1 ppm, although this value varies considerably depending on the element and the matrix in which it is located.

The detection limit is determined by the background intensity obtained for a given mass and a set of analysis conditions [6, 19, 20, 21]. The most important background sources in SIMS (mass interference, residual gas on the sample surface, memory effects, etc.) have been studied by many authors [3, 19, 20, 22, 23, 24, 25].

3. Methodology

3.1 Static and dynamic

When the sample is bombarded with a primary ion of high enough density, there is a significant erosion of the surface and these surface atomic layers are lost. This corresponds to the **dynamic SIMS** regime [3, 26, 27]. From the data given by the mass spectrometer as a function of time, it is possible to infer the composition of the material not only on the surface but also in depth. If the

applied ion density is low enough, it will lead to a situation in which the primary ions are unlikely to affect an area previously affected by the incidence of another ion fallen before. Under these conditions, most primary ions impinge on an unexposed surface area, not previously bombarded. This situation is known as the **static SIMS** regime (SSIMS), and corresponds to a purely technical analysis of surfaces [3, 5, 7, 28]. The SSIMS condition decreases with bombarding time so the analysis must be performed in the limited time before this condition is substantially lost. The instruments implementing a SSIMS require high-transmission analyzers. Instruments devoted to SSIMS are usually highly specialized in this type of analysis and are mainly applied in organic chemistry and biology.

3.2 Bulk analysis

The easiest SIMS analysis is to make impinge a relatively focused ion beam firmly on a surface and record the secondary signals obtained in a range of masses. The ion beam produces a crater with a shape resembling an inverted Gaussian. The ions are extracted from different parts of the crater (one of the walls, some part of the bottom) and it is not possible to associate a well defined depth to each of the signals being measured. The measurement of secondary signals informs us about the composition of the material at an average depth between the surface and the bottom of the crater. This volume analysis which will be more representative of the material as a whole the more homogeneous the material in depth is. This method, although it cannot distinguish variations of elements with depth, has a very simple implementation and is useful for identifying components of a material or the presence of impurities.

3.3 Depth profile

Working in dynamic regime, secondary ions are detected from a certain depth at short intervals of time, and therefore a collection of intensities as a function of depth can be obtained. This type of measurement is called a depth profile and it is probably the most widely used method in SIMS. In practice, the signals are obtained directly in terms of bombarding time and not in terms of depth. In order to re-scale the graph from bombarding time to depth units, it is necessary to know the sputter rate ż [29, 30, 31]. Figure 3 shows an example of depth profile obtained in our instrument for a diamond thin film on a Mo substrate, bombarded by $O2^{+}$.

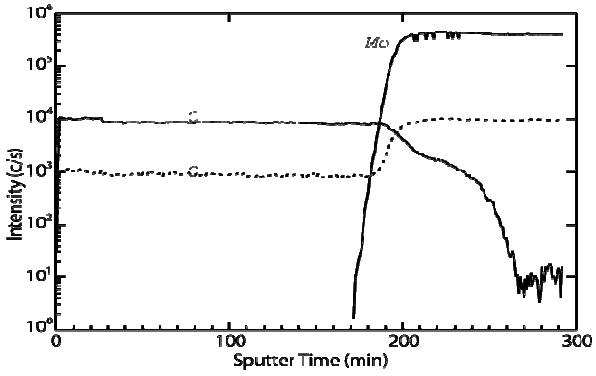

Figure 3: In depth profile obtained with our instrument on a diamond thin layer.

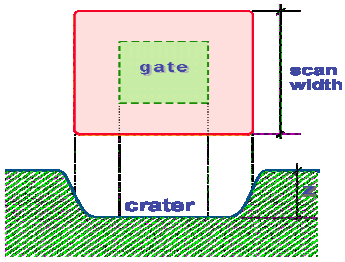

Figure 4: Main parameters in a SIMS crater squared shaped with x/y scan

To obtain reliable depth profiles, the detected species must come from a specific depth. Therefore, this technique seeks to produce a crater that has a flat bottom and consider only the species that come from this area. One way to achieve this is by scanning the primary beam so that it scrolls regularly and homogeneously a controlled area of the surface, usually square-shaped. In this way, a flat bottomed crater is obtained, although the section of the beam is not of constant ionic strength. In synchronism with the primary beam tracking, a window centered in the scanning zone

that records only the ions from this area can be defined by electronic switching. Figure 4 illustrates the concepts mentioned in a square-shaped crater with swept x/y.

3.4 Dynamic range

An important feature of SIMS is its large dynamic range. This is defined as the ratio between the maximum and minimum intensities of a particular secondary species that can be measured in an in-depth profile. The minimum intensity is determined by the background signal corresponding to the secondary ion being measured, and it may depend on the element and the conditions of the analysis. The value of the dynamic range reaches more than 6 orders of magnitude for many elements depending on the species, the material and test conditions. In profiles of B implanted in Si, dynamic ranges > $5x10^5$ are obtained. This characteristic explains why SIMS measurements are usually expressed in logarithmic scale. In this representation, it is possible to see simultaneously the major and trace signals in the same graph.

3.5 Depth resolution

The atomic mixing produced by the primary ion bombardment limits the depth resolution at which elements are detected. Basically, the depth resolution depends on the mass and energy of the primary species, and their interaction with the target matrix [3, 32, 26, 6, 10]. In practice, the final depth resolution in a profile may also depend on other geometric factors such as the flatness of the crater or the roughness of the sample surface. Another factor that may be important is the roughness induced by the bombardment [24, 33].

3.6 Mass Spectrum

A mass spectrum consists of recording the intensity of a range of secondary species as a function of mass (exactly in terms of m/q). The spectrum will contain information about the elements present on the surface. A mass spectrum could be obtained after previous bombardment of the surface in dynamic regime, in order to position the primary ions at a certain depth and to know the composition of the material at a distance from the surface. Figure 5 shows a mass spectrum obtained with our instrument for a Ti alloy bombarded with oxygen primary ions. Signals of mono-atomic elements and also aggregates formed by atoms of O and Ti can be observed.

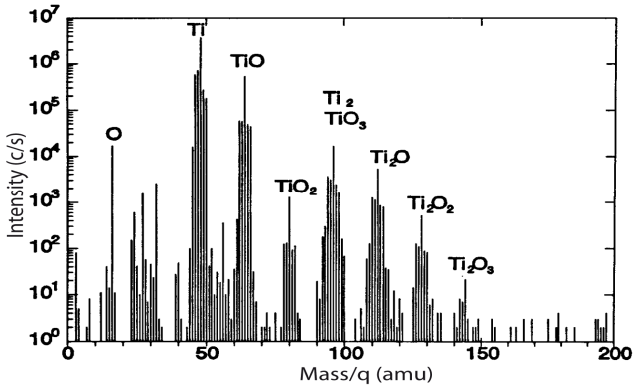

Figure 5: Mass spectrum in a Ti alloy bombarding with 0_2^+.

4. Instrumentation, ion micro-probe Atomika A-DIDA 3000-30

4.1 Presentation

The basic instrumentation required for SIMS was indicated in paragraph 1. This section briefly gives particular details of the components and characteristics of our instrument, an ion micro-probe A-DIDA3000-30 [34].

The ion micro-probe A-DIDA 3000-30 is a compact SIMS manufactured by the german company Atomika. This SIMS is of general use, relatively versatile, suitable for routine applications but mainly focused on analysis by depth profiling. It is of relatively simple structure compared with models from other companies, but with acceptable performance and versatility. The

most important technical specifications of the ion micro-probe Atomika A-DIDA 3000-30 are shown in Table 1.

Figure 6: Main front view of the ion micro-probe A-DIDA 3000-30.

Figure 7: Enlarged view of main chamber

4.2 Vacuum system

SIMS experiments are carried out in ultra-high vacuum for two different reasons: firstly, to prevent the spread of primary and secondary ions along its path, and secondly, to avoid interference of the gases that are deposited on the surface to investigate. A wide variety of vacuum pumps are used such as turbo-molecular pumps, ionic, diffusion, Ti sublimation, cryogenic wall, etc. Some of them are coupled in tandem with another pump so that each one works within a suitable pressure range.

4.3 Ion gun

Our complete ion gun consists of an ion source, an ion extraction system inside of it, an acceleration system through a potential difference (0.5 to 15 kV) to determine the final energy of the beam, a system of deflectors for alignment of the beam, a focusing lens system to collimate the beam, and a deflector x/y to position the beam and to scan it. The set of ion extraction system, acceleration, deflection, alignment, focus and mass filter is called primary ion optics. Figure 8 shows a schematic diagram of the main elements that make up the A-DIDA ion gun.

Table 1. Summary of major technical specifications of the Atomika ion micro-probe A-DIDA 3000-30.

Priamary ions species	Ar^+, O_2^+
Angle of incidence	2° (almost normal)
Primary ion energy	0.5 keV to 15 keV
Primary ion current	$<10^{-10}$ A to $2x10^{-6}$ A
Densidad de corriente iones primarios	$<10^{-9}$ A/cm^2 to $2x10^{-2}$ A/cm^2
Primary ion source size	5-10 µm to 2 mm
Voltage of sample holder	[-60 V, +60V]
Beam scanning amplitud	0 to 1-2 mm energy as
Base pressure	$10^{-7} \div 10^{-8}$Pa
Extraction voltage for secondary ions	±100 V
Mass range	0-350 amu
Mass resolution at 28 amu	0.05 amu

4.4 Mass Spectrometer

The other essential part of a SIMS is the mass spectrometer, which is responsible for measuring the mass of secondary ions. In the micro-probe A-DIDA, the mass spectrometer consists of a quadrupole mass filter with a high transmission and a special secondary optics in the entry for

capturing and filtering in energy the secondary ion, and a detector device for individual particles of the electron multiplier type (chaneltron). Figure 9 shows a schematic diagram of the spectrometer with the main elements.

The use of quadrupole spectrometers has some advantages such as few memory effects, few problems in the analysis of insulating materials, fast switching between modes of detection of positive and negative ions, support for easy positioning of the sample, operation and maintenance.

4.5 Computerized system

The data acquisition, program analysis and automation system are entrusted to a personal PC computer system with IEEE and RS232 standard communications. The control software has been programmed in Visual-Basic language and entirely developed by the author. The user Interaction runs in a Windows environment and the graphs and data are saved in standard ASCII format, compatible with most software applications.

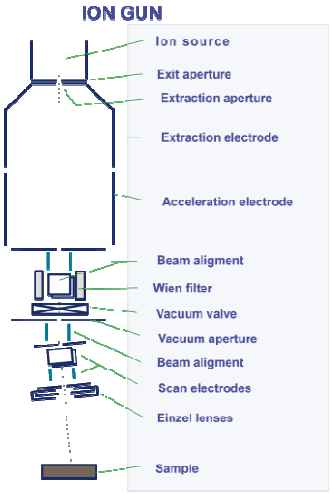

Figure 8: Schematic view of the main elements constituents of the A-DIDA3000 ion gun.

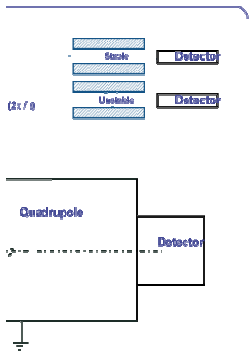

Figure 9: Schematic diagram of the quadrupole spectrometer with the main elements.

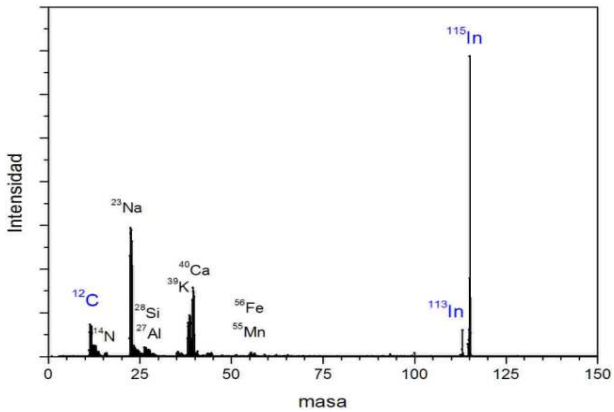

Figure 10: Mass spectrum in the metallic coating of a car emblem

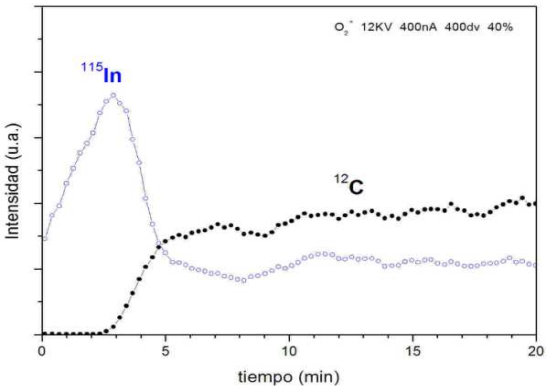

Figure 11: In-depth profile on the same sample

5. Examples of applications

The SIMS technique is applied in a wide variety of fields related with the sciences of new materials thanks to its versatility. It is an indispensable tool in many fields such as electronics, optics, metallurgy, superconductors, geology, etc. Nevertheless its biggest drawback must be indicated: the

difficulty to quantify. In the following, I will show some illustrative examples of applications where our instrument has been used for the described measurements.

5.1 Analysis of the metallic coating of a car emblem

Firstly, the sample was subjected to a spectral analysis in order to identify the main components of the alloy. A mass spectrum from a mass range of 3-150 amu was performed. The result is shown in Figure 10, where the presence of In can be identified as the main constituent of the coating. Also C is detected (probably from the plastic material of the substrate) along with some contaminants.

Once In and C were identified as main elements, we planned to do a Dynamic Analysis. An in-depth profile was carried out following the In and C signals. The result is shown in Figure 11, and confirms the presence of a thin coating (≈100 nm) of In deposited on the plastic substrate.

5.2 Cathodic chromium carbide coatings

In this application, chromium carbide coatings deposited on hardened steel probes were analyzed. The coatings were obtained by cathodic arc evaporation (CAE) from chromium targets in reactive acetylene gas [35]. The effect of the deposition parameters on composition and crystalline structure was characterized by means of SIMS among other techniques. Figure 12 shows the SIMS analysis of the sample. The depth composition profiles of Cr and C reveal a good uniformity in the chromium carbide region, a sharp transition between the chromium carbide and the chromium nitride regions and a two-fold higher erosion rate for the nitride than for the carbide.

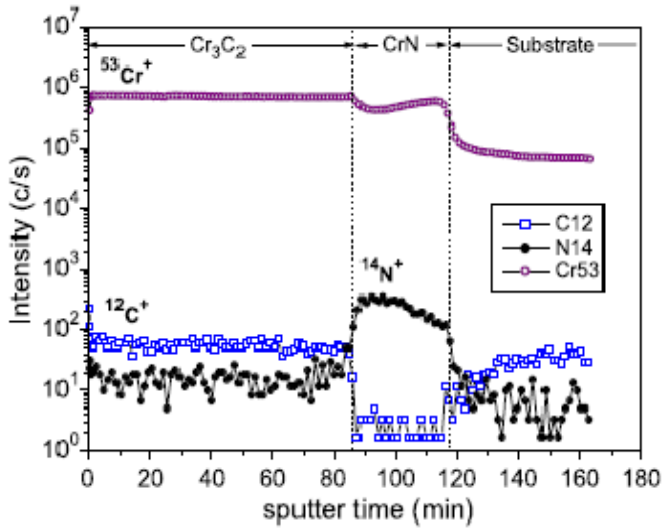

Figure 12: SIMS profile of a Cathodic chromium carbide sample: CrN (1.5 µm) + CrC (1.5 µm).

5.3 Nanometer-metal multilayer

In this work, the depth resolution (interface width) in elemental analysis and depth profiling of complex layer systems of three ion-probing techniques including SIMS was analyzed. Each technique has advantages and drawbacks [36]. From the results, it was concluded that SIMS is suitable and complementary technique for in-depth elemental analysis of metal-multilayer stacks of nm individual thickness. A very good correlation between nominal thickness and calculated values was found between the depth profiles obtained using SIMS and those obtained by other techniques, in spite of the fact that the analytical methods were very different in each case.

5.4 Nanometric chromium/chromium carbide multilayer

This example shows the analysis of metal/ceramic multilayer with periods in the nanometric range [36]. These materials have been proposed as protective coatings due to their improved tribological and mechanical properties as compared to single coatings. Secondary ion mass spectrometry confirmed the periodic multilayered structure.

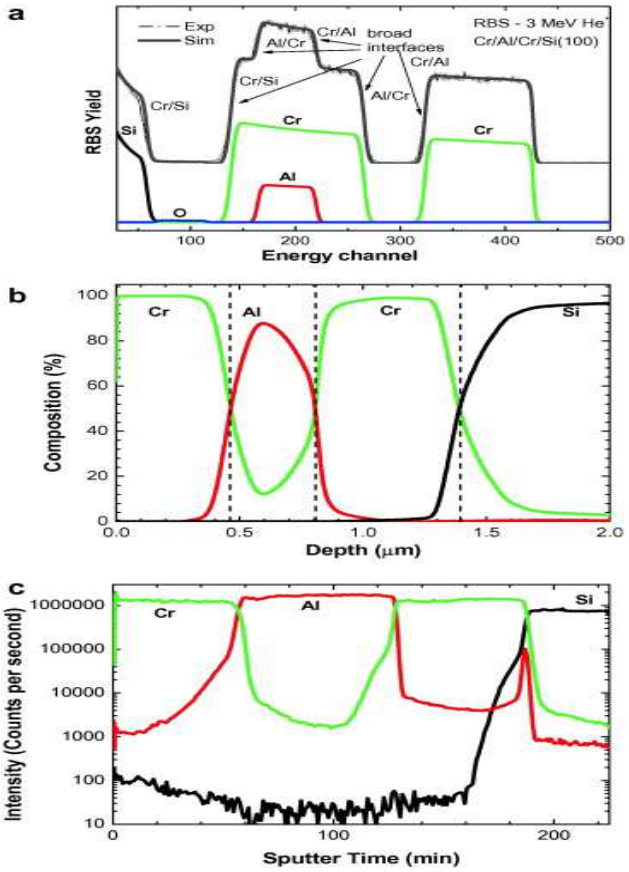

Figure 13: Depth profiles of a 450 nm Cr / 400 nm Al / 450 nm Cr tri-layer film obtained by a) Rutherford Backscattering (RBS), b) Glow-Discharge Optical Emission Spectrometry (GDOES) and c) SIMS. In a), the experimental data and the global fit have been shifted vertically from the contributions of the elemental spectra (lower part of the graphs). The dashed vertical lines in b) indicate the location of the different interfaces. Notice that, in c), the vertical axis (intensity) is in logarithmic scale.

5.5 Hydrogenated amorphous carbon films on silicon

Hydrogenated amorphous carbon films deposited on silicon by r.f. Plasma decomposition of methane were analyzed by SIMS [37].

The dependence of the Si-C transition width on substrate temperature and homogeneity of the carbon layer were studied. For films deposited on refrigerated substrates, the Si-C transition width was found to be two-fold higher than for the films deposited on unrefrigerated substrates. The secondary-ion mass spectrometry signal intensities of the main constituents are constant over the whole carbon layer (see Fig. 15). The C^{+2}-to-C^{+3} signal ratio is constant in the deep region but it increases towards the surface; this result seems to indicate that some degradation of the film occurs during the growth process.

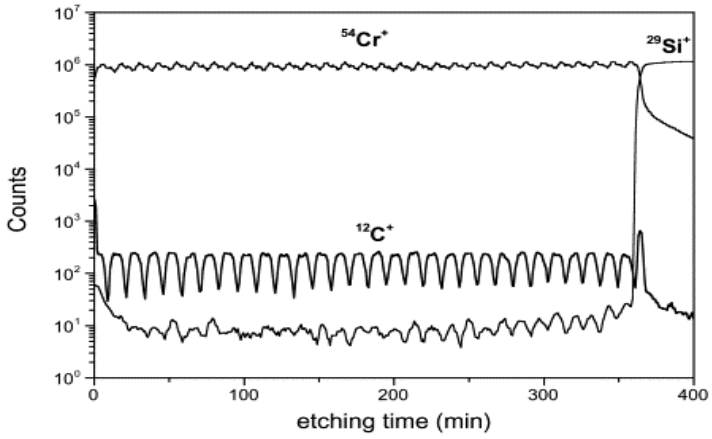

Figure 14: SIMS depth profile analysis of the 30/30 nm Cr/CrC multilayer.

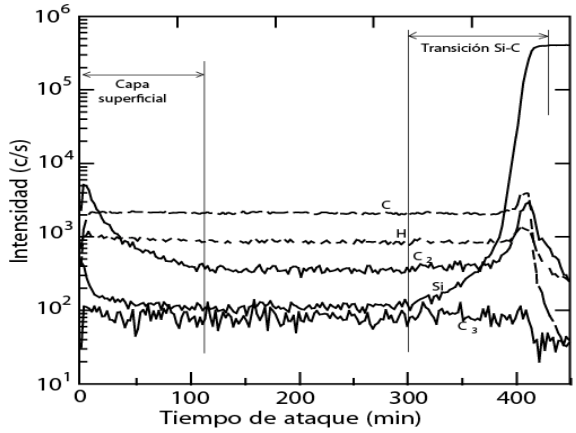

Figure 15: SIMS depth profile in the film deposited at 450 V on a refrigerated substrate.

Acknowledgments

The author wishes to thank Dr. Arturo Lousa for allowing the use of Figures 12, 13 and 14. Thanks also to Dr. Joan Esteve, Dr. María-Victoria Garcia-Cuenca and Dr. Josep Lluís Morenza, from the department of Física Aplicada i Óptica of the Facultat de Física, for their help and collaboration, and the staff of the Taller d'Electrònica and Taller de Mecànica for the services provided.

References

[1] Blattner R.J. and Evans C.A., Jr., *Scanning Electron Microscopy*, **IV**, (1980).

[2] Feldman L.C. and Mayer J.W., *Fundamentals of Surface and Thin Film Analysis*, (Elsevier, New York, 1986).

[3] Benninhoven A., F.G. Rdenauer and H.W. Werner, *Secondary Ion Mass Spectrometry: Basic Concepts, Instrumental Aspects, Applications and Trends*, (Wiley, New York 1987).

[4] Adams F., F. Michiels, M. Moens y P. Van Espen, *Analytica Chimica Acta*, **216** (1989) 25.

[5] Briggs D., A. Brown and J.C. Vickerman, *Handbook of Static Secondary Ion Mass Spectrometry*, (Wiley, New York, 1989).

[6] Wilson R.G., F.A. Stevie and C.W. Magee, *Secondary Ion Mass Spectrometry*, (Wiley, New York, 1989).

[7] Vickerman J.C, in *Secondary Ion Mass Spectrometry: Principles and Applications*, eds. J.C. Vickerman, et al.(Oxford, New York, 1989a,b,c,d,e) p. 1, p. 9, p. 35, p. 149, p. 272.

[8] Abel F., B. Agius, G. Blaise and A. Huber, en *Surfaces Interfaces et Films Minces*, ed. B. Agius, M. Froment and co-autores, (Bordas, Paris, 1990) p. 237.

[9] Behrisch R. and K. Wittmaack, in *Topics in Aplied Physics: Sputtering by Particle Bombardment III*, Eds: R. Behrisch and K. Wittmaack, Vol. **64**, (Springer-Verlag, Berlin, 1991), p. 15.

[10] Wittmaack K., in *Practical Surface Analysis* Eds: D. Briggs and M.P. Seah, Vol. **2**, (Wiley, New York, 1992) p. 105.

[11] Yu M.L. in *Topics in Aplied Physics: Sputtering by Particle Bombardment III*, Eds: R. Behrisch and K. Wittmaack, Vol. **64**, (Springer-Verlag, Berlin, 1991), p. 91.

[12] Wach W. and K. Wittmaack, Nucl. Instrum. Methods, **149**, 259 (1978).

[13] Thompson M.W., *Philos. Mag.*, **18** (1968) 377.

[14] Hofer W.O., in *Topics in Aplied Physics: Sputtering by Particle Bombardment III*, Eds: R. Behrisch and K. Wittmaack, Vol. **64**, (Springer-Verlag, Berlin, 1991), p. 15.

[15] López F., M. V. García-Cuenca, J. L. Andújar and J. L. Morenza, in: Secondary Ion Mass Spectrometry SIMS VIII, ed. by A. Benninghoven et al.(Wiley, New York, 1992), p.459.

[16] Williams P., in *Practical Surface Analysis*, **Vol.2**, eds. D. Briggs and M.P. Seah, (Wiley, New York, 1992) p. 177.

[17] Homma Y. y Kurosawa S.; Yoshioka Y.; Shibata M.; Nomura K.; Nakamura Y., *Anal. Chem.*, **57** (1985) 2928.

[18] Smith H.E. y Morrison G.H., *Anal. Chem.*, **57** (1985) 2663.

[19] Kobayashi J., M. Nakajima y K. Ishida, *J. Vac. Sci. Techonol.* **A6** (1988) 86.

[20] Kobayashi J., M.Nakajima y K. Ishida, J. Vac. Sci. Techonol. **A7** (1989) 2542.

[21] Wittmaack K., in "Sputtering by Particle Bombardment III", *Topics in Aplied Physics*, Eds: R. Behrisch y K. Wittmaack, Vol. **64**, (Springer-Verlag, Berlin, 1991), p. 161.

[22] Magee C.W., R.E. Honig and C. A. Evans, Jr., in *Secondary Ion Mass Spectrometry SIMS III*, ed. by A. Benninghoven, J. Giber, M. Riedel and H.W. Werner, (Springer-Verlag, Berlin, 1982) p. 172.

[23] Frenzel H. and Maul J. L., in *Secondary Ion Mass Spectrometry SIMS III*, ed. by A. Benninghoven, J. Giber, M. Riedel and H.W. Werner, Springer-Verlag, Berlin (1982), p.94.

[24] Hofman S. in *Secondary Ion Mass Spectrometry SIMS III*, ed. by A. Benninghoven, J. Giber, M. Riedel and H.W. Werner, Springer-Verlag, Berlin (1982), p. 186.

[25] Clegg J.B., in *Secondary Ion Mass Spectrometry SIMS V*, ed. by A. Benninghoven, R.J. Colton, D.S. Simons and H.W. Werner, Springer-Verlag, Berlin (1986), p. 112.

[26] McPhail D.S., in *Secondary Ion Mass Spectrometry*, eds. J.C. Vickerman, A. Brown and N.M. Reed, (Oxford, New York, 1989) p.105.

[27] Dowsett M.G. and E.A. Clark, in *Practical Surface Analysis* Eds: D. Briggs and M.P. Seah, Vol. **2**, (Wiley, New York, 1992) p. 229.

[28] Briggs D. in *Practical Surface Analysis* Eds: D. Briggs and M.P. Seah, Vol. **2**, (Wiley, New York, 1992) p. 367.

[29] Kempf J.E. and Wagner H.H., in *Thin Film Depth Profile Analysis*, H. Oechsner, Springer-Verlag, Berlin (1984) p. 87.

[30] Kirschner J. and H.-W. Etzkorn, in *Thin Film Depth Profile Analysis*, ed. H. Oechsner, (Springer-Verlag, Berlin, 1984) p. 103.

[31] López F., M.V. García-Cuenca, J.M. Asensi and J.L. Morenza, Applied Surface Science, Volumes 70-71, Part 1, 2 June 1993, Pages 68-72.

[32] Meuris M., Vandervorst W., De Bisschop P. y Avau D., *Appl. Phys. Lett.*, **54** (1989) 1531.

[33] Vajo J.J. y Cirlin E.-H., Wilson R.G. y Hasenberg T.C., en *Secondary Ion Mass Spectrometry SIMS VIII*, Wiley (1992).

[34] Maul J.L. y Frenzel H. in *Ion Implantation Techniques*, ed. by H. Ryssel y Glawischnig, Springer-Verlag, Berlin (1982), p.361.

[35] Esteve J., J. Romero, M. Gómez, A. Lousa., Surface & Coating Technology, 188-189 (2004) 506-510.

[36] Escobar R., R. Gago, A. Lousa and J.M. Albella, Trends in Analytical Chemistry, Vol. **28**, No. 4, 2009.

[37] Romero J., A. Lousa, E. Martınez and J. Esteve, Surface and Coatings Technology, 163 – 164 (2003) 392–397.

[38] López F, M.V. Garcia-Cuenca, C. Serra and J.L. Morenza, Diamond and Related Materials, Volume **2**, Issues 2-4, 31 March 1993, Pages 229-232.

Crystal Engineering Studies: polymorphs and co-crystals

Rafel Prohens and Cristina Puigjaner

Plataforma de Polimorfisme i Calorimetria, CCiTUB, Universitat de Barcelona. Parc Científic de Barcelona. Baldiri Reixac, 10. 08028 Barcelona.

email: *rafel@ccit.ub.edu, cris@ccit.ub.edu*

Abstract. We review the key topics of one of the areas with the biggest impact of the last years in the chemical and pharmaceutical industry that is Crystal Engineering. The relevance of polymorphs and co-crystals from different points of view is been highlighted and broadly illustrated by means of several recent examples of studies carried out in this field. In addition, the most suitable instrumental techniques and the intellectual property implications are reviewed.

1. Introduction

Crystal engineering is the rational design of functional molecular solids from neutral or ionic building blocks, using intermolecular interactions in the design strategy [1]. This field has its origins in organic chemistry and in physical chemistry. The expansion of crystal engineering during the last years as a research field has gone parallel with a significant interest in the origin and nature of intermolecular interactions and their use in the design and preparation of new crystalline structures.

Active pharmaceutical ingredients (APIs) represent a particularly great challenge to crystal engineers because of both fundamental and applied reasons. APIs are inherently predisposed for self-assembly since their utility is normally the result of the presence of one or more supramolecular synthons. The crystalline materials obtain their fundamental physical properties from the molecular arrangement within the solid, and altering the placement and/or interactions between these molecules can have a direct impact on the properties of a particular solid. Usually, solid-state scientists call upon a variety of different strategies when trying to modify the chemical and physical solid-state properties of APIs, namely, the formation of polymorphs, hydrates, solvates, salts and co-crystals [2] (Fig. 1).

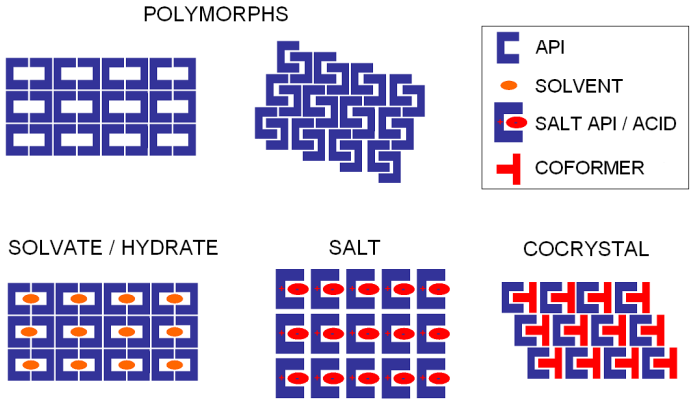

Figure 1. Different solid forms of an API: polymorphs, solvates/hydrates, salts and co-crystals.

Polymorphism is the ability of a substance to crystallize in different crystal modifications, each of them having the same chemical structure but different arrangements or conformations of the molecules in the crystal lattice. Polymorphs can differ in their chemical, physical and biological properties. There are many cases where insufficient exploration of possible crystallization and interconversion conditions caused serious delays in market launch and losses of revenue. Hence, the understanding and control of polymorphism and polymorphic behaviour is of considerable fundamental and practical importance. Moreover, a metastable polymorph is sometimes accepted for example to provide better handling/processing properties [3].

Crystallizing the API as a multicomponent crystal has been another accepted approach to generating form and physical property diversity. Hydrate and salt formation are the most common applications of this concept. Pharmaceutical hydrates are important due to the presence of water molecules in so many pharmaceutical drugs. On the other hand, it is estimated that over half of the medicines on the market are administered as salts. However, a major limitation within this approach is that the API must possess a suitable (basic or acidic) ionisable site. In comparison, the emerging field of pharmaceutical co-crystals (multicomponent assemblies held together by freely reversible, noncovalent interactions) offer a different pathway, where any API regardless of acidic, basic or ionisable groups, could potentially be co-crystallized [4].

2. Methodology and Applications

2.1. Relevance of polymorphs and co-crystals in the pharmaceutical and agrochemical industry
Crystal polymorphism is a common phenomenon in the pharmaceutical industry because the solid-state form is a significant quality attribute of a crystalline drug compound. The control of the desired crystal form during the manufacturing, storage or transport of a pharmaceutical substance is a key issue and losing this control can have serious economical effects due to the infringement of the intellectual property [5].

In addition, intrinsic properties of a drug substance candidate like its solubility or its chemical stability can be affected by its solid state. Poor physical properties of drug substances may be improved by using different crystal forms. Pharmaceutical formulations are developed in order to affect and improve solid-state properties of the drug substance in the final product [6].

Although polymorphism is a less frequent issue in agrochemicals, some important compounds, including pesticides and herbicides such as metazachlor exist in different polymorphic modifications [7] and their different solubility can affect the efficiency and toxicity of the pesticide.

Finally, co-crystals of APIs represent a class of multi-component crystalline forms that are of interest for their advantageous physical properties and for intellectual property implications [8]. In the last years, a great number of patents have been issued involving new co-crystals of APIs together with pesticides, herbicides and fungicides.

2.2. Polymorphs and co-crystals screening
During the last decades, high-throughput methodologies have been developed to look for new polymorphs and co-crystals of relevant drug compounds. Initially, the design of screening methods was based on solution growth. However, other methods such as solvent-drop grinding, slurring and the use of experimentally-determined phase diagrams have been developed in order to screen as much as possible the polymorphic landscape of a target compound. Due to the fact that all these screening methods are very time consuming and expensive, modern computational virtual screening methodologies for co-crystals have appeared recently with very promising results [9].

2.3. Analytical Techniques
Polymorphs and co-crystals represent different crystal structures of a compound. In principle, any physical or chemical property can a priori vary along the crystalline landscape of a compound and thus, practically any analytical technique able to measure properties of a crystalline material is suitable to study the solid state behaviour of a given compound. In this sense, the most useful techniques are:

2.3.1. Differential Scanning Calorimetry (DSC). This technique measures the difference in the amount of heat required to increase the temperature of a sample and a reference as a function of temperature. Pure crystalline forms are characterized by their melting process and the polymorphic behaviour can be studied through the observed onset and enthalpy of any thermal phenomenon which can be accurately measured. Endotherms represent phenomena such as desolvation, phase transitions and melting. On the other side, exotherms are associated with crystallization, phase transitions and decomposition reactions.

2.3.2. Thermogravimetry (TGA). Thermogravimetric analysis records the mass changes of a sample as a function of time and temperature under a controlled atmosphere. Although this technique does not give direct information about the existence of polymorphism, since all polymorphs have the same mass, it is crucial in determining the existence of solvates and the determination of their stoichiometries. During polymorph screening of drugs, TGA helps to confirm or discard the appearance of a new polymorph.

2.3.3. X-ray Diffraction (XRD). This technique is probably the most useful in the detection of a new polymorph, co-crystal and solvate. There exist two different methodologies of application

depending on the sample: powder diffraction for those polycrystalline samples and single crystal diffraction when a single crystal can be isolated. Usually powder methods are used to characterize qualitatively a new crystal phase while the single crystal method is used to determine the crystal structure. However, recently powder methods are being applied also to solve the crystal structure of microcrystalline solids.

2.3.4. Thermomicroscopy. Hot stage microscopy consists of a hot stage and a microscope equipped with a digital camera which provides useful information about thermal events, including meltings, solid-solid transitions, crystallizations, sublimations, desolvations and co-crystallizations. Although the visual observation of a polymorphic transition or a melting onset is subjective, this technique can provide very useful qualitative information about the polymorphic system under study. In addition, the observation of changes in size, shape, colour, etc. during hot stage experiments can be useful to detect the existence of polymorphism in a rapid screening study.

2.3.5. Other Techniques. Spectroscopic techniques such as Infrared, Raman and solid-state Nuclear Magnetic Resonance (NMR) can also provide useful information about different crystalline forms of the same organic compound and can be used to identify a pure crystal form and quantify a mixture of two forms.

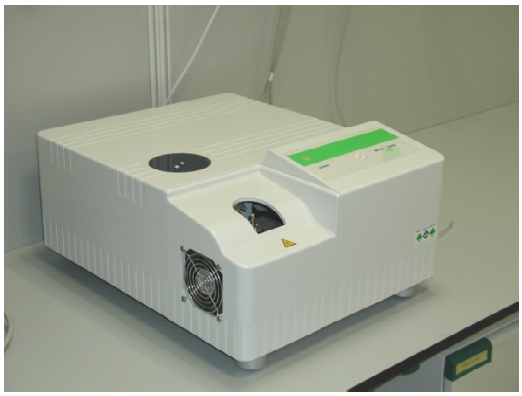

Figure 2: Differential Scanning Calorimeter.

Figure 3: Thermomicroscope.

2.4. Crystal Engineering and intellectual property

Polymorphs and co-crystals of a drug can be protected by patents since they represent different crystal forms of the same compound with different properties. The relevance of this issue in the pharmaceutical industry is extreme because the discovery of a new polymorph can be translated into the filing of a new patent application with important economical consequences. In this sense, a new polymorph (or a co-crystal) with improved properties such as stability or solubility could be marketed and displace other commercial polymorphs of the same API. Many examples in recent years, such as the Zantac or Cefadroxil cases (involving huge amounts of money) highlight the importance of having a deep knowledge of the polymorphic landscape during the development of a new drug. This is particularly relevant since generics started to be commercialized.

3. Examples of applications

In this section, we show some case studies conducted in our facilities which briefly illustrate the key topics of crystal engineering in reference to the pharmaceutical industry and new materials.

3.1. Norfloxacin

This API is a synthetic broad antibacterial fluoroquinolone compound used in the treatment of gonorrhea, prostate and urinary tract infections [10].

3.1.1. Anhydrous forms of Norfloxacin. The polymorphism screening on Norfloxacin conducted in our laboratory revealed the existence of up to three different anhydrous forms [11]. These three forms were characterized by means of X-ray Powder Diffraction (XRPD) (Fig. 4) and DSC (Fig. 5).

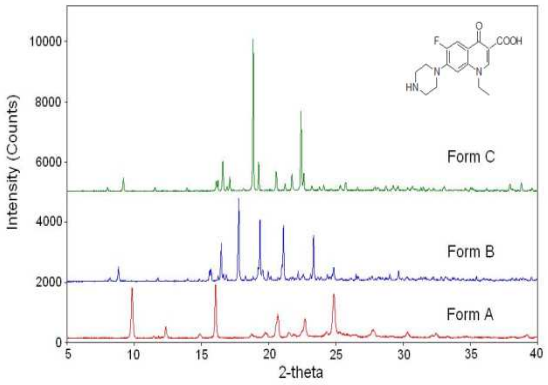

Figure 4: XRPD of forms A, B and C of Norfloxacin

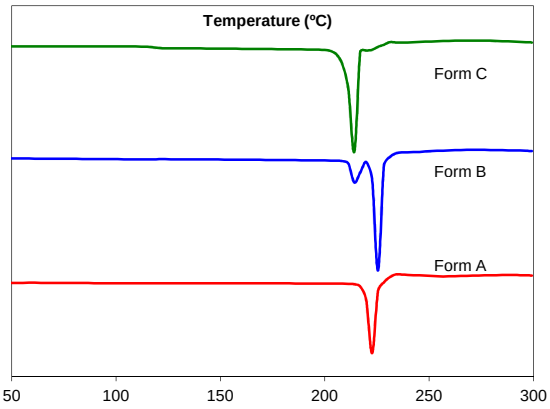

Figure 5: DSC thermograms of forms A, B and C of Norfloxacin

Form A is the higher melting form (219ºC) and form C melts at 207ºC. On the other hand, the DSC thermogram of form B shows the melting endothermic process of form B followed by an exothermic process (crystallization of the higher melting form A, the most stable at melting temperature) which happens simultaneously, being the net heat flow smaller than the expected for the melting of form B. Finally, melting of crystallized form A occurs. Occasionally, samples of pure polymorph B show endothermic solid-solid transition of form B to form A, followed by melting of remaining form B and subsequent melting of form A (Fig. 6).

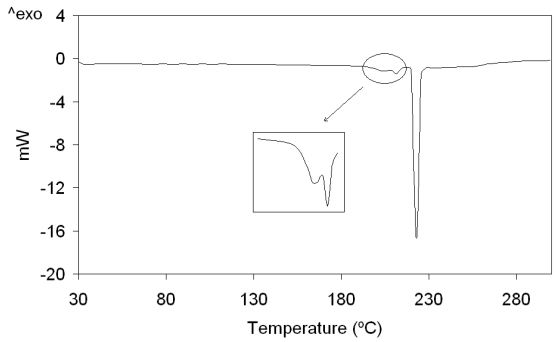

Figure 6: DSC of form B showing rare occasions when the sample underwent partly a solid-phase conversion at 196 ºC before melting

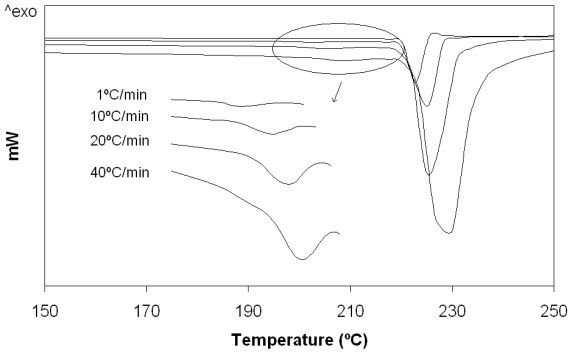

Figure 7: DSC of form A mixed with small amounts of form B, recorded at the heating rates of 1-40 ºC/min

When polymorph A is mixed with small amounts of polymorph B, an endothermic phenomenon is observed at 196 ºC in a DSC experiment at 10 ºC/min, followed by melting of form A. Heating rate influences the onset temperature of the first endotherm whereas the onset temperature of the melting of form A is not affected (Fig. 7), thus confirming that the first endotherm is a solid-solid transition.

It is of practical interest to know the relative thermodynamic stability of all forms. The main questions to solve are whether two polymorphs are monotropically (one form is more stable than the other at any temperature) or enantiotropically (a transition temperature exists, below and above which the stability order is reversed) related, and for an enantiotropic system, where transition

temperature lies. According to the "heat of transition rule" of Burger and Ramberger [12], forms A and B are enantiotropically related. Based on physicochemical data, a semi-schematic energy/temperature diagram was constructed in order to display the thermodynamic relationship of the three polymorphs at different temperatures (Fig. 8).

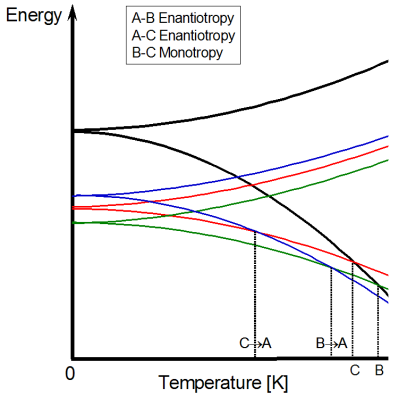

Figure 8. Semi-schematic energy/temperature diagram of Norfloxacin.

3.1.2. Hydrates of Norfloxacin. Pharmaceutical hydrates are important due to the presence of water molecules in so many pharmaceutical drugs, which affects to a variety of physical and chemical properties such as the stability, solubility and dissolution rate. Usually, hydrates are less soluble than their anhydrous forms because the interaction between the compound and the water molecules confers an extra thermodynamical stability [13]. Norfloxacin is an example which contradicts that general rule because the hydrated forms are more soluble than the anhydrous one. This implies that the hydration process plays an important role in influencing the bioavailability of Norfloxacin and it has made its hydrates an interesting object of study.

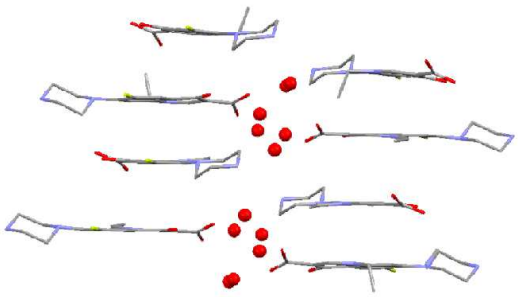

Figure 9: Water molecules forming channels in the crystal structure of form II

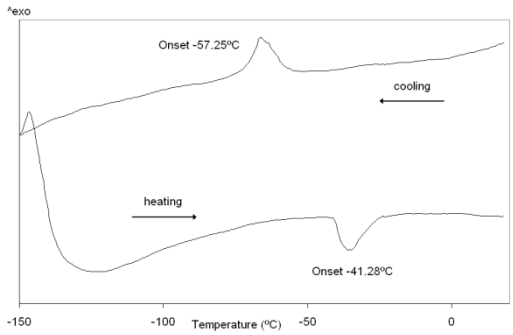

Figure 10: Cooling-heating DSC experiment, where the reversibility of the solid-solid transition of NF sesquihydrate can be observed

During this study, two polymorphs of Norfloxacin sesquihydrate were discovered and their crystal structures solved, one of them at low temperature [14] (Fig. 9). Taking into account that there could be a possibility for a phase transition while cooling, we decided to perform a DSC experiment cooling from room temperature to -150ºC and heating from -150ºC to room temperature. As it can be seen in Figure 10, a reversible solid-solid transition was observed at -57ºC while cooling and at -41ºC while heating. This experiment allows us to establish the relative thermodynamic stability between both forms, which is a matter of great relevance. According to the heat of transition rule forms I and II are enantiotropically related, being form I the most stable at room temperature and form II the most stable under approximately -40ºC. It was also possible to study the reversible phase transition of form I to form II by means of thermomicroscopy (Fig. 11).

Moreover, the variable temperature XRPD experiment demonstrates that form I of NF sesquihydrate undergoes a phase transformation into form II while cooling down (Fig. 12).

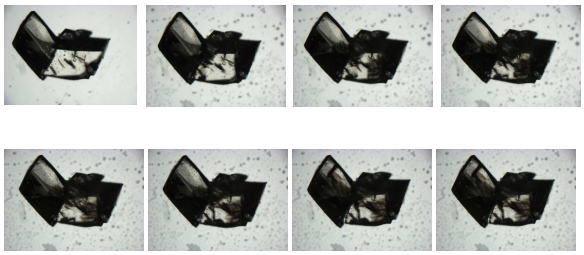

Figure 11: Photomicrographs of NF Sesquihydrate in polarized light.

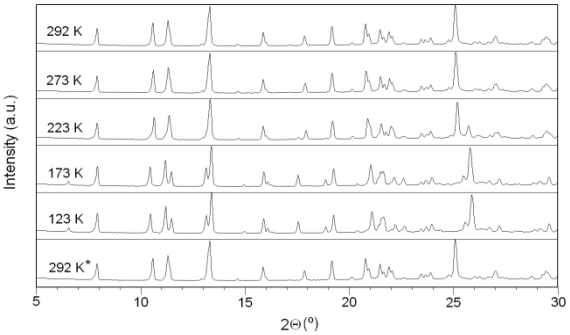

Figure 12: Variable XRPD of NF sesquihydrate showing the phase transition from form I to form II

ChT.1

3.2. Ziprasidone

Ziprasidone is a poorly soluble drug in water, a factor that unfavorably affects its bioavailability [15]. Ziprasidone, an antipsychotic agent useful for the treatment of psychotic disorders of the schizophrenic types [16], is marketed under the name GEODON as an oral capsule and as an injectable drug. GEODON capsules contain the monohydrate hydrochloride salt of ziprasidone, whereas GEODON for injection contains ziprasidone mesylate trihydrate. The need for improved water soluble forms of ziprasidone has been recognized during the last years. Salts are usually employed for increasing aqueous solubility [17].

It is commonly accepted that the formation of a stable salt requires a difference of at least three units between the pK_a value of the ionisable group and that of the counterion [18]. So, we selected a range of acids according to this information. A microscale screening allowed us to discard some acids from the selected list before completion of the study because no salt was isolated from these acids. Next, a screening at a larger scale was developed with the remaining acids. The obtained salts were characterized by DSC, XRPD, IR and ^{1}H-NMR. Additionally, the aqueous solubility of these salts was determined in order to compare the data obtained with the previously known solubilities of hydrochloride and mesylate salts [19]. Results are reported in table 1.

Table 1 Aqueous solubilities of ZP salts by HPLC at 25ºC

Salt	Aqueous solubility (μg/mL)[a]
Free base	0.3
Hydrochloride	80
Mesylate	1000
Phosphate	28
Citrate	30
Fumarate	55
Oxalate	236
Isethionate	1121
Malate	475

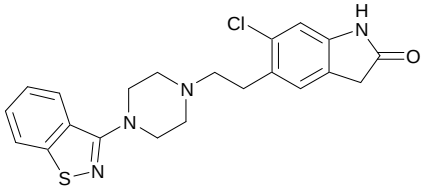

[a]Solubility values indicate the weight in μg of Ziprasidone calculated as the free base, per mL of water.

As it can be seen, isethionate salt is the one with the highest solubility. However, the appearance of coloured impurities during its isolation together with the poor recovery forced us to reject this salt. Then, our efforts were directed towards the malate salt as the selected target for further studies due to its good solubility. Moreover, malic acid is generally regarded as safe (GRAS) by the Food and Drug Administration (FDA) and has previously been used in FDA-approved marketed drugs.

The malate salt of ZP was found to exist in three anhydrous crystalline forms. Each form was characterized by means of DSC, XRPD, IR and ^{1}H-NMR spectroscopy. The aqueous solubilities of the ZP malates were also evaluated (table 2). Interestingly, forms B and C show an improved, highly solubility value of 989 and 1084 µg/mL respectively, if compared to malate form A. In addition, these solubility values are in the same range as that of mesylate. In this sense, malate salts of ZP are good candidates for further pharmaceutical development.

Table 2 Aqueous solubilities of the malate salts of ZP by HPLC

Salt	Aqueous solubility (µg/mL)[a]
Malate form A	475
Malate form B	989
Malate form C	1084

[a]Solubility values indicate the weight in µg of ziprasidone calculated as the free base, per mL of water

ChT.1

3.3. Triphenylglycol

(*S*)-triphenylglycol is a chiral auxiliary reagent which has found wide application in asymmetric aldol additions and ester enolate imine condensations. It has been used also in synthesis of natural products and biological active compounds. Furthermore it has applications as a chiral solvating agent in NMR spectroscopy [20]. In order to explore the possible polymorphic behaviour of triphenylglycol, we decided to study by thermal analysis the amorphous form obtained from quenching the melt, instead of performing classical crystallizations methods [21]. Interestingly, the heating of the amorphous form in a DSC experiment shows a collection of crystallization and melting phenomena demonstrating the complex polymorphic system (Fig. 13). From the glassy state (glass transition at 32 ºC) form D crystallizes first and melts (mp 72 ºC) with crystallization of other phases. With continuous heating, forms E (mp 110 ºC), F (mp 116 ºC), B (mp 119 ºC) and A (mp 127 ºC) melt successively. It has been found that a heating rate of 10 ºC/min must be applied in order to observe the maximum number of polymorphs in a DSC experiment. Lower heating rates lead to the crystallization of fewer forms whereas higher heating rates are not suitable due to a loss in the resolution. The cooling rate during quenching seems to have no influence on the result.

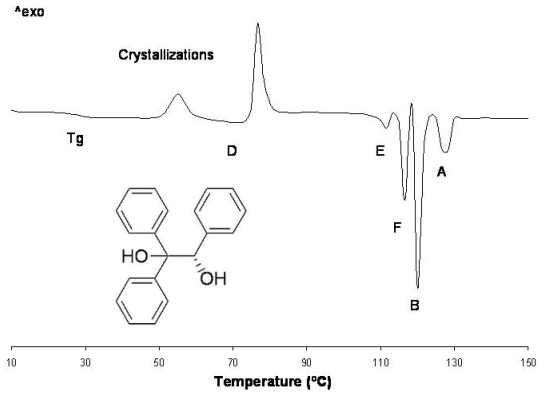

Figure 13: DSC of a quenched from the melt sample.

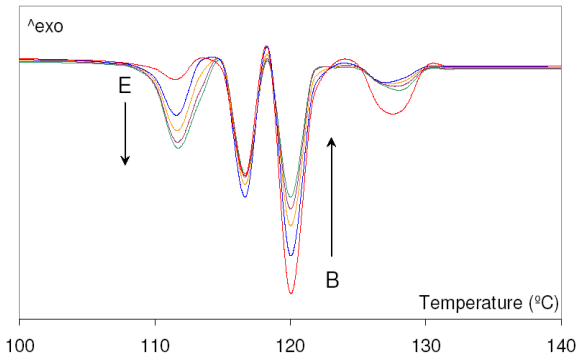

Figure 14: DSC of five successive heating/cooling cycles.

Since we were not able to isolate forms D, E and F by conventional crystallization methods, we explored alternative approaches in view of the observed thermal behaviour by DSC. After some heating/cooling cycles (Fig. 14) starting from form A in a DSC (heating rate 10 ºC/min), form E grows at expenses of form B. Crystallization of the various polymorphic forms are time and temperature dependent, and a thermodynamic/kinetic competition in the crystallization of the different forms from the melt is observed. This can be explained by some kind of kinetical amplification process leading to the metaestable form E. After four cycles, the relative intensities of

all forms remain invariable. This suggests that form E is the first crystallizing form which transforms into the other three forms by crystallization from the melt during heating.

3.4. Dibenzylsquaramide

Secondary squaramides are a family of synthetic compounds that exhibit interesting and useful properties as supramolecular synthons. Previous studies of secondary squaramides in solution demonstrate that these compounds can exist in several conformations due to the partially restricted rotation of the C-N bond (anti/anti and anti/syn conformers) [22]. We have studied the solid state behaviour of secondary squaramides in order to establish relations between the aforementioned properties and their possible polymorphism.

In this example we have chosen dibenzylsquaramide (DBZSQ) as the model compound to explore its possible polymorphic behaviour [23]. In order to obtain as many crystal forms as possible a polymorphic screening was carried out. DBZSQ is only soluble in polar media such as dimethyl formamide (DMF) and dimethyl sulfoxide (DMSO). Therefore different combinations of those solvents with polar and non polar antisolvents were tested at several concentrations and temperatures, with variable cooling rates, in both thermodynamic and kinetic conditions, revealing a polymorphic system consisting of three polymorphs according to their different X-ray patterns.

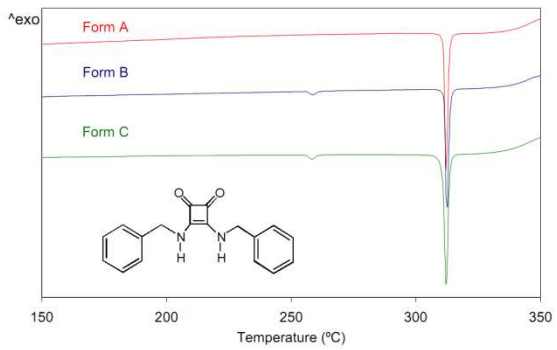

Figure 15: DSC of a quenched from the melt sample.

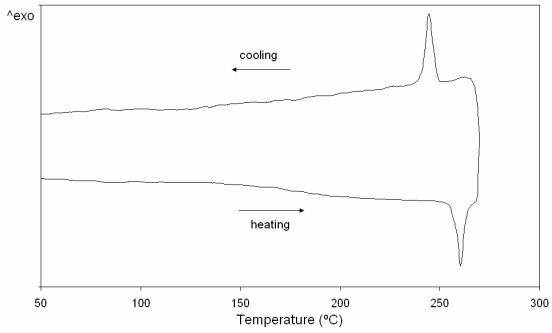

Figure 16: DSC of five successive heating/cooling cycles.

The DSC analysis of the three forms show the same sharp endothermic phenomenon at 311ºC but two of them also show a low intensity broad endothermic phenomenon at 257ºC (Fig. 15). Variable heating rates confirm that the first phenomenon is a solid-solid transition, with the second one being a melting process. This can be interpreted in the following manner: two forms (B and C) transform during the DSC analysis in the same polymorph (A) which melts at 311ºC.

Curiously, the transition temperature is observed around the same value in all the cases. Although several polymorphs can present the same melting value (e.g. conformational polymorphism), to the best of our knowledge this is the first time that two forms share the same transition temperature. Therefore, a misleading interpretation of this system could be concluded if based only on the DSC analysis.

According to the heat of transition rule [12] forms B and C are enantiotropically related to form A. This means that form A is a metastable form at room temperature. In addition, the reversibility of the solid transition could be observed in both cases by a heating-cooling DSC experiment (Fig. 16). Both forms B and C return to form B after cooling (confirmed by XRPD).

All the examples reviewed highlight the necessity of a multidisciplinary approach to solve a polymorphic problem or to design new crystal structures. Scientists from diverse areas such as physical-organic chemistry, supramolecular chemistry, physics or X-ray diffraction spectroscopy usually work together in ambitious research projects looking for new crystalline solids with improved properties.

References

[1] Desiraju G.R. 2007, *Angew Chem Int Ed* **46** 8342-8356.
[2] Shan N., Zaworotko M.J. 2008, *Drug Discovery Today* **13** 440-446
[3] Bernstein J. 2002 *Polymorphism in Molecular Crystals*, Oxford Science Publications, Oxford
[4] Schultheiss N., Newman A. 2009, *Crystal Growth & Design* **9** 2950-2967
[5] Lee A.Y., Erdemir D, Myerson A.S. 2011 *The Annual Review of Chemical and Biomolecular Engineering*
[6] Giron D., Mutz M., Garnier S. 2004 *Journal of Thermal Analysis and Calorimetry* **77**, 709-747
[7] Griesser U. J., Weigand D., Rollinger J. M., Haddow M., Gstrein E. 2004 *Journal of Thermal Analysis and Calorimetry*, **77**, 511–522
[8] Lara-Ochoa F., Espinosa-Pérez G. 2007, *Crystal Growth & Design* **7** 1213-1215
[9] Musumeci D., Hunter C. A., Prohens R., Scuderi S., McCabe J. F. 2011 *Chem. Sci*., **2**, 883-890
[10] Mazuel C. 1991, *Analytical Profiles of Drug Substances* **20** 557
[11] Barbas R., Prohens R., Puigjaner C. 2007, *Journal of Thermal Analysis and Calorimetry* **89** 687-692
[12] This rule states that if an endothermal transition (for a solid-state conversion) is observed at some temperature, it may be assumed that there is a transition point below it; i.e., the two forms are related enantiotropically
[13] Khankari R.K., Grant D.J.W. 1995, *Thermochimica Acta* **248** 61-79
[14] Puigjaner C., Barbas R., Portell A., Font-Bardia M., Alcobé X., Prohens R. 2010, *Crystal Growth & Design* **10** 2948-2953
[15] Turczyn E., Cieplucha A., Khan Z., Wloch T., Dyba R. 2007, *PCT Int. Appl.* WO 2007126322
[16] Caley C.F., Cooper C.K. 2002, *Annals of Pharmacotherapy* **36** 839
[17] Srivijaya R., Vishweshwar P., Sreekanth B.R., Vyas K. 2008 *CrystEngComm* **10** 283
[18] Bastin R.J., Bowker M.J., Slater B.J. 2000, *Org. Process. Res. Dev.* **4** 427
[19] Portell A., Barbas R., Font-Bardia M., Dalmases P., Prohens R., Puigjaner C. 2009, *CrystEngComm* **11** 791-795
[20] Ridder D., Wunderlich H., Braun M. 1998 *Eur. J. Org. Chem.* 1071; Braun M., Sacha H., Galle D., Baskaran S. 1996 *Pure Appl. Chem.* **68** 561
[21] Barbas R., Polito M., Prohens R., Puigjaner C. 2007, *Chem.Commun.* 3538-3540
[22] Rotger M.C., Piña N., Frontera A., Martorell G., Ballester P., Deyà P.M., Costa A. 2004 *J. Org. Chem.* **69** 2302-2308
[23] Portell A., Barbas R., Braga D., Polito M., Puigjaner C., Prohens R. 2009 *CrystEngComm* **11** 52-54

Raman spectroscopy as a powerful analytical tool: probing the structure of matter

Tariq Jawhari

Unitat d'Anàlisi Molecular, CCiTUB, Universitat de Barcelona. Lluís Solé i Sabaris, 08028 Barcelona, Spain.

email: *jawhari@ccit.ub.edu*

Abstract. This article reviews the basic principles and instrumentation of Raman spectroscopy, discusses its advantages and limitations and gives examples of applications that illustrate the capabilities of the technique.

1. Introduction: some historical features

We shall see, in this contribution, the enormous possibilities that offer Raman Spectroscopy when identifying not only molecules but also in determining its structure and properties. So the obvious question that immediately arises is why, if Raman spectroscopy is such a powerful analytical technique, the method was for nearly half a century, mainly restricted to academic and research groups? Well, in fact, this is not totally exact: immediately after that Chandrasekhara Venkata Raman discovered in India in 1928 this new scattering effect, the method was enormously and uncommonly used during more than 10 years, founding the basis of molecular spectroscopy. Infrared spectroscopy (IR), the other fundamental molecular spectroscopy, which was discovered during the 19th century, was mainly restricted to some few laboratories due to some huge instrumental difficulties at this time. Soon after Raman published this new scattering phenomenon, obtained with a ridiculous simple experimental set-up†, many groups over the world began to record Raman spectra: 58 publications appeared in the same year of the discovery and more than 2500 compounds were studied in less than 10 years!

However, this initial momentum of research stopped at the end of the 2nd World War when the first commercialized infrared spectrometers using photoelectric detectors were presented, as a result of an initiative of the US Government to produce a batch of infrared spectrometers for special government projects. During the next 20 years, Raman spectroscopy became a technique limited to some fundamental research in the academic world. The renaissance of Raman spectroscopy began in the sixties with the discovery of the laser: laser is the ideal source for Raman experiments since it provides highly intense monochromatic coherent radiation, with well defined polarization in a narrow non-diverging beam which can be focused to a diffracted limited spot. In the 70's, the typical Raman spectrometer consisted of a laser, a double-grating monochromator, which allows to diminish drastically the straight-light, and photo-multipliers tubes (PMT), which improve the detection of weak signals. In 1974, the first Raman microscope was presented separately in Lille (France) and at National Bureau of Standards (Washington).

During the last 25 years, the huge improvement made in instrumentation, mainly in compact air-cooled solid state lasers, holographic notch and edge filters to eliminate the strong laser line and high quantum efficiency and low-noise detectors such as charge-coupled devices (CCD), improved both the sensitivity and the simplicity of the Raman systems and opened the applications of Raman spectroscopy to many new fields of science. Raman spectroscopy which was basically known as a technique restricted to research labs, started to penetrate into the industrial world.

In the mid-80's, the first Fourier Transform (FT) Raman instruments began to appear in the

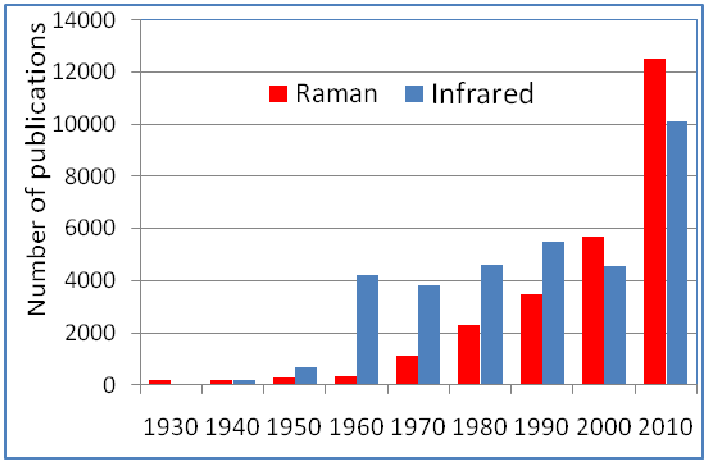

man and infrared
shed over the last
ata obtained with
arch program**).**

† The first experiment was obtained in February 1928 in Calcutta, using the sun as a source, a filter, a prism and the eyes as a detector. Two weeks later, the experiment was improved introducing an Hg-arc as a source and a photographic plate to record these new lines, in order to confirm these initial results, which were published in Nature on April 21 of the same year!!! Soon after Rutherford ranked the Raman effect as one of the best three discoveries in experimental physics in the decade and 2 years later, the Nobel's prize was conceded to Raman, the first Asian fellow to receive it.

market. Few years later, Raman instruments coupled with optical fibres, Raman mapping spectrometers and confocal Raman microscopes were offered. Nowadays both complex and large Raman instruments working with 4 or 5 lasers, in the ultraviolet (UV), visible and Near infrared (NIR) with a triple grating monochromator or very small miniaturized systems that can fit in a bag and can be used outdoor, are commercially offered. Finally, the evolution of Raman spectroscopy over the last 80 years can be followed, in table 1, by comparing the numbers of publications including "infrared" and "Raman" entries, respectively.

2. The Raman effect

When monochromatic radiation of frequency ν_0 is passed through a transparent medium, most of it is transmitted, some of it is absorbed and a small amount is scattered (less than 10^{-5} of the intensity of the exciting source). Most of this scattered light is at the same frequency as the incident radiation (called elastic o Rayleigh scattering) whilst a very small amount (10^{-3} to 10^{-4} of the Rayleigh intensity) is scattered at a frequency higher or lower than that of the incident radiation. It is this inelastic scattering that is referred as Raman Scattering.

Molecules are continuously vibrating. Both Raman and infrared spectroscopy detect and analyze the energy of the different vibrations that take place in the molecule, which will produce a spectrum. Every molecule or crystal has its own specific and unique Raman/IR spectrum. The way in which radiation is employed in Raman and infrared spectroscopy is different: in infrared spectroscopy a whole range of radiation, covering all IR spectrum, is directed onto the sample and absorption takes place when the frequency of the radiation matches precisely that of the vibration. In contrast, Raman spectroscopy uses a single frequency source to irradiate the sample and it is the scattered light from the molecule which is detected in the Raman experiment. The Raman scattering process can be easily explained by a simple quantum mechanical description (see figure 1): a photon of energy $h\nu_0$ colliding with a molecule can either be scattered elastically (Rayleigh)

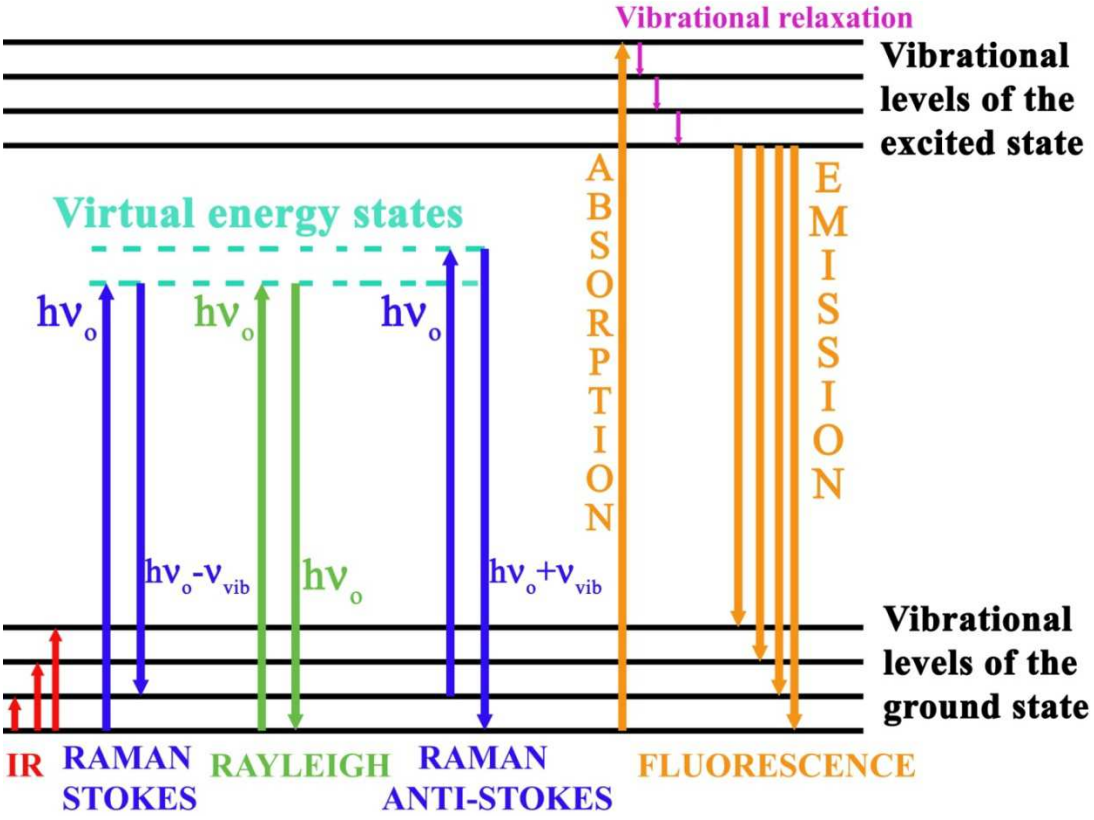

Figure 1: Vibrational and electronic energy-level diagram of a molecule showing the processes of IR absorption, Raman and Rayleigh scattering and fluorescence emission.

or inelastically (Raman). In the latter case, the collision with photons induces the molecule to undergo a transition between two vibrational energy levels of the molecule and the resulting scattered radiation has a different frequency than the incident photon. If during the collision, the molecule gains some energy $h\nu_{vib}$, the photon will be scattered at the frequency $h\nu_0 - h\nu_{vib}$, which is referred to as Stokes Raman scattering. Conversely, if the molecule loses some energy by relaxing from an excited vibrational level to the ground state, then the scattered energy will be at $h\nu_0 + h\nu_{vib}$, i.e. anti-Stokes Raman scattering[†]. Raman spectra are usually represented in wavenumbers shift (ν_{vib}), relative to the excitation line. The advantage of using such a shifted scale is that it allows working with a spectrum that gives directly the frequency of the molecular vibrations.

The relative intensities of the two processes depend on the population of the various states of the molecules, which is given by Boltzman distribution. At room temperature, the probability to have molecules in an excited vibrational state is low, therefore anti-Stokes scattering will be weak compared to Stokes intensity, and will become weaker as the frequency of the vibration increases (see Figure 2). This is why the Raman spectrum is usually limited to the Stokes region. In some cases, both Stokes and anti-Stokes band intensities are measured in order to determine the temperature *in situ* at the microscopic level in some specific positions of the sample.

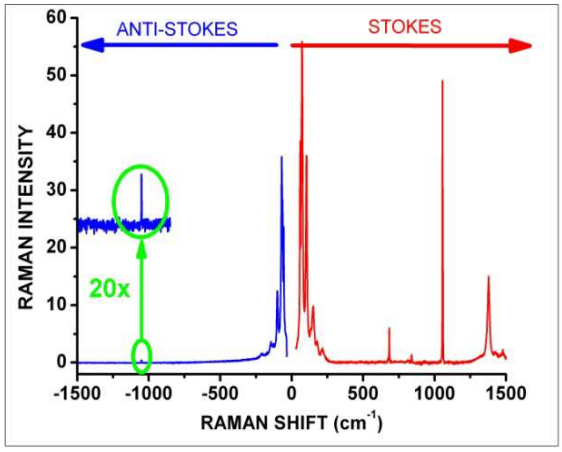

Figure 2: Stokes and anti-Stokes Raman spectra of cerussite ($PbCO_3$)

3. Instrumentation

Due to the immense technological advances in the last 20 years, many types of Raman instruments, from very large systems to miniaturized ones, working in different ranges of the spectrum, are found in the spectroscopy market. Very often, the difficulty for non specialist Raman users, is to decide what type of Raman instruments and conditions should be used for different kinds of samples or experiments. Basically, a Raman spectrometer is made of 4 main parts: a laser source, an optical system to illuminate the sample and collect the Raman signal, a "dispersive" system and a detector.

One of the most typical collecting systems is the so-called back-scattering geometry where the laser light is focused with the collection lens onto the sample and the scattered Raman collected by the same lens system and sent to the entrance slit of the spectrometer. Another possibility is to recollect the scattered light at 90°. The Raman microscope is a special back-scattering illumination-collecting system, where a typical optical microscope is used to both visualize and focalize the laser onto a microscopic region of the sample and to recollect the Raman signal. The dispersive system, which is a fundamental part of the spectrometer since it discriminates the weak Raman scattering from the intense laser line, is usually formed of several holographic gratings. Nowadays, the CCD is the typical detector used for Raman spectrometers. These detectors are often cooled at liquid nitrogen temperature in order to decrease the noise permitting therefore the detection of very weak signals.

More compact systems and miniaturised Raman instruments use filters technology with only one short focal length grating, often combined with optical fibres. These much cheaper instruments,

[†]During his studies on fluorescence in the mid-19th century, Sir G. Stokes postulated that the wavelength of a radiation emitted through a process of fluorescence is always higher than the excitation source wavelength. By analogy, the Raman lines are named Stokes and Anti-Stokes.

have a lower spectral resolution but are much more robust, easy to use and can be truly portable (i.e. dimension as low as 4"x2"x2").

Another type of Raman instrument is the Fourier Transform FT-Raman system, which uses the Michelson interferometer, instead of a dispersive unit, with a NIR source and an InGaAs detector [1]. FT-Raman and FTIR instruments can be very easily coupled which allow getting, with a unique system, a complete vibrational description of materials.

Nowadays, Raman microscopy is a very demanded and popular technique and most of the spectrometers proposed on the market are now furnished with an optical microscope. Such evolution is probably explained by the great advantage that the micro-Raman method offers to the microspectroscopist: it is possible to look at extremely small samples and get structural information at the submicrometric level. In fact, Raman microscopy is the method that offers the highest spatial resolution (both lateral and axial) of all molecular spectroscopies.

4. Advantages and limitations of Raman spectroscopy

4.1. Advantages

Raman spectroscopy is a practical method that offers a large series of advantages:

- No sample preparation; all types and sizes of samples can readily be analyzed as received.
- Very high spatial resolution ($\approx 0.5\mu m$) and very little sample required ($\approx 10^{-9}$ l or $\approx 10^{-12}$ g).
- Glass does not interfere with Raman spectrum thus traditional optics are suitable for Raman spectroscopy; simple accessories can be easily adapted for Raman measurements such as temperature and pressure cells, reactors for in-situ experiments, optical fibres for remote analysis.
- Common glass recipients such as vials or capillary tubes are used for solids, powder, liquids and gases. Plastics, quartz and even amber container, that can be sealed, can be utilized.
- Raman spectrum of water is weak which allows vibrational studies of aqueous solutions.
- The whole vibrational spectrum from 5 cm^{-1} to 4500 cm^{-1} is readily obtained which gives both information of the lattice modes at very low frequencies and internal modes.
- Standard Raman systems now offer the possibility to record both Raman and photoluminescent measurements in the UV, visible and near-infrared.
- Raman bands are usually well defined and resolved and the baseline is quite flat (if no fluorescence occurs) which makes the technique very powerful for structural characterization.
- Raman intensity is proportional to concentration therefore quantitative analysis is relatively simple.
- The possibility to couple optical fibres to Raman spectrometers has been largely used for remote in-process control and monitoring especially in industrial plants where the quality control laboratory is often separated from the process line.

4.2. Drawbacks

Basically, Raman spectroscopy has only one major limitation, but it is of considerable matter: Raman scattering is extremely weak[†]! As a result, the technique was known to be a complicated method when analyzing low concentration mixtures (below 1%) and material that fluoresces or samples with fluorescing impurities, since the large fluorescence background will strongly interfere with Raman signal. Fortunately, the new Raman systems with several laser sources permit to avoid fluorescence. Further, the recent technological developments of methods that increase the efficiency of Raman signal such as Raman resonance or surface enhanced Raman spectroscopy (SERS) have been successfully applied to detect and identify traces of chemical contaminants.

[†]Raman scattering cross section~$10^{-31}cm^2$; Infrared absorption cross section~10^{-18} cm^2; Fluorescence cross section~$10^{-15}cm^2$

5. Applications of Raman spectroscopy

In this part we shall review the different types of information on the microstructure and physical parameters of the condensed matter that can be obtained from the Raman spectrum:

5.1. Frequency

The frequency of the Raman band depends on the masses and positions of the atoms, the interatomic forces (i.e. force constants of the bonds) and the bond length. Therefore, any effects altering these features will produce a change in the frequency of the band. For instance, this is the reason why the band position is sensitive to the presence of stresses or strains: a tensile stress will determine an increase in the lattice spacing and, hence, a decrease in the wavenumber of the vibrational mode. In the case of compressive strain, the decrease of the lattice parameter yields a corresponding increase of the vibrational frequency. If the deformation of the structure follows an elastic behaviour, the shift will vary linearly with the magnitude of the stress, and as a result, the position of the Raman band can be used to measure the stress. It is well known that sharp Lorentzian band at 520 cm^{-1} of the first order Raman spectrum of crystalline silicon is quite sensitive to the presence of stress. For a biaxial stress in elastic regime, the stress $\boldsymbol{\varepsilon}$ in silicon can be obtained from

$$\boldsymbol{\varepsilon} = 250\ \boldsymbol{\Delta\nu}\ \text{Mpa/cm}^{-1},$$

where $\boldsymbol{\Delta\nu}$ is the Raman shift in wavenumber. Since the fabrication processes of semiconductors devices often produce strains in some localized microscopic regions, the Raman microprobe was found very useful in analyzing these micro-domains. This technique is now recognized as a powerful tool in identifying stress and strain in polycrystalline silicon structures used for the fabrication of large polysilicon micromechanical structures. These micromechanical systems based on surface-micromachining technologies can have serious stress effects that can cause mechanical device failure, curling or fracture, therefore, the micro-Raman system can be used as a quality control method and to improve several technological parameters.

Further, the presence of crystalline disorder also produces changes in the frequency of the band, usually towards lower wavenumbers. These are related to the breaking of translational symmetry in the crystal, which can be due to structural defects such as grain boundaries in nanocrystalline materials or dislocations. The position and shape of the Raman band can be simulated with a correlation length model [2] which allows to estimate the value of the correlation length **L**. **L** is defined as the characteristic size of crystalline domains where the translational symmetry of the crystal holds, and is related to the average grain size for nanocrystalline materials or to the average distance between defects for damaged crystals.

The presence of chemical impurities in the crystalline network may also give rise to changes in the mass of the atoms in the lattice sites which will shift the phonon frequency. For example, the presence of Ge atoms at substitutional positions in the silicon network produces a decrease in the frequency of the vibrational modes, due to a higher mass. This is known as the chemical effect and it has been used to characterize heteroepitaxial layers. For instance, the Raman spectrum of a typical $SiGe_x$ alloy, as shown in Figure 3, presents three main bands, related to Si-Si, Si-Ge and Ge-Ge vibrational modes. The wavenumber of these modes follows a linear relationship with both chemical composition and strain [3]:

$$\boldsymbol{\nu}_{\text{Si-Si}} = 520 - 68\ \mathbf{x} - 830\ \boldsymbol{\sigma}$$
$$\boldsymbol{\nu}_{\text{Si-Ge}} = 500.5 + 14.2\ \mathbf{x} - 575\ \boldsymbol{\sigma}$$
$$\boldsymbol{\nu}_{\text{Ge-Ge}} = 282.5 + 16\ \mathbf{x} - 384\ \boldsymbol{\sigma}$$

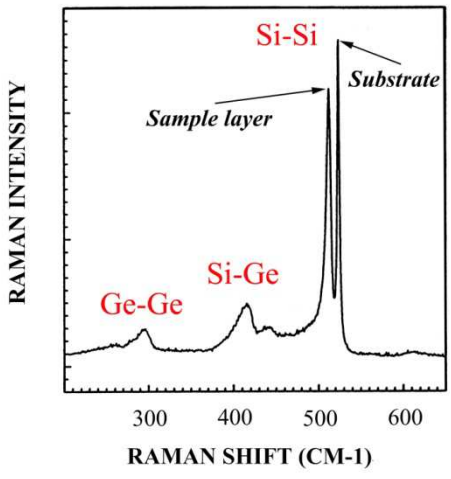

Figure 3: Raman spectrum of $SiGe_{0.3}$

where **ν** is the wavenumber of the Raman mode, **x** the chemical composition and **σ** the strain parallel to the substrate. Using these relationships, a single Raman spectrum of $SiGe_x$ allows the determination of silicon and germanium contents as well as strain. Similar relationships have also been proposed for SiC_y as well as for more complex $SiGe_xC_y$ and $SiGe_xB_y$ ternary alloys [4].

5.2. Raman bandwidth

Raman bandwidth and bandshape are closely related to the crystalline order. In principle the bandwidth is related to the lifetime of the phonons. The presence of crystalline disorder produces a decrease of the phonon lifetime which thus generates an increase of the bandwidth. Therefore the density of defects can be evaluated from the bandwidth.

On the other hand, the bandshape of the Raman line is also affected by confinement of phonons being that given by the correlation length model [2]. This model allows the estimation of both the correlation length **L** and the average stress. This is interesting when studying nanocrystalline materials since the average grain size is given by **L**. The main limit for this measurement is that phonon confinement only occurs for sizes in the nanometric range (**L** < 20nm for silicon). The changes in the bandshape and position of the Raman band related to phonon confinement permits the assessment of the average grain size and stress in nanocrystalline Si layers [5], as well as the density of defects in highly damaged Si films [6]. Figure 4 shows the spectra simulated for Si assuming spherical confinement and different values of the correlation length.

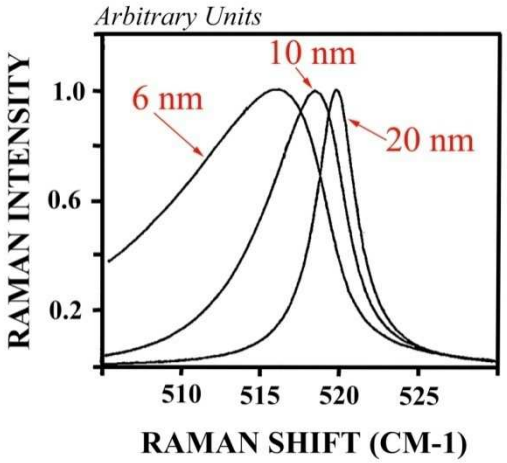

Figure 4: Simulation of silicon first order phonon mode assuming a spherical confinement L of 6 nm, 10 nm and 20 nm, respectively.

5.3. Raman intensity

The intensity of the Raman band is also very sensitive to the structure of crystals and as a result significant information can be obtained from intensity measurements. Damage in the lattice leads to a decrease of the intensity of the Raman modes, related to the breaking of bonds and changes in atomic forces displacements, and, hence produces a decrease of the Raman polarizability tensors. For instance, typical ion bombardment during doping process will alter the original crystal with a consequent reduction of the Raman signal intensity. The measurement of the Raman band intensity has therefore been applied to quantify the residual damage in processed wafers, such as ion implanted structures. Figure 5 shows an example on the quantification of the implanted induced damage in wafers of 6H-SiC (a hexagonal polytype of SiC) implanted with different doses of Ge+ ions [7]. This is determined through the normalised intensity In=(Io-I)/Io, where I is the intensity of the Raman band measured in the implanted layer and I_o is the intensity of the Raman band measured in a virgin non-processed sample. For a low degree of damage, I is very similar to I_o and I_n is close to 0. As damage increases, I decreases and $I_n$tends to the maximum value of 1. This last value gives a 100% of

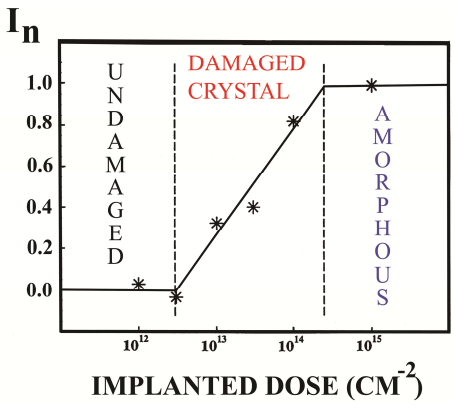

Figure 5: Relative micro-Raman intensity of the Longitudinal Optical mode of 6H-SiC versus the implantation dose

damage which corresponds to the damage level for which fully amorphization of the implanted layer occurs. In this case, all the crystalline modes vanish from the spectrum, and I becomes 0. This method permits to check the degradation of the crystalline structure and is also used for optimizing annealing process after ion implantation in order to eliminate the induced damage.

Intensity measurement is also performed for quantitative analysis of different polymorphisms, defects, disorder, micro-inhomogeneities, etc. Micro-Raman mapping measurements can also be carried out in order to determine, in a non destructive and simple way, the thickness and structural uniformity of thin films, such as cobalt silicide films ($CoSi_2$) deposited on Si used for IR detectors technology [8]. This was obtained by measuring the intensity of the Raman signal from the Si substrate at different points on the surface. As can be seen in Figure 6, the intensity of the Raman line of the substrate decreases in an exponential way, as the thickness of the layer increases. This is due to absorption of light in the layer. This method allows detection of $CoSi_2$ films as thin as 3-4 nm, and the $CoSi_2$ film thickness can be measured in the range between 10 and 100 nm with an uncertainty below 10%. More applications of Raman microspectroscopy on semiconducting materials can be found in Refs. [9-11].

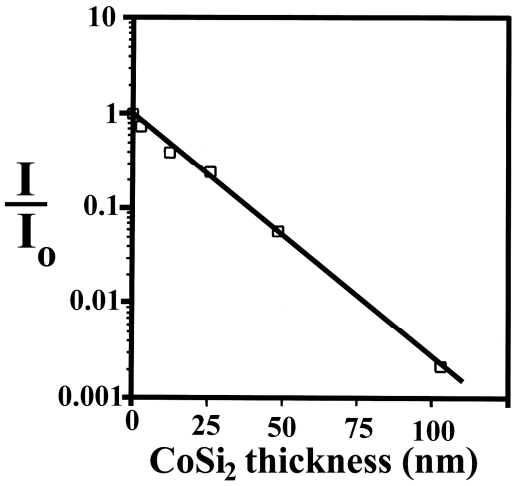

Figure 6: Relative Raman intensity of the 1st order Si mode in function of $CoSi_2$ layer thickness.

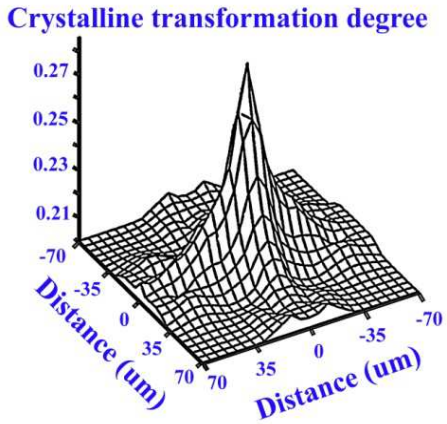

Figure 7: three-dimensional map showing the variation of the crystalline transformation degree along the Vickers micro-indentation.

Raman microscopy has been used to analyze at the molecular level polymeric materials submitted to different types of stresses in order to get a more complete understanding of the process of deformation in these samples. For example, the distribution of stress in the residual deformed micro-region produced by a process of microindentation in both poly(3,3-dimethyl oxetane) (PDMO) and polyvinylidene fluoride (PVF_2) was examined using the Raman microprobe [12-14]. Although the microhardness test, which basically consists in the impression of a microindenter of known geometry on the surface of the sample to study, is widely used for measuring the strength of materials, it remains one of the least fundamentally understood mechanical-analysis methods. The main reason for the lack of information about the process of deformation during the application of an indenter in a material is the difficulty of detecting experimentally the effects of the process of microindentation inside and around the impression. Micro-Raman spectroscopy is one of the few methods that enable to analyze structural changes along the microindentation without requiring any sample preparation that would alter the microstructure in the zone of interest. PVF_2 present a crystalline transformation, from the non planar (TGTG') conformation [form II(α)] to the planar zigzag (TTTT) structure [form I(ß)], that is sensitive to the degree of stress submitted to the sample. The crystal transformation from II(α) to form I(ß) can be followed by measuring the intensity of the two bands at 799 and 840 cm^{-1}, respectively, and the relative degree of crystalline modification is given by the coefficient $R = 100\ I_{840cm-1}/(I_{840cm-1} + I_{799cm-1})$. Raman mapping of the microdeformed zone produced by Vickers indenter microhardness techniques in PVF_2 (see Figure 7) reveals the

existence of three zones which appear to depend on the elastoplastic behaviour of the material and on the type of deformation to which the material is subjected, mainly determined by the geometry of the indenter [13].

Micro-Raman analyses of the transition front in the neck region of stretched polymers have also been carried out [15-16]. The change in the crystalline structure that takes place in the transition front between the isotropic and oriented regions in uniaxially cold drawn PVF_2 can readily be followed by Raman micro-spectroscopy. The Raman mapping of the transition region allows to provide the distribution of crystalline phase transformation along the neck (see Figure 8). Further, micro-Raman polarized measurements carried out along the neck region in uniaxially stretched polypropylene allowed to determine the evolution of the polymer chain orientation along the transition zone as a function of the drawing rates, which was correlated with other parameters associated with the drawing response of these polymers [16].

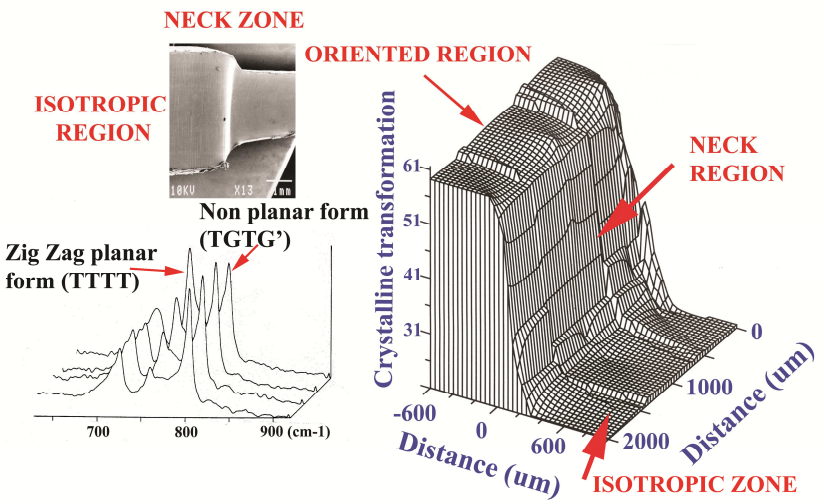

Figure 8: Raman mapping of the neck region of uniaxially cold drawn PVF_2.

Raman microscopy was found to be a powerful technique in the identification of multilayer polymer structures [17], which are commonly used as food packaging containers, and in some cases to probe the quality of the adhesion between layers. The whole operation just takes some few minutes since no sample preparation is needed: the different layers are easily characterized after having cut the multilayer with a typical razor blade and holding it under the microscope objective with an ordinary clip. Micro-Raman spectroscopy is also a very helpful technique in characterizing different morphological features and micro-damaged or degradation in some localized region of materials[9]: for instance, Figure 9 shows the transmitted crossed polarized light micrograph of polymeric composite interface between a fibre of polyethylene terephtalate (PET) and polypropylene (PP) matrix, which allows the visualization and location of two different morphologies, i.e. the transcrystalline zone near the fibre and the typical spherulitic structure away of the interface. In this example, combining transmitted crossed polarized light microscopy with micro-Raman spectroscopy allows to get information on the different types of polymer chains orientation that prevail in each of the two different morphological species. Further, the use of polarized Raman microscopy with polarized light microscopy enabled the characterization of the banded structures that are often observed in the spherulites of polymers. The evolution of the lamellae orientation along the periodical ring pattern structure observed in the crossed polarized micrograph was determined by exploiting the high resolving power of the micro-Raman instrument.

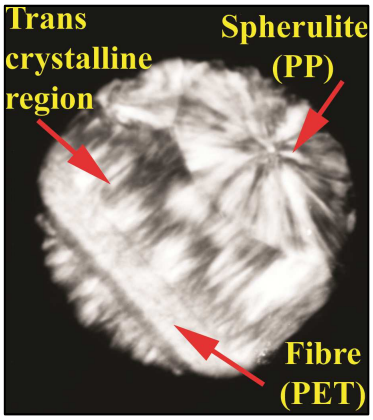

Figure 9: Crossed polarized optical micrograph of a polymeric composite

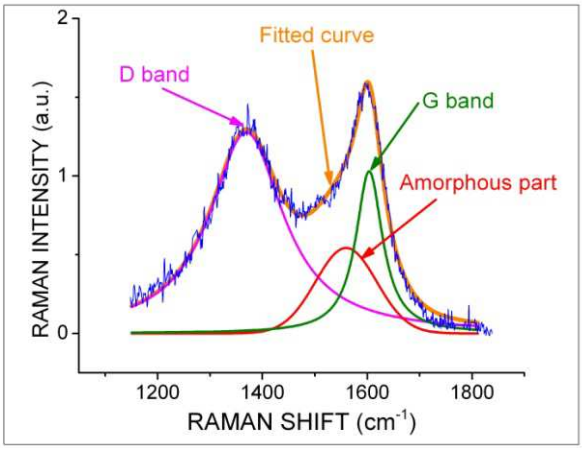

Figure 10: Curve-fitting of black carbon Raman spectrum

In the research field of carbonaceous materials, micro-Raman spectroscopy is a fundamental tool for their characterization since the different allotropes of carbons, such as diamond *(sp^3)* or graphitic *(sp^2)* structures, can be straightforwardly differentiated by the method. Further, the Raman signal is sensitive to short range disorder which allows the determination of the amorphous phase as well as crystals size. Figure 10 shows the micro-Raman spectrum of an individual black carbon particle. A curve fitting was carried out in order to determine with great accuracy the spectroscopic parameters such as peak position, bandwidth, lineshape and band intensity. The spectrum is formed of 3 bands: the D (diamond-like) band and G (graphitic-like) band, both with a Lorentzian shape, at 1370 and 1603 cm^{-1}, respectively, and a broader Gaussian feature centered at about 1550 cm^{-1} assigned to amorphous graphitic phase. The Raman analysis shows that this material has a high degree of disorder and consists principally of non-hydrogenated sp^2 carbon bonds [18]. The microcrystalline planar crystal size was also determined from the following relationship:

$$L_a = [I(D)/I(G)]^{-1},$$

where I(D) and I(G) are the integrated intensities of the D and G bands, respectively. The sample analyzed here has a low microcrystalline planar size, i.e. L_a is of the order of 2 nm. Since Raman spectrum of carbons is sensitive to its microstructure, Raman spectroscopy is a very valuable method in characterizing new synthesized carbons-based materials such as fullerenes, graphenes, fullerites, nanotubes, carbon fibers, layered intercalate carbon-based structures, etc. [19-23]. Further, Raman spectroscopy can give some valuable information on doping, temperature and pressure response in C60 and C70, allows to identify MWCNT (multi-wall carbon nanotubes) and SWCNT (single-wall carbon nanotubes), to determine directly the stress, strain as well as diameter size of carbon nanotubes, and finally to find out the number of graphene layers.

Geologists have been particularly interested in laser Raman microspectroscopy as a mean of nondestructive analysis of single fluid inclusions. Fluid inclusions are multiphase systems of minuscule volumes (tens of cubic micrometers) - often with coexisting liquid, gaseous or solid phases - trapped within a mineral host. The coupling of Raman microscopy with microthermometry is still the only viable option to obtain the composition of individual fluid inclusions. For example, Figure 11 shows the Raman spectra of a liquid and vapour phase inclusion in a quartz matrix. Due to the complex histories of many geological environments, individual minerals may contain several generations of fluid inclusions which are a direct source of information on the initial environment of rock and their subsequent geological history. The chemical analysis of fluid inclusions provides important data related to many mineralogical, geochemical and geological processes. In gemology, Raman is now commonly used for the detection of jewels treatments and the analysis of the nature and identification of gemstones.

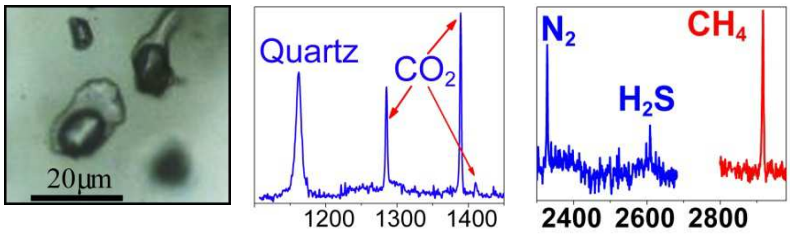

Figure 11: Raman spectra of a microinclusion in quartz.

Raman spectroscopy was found very useful for process monitoring both in industrial plants and quality control laboratory. For example, it was applied to thin film chalcopyrite photovoltaic

technologies: Raman modes from the chalcopyrite layers are very sensitive to features related to their crystalline quality, chemical composition and the presence of secondary phases that are relevant for the optoelectronic properties of the absorbers and the efficiency of solar cells [24-25]. Measurements performed at different process steps allow for the monitoring of the synthesis process of the chalcopyrite layers, giving information directly related to their processing conditions. Experimental configurations have been successfully applied for the monitoring at on-line and in-situ real time levels of the electro-deposition processes involved in the fabrication of low-cost electrochemical based chalcopyrite solar cells [26].

At low frequencies, the lattice modes corresponding to intermolecular collective vibrations and semi-internal motions associated to the rotation of groups of atoms within the molecule, are easily detected with a Raman spectrometer. These modes are very sensitive to polymorphic structures and have been largely used in the pharmaceutical analysis to characterize pharmaceutical solid-state transformations, such as amorphization, crystallization, hydrate formation/dehydratation, co-crystal formation, etc.

During the last two decades, Raman spectroscopy has been widely used in the field of Art and Archeology, in collaboration with conservation scientists, art historians, archaeologists, and applied to the study of pigments in manuscripts and artwork, textiles, enamels, mummies, bio-deteriorated wall paintings, resins, ivories etc. The technique can be utilized to date artwork and even to establish forgery and frauds. Also, a procedure was proposed to determine in a non destructive way the colour printing order in multilayer artistic prints [27].

More recently, Raman spectroscopy has become a useful analytical tool in biomedical science to differentiate between healthy and diseased tissues. The method generates information about the molecular composition, molecular structures, and molecular interactions in a cell and tissue. Raman spectroscopy provides a measure of biologically important molecular group such as lipids, proteins and nucleic acids since most of these molecules are Raman actives and their spectra can be considered as specific fingerprints. As the transformation from normal to cancerous tissues is characterized by molecular changes of tissues constituents, these variations should be reflected in the Raman spectra and can be used as phenotypic markers of the disease. The monitoring of these molecular changes within the tissues can provide diagnostic and prognostic information for early detection of tumour. Indeed, Raman spectroscopy was proposed as a diagnostic method, complementary to histopathology or immunochemistry. Now, the ultimate objective in cancer research is the replacement of biopsy with fiber-optic Raman spectroscopy.

References

[1] Ellis G., Hendra P.J., Hodges C., Jawhari T., Jones C., Le Barazer P., Passingham C., Royaud I., Sanchez-Blasquez A., Warnes G. 1989 *The Analyst* **114** 1061

[2] Fauchet P.M., Campbell H.I. 1988 *CRC Crit. Rev. Solid State Mater. Sci.* **14** S79

[3] Tsang J.C., Mooney P.M., Dacol F., Chu J.O. 1994 *J. Appl. Phys.* **75** 8098

[4] Pérez-Rodríguez A., Romano-Rodríguez A., Cabezas R., Morante J.R., Jawhari T., Hunt C.E.
1996 *J. Appl. Phys.* **80** 5736

[5] Achiq A., Rizk R., Gourbilleau F., Madelon R., Garrido B., Pérez-Rodríguez A., Morante J.R.,
1998 J. Appl. Phys. **83** 5797

[6] Macía J., Martin E., Pérez Rodríguez A., Jiménez J., Morante J.R., Aspar B., Margail J.
1997 *J. Appl.Phys.* **82** 3730

[7] Pérez-Rodríguez A., Pacaud Y., Calvo-Barrio L., Serre C., Skorupa W., Morante J.R. 1996 *J. Electr. Mater*. **25** 541

[8] Pérez-Rodríguez A., Roca E., Jawhari T., Morante J.R., Schreutelkamp R.J. 1994 *Thin Solid Films* **251**, 45

[9] Jawhari T. 1995 *Handbook of Advanced Materials Testing*, Marcel Dekker, New York

[10] Jawhari T., Pérez-Rodríguez A. 1999 *The Internet Journal of Vibrational Spectroscopy*,

II(4)
41 (http://www.ijvs.com/volume2/edition4)
[11] Jawhari T. 2000 *Analusis* **28** 15
[12] Jawhari T., Merino J.C., Pastor J.M. 1992 *J. Mater. Sci.* **27** 2231
[13] Jawhari T., Merino J.C., Rodriguez-Cabello J.C., Pastor J.M. 1993 *Polym.* **34** 613
[14] Jawhari T., Merino J.C., Pastor J.M. 1992 *J. Mater. Sci.* **27** 2237
[15] Jawhari T., Merino J.C., Rodriguez-Cabello J.C., Pastor J.M. 1992 *Polym. Comm.* **33** 4199
[16] Pastor J.M, Jawhari T., Merino J.C., Fraile J. 1993 *Makromol. Chem. Macromol. Symp.* **72** 131
[17] Jawhari T., Pastor J.M. 1992 *J. Mol. Struct* **266** 205
[18] Jawhari T., Roig A., Casado J. 1995 *Carbon* **33** 1561
[19] Afanasyeva N.I., Jawhari T, Klimenko I.V., Zhuravleva T.S. 1996 *Vibrat. Spectrosc.* **11** 79
[20] Klimenko I.V., Zhuravleva T.S., Jawhari T. 1996 *Synth. Met.* **86** 1
[21] Afanasyeva N.I., Belogorokhov A.I., Blank V.D., Jawhari T., Ovchinnikov A.A. 1997 *Macromol. Symp.* **119** 207
[22] Klimenko I.V., Zhuravleva T.S., Afanasyeva N.I., Jawhari T. 1996 *Polym. Sci.* ***A*12** 1336
[23] Klimenko I.V., Zhuravleva T.S., Geskin V.M., Jawhari T. 1998 *Mater. Chem. Phys.* **56(1)** 14
[24] Rudigier E., Pietzker Ch., Wimbor M., Luck I., Klaer J., Scheer R., Barcones B., Jawhari T., Alvarez-Garcia J., Perez-Rodriguez A., Romano-Rodriguez A. 2003 *Thin Solids Films* **431** 110
[25] Rudigier E., Barcones B., Luck I., Jawhari T., Perez-Rodriguez A., Scheer R. 2004 *J. Appl. Phys.* **95** 5153
[26] Izquierdo-Roca V., Saucedo E., Jaime-Ferrer J.S., Fontané X., Pérez-Rodríguez A., Bermúdez V., Morante J.R. 2011 *J. Electrochem.Soc.* **158** 521
[27] Vila A., Jawhari T., García J.F 2007 *J. Raman Spectrosc.* **38** 1267

Applications of Fourier transform infrared spectroscopy

Núria Ferrer

Unitat d'Anàlisi Molecular, CCiTUB, Universitat de Barcelona. Lluís Solé i Sabarís, 1-3. 08028 Barcelona. Spain.

email: *nferrer@ccit.ub.edu*

Abstract. This article summarizes the basic principles of Fourier Transform Infrared Spectroscopy, with examples of methodologies and applications to different field sciences.

1. Introduction

Infrared spectroscopy is an analytical technique applied to the characterization of molecules.
It is based in the fact that molecules absorb specific frequencies that are characteristic of their structure. These absorptions are related to the strength of the bond.

In order for a vibrational mode in a molecule to be active in the infrared region, it must be associated with changes in the permanent dipole. The interaction between electromagnetic light and a molecule produce a change in its permanent dipole, and when the frequency of the infrared light is the same as the vibrational frequency of a bond, absorption occurs.

Although this technique has been used for many years, conventional dispersive infrared spectrometers have been replaced by Fourier Transform infrared equipment, which incorporates a Michelson interferometer and presents an improvement of energy and the simultaneous measurement of the whole spectral range.

The Michelson interferometer consists of a fixed mirror, a moving mirror and a beamsplitter. The beamsplitter is made of a material that transmits and reflects light equally. The two beams reflects back to the beamsplitter from the mirrors and interfere constructively and destructively according to the optical path difference produced by the moving mirror.

Owing to these improvements, infrared spectroscopy has undergone a marked development in the last years because of the possibility of adapting new accessories to the spectrometers and, therefore, of analyzing all kind of samples in the solid, liquid or gaseous state.

The possibility of analyzing and identifying macroscopic or microscopic samples, the accurate comparison of samples from different origins and the fact that the sample is not destroyed, have converted the FTIR technique into a valuable tool. Moreover, the possibility to obtain an infrared spectrum in few minutes and the selectivity of the technique, like a fingerprint of the substance, makes it a first step choice in any conventional analysis.

Kinetics, surface analysis, in vivo measurements are also fields of interest.

Mapping and imaging instrumentation, provide an interesting tool for obtaining large amount of spectra and applying chemometrics measurements.

2. Methodologies and main accessories

Depending on the size of the sample and difficulties regarding handling, different accessories and methodologies can be applied to Fourier Transform Infrared Spectrometers.

2.1. Accessories for macro samples

2.1.1. Transmission

Samples which are between 2 and 10 mm in diameter and below 100 microns thick, can be analysed placing them directly in the middle of the beam. In the same cases, they can be prepared mixing particles with an infrared transparent compound, such as potassium bromide, sodium chloride, cesium iodide or other ionic compounds, and pressing it to make a pellet.

Liquids and gases can also be measured by transmission using special cells with transparent windows in the infrared regions of interest.

2.1.2. Diffuse reflection (DRIFT)

Diffuse reflectance may be considered as a result of multiple reflection, refraction and diffraction processes on solid particles. It is a common accessory used for surface analysis when samples show a diffuse component of reflected light. Samples which can be a powder or a piece of paper or textile, or a stone, are placed on a cubette or flat support, and the diffuse light emitted is recovered by a semispheric mirror and sent to the detector.

Some good examples to be analysed using this accessory are gemstones. Specially cut gemstones like brilliants, show a very neat spectrum because of its property to diffuse light in all directions.

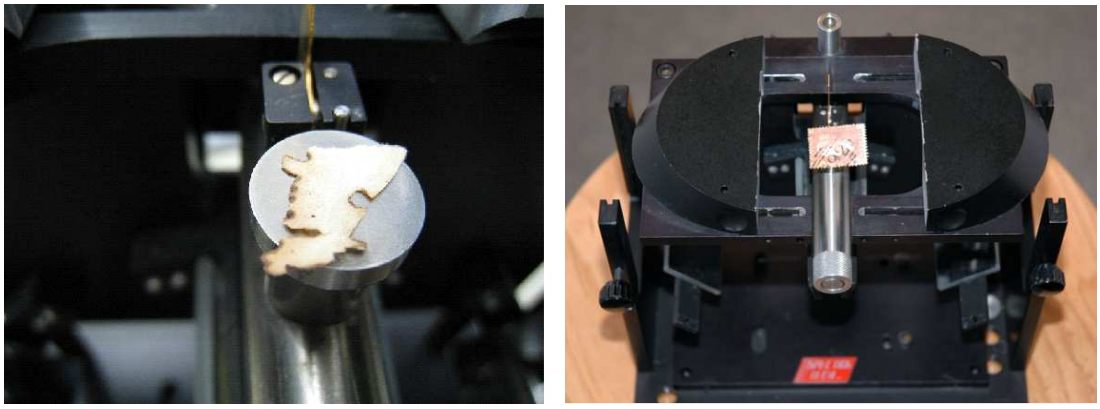

Figure 1. Detail of the sample holder for the DRIFT accessory

2.1.3. Specular Reflection

Samples that can not be manipulated at all and have a specular or polished surface, can be placed on a flat support and be analysed collecting the light reflected in the same direction that the one inciding on the surface. Metal surfaces, thin organic or inorganic layers over metals, semiconductors, are commonly analysed using this methodology.

2.1.4. Attenuated Total Reflectance (ATR)

Internal reflection spectroscopy is an infrared technique in which the infrared radiation is passed through an infrared transmitting crystal of high-refractive index. Radiation is directed up to the input face of the crystal. It reflects through the crystal, passing into the sample a finite amount with each reflection along the top surface. The radiation is reflected one or more times depending on the length of the crystal, the refractive index and the angle of incidence of the light.

Attenuated total reflectance is applied to samples where the composition of the surface needs to be measured. It is applied to soft samples such as paper, polymers, textiles, which can achieve good contact with the crystal used. The only consideration to be borne in mind is the need to obtain good optical contact between the surface of the sample and the crystal of the accessory, which can be made of diamond, Germanium, Zinc Selenide, etc. It is also used for liquid, viscous or sticky samples.

When the sample is big enough to cover a long ATR crystal, the possibility of multiple reflections on the surface of the sample, makes it possible to obtain a good infrared spectrum. This is also a solution for liquid samples. Some macro ATR accessories, have a cuvette form to fit liquids inside.

Nowadays, many instruments have the unique internal reflection ATR crystal. The sample is just pressed against it or a drop is placed on the crystal, and a good spectrum can be obtained in few seconds.

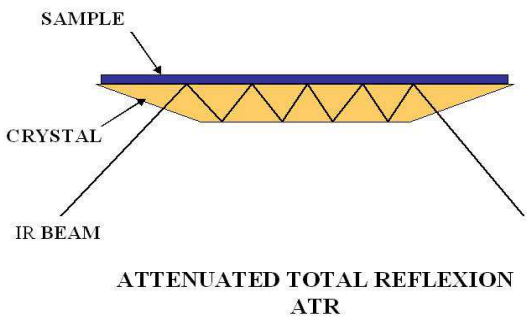

Figure 2. Detail of sample handling in a multireflection ATR accessory

2.2. Accessories for microscopes

2.2.1. *Diamond Cell*

Diamond cell is one of the most frequently used accessories in infrared microscopy. It is normally used when samples are very small, but can be separated from the matrix. The particle or fibre is placed on a diamond window and put under pressure with the help of another diamond window. The pressure of the cell allows the sample to spread over the diamond increasing its surface area while decreasing in thickness. In this way, the infrared radiation is able to go through the sample and, therefore, its infrared spectrum can be obtained by transmission.

Despite the absorption of diamond in the mid infrared, the excellent wavenumber reproducibility of Fourier Transform instruments, makes it possible to substract the diamond spectrum and to obtain clean spectra of the sample.

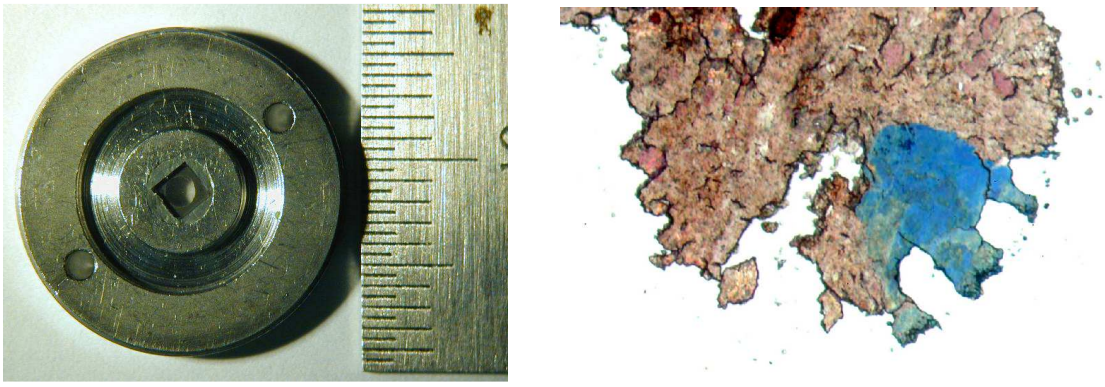

Figure 3. Diamond cell and a pressed sample on a diamond cell

2.2.2. Micro Attenuated Total Reflectance (ATR)

The ATR crystal is a part of an objective that can be coupled to the microscope. A unique internal reflection over the sample in touch with the crystal is enough to obtain the spectrum. This is the alternative when even a single particle cannot be removed from the matrix, which is the case for very ancient or valuable samples such as manuscripts, books or paintings. In forensic science, when the sample needs to be recovered for other analysis, ATR is a well known alternative.

Figure 4. ATR Germanium tip

2.2.3. Cross sections

In same cases, samples contain several thin layers of different materials. Layers can be as small as 5 microns, and can not be removed separately. This is the case of multilayer commercial polymers, multilayers from paintings or sculptures, etc. Embbebing the sample in different materials, such as paraffin, polyester or epoxy resins, permits to cut it in thin layers with a microtome and therefore to analyse it in transmission. Another option is to polish the block where the multilayer is embebbed until the sample appears on its surface and apply reflectance measurements.

2.2.4. Mapping and Imaging

Most of the modern infrared spectrometers with a coupled microscope, have a motorized stage for samples and therefore it is possible to analyse regions of samples. This can be accomplished by mapping or imaging.

In a mapping analysis, a sequential acquisition of adjacent regions is measured, either moving the stage to the last point of the previous regions, or overlapping it using a fixed step size.

In an imaging analysis, a region of the sample to be measured is focused on the array detector and each pixel is analysed simultaneously.

This has produced an enormous advantage both in speed, a big area can be measured without personnel intervention, and in spectral interpretation, because each band of interest shows an intense colour in the image. Distribution of colours through the image allows the location of its compounds.

3. Examples of applications

Applications to all fields have been developed in our laboratory [1]. They include subjects such as:

- Food analysis: additives, preservatives, colorants
- Environmental analysis: water, atmospheric particles, gases
- Conservation and restauration of heritage: paintings, sculptures, ceramics, fossils, ivories.
- Forensic science: paints, textiles, cosmetics,
- Semiconductor analysis
- Pharmaceuticals.
- Physiciological samples: malignant cells, bones, hairs
- Multilayer compounds: polymers, paintings, films
- Geological samples: inclusions in stones

3.1. Gemstones

Infrared spectroscopy applied to gemstones in order to distinguish natural or synthetic pieces, or even to analyze its composition, has provided an objective evidence for its characterization and has proved to be an important tool for both identification and certification purposes in commercial and legal practices. Emeralds, diamonds, topazs, aquamarines, show characteristic infrared absorptions. Gemstones, specially those with a brilliant cut, diffuse light in all directions, therefore, the diffuse reflectance accessory provides a useful way to analyse them quickly.

Natural diamonds without impurities have a characteristic spectrum with bands that are common to both natural and synthetic pieces, but most diamonds also present bands caused by defects in the crystalline lattice. Two different ranges in the infrared spectra are interesting for identification purposes: the first one corresponds to the interval between 5000 and 2700 cm^{-1} and is the range where the bands corresponding to hydrogen impurities in natural diamonds appear, the second one , between 1400 and 1000 cm^{-1}, identifies the impurities due to nitrogen (Figure 5). According to the type of nitrogen substitution, there are also different kinds of diamonds [2].

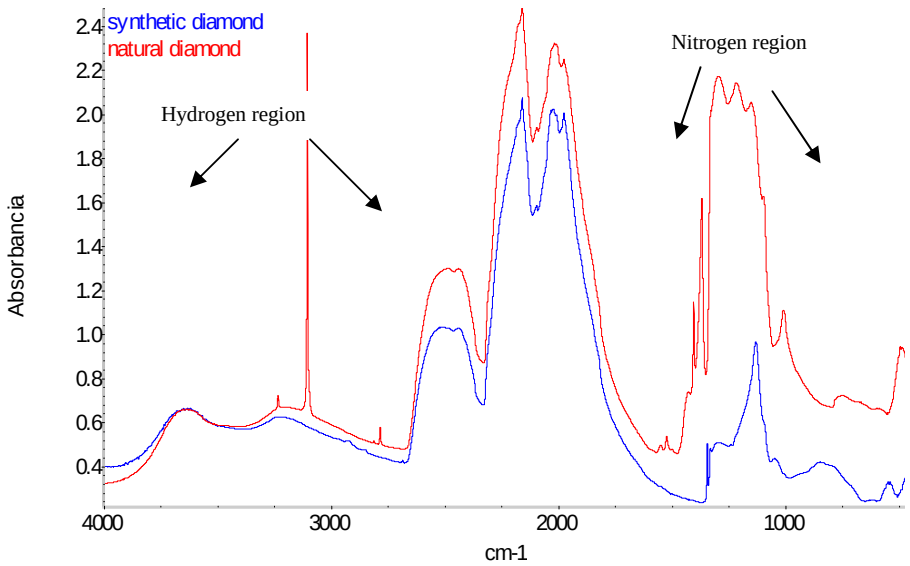

Figure 5. comparison between a natural and a synthetic diamond.

3.2. Analysis of multilayer samples

Some of the samples of interest to be measured using mapping or imaging infrared spectroscopy are those from pictures, walls, murals, sculptures…

The purpose is not only to know the pigment or substract of the painting, but also the binding media used to fix pigments. A cross section of multilayer samples makes it possible to analyse the different layers. Figure 6 shows a little piece of a mural painting. Mapping of the sample allows us to place the different materials.Infrared spectra of the layers show calcium sulphate, calcium carbonate, Prussian blue, quartz and carboxilates coming from metal soaps, which makes it possible to recognize oil as a binding material.

Figure 7 shows the spectrum of the Prussian blue region. Figure 8 shows the spectrum of oil and carboxilates placed on the external surface of the mural painting. Figure 9 shows the spectrum of a quartz particle in the inner part of the painting.

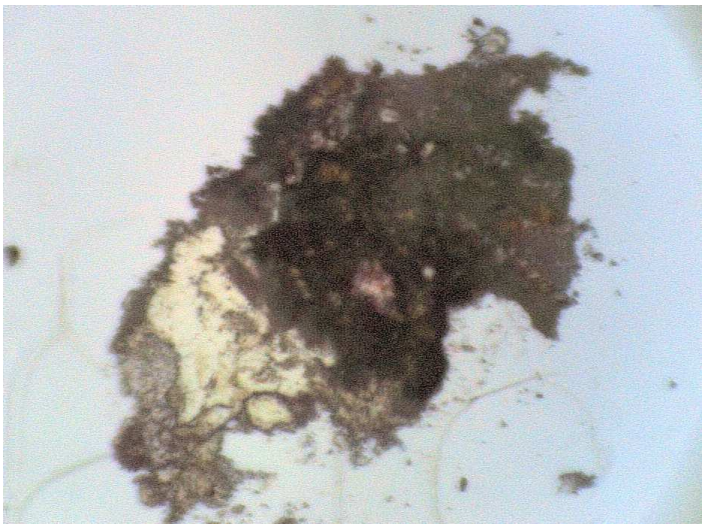

Figure 6. Cross section of a piece of a mural painting (about 300 microns long)

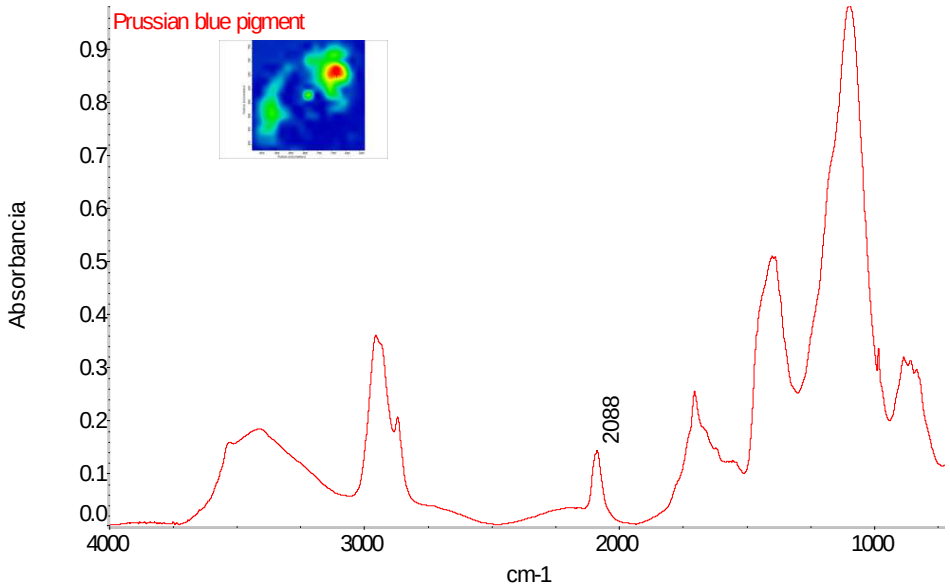

Figure 7. Spectrum of a region containing Prussian blue

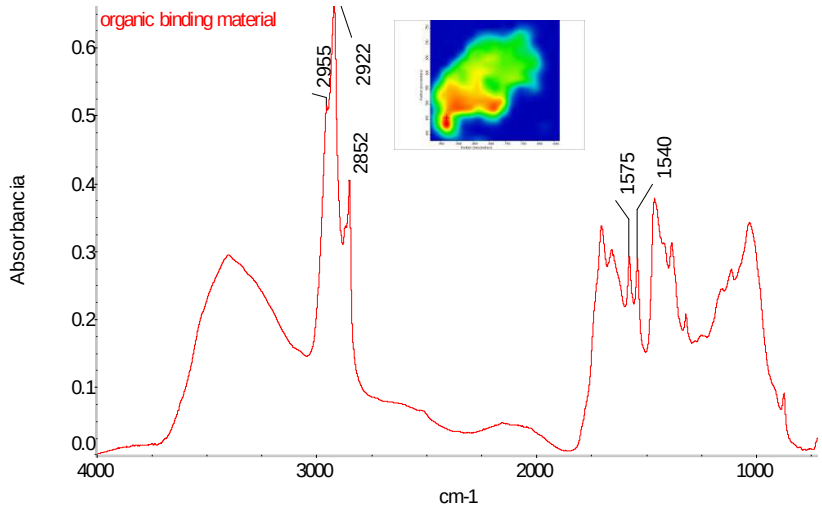

Figure 8. Spectrum of a region containing binding material

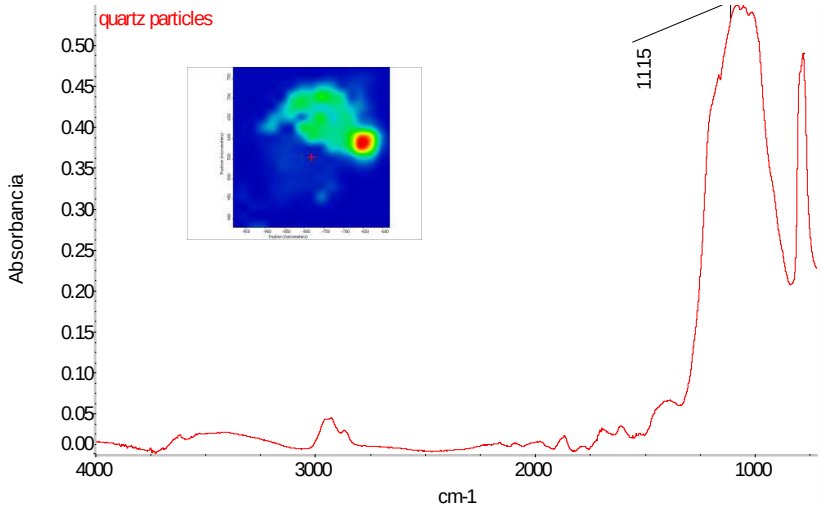

Figure 9. Spectrum of a region containing quartz

Multilayer films of polymers are also a common sample that can be analysed using mapping or imaging infrared spectroscopy. Figure 10 shows the image of a 3 component multilayer film used to contain farmaceuticals and figure 11 shows the spectra of polyethylene and polypropylene found in two layers.

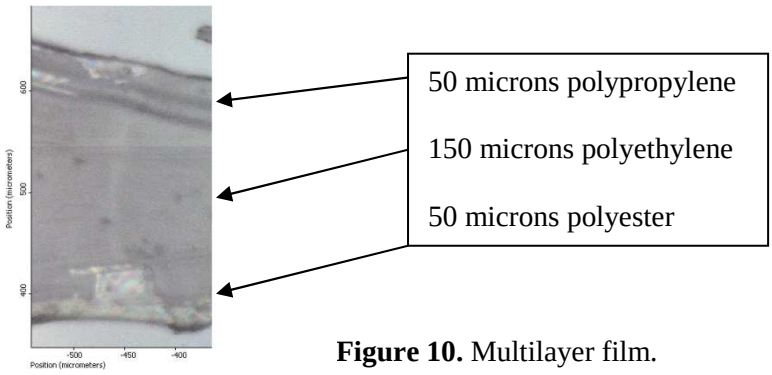

Figure 10. Multilayer film.

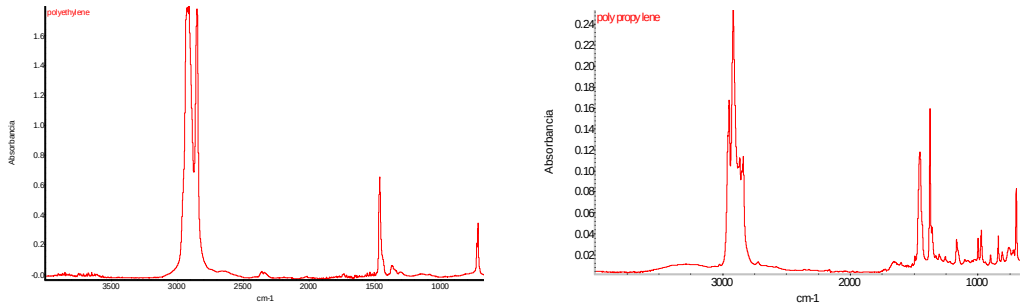

Figure 11. Spectra of polyethylene and polypropilene

3.3. Analysis of papers and inks

Analysis of papers, parchments and inks in ancient manuscripts which are nearly destroyed and need to be restored, has been one of the goals in archives and libraries containing valuable and incunable books. Determining the composition of papers and inks is important to understand the reaction mechanisms involved in its damage [3]. Corrosion in manuscripts involves acidity and oxidation processes. Iron ions have an important role in the oxidation of cellulose. Acidity of paper is also another parameter to measure in order to postulate degradation mechanisms. Some compounds found over ferrogallic inks are: oxalates, sulfates, carbonate, etc.

Extraction of single particles as small as 10 microns in size, or micro ATR techniques are used for these samples whose handling needs to be not destructive at all. Figure 12 shows two pictures of parchment and paper with inks. Figure 13 shows a spectrum of a single particle from an ancient parchment. Bands at 1663, 1375, 1320 and 827 correspond to magnesium oxalate. Bands at 1195, 1080 and 999 correspond to iron sulphate.

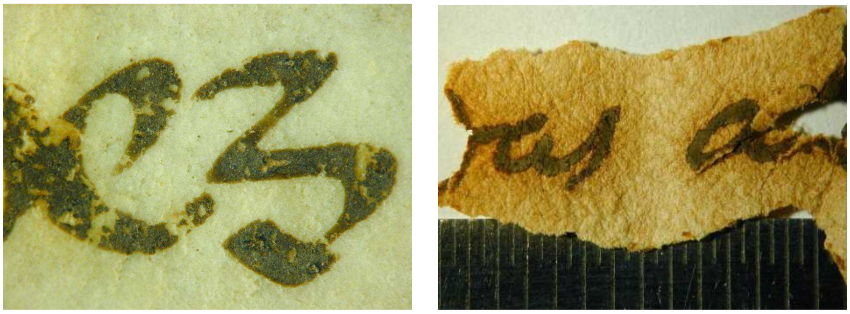

Figure 12. Pictures of a parchment manuscript and a paper manuscript. Both with ink.

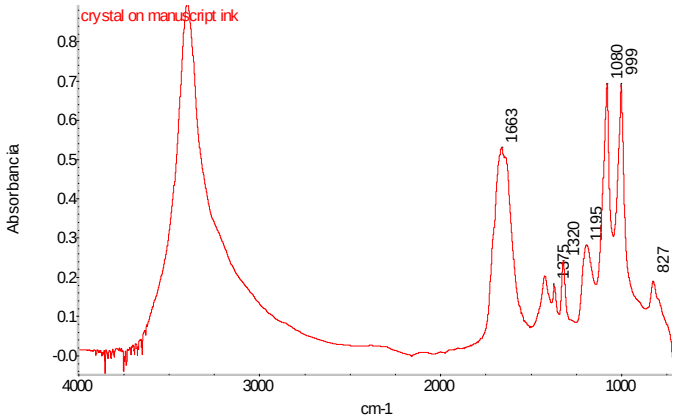

Figure 13. Spectrum of a single crystal on the surface of a parchement sample with ink

Analysis of modern printing inks has also been developed in our centre [4]. Analysis of inks in printings needs a special handling because of the cellulose matrix. Sometimes the accurate comparison between a clean fibre and a fibre with ink is enough to characterize the pigment. (Figure 14)

Figure 15 shows the spectra of blue and red pigments found in damaged stamps. Blue colour was associated to Prussian Blue and red colour to lead chromate.

Figure 14. One penny postage stamps printed 1841-1880 with a blueing effect

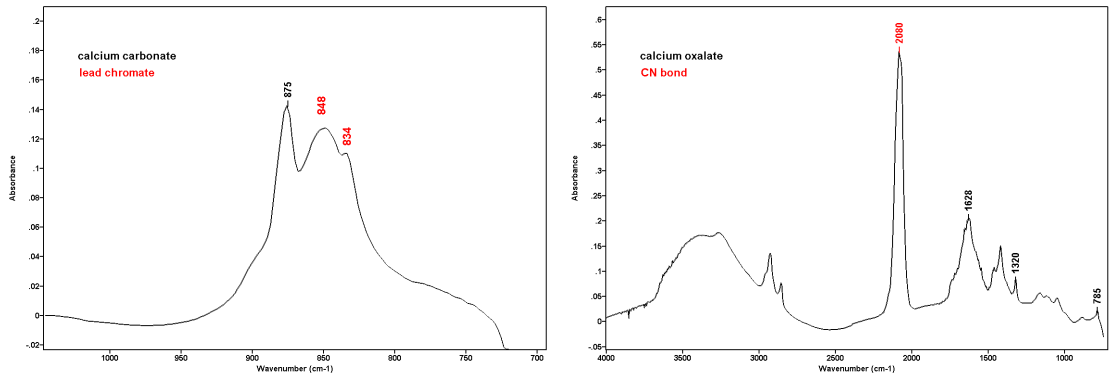

Figure 15. Spectra of Prussian blue and lead chromate. Both pigments were found in damaged stamps.

3.4. Quantitative and qualitative analysis of oils and greases

An alternative procedure using solid phase extraction for the analysis of oil and grease in waters was developed in our laboratory [5]. The use of a teflon filter as a solid phase allowed retention of oil and grease and further analysis of carbon-hydrogen bonds could be run over the filter. Teflon has only carbon-fluor bonds and therefore the region where carbon-hydrogen bands absorb is clean. This method avoided the use of any kind of solvent. Standard methods used carbon tetrachloride or trichlorotrifluoroethane extractions, which should be avoided according to the Montreal Protocol [6].

Experiments used n-hexadecane as a standard oil in different water matrices. The detection limit was 0.034 mg/l. Recoveries of diesel oil, pump vacuum oil, olive oil, sunflower oil and mixture of oils, depend strongly on the oil used for the calibration line, but in general satisfactory results were obtained. The method was fast, clean and sensitive, and represented a way of measuring oil and grease in water with high reproducibility. Qualitative differences could also be detected, depending on the relationship among the intensities of the CH3 and CH2 symetric stretching bands. A small shift in the position of both bands, could also be seen.

Figure 16 shows the comparison among different oils used to prepare synthetic samples.

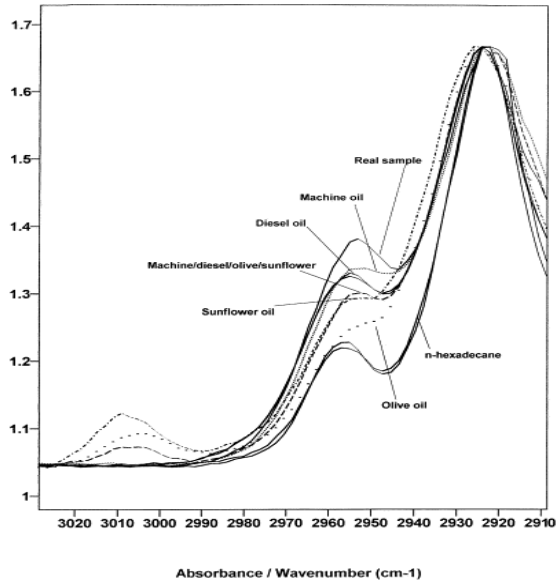

Figure 16. Comparison of infrared absorptions among different oils.

Acknowledgements

To the people who contributed to the development of new methodologies in our laboratory, and to Juan José Gámez, Maite Romero, Josep Mª Socias and Anna Vila.

References

[1] N. Ferrer, Forensic Science, Applications of IR Spectroscopy, Encyclopedia of Spectroscopy and Spectrometry, Academic Press 2000, Vol 1, pp 603-615

[2] N.Ferrer and J.M. Nogués, Characterisation study of cut gem diamond by IR spectroscopy Diamond and Related Materials 5 (1996) 598-602

[3] N.Ferrer and M.Carme Sistach, Characterisation by FTIR Spectroscopy of Ink Components in Ancient Manuscripts, Restaurator, 2005, 105-117

[4] N. Ferrer and A. Vila, Fourier transform infrared spectroscopy applied to ink characterization of one-penny postage stamps stamps printed 1841-1880. Analytica Chimica Acta 550 (2006)161-166

[5] M.T. Romero and N. Ferrer, Determination of oil and grase by solid phase extraction and infrared spectroscopy, Analytica Chimica Acta 395 (1999) 77-84

[6] http://ozone.unep.org/Publications/MP_Handbook/Section_1.1_The_Montreal_Protocol/

Nuclear Magnetic Resonance

Miguel Feliz, Maria Antònia Molins, Margarida Gairí, Victòria Muñoz-Torrero, and Teresa Gonzalez

Unitat de Ressonància Magnètica Nuclear, CCiTUB, Universitat de Barcelona. Parc Científic de Barcelona. Baldiric Reixac, 10. Edifici Cluster. 08028 Barcelona. Spain.

email: *informn@ccit.ub.edu*

Abstract. This article reviews the principles and methods of nuclear magnetic resonance spectroscopy, and gives examples of applications carried out at our Facility, which illustrate the capabilities of the technique.

1. Introduction

Nuclear Magnetic Resonance (NMR) is a useful tool for the determination of chemical compound structures. It is a powerful technique for dealing both with static and dynamic problems, and with molecular interactions. This ability makes it an essential tool in many scientific areas such as chemistry, biology, biochemistry, metabolomics and genomics and it has been of crucial importance for their research acceleration and dynamization, especially in the pharmaceutical industry.

NMR is a technique based on a physical property of certain nuclei that get oriented in the presence of an external magnetic field and its principles where established in 1938. The first measurements were done by Felix Bloch and Edward M. Purcell en 1945[1] and the most studied nucleus at these early times was ^{1}H. In 1950 the concept of chemical shift was introduced connecting it with chemical environment of protons on the molecule, and in mid 50's, the splitting of signals in the spectrum was connected with interactions between different nuclei. These early concepts, together with information coming from decoupling techniques and the Nuclear Overhauser Effect (NOE), are nowadays crucial for the determination of chemical structures. Since 1957, the development of ^{13}C NMR has opened the technique to the study of other nuclei such as ^{15}N, ^{31}P, ^{19}F or ^{113}Cd, some of them are essential today in the study of high-biological interest compounds.

In 1966 Richard R. Ernst[2] and Weston A. Anderson took a step forward in increasing the intrinsic low sensitivity of the technique by developing Fourier Transform pulsed NMR which allows simultaneous observation of the same species of nuclei on a wide range of frequencies, making feasible the co-addition of spectra. In 1970 Jean Jeneer conceived the idea of bidimensional experiments later developed by R. R. Ernst. The widespread use of 2D and 3D experiments has contributed to extend the technique to increasingly complex molecules, being essential today in the study of proteins[3].

Although the initial development of NMR focused on liquid state, overcoming of problems derived from strong interactions present in solid samples, allowed its extension to the latter samples (1960-1970). This application has increasing significance, not only for the study of materials, but also in the field of Biochemistry, as it allows the study of non-soluble great-sized proteins. Solid state NMR provides tools to better understand protein aggregation processes which happen to occur in the vast majority of neurodegenerative diseases.

The development of superconducting magnets has pushed forward stronger, more stable and more homogeneous magnets which has end up with improvements on sensitivity and spectral resolution. Latest advances on magnets are focused on decreasing their maintenance by lowering their cryogenic liquids demand and on ultrashield magnets which decrease magnetic field interferences in surrounding areas. More information on basic NMR can be found elsewhere[4,5].

Since 1982, the NMR Facility of the University of Barcelona, nowadays assigned to the Scientific and Technological Centers (CCiTUB), provides access to NMR instrumentation and scientific and technical support on NMR. Its activity is opened to researchers coming from both private and public institutions. The large number of instruments (12 magnets with "fields" ranging from 800 to 250 MHz) together with experienced staff converts this facility in a reference point in our state.

2. Applications and Methodology

The relationship between chemical shift and nuclei electronic environment is a key tool for structure determination. NMR spectrometers are able to detect subtle differences of chemical shifts providing identification of neighbouring chemical functionalities, changes on substitution, etc. It affords, too, a quick tool to differentiate among similar compounds, as illustrated in the detection of oversulfated Condriotin Sulfate (OSCS) as a contamination of Heparin; in this particular case the analysis is based on the differentiation between OSCS N-Ac methyl and heparin N-Ac methyl. In spite of the proximity of signals and of the great difference in intensity, it is possible to detect even

less than 1% of OSCS (Example 3.1). In fact, working with a 500 MHz NMR spectrometer, a detection limit of 0.01% of contamination has been established on an active pharmaceutical ingredient (API) analysis.

NMR technique affords also quantitative information (qNMR), as it is possible to correlate between the NMR signal area and the number of protons involved. With signal integration and a U.S. Pharmacopeia (USP) protocol, it has been possible to determine poloxamer composition (Example 3.2). In case no USP protocol or similar is available, a validation of protocols used in qNMR is necessary because the reliability of results is determined by sample characteristics and experimental conditions.

Stereochemical information can be inferred from scalar coupling constants (J_{HH}) on proton spectra and from dipolar coupling constants in NOE experiments. Scalar coupling data can afford direct information about, for instance, a cis/trans arrangement in a double bond or it also can be used both, directly or indirectly, in multiple bidimensional experiments. A simple example is the COSY experiment, where the correlation signals originate from magnetization transfer between scalar-coupled protons. The 2D experiments are very useful to study complex molecules since in these cases the mono-dimensional spectrum is pretty crowded and severe overlapping of the signals interferes with data interpretation. Some examples of 2D experiments are ^{1}H-^{1}H homocorrelation (COSY or TOCSY) where different fragments of structure can be identified, or ^{1}H-^{13}C heterocorrelation (HSQC) where directly bonded proton and carbon can be connected, taking advantage of the great carbon spectral width which reduces significantly overlapping. Some long range ^{1}H-^{13}C experiments (HMBC) are possible too. An appropriate combination of bidimensional experiments allows structure determination of natural products or synthetic compounds (Example 3.3).

The study of complex molecules such as proteins, DNA or RNA requires complex 2D and 3D experiments including some heteronuclei as ^{13}C and ^{15}N for proteins or ^{13}C and ^{31}P for nucleic acids. Professor K. Wutrich was the first to develop pulse sequences and assignment strategies for the study of proteins[3]. The low sensitivity of the technique and the complexity of this kind of samples requires ^{15}N labelling and often ^{13}C labelling too. For proteins larger than 250 residues, the use of ^{2}H labeling and TROSY[6] methodology in very-high-field instruments are necessary. An example of the largest macromolecular complex studied by NMR with this methodology is the GroEL-GroES complex, as big as 900 KD, carried out by Professor Wutrich[7]. In our NMR facility, protein studies are carried out on 600 and 800 MHz instruments where a wide variety of TROSY 2D and 3D sequences have been implemented (Example 3.8).

Detecting active sites and ligand-binding interactions is of great importance in the study of potential drug molecules. NMR can deal with it from two different approximations:

- Study of small chemical shift changes caused to nuclei close to the active site during binding. ^{1}H-^{15}N HSQC can be useful to detect these changes and has been used in our facility to study interactions of P53 tetramer and arginine enriched peptides[8].
- Study of changes caused to ligand when bound to a large molecule as it adopts characteristics of the latter as far as correlation time or relaxation concerns. “Information” from the bound state is transferred to the free ligand during the equilibrium between both species. In our facility, these kind of studies are run on 500 MHz instruments with autosampler. STD, Waterlogsy, CPMGT2, or NOE Transfer[9] experiments are commonly used (Example-3.5). If higher sensitivity is required 600 MHz instruments are used instead.

NMR is useful not only for ^{1}H, ^{13}C and ^{15}N nuclei, as there is a wide range of NMR active nuclei. ^{31}P and ^{19}F are widely used for the study of organometalic and fluorinated compounds, respectively. Experiments which combine both nuclei can provide simplified spectra (Example 3.6). Currently, ^{19}F NMR is used in our laboratory to determine association with proteins. Our facility can tackle with these nuclei and other less common such as ^{113}Cd, ^{195}Pt, ^{11}B, ^{29}Si, ^{27}Al, etc.

All instruments present in our facility are prepared to work with solution samples. In addition to that, our High Resolution Magic Angle Spinning (HRMAS) probe allows working with semi-solid samples such as tissues, resins chromatographic supports, gels, etc. Metabolite determinations on

tissues, stability of almond pulp or solid phase synthesis control are some examples of work done with this probe in our lab (Example 3.7).

Magnetic field strength determines the sensitivity and spectral dispersion of NMR spectra. Sensitivity increases in a relation of 7/4 with magnetic field B_0. The increase in spectral dispersion makes evident an smaller overlapping of signals (Figure 1). Occasionally, a simplification of coupling systems can also be obtained.

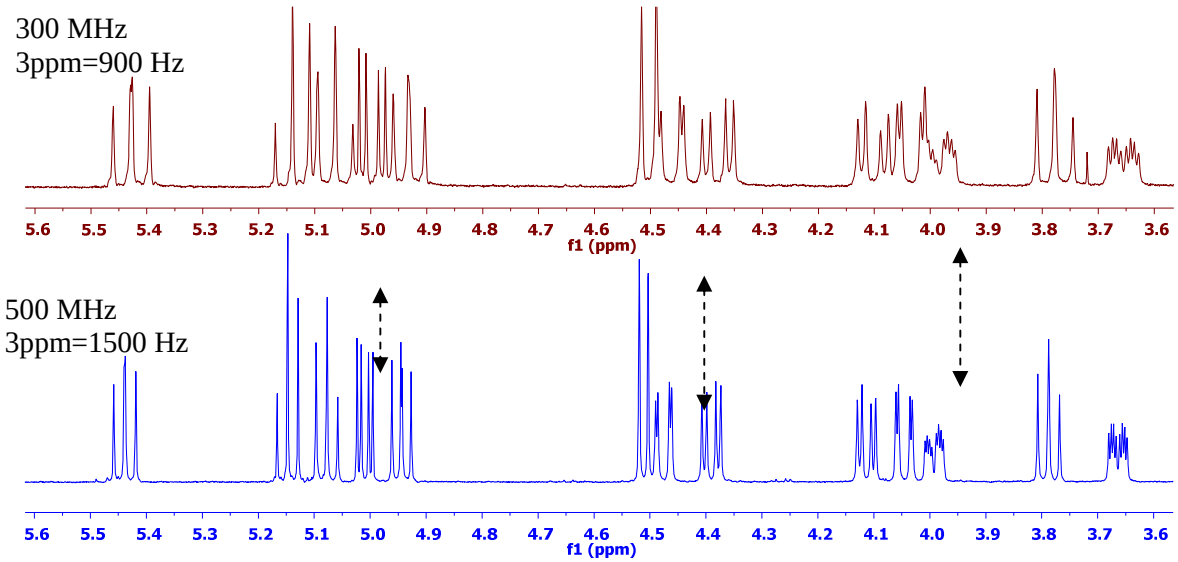

Figure 1 Expansion of a ^{1}H spectrum acquired in a 300 and 500 MHz spectrometer

The choice of spectrometer is determined by the complexity and availability of the sample under study. Generally speaking instruments with observation proton frequencies ranging from 300 to 500 MHz are suitable for the study of small and medium-sized molecules. In our facility the 800 MHz instrument is mainly used for the study of dynamic problems, biomolecular interaction or structure determination of high-molecular weight compounds such as proteins and nucleic acids. The 600 MHz instrument is used both for medium-sized molecules and initial studies with high molecular weight molecules. An important point to have into account in the choice of the best spectrometer is its particular characteristics, sensitivity (Table 1) and available probes. Detailed information on available spectrometers and probes can be found in our web site[10].

Table 1 S/N ratio on our main instruments (sample test 0.1% Etilbenzene in $CDCl_3$)

Nucleus	B800	B600-II	B600-I	V500S	V500	M400
^{1}H	>7000:1	>7000:1	700:1	730:1	720:1	220:1
^{13}C	> 700:1	> 750:1	335:1	240:1	83:1	158:1
^{31}P	---	---	200:1	135:1	24:1	183:1
^{19}F	---	---	450:1	450:1	---	200:1

3. Examples of applications performed in the NMR Facility

3.1. Heparin Analysis

Heparins are a complex mixture of highly sulfated glycosaminoglycans (CAGs) isolated mainly from the intestinal mucosa of pigs or bovine lungs and are widely used as anticoagulant and antithrombotic agents. The heparin consist of a mixture of sulfated disaccharide units, the major component is a 2-O-sulfated iduronic acid and 6-O-sulfated, N-sulfated glucosamine IdoA(2S)-GlcNS(6S).

The differences in the production processes of heparin lead to changes in the content of minor compounds. Some of these native impurities such as Dermatan sulfate (DS) are accepted with

restrictions but others such as Oversulfate Chondroitin sulfate (OSCS)[11], a non-native contaminant, are not allowed.

In 2008, there were an increase of incidents and deaths associated with allergic reactions caused by adulterated heparin. The Food and Drug Association (FDA) and several research groups identified OSCS as a heparin contaminant associated with adverse reactions. International organizations such as EP (European Pharmacopoeia) and USP included the use of NMR technique in heparin analysis[12] procedure to assess the presence of OSCS in the samples (Figure 2).

The proton spectrum of heparin must show, among others, characteristic signals at δ 2.04, 3.27 ppm (doublet), 4.34 ppm, 5.22 ppm, and 5.42 ppm (all with less than ± 0.03 ppm deviation). The chemical shift for OSCS N–Ac group in heparin sodium is reported at 2.16 ± 0.03 ppm and in any case it should not be observed. Subsequent revisions of the monographs include additional requirements on the profile of intensities of some signals of heparin in the proton spectrum. The latest methods are:

- USP monograph appeared in USP32; Pharmacopeia Forum 35(5) Oct 2009.
- European Pharmacopoeia 7.0 (8/2010:0333)

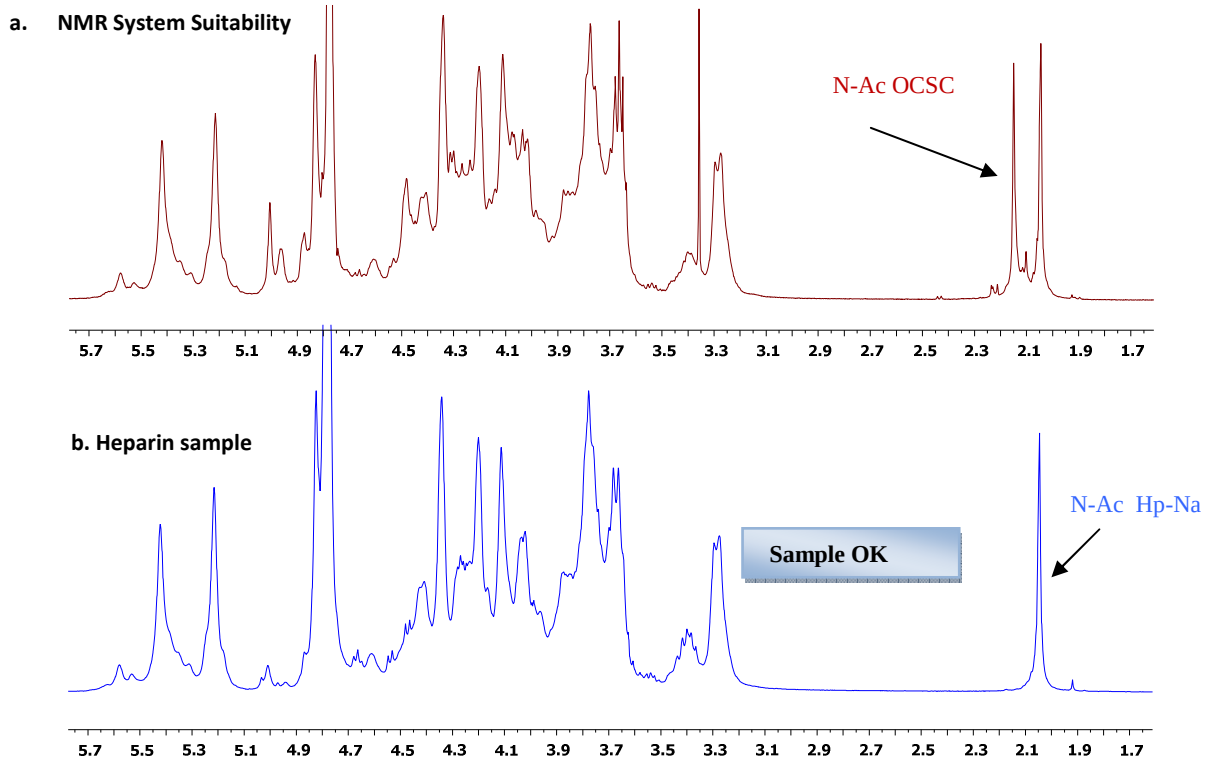

Figure 2 Upper spectrum: heparin System suitability sample spiked with OSCS. Lower spectrum shows heparin sample (suitable for marketing)

In our NMR Facility, heparin analyses are performed on NMR 500 MHz spectrometers, since it is essential to obtain a good separation and definition of the broad signals of the N-acetyl. It is also necessary that the signal to noise ratio in the area to examine must be higher than 1000:1. The ability to observe the ^{13}C satellites in the N-acetyl of the major components is an indication that the detection limit is higher than 0.5%.

Depending on the user's needs, a specific Standard Operating Procedure (SOP) can be elaborated. With NMR systems ISO9001 and GMP compliant

If the content of OSCS is small, the N-Ac peak of the impurity can be confused with the ^{13}C satellites of N-acetyl of the major components. In this case, acqusition of the proton spectrum with ^{13}C decoupling is necessary, as shown in Figure 3c.

When experiments are run in a 600 MHz spectrometer, ^{13}C decoupling is recommended.

3.2. Polaxamer Analysis.

A poloxamer is a synthetic triblock copolymer of ethylene oxide (EO) and propylene oxide (PO), with a general formula $HO(C_2H_4O)_a(C_3H_6O)_b(C_2H_4O)_a OH$. The ability of poloxamers to form micelles makes them interesting for the pharmaceutical industry as drug-delivery vehicles. It is also used in pharmaceutical formulations because of its ability to form thermo-reversible gel, which at low temperatures, is a low viscosity liquid and at high temperatures a gel.

Figure 4 shows a proton poloxamer spectrum of the sample dissolved in $CDCl_3$. The oxypropylene units are characterized by a series of doublets centered at 1.08 ppm due to CH3 groups (region **A**). The signals from 3.2 to 3.8 ppm (region **B**) are due to the CH_2O groups of oxyethylene units, and also the CH_2O/CHO groups of the oxypropylene units.

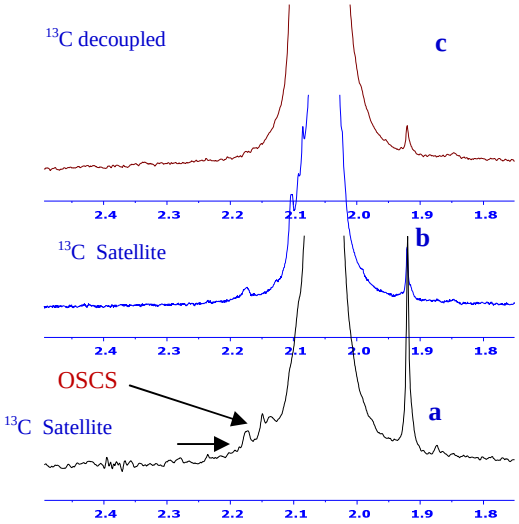

Figure 3: **a)**. ^{1}H-RMN of System suitability sample with the corresponding N-Ac of OSCS and ^{13}C satellite peaks. **b).** A typical spectrum of heparin sample (not containing OSCS) with the signal at δ 2.17 ppm attributed to the ^{13}C satellite. **c).** The proton spectrum of the previous sample performed with ^{13}C decoupling. Notice that the signal at δ 2.17 ppm disappears.

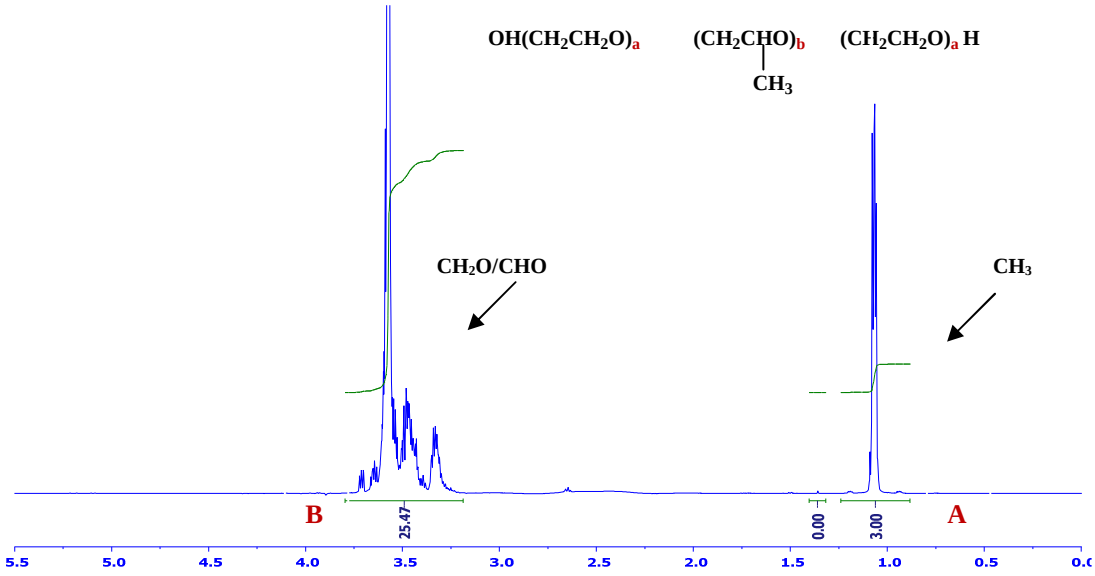

Figure 4. Proton spectrum of a poloxamer sample

In monograph USP32-NF27, a procedure to determine the ratio of oxyethylene/oxypropylene, using a Relative Method of Quantization <761> is described. The percentage of oxyethylene, by weight, in the Poloxamer is calculated by the following formula[13]

$$\text{Weight \% oxyethylene} = 3300\alpha / (33\alpha + 58) \quad \text{being } \alpha = (B / A) - 1.$$

Applying this formula to the spectrum of Figure 4**,** a value of 80.9% EO is obtained.

At the NMR Facility, poloxamer analysis are performed using 500 MHz spectrometers that fulfill ISO 9001-2008 regulations and GMP quality system.

3.3. Structural Elucidation by NMR Spectroscopy (small and medium size Organic Compounds)
An essential need of synthetic or chemical isolation processes is to unequivocally identify the obtained compounds.

Routine spectrometers in our facility are prepared with a series of tools which provide a friendly access to a wide variety of NMR experiments even for non-expert NMR users. Research users of Chemical and Pharmaceutical industry can make use too of these possibilities, depending on their particular demands, with no need to invest in high cost instrumentation.

NMR staff contribution to studies coming from industry can include data interpretation and fully elaborated documentation

The most frequently used strategy for structure determination of small and medium-sized molecules begins with a detailed study of proton 1D spectrum. Further information is obtained in a next step by ^{1}H-^{13}C heterocorrelation (either by HSQC or HMQC), which, if edited, affords differentiation between carbons according to the number of protons directly attached (**Figure 5**). Spin systems can be identified by ^{1}H-^{1}H homocorrelation experiments (COSY, DQF-COSY, TOCSY, etc). Assigned fragments obtained can be interconnected by long-range ^{1}H-^{13}C heterocorrelation (HMBC). Finally, a study of coupling constants and NOE data can define compound stereochemistry.

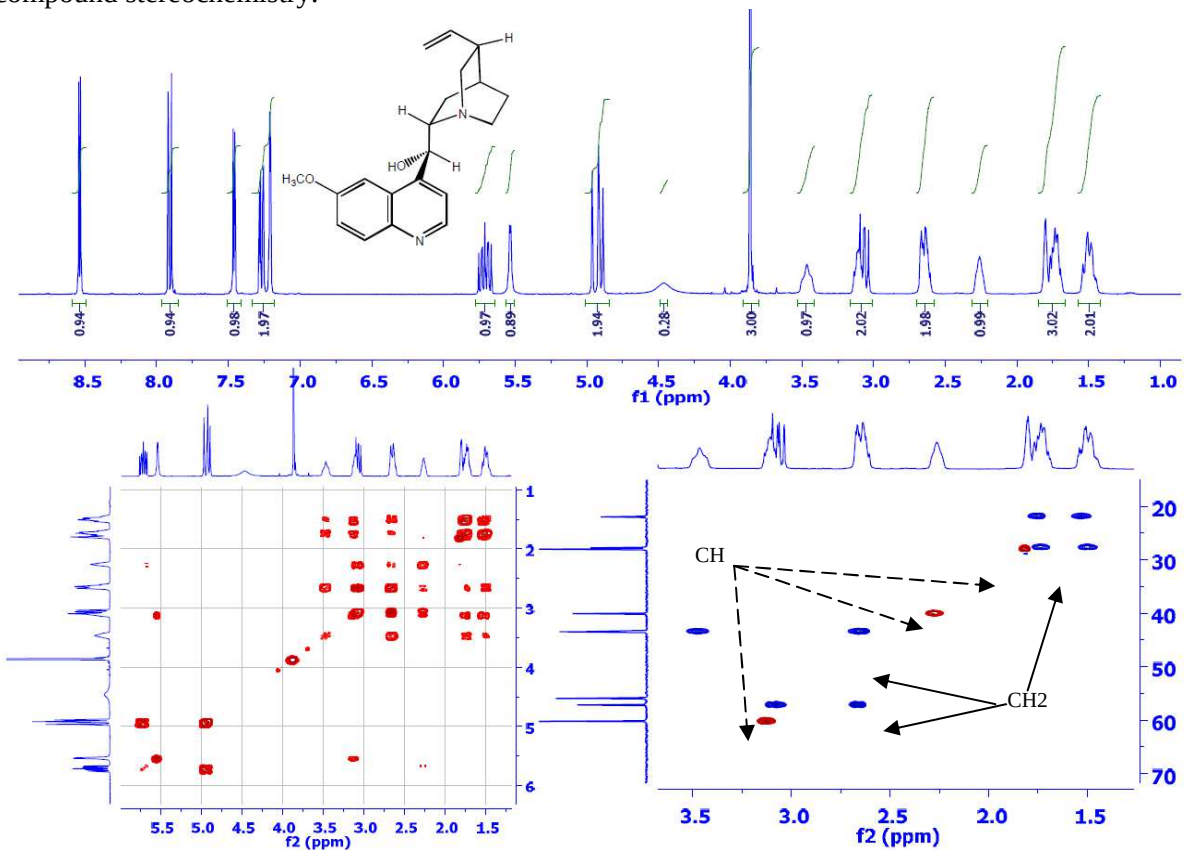

Figure 5. Basic experiments used for assignment 1D^{1}H, 2D COSY and 2D HSQC of Quinine in $CDCl_3$

A detailed example of a combined use of multiple 2D experiments for the study of Quinine is available on our web site as a tool for beginners on NMR in order to help them to choose proper experiments.

3.4. Fast 2D-NMR ligand screening using Hadamard spectroscopy[14]
The following is an example of methodological development carried out in the NMR facility in collaboration with the research group of Prof. Miquel Pons.

Chemical shift perturbation NMR experiments are widely used for structure-based drug discovery. The main advantage of NMR methods based on protein observation is the possibility to map the ligand interaction site, due to the single residue selectivity offered by 2D HSQC experiments.

There is an increasing interest in new NMR methods that can reduce the time needed to record 2D correlation spectra (SOFAST, Hadamard). Recent applications of Hadamard encoded spectroscopy allow a very fast acquisition of the spectrum , while maintaining a high-spectroscopic resolution in the 2D spectra. In ligand-screening experiments, the signals involved usually experience only small frequency changes (no more than 50-100 Hz). The knowledge of initial free protein spectrum can be used to speed up spectral acquisition using Hadamard encoding of the frequencies of interest. In Hadamard spectroscopy, the evolution time in the indirect dimension is replaced by phase modulated multisite selective excitation. In this way, only selected regions are being measured and the sensitivity per unit time can be increased by more than one order of magnitude.

Hadamard-encoded HSQC spectra only contain cross-peaks with selected heteronuclear frequencies (e.g. ^{15}N). The disappearance of a correlation signal of an amide proton (^{1}H-^{15}N) indicates that is involved in ligand-binding process. When the ligand-induced ^{15}N shifts exceed the excitation bandwidth, it results in the disappearance of the cross-peak. While this may be enough for screening applications, no information on the magnitude and direction of the shift is obtained. This information can be recovered by generating three frequencies for each signal to be studied. The excitation frequencies are those of the unperturbed signal (center) or have an offset of plus or minus 10 Hz. As shown in Figure 6 (residues 1 and 3), a signal intensity decrease in the Hadamard spectrum with the excitation frequencies of the free protein identifies the observed residues that are affected by ligand binding. Signals in Hadamard spectra with excitation frequency offsets provide information on the sign of the induced shifts.

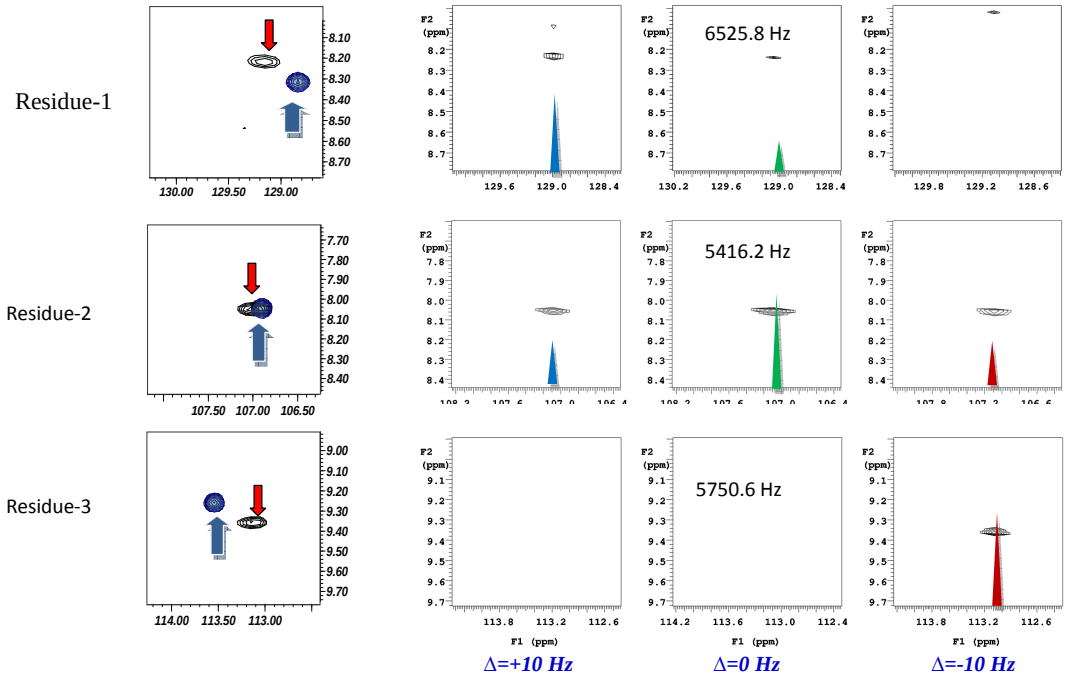

Figure 6. The top and bottom rows are from ligand shifted residues. The centre row is from an unperturbed residue. The leftmost column is a superposition of HSQC cross-peaks of a ^{15}N-labeled WW domain in the absence (↑) and in the presence (↓) of ligand. The other three columns to the right are expansions of Hadamard spectra in the presence of ligand at excitation frequencies corresponding to offsets of +10Hz, 0 Hz, and -10Hz, respectively, with respect to the frequencies in the free protein.

3.5. Saturation Transfer Difference a Method for HTS

The Saturation Transfer Difference (STD) was developed by M. Mayer and B. Meyer[15]. Using this method two experiments are acquired: in the first the selective saturation is applied on the target resonances (protein methyl's ~ 0 ppm); the second experiment is acquired with the irradiation off resonance (~ -35 ppm). Both spectra are subtracted and only the signals affected by the saturation are present. The saturation is transferred to all protein residues by diffusion mechanism, and also to the ligand bounded to protein, but the other ligands remain unaffected (Figure-7).

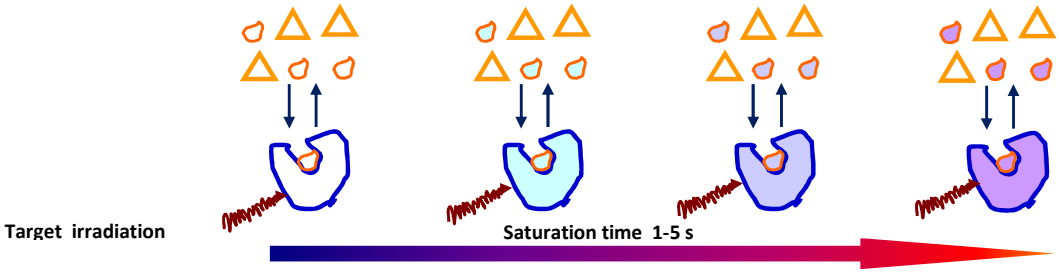

Figure 7: Schematic representation of the evolution of the STD effect

The degree of saturation in ligand resonance signals depend on the distance of the protons involved in the binding. Protons close to the target molecule are saturated in more extension and have a stronger STD effect. This information can be used to find the part of the ligand more involved in the association (*binding epitope on ligand*). The STD experiment is useful in the case of low and medium binding interaction. It can be applied to medium and large size proteins. No detailed protein information is required, and the concentration of the protein may be relatively low.

At In the NMR Facility this method, is regularly used by several public and private research groups. An example of this application is the collaboration with the research group of Dr. Ignasi Fita[16]. The STD experiment has enabled to check and complete the results of crystallographic studies on the binding sites on protein catalase-peroxidase KatG with INH and NAD^+.

The STD experiments of INH-KatG mixtures confirmed that the protons H2/H6 and H3/H5 of INH make interaction with the protein (Figure 8 (left)), consistent with the X-ray structures. The STD experiment also allows a mapping of binding epitope. In KatG/NAD^+ the H8 adenine ring and H1' of the adenosine ribose exhibit stronger STD signals than the others protons of NAD^+ , as it can be observed in the STD spectrum (Figure 8 (right))

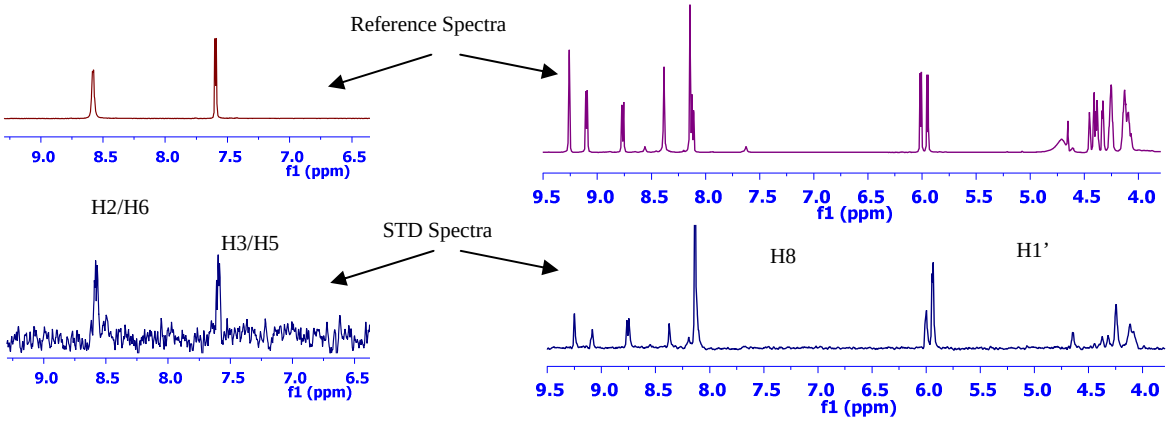

Figure 8. STD experiment of INH-KatG (left); STD experiment KatG/NAD^+ (right)

The protocol used in our NMR Facility for the study of chemical libraries includes an experiment CPMGT2 to confirm the results of the STD. The method allows the study of various ligands at the same NMR sample. The time required for the study of each sample varies between 30 and 100 minutes depending on intensity threshold set in the STD experiment.

3.6. ^1H-^{19}F Double resonance experiments

The high sensitivity of ^{19}F (83% of the ^{1}H sensitivity), makes ^{19}F NMR a powerful tool for analyzing different kind of compounds. However, often the spectra of ^{1}H and ^{19}F of these compounds are complex. This is so because ^{1}H and ^{19}F couple to each other ($^{2}J_{HF}$=50-45Hz; $^{3}J_{HF}$=27-7 Hz) , creating complex splitting patterns. The spectra can be simplified by decoupling techniques resulting in clearer assignments, more visible impurities and more reliable confirmations.

The application of $^{19}F\{^{1}H\}$ or $^{1}H\{^{19}F\}$ NMR methods is not always a routine. They need specialized hardware requirements:

- A probehead that can simultaneously be tuned to ^{1}H and ^{19}F.
- A console able to generate two high-band frequencies (^{1}H and ^{19}F) and often additional amplifiers.

These requirements are becoming more frequent in the latest generation of spectrometers, and are not as common in older instruments. Several spectrometers in our NMR Facility allow simultaneous work with ^{1}H and ^{19}F. Acquisition of ^{19}F spectra with ^{1}H decoupling in broadband mode is possible in our Varian Inova-300 spectrometer (Figure 9).

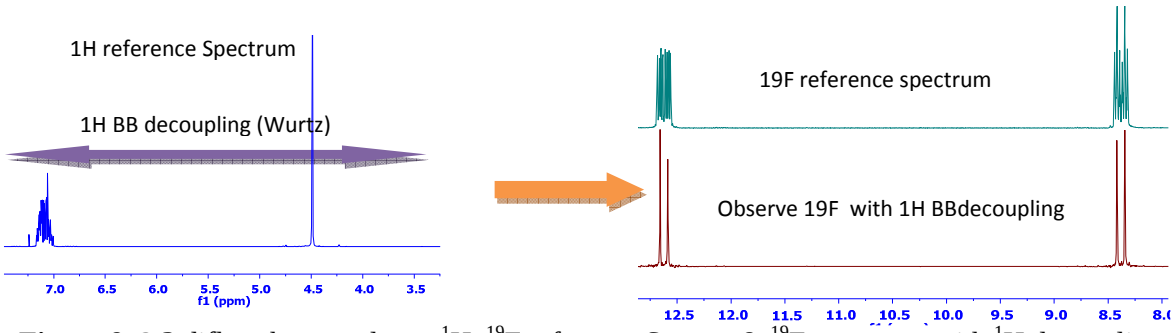

Figure 9. 2,3 difluro bromotoluene ^{1}H, ^{19}F reference Spectra & ^{19}F spectrum, with ^{1}H decoupling

The selective decoupling experiments (^{1}H or ^{19}F) may be useful to identify and measure J_{19F1H} . In the BrukerAvance 600 with a probehead (BBO BB/19F-1H/D), it is possible to carry out all 1D experiments $^{19}F\{^{1}H\}$ or $^{1}H\{^{19}F\}$ in broadband or selective mode, and also 2D NOESY ^{1}H-^{19}F.

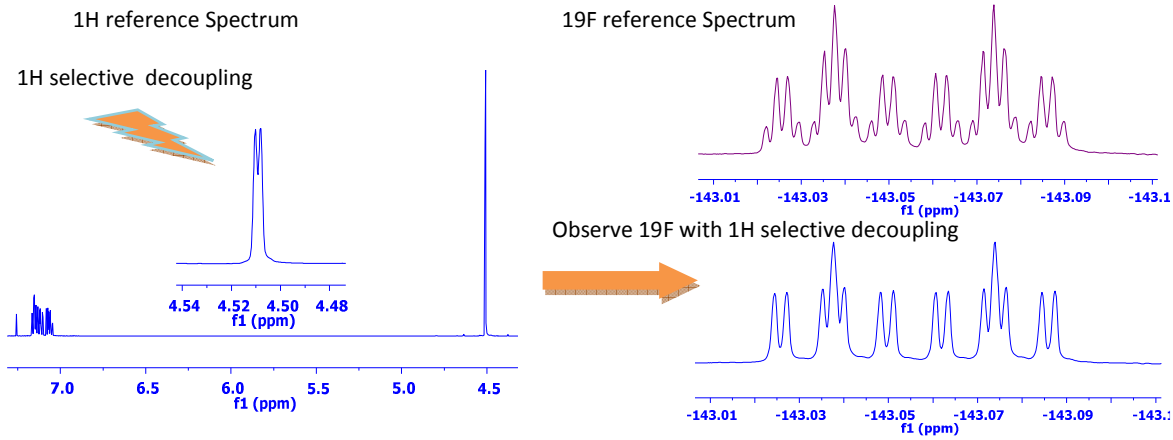

Figure 10 ^{19}F spectrum of 2,3 difluro bromotoluene with ^{1}H selective decoupling

Figure 10 shows the spectrum of ^{19}F with selective ^{1}H decoupling of the CH_2Br group, which allows checking the assignment of the signal at -143 ppm as the ^{19}F at position 2.

3.7. HRMAS (High Resolution Magic Angle Spinning)

There is a wide variety of samples unsuitable to be studied with common liquid-state NMR probes. The nature of these samples can be as different as polymer gels, lipids, biological tissues, swollen resins, food, etc. What they have in common is heterogeneity and restricted or anisotropic motion which results in broad NMR signals.

Figure 11. Small rotor being inserted into the magnet

High Resolution Magic Angle Spinning (HRMAS) NMR technique allows extending NMR studies to these heterogeneous samples. A special probe designed to perform solution type experiments while spinning the sample up to 16 kHz at the magic angle (θ=54.74°) is used. Under such conditions, broadening of NMR signals coming from differences in magnetic susceptibility is reduced, and leads to NMR spectra that display resolution approaching that of liquid samples. The quality of spectra depends only on the degree of mobility of the sample. All usual NMR experiments available on liquid probes (both 1D and 2D) are able to be run on a HRMAS probe.

ChT.4

Samples under study for this probe are prepared with some amount of solvent in specially designed zirconium oxide rotors with a final sample volume ranging from 12 or 80 µL (see on Fig. 11 a small white rotor being inserted into the magnet). Solvent added helps in increasing mobility.

Different nature of samples has been studied in our facility with this probe, and a pair of examples is shown in next figures. Figure 12 corresponds to an aminomethylated resin swollen in $CDCl_3$ and subsequent inclusion of a handle, characterized by an aldehyd function, easily detected on the spectrum by the characteristic signal at low field.

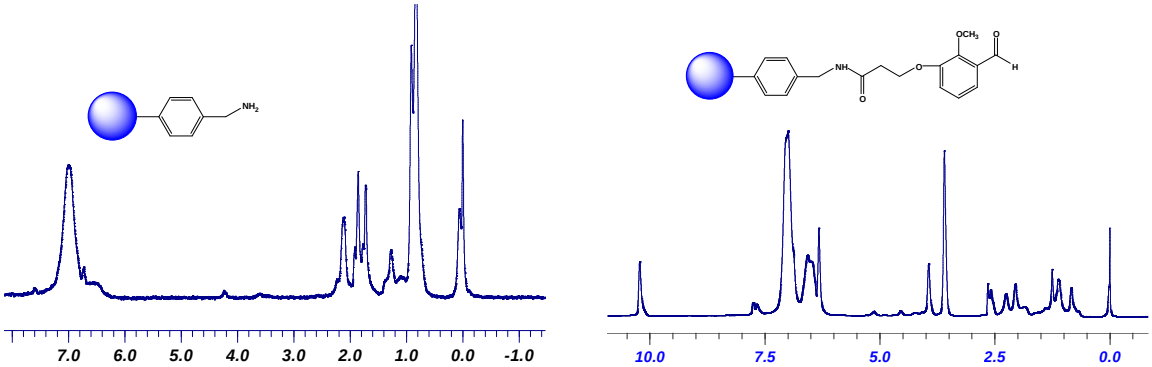

Figure 12 Anchoring of a handle in a resin followed by HRMAS

In our lab, in collaboration with Prof. C. Arús research group (UAB)[17] HRMAS has been used in a study to validate brain tumour biopsy classification by comparing meningiomas (MM), a benign tumour, with glioblastoma multiform (GBM), an aggressive tumour. Initial studies of this

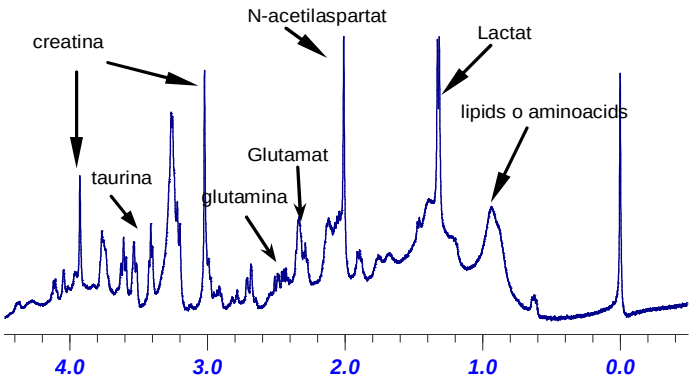

Figure 13. HRMAS spectrum of mouse brain sample

kind of samples with the aim to identify different metabolites on brain were run on mouse brain samples (Figure 13).

3.8. Structural and dynamic studies of proteins in solution by NMR Spectroscopy

NMR spectroscopy is a powerful tool for protein 3D structure determination at atomic resolution, as well as for the study of protein recognition processes and dynamic features of these macromolecular structures.

Strategies for structural studies by NMR largely depend on protein size. Peptides and small proteins (up to 10-12 kDa) can be studied with ^{1}H NMR spectroscopy using 2D TOCSY and DQF-COSY experiments to identify amino acid spin systems and 2D NOESY experiments to carry out the sequential resonance assignment[3], as the first step of the process. Secondly, structural restraints needed for structure determination, such as inter-proton distances and torsion angles, are calculated from NOE intensities in NOESY spectra and coupling constants in DQF-COSY, respectively. Finally, a computing algorithm is used to calculate a set of structures compatible with those NMR-derived constraints. Experiments above are regularly used in the high-field instruments in our NMR Facility and we have applied the described methodology to calculate the structure of several small proteins and peptides (see Figure 14 as an example), in collaboration with Prof. Ernest Giralt[18,19]

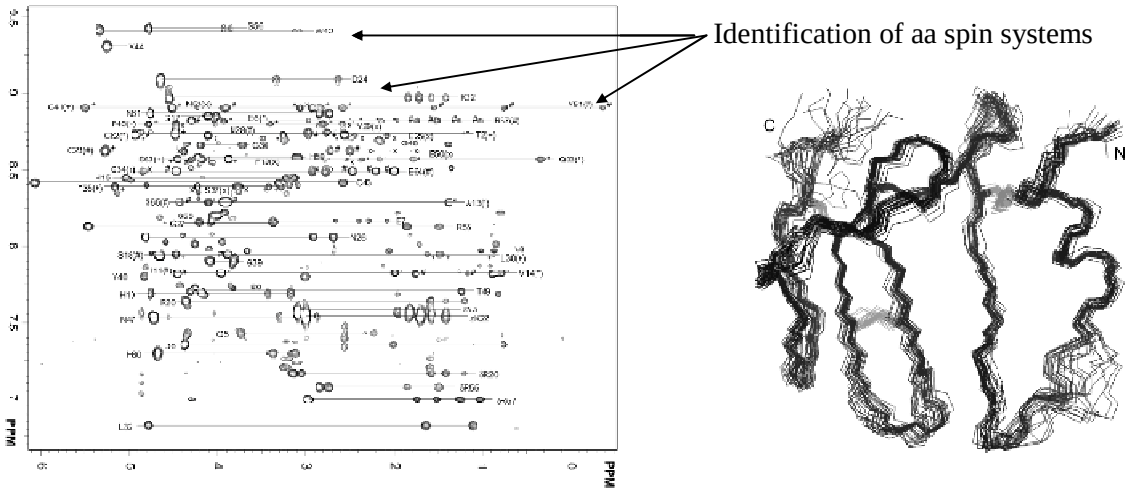

Figure 14. Region of a 2D TOCSY spectrum of the P41icf protein[16] (1mM, 15% D2O/ H2O, pH 5.7) recorded at 800 MHz and 288 K (left). Superposition of the 30 calculated structures of P41icf obtained by ^{1}H NMR spectroscopy (right).

The study of proteins up to 25-30 kDa requires the incorporation of isotopic labels (^{15}N, ^{13}C) to the protein to solve signal overlap problems in ^{1}H spectra. In this case, protein assignment[20] is based on 3D ^{15}N-edited TOCSY/ NOESY experiments and/or 3D triple resonance experiments correlating ^{1}H, ^{15}N and ^{13}C frequencies. A large set of 3D experiments is fully implemented in our 600 and 800 MHz spectrometers for the purpose of resonance assignment. Protein perdeuteration and/or the use of Transverse Relaxation Optimized Spectroscopy (TROSY)[5] are necessary to study proteins larger than 25 kDa in order to decrease transverse relaxation rates and to obtain satisfactory signal line widths. TROSY methodology applied to ^{1}H-^{15}N HSQC spectra combined with ^{15}N-selective labeling prove to be very useful in the study of binding events of large proteins, where the whole resonance assignment is not necessary, as has been demonstrated with POP, a serine protease of 80 kDa, one of the largest proteins studied in our Facility in collaboration with Prof. Giralt[21]

In addition to structural information, dynamics and stability of globular proteins can also be studied by NMR spectroscopy through hydrogen/deuterium (H/D) exchange experiments, by measuring the protection of labile hydrogen's against exchange with solvent deuterons. A very interesting example involves the H/D exchange study of amyloid fibrils formed from the SH3 domain of the α-subunit of bovine phosphatidylinositol-3'-kinase (PI(3)K-SH3) at pH 1.6, carried

out in our Facility in collaboration with Dra. Natàlia Carulla[22]. The site-specific hydrogen exchange behavior of this protein within amyloid fibrils was analyzed by 2D ^{1}H-^{15}N HSQC spectroscopy. Resonance assignment of the protein was previously done by standard 3D ^{15}N-edited TOCSY and NOESY experiments and 3D triple resonance experiments, CBCA(CO)NH and CBCANH. The degree of exchange was calculated for each hydrogen amide in the protein backbone from peak volumes in ^{1}H-^{15}N HSQC spectra (Figure 15, left) recorded after H/D exchange (V_{D2O}) relative to those before exchange (V_{H2O}), where V_{D2O}/ V_{H2O} =1 means no exchange (Figure 15, right). H/D exchange results indicated that SH3 molecules are highly resistant to exchange when incorporated into fibrils and that the majority of residues exchange to a similar degree. Complementary information derived from electrospray ionization mass spectrometry highlights that exchange is dominated by a mechanism of molecular recycling within the fibril population revealing the dynamic nature of amyloid fibrils.

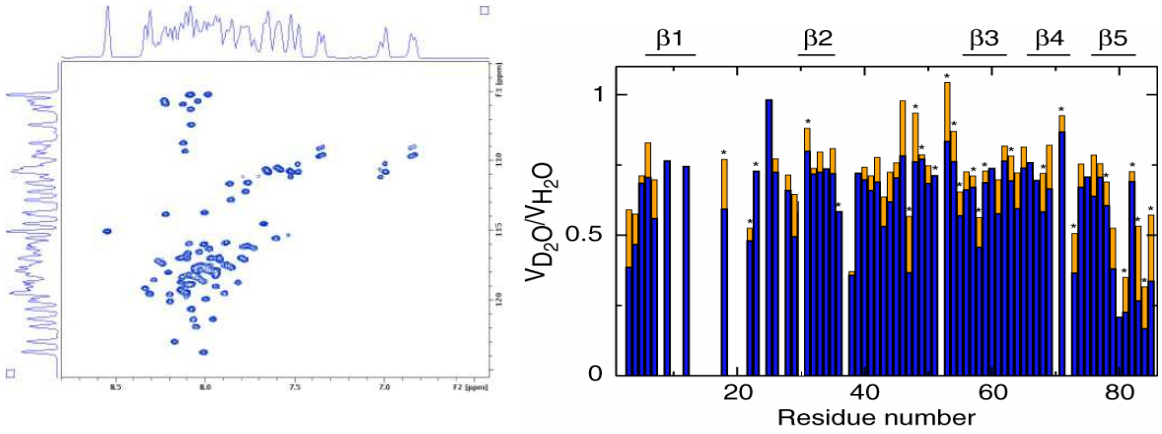

Figure 15. ^{1}H-^{15}N HSQC spectra of PI(3)K-SH3 at 800 MHz (left). H/D exchange of PI(3)K-SH3 amyloid fibrils monitored by NMR spectroscopy (right).

Acknowledgments

We thank Dr. Miquel Pons, Dr. Ernest Giralt, Dr. Natalia Carulla, Dr. Carles Arús, Dr. Xavier Salvatella and Dr. Ernesto Nicolás for their collaboration and permission to use part of their data in this document. We also wish to thank everyone who in one way or another has contributed to the completion and revision of this document, especially to all the technical staff of the NMR facility for their interest and dedication. We thank the Spanish Ministerio de Ciencia y Innovación (MICINN) for funding most of the high-field instrumentation and the European Regional Development Fund (ERDF) for funding the shielded Bruker 600 instrument.

References

[1] 1952 Nobel Prize: Felix Bloch & Edward Mills Purcell "for their development of new methods for nuclear magnetic precision measurements and discoveries in connection therewith" http://nobelprize.org/nobel_prizes/physics/laureates/1952.

[2] Nobel Prize1991: Richard R. Ernst "for his contributions to the development of the methodology of high resolution nuclear magnetic resonance (NMR) spectroscopy" http://nobelprize.org/nobel_prizes/chemistry/laureates/1991.

[3] K. Wuthrich; NMR of Proteins and Nucleic Acids (1986), Wiley, New York
Nobel Prize 2002: Kurt Wuthrich- "for his development of nuclear magnetic resonance spectroscopy for determining the three-dimensional structure of biological macromolecules in solution" http://nobelprize.org/nobel_prizes/chemistry/laureates/2002.

[4] High-Resolution NMR Techniques in Organic Chemistry, Volume 27, Second Edition (Tetrahedron Organic Chemistry) [Paperback] T.D.W. Claridge

[5] A Complete Introduction to Modern NMR Spectroscopy, Wiley-Interscience (November 26, 2008), Roger S. Macomber

[6] K. Pervushin, R. Riek, G. Wider, K. Wüthrich; "Attenuated T2 relaxation by mutual cancellation of dipole–dipole coupling and chemical shift anisotropy indicates an avenue to NMR structures of very large biological macromolecules in solution"; Proc. Natl. Acad. Sci. USA (1997) 94, 12366–12371

[7] Jocelyne Fiaux, Eric B. Bertelsen, Arthur L. Horwich and Kurt Wüthrich; *"NMR analysis of a 900K GroEL–GroES complex"; Nature* 418, 207-211 (11 July 2002)

[8] M. Martinell, X. Salvatella, J. Fernández-Carneado, S. Gordo, M. Feliz, M. Menéndez, and Ernest Giralt. *"Synthetic Ligands Able to Interact with the P53 Tetramerization Domain. Towards Understanding a Protein Surface Recognition Event*" ChemBioChem7, 1005 (2006)

[9] Brian J. Stockman, and Claudio Dalvit, "*NMR screening techniques in drug discovery and drug design*" Progress in NMR Spectroscopy 41, 187 (2002)

[10] http://www.rmn.ub.es/cat/servicios/equipos/equipos.php

[11]http://www.fda.gov/Drugs/DrugSafety/PostmarketDrugSafetyInformationforPatientsandProviders/UCM112597

[12] http://www.usp.org/hottopics/heparin.html and http://www.edqm.eu/en/Search-519.html.

[13] USPC Official 12/01/09-4/30/10 NF Monographs Poloxamer; Pharmacopoeial Forum: Volume No. 33(4) Page 714; *European Pharmacopoeia* 01/2008 1664 E

[14] Miguel Feliz, Jesús García, Eric Aragón, and Miquel Pons* "*Fast 2D NMR Ligand Screening Using Hadamard Spectroscopy*"; *J. Am Chem Soc.* Vol 128,No 22, 7146 (2006)

[15] Mayer, M. and B. Meyer, *"Characterization of ligand binding by saturation transfer difference NMR Spectroscopy"*. Angewandte Chemie-International Edition 38 1784 (1999)

[16] Ben Wiseman, Xavi Carpena, Miguel Feliz, Lynda J. Donald, Miquel Pons, Ignacio Fita and Peter C. Loewen. *"Isonicotinic Acid Hydrazide Conversion to Isonicotinyl-NAD by Catalase-peroxidades ". Journal of Biological Chemistry* , 85, 26662 (2010)

[17] Daniel Valverde-Saubí, Ana Paula Candiota, Maria Antònia Molins, Miguel Feliz, Óscar Godino, Myriam Dávila, Juan José Acebes, Carles Arús; *"Short-term temperature effect on the HRMAS spectra of human brain tumor biopsies and their pattern recognition analysis"*; Magn Reson Mater Phy (2010) 23:203–215

[18] C. Chiva, P. Barthe, A. Codina, M. Gairí, F. Molina, C. Granier, M. Pugnière, T. Inul, H. Nishi, Y. Nishiuchi, T. Kimura, S. Sakakibara, F. Albericio, E. Giralt; "Synthesis and NMR structure of P41icf, a potent inhibitor of human Cathepsin L"; J. Am. Chem. Soc. (2003), 124, 1508-1517

[19] M. Gairí, P. Saiz, S. Madurga, X. Roig, J. Erchegyi, S. C. Koerber, J. C. Reubi, J. E. Rivier, E. Giralt;"Conformational analysis of a potent SSTR3-selective somatostatin analogue by NMR in water solution"; J. Pept. Sci. (2006) 12, 82-91

[20] M. Sattler, J. Schleucher, C. Griesinger; "Heteronuclear multidimensional NMR experiments for the structure determination of proteins in solution employing pulsed field gradients"; Progress in NMR Spectroscopy (1999) 34, 93-158

[21] T. Tarragó, B. Claasen, N. Kichik, R. Rodríguez-Mias, M. Gairí, E. Giralt; "A cost-effective labeling strategy for the NMR study of large proteins: selective 15N-labeling of the Trp side chains of Prolyl Oligopeptidase"; ChemBioChem (2009) 10, 2736-2739

[22] N. Carulla, G. L. Caddy, D. R. Hall, J. Zurdo, M. Gairí, M. Feliz, E. Giralt, C. V. Robinson, C. M. Dobson; "Molecular recycling within amyloid fibrils"; Nature (2005) 436, 554-558. DOI: 10.1038/nature03986

Basics of Mass Spectrometry

Lourdes Berdié[1], Isidre Casals[2], Irene Fernández[3], Olga Jáuregui[2], Rosa Maria Marimon[4], Joaquim Perona[4], and Pilar Teixidor[1]

[1] Unitat de Cromatografia de Gasos i Espectrometria de Masses, CCiTUB, Universitat de Barcelona. Lluís Solé i Sabarís 1-3. 08028 Barcelona, Spain.

[2] Unitat de Tècniques Separatives d'Anàlisi, CCiTUB, Universitat de Barcelona. Parc Científic de Barcelona. Baldiri Reixac, 10. 08028 Barcelona, Spain.

[3] Unitat d'Espectrometria de Masses de Caracterització Molecular, CCiTUB, Universitat de Barcelona. Fac. Química. Martí i Franquès s/n. 08028 Barcelona, Spain.

[4] Unitat de Medi Ambient, CCiTUB, Universitat de Barcelona. Fac. Geologia. Martí Franquès, s/n. 08028 Barcelona, Spain.

email: *ifernandez@ccit.ub.edu, isidre@ccit.ub.edu, marimon@ccit.ub.edu, teixidor@ccit.ub.edu*

Abstract. This article summarizes the basic principles of mass spectrometry instrumentation with special emphasis in sample introduction methods, ionization techniques and mass analyzers used in the different mass spectrometry techniques.

1. Introduction

Mass spectrometry (MS) is a powerful analytical technique [1, 2]. Over the past decades, mass spectrometry has undergone tremendous technological improvements that have made it an essential analytical tool in chemistry, biochemistry, pharmacy and medicine. Mass spectrometry is employed to analyze combinatorial libraries, sequence biomolecules, structural elucidation of unknowns, environmental and forensic analysis, quality control of drugs, flavours and polymers. Mass spectrometry has both qualitative and quantitative uses.

To achieve these goals, a mass spectrometer ionizes the chemical compounds to generate charged molecules or molecule fragments and measures their mass-to-charge ratios (m/z).

A mass spectrometer [3] consists of an ion source (ionization), a mass analyzer (separation of ions) and a detector (detects and measures the number of ions formed). Mass analyzer, detector and some ion sources operate under high- vacuum conditions in order to allow ions to reach the detector without colliding with other gaseous molecules or atoms (see Fig. 1). Sample molecules are introduced into the instrument through a sample inlet.

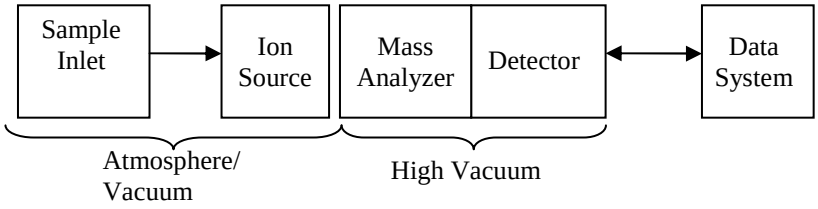

Figure 1. Schematic diagram of the mass spectrometry technique

Results are presented as a *Mass Spectrum:* a two-dimensional representation of signal intensity (abundance of ionic species) (ordinate) versus m/z (abscissa). The most intense peak of a mass spectrum is called *base peak*. In most representations of mass spectral data, the intensity of the base peak is normalized to 100% of relative intensity.

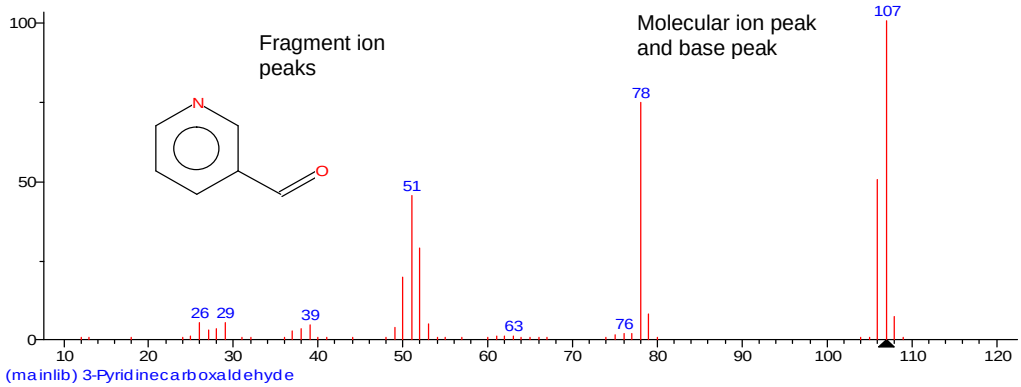

Figure 2. Typical mass spectrum of a 3-Pyridinecarboxaldehyde

Ionization of compounds can be achieved by several mechanisms in the source: ionization of a neutral molecule through electron ejection, electron capture, protonation, cationization, deprotonation, transfer of a charged molecule to the gas phase. Ionic species obtained correspond to whole molecule or fragments.

Mass spectrometry is used with direct insertion probes, but also in tandem with gas chromatography (GC-MS), liquid chromatography (LC-MS) or other separation techniques, fitted with different kind of ionization sources. The basis of these combined techniques is reviewed in this contribution. Examples of applications will be given elsewhere in this Handbook.

2. From sample to mass spectrometer

2.1. Sample introduction in GC-MS

When an analysis of a sample is to be performed by GC-MS, it is necessary to plan some previous steps. Often, if the sample is introduced as it is, no information is obtained, and, in some cases, the apparatus can be damaged. In a gas chromatograph, the sample is introduced in an injector where the gases or vapours resulting from the sample are normally split and part of them are introduced into the chromatographic column by means of a carrier gas. As a result the effluent enters continuously in the ionization source. There are other injection configurations such as splitless (where there is no split of the vapour gases before the column), on column and other specific for large volumes.

The first condition that analytes have to fulfill is to be volatile and thermostable. Some small molecules are volatile and, as a result, no preparation is needed if a convenient column to analyse them is used. But many molecules are not volatile enough, especially if they are polar. Therefore, chemical strategies must be planned to improve their volatility. There are many derivatization reactions for gas chromatography described in the literature, the most used among them, are methylation and silylation of polar functional groups such as –OH and $–NH_2$.

Different injection ports are available to inject different kind of samples.

- Direct injection; liquid or gas samples can be injected into the injection port using a syringe. Packed columns can analyze some hundred micrograms of analytes meanwhile capillary columns can only be charged with less than ten micrograms.
- Head-space injector is a common system used to analyse gases and vapours in equilibrium with liquid or solid samples (studies of residual solvents, contaminants, etc). The sample is introduced in a vial, stopped with a septum, closed hermetically, and placed on a thermostatic block at a determined temperature. After an equilibration time with the inner atmosphere, an aliquot of that vapour phase is injected into the column.
- Cooled injection devices are very versatile. In the past, they were designed for the analysis of very volatile molecules, but today combinations of cooled and heated areas (liquid N_2, decompression of CO_2, peltiers and electrical resistances) give to this devices a wide applications range. They allow venting the solvent, avoiding its entrance in the column, and focusing the analytes in bands of its chromatographic analysis. A simple injector of this kind is used in mineral analysis to trap CO_2 to be analyzed by isotope ratio mass spectrometry (IRMS).
- Pyrolysis of the sample is useful in some applications, such as in oil and polymer studies. The sample is introduced in a high temperature oven and a ramp of temperature is activated (50 – 1000 ºC). During the ramp heating, the sample decomposes and the fragments of the molecules resulting from the pyrolysis are analysed.
- Elemental analyzers fitted with GC are also used to introduce the gases resulting from the combustion or pyrolysis of a sample into a mass spectrometer. N_2, CO_2, H_2O and SO_2 yielded by combustion, or CO and H_2 coming from pyrolysis of a sample are analysed in a mass spectrometer, usually to study the isotopic composition of the elements N, C, H, O and S in the analyte.
- Fibers and other absorbents or adsorbents are also used as a trap for specific substances in liquid or gaseous samples (water, atmosphere…). The material in which the analytes are adsorbed is introduced in the injector and heated to desorb the analytes, which are then separated and analyzed in the mass spectrometer.

2.2. Ionization Sources for GC-MS

2.2.1. Electron Impact Ionization

In a vacuum region, a current passes through a metallic filament, chosen as the source of electrons. An electrostatic field is used to detach electrons from the heated filament, which are focused so as to form a beam of electrons that will impact into the analyte area. This area is the end of the

column or the cup of a direct introduction probe, in its way to the counter electrode. As a result of electron impact (EI), the analyte molecules are ionized and fragmented. Using electric fields and lens, the resulting ions are driven into the spectrometer where they are analyzed. Usually, a wide range of molecular fragments is obtained, increasing in number when the energy of the electron beam increases. Usually only positive ions are analyzed. Extensive EI ionization spectra databases are available in the literature.

2.2.2. Chemical Ionization

While EI is a very strong form of ionization, chemical ionization (CI) is very gentle. Usually EI results in a great number of fragments of the molecule and often the molecular ion signal cannot be observed. In CI, the number of signals is less than in EI and, as a result, the pseudomolecular ion yields a high signal. A reagent gas is ionized in the ion source by electron impact, and the resulting ions are accelerated and they impact against the analyte molecules. The obtained fingerprint depends on the energy, pressure, temperature, purity, and nature of the gases used to ionize. Methane and ammonia are the most common used gases. The mechanisms of ion formation are: proton transfer, exchange of charge, formation of adducts and abstraction of an anion. In each experiment, the identification of the ions must be studied.

2.3. Sample introduction in LC-MS

The preparation of the sample is very important before attempting its analysis by LC-MS. It is important to choose a suitable solvent in order to get the maximum ionization efficiency of the analyte, because using a mass spectrometer we will only analyze ions: positive or negative. The simplest case is an aqueous solution of an ionic salt: it yields solvated anions and cations in solution. But many substances are not ionic and then ionization is not possible or only in a very small degree.

The election of the solvent depends on both the nature of the analyte and the ionization source of the spectrometer. When the sample is introduced via direct infusion, the solvent and the liquid carrier are usually the same. In this case, a syringe is used to push the liquid solution to the interface. If we use a liquid chromatograph, the composition of the mobile phase is usually different from the solvent of the sample and, in addition, it can vary with time (gradient). In general, the solvents used in LC-MS must be volatile or vaporizable, free of crystallizations or other solid formations when they are vaporized to avoid obstruction of the capillary entrance to the mass spectrometer.

2.4. Ionization sources for LC-MS

2.4.1. Electrospray Ionization

Nowadays the most universal ion source in High Performance LC-MS is electrospray ionization (ESI). In fact, we would say nitrogen- assisted electrospray, usually named by its acronym ESI. The liquid that carries the analytes is pushed to a nebulizer installed into a chamber at atmospheric pressure. The chamber is placed in front of a cone that has a capillary orifice, allowing the entrance of the ions in the mass spectrometer. There is a potential difference between the cone and the spray tip, that is, an electrostatic field. The polarity of this field determines the ions to be analyzed. In addition, the chamber is heated in order to evaporate the solvent. In these conditions, the ions that are in solution are both desolvated and attracted to the entrance of the spectrometer.

2.4.2. Atmospheric Pressure Chemical Ionisation

Atmospheric pressure chemical ionization (APCI) sources can be considered as a variant of ESI sources, in which a discharge needle is added in the chamber. Between the needle and ground, a high difference of potential is established, which creates a corona discharge that ionizes molecules present in the spray (mainly from the solvent). In ESI sources, the ions must be present in the sprayed solution, while in APCI sources, the ions formed are accelerated in the electrostatic field originating at the tip of the cone. In this pathway, the formed ions impact on the neutral analyte

molecules and transfer the electrical charge to them. As a result, the analyte molecules become ions, which are "visible" for the mass spectrometer.

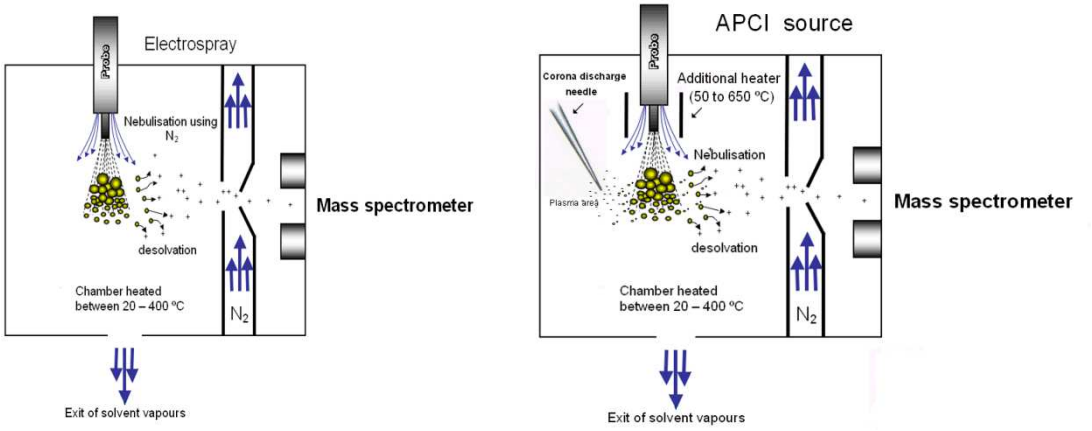

Figure 3. Schematic representation of ESI and APCI sources

2.4.3. Atmospheric Pressure Photoionization

In atmospheric pressure photoionization (APPI) sources, the ionization of the solvent molecules, which will ionize the analyte molecules by charge transfer, is produced by an intense source of ultraviolet light that illuminates the spray.

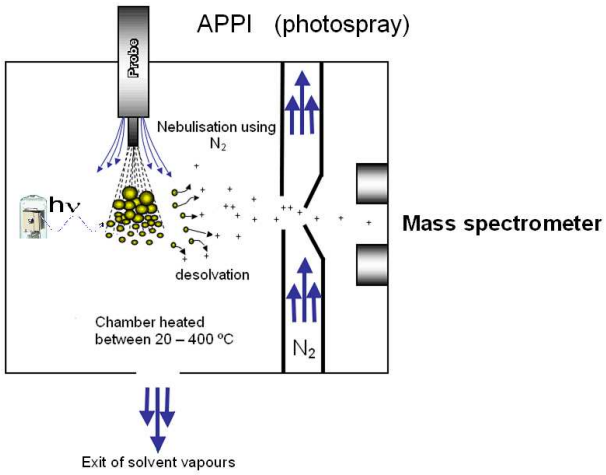

Figure 4. Schematic representation of an APPI source

2.4.4. Plasma torch

When elemental analysis is the goal using a mass spectrometer, a plasma torch is the ionization source of choice. The resulting technique is referred to as inductively-coupled plasma mass spectrometry (ICP-MS). Usually three concentric flows of argon are used in this source: in the centre a nebulizer is used to spray the analytical solution, a second flow of argon is used in a corona to generate the plasma inside a strong radiofrequency field, and finally a third argon flow protects the instrument parts from the high temperatures reached in the plasma region (up to 10,000 K). When a nebulized sample enters into the plasma region, almost all the molecules break down in their atomic components and many of the atoms lose one electron becoming single charged ions. Aided by an electrostatic field and often by the aspiration of a vacuum pump, the created ions follow a beam toward the tip of the sampling cone, where a capillary hole allows their entrance into

the mass spectrometer for mass analysis. The ICP-MS coupling results in a powerful elemental analyzer, very sensitive and capable to cover almost all the elements of the periodic table. For many metals and non metals, it reaches parts per trillion of the element in the analytical solution.

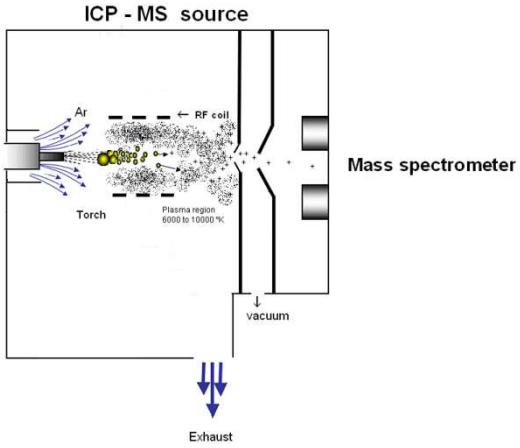

Figure 5. Schematic representation of an ICP-MS source

2.4.5. Matrix Assisted Laser Desorption/Ionization

Matrix-assisted laser desorption/ionization (MALDI) is an ionization technique mainly used with time-of-flight (TOF) mass spectrometers. Samples are prepared as solid solutions, where the solvent is a substance, named matrix, able to be ionized by a laser beam. When the solid solution is irradiated with a pulsed laser beam (in the ultraviolet range) the heat evaporates small quantities of the solid and a small part is ionized mainly by charge transfer. An electrical field attracts the ions into the spectrometer.

Polymers and biopolymers are the main substances analyzed by using this technique, but it can also be used for the analysis of many organic molecules, inorganic complexes and minerals. Its characteristic is the softness, and usually only single charged ions are obtained. When combined with the high resolution of a TOF analyzer, results in a very good tool to determine molecular weights with high accuracy.

The solid solution is prepared from a liquid solution of the matrix in a volatile solvent in which the sample is also dissolved. A small drop of few microliters of the solution containing the sample and the matrix is placed on a plate and the liquid solvent is allowed to evaporate (acetonitrile, methanol, aqueous trifluoroacetic acid…). The result is a small dry spot on which a laser beam is focused. The more common matrices are 2, 5-dihydroxybenzoic acid (DHB); alpha-cyano-4-hydroxycinnamic acid; 3,5-dimethoxy-4-hydroxycinnamic acid (sinapinic acid); ferulic acid, picolinic acid, and other molecules with aromatic rings or conjugated double bonds.

Many of the novel sources being studied nowadays are variants of those described above, while others are innovative. All these novel sources are aimed at improving sensitivity, stability and easy operation.

3. Mass analyzers

The mass analysis of ions in the gas phase is based on the interactions of ions with electric and magnetic fields. Until the 1960s, most of the mass spectrometers were dedicated to physics, organometallics and organic chemistry and were based on magnetic sectors. In these spectrometers, high-resolution conditions were generally achieved by means of an electrostatic sector. The double-focusing systems were instruments of larger dimensions and difficult to use, and were mainly used in high-level and academic environments. The development of devices based on electrodynamic fields led to the production of quadrupoles and ion traps of small dimensions and mass spectrometers became bench-top instruments. Their easiness of use, as compared to double-

focusing instruments, and the possibility of interfacing them easily with data systems moved mass spectrometry to the application labs.

The mass analyzer is the portion of the mass spectrometer where charged analyte molecules are separated based on the *m/z* ratio. In addition to the choice of ionization source, many different types of mass analyzers can be chosen. These include magnetic sector, ion trap (IT), quadrupole systems, TOF and Fourier transform mass analyzers. Each mass analyzer has its advantages and disadvantages. Here, a description of the currently most widely employed analyzers is given.

3.1. Time-of-flight

The linear TOF mass analyzer is, from the theoretical point of view, the simplest mass analyzer. It simply consists of an ion source and a detector, and between them is a region under vacuum. It is based on accelerating a group of ions towards the detector where all the ions are given the same amount of energy through an accelerating potential. Because the ions have the same energy but different mass, the lighter ions reach the detector first because of their greater velocity. As a result ions with different *m/z* ratios reach the detector at different times, which is proportional to the square root of their *m/z* value. The calibration of the time scale with respect to the *m/z* value can be easily obtained by injection of samples of known mass (standards of calibration). When compared to quadrupole (Q) and sector systems, this analyzer cannot operate in a continuous mode. The main advantages of this analyzer are its high speed and wide mass range (when analyzing high-molecular weight compounds such as polymers or biomolecules, TOF mass analyzers are often employed due to their virtually unlimited mass range).

In its hybrid configuration, the Q-TOF instrument is capable of performing MS/MS analysis. The ions of interest generated in the source, are selected by the quadrupole mass filter Q1. The collision takes place in Q2. The product ions are analysed by the TOF analyzer, and thus accurate masses of the collisionally generated product ions (as well as their precursors) can be easily obtained, allowing the determination of their elemental composition. The resolution of TOF instruments can be improved by using a reflectron. Today, resolutions up to 20.000 are achieved by commercial instruments.

With the same aim (MS/MS analysis) modern instruments with two TOF analyzers (TOF/TOF configuration) are available.

3.2. Fourier transform ion cyclotron resonance

Fourier transform ion cyclotron resonance (FTICR) is a type of mass analyzer which involves accelerating ions in a particle accelerator known as cyclotron. The charged particles move in circular paths perpendicular to a uniform magnetic field at a characteristic frequency known as the cyclotron frequency, which is dependent on the *m/z* ratio. Pulsed radiofrequency (RF) radiation is used to excite ions to paths of larger radius and this radiation causes them to move in phase, which creates an image current. A Fourier transform is then employed to obtain oscillation frequencies for ions with different masses, resulting in an accurate reading of their *m/z* ratio and high-mass resolution. The FTICR analyzer differs from other kinds of mass analyzers in that ions are not separated prior to detection. Thus, the different ions are not detected in different places as sector instruments or at different times as in TOF instruments, but all ions are detected simultaneously over a given period of time. This technique offers very high resolution (up to 100.000) that can be increased (up to 1.000.000) by increasing the magnetic field strength of the magnet or by increasing the detection duration. It is important to note that a signal is generated only by the coherent motion of an ion under ultra-high vacuum (10^{-11}-10^{-9} Torr) and that the signal has to be measured for a minimum time (from 500 ms to 1s) to provide high resolution. This could be a drawback, if compared to TOF systems, in order to couple them with ultra-performance liquid chromatography (UPLC) systems.

Nowadays, some hybrid instruments using this technology such as the Orbitrap are available. These instruments allow MS^n experiments to be performed previous to the FTMS analyzer, thus providing ultra-high resolution and accurate mass data both in precursor and in product ions.

3.3. Quadrupole mass filter

Quadrupole mass analyzers are still the most common mass analyzers in existence today. In the quadrupole mass filter, the application of a particular combination of DC and RF voltages to four parallel metal rods creates a filtering device through which only ions of a defined *m/z* value are transmitted. Changing the ratio of the voltages changes the *m/z* value of the ion that is passed through the detector. The quadrupole mass filter can also be operated in other modes, such as passing a mass range of ions through the detector. If only the rf portion of the voltage is applied to the rods, essentially all ions are passed through to the detector. Quadrupole instruments can typically resolve ions that differ by one mass unit. Hexapole and octapole ion guides have also been devised, and they operate under similar principles. Quadrupoles offer three main advantages: they tolerate relatively high pressures, they have significant mass range with the capability of analyzing up to an *m/z* of 4000 and they are relatively low cost instruments. The triple quadrupole mass spectrometer consists of three quadrupoles connected in tandem. The first and third quadrupoles act as mass filters, while the second quadrupole (non-mass filtering) serves as a collision chamber. In this way, tandem mass spectrometry can be accomplished through different MS/MS experiments: the product ion scan (where the product ions from a precursor were scanned), the precursor ion scan (where one examines all of the precursor ions capable of fragmenting to produce a particular product ion), the neutral loss scan (that involves looking at pairs of precursor and product ions that differ by a defined constant neutral loss) and the selected reaction monitoring (SRM). This one is the most sensitive mode and consists in simultaneously monitoring multiple precursor-product ion pairs.

3.4. Quadrupole Ion trap analyzer

The difference with a quadrupole is that ions, rather than passing through a quadrupole analyzer with a superimposed radio frequency field are trapped in a radio frequency field. An ion trap analyzer consists of two hyperbolic endcap electrodes and a ring electrode into a compact device that serves as mass analyzer. The motion of the ions induced by the electric field of the ions allows them to be trapped or ejected from the ion trap. In the normal mode, the radio frequency is scanned to resonantly excite and, therefore, eject ions through small holes in the endcap to the detector. As the RF is scanned to higher frequencies, higher m/z ions are excited, ejected and detected. A very useful feature in ion traps is that it is possible to isolate one ion species by ejecting the rest from the trap. The isolated ions can be fragmented by collisional activation and the fragments detected. As a result, quadrupole ion traps have been used in MS^n applications. The advantages of quadrupole ion traps include the possibility of performing LC-MS/MS in real time, their compact size and their ability to trap and accumulate ions to provide a better ion signal.

3.5. Linear Ion Trap

The linear ion trap differs from the 3D ion trap as it confines ions along the axis of a quadrupole mass analyzer using a two dimensional (2D) RF field with potentials applied to end electrodes. It has a greater dynamic range and an improved quantitative range of quantitative analysis if compared to the 3D trap.

3.6. Double-Focusing Magnetic Sector

In the double-focusing magnetic sector, ions are accelerated into a magnetic field using an electric field. A charged particle traveling through a magnetic field will travel in a circular motion with a radius that depends on the speed of the ion, the magnetic field strength and the ion's *m/z* ratio. To increase the drawback of its low resolution, an electrostatic analyzer is added to focus the ions but this technique results in a decrease in sensitivity. These are called double-sector instruments and are used with ESI, FAB and EI ionization. However, they are not widely used today mainly because of their large size and the success of TOF, quadrupole and FTMS analyzers.

References

[1] G. Siuzdak, “The expanding role of mass spectrometry in biotechnology”, Ed. MCC Press (2006).
[2] I. Lavagnini et al. “Quantitative applications of mass spectrometry”, Ed. John Wiley & Sons LTD., (2006).
[3] Jürgen H. Gross, “Mass Spectrometry. A Textbook”, Ed. Springer (2004).

Gas Chromatography - Mass Spectrometry

Lourdes Berdié[1], Irene Fernández[2], and Pilar Teixidor[1]

[1] Unitat de Cromatografia de Gasos i Espectrometria de Masses, CCiTUB. Lluís Solé i Sabarís 1-3. 08028 Barcelona, Spain.

[2] Unitat d'Espectrometria de Masses (Química), CCiTUB. Facultat de Química. Martí i Franquès s/n. 08028 Barcelona, Spain

email: *lourdesb@ccit.ub.edu, i.fernandez@ccit.ub.edu, teixidor@ccit.ub.edu*

Abstract. This article briefly describes the possible configurations of the gas chromatography- mass spectrometry (GC/MS) technology available at the CCiTUB. Some developed examples of different applications are shown.

1. Introduction

The technology of gas chromatography-mass spectrometry (GC/MS) combines the fine separating power of GC (complex mixtures of hundredths of compounds) with the two main competences of MS:

- Powerful detection
- Strong capacity of unknown identification

The applied GC/MS unit of the Scientific and Technological Centers has the ability to select, practice and develop the different appropriated methods of extraction, clean-up, concentration and derivatization of organic compounds in a great variety of natural and synthetic samples, from mineral to biological world in order to analyze the prepared extracts by GC/MS towards the process of identifying and quantifying the extracted organic compounds.

Method developments and subsequent validation following the International Conference of Harmonization (ICH) guidelines are also performed if they are required.

2. Methodology

Several GC/MS systems with capillary column separation and different ionization methods are available in the Unit. These systems are summarized in Table 1.

Table 1. Summary of the different GC/MS systems available at the CCiTUB

Ionization method	**Analyzer**	
Electron ionization (EI)	Quadrupol Mass Filter	IonTrap Quadrupol
Positive chemical ionization (PCI)	Quadrupol Mass Filter	
Negative chem. ion. (NCI)	Quadrupol Mass Filter	

The detection in the Quadrupol mass filter MS instruments can be performed in scan or single-ion monitoring (SIM) mode. In the scan mode, a specified mass range is scanned at regular intervals during the chromatographic process and stored in the data system. This mode provides reproducible mass fragmentation patterns that originate the mass spectra. With this information it is often possible to identify the GC separated unknown compounds. There are some spectral databases (commercial libraries) that assist the analyst in the process of identification. In spite of this, experienced analysts are required and considerable care must be exercised in interpreting the results of such comparisons. The identifying process can be assisted by the additional measurement of the retention index for each peak eluted and quantification is also possible by integration of the different ion peaks present in the chromatogram using internal and/or external standards.

With the MS^n ability of the ion trap analyzer, the possibility to detect an unknown in a complex mixture is enhanced and this tandem mode also provides additional structural information to help in the identifying process.

According to the nature of the sample and the volatility of compounds to be analyzed, some different sample introduction systems can be applied:

- Static Head Space (HS)
- Solid phase microextraction (SPME)
- Thermal desorption (TD)
- Direct liquid/gas injection

A summary of the different sample introduction systems used for volatile and semivolatile compounds is given in Table 2.

Table 2. Summary of the different sample introduction systems for volatile (VOC) and semivolative (SVOCs) compounds

Compound	**Sampling**			
VOCs	HS	TD	SPME	Direct
SVOCs	Direct		SPME	

Volatile compounds (VOCs): This group includes low-molecular weight compounds (ca < 250 uma) with high-vapour pressures and low-to-medium water solubilities. Some of them have natural origin but the majority is anthropogenic, which are used and produced in the manufacture of cleansers, paints, adhesives, plastics, pharmaceuticals, refrigerants, etc. They often are compounds of fuels, solvents, lubricants, paint thinners and dry-cleaning agents commonly used in urban settings. Most of them cause environmental problems and are potential carcinogens, and therefore, their control becomes obligatory and regulated.

Semivolatile compounds (SVOCs): There are organic compounds with molecular weights up 1000 amu, which may vaporize when exposed to temperatures above room temperature (usually with a boiling point >100ºC). In this group, some compounds such as common pesticides (OC's, OP's, triazines), persistent pollutants (phthalates, nonylphenols, PCBs, PAHs), neutral lipids, small metabolites, aliphatic and aromatic hydrocarbons, fragrances, essential oils and relatively non-polar drugs are analyzed in different matrices. In order to increase the volatility of compounds containing polar functional groups (-OH, -COOH, $-NH_2$, etc.), chemical derivatizations, e.g. silyl derivatives for alcohols and amines, methyl esters, transterification, are often employed in order to extend the range of suitable analytes to such compounds as steroids, polar drugs, polar lipids, organic acids, and aminoacids.

3. Examples of applications

3.1. Authentication analysis of personnel care products

In order to detect differences between two similar commercial deodorant spray samples (original branded and imitation), the analysis of volatile organic compounds was performed. The obtained results revealed multiple coincident compounds in both samples but the synthetic musk galaxolide (1,3,4,6,7,8-Hexahydro-4-6-6-7-8-8-hexamethyl cyclopenta-[g]-2-benzopyran) was only detected in the original spray. However, in the imitation sample, high amount of ethanol was found and floropal (2,4,6-Trimethyl-4-phenyl-1,3-dioxane) was detected instead of the polycyclic musk. The GC/MS ability to filter specific ions permitted to detect this 1,3-dioxane odorant which coeluted with a menthol derivative. The different chromatograms and mass spectra obtained in this example are shown in Figs. 1-5.

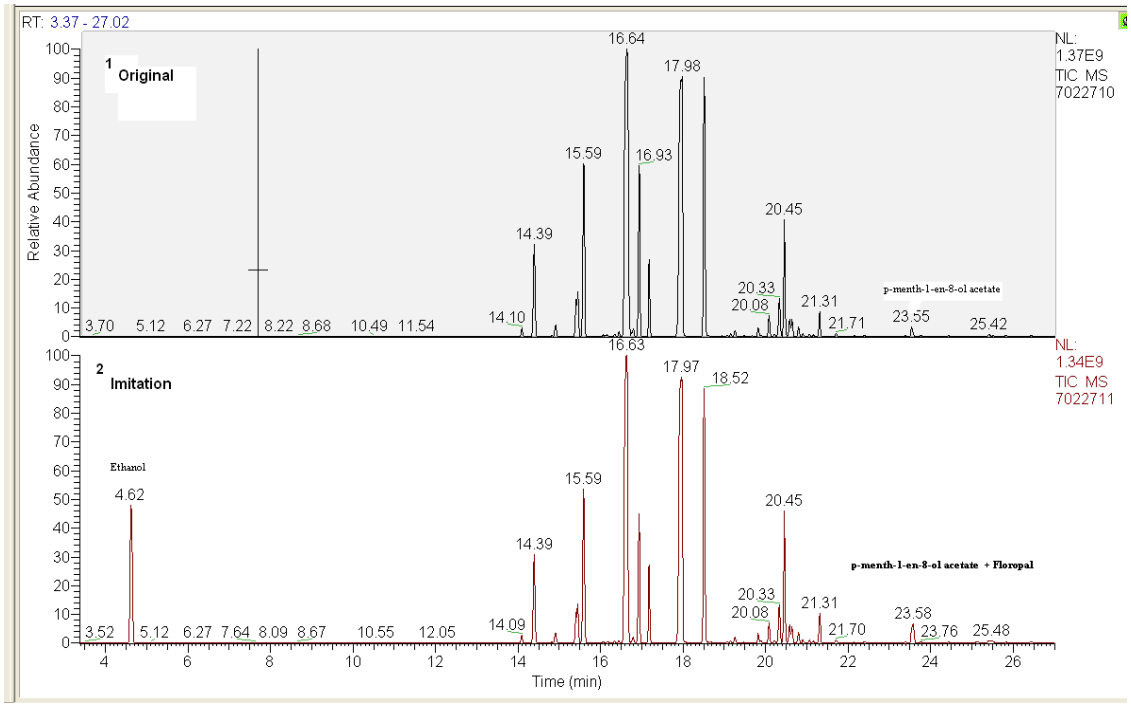

Figure 1. Comparison of the chromatograms corresponding to the original and defective samples obtained by HS-GC/MS on a DB-624 column. Note: Coelution between p-menth-1-en-8-ol acetate and floropal (only in sample 2).

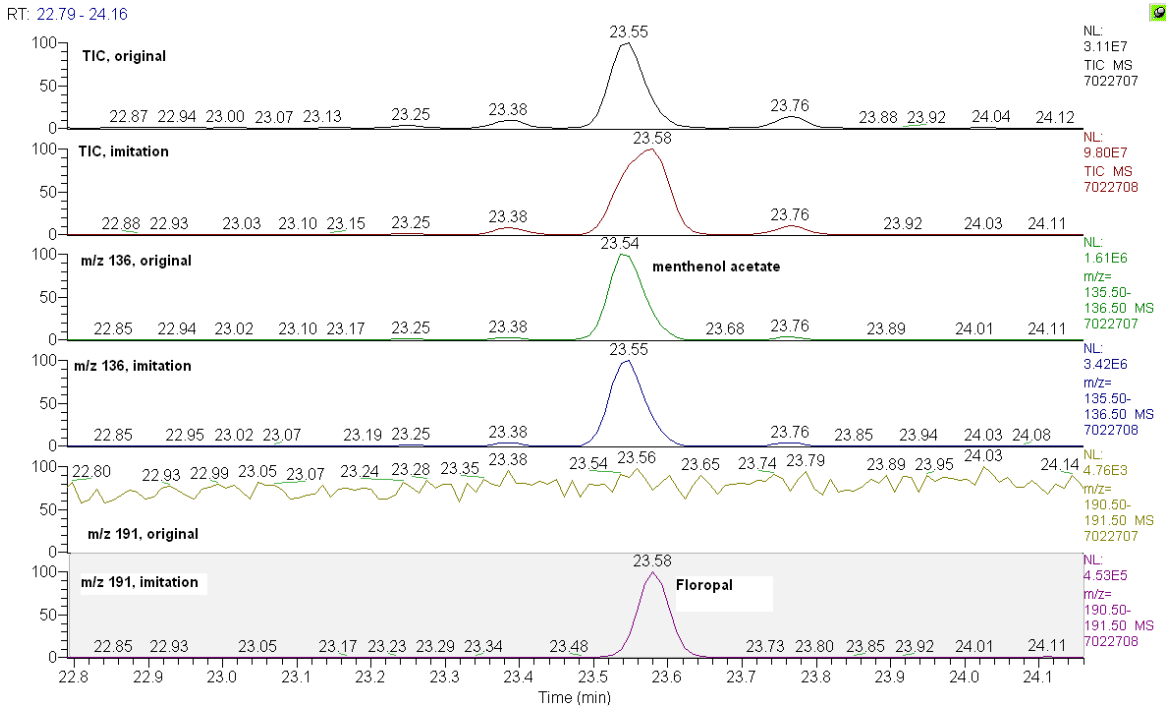

Figure 2. Mass chromatograms corresponding to the original and defective samples. Trace ions m/z 136 corresponding to p-menth-1-en-8-ol acetate and m/z 191 to floropal

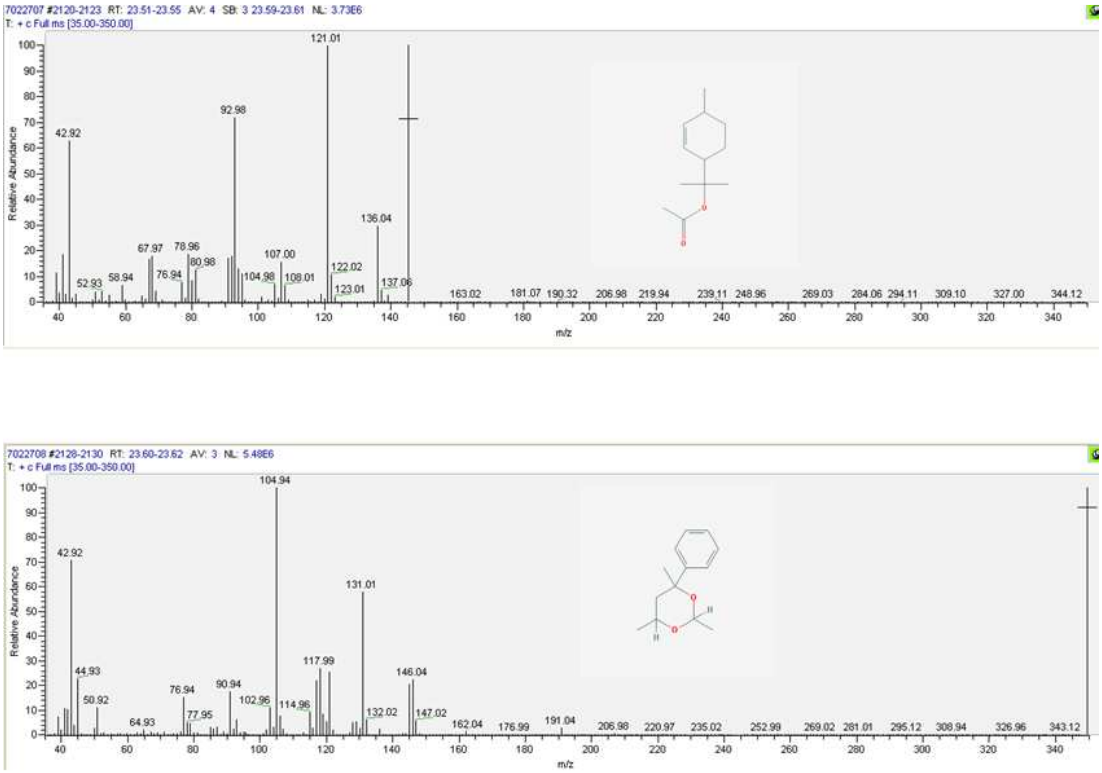

Figure 3. Mass spectra of p-menth-1-en-8-ol acetate (top) and floropal (bottom)

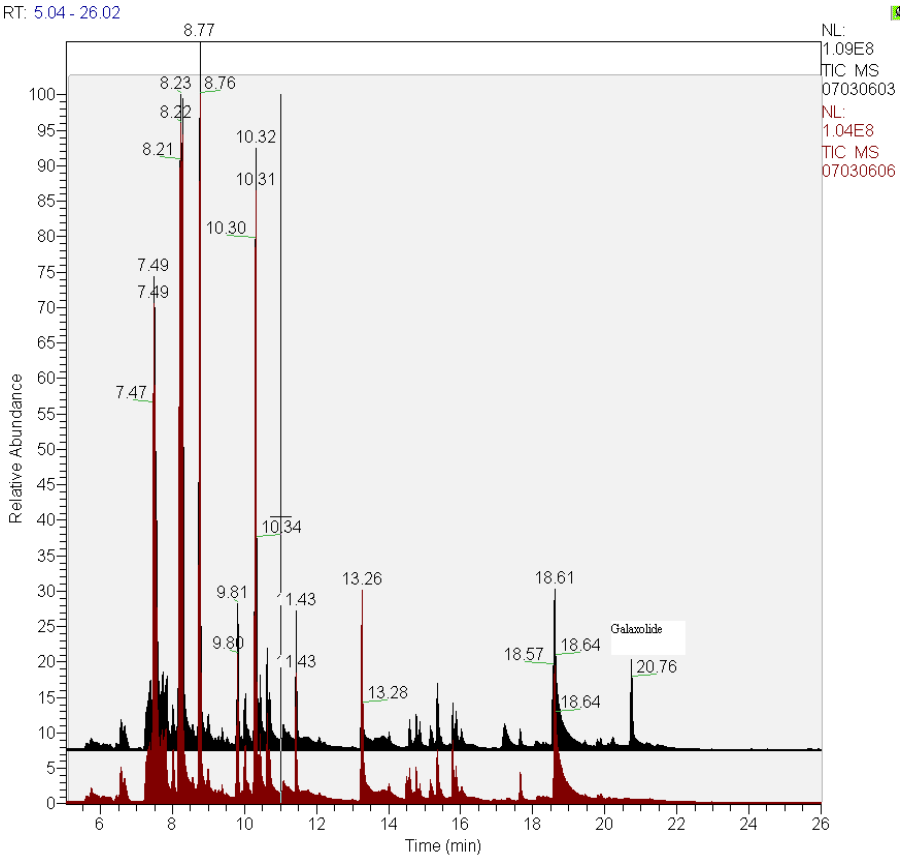

Figure 4. Comparison of the chromatographic profiles corresponding to the original and defective samples obtained by GC/MS on a VF-5MS column.

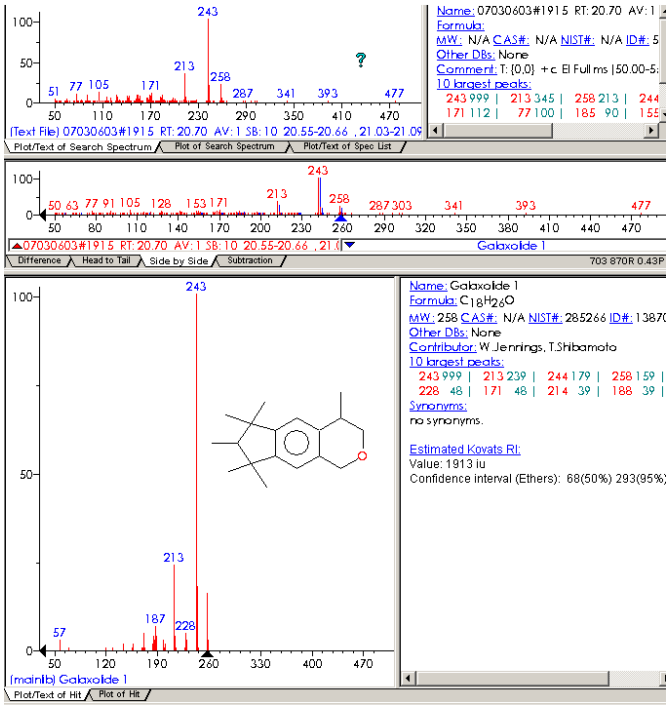

Figure 5. Mass spectrum of galaxolide with the corresponding library search result.

The original deodorant could be distinguished from the copy with the GC-MS technique. Even in the case of a coelution, it was possible to find differences between both samples.

3.2. Odour markers in food containers

In order to detect some odour markers in defective tin containers, samples were analyzed by head-space gas-chromatography mass spectrometry (HS-GC/MS). The VOCs chromatograms revealed some significant quantitative differences between a blank sample (correct) and an odorant sample (defective). In the latter sample, higher concentrations of chlorinated compounds and phenol were detected. These compounds could be responsible for the unpleasant odour (see Fig. 6)

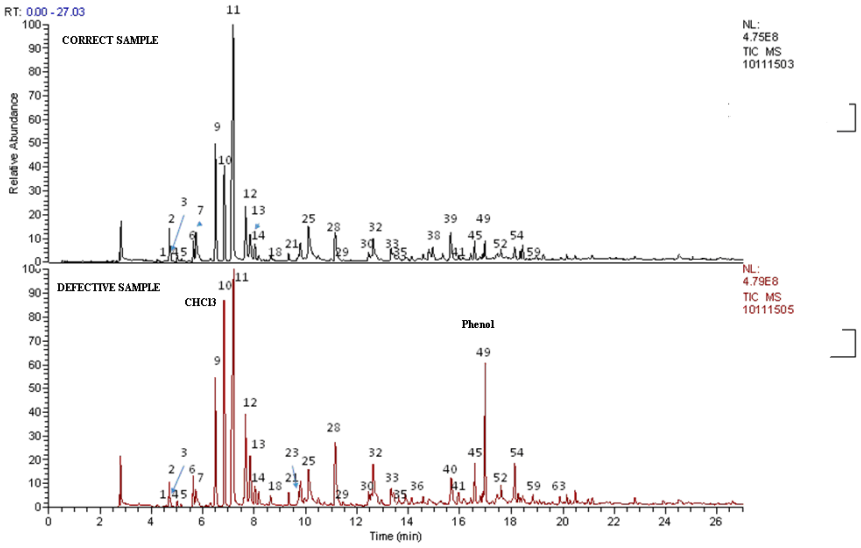

Figure 6. Comparison of the chromatographic profiles corresponding to the original and defective samples obtained by HS-GC/MS on a DB-624 column

3.3. Biomarkers in archaeological residues

Lipid biomarkers extraction and analysis of cooking wares residues (5th century AD) from Sa Mesquida (Mallorca, Spain) were performed by GC/MS. The origin of food contained in the archaeological ceramics could be distinguished from the fatty acids profile (Pecci) .

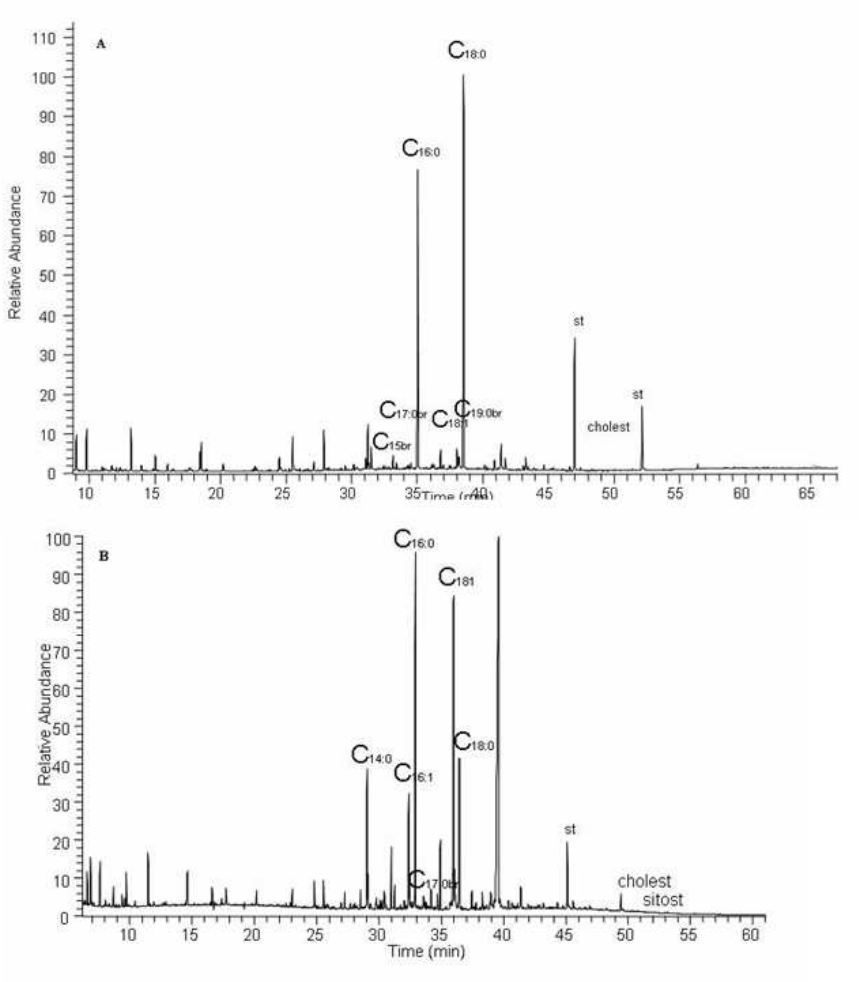

Figure 7. Chromatograms corresponding to a different total lipid extract samples. The fatty acids profile in sample A, where the saturated acids are clearly dominant, suggests an animal fat trace. In contrast, the fatty acids pattern showed in sample B suggests that a vegetal fat origin as unsaturated acids is relevant.

3.4. Determination of fenthion in liver samples (GC/MS^n example)

Fenthion is an organophosphorous (OPs) pesticide of regulatory concern for health and safety problems due to its lipophilic properties and large degree of persistence in the environment. One of the most important organophosphorous compounds reactions is water hydrolysis. Moreover, OPs inhibit the phosphorylate esterases, particularly the enzyme acetylcholinestarase, thus causing an accumulation of the neurotransmitter acetylcoline. Other effects are mutagenicity and carcinogenicity as well as specific organ toxicity to heart, liver, kidney and other organs.

For this compound, extraction and clean-up procedures are long and generally involve several steps (e.g. extraction, GPC and SPE clean-up), which can imply systematic losses and consequent inaccuracy (Russo et al., 2002). Ion trap tandem mass spectrometry is a useful approach to reduce clean-up steps in such a complex matrix. Using this technique, analysis of fenthion in liver samples can be achieved with a simple extraction (Figs. 8-11)

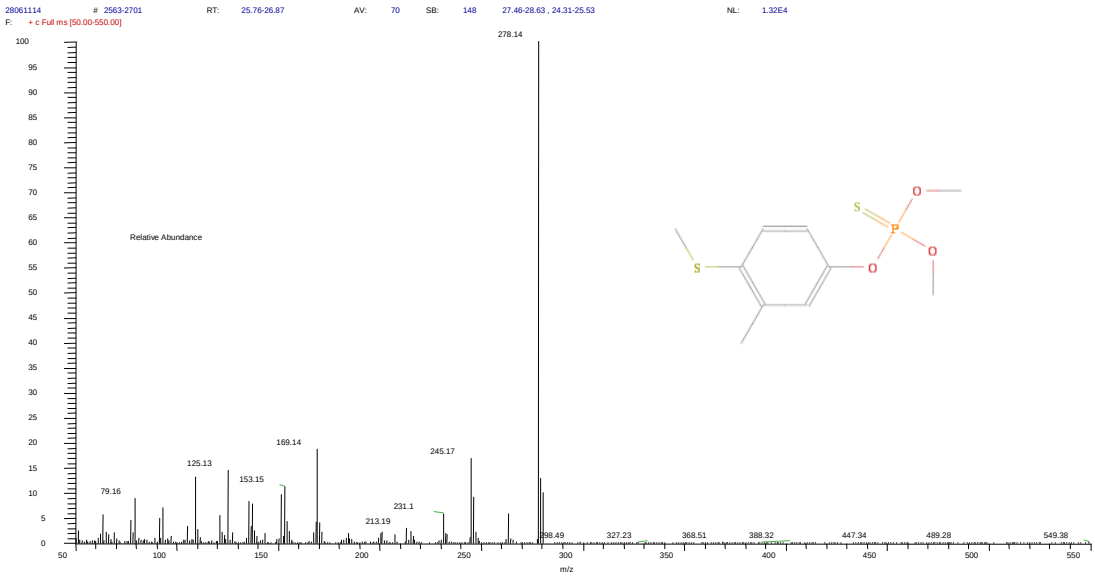

Figure 8. Fenthion mass spectrum (EI) obtained in an ion trap analyzer from a 2 ppm standard solution

In a liver sample, a coelution at 25.98 min is observed due to palmitic acid present in the liver.

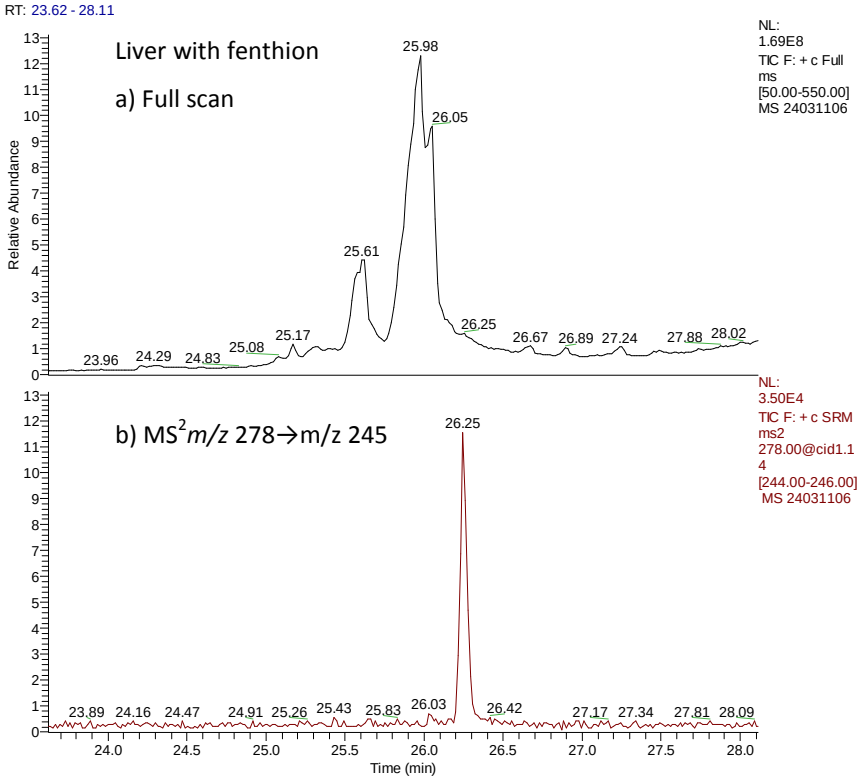

Figure 9. Liver extract zoom chromatogram. a) TIC chromatogram and b) SRM 278 to 245 amu

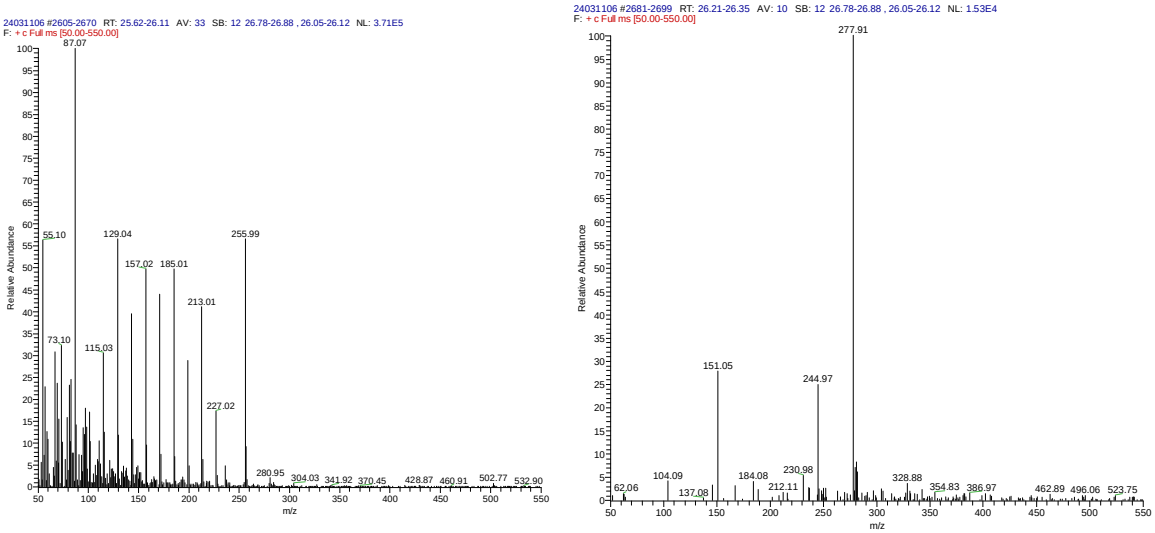

Figure 10. Mass spectra of palmitic acid (left) and fenthion (right) in liver extract.

Signal to noise ratio observed for SRM from 278 to 245 amu is better than that observed for the 278 mass chromatogram.

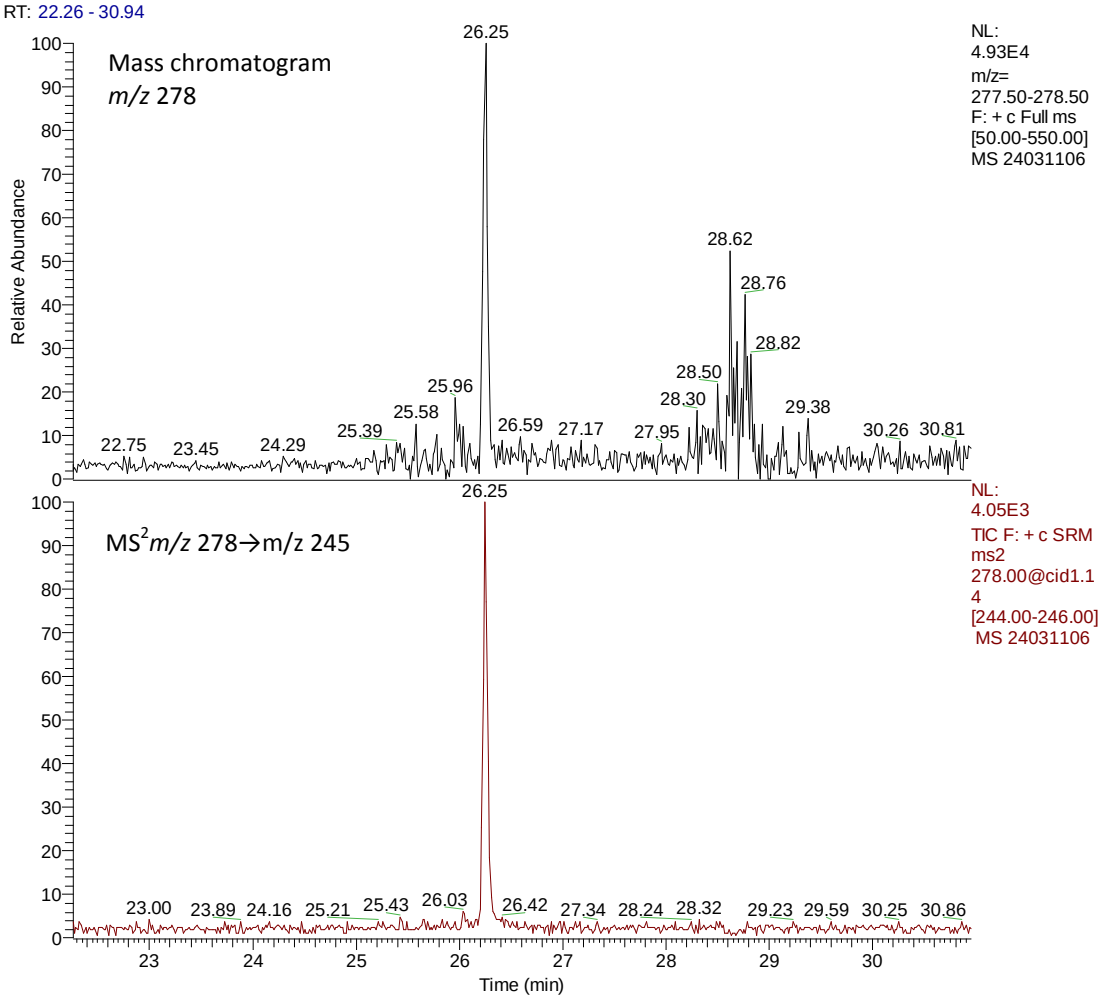

Figure 11. Mass chromatogram m/z 278 and SRM from 278 to 245 amu.

3.5. GC-MS Structural Characterization of polyesters produced from Linseed Oil by *P. aeruginosa 42A2*

Poly[3-hydroxyalcanoates] (PHAs) are optically active polyesters. The PHA synthesized by numerous bacteria are high-molecular weight polymers which form intracellular inclusion bodies such as carbon and energy reservoir. These polymers are environmentally friendly, biodegradable and may become an alternative for biocompatible materials. The native polymer has a random composition of monomers ranging from C6 to C14 with 20% of the alkyl side chains exhibiting unsaturation at C12 and C14 alkyl side chains. A strategy for the study of the nature of these PHA by GC/MS has been developed in our Unit. Biodegradable polymer was extracted from lyophily zed cells with $CHCl_3$ and after purification (MeOH precipitation) was hydrolyzed ($CHCl_3$, H_2SO_4, MeOH, 100C, 3h) in order to obtain the monomers (3-hydroxy-methylesters). The monomers were silylated and characterized by GC-MS (see Figs. 12-14).

ChT.6

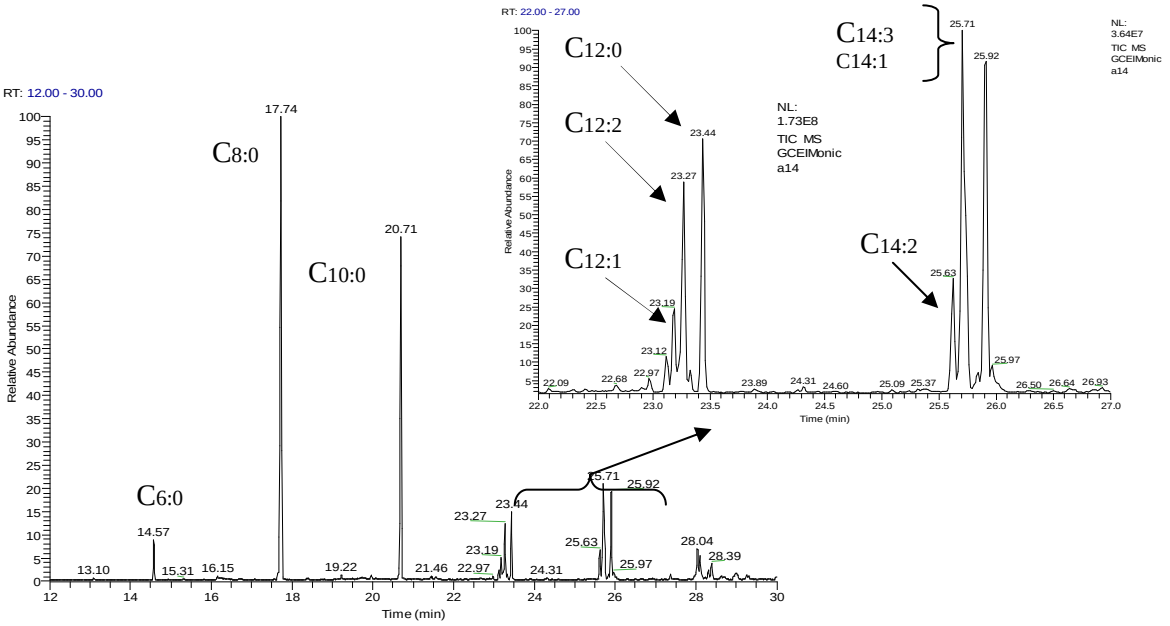

Figure 11. Ion Chromatogram (TIC) of the trimethylsilyl derivatives of (3-hydroxy-methyl esters) monomers.

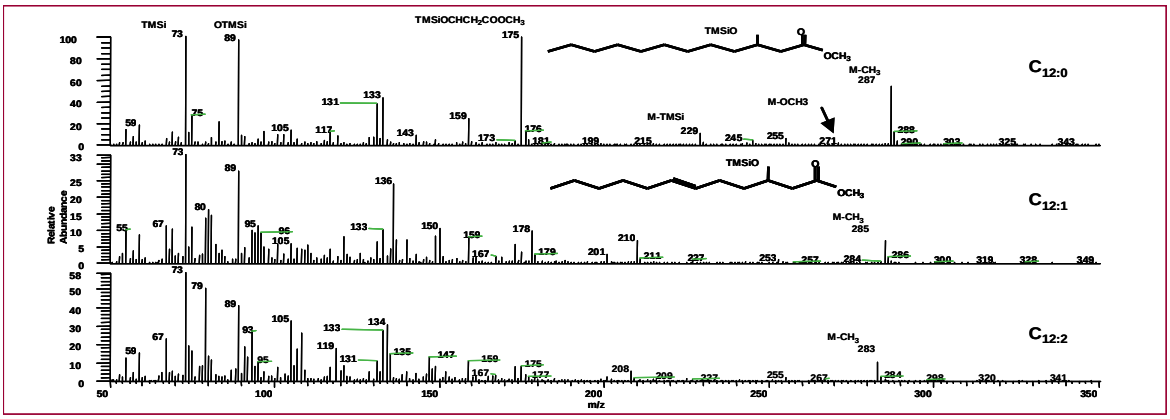

. **EI** mass spectra correspondig to the C_{12} family

Figure 12. EI mass spectra corresponding to the C_{12} family

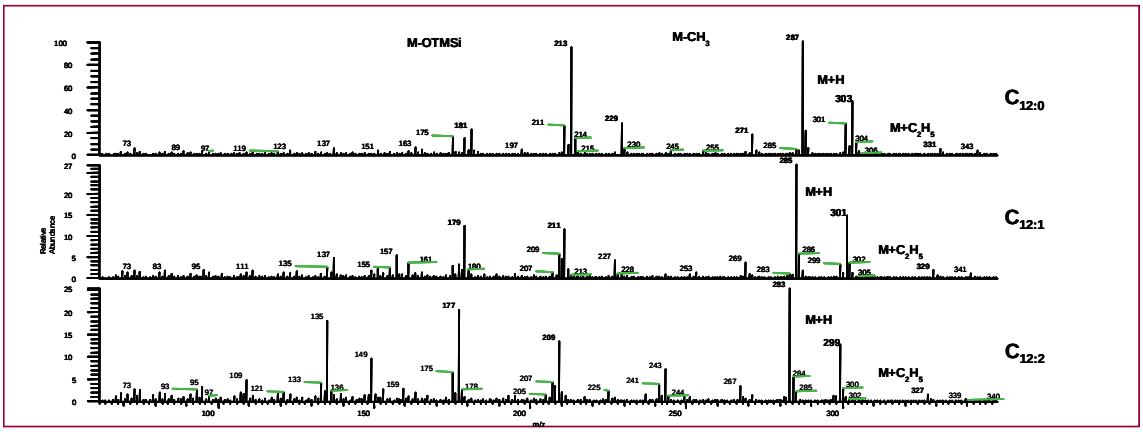

CI (CH_4) mass spectra correspondig to the $C_{12:0}$ monomers.

Figure 13. CI (CH_4) mass spectra corresponding to C_{120} monomers

Acknowledgements

We thank the Unitat de Toxicologia Experimental y Ecotoxicologia (UTOX)-Parc Científic de Barcelona for providing the samples of section 3.4.

References

I. Fernández, M. Bassas and A. Manresa. "GC-MS Structural characterization of polyesters produced from linseedoil by *Paeruginosa 42A2*".11as Jornadas de Análisis Instrumental "JAI". Barcelona 2005.

A. Pecci (ERAA-UB), IEF-FP7 Profolant Marie Curie Project

Russo et al., 2002 Journal of Chromatography B, 780:431-434

Liquid Chromatography - Mass Spectrometry

Olga Jáuregui[1], Isidre Casals[1], and Irene Fernández[2]

[1] Unitat de Tècniques Separatives d'Anàlisi, CCiTUB, Universitat de Barcelona. Parc Científic de Barcelona. Baldiri Reixac, 10. 08028 Barcelona, Spain.

[2] Unitat d'Espectrometria de Masses (Química), CCiTUB, Universitat de Barcelona. Fac. Química. Martí i Franquès s/n. 08028 Barcelona, Spain.

email: *ojauregui@ccit.ub.edu, isidre@ccit.ub.edu, ifernandez@ccit.ub.edu*

Abstract. In this article, selected examples of applications of liquid chromatography coupled to mass spectrometry are given. The examples include the analysis of i) impurities in manufactured, pharmaceutical or synthesis products, ii) polyphenols in natural products, and iii) phytohormones in plant extracts. Finally, examples of applications of molecular characterization via flow injection analysis by electron spray ionization mass spectrometry (ESI-MS) are also given.

1. Introduction

Liquid Chromatography – Mass Spectrometry (LC-MS) is a hyphenated analytical tool that has become popular from the middle nineties of the twenty century. It is a relatively young technique that has evolved quickly reaching a wide range of applications, from inorganics to biological macromolecules. The advantage of LC-MS is that non-volatile molecules of interest can be studied without the need of derivatization reactions, making easiest the sample preparation.

Some of the applications performed in our units are the following: analyses of molecules involved in animal/vegetal metabolism (natural or xenobiotics), analyses of impurities in products from synthesis (fine chemicals/biochemicals), analyses of degradation products and biotransformations, analyses of natural products (antioxidants, new drugs, industrial products), analysis for bromatolgy (additives, organoleptic modifiers), toxicological and forensic analyses (natural toxins, toxical additives, preservatives), molecular weight determinations, structural studies of unknown molecules, among many other applications.

2. Methodology

The available instruments in our Units allow us to use chromatographs and spectrometers from different brands, with diverse capabilities. Mass spectrometers fitted with different ionization sources such as electron spray ionization (ESI), atmospheric pressure chemical ionization (APCI), atmospheric pressure photoionization (APPI) and different kind of mass analyzers such as single quadrupole (Q), triple quadrupole (QQQ), ion trap (IT), orbitrap (OT), and time of flight (TOF) are available. This combination of techniques makes it possible to work using a wide variety of experiments, namely LC-MS, LC-MS/MS, LC-MS^n, LC-HRMS, etc. being LC any of the following modes of work: gel permeation chromatography (GPC), high-performance liquid chromatography (HPLC), ultra-high-performance liquid chromatography (UHPLC) and flow-injection analysis (FIA). As a result, a wide variety of analytical problems can be addressed using our facility. The basis of the above mentioned mass spectrometry techniques has been described elsewhere in this Handbook.

In the following, examples of applications of different LC-MS techniques are given.

3. HPLC-HRMS for identification of impurities in chemical products

Several strategies for drug impurity profiling have been reported in the literature, all of them stressing the importance of qualitative data from hyphenated chromatography-mass spectrometry like HPLC-MS. Among the different analyzers, those providing high-resolution such as TOFs and Fourier transform mass spectrometers would be the instruments of choice. Hybrid instruments (such as Q-q-TOF or IT-FTMS) can produce high quality MS/MS spectra including high-resolution data for the determination of molecular formulae. Both single MS and MS/MS experiments can be performed at good accuracy and high resolution.

Typically, our approach involves the installation of a suitable HPLC method or modification of an existing method for use with volatile buffers that are compatible with a mass spectrometer. The goal is to assure adequate separation of the active ingredient and the impurity or degradation product(s). Normally, the analyses are done in QTOF or LTQ-Orbitrap mass spectrometers that allow the obtention of some formulae for the impurities of interest. Once separation is achieved, we obtain the full scan and MS/MS spectra of the product(s) of interest. This approach helps us to develop a relational understanding of molecular structure to mass spectrometric fragmentation patterns, which then are used to identify putative structures. The customer report will include the ultra-violet (UV) chromatograms, the trace mass chromatograms, the mass spectra obtained at resolution between 10.000 and 30.000 (if desired, up to 100.000) and if possible, the MS/MS spectra. In addition, if the customer gives us possible elements, we can also include possible empirical formulae with the associated error (always below 2 mDa) that could help in the interpretation of results.

In the example of Fig. 1 we can see the UV chromatogram (Fig 1A), the total ion current (TIC) (Fig 1B) and the trace mass chromatogram (Fig 1C and 1D) for the two impurities scope of the work (those at 4.04 and 4.22 min in the UV chromatogram). The high-resolution mass spectrum allows the clear identification of double-charged species in impurity at 4.22 min as it can be seen in Fig. 1G where 0.5 Da spaced ions are observed. The hybrid instrument IT-FTMS allows the MS^2 and MS^n spectra to be acquired (Fig. 1H and 1I). A list of some empirical formulae is obtained for all the fragments with errors between 0.5 and 2.0 mDa.

4. Characterization of polyphenols in natural products by HPLC-MS/MS in a triple quadrupole instrument and by HPLC-HRMS in an IT-FTMS instrument

In the HPLC-MS laboratory of the CCiTUB, we have a large experience in the characterization of polyphenols and related substances in natural products such as apples, artichokes, plants, beer, cocoa, wine, et Identification of phenolic compounds in food matrices is a complex task, compared to the identification of enriched supplements or drugs, due to the wide variety of structures present in nature and the lack of standard polyphenols commercially available. During several years the characterization of phenolic compounds was done using triple quadrupole instruments through MS/MS experiments such as Product Ion Scan, Precursor Ion Scan and Neutral Loss Scan. The full scan in quadrupole instruments shows a poor signal-to-noise ratio but the MS/MS experiments such as precursor or neutral loss allow the screening of families of polyphenols. Figure 2 shows an example of the use of a triple quadrupole for characterization of the polyphenolic profile in artichokes [1]. Here, we can see the ability of the precursor ion experiment to clarify the chromatogram and facilitate the screening of compounds family (Fig 2A versus Fig 2C).

The arrival of HRMS instruments has improved the full scan experiments and, moreover, it has facilitated the identification and confirmation tasks through the generation of empirical formulae with a very good mass accuracy. In this example, the characterization of polyphenols in tomato samples is presented using both triple quadrupole and IT-FTMS instruments [2].

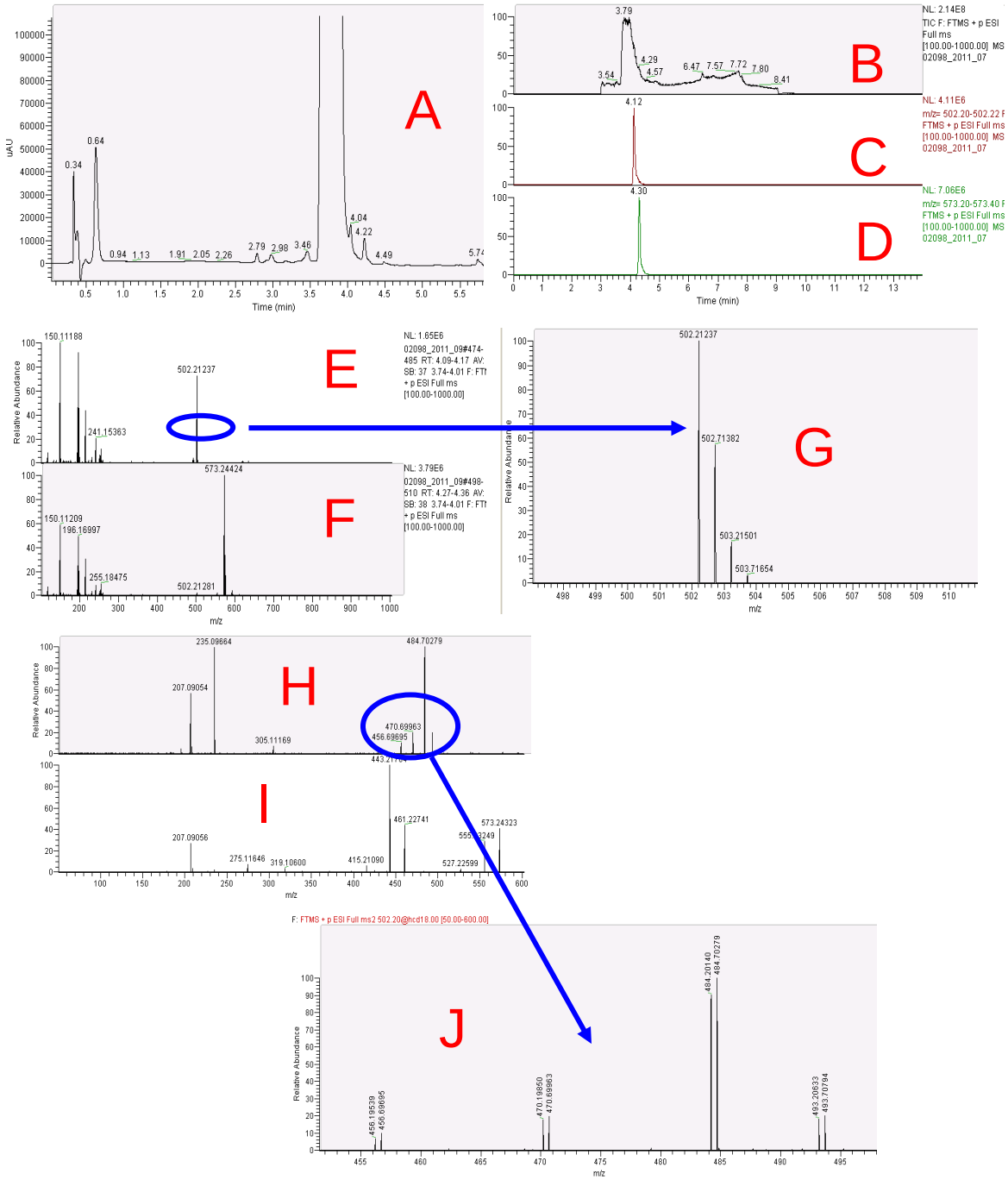

Figure 1. A) UV chromatogram; B) TIC; C) and D) trace chromatogram for each impurity. E) Mass spectrum for impurity at 4.04 min and F) Mass spectrum for impurity at 4.22 min. G) Enlargement of mass spectrum for impurity at 4.22 min. H) MS^2 spectrum for impurity at 4.04 min and I) for impurity at 4.22 min. J) Enlargement of mass spectrum on H.

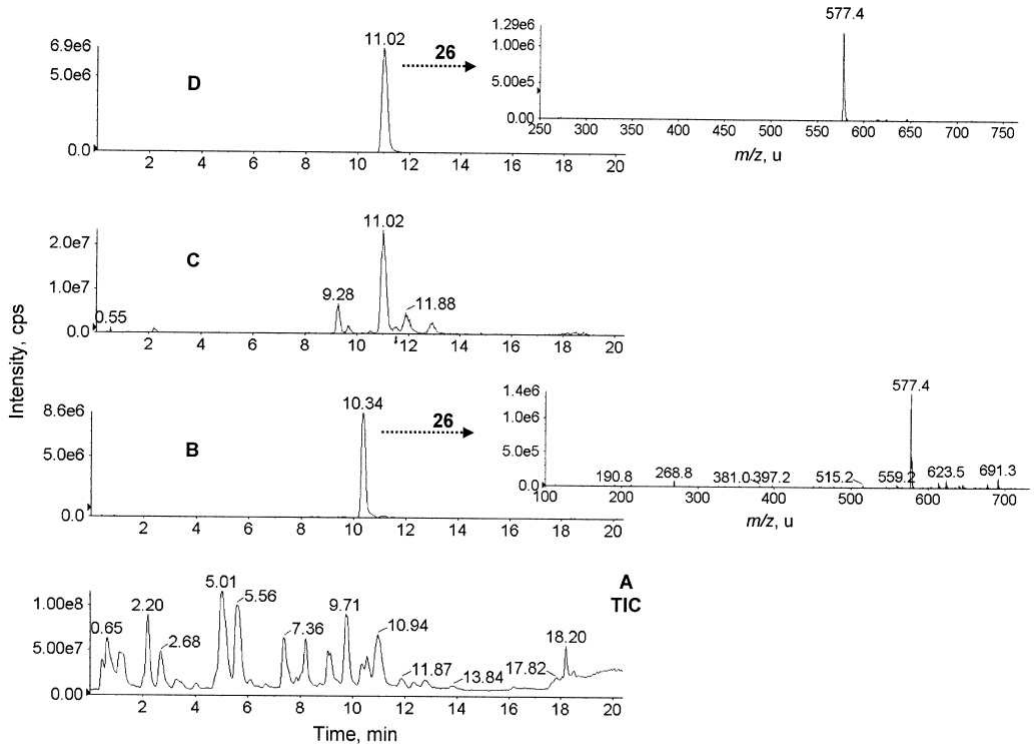

Fig. 6. TIC, trace chromatograms and mass spectra of subfraction C injected in full scan mode, and in precursor ion scan mode of 269 u. (A) TIC in full scan mode; (B) trace chromatogram of m/z 577 in full scan mode and mass spectrum of peak 26 (isorhoifolin); (C) TIC in precursor ion scan mode of 269 u; (D) trace chromatogram of m/z 577 in precursor ion mode of 269 u and mass spectrum of peak 26.

Figure 2. TIC, trace chromatograms and mass spectra corresponding to the analysis of the polyphenolic profile in artichokes [1].

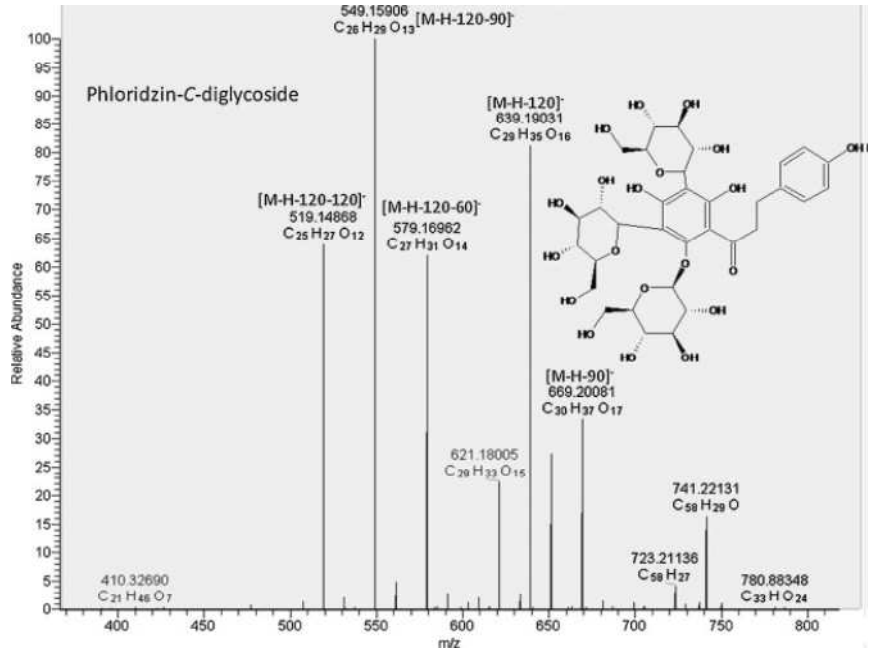

Figure 3. Identification of phloridzin-C-diglycoside in tomato samples [2].

The main advantage of the triple quadrupole is its capability of prescreen several compounds in a few experiments of, for instance, neutral loss scan of 162 (for hexosides). The use of HRMS instruments gives the error in the determination of the mass accuracy in both parent and product

ions. Figure 2 shows the identification of a *C*-diglycoside through MS^2 experiments in an IT-FTMS instrument.

In conclusion, the use of the LTQ-Orbitrap has been crucial for the structural determination of unknown compounds that could not be identified in the triple quadrupole system, probably due to their low concentration (see Table 1).

Table 1. List of compounds identified in tomato samples [2].

Compound	rt (min)	[M–H]	MS/MS ions (% intensities)	NL	PI	Acc. mass	mDa	MF
Gallic acid*	0.97	169	169 (55), 125(100)			169.0142	0.28	$C_7H_6O_5$
Protocatechuic acid*	2.08	153	153 (30), 109 (100)			153.0193	0.11	$C_7H_6O_4$
Caffeic acid-*O*-hexoside 1	2.98	341	341(25), 179 (100), 135 (10)	162	179	341.0877	0.12	$C_{15}H_{18}O_9$
Caffeic acid-*O*-hexoside 2	3.29	341	341(25), 179 (100), 135 (10)	162	179	341.0877	0.10	$C_{15}H_{18}O_9$
Neochlorogenic acid (3-caffeoylquinic acid)	3.36	353	191 (100), 179 (80),135 (45)	162		353.0877	0.02	$C_{16}H_{18}O_9$
Caffeic acid-*O*-hexoside 3	4.39	341	341(25), 179 (100), 135 (10)	162	179	341.0877	0.09	$C_{15}H_{18}O_9$
Homovanillic acid-*O*-hexoside	4.97	343	181 (100), 137 (20), 121 (5)	162		343.1034	0.07	$C_{15}H_{20}O_9$
Feruoylquinic acid-*O*-hexoside	5.56	529	529 (100), 367 (25), 191 (10)			529.1561	0.21	$C_{25}H_{30}O_{14}$
Ferulic acid-*O*-hexoside	5.78	355	355(40), 193 (100), 178 (30)	162		355.1034	0.04	$C_{16}H_{20}O_9$
Caffeic acid-*O*-hexoside 4	5.80	341	341(25), 179 (100), 135 (10)	162	179	341.0877	0.12	$C_{15}H_{18}O_9$
Coumaric acid-*O*-hexoside	6.41	325	325 (70), 187 (40), 163(100)			325.0928	0.95	$C_{15}H_{17}O_8$
Caffeic acid*	6.85	179	179 (40), 135 (100)			179.0349	0.34	$C_9H_8O_4$
Chlorogenic acid (5-caffeoylquinic acid)*	7.15	353	191 (100), 179 (<5)	162		353.0877	0.03	$C_{16}H_{18}O_9$
Cryptochlorogenic acid (4- caffeoylquinic acid)	8.28	353	191 (40), 179 (70), 173 (100), 135 (25)	162		353.0877	0.02	$C_{16}H_{18}O_9$
Naringenin-*O*-dihexoside 1	8.53	595	595 (20), 433 (100), 271 (30)	162		595.1665	0.33	$C_{27}H_{32}O_{15}$
Rutin-*O*-hexoside-pentoside	8.64	903[a]	741 (100), 609 (70), 300 (100)[a]			903.2411	0.58	$C_{38}H_{48}O_{25}$
Naringenin-*O*-dihexoside 2	8.89	595	595 (20), 433 (100), 271 (30)	162		595.1665	0.30	$C_{27}H_{32}O_{15}$
Rutin-*O*-hexoside	8.97	771	771 (100), 609 (50)		301	771.1989	0.42	$C_{33}H_{40}O_{21}$
Naringenin-*C*-diglycoside	9.01	595	595 (100), 475 (30), 385 (45), 355 (30)			595.1667	0.13	$C_{27}H_{32}O_{15}$
Coumaroylquinic acid	9.28	337	191 (100), 163 (10)			337.0930	0.13	$C_{16}H_{17}O_8$
Ferulic acid*	9.56	193	193 (20), 178 (70), 149 (20), 134 (100)			193.0506	0.41	$C_{10}H_{10}O_4$
Kaempferol-*O*-rutinoside-hexoside	9.72	755[b]	593 (100), 285 (5)[b]			755.2039	0.40	$C_{33}H_{40}O_{20}$
Naringenin-*O*-hexoside 1	10.11	433	433 (45), 271 (100)	162		433.1140	0.10	$C_{21}H_{22}O_{10}$
Phloridzin-*C*-diglycoside	10.37	759	741 (20), 669 (30), 639 (80), 621 (20), 579 (60), 549 (100), 519 (65)			759.2346	0.70	$C_{33}H_{44}O_{20}$
Naringenin-*O*-hexoside 2	10.57	433	433 (45), 271 (100)	162		433.1140	0.08	$C_{21}H_{22}O_{10}$
Rutin-*O*-pentoside	10.93	741	609 (60), 300 (100)	132	301	741.1883	0.85	$C_{32}H_{38}O_{20}$
Rutin(quercetin 3-*O*-rhamnosyl-glucoside)*	11.16	609	609 (100), 300 (50)		301	609.1460	0.49	$C_{27}H_{30}O_{16}$
Phloretin-*C*-diglycoside	11.25	597	597 (30), 477 (50),417 (40) 387 (90), 357 (100)			597.1819	0.10	$C_{27}H_{34}O_{15}$
Kaempferol-3-*O*-rutinoside*	11.35	593	593 (100), 285 (80)			593.1511	0.58	$C_{27}H_{30}O_{15}$
Prunin (Naringenin-7-*O*-glucoside)*	11.45	433	433 (45), 271 (100)	162		433.1140	0.10	$C_{21}H_{22}O_{10}$
Eriodictyol-*O*-hexoside	11.50	449	449 (20), 287 (100), 151 (30)	162		449.1089	0.12	$C_{21}H_{22}O_{11}$
Dicaffeoylquinic acid 1	11.52	515	515 (65), 353 (50), 191 (100)	162		515.1194	0.03	$C_{25}H_{24}O_{12}$
Dicaffeoylquinic acid 2	11.62	515	515 (65), 353 (50), 191 (100)	162		515.1194	0.02	$C_{25}H_{24}O_{12}$
Naringenin-*O*-hexoside 3	11.64	433	433 (45), 271 (100)	162		433.1140	0.09	$C_{21}H_{22}O_{10}$
O-acetylprunin	11.68	475	433 (15), 271 (100)			475.1245	0.07	$C_{23}H_{24}O_{11}$
Kaempferol-3-*O*-glucoside*	11.76	447	447(100), 285 (20)	162		447.0932	0.14	$C_{21}H_{20}O_{11}$
Naringenin*	12.07	271	271 (100), 177 (20), 151(100), 119 (30)			271.0611	0.03	$C_{15}H_{12}O_5$
Quercetin*	13.63	301	301(60), 151(100)			301.0353	0.15	$C_{15}H_{10}O_7$

* Comparison with standard.
rt, retention time; NL, neutral loss; PI, precursor ion scan; Acc. mass, accurate mass; MF, molecular formula; mDa, millidaltons of error between the mass found and the accurate mass of each polyphenol.
[a] MS^2 of 903 and MS^3 of 741

5. Quantitation of phytohormones in plant extracts by HPLC-ESI-MS/MS

The main applications in the HPLC-MS laboratory of the CCiTUB involve quantification of small molecules in different kind of samples as mentioned in the introduction. We analyse, for instance, plant extracts after a simple extraction (acetone/water/acetic acid (80:19:1, v/v)) by vortex, centrifugation and filtration. The most valid approach that guarantees an equal efficiency of extraction of both the analyte and the internal standard and it also compensates the non-specific matrix effects caused by co-eluting components is the well-known isotopic dilution method. This method is based on the addition of deuterium-labeled internal standards to the extract. In this example [3], we used d_6 and d_5 deuterium-labeled standards for abscisic acid (ABA) and absicisic acid-glucose ester (ABA-GE) respectively. A mass difference of 4 Da between the compound and the analogue deuterated avoids the need to correct for overlap between the ^{13}C isotopic peaks of the former and the monoisotopic peak of the latter during LC–MS–MRM (multiple reaction monitoring). The quality parameters of the method showed LODs between 1 and 7 ng g^{-1} f.w. The high specificity of the MRM acquisition mode allowed us to obtain clean chromatograms from non-purified crude plant extracts, thus avoiding possible interferences to the analysis. This can be seen in Fig. 4, which shows the trace chromatograms.

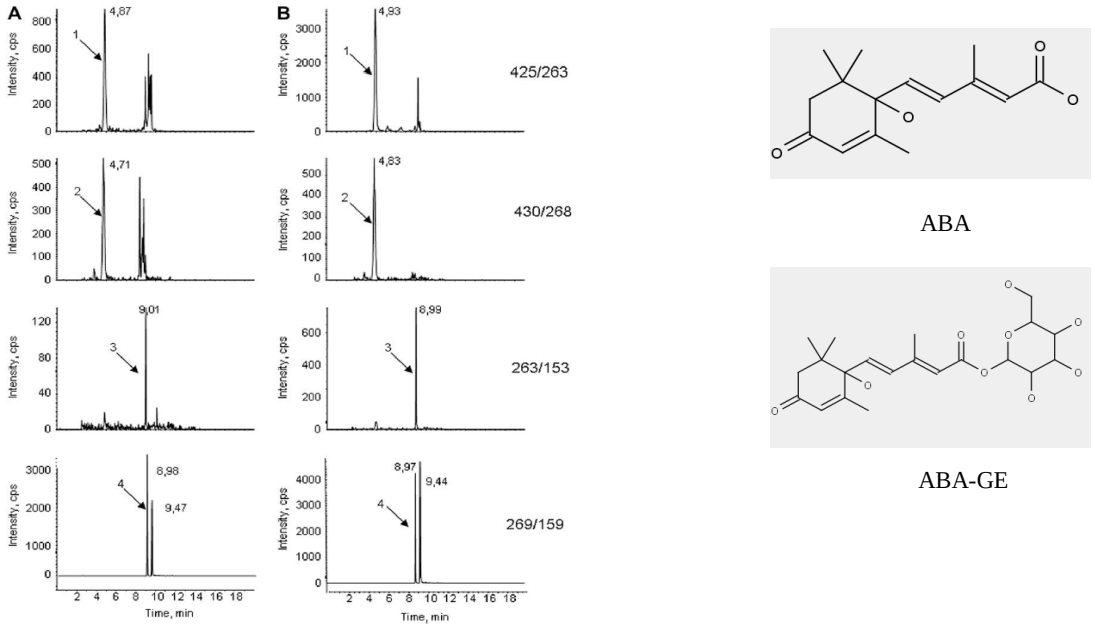

Figure 4. Trace chromatograms of *Cistus Albidus* plant. A) January sample and B) August sample (stressed). The peaks corresponding to MRM transitions are: (1) ABA-GE (425/263), (2) d5-ABA-GE (430/268), (3) ABA (263/153) and (4) d6-ABA (269/159) [3].

6. Molecular Characterization by ESI

The ESI method enables a wide variety of analysis due to its characteristic softness ionization process, as we have seen in the case of characterization of organic compounds by LC/MS. But the field of applications ranges from small organic/inorganic compounds to biomolecules (Proteins, DNA, RNA). The use of the LC/MS version, or by direct infusion of the compounds to the source, has become one of the principal methods to study the structure of biomolecules (studies of the primary, secondary, tertiary and quaternary structure), non-covalent complexes such as metal-binding proteins and organometallic compounds, among others.

The two examples below show some of the above mentioned applications.

6.1. ESI-MS Analysis of Non covalent complexes: Myoglobin–heme complex

There are several instrumental methods that have been applied to the study of macromolecular interactions such as circular dichroism, light scattering, fluorescence, or calorimetry.The softness of ESI preserves higher order protein structure in the gas phase, which makes this technique very useful for the study of noncovalent interactions such as protein-protein and protein-ligand interactions. The high-resolution capabilities of the analyzers also enable charge state identification for the multiple charged species of many compounds produced in the ionization processes. For the high-molecular weight compounds like biomolecules, very powerful deconvoluting softwares (Max Entropy) can help in their characterization.

Figure 5 illustrates the presence of the Myoglobin-heme complex characterized by ESI/MS.

6.2. ESI-MS Analysis of Pt(II)-Complexes:

Organometallic compounds such as Palladium and Platinum derivatives are becoming of great interest due to their numerous applications in many fields such as organic synthesis, design of biologically active compounds and others. Characterization of the new compounds is made by several techniques including Elemental Analysis, Nuclear Magnetic Resonance (NMR) and ESI. The characteristics of the latter method, with the improvement of mass analyzers so as to obtain better resolution, accuracy (< 5 ppm) and reproducibility, enable accurate mass measurements for molecular formula generation and Isotope Pattern determination, facilitating identification of

compounds in complex mixtures. Structural information can be obtained for isolated compounds by in-source fragmentation, with the same resolution and accuracy of mass measurements than those obtained by MS/MS experiments.

Figure 6 shows spectra that illustrate the characterization of the Pt organometallic compound **a** (C33H28NPPtClBr).

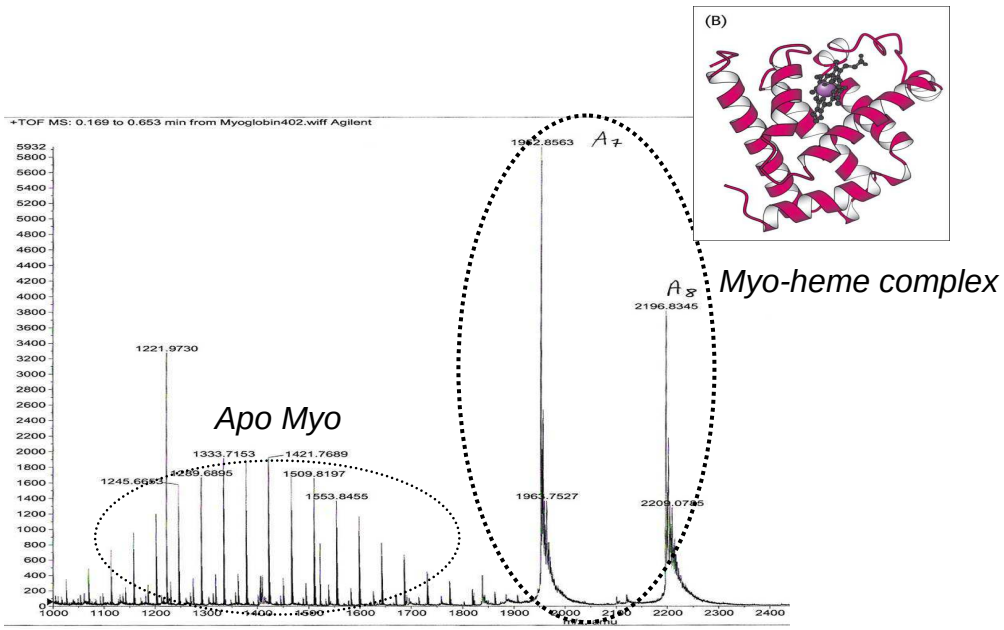

Figure 5. Positive ion ESI mass spectrum (LC/MSD-TOF instrument) of Horse Heart Myoglobin (1µM) in 10mM ammonium acetate. Signals on the left correspond to ions for the apo-protein. The two large signals on the right correspond to ions for the Myoglobin-heme complex.

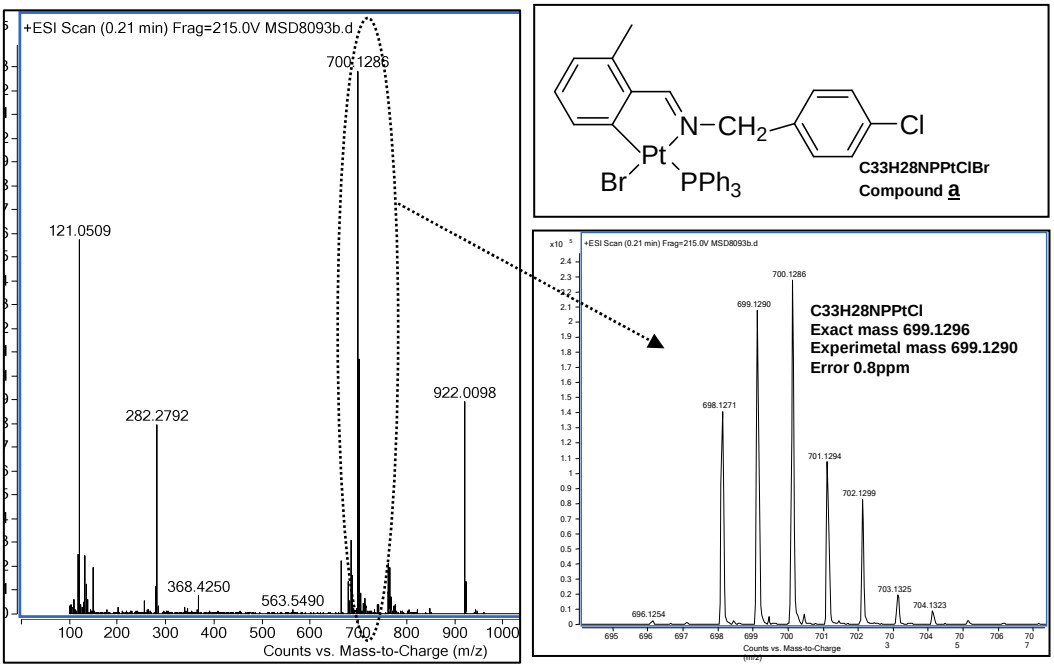

Figure 6. Left: Spectrum of Pt organometallic compound **a**. (LC/MSD-TOF instrument; 121.0509 and 922.0098 are internal reference compounds). Right: Enlarged Isotope pattern and mass accuracy result measurements for the molecular formula generated.

References

[1] F. Sánchez-Rabaneda *et al.* Journal of Chromatography A 1008 (2003) 57–72
[2] A. Vallverdú-Queralt *et al.* Rapid Commun. Mass Spectrom. 2010; 24: 2986–2992
[3] M. López-Carbonell *et al*. Plant Physiology and Biochemistry 47 (2009) 256–261

Isotope Ratio - Mass Spectrometry

Rosa Maria Marimon[1], Joaquim Perona[1], and Pilar Teixidor[2]

[1] Unitat de Medi Ambient, CCiTUB. Facultat de Geologia. Martí Franquès, s/n. 08028 Barcelona, Spain.

[2] Unitat de Cromatografia de Gasos i Espectrometria de Masses. CCiTUB, Lluís Solé i Sabarís 1-3. 08028 Barcelona, Spain.

email: *marimon@ccit.ub.edu, jperona@ccit.ub.edu, teixidor@ccit.ub.edu*

Abstract. This article summarizes the configurations involving isotope ratio mass spectrometry (IRMS) technology available at the CCiTUB and the wide range of possible applications. Some examples of these applications are shown.

1. Introduction

The natural abundances of stable isotopes for any given element are not constant in nature due to a great variety of physical and chemical fractionation processes that constantly occur. The isotope ratio mass spectrometry (IRMS) is a technology that allows us to measure these small variations in isotopic abundances of the major light elements in nature (H, C, N, O, S) with high precision.

2. Methodology

An isotope ratio mass spectrometer consists of three main parts:

- Electronic ionization source (high stability and yield of ionization)
- Magnetic field analyzer (effective separation of different ion beams)
- Multiple Faraday cups detector (robust collection of the specific ions)

Gas sample introduction can be performed directly by means of dual inlet (DI) systems or via an additional hyphenated technique, referred to as continuous flow (CF) systems, through a carrier gas, e.g. chromatography, elemental analysis, pyrolysis. Both systems are available at the Scientific and Technological Centers of the University of Barcelona, comprising several isotope ratio mass spectrometers with different sample preparation devices. These peripherals are carbonate device, equilibration-GC system (gas bench, GB), elemental analyzers (EA), pyrolyzers (TC/EA), gas chromatographs (GC) and liquid chromatograph (LC).

Such variety of configurations allows a full range of applications in different areas:

- Life and Earth sciences (physiology, ecology, hydrology, climate, marine geosciences, biogeochemistry)
- Health sciences (biochemistry, metabolism, physiology, nutrition)
- Forensic science
- Archaeology

The different applications comprise the analysis of samples of natural isotopic composition and low level of enrichment (up to 2-3% heavy isotope), where isotopes can be used as tracers of metabolic and fluxomic pathways.

In our laboratories we have implemented several routine measurements for specific type of samples, covering inorganic and organic fields. The stable isotope analyses that we perform in our laboratories are shown in Table 1.

3. Examples of applications

3.1. DI-IRMS. Carbonate analysis in foraminifera.

Foraminifera have been distributed widely in the ocean from the Cambrian period to the present. Their hard shells, mainly consisting in $CaCO_3$, are often preserved within seafloor sediment as microfossils. The analysis of their stable carbon and oxygen isotopic compositions ($\delta^{13}C$ and $\delta^{18}O$) is useful because these parameters are paleoindicators of the paleoenvironment at the time when they were alive.

To analyse the stable isotopic composition of foraminiferal shells, more than 20 micrograms of $CaCO_3$ are needed. In order to obtain a reliable result, the weight of samples and reference materials should be similar. This is why samples are weighted prior to be transferred to a reaction tube, which is placed in the automatic carbonate device feed system. The carbonate device works according to the McCrea method (McCrea, 1950). This method releases CO_2 from the $CaCO_3$ and the gas flows into the IRMS (see Fig. 1).

Table 1. Stable isotope analyses performed at the CCiTUB by using different IRMS configurations

Technique	$\delta^{13}C$	δD	$\delta^{15}N$	$\delta^{18}O$	$\delta^{34}S$
DI-IRMS	Carbonate microsamples			Carbonate microsamples	
GB-IRMS	CO_2 from air	Water samples		Water samples	
	DIC in water samples			CO_2 from air	
EA-IRMS TC/EA-IRMS	Solid and liquid bulk material	Solid and liquid bulk material	Solid and liquid bulk material	Solid and liquid bulk material	Solid and liquid bulk material
GC-IRMS	Specific Organic compounds (VOCs and SVOCs)	Specific Organic compounds (VOCs and SVOCs)	Nitrogenated organic compounds		
LC-IRMS	Water soluble organic compounds (total extract and compound specific)				

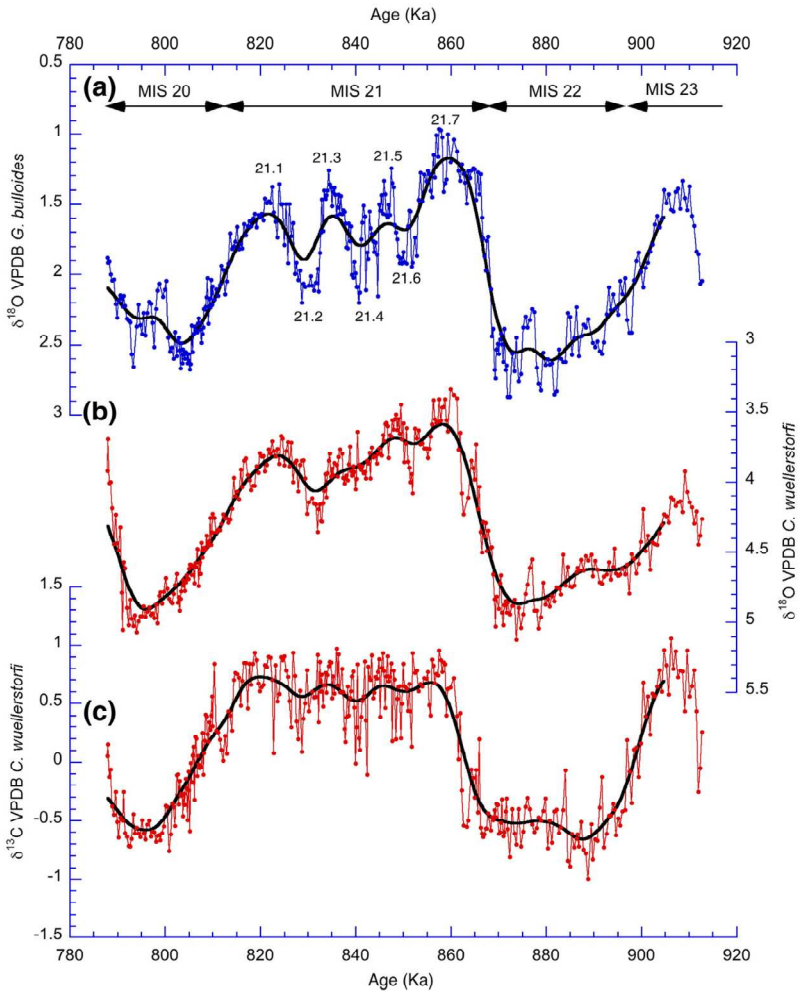

Figure 1. Example of isotope records in an oceanic core (Ferretti et al, 2010).

3.2. CF-IRMS

At our IRMS facilities, several methodologies have been developed in CF-IRMS. Some of them are focused to environmental applications as the stable isotopes signatures contribute to the knowledge of the origin and fate of specific pollutants found in different areas. Moreover, the isotopic analyses contribute to control the natural or induced degradation processes (remediation). Other applications are related to metabolism and physiology, where stable isotopes are used as tracers of different processes.

3.2.1. $\delta^{15}N$ and $\delta^{18}O$ of dissolved nitrates in waters .

The analysis of the isotopic composition of the ions involved in the denitrification reactions allow us to determine which processes control the natural attenuation (Otero et al., 2007).

In this example sample preparation is as follows. For the $\delta^{15}N_{NO3}$ and $\delta^{18}O_{NO3}$ analysis, dissolved nitrates are concentrated using anion-exchange columns, after extracting the sulphates and phosphates by precipitation. Afterwards, dissolved nitrates are eluted with HCl and converted to $AgNO_3$ by adding silver oxide. The liophilised $AgNO_3$ is enclosed in a Sn and/or Ag capsule for the subsequent $\delta^{15}N$ and/or $\delta^{18}O$ analysis by EA-IRMS and/or EA/TC-IRMS.

The isotopic values $\delta^{15}N$ vs. $\delta^{18}O$ of dissolved NO_3^- found in different sampling sites of a regional area near Barcelona (Spain) are shown in Fig.2. The isotopic composition of nitrates indicates that dissolved nitrate is mainly derived from pig manure ammonium which is nitrified at the aerobic zone. It is worth noting that the $\delta^{18}O_{NO3}$ indicates that nitrate is derived from fertiliser NH_4, which has been nitrified. There is no evidence of the contribution of "direct" nitrate from fertilisers. Samples show a coupled increase in $\delta^{15}N$ and $\delta^{18}O_{NO3}$, with a slope 2:1. This correlation indicates the existence of denitrification processes, in almost one third of the samples.

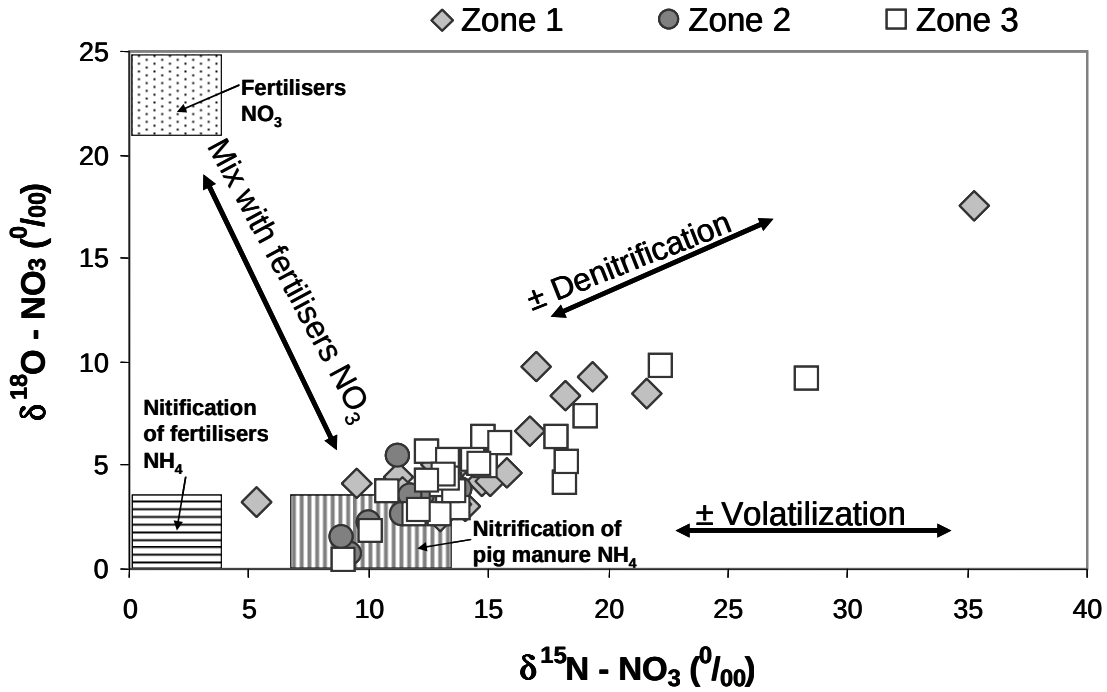

Figure 2. Isotopic values $\delta^{15}N$ vs. $\delta^{18}O$ of dissolved NO_3^- found in different sampling sites of a regional area near Barcelona (Spain). . Arrows indicate the isotopic changes linked to the different processes.

3.2.2. Compound specific carbon isotope analysis of volatile organic compounds

Using head space-solid phase microextraction (CAR-PDMS fiber) as a preconcentration technique, it is possible to detect trace levels (LOQ <10 ug/l) of halogenated and non-halogenated volatile compounds and analyze its isotopic composition with optimum precision (J.Palau *et al*., 2007)

As in-situ chemical oxidation has emerged as an effective and low-cost method for contaminated groundwater remediation, analysis of the variation of the isotopic composition of the halogenated contaminants during different oxidation conditions was performed in order to evaluate them as a potential tool to monitor the performance of the oxidative processes applied. The observed trend in the isotopic values of $\delta^{13}C$ allowed the quantification of the enrichment factor using Rayleigh equation (see Figs. 3 and 4).

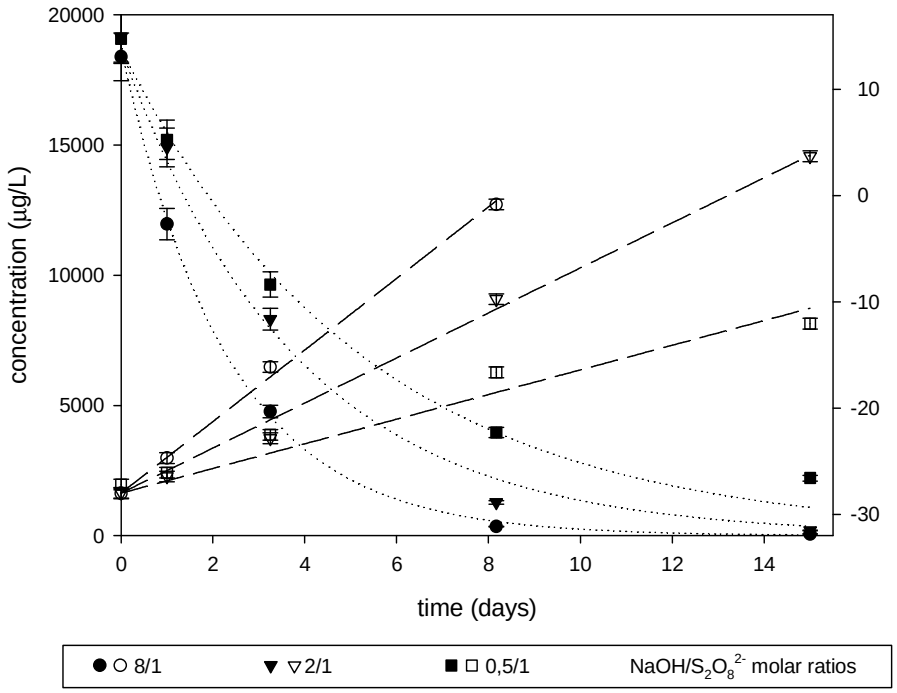

Figure 3. Concentration (black symbols) and $\delta^{13}C$ values (white symbols) of TCA for different $NaOH/S_2O_8^{2-}$ molar ratios (Marchesi *et al*., 2009).

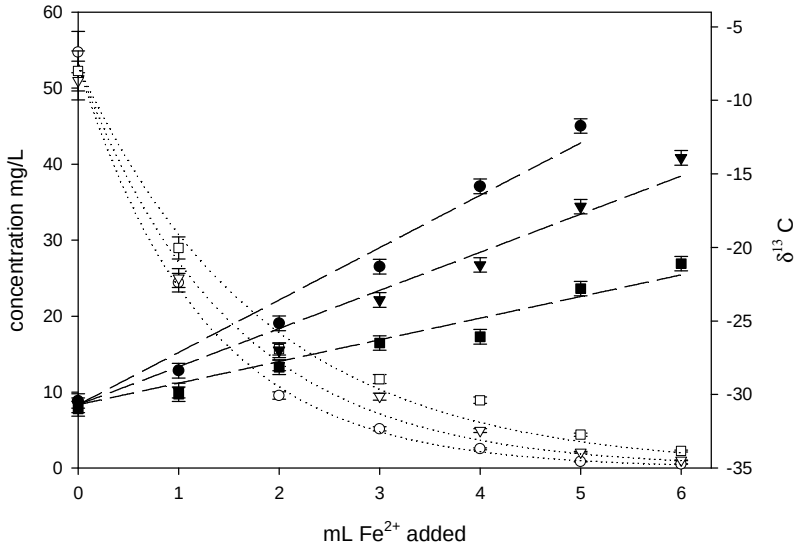

Figure 4. Concentration (white symbols) and d13C values (black symbols) of PCE for different S2O82-/Fe2+/PCE molar ratios (Marchesi *et al*., 2009)

3.2.3. Study of ^{13}C and ^{15}N isotopic labeling on amino acids in plants by GC/C/IRMS

We have developed a methodology that allows the detection and quantification of both unlabelled and isotopically labeled amino acids so that it can be applied in a broad range of metabolomic and fluxomic studies in which stables isotopes can be used as a tracers (G. Molero et al., 2011). Typical results are shown in Figs. 5 and 6.

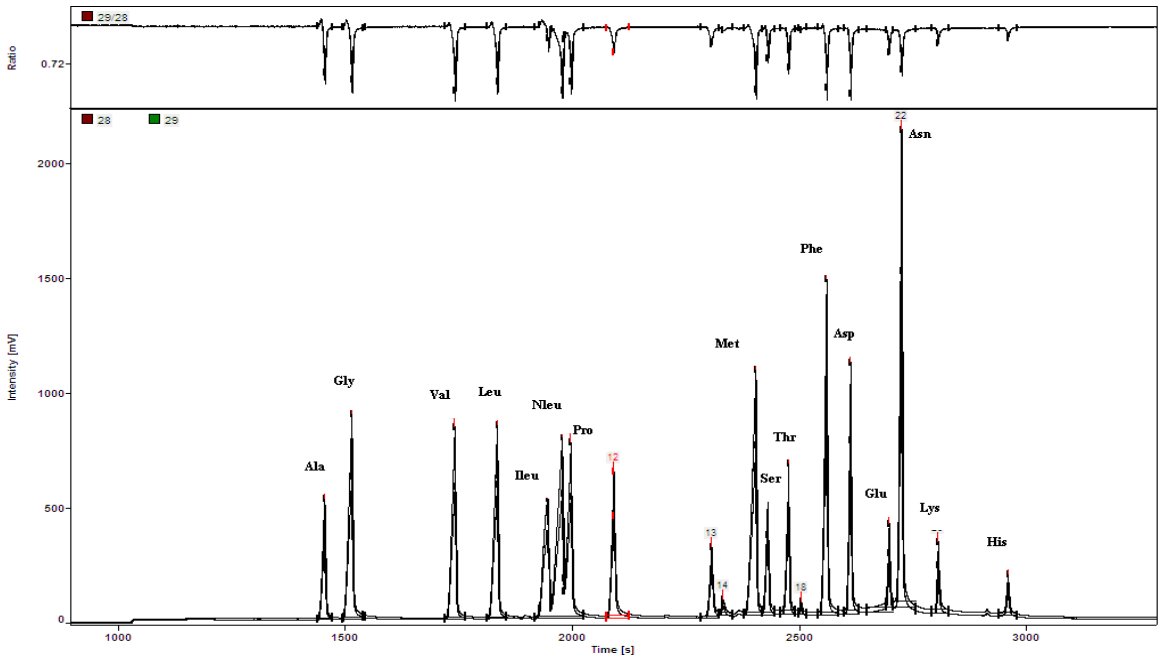

Figure 5. GC/C/IRMS chromatogram obtained from a mixture of aminoacids (MTBDMS-derivatives) on a PT-5 column

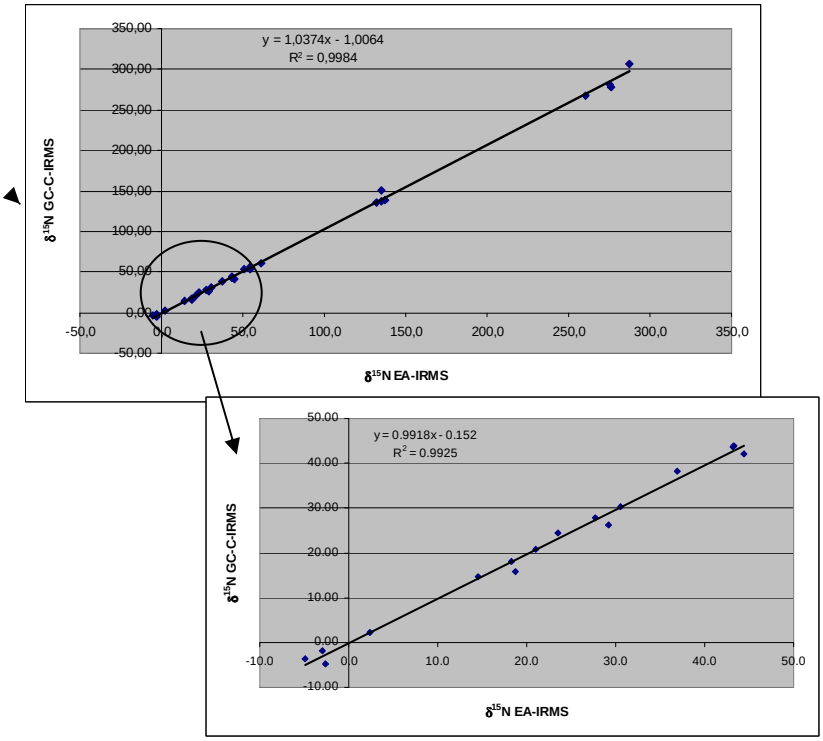

Figure 7. Comparison between $\delta^{15}N$ values obtained by EA-IRMS and GC-C-IRMS

A good linearity correlation (r^2> 0,99) was observed between $\delta^{15}N$ signature values (n= 28) obtained by EA-IRMS *vs.* GC-C-IRMS of four amino acids (Ala, Phe, Asp, Glu), ranging from natural to enriched (up to 300 per mil) isotopic composition. As a result, the developed methodology is applicable for natural abundance as well as for enriched materials.

3.2.4. Analysis of $\delta^{13}C$ in water soluble compounds by FIA-IRMS and LC-IRMS

The flow injection analysis FIA-IRMS technology allows us to analyse fast the bulk carbon isotopic composition of very small water soluble samples (50ul, 100ngC) without the complex sample preparation required for EA-IRMS analysis (see Figs. 8).

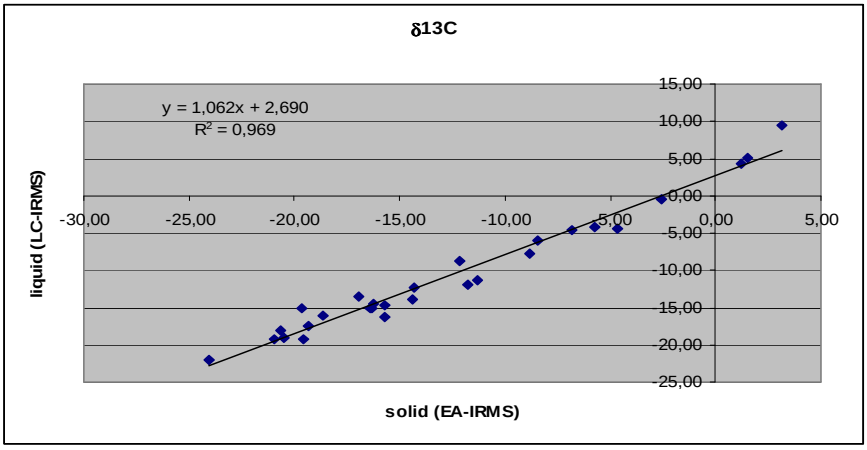

Figure 8. Comparison between $\delta^{13}C$ values (water soluble compounds from plants) obtained by EA-IRMS and FIA-IRMS

The methodology has been applied to assess the performance of plants exposed to contrasted conditions of depleted CO_2, temperature and water availability (.Aranjuelo, 2011). The technology is useful as a fast screening method for metabolic response as the recently assimilated compounds are measured (Fig. 9).

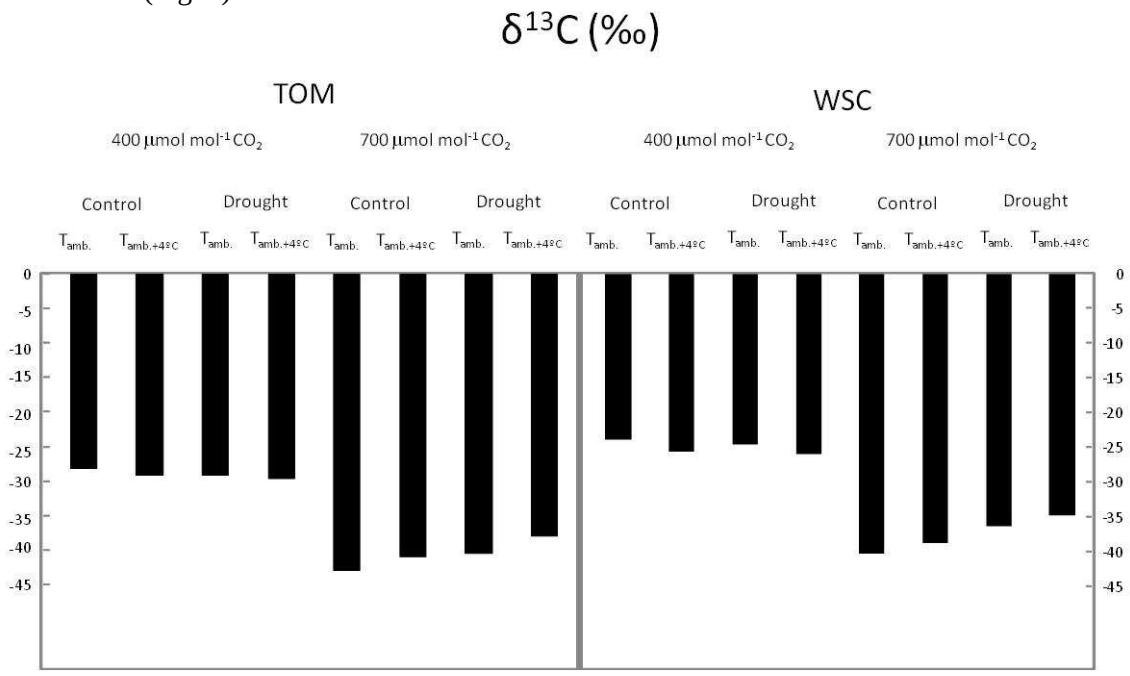

Figure 9. The $\delta^{13}C$ values obtained from WSC are less ^{13}C depleted in comparison to those obtained from total organic matter by EA-IRMS, which reflect better the stressful conditions applied.

References

- Aranjuelo I, 2011 (unpublished).
- Ferreti et al 2010 Patrizia Ferretti, Simon J. Crowhurst, Michael A. Hall, Isabel Cacho.
- (2010): North Atlantic millennial-scale climate variability 910 to 790 ka and the role of the equatorial insolation forcing. Earth and Planetary Science Letters, 293, 28–41.
- Marchesi *et al*., 2009. 8th International Symposium on Applied Isotope Geochemistry.
- J.M. McCrea (1950): On the Isotopic Chemistry of Carbonates and a Paleotemperature Scale. The Journal of Chemical Physics, vol.18, n.6, p.849-857.
- G. Molero, et al., 2011 Rapid Commun. Mass Spectrom. 2011, 25.599-607.
- Otero et al. 2007 Multi-isotopic methods applied to monitoring groundwater nitrate attenuation in a regional system, in *Towards a better efficiency in N use*, Bosch Eds. 446.471.
- J. Palau *et al*., 2007, J. Chromatogr. A, 1163:260-268.

3D Solutions in Transmission Electron (Cryo) -Microscopy in Biology

Lídia Delgado, Gemma Martínez, Yolanda Muela, Nieves Hernández, and Carmen López-Iglesias

Unitat de Crio-Microscòpia Electrònica, CCiTUB, Universitat de Barcelona. Parc Científic de Barcelona. Baldiri i Reixac, 10. 08028 Barcelona. Spain.

email: *carmenli@ccit.ub.edu*

Abstract. One of the main problems in transmission electron microscopy in the biological field is the tri-dimensionality. This article explains the technical procedures and requirements to prepare biological specimens preserving them closest to their native state to perform 3D reconstruction of the macromolecular complexes and cellular structures in their natural environment.

1. Introduction

Transmission electron microscopic (TEM) studies of biological samples are limited by four general factors:

- Electrons need high vacuum to form a beam able to traverse the sample and to form an image from it.
- Electrons heat the sample.
- The penetration power of electrons is very low.
- The image is a 2D projection of the specimen.

Therefore, the followings points must be considered:

- Firstly, the specimens cannot be alive, they must be immobilized or fixed. The high water content of cells (around 80%) needs to be removed or, preferably, stabilized by freezing [1].
- Secondly, the samples have to be dried, embedded in a resin resistant to heating or the electron microscope (EM) must be able to work under particular conditions ("low dose" of electrons) without damaging the sample [2].
- Thirdly, the thickness of the sample has to be between 50 and 400 nm, depending on the voltage of the EM.
- Finally, the viewing of 3D images from the specimen requires certain strategies in working with the EM and special software, called generally: "single particle analysis/reconstruction" and "electron tomography" [3].

BT.1

3D solutions in EM refer to technical procedures that bring the electron microscopic study closer to the native "hydrated" and "three-dimensional" state of biological specimens. These technical procedures are summarized as follows (see Table 1):

- *CRYO-IMMOBILIZATION:* The optimal way to immobilize or fix biological specimens in a close-to-native state, using physical procedures based on freezing. It is the recommendable first step in any 3D procedure. The goal is to get "vitreous" or amorphous ice from the cell water after ultrarapid freezing, without destroying cell structures and preserving their *in vivo* rapidly changing interactions. Vitrification allows spatial and temporal resolution of cellular events.
- *VITREOUS SECTIONING & FREEZE-SUBSTITUTION*: Two procedures to prepare bulk specimens for three-dimensional reconstruction. Cryo-sectioning of vitreous samples allows thin sections of cells or tissues at low temperatures to be taken without loss of their vitreous state. Freeze-substitution consists of the substitution of the vitreous ice by an organic solvent followed by embedding in a resin which after polymerization leads to thin sections of the specimens
- *FREEZE-DRYING & FREEZE-FRACTURE***:** Two different procedures to prepare bulk specimens for three-dimensional view but not for 3D-reconstruction. Freeze-drying allows to dry vitreous samples keeping all the nano-features immobilized by vitrification. Freeze-fracture opens lipid bilayers showing intra-membrane proteins. In both cases, a replica of the rough surface obtained by drying or fracture of the vitreous sample, is performed by shadowing with platinum (or tantalum) and carbon.
- *ROOM TEMPERATURE 3D ELECTRON MICROSCOPY*: Possibilities for 3D imaging of molecular or cell structures at room temperature. The procedures for the preparation of the samples for room temperature 3D-reconstruction and tomography are: i) negative staining (for small isolated particles) and ii) vitrification followed by freeze-substitution and resin embedding allowing sectioning at room temperature (for bulk specimens)
- *3D CRYO-ELECTRON MICROSCOPY*: The same three-dimensional reconstruction strategies mentioned above, but working under cryo-conditions (keeping the sample at a temperature below -170ºC and working with a "low dose" of electrons). The procedures for

the preparation of the samples for 3D Cryo-EM are: i) vitrification (for small isolated particles) and ii) vitrification followed by cryosectioning (for bulk specimens)

- *COMPUTATIONAL METHODS FOR 3D-RECONSTRUCTION*: After image acquisition, different software are used for data alignment, reconstruction and viewing. The reconstruction can be considered as the inversion of the imaging process. The projections obtained from the 3D-specimen at different angles or orientations are deprojected into the reconstructed volume.

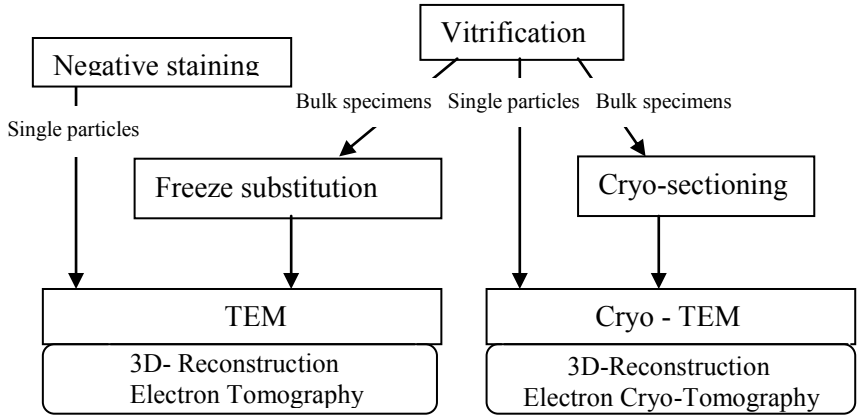

BT.1

Table 1. Technical procedures for 3D solutions in EM

2. Methodology

2.1. Cryo-immobilization

The first step in the 3D reconstruction of cells or molecules in EM is the preservation of the biological specimens in a close-to-native state.

In the EM, samples have to be observed under high vacuum and the electron beam leads to the destruction of native biological structure. Furthermore, the electron beam cannot usually penetrate an entire cell, so cells and tissues have to be cut into thin sections (50-400 nm in thickness depending on the voltage of the EM used) for observation. A conventional and classic way to solve these problems involves chemical fixation of the specimens, followed by dehydration or drying by various methods. Usually, chemical fixation is achieved by aldehydes such as glutaraldehyde and paraformaldehyde in a buffer. These mixtures fix the structures by selective cross-linking between certain amino acid residues of proteins. The rest of the macromolecules, small molecules and ions are not immobilized by this method. Thus, they are easily removed or re-distributed during the dehydration or drying. Another important drawback of conventional chemical methods is the time needed for the fixation. The chemicals penetrate the sample by diffusion. For thin samples, less than a few micrometers in the shortest dimension, diffusion is fast enough to give rapid fixation, but for larger pieces of tissue or organisms with natural diffusion barriers, such as cell walls, exoskeletons or special layers of embryos, diffusion throughout all cells is very slow. During this time, up to hours in some cases, the cell structure outside its natural environment is slowly destroyed.

In contrast to these conventional methods, ultrarapid freezing immobilizes all molecules in a cell within milliseconds. It is also called “quick freezing” “cryo-immobilization” or “cryo-fixation”. Ultrarapid freezing is highly desirable, because it allows the instantaneous fixation of all molecules in their current position. After this instantaneous immobilization it is very important to maintain this situation until the observation or image acquisition in the EM, in order to have a true snapshot of the cell at the moment of freezing [4].

The next optional steps are explained in the “*Cryosectioning and Freeze-substitution”* and *“Cryo-Electron Microscopy”.*

There are several methods of freezing cells, but they all have the same goal of removing heat from the sample so quickly that water molecules form an amorphous or vitreous non-crystalline ice. Thus, the optimal cryofixation is "vitrification". Such samples are called: frozen-hydrated or vitreous samples.

The methods to cryo-immobilize cells and molecules are:

- Plunge freezing
- Impact freezing (or slam- freezing)
- High pressure freezing
- Self-pressurized rapid freezing

For freezing suspensions or molecules or even small cells, plunging into a cooled cryogen, such as ethane or propane, is a common method. Another method, faster than plunging in its heat transfer, is slamming cells or tissues against a cooled metal block. For both impact- and plunge-freezing, it is possible to achieve up to 2-20 microns of good freezing depth. Beyond that, ice crystals form and destroy the tissue. However, most cells and tissues are much larger than a few microns, so we need another method to freeze them without ice crystal damage. The best method in these cases is High-Pressure Freezing (HPF), which freezes samples with liquid nitrogen under high-pressure conditions. Using HPF, relatively large volumes (200 microns and more) can be frozen without ice crystal damage.

BT.1

2.1.1. Plunge freezing

Plunging samples into a cooled cryogen is a common method for freezing suspensions (viruses, liposomes, bicelles, micelles...), molecular assemblies (proteins, nucleic acids...), isolated organelles and cell structures and small cells (bacteria, parasites...) [5].

Two types of gas can be used: ethane and propane. Both of them are gases at room temperature and become liquids at low temperature: Propane is liquid between - 42ºC and -188ºC; and ethane, between -88ºC and -172ºC. They are transferred from a gas bottle to a container cooled by liquid nitrogen at -196ºC and they liquefy instantaneously. They are used because of their low temperature in liquid state, which allows plunging for freezing, and for their high thermal conductivity, which allows a quick transfer of heat from the sample to the liquid. They are kept in liquid nitrogen during the freezing process to ensure that they remain liquid and at the lowest temperature.

The samples must be immersed at high speed into the liquid coolant to optimize the heat exchange required to vitrify the specimen. Usually, acceleration 3 times greater than the gravitational force is required. Under these conditions, high freezing velocity, around 10^4 ºC/sec, is attained.

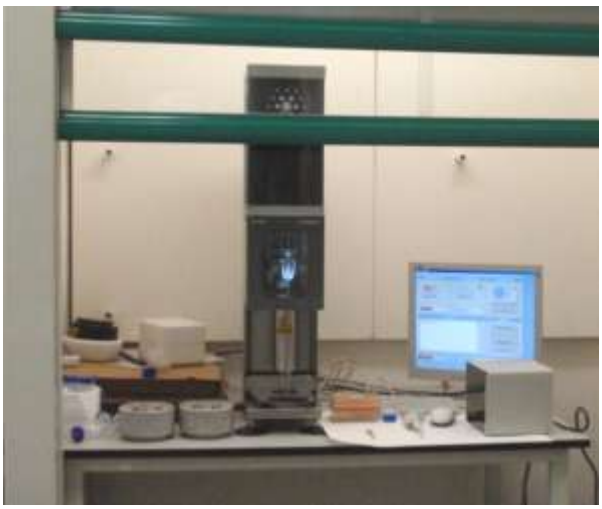

Figure 1. Plunge freezing equipment: Vitrobot Mark III (FEI Company) atthe CCiTUB Cryo-EM laboratory.

2.1.2. Impact freezing

Slamming or impact-freezing or "metal-mirror" is a process of rapidly projecting cells or tissue onto a cooled metal block. The copper block is cooled by liquid nitrogen or liquid helium from a Dewar flask. Some instruments have the copper block placed in a vacuum chamber in order to avoid any moisture contamination on the block surface. Good structural preservation, without ice crystal damage, goes from 10 to 30 microns in depth.

Impact-freezing is used to cryofix cells and tissues for further freeze-substitution or freeze-drying, or even for cryo-sectioning and cryo-EM [6].

The main advantage of this method is the possibility of vitrifying surface regions of quite large samples, nearly as large as the cooling block (between 1 and 3 cm in diameter, depending on the type of instrument). Another advantage, compared with plunge-freezing, is the high thermal conductivity of copper, much higher than organic liquids. The same amount of heat is transferred 10,000 times faster through copper than through liquid cryogen. This is why it is used for samples larger than "single particles" (seen in plunge-freezing).

Figure 2. Impact freezing equipments: Leica EM-CPC cooled by liquid nitrogen and Leica Cryoblock, cooled by liquid nitrogen or liquid helium. Both at the CCiT Cryo-EM Laboratory.

2.1.3. High-pressure freezing

High pressure freezing freezes samples with liquid nitrogen under high pressure conditions. Using HPF, relatively large volumes (200 microns and more) can be frozen without ice crystal damage [7] [8]. This is possible because at high pressure (about 2,000 atmospheres or bar) ice crystal nucleation and growth are slowed down (homogeneous nucleation of water molecules to form crystals starts at -40ºC at ambient pressure and drops to -90ºC at 2,000 bar; and water is 1,500 times more viscous than at ambient pressure, reducing the ice crystal growth rate). High pressure lowers the freezing point of water (at 2,000 bar the freezing point is at a minimum of -22ºC) [9].

When freezing at ambient pressure, it takes a very high freezing rate to achieve good preservation, between 10^5 and 10^6 ºC/sec. In very viscous water under high pressure the cooling rate can be much lower, in the range of 10,000 to 30,000ºC/sec.

In HPF machines the pressure increase is synchronized with the temperature decrease. Pressure can be harmful when applied for too long times (>100 ms) to a biological sample. Therefore, pressure and cold must be simultaneously applied to the sample to achieve vitreous ice. The only problem in freezing a sample with HPF is the gaseous compartments, because these are compressed and their collapse may distort the sample. However, the aqueous phase is almost incompressible.

2.1.4. Self-pressurized rapid freezing (SPRF)

This new rapid-freezing method uses the increase of volume of water when it freezes naturally. The sample, preferably in an aqueous medium or buffer, is located into a thin-copper tube, which is projected into liquid ethane or propane in two speed steps. Thus, the cooling rate is slow at the ends of the copper tube and very fast in the middle of it. Therefore, the increasing of water volume at the

ends of the copper tube by ice crystals formation pressurizes the middle of the tube at the same time that freezing takes place in this part.

SPRF is a totally new technology described by Leunissen et al [10] recently.

Figure 3. High-pressure freezing Leica EMPact machine at the CCiT Cryo-EM Laboratory.

2.2. Cryo-sectioning of vitreous samples & Freeze substitution

2.2.1. Cryo-sectioning of vitreous samples

Cryo-sectioning of vitreous samples allows thin sections of cells or tissues at low temperatures to be taken without loss of their vitreous state. Most cells are too big to be imaged by EM, so microtomy is needed to make samples thin enough to be viewed under the electron beam. Even if the cells are small enough to be imaged by an EM of a certain voltage, it has been tested that the resolution is higher after sectioning.

Cryo-tomography of vitreous sections allows 3D reconstruction of macromolecular complexes within the natural cell environment [11].

The necessary instrumentation for vitreous sectioning is a cryo-ultramicrotome in an atmosphere totally free of moisture. One option is an anti-contamination glove box covering the cryo-ultramicrotome where it is possible to reach 0% of relative humidity (Fig. 4).

Figure 4. Cryo-ultramicrotome Leica UC6/FC6 with an anti-contamination glove box based on the prototype of Peters Lab. [12], at the CCiTUB Cryo-EM Laboratory.

2.2.2. Freeze substitution

Freeze substitution consists of the substitution of the vitreous ice by an organic solvent followed by embedding in a resin which after polymerization allows to take thin sections of the specimens. The samples are cryo-immobilized to get vitrification of the cell water and the amorphous ice is dissolved by the solvent at about -90ºC during freeze substitution. The samples are put in a medium composed by acetone, methanol or ethanol containing chemical fixatives such as uranyl acetate, osmium tetroxide, or glutaraldehyde, in different mixtures and different concentrations, depending on the type of sample and on the technique to be carried out later [13]. The samples are kept in the chosen medium at about -90ºC from several hours to 3 days. The freeze substitution time is dependent on the specimen, e.g., for culture cells we use 24 hours or less and for yeast or plant cells, 72 hours. After substitution the temperature is raised to the appropriated embedding temperature depending on the resin used. Epoxy resins are used for structural and tomographic studies without molecular labels and they polymerised at room temperature. Acrylic resins are used for immunolabeling, *in situ* hybridization and also for tomographic studies searching for their higher transparency [14].

Freeze substitution protocol for tomography

0.5% uranyl acetate in acetone

Step	Time	Temperature	Slope
T1	24 h	- 90˚C	
S1	2,5 h	until -40ºC	20˚C/h
T2	2h	- 40˚C	

Followed by Lowicryl HM 23 embedding at -40ºC.

Figure 5. Leica EMAFS (Automatic Freeze Substitution System) at the CCiTUB Cryo-EM Laboratory

2.3. Freeze drying and freeze fracture

2.3.1. Freeze drying

This term refers to the removal of ice from the vitrified sample by vacuum sublimation, before a heavy metal-carbon replica of the tri-dimensional surface is made. The replica is obtained by oblique and rotary deposition of a heavy metal, usually platinum, followed by coating with a strengthening layer of electron-translucent carbon. The angle of platinum deposition is 45º in a standard way, but it is changed depending on the height of the structure to be shadowed. For example, for caveolae, 23º are used and for DNA, around 8º. Then, the biological material is removed and the cleaned replica is mounted on a grid for examination in the TEM [6] [15].

2.3.2. Freeze fracture

The freeze-fracture technique involves physically fracturing a suitably frozen sample, making a metal-carbon replica of the frozen fractured surface under vacuum. The replica is made by oblique and unidirectional deposition of a heavy metal followed by carbon as it was explained before. The difference with the freeze-drying process is the uni-directionally of the shadowing [15].

Improved resolution in all replication techniques can be achieved using a mixture of tungsten/tantalum instead of platinum, but this metal mixture is more difficult to use reproducibililty.

In frozen cells the preferably planes of fracture are the interior of lipid bilayers of cell membranes [16]. For this reason, freeze-fracture is very useful to study intra-membrane proteins.

Figure 6. Freeze-etching system BAF 060 from BalTec at the CCiTUB CryoEM Laboratory

2.4. Room temperature 3D electron microscopy

This subsection refers to the possibilities for 3D imaging of molecular or cell structures at room temperature. In general, the term 3D reconstruction is used when images are acquired in the EM in only one direction of the electron beam. One case is the reconstruction from the different orientations of a single particle on a grid. Single particles are isolated macromolecules, molecular assemblies, small organelles, small cellular structures or small organisms not needing sectioning. Another case is the reconstruction of a cell structure or organism from images obtained from serial sections.

The term electron tomography is commonly used when images from a specimen in the EM are recorded in as many directions of the electron beam as possible. This is achieved by tilting the holder supporting the grid containing the specimen. The sample can be an isolated specimen not needing sectioning or a structure inside a section. In practice, we tilt the grid around a tilt axis of the goniometer, typically over the range from -70º to +70º, recording images at regular tilt intervals of 1º for example. These tilted images form a tilt series and are processed by software. Then, the acquired images are aligned with each other using suitable software, and from them a three-dimensional volume consisting of a stack of parallel images is reconstructed. The next step is the visualization or modelling of the 3D-structure. Summarizing, acquisition, alignment/reconstruction and modelling are the three steps in tomography.

There are two ways of preparing samples for EM 3D studies at room temperature: negative staining and freeze substitution. Negative staining is used for single particle analysis and reconstruction. It is a very simple technique based on the use of salts containing heavy metals such as uranyl acetate or formiate, ammonium molibdate or phosphotungstic acid. They provide an electrodense background to the grids and the single particles protrude from it. As a result, the image presents a negative contrast, the particles become clear over a dark background. On the other hand, freeze substitution is used, as it was mentioned before, to enable thin sectioning of bulk cells or specimens [17].

2.5. 3D Electron Cryo-Microscopy

This subsection refers to the possibilities for 3D imaging of molecular or cell structures in cryo-conditions. Single particle analysis of vitrified samples and electron cryo-tomography of vitreous specimens or sections differs from room temperature 3D EM in the temperature used to observe and image the specimen and enables a three-dimensional visualization of the macromolecular complexes, cells or tissues in a quasi-native environment [18] [19]. The temperature of the vitrified

sample during the cryo-work should be below -170ºC and the specimens aren't chemically fixed and stained with heavy metals. Although the radiation sensitivity of vitrified samples and their low contrast pose problems for information imaging, methods used now like low- dose of electrons imaging and high resolution CCD cameras make more efficient the cryo-EM work.

The procedures for sample preparation for 3D Cryo-EM are: vitrification for small isolated particles and vitrification followed by cryo-sectioning for bulk specimens.

Figure 7. Tecnai Spirit electron microscope, equipped for cryo and tomography at the CCiT Cryo-EM Laboratory.

Figure 8. Tecnai F20 200 kV and field-emission gun (FEG) electron microscope. It is equipped for cryo and tomographic work with an anti-contamination device, the cryo-box, a low dose imaging mode, a 4k x 4k CCD Eagle camera and the FEI tomography software package. At the CCiT Cryo-EM Laboratory

3. Examples of applications

In the next plates, different examples of the describedr procedures are showed. They are focused mainly onthe optimal preparation methods to do three-dimensional studies in biological structures.

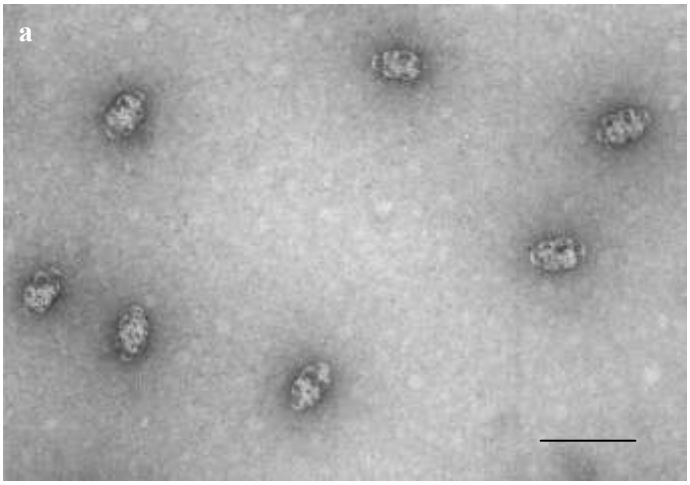

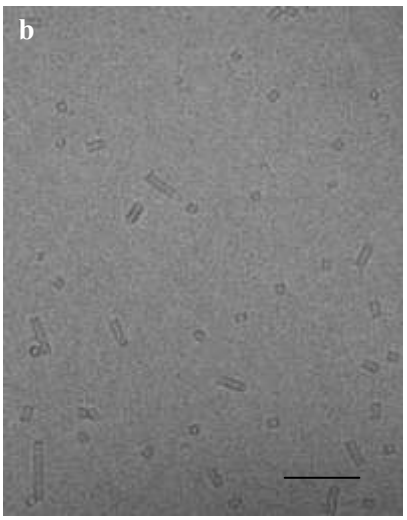

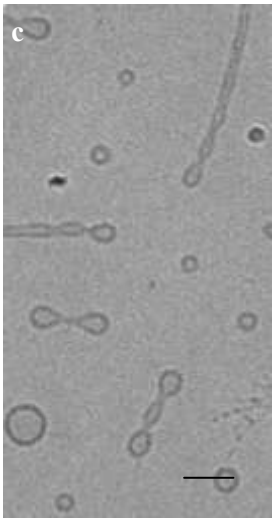

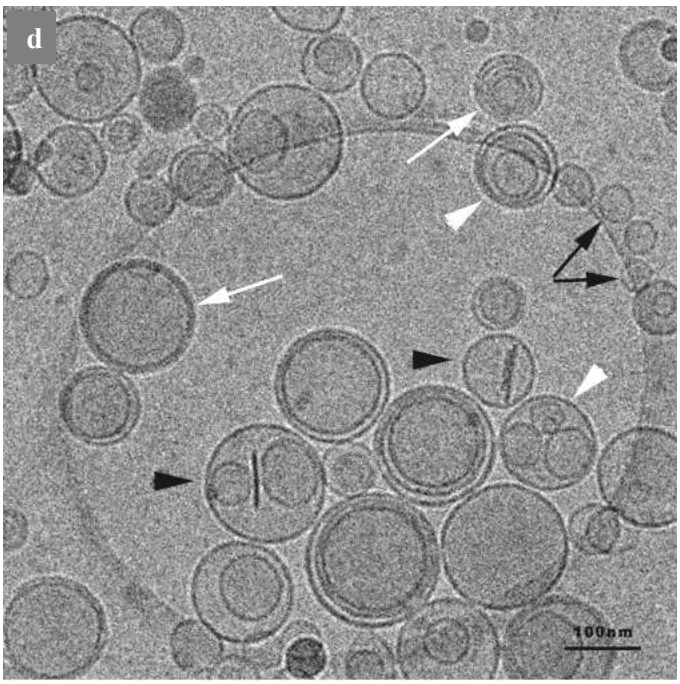

Figure 9. Single particles

a.Vaults imaged after negative staining with 2% uranyl acetate in water.
This image belongs to an study of these ribonucleoprotein particles [20]. It shows the high resolution that can be achieved with basic techniques such as negative staining to perform 3D-studies.

b. Hemocyanin protein . A solution of this protein was vitrified by plunge freezing in ethane using the Vitrobot. 3 µl of the solution were deposited on a holey carbon copper grid, kept during 30 seconds in a 100% humidity chamber and blotting with filter papers before plunging in the liquid ethane cooled by liquid nitrogen.
This is a second way to prepare single particles to perform 3D-studies. In this case the observation and imaging were made in an electron cryo-microscope.

c. Vesicles isolated from the extracellular matrix in a bacterial colony. The vesicles were vitrified by plunging in ethane and directly transferred into liquid nitrogen to the electron cryo-microscope and imaged at -180ºC.

d. Bicosomes: liposomes containing bicelles.This image was taken at -180ºC in the F20 cryo-microscope after vitrification in liquid ethane. Bicellar systems are mixtures of aliphatic long chain and short-chain phospholipids. Their morphology depends on the composition, temperature, hydration and the long/short chain phospholipid molar ratio. These systems may form spherical micelles, discoidal bilayers, rod-like micelles and perforated bilayers. Freeze-fracture EM and cryo-TEM are the most suitable techniques to study these systems [21].

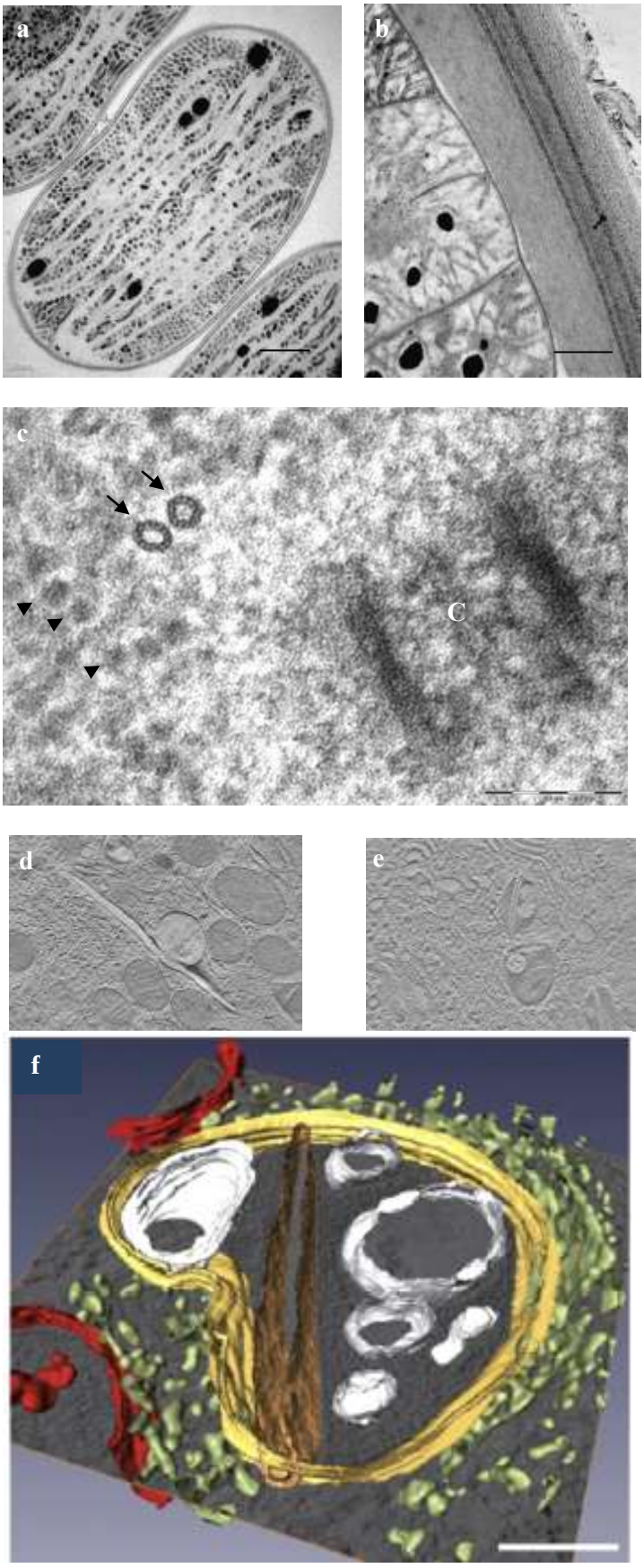

Figure 10. Bulk specimens

Freeze substitution:

a & b. Cianobacteria. High pressure freezing without any cryoprotectant and filler. Once frozen, they were freeze-substituted in 2% osmium tetroxide and 0.1% uranyl acetate in acetone and embedded in Epon resin [see 22].

c. Centrosome area of a neuroblast in the brain of a Drosophila embryos. A centriole (c), two microtubules (arrows) with the typical subunits and the ribosomes (arrowheads) out of the area surrounding the centrioles can be seen. The embryos brain was cryofixed by high pressure freezing using a mixture of yeast paste and dextran like filler. Then, it was freeze-substituted and embedded in Epon.

d. & e. Computational tomographic slides (~3 nm) of the tomogram obtained from 200 nm sections of high-pressure frozen, freeze-substituted with 0.5% uranyl acetate in acetone and Lowicryl HM23 embedded Rubella infected cells. To stabilize the sections under the electron beam they were collected on holey carbon Quantifoil® grids. Rubella virusbuilds a factory around modified lysosomes, known as "cytopathic vacuoles" or "CPVs", by recruitment of mitochondria, rough endoplasmic reticulum elements and Golgi stacks [23].

f. 3D model after segmentation and visualization of the CPV of a Rubella replicon transfected cell. Single axis tilt series were obtained with angle ranges between -60 and +60º and a 2º angular increment. Color code is as follows: CPV,yelow; straight sheet, brown; RER, green; mitochondria, red; nucleus, pink; vesicles and vacuoles, white; cytoplasm, grey [23].

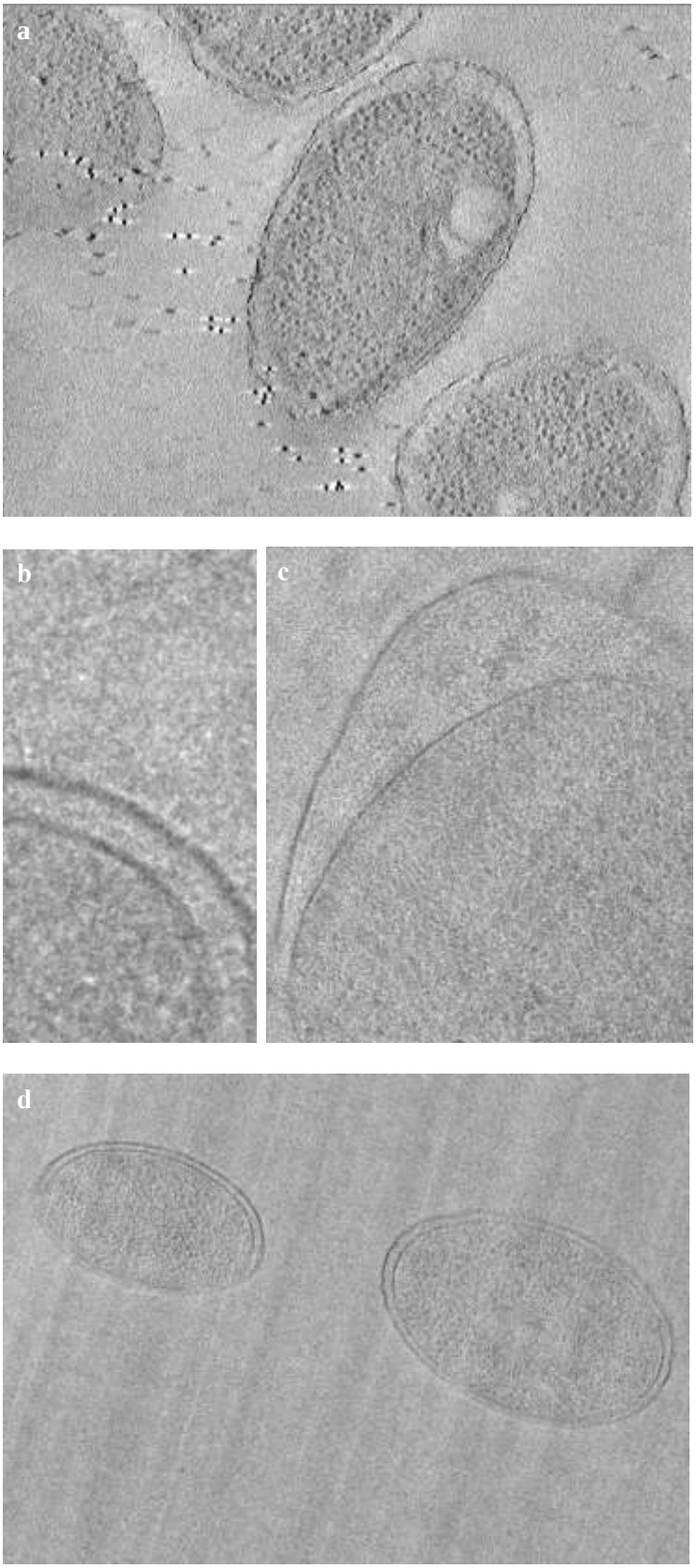

Figure 11. Bulk specimens

a.Antarctic bacteria *Pseudomonas deceptionensis* .

Computational tomographic slides (~3nm) of the tomogram obtained from 200 nm sections of high pressure frozen, freeze-substituted with 2% osmium tetroxide /0.1% uranyl acetate and Epon embeddedAntarctic bacteria.
Gold particles used as fiducial markers for tomography can be seen in the image with a shadow after tilting.

Cryosectioning of vitreous samples:

b, c & d. *Ps. deceptionensis.*
Cryosections of vitreous samples observed in an electron cryo-micoscope (CEMOVIS: Cryo-electron microscopy of vitreous sections).
Bacteria colonies were mixed with dextran at a final concentration of 20%-30% and frozen by high pressure freezing into small copper tubes. The tubes were sectioned at -150ºC in a cryo-ultramicrotome equipped with an anti-contamination glove box. Cryosections of 50 nm were collected on holey carbon Quantifoil grids.
Details of the bacteria envelope and extracellular area is shown in b, periplasmic space in c and a panoramic view of this kind of sections in d. CEMOVIS allows the study of the macromolecular structures inside the cell (*in situ)* in the closet to the native state conditions.

The final goal of this technique in development known as CETOVIS (cryo-electron tomography of vitreous sections) is to have the 3D-information of the cellular nano-machines in their natural environment.

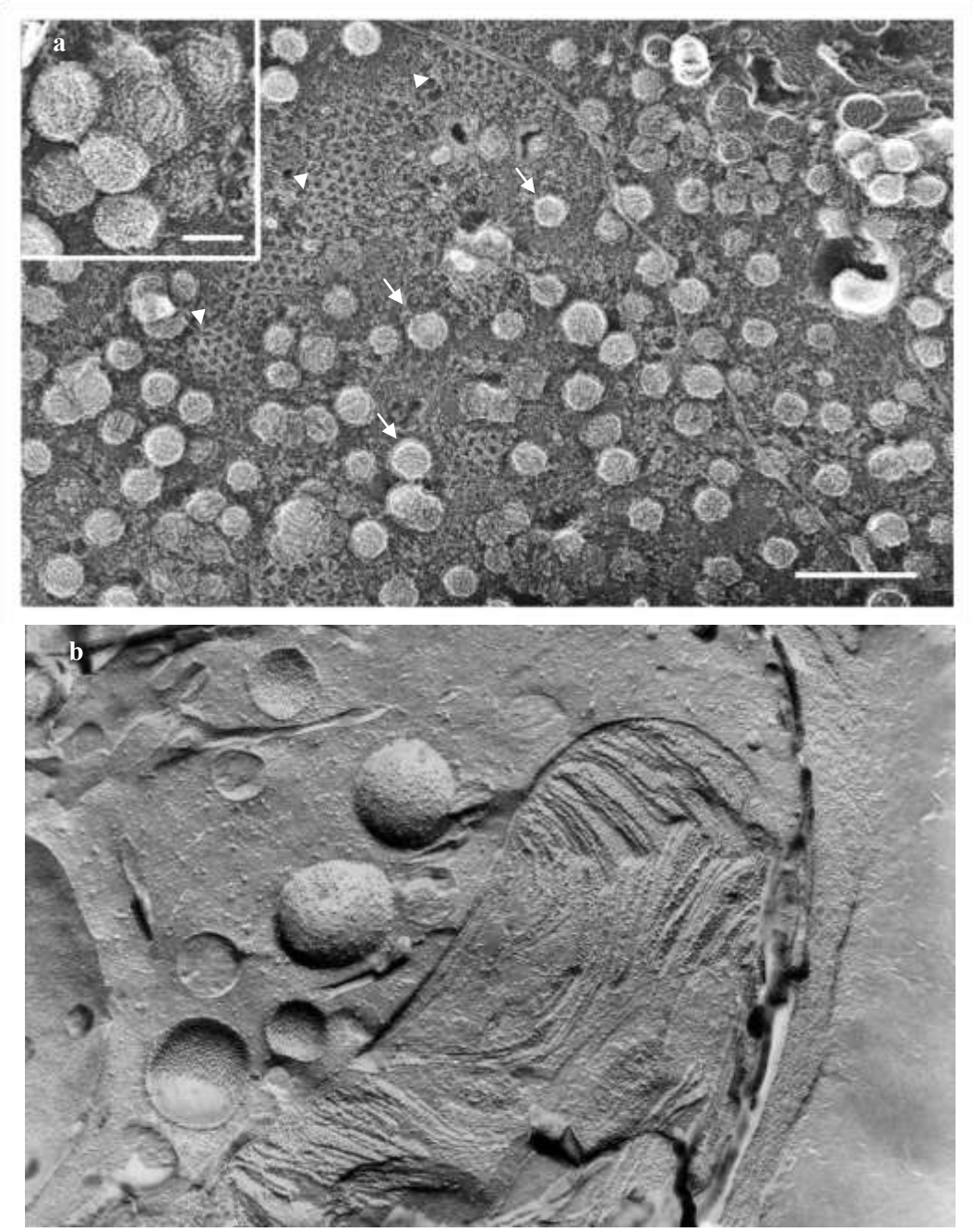

Figure 12.
a. Plasma membrane lawn of the ventral membrane of a 3T3 adipocyte. Membranes attached to a substrate were frozen by impact freezing and dried at 10^{-7} mbar and -90ºC . The dried surface was shadowed with platinum and carbon in a rotator way in order to make a replica of it. Caveolae (arrows) and clathrin lattices (arrowheads) are revealed [24].
b. Alga frozen by propane immersion which was freeze-fractured at -150ºC and the rough surface obtained was shadowed with platinum at 45º and carbon at 90º in an unidirectional way. Intramembrane proteins can be studied with this technique [13].

Acknowledgments

The authors would like to thank all users with whom they collaborate, especially l Núria Verdaguer, Elena Mercadé, Olga López, Cayetano González, Xavier Huete, Cristina Risco, Marta Camps and Mariona Hernández-Mariné, for allowing to use in this article images belonging to their studies. They also acknowledge David Bellido, Sonia Ruíz and Elisenda Coll for actively contributing to these studies in the course of their professional life.

References

[1] [Echlin P. 1992 *Low Temperature Microscopy and Analysis*, Plenum Publishing Corporation, New York
[2] [Steinbrecht R.A, Zierold K. 1987 *Cryotechniques in Biological Electron Microscop,y* Springer-Verlag
[3] Frank J. 2006 *Three-dimensional electron microscopy of macromolecular assemblies: visualization of biological molecules in their native state,* Oxford University Pres
[4] Cavalier A., Spehner D, Humbel B.M. 2008 *Handbook of Cryo-preparation Methods for Electron Microscopy*, CRC Press
[5] Dubochet J., Adrian M., Chang J-J., Homo J-C., Lepault J., McDowall A.W., Schulz P. 1988 *Quarterly Review of Biophysics* **21** 129
[6] Ros-Baro A., López-Iglesias C., Peiro S., Bellido D., Palacin M., Zorzano A., Camps M. 2001 *Proc Natl Acad Sci U S A* **98** 12050
[7] Galy V., Askjaer P., Franz C., López-Iglesias C., Mattaj I.W. 2006 *Curr Biol.* **16** 1748.
[8] Nebot M., Deroncele V., López-Iglesias C., Bozal N., Guinea J., Mercade E. 2006 *Microb Ecol*. **51** 501
[9] Studer D., Humbel B. M., Chiquet M. 2008 *Histochem. Cell Biol.* **130** 889
[10] Leunissen J.L.M., abd Yi H. 2009 *J. Microsc.* **235** 25
[11] Pierson J., Sani M., Tomova C., Godsave S., Peters P.J. 2009 *Histochem Cell Biol.* **132** 253
[12] Pierson J., Fernández J.J., Bos E., Amini S., Gnaegi H., Vos M., Bel B., Adolfsen F., Carrascosa J.L., Peters P.J. 2010 *J Struct Biol.* **169** 219
[13] Porta D., López-Iglesias C. 1998 *Tissue Cell.* **30** 368
[14] Visa N., Quintana C., López-Iglesias C., Fibla J., Gonzàlez-Duarte R., Santa-Cruz MC. 1993 *Microsc Res Tech*. **24** 453
[15] Severs J., Shotton D.M. 1995 *Rapid freezing, freeze fracture and deep etching.* Wiley & Sons. New York
[16] López O., López-Iglesias C., Cócera M., Walther P., Parra J.L., De La Maza A. 2004 *J Struct Biol*. **146** 302
[17] McIntosh J.R. 2007 *Methods in Cell Biology*. Vol.**79**. Elsevier
[18] Baumeister, W. 2002 *Curr Opin Struct Biol* **12** 679
[19] Al-Amoudi, A., Chang J.J., Leforestier, A., McDowall, A., Salamin, L.M., Norlen, L.P.O., Richter, K., Sartori Blanc, N., Studer, N. and Dubochet, J. 2004 *EMBO J.* **23** 3583
[20] Querol-Audi J., Pérez-Luque R., Fita I., López-Iglesias C., Castón J.R., Carrascosa J.L, Verdaguer N. 2005 *J.Struct. Biol.* **151** 111
[21] Rodríguez G., Soria G., Coll E., Rubio L., Barbosa-Barros L., López-Iglesias C., Planas A.M.., Estelrich J., de la Maza A., López O. 2010 Biophys J. **99** 480
[22] Frias A., Manresa A., de Oliveira E., López-Iglesias C., Mercade E. 2010 *Microb Ecol.* **59** 476
[23] Fontana J., López-Iglesias C., Tzeng W.P., Frey T.K., Fernández J.J., Risco C. 2010 *Virology* **405** 579
[24] González-Muñoz E., López-Iglesias C., Calvo M., Palacín M., Zorzano A., Camps M. 2009 *Endocrinology* **150** 3493

Transmission Electron Microscopy in Cell Biology: sample preparation techniques and image information

Núria Cortadellas, Almudena Garcia, and Eva Fernández

Unitat de Microscòpia Electrònica, CCiTUB, Universitat de Barcelona. Facultat de Mediciona. Casanova, 143, 6ª pl. Ala Nord. 08036 Barcelona.

email: *nuriac@ccit.ub.edu*

Abstract. Transmission electron microscopy is a proven technique in the field of cell biology and a very useful tool in biomedical research. Innovation and improvements in equipment together with the introduction of new technology have allowed us to improve our knowledge of biological tissues, to visualize structures better and both to identify and to locate molecules. Of all the types of microscopy exploited to date, electron microscopy is the one with the most advantageous resolution limit and therefore it is a very efficient technique for deciphering the cell architecture and relating it to function. This chapter aims to provide an overview of the most important techniques that we can apply to a biological sample, tissue or cells, to observe it with an electron microscope, from the most conventional to the latest generation. Processes and concepts are defined, and the advantages and disadvantages of each technique are assessed along with the image and information that we can obtain by using each one of them.

1. Introduction

The preparation of a biological sample, cells or tissue, for transmission electron microscopy (TEM) requires several stages, some of which are quite complicated and some are critical. There is a wide range of possible techniques and processes and the use of one particular process rather than another will depend on the sample (type of tissue, cells, biofilm, etc.), on the size of the specimen being studied, on how the sample is obtained (in a laboratory, a hospital, or in the field, etc.), on the equipment that is available to us and finally, and very importantly, on what type of study we wish to carry out (ultrastructural, molecular localization, immunolocalization, electron tomography, correlative techniques, etc.). There are different possibilities for each type of study and before starting, it is necessary to decide which is the best option or options that we can use based on the information that we want to obtain from the sample and on the equipment that is available to us to carry out the study.

The first stage in preparing a biological sample is the fixation**,** one of the most important and most critical stages. The objective of this is to halt cellular activity without altering the cellular characteristics, the components that make up the sample or their distribution: to preserve the internal three-dimensional organization, the size and the shape of the sample.

The fixation process can be carried out in two different ways, by chemical fixation or by cryofixation. Chemical fixation [1,2] has been used since the 1950s and consists of the use of a whole range of chemical components (glutaraldehyde, paraformaldehyde, acrolein, osmium tetroxide, uranyl acetate, etc.) which, when used separately or in combination, in different proportions and dissolved in a buffer solution that acts as a vehicle, will serve as the fixative, by combining with the components of the cell and halting its processes. Within what is known as chemical fixation there are different systems, perfusion, immersion, by vapour, etc., and the use of one or another will depend on different factors: the type of sample, its size, etc. However, we need to bear in mind that chemical fixation produces structural artifacts and can result in the redistribution of ions and small soluble proteins in the sample [15].

The best way to immobilize and preserve the cell architecture is probably cryofixation, which consists of freezing the sample very quickly without crystals formation. There are different systems and equipment for carrying out the process: immersion in a liquid agent, impact on a pre-cooled metallic block, high pressure, etc. The use of one or another will depend on the type of sample and also on the equipment that can be used. However, the only system that permits maximum depth of cryofixation, of around 200 μm, is high pressure freezing (HPF). This consists of stopping cellular activity by freezing a sample at a rate of more than 10,000ºC/s and at a pressure of around 2100 bars [5]. At this rate of freezing and this pressure, the water molecules lose their usual mobility and crystals do not form (this is the phenomenon of nucleation) resulting in what is called vitreous ice [14]. However, in many cases the sample has to be treated with cryoprotectants prior to cryofixation [3,4]. Cryofixation is the most modern method for preserving the ultrastructure, but we must bear in mind that the instability and the anoxic sensitivity of tissues prior to cryofixation mean that in some cases and for certain types of samples a combination of chemical fixation with cryofixation by HPF can be a very useful compromise [4,9].

2. Methodology

After the fixation stage, the sample can be processed by different routes before it is studied in the electron microscope. The most common routes are indicated in the following schematic diagrams: Chemical fixation (Fig.1) and Cryofixation (Fig.7).

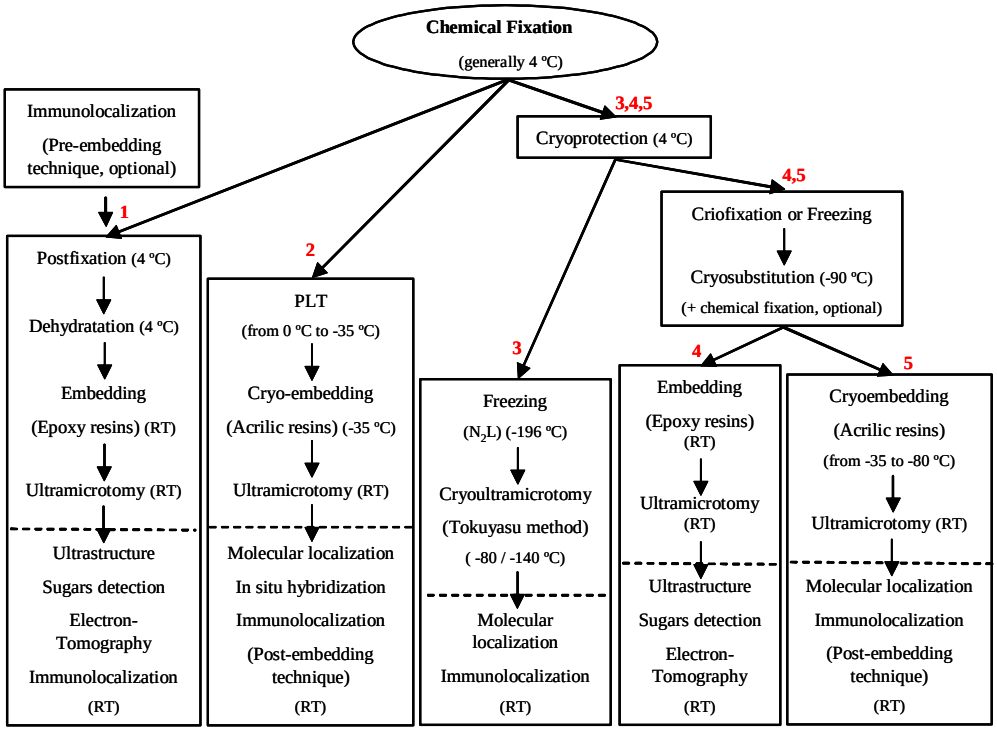

Figure 1. Chemical fixation. The most important processing routes for a biological sample based on chemical fixation.

BT.2

2.1. Chemical fixation – dehydration – embedding (see Fig. 1, technique 1) [1,2,18].

If the sample has been chemically fixed (see Fig. 1), it can then undergo some postfixation, which is usually performed using osmium tetroxide, to improve the quality of the fixation and especially to preserve the lipid part of the sample. Afterwards, it is dehydrated in an organic solvent (alcohol, acetone, propylene oxide, etc.) in order to eliminate the water from the sample and to embed it in an epoxy-type resin that is not miscible with water (Epon 812, Spurr, Araldite, etc.). The sample will then be sectioned, contrasted with heavy metals and observed in a TEM.

Advantages:

- Most biological samples can be fixed and processed using this method.
- The process of chemical fixation requires no special equipment and it can be carried out in any setting (laboratory, operating theatre, in the field, onboard ship, etc.).
- The block containing the sample can be stored for many years.
- The sample can be redirected, after dehydration, to the critical point process so that it can later be observed in a scanning electron microscope (SEM).

Disadvantages:

- It can create structural artefacts.
- Modifications may be produced in the cellular volume due to osmotic changes.
- It can lead to the redistribution of ions and of small soluble proteins.

Image and information:

- The image that is obtained is a contrasted image, with well-defined membranes, and it is easy to bring into focus in the TEM.
- We can work with a large area of the specimen and the fixation is homogeneous.
- This processing route allows us to carry out optical studies, ultrastructural studies, detection and localization of sugar residues using lectins and colloidal gold, cytochemical techniques, enzymatic digestions, electron tomography and molecular localization techniques with nanogold or quantum-dots (pre-embedding technique) (see Fig. 1).
- It allows correlatives techniques to be used: optical microscopy–electron microscopy.

- It also allows the elements of the sample to be analysed by energy filtered transmission electron microscopy (EFTEM) or by secondary ion mass spectrometry (SIMS).
- Semithin sections can be observed by SEM.

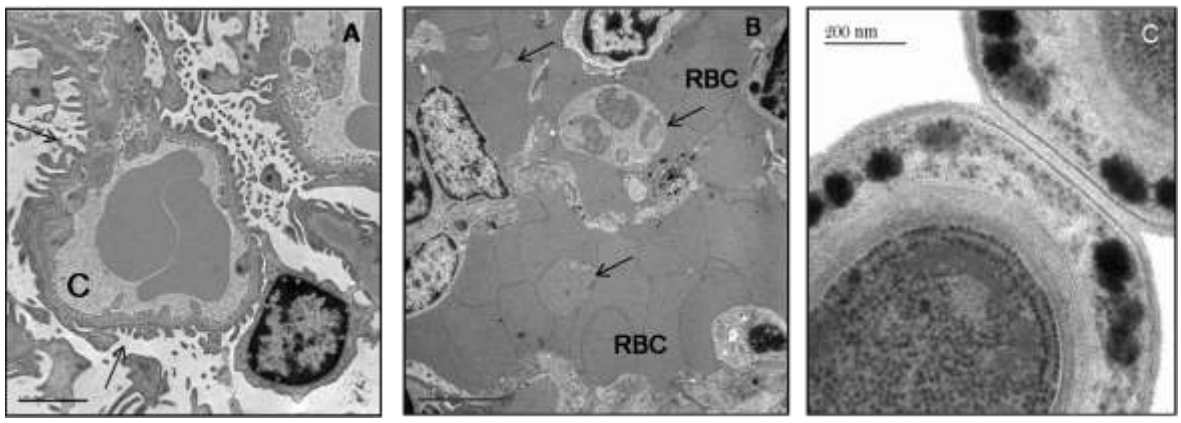

Figure 2. Chemical fixation – dehydration - embedding (A) Kidney capillary and filtration barrier. Bar 2 µm. (Courtesy F..Pardo and R. Gomis, Idibaps), (B) Spleen malaria infection , *Plasmodium yoelii* (→). Bar 5 µm. (Courtesy H. del Portillo, L. Martin, M. Ferrer – Cresib), (C) Bacteria detail of *Clostridium bifermentans*. Bar 200 nm. (Courtesy of R. Guerrero and L.Villanueva - UB).

BT.2

2.2. Chemical fixation–PLT–cryoembedding method. (see Fig. 1, technique 2) [5,6,7].
After chemical fixation we can also perform what is called progressive lowering of the temperature (PLT), which is specific for immunolocalization techniques and molecular localizations such as "in situ" hybridization. The technique uses a gentle aldehyde fixation followed by dehydration of the sample which is achieved by progressively lowering the temperature from 4ºC to –35ºC **[5,6]**. This method, working at temperatures below 0ºC, reduces the loss of components from the sample and minimizes the denaturization of the proteins. Afterwards, the sample is embedded at –35ºC in an acrylic resin (Lowicryls, LRWhite, LRGold, etc.) that has low viscosity and is miscible with water Most of the resins are hydrophilic and they have good electron beam stability when they are polymerized [7]. Furthermore, they polymerize with ultraviolet light, which means that the antigenicity of the tissue is preserved.

Advantages:
- The method is fast and an easy way to localize proteins or a genetic sequence by "in situ" hybridization.
- Labelling or co-localization can be performed using different sizes of colloidal gold.
- This method allows co-localization with antibodies from the same species to be performed, incubating both sides of the ultrathin slice.
- The use of acrylic resins allows 5% of the content of the sample to be water.
- The sectioning is not easy but, with experience in ultramicrotomy, very good quality slices can be obtained.
- The block containing the sample can be stored for years.

Disadvantages:
- If the quantity of protein to be localized or the genetic sequence is small, it is difficult to obtain a signal using this method and so it will be better to use the Tokuyasu method which is more sensitive.
- The technique requires commercial equipment or a homemade system.

Image and information:

- The image allows the structures to be clearly identified, but even so it is useful to know the tissue well at the ultrastructural level by other methods.
- Since osmium tetroxide is not used, the membranes are not very electrodense and in general the sample has a gentle contrast, which means that the gold labelling stands out clearly over the structure that we are labelling.
- It is a good technique for immunolocalization and "in situ" hybridization techniques. This can be performed using an optical microscope, on semithin slices, using colloidal gold and intensification in silver or directly on ultrathin sections with colloidal gold.
- It is suitable for correlative techniques (optical–electron microscopy).

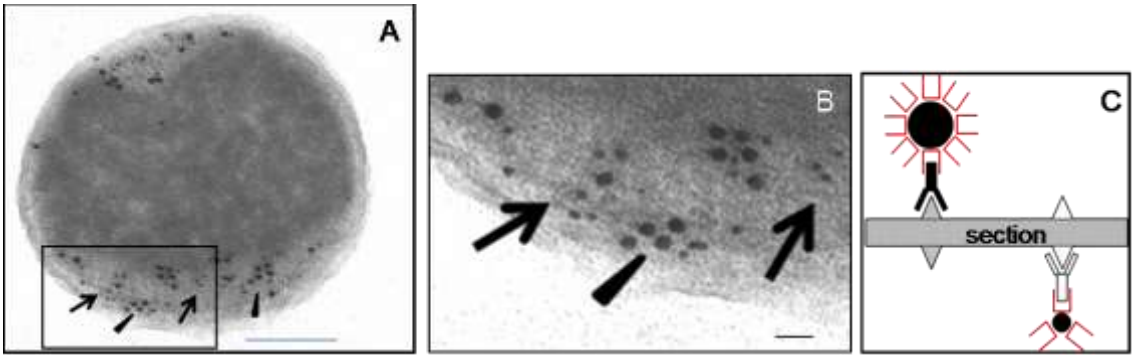

Figure 3. Technique Chemical fixation–PLT–cryoembedding method**.** Immunolocalization (A) Double detection of chaperones DnaK (►) (15 nm gold) and GroEl (→) (5 nm gold) in *E. coli* inclusion bodies using antibodies from the same species. (Bar 200 nm). (B) Detail inset in A. (Bar 50 nm). (C) Technique detail. (Courtesy of M. Carrió and A. Villaverde – UAB).

2.3. Chemical fixation–Tokuyasu method (see Fig. 1, technique 3) [7,8]

The Tokuyasu method is based on cryosectioning of the sample and is used for immunolocalization techniques. In this case, the chemical fixation that is carried out is at low concentrations of aldehydes in order to preserve the antigenicity of the sample and so that molecular detection can be performed afterwards. The chemically fixed sample is enveloped in gelatine and is then impregnated with sucrose or with a sucrose/polyvinylpyrrolidone mixture. After that, it is mounted on a special sample holder and frozen immediately in liquid nitrogen. Finally, it is cryosectioned in a cryoultramicrotom at a temperature between -80ºC and -140ºC. The immunolocalization is carried out on ultrathin sections (80-100 nm) and finally these slices have to be contrasted and embedded in methyl cellulose (a thin layer which embeds the slices and allows them to be embedded and dried without the sample shrinking).

Advantages:

- The sample is not dehydrated or embedded in resin: the proteins remain in their aqueous state.
- The immunolocalization is highly efficient; this is extremely useful for antigens that are present in small quantities.
- Very high definition of the intracellular membrane systems.
- The method is very quick and results can be obtained in a day, if necessary.

Disadvantages:

- Cryoprotection in sucrose can cause problems of a reduction in cellular volume and soluble proteins can be lost, since the fixation that is usually used is gentle.
- The level of contrast is generally low and depends on the fixation; strong fixation leads to less loss of proteins.

- The sectioning and handling of the slices can lead to relocalization of antigens and the loss of material.
- The difficulty involved in cryosectioning certain samples.
- The sample has to be kept frozen in liquid nitrogen.

Image and information:

- In general, the sample exhibits only a gentle contrast, but the membranes and cellular compartments can be very clearly observed.
- It is a specifically aimed at molecular localization techniques and is very useful for these.
- The technique can be used to work on semithin sections with gold and silver intensification or on ultrathin sections with colloidal gold.
- The sectioned side of the block can be observed by cryo-SEM.

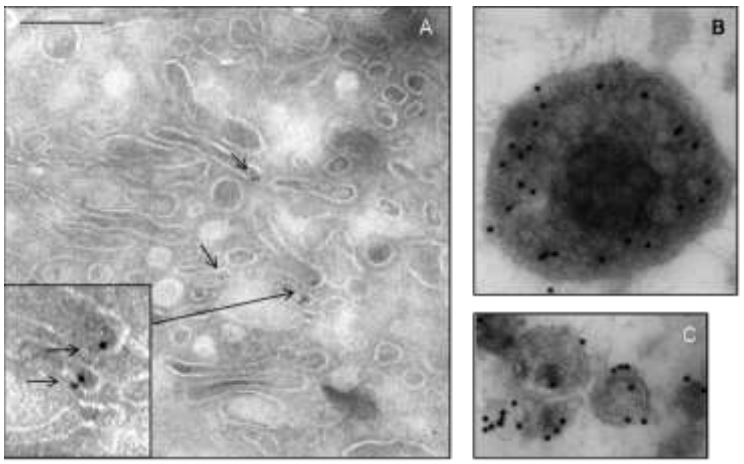

Figure 4. (A) Caveolin (→) localization in CHO cells. Bar 0.1 µm. (B and C) Multivesicular bodies isolated from rat liver and labelled with anti- annexin A-6 (Courtesy of C.Enrich – UB).

2.4. Chemical fixation – cryofixation - (hybrid method) – embedding (see Fig. 1, technique 4).
There is evidence that the chemical fixation itself produces fewer alterations or artefacts than the later stages after fixation, such as osmium tetroxide postfixation and the process of dehydration. The hybrid method consists of chemical fixation of the sample and then cryoprotection (usually in sucrose) and cryofixation (by HPF, for example) or freezing in liquid nitrogen (if the sample is large in size). The sample then undergoes the process of freeze substitution (FS), which consists of eliminating the water from the sample at a temperature around -90ºC through the use of organic solvents, and in this case we use methanol as the organic solvent, since it is miscible with sucrose. This freeze-substitution medium will also contain different types of chemical fixatives (glutaraldehyde, osmium tetroxide, uranyl acetate, etc.) which will depend on the sample and the type of study that we wish to carry out and will provide better contrast and ultrastructural preservation **[4,9].**

Advantages:

- If a long dissection time is required to localize the area before cryofixation, then anoxia can be avoided if they are first fixed chemically (for example, nervous system)
- We replace the dehydration process by FS which is less aggressive since it is carried out at very low temperatures (-90ºC) and it reduces the loss of components from the sample.
- It is possible to work with large samples and to obtain homogeneous fixation.
- The block can be stored for years.

Disadvantages:

- The process starts with chemical fixation that can cause structural changes in the sample.

- Commercial equipment or a homemade system is required (in the latter case there are certain difficulties in controlling the stability of the temperature and the rates of temperature increase).

Image and information:

- It preserves the ultrastructure well and produces an image similar to cryofixation.
- It is useful for ultrastructural studies, detection of sugar residues, cytochemical techniques, enzymatic digestion, correlative techniques (optical–electronic), electron tomography by TEM, and electron tomography by SEM.

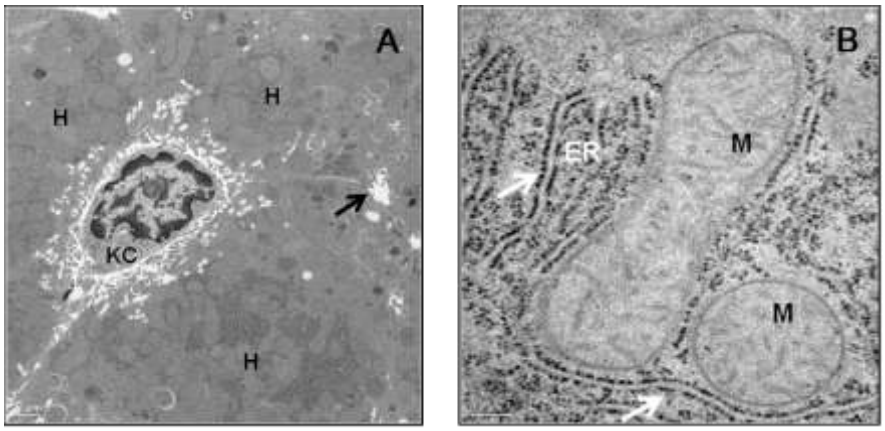

Figure 5. Chemical fixation – cryofixation - Hybrid method, (A) Liver general view. Hepatocytes (H), bile canaliculus (→), Kupffer cell (KC) in a sinusoid. Bar 1 µm. (B) Liver cytoplasm detail. Mitochondria (M) endoplasmic reticulum (ER) and ribosome (→). Bar 0.2 µm.

2.5. Chemical fixation– cryofixation (hybrid method) – cryoembedding (see Fig. 1, technique 5) [4,9].

The hybrid method can also be used to carry out immunolocalization, in which case the aldehyde-type chemical fixation will have to be gentle in order to preserve the antigenicity of the sample. The sample is then cryoprotected in sucrose and afterwards we perform FS at -90ºC using methanol as the organic solvent. Different types of chemical fixatives, or a mixture of different proportions of several fixatives, can also be added to the FS medium. Once FS has been carried out, the temperature is raised in order to embed the sample in acrylic resin. How the temperature is raised will depend on the type of resin in which we wish to embed the sample; so, for example, we raise it to -35ºC for Lowicryl K4M or to -50ºC for Lowicryl K11M. Finally we polymerize it with ultraviolet light at the chosen temperature.

Advantages:

- FS allows a better preservation of cellular structures.
- This method allows us to embed the sample in different types of acrylic resin at different temperatures.

Disadvantages:

- Commercial equipment or a homemade system is required (see the explanation of the previous technique).
- The difficulty involved in visualizing and orienting the sample.
- The difficulty involved in sectioning, depending on the type of acrylic resin used.

Image and information:

- The contrast is gentle, which means that labelling with gold can easily stand out over the structure that we are labelling.

- It is a good technique for immunolocalization and "in situ" hybridization. It can be performed both by optical microscopy (semithin section) with colloidal gold labelling and silver intensification or by electron microscopy (ultrathin section) with colloidal gold labelling, or by correlative techniques.

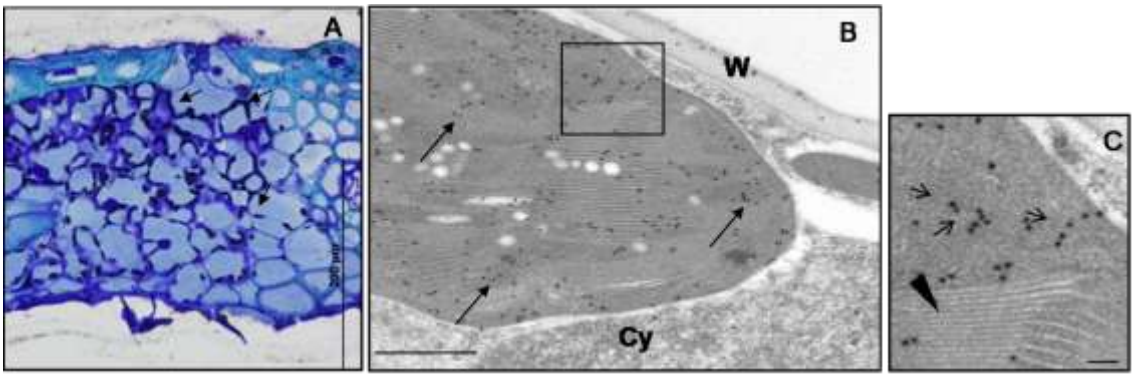

Figure 6. Glutamine synthetase immunolocalization in wheat flag leaf mesophyll spongy parenchyma cell. (A) Light microscopy image – gold silver enhancement (→). Bar 200 µm. (B) Electron micrograph spongy cell chloroplast. Bar 0.5µm (C) Inset detail. Bar 50 nm. Arrows indicate immunogold label, Cytosol (Cy), cell wall (W) and thylakoid (arrowhead). (Courtesy of M. Lopes and JLL. Araus – UB).

BT.2

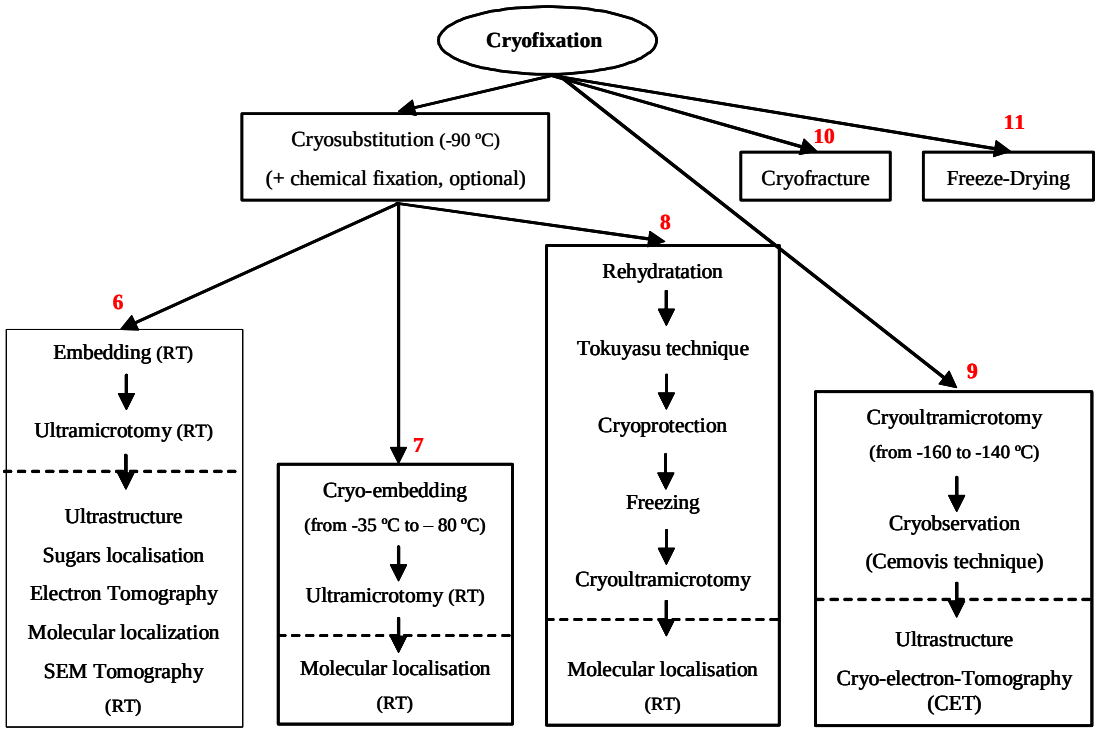

Figure 7. Cryofixation. The most important processing routes for a biological sample, based on cryofixation.

2.6. Cryofixation–FS–embedding (see Fig. 2, technique 6). [14,15,16,17, 18].
A sample that has undergone cryofixation by HPF can be processed by different routes (see Fig. 2). One route is to carry out FS using different organic solvents (acetone, alcohol, methanol, etc.) in order to replace the aqueous content of the sample by an organic solvent that allows us to embed the sample afterwards. We can add different types of chemical fixatives (glutaraldehyde, osmium tetroxide, uranyl acetate, etc.) to the FS medium in different proportions (depending on the sample

and the type of study we wish to perform) in order to preserve the structures better and to intensify the contrast. During the heating process the chemical fixatives begin to act: uranyl acetate as soon as the negative charges of the nucleic acids and phosphate groups become accessible; osmium tetroxide at -70ºC and glutaraldehyde between -40ºC and -30ºC. Since FS is usually carried out at around -90ºC, afterwards the temperature of the sample is gradually increased to room temperature and then the sample is embedded in epoxy resin, followed by sectioning and observation of the sample.

Advantages:

- It is the best way to preserve the cell architecture.
- The processing time of cryoimmobilized samples is no greater than it is for chemical methods.
- The quality of the fixation depends on the size of the specimen and on its composition, e.g., whether the sample naturally contains antifreezing agents or whether it has a low water content.

Disadvantages:

- Although there are routine protocols, on many occasions it is necessary to experimentally work out the necessary conditions for each sample in order to avoid the formation of crystals (the type of cryoprotectant, type of sample holder, etc.).
- The sample must be of the order of 2 mm in diameter and 200 μm thick.

Image and information:

- Very good ultrastructural preservation, the images give a feeling of turgidity, the microtubules are preserved, but it does not have the membrane definition that we achieve with chemical fixation.
- This processing route allows us to perform optical studies, ultrastructural studies, detection and localization of sugar residues using lectins and colloidal gold, cytochemical techniques, enzymatic digestions, electron tomography, elemental analysis by energy-filtered transmission electron microscopy (EFTEM) or by secondary ion mass spectrometry (SIMS).

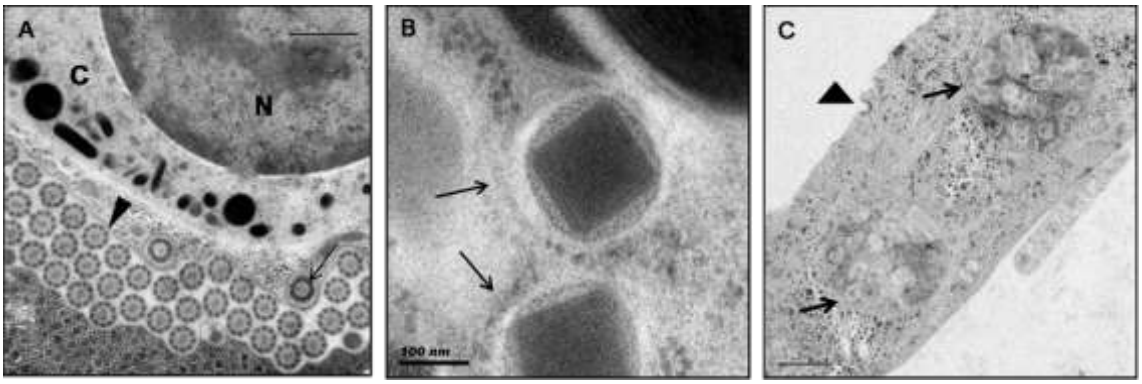

Figure 8. Technique 6. Cryofixation – FS- embedding (A) Embryonic structure (miracidium) from *Mediogonimus jourdanei* (Trematode), centriole (→) , ciliums (►), nucleus (N) and cytoplasm (C) (Bar 0.5μm). (Courtesy of J. Miquel – UB). (B) Trichocist (→) of a dinoflagellate, an organelle that releases long filamentous proteins (Courtesy of E. Garces, ICM-CSIC). (C) Caco-2 cells directly cryofixed without cryoprotection, coated-pit (arrowhead) and autophagosomes (→).

2.7. Cryofixation–FS–cryoembedding (see schme 2, technique 7) [14,15,16,17,20].

Starting from cryofixation we can also perform "in situ" hybridization and immunolocalization techniques. The process is similar to that above described, although generally acetone is used as the

organic solvent and we always have to be careful with the type of chemical fixatives used and in what proportions (we have the option of not using any chemical fixative) as the antigenicity of the sample has to be preserved. After FS and similarly as in Technique 5 above, we can embed the sample in different types of acrylic resin at different temperatures and finally polymerize it with ultraviolet light**.**

Advantages:

- FS together with cryofixation preserves the cellular structures very well while, at the same time, maintaining the antigenicity of the sample.
- The method allows us to embed the sample in different types of acrylic resins and at different temperatures.
- The block can be stored for years

Disadvantages:

- The same as for the previous process of cryofixation-FS-cryoembedding
- Visualization of the sample during the process, making the blocks and the orientation of the sample all involve a certain degree of difficulty

Image and information:

- Good preservation for molecular localization (immunolocalization, "in situ" hybridization, etc.)
- This processing route allows us to carry out optical studies with colloidal gold and silver enhancement in semithin sections, and immunolocalization using colloidal gold on ultrathin sections.

2.8. Cryofixation–FS–rehydration–Tokuyasu method. (see Fig. 2, technique 8) [19].
A sample that has been cryofixed by HPF and freeze substituted can be rehydrated, and then we can apply the Tokuyasu method to cryosection it.

Advantages:

- This technique combines the ultrastructural preservation of cryofixation with a very efficient immunolocalization system.
- Chemical fixation during FS is useful for antigens that are sensitive to fixation. It may be used for samples for which chemical fixation is difficult, such as yeasts, bacteria, plants, insects, etc

Disadvantages:

- The size of the sample is small given that we start with cryofixation.
- Artefacts may be caused during rehydration

Image and information:

- The image is very similar to that obtained by the Tokuyasu method, a gentle contrast, but the membranes and the cellular compartments can be seen very well.
- It is a specific technique which is useful for molecular localization techniques of samples that may be difficult to fix chemically.

However, starting from a cryofixed sample, we can use other techniques (all of them require special equipment) such as:

- **Freeze-fracturing**, which consists of freezing the sample and fracturing it in such a way that we obtain a double-sided fracture, a replica of the sides is made using platinum-carbon at different angles and they are observed in the microscope. There is also the "freeze-

etching" variation in which the fracture face is gently freeze dried. This is a technique for studying membranes and for localization and distribution of membrane proteins [3].

- **Freeze-Drying**, this technique consists of cryofixation of the sample and extraction of the water from the sample in order to sublimate it at low temperatures in a vacuum; once it is dry, it can be embedded in any type of resin and sectioned [12].
- **CEMOVIS**: it consists in freezing the sample at high pressure, cryosectioning it and cryoobserving it directly on the electron microscope; this technique allows us to see the tissue in its hydrated state, without the necessity to remove the water from the sample and therefore in its most natural state [13].

3. Examples of applications

All these techniques can be applied to:

- Animal tissues (ex. liver, spleen, bone...) (see Fig. 2A/B, 4A, 5A/B, 5A)
- Cell culture (in liquid medium, on substrate...) (see Fig. 8C)
- Bacteria, cellular organelles, biofilms, … (see Fig. 2C)
- Plant tissues (ex. seeds, pollen, leaves...) (see Fig.6)

4. Conclusions

Electron microscopy is essential to understanding how cells and tissues work; it allows us to visualize structures with high resolution and to relate their functions of the components as well as being able to detect and localize molecules "in situ". It is very important to consider the different techniques, be able to work with several of them, and assess and compare them in order to arrive at a good final conclusion.

Acknowledgments

The authors would like to thank all the users of the Electron Microscopy Unit.

References

[1] Mascorro J.A. and Bozzola J.J. Processing biological tissues for ultrastructural study. In: Electron Microscopy. Methods and Protocols. Methods in Molecular Biology. Ed. John Kuo. Human Press. (2007)

[2] Hayat, M.A. Principles and Techniques of Electron Microscopy, Biological Applications, fourth ed. Cambridge University Press, Cambridge (2000).

[3] Cryo-preparation Methods for Electron Microscopy. Methods in visualization series. Ed. By A. Cavalier, Danièle Spehner and Bruno M. Humbel. CRC Press (2009).

[4] W. Möbius. Cryopreparation of Biological Specimens for Immunoelectron Microscopy. Annals of Anatomy 191 , 231-247, 2009.

[5] Vanhecke D. and Studer D. High-Pressure freezing Leica EMPACT. Cryo-preparation Methods for Electron Microscopy. Methods in visualization series. Ed. By A. Cavalier, Danièle Spehner and Bruno M. Humbel. CRC Press (2009).

[6] Hobot, J.A. Lowicryls and low temperature embedding for colloidal gold methods, in Colloidal Gold:Principles, Methods and Applications, Hayat, M.A., ed., Academic Press, San Diego, CA, USA, 75, 1989.

[7] Carlemalm, E., Garavito, R.M., and Villiger, W. Resin developmentt for electron microscopy and an analysis of embedding at low temperature. J. Microsc., 126, 123, 1982.

[8] Tokuyasu, K.T. A technique for ultracryotomy of cell suspensions and tissues. J. Cell Biol., 57, 551, 1973.

[9] Liou, W., Geuze, H.J., ans Slot. J.W. Improving structural integrity of cryosections for immunogold labelling. Histochem. Cell Biol., 106, 41, 1996.

[10] Sosinsky G.E., Crum, J., Jones, Y.Z. Jones, Lanman J., Smarr B., Terada M., Martone M.E., Deerinck T.J., Johnson J.E. and Ellisman M.H. The combination of chemical fixation procedures with high pressure freezing and freeze substitution preserves highly labile tissue ultrastructure for electron tomography applications. J. of Structural Biology, 161, 359-371, 2008.

[11] Ripper, D., Schwarz, H., and Stierhof, Y. –D. Cryo-section immunolabelling of difficult to preserve specimens: advantges of cryofixation, freeze-substitution and rehydration, Biol. Cell, 100, 109, 2008.

[12] Edelmann, L. Freeze-dried and resin-embedded biological material is well suited for ultrastructure research. J. Microsc., 207, 5, 2002.

[13] Al-Amoudi, A. et al. Cryo-electron microscopy of vitreous sections of native biological cells and tissues. J. Struct. Biol., 148,131,2004 .

[14] Dubochet, J. et al. Cryo-electron microscopy of vitrified specimens, in Cryotechniques in Biological Electron Microscopy. Steinbrecht, R.A. and Zierold, K., eds., Springer, Berlin, Germany, 1987, 114. 1987.

[15] Koster A.J. and Klumperman J. Electron microscopy in cell biology: integrating structure and function. Nat Rev Mol Cell Biol Suppl: SS6-S10, 2003.

[16] Giddings T.H. Freeze-substitution protocols for improved visualization of membranes in high-pressure frozen samples. J. of Microscopy, vol. 212, 53-61, 2003.

[17] McDonald K.L. A review of high-pressure freezing preparation techniques for correlative light and electron miccroscopy of the same cells and tissues. J. of Microscopy, vol. 235, 273-281, 2009.

[18] Douglas K. R. And Tyla S.F. Transmission electron microscopy of cartilage and bone. Methods in Cell Biology 96: 443-73, 2010.

[19] Ripper D., Schawrz H. and Stierhof Y-D. Cryo-section immunolabelling of difficult to preserve specimens: advantage of cryofix, freeze-substitution and rehydratation. Biology of the Cell, 100, pp. 109-123, 2008.

[20] Sobol M. Comparasion methods of high-pressure freezing and automated freeze-substitution of suspension cells combined with LR-White embedding. Histochemistry and Cell Bio, vol 134, 6, 631-641, 2010.

Biomedical and Biological Applications of Scanning Electron Microscopy

Núria Cortadellas, Eva Fernández, and Almudena Garcia

Unitat de Microscòpia Electrònica (Casanova), CCiT-UB, Universitat de Barcelona. Facultat de Medicina. Casanova, 143, 6ª pl. Ala Nord. 08036 Barcelona.

email: *nuriac@ccit.ub.edu*

Abstract. This article summarizes the basic principles of scanning electron microscopy and the capabilities of the technique with different examples of applications in biomedical and biological research.

1. Introduction

The scanning electron microscope (SEM) (see Fig. 1) uses electrons to form an image. A beam of electrons is produced at the top of the microscope (electron gun) and follows a vertical path through the column of the microscope, it makes its way through electromagnetic lenses which focus and direct the beam down towards the sample. The beam passes through pairs of scanning coils or pairs of deflector plates in the electron column, typically in the final lens, which deflect the beam in the x and y axes so that it scans over a rectangular area of the sample surface (see Fig. 2) [1,9].

Figure 1. Zeiss DSM 940A SEM electron microscope at the CCiT-UB (Medical school)

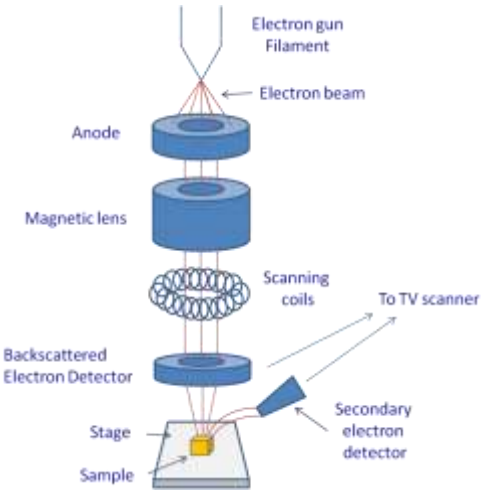

Figure. 2. Diagram of a Scanning electron microscope

The focused beam of high-energy electrons generates a variety of signals at the surface of solid specimens. The signals that derive from electron-sample interactions reveal information about the sample including external morphology or surface topography, chemical composition, and others properties such as electrical conductivity (see Fig. 3).

Different detectors collect the signals, and convert them into another signals that are sent to a viewing screen similar to the one in an ordinary television, producing an image. This image is then digitally captured and displayed in a computer monitor. Magnification in a SEM can be controlled over a range of about 10 to 500,000 times or more.

The spatial resolution of the SEM depends on the size of the electron spot, which in turn depends on both the wavelength of the electrons and the electron-optical system which produces the scanning beam. Depending on the instrument, the resolution ranges between 1 and 20 nm.

The signals result from interactions of the electron beam with the atoms at or near the surface of the sample. The type of signals produced by a SEM include secondary electrons, back-scattered electrons (BSE), characteristic X–rays, light (cathodoluminiscence), specimen current and transmitted electrons (see Fig. 3) [5,9].

Secondary electrons. The most common imaging mode collects low-energy (<50 eV) secondary electrons that are ejected from the k-orbitals of the specimen atoms by inelastic scattering interactions with the beam electrons. Due to their low energy, these electrons originate within a few nanometers from the sample surface. Secondary electrons can produce very high-resolution images of a sample surface, revealing details about less than 1 to 5 nm in size. Due to the very narrow electron beam, SEM micrographs have a large depth of field yielding a characteristic three-dimensional appearance useful for understanding the surface structure of a sample.

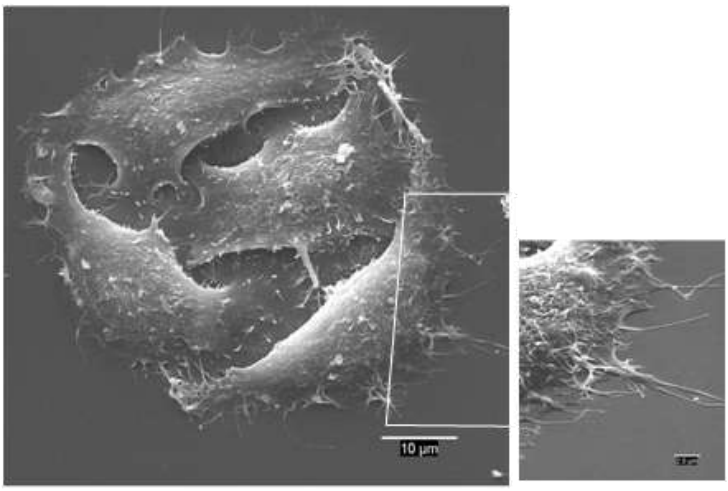

Figure 2. Hela Cells on glass coverslips substrat. Detail: tilt image (35º).
(Courtesy of Carles Enrich, University of Barcelona).

Backscattered electrons (BSE). Back-scattered electrons (BSE) are beam electrons that are reflected from the sample by elastic scattering. As a result, the intensity of the BSE signal is strongly related to the mean atomic number (Z) of the specimen, and BSE images can provide information about the distribution of different elements in the sample. Since heavy elements (high atomic number) backscatter electrons more strongly than light elements (low atomic number), and thus appear brighter in the image, BSE are used to detect contrast between areas with different chemical compositions. For the same reason, BSE imaging can image colloidal gold immuno-labels of 5 or 10 nm in diameter which would otherwise be difficult or impossible to detect in secondary electron images in biological specimens.

Characteristic X-rays. Characteristic X-rays are emitted when the electron beam removes an inner shell electron from the sample, causing a higher energy electron to fill the shell and release energy. These characteristic X-rays are used to identify the composition and measure the abundance of elements in the sample.

Cathodoluminescence. The highly focused beam of electrons impinges on a sample and induces it to emit light from a localized area by scanning the microscope's beam in an X-Y pattern and measuring the light emitted with the beam at each point, a map of the optical activity of the specimen can be obtained.

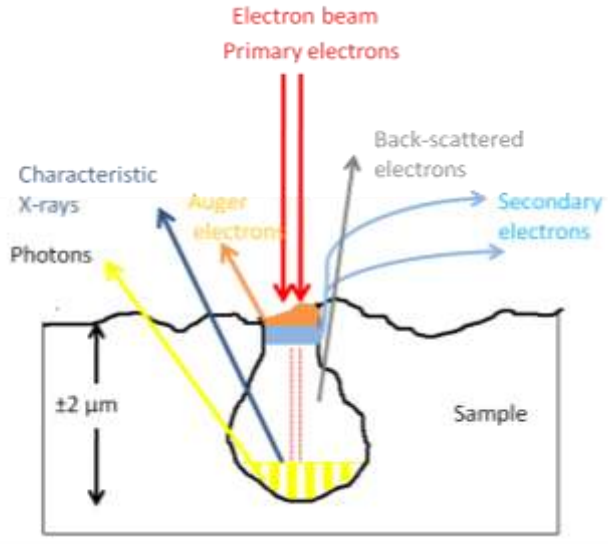

Figure 3. Electron beam interaction and signals

2. Methodology

For SEM, a specimen is normally required to be completely dry, since the specimen chamber is at high vacuum. For conventional imaging in the SEM, specimens must be electrically conductive at least at the surface, and electrically grounded to prevent the accumulation of electrostatic charge at the surface. All samples must also be of an appropriate size to fit in the specimen chamber and are generally mounted rigidly on a specimen holder called a specimen stub [1,2,6,8].

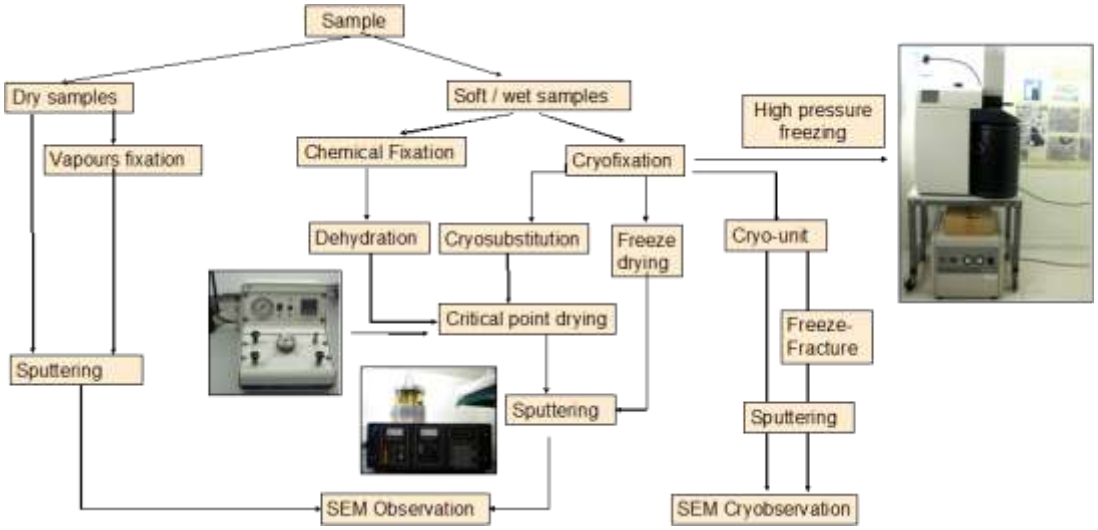

Figure 4. Schematic diagram of the sample preparation methods for the observation with the scanning electron microscope

Hard, dry materials such as bone, wood, dried Insects, seeds or teeth can be examined with little further treatment or directly. Living cells and tissues, soft-bodied organisms usually require fixation to preserve and stabilize their structure (see Fig. 4) [1,4,5,6,8]. Fixation is usually performed by incubation in a solution of a buffered chemical fixative or by cryofixation [1,2]. The fixed cell or tissue is then dehydrated or cryosubstituted. Because air-drying causes collapse and shrinkage, this is commonly achieved by critical point drying. Critical point drying involves replacement of organic solvents such as ethanol or acetone, and replacement of these solvents in turn with a transitional fluid such as liquid carbon dioxide at high pressure. The carbon dioxide is finally removed while in a supercritical state, so that no gas-liquid interface is present within the sample during drying. The dry specimen is usually mounted on a specimen stub using colloidal silver and sputter coated with gold, carbon or gold/palladium alloy before examination in the microscope [1,2,4,6].

If the SEM is equipped with a cold stage for cryo-microscopy, cryo-fixation may be used and low-temperature scanning electron microscopy performed on the cryogenically fixed specimens. Cryo-fixed specimens may be cryo-fractured under vacuum in a special apparatus to reveal internal structure, sputter coated and transferred onto the SEM cryo-stage while still frozen [9].

3. Application Examples

3.1. Parasite study by scanning electron microscopy

SEM allows us to visualize external morphological characteristics and is a very useful tool for obtaining data on systematic and taxonomic studies of parasites in general. The parasitological studies of these hosts allow us to learn the composition of their communities and thus the parasite biodiversity, providing as well interesting information as to the complex life cycles of these parasites (see Figs. 5, 6 and 7).

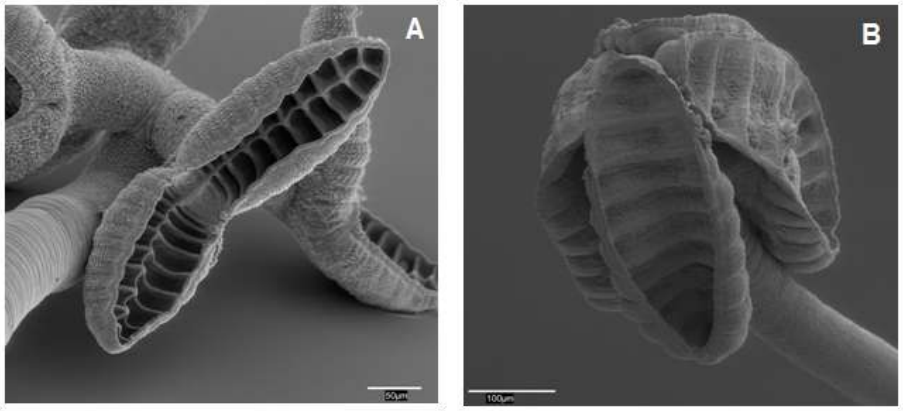

Figure 5. A. *Rhinebothrium* sp., cestode of the order Rhinebothriidea: detail of one of the bothridia in which the morphology of the loculi can be seen. B. *Scalithrium minimum*, cestode of the order Tetraphyllidea: general view of the scolex with its 4 bothridia. (Courtesy of Jordi Miquel, University of Barcelona).

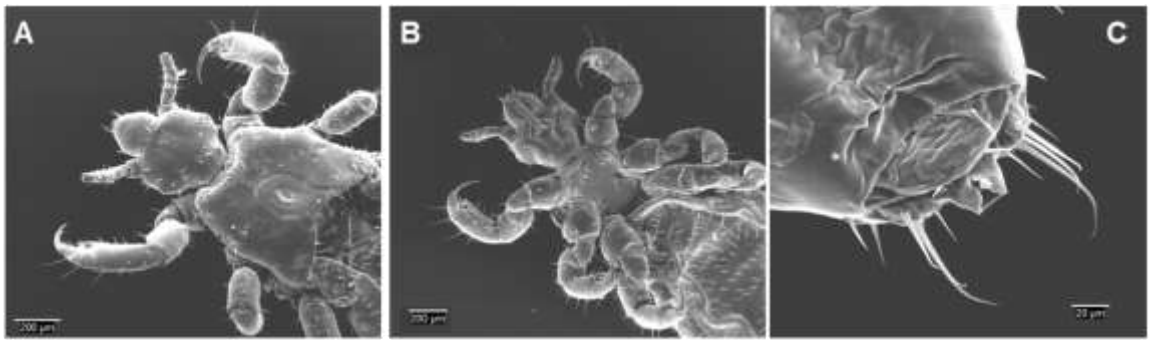

Figure 6: A. *Pediculus humanus capitis* head and thorax dorsal view. B. Ventral view. C: Female's abdomen detail.

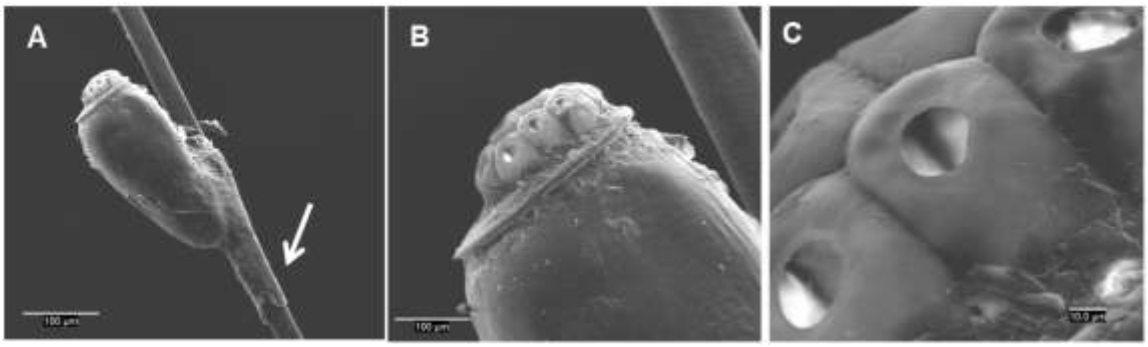

Figure7: A. Nit general view, hair (→). B. Operculum detail with aerial cameras. C. Aerial cameras detail**.**

3.2. Alveolar-capillary barrier

Acute lung injury (ALI) and acute respiratory distress syndrome (ARDS) are clinical manifestations of acute and constant respiratory failure caused by lung inflammation and the disruption of the alveolar-capillary barrier with a subsequent infiltration of protein-rich oedema fluid and inflammatory cells into the alveolar space. Some inflammatory and coagulation mediators overexpressed in these diseases may modulate alveolar-capillary barrier integrity (see Fig. 8).

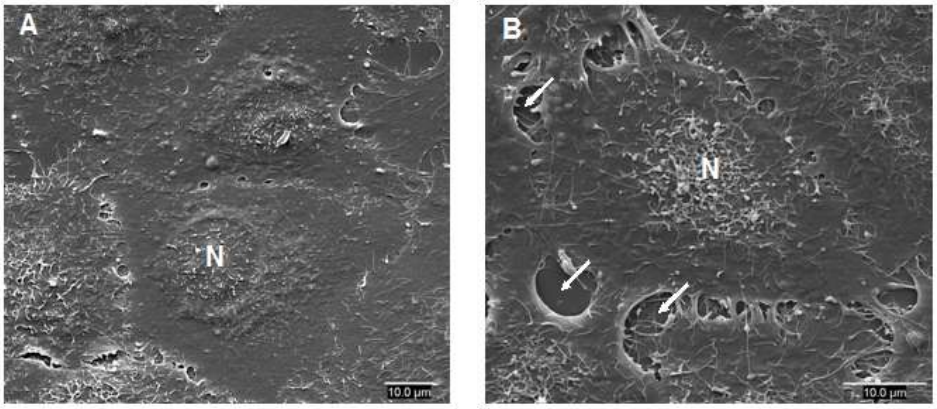

Figure 8. A. Alveolar epithelial monolayer. Nucleus (N). B. Alveolar epithelial cells challenge by Thrombin, a pro-coagulant serine protease that forms intercellular gaps (→), Nucleus (N). (Courtesy of F. Puig, G. Fuster, J. Tijero, L. Blanch, and A. Artigas, Sabadell Hospital, and R. Nieto, D. Navajas and R. Farré, University of Barcelona).

3.3. Pro-inflammatory stimuli activate dendritic cells, important players in the battle against diseases

BT.3

Dendritic cells (DCs) are the sentinels of the body, playing a key role in the initiation and regulation of the immune and inflammatory responses. Under a pro-inflammatory stimulus or pathogen, immature DCs (iDCs) experience a profound molecular and morphological transformation toward a "mature" state (mDCs). Scanning electron microscopy (SEM) is a powerful tool to visualize such morphological variations occurring on the DC cell surface upon activation, such as extended dendrite formation and clustering, allowing efficient antigen presentation.

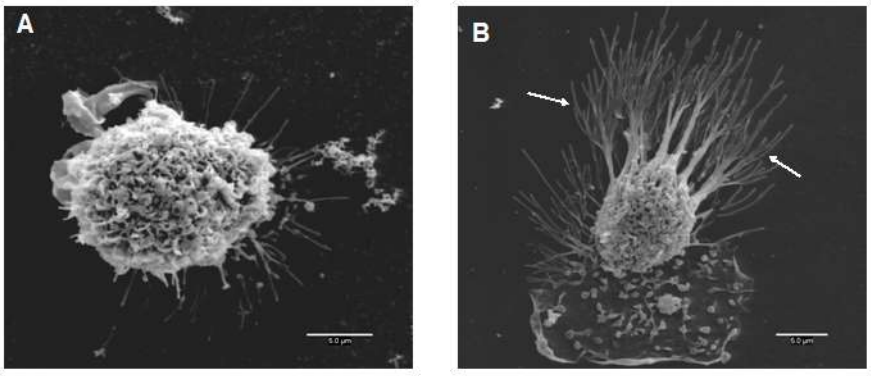

Figure 9. The images shown are SEM micrographs of monocyte-derived human dendritic cells (DCs) either untreated (iDCs) (A) or treated for 48 h with 5 µg/ml of bacterial lipopolysacharide (LPS) (pro-inflammatory stimulus) (mDCs) (B). Note the increased and polarized dendrites (→) in mDCs stimulated with LPS. (Courtesy of Rut Olivar and Josep M. Aran. IDIBELL).

3.4. Intestinal epithelium

The main objective of the project is to study the effect of different natural substances on the control of the prevalence of *Salmonella* in chicken intestine.

3.5. Biofilm formation in endotracheal tubes of mechanically ventilated pigs with pneumonia

Biofilms are bacterial communities that adhere to a surface and grow in a self-produced polymeric matrix difficult to disrupt. Bacteria in biofilm increase their ability to survive, usually altering their resistance pattern.

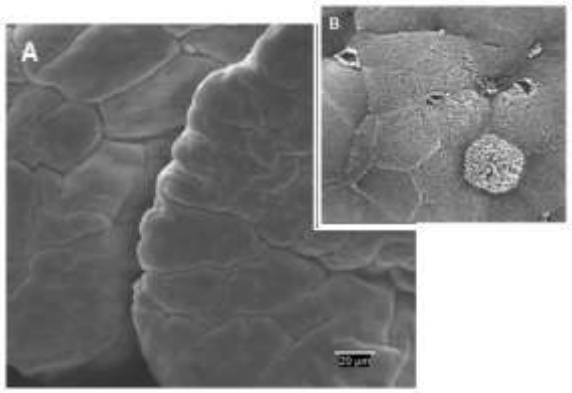

Fig. 10. Intestinal epithelium of a 21-day old chicken: A. villi, and B. surface of the enterocytes and goblet cells (mucus secreting cells). (Courtesy of M.T. Brufau, , A. Guerrero-Zamora, R. Martín-Venegas. and R. Ferrer, R-, University of Barcelona, and B. Vila, and J. Brufau, IRTA).

In tracheally intubated patients, biofilm, which is universally present in endotracheal tubes, comprises bacteria, bacterial polysaccharides, host cellular detritus and respiratory secretions. With the ventilatory flow, biofilm particles can be dislodged into the lungs and develop into responsible for persistent lung infection

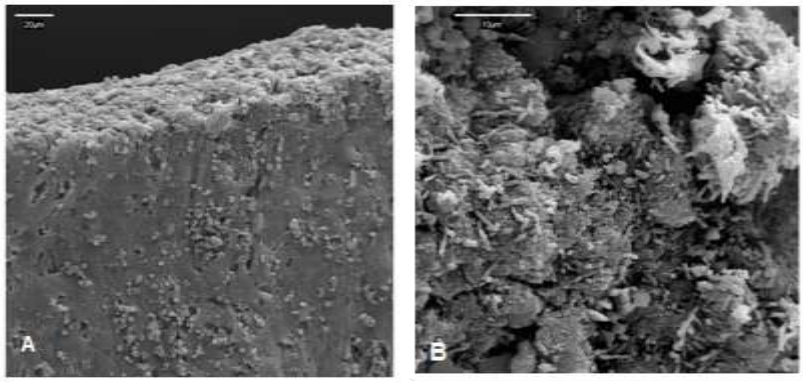

Figure 11. SEM micrographs showing the morphology (A) and bacteria-like structures (B) of a biofilm from an animal model (Courtesy of Laia Fernández-Barat, Miquel Ferrer, Gianluigi Li Bassi, and Antoni Torres. Hospital Clínic-IDIBAPS and University of Barcelona).

3.6. Human Embryo Development by Scanning Electron Microscopy.

Figure 12 shows a SEM of a of a lower limb of a human embryo after 10 weeks' development. The presence of a tactile metatarsal prominence can be seen (→) on the distal tips of the fingers. In addition, one can see how, at this stage of development, the fingers are already independent of each other.

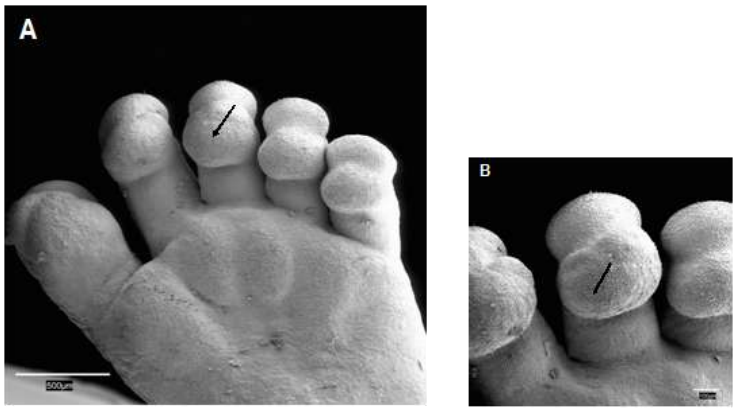

Figure 12. A. SEM micrograph of a lower limb of a human embryo after 10 weeks' development. B. Detail. Plantar view. (Courtesy of Rosa Artells, Alfons Navarro, Tània Díaz, Ruth Tejero, Victor Ciria, Dolors Fuster, Carmen Muñoz, and Mariano Monzó, University of Barcelona)

3.7. Plants diseases

Sclerotinia sclerotiorum is a plant pathogenic fungus that cause a disease called cotton rot or watery soft rot in several crops, like lettuce. This pathogen has the ability to produce a black resting structure known as sclerotia.

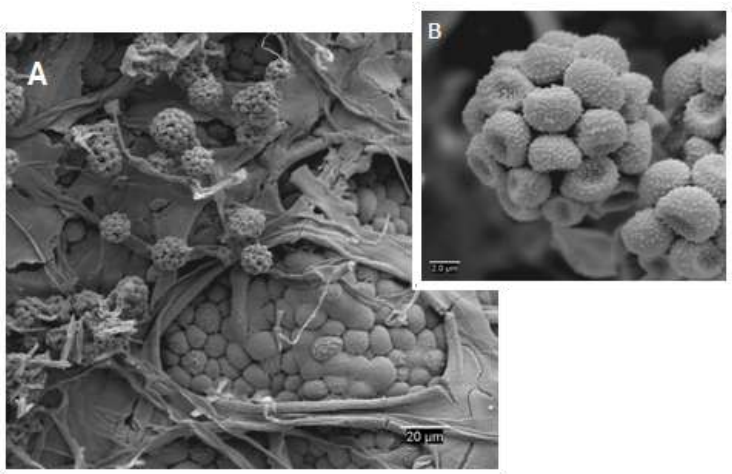

BT.3

Figure 13. SEM micrographs of sclerotia of *Sclerotinia sclerotiorum* parasitized by another fungus (*Trichoderma asperellum*, strain T34) inhibiting the pathogen growth and the development of the disease (A). Detail of the conidia of the beneficious fungi (Trichoderma asperellum, strain T34) (B). (Courtesy of Maribel Trillas, University of Barcelona).

3.8. Leukocyte-Endothelium Interactions during the Inflammatory Response

Single layer of human endothelium treated with proinflammatory stimuli in which human lymphocytes and monocytes from peripheral blood have been perfused with a physiological flow (1,8 din/cm^2). Several non-polarized leucocytes have established contact with the endothelium and have been captured during the process of rolling (see Fig. 14).

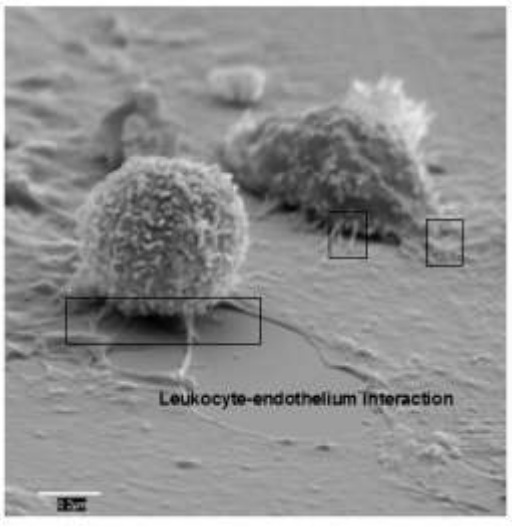

Figure 14. Interaction of the lymphocytes with the apical membrane of endothelial cells subject to flow. (Courtesy of Olga Barreiro, Universidad Autónoma de Madrid and Francisco Sánchez-Madrid, Centro Nacional de Investigaciones Cardiovasculares)

3.9. Erythrocytes morphology with amino acid-based surfactants

The erythrocytes present a characteristic morphology (discocytes, see Fig. 15 A), which enables their function of transporting oxygen. Any alteration in this morphology will cause a reduction in their capacity to transport oxygen. The surfactants interact with the erythrocytes membrane causing

changes in the structure of membrane proteins and lipids, which can induce some alterations in the external surface of the cells (see Fig. 15B).

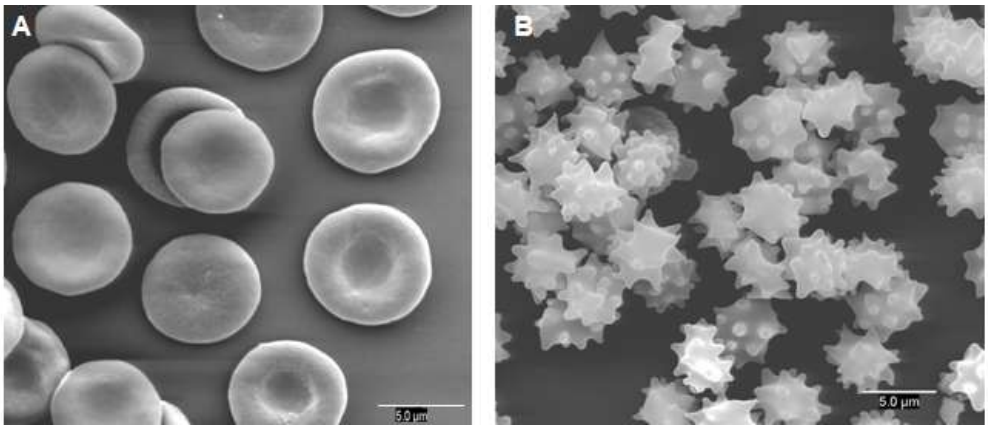

Figure 15. SEM micrograph showing the typical form of the erythrocytes (discocytes) (A), and alterations induced by the presence of surfactants at a physiological pH (echinocytes) (B) (Courtesy of Daniele Rubert, Montse Mitjans and Pilar Vinardell, University of Barcelona).

3.10. Characterization of an In Vitro Model of Mucosal and Nasal Polyp Epithelial Cells Cultured in the ALI System (Air-Liquid Interface)

In the dedifferentiation process the epithelial cells arising from the mucosa and nasal polyp undergo on being cultured in the ALI system of culture (Air-Liquid Interface). In this system, cell culture is developed on a porous support called insert or transwell that allows the cells to be exposed to air at their apical zone whilst remaining in contact with the culture medium at their base. On day 0, one can observe a single layer of dedifferentiated cells, without ciliated cells. However, ciliated cells can be seen after 14 days of culture (see Fig. 16-A) and after 28 days these cells can be seen in greater numbers and with a greater development of cilia (see Fig. 16-B). The different degrees of ciliogenesis observed at different times, indicates that the epithelial cells are becoming dedifferentiated during culture.

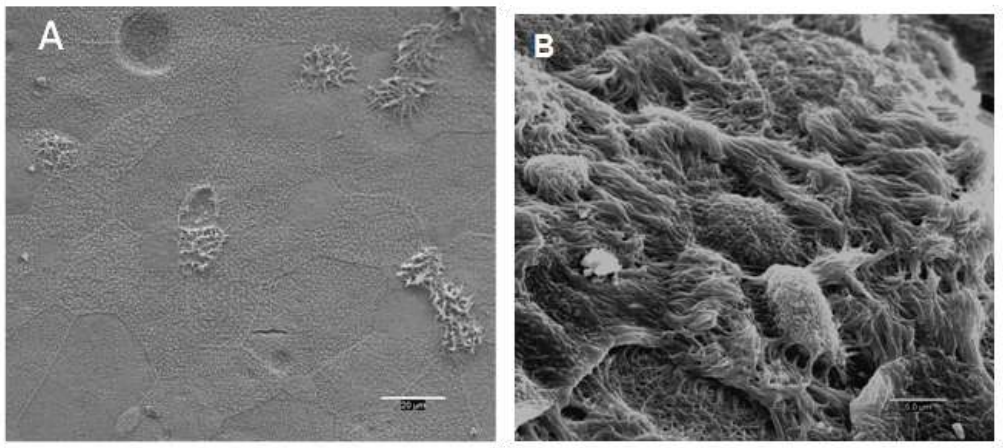

Figure 16. These images contribute, in part, to the characterization that has been carried out of the in vitro model of epithelial cells of the mucosa and nasal polyp cultured in the ALI system. SEM micrographs corresponding to days 14 (A) and 28 (B) of a cell culture under ALI conditions. (Courtesy of Francisco de Borja Callejas, Asunción Martínez-Antón, César Picado, and Joaquin Mulloll, IDIBAPS, and Eva Donet, Instituto Carlos III).

Acknowledgments

The authors would like to thank all the users of the Electron Microscopy Unit.

References

[1] Bozzola, J..J. and Russell. L.D. Electron Microsscopy Principles and Techniques for Biologists. Jones and Bartlet Publishers. Sudbury. M.A., 1999.
[2] Kuo J. Electron Microscopy. Methods and Protocols. Humana Press , 2007.
[3] Smith L..E. et al. A comparision of imaging methodologies for 3D tissue engineering. Mic. Research and Technique, vol. 37, 1123-1133, 2010.
[4] Pollack A. and Tadmor T. Surface topography of hairy cell leukemia cells compared to other leukemias as seen by scanning electron microscopy. Leukemia and lymphoma, 52 (S2): 14-17, 2011.
[5] Echlin P. Hanndbook of sample preparation for scanning electron microscopy and X-ray microanalysis. Ed. Springer., 2009
[6] Passey S et al. Scanning electron microscopy of cell surface morphology. Current protocols in Cell Biology, unit 4.17, 2007.
[7] Goldstein , J.I. et al. Scanning electron microscopy and X-ray microanalysis : A text for biologists, materials scientists, and geologists. New York: Plenum Publishing Cor., 673 pp. 1981.
[8] Murphy, J.A., and G.M Roomans, eds, Preparation of biological scpecimens for scanning electron microscopy. Scanning Electron Microscopy, Inc., AMF O'Hare, II, 344 pp. 1984.
[9] http://www.purdue.edu

Advanced Light Microscopy Techniques

Manel Bosch[1], Benjamín Torrejón-Escribano[2], Anna Bosch[3], and Maria Calvo[3]

[1] Unitat de Microscòpia Confocal, CCiTUB, Universitat de Barcelona. Fac. Biologia, 645. 08028 Barcelona, Spain.

[2] Unitat de Biologia (Bellvitge), CCiTUB, Universitat de Barcelona. Feixa Llarga s/n. 08097 L'Hospitalet de Llobregat, Spain.

[3] Unitat de Microscòpia Confocal, CCiTUB, Universitat de Barcelona. Fac. Medicina, Casanova, 143. 08036 Barcelona, Spain.

email: *mcalvo@ccit.ub.edu*

Abstract. This article summarizes the basic principles of light microscopy, with examples of applications in biomedicine that illustrate the capabilities of the technique.

1. Introduction

An optical microscope uses lenses and properties of light to magnify and resolve laterally small objects in the sample, with a maximum precision of 200 nm, under conventional conditions.

Due to the useful properties of light microscopy applied to biological samples, it has become a fundamental technique in biomedicine. Biological samples that can be studied are fixed or live, cells, tissues, organs, embrios and small animals. Studies of materials surface or solutions can also be performed.

One of the most important advantages of light microscopy is that the tridimensional structure and integrity of the sample can be very well preserved after its processing for observation. In addition, the almost non-invasive properties of light allow studying living cells, tissues and whole organisms.

By using optical microscopes with different light contrast techniques and a wide range of labellings, the different features of the samples such as morphology, structure and components can be highlighted. From among all light-contrast techniques, fluorescence is probably the most widely used. This is due to its multiple properties and advantages versus other light-contrast techniques. One of the advantages of fluorescence is its specificity. Fluorescent molecules are identified and discriminated from the others by their individual light absorption and fluorescence emission spectra. A particular fluorophore can be detected by using specific excitation light and emission range. This detection can be performed with a high contrast. Fluorescent molecules glow in a dark background and their signals can be isolated easily from the surrounding. Another important advantage is that fluorophores have several physical and chemical properties (lifetime, absorption and emission spectra, intensity, etc.) which are sensitive to environmental conditions (pH, temperature, concentration, molecular interaction, etc.) or can be used to make some processes evident; thus, a wide range of fluorophores are used as specific reporters of particular situations such as environmental conditons, molecular reactions or dynamics.

Recently, the discovery of fluorescent proteins from different organisms and subsequent genetic engineering has made it possible to express, in living cells, the proteins of interest tagged with these genetically encoded fluorescent proteins [1]. Numerous variants of fluorescent proteins have been developed for protein labelling or as reporters of specific conditions. The combination of this development together with the properties of fluorescence has revolutionized the study of localization and function of proteins in its natural environment, the living cell.

As a result, there has been an important development of advanced techniques which provide novel information about how, when and where changes in molecular states, dynamic processes and reactions occur in biological samples. Recently, some techniques have increased the conventional optical resolution up to 10 times [2]. Advanced optical microscopy techniques combine and take advantage of the properties of light, design and improvement of probes, progress in image analysis tools, new imaging techniques and development and commercialization of equipment and software that provide solutions to these new applications.

Light microscopy has become prevailing in biomedical research and, furthermore, the incoming techniques point out to give new insights into cell biology and molecular mechanisms.

This chapter summarizes some light microscopy techniques with examples of applications based on our specialization and experience.

2. Contrast Techniques in Light Microscopy

2.1. Transmitted light contrast techniques

2.1.1. Brightfield microscopy

Brightfield microscopy is the simplest of all optical illumination techniques. It yields an image with the sample appearing black, surrounded by a bright background. This contrast is due to the absorption of light by dense areas of the sample. Most biological samples, however, have a low contrast and, therefore, they have to be observed using other methods. Staining the samples

increases this contrast but it is not always possible or convenient, especially in the case of living cells. There are special optical contrast-enhancing techniques based on changes in the phase of light due to differences in thickness and refractive index between the specimen (phase specimens) and the surrounding medium. These differences are converted in differences in colour or intensity of the image. Some of these contrast-enhancing techniques are: phase contrast or differential interference contrast (DIC).

2.1.2. Phase contrast

Phase contrast enhances the differences in the phase of the light between waves traversing the sample (diffracted) and waves passing through the surrounding medium (undiffracted). When both waves are combined, the resulting interference makes the phase variations observable in the image and, therefore, it is possible to distinguish the structure from the surrounding medium. It is a high-resolution technique and is ideal for fairly thin and uniform specimens, such as monolayers of cells. Some problems, however, may appear with very thick o highly refractile objects.

2.1.3. Differential interference contrast

Differential interference contrast (DIC), also known as Nomarski microscopy, generates contrast from local changes in refractive index of the specimen. The resulting images give the appearance of a three-dimensional physical relief, though not providing a topographically accurate image. DIC does not give much contrast when working with a thin object but it is the technique of choice for thick samples such as protozoa, embryos and small organisms.

2.2. Fluorescence as a contrast technique

Fluorescence microscopy has become an essential tool in biology and in the biomedical sciences, as well as in materials science due to its attributes that are not readily available in other contrast modes within traditional optical microscopy. It gives the possibility to label individual structures, molecules, or cell compartments, so that their observation under the microscope, and even the dynamics of the living cells, is possible. Moreover, it is possible to use several fluorescence probes at the same time to identify several target molecules simultaneously. Although the fluorescence microscope cannot provide spatial resolution below the diffraction limit of specific specimen features, the detection of fluorescing molecules below such limits is readily achieved. There are many fluorescent microscopes that provide different imaging solutions achieved by the variations in the different components of the microscope.

2.2.1. Fluorescence process

When specimens, living or non-living, organic or inorganic, absorb and subsequently re-radiate light, the process is described as photoluminescence. If the emission of light persists only during the absorption of the excitation light, the phenomenon is known as fluorescence. Fluorescence is the light emitted during the rapid relaxation of fluorescent molecules following excitation by light absortion.

The process consists of three phases (Fig. 1a). Briefly, in the first phase (absorption) a photon collides with a molecule that absorbs it. This process excites and promotes the atomic electrons of the molecule to a higher-energy level. In a second phase (relaxation), the excited electrons undergo a transition to the lowest excited state, losing energy as heat. Finally, in the third phase (emission), the electrons drop back to the ground state via a number of processes. One of these processes is the emission of light. As a consequence of this process, the energy of emitted light is lower than that of the absorbed light and, therefore, the wavelength of the emitted light is longer than that of the absorbed radiation. Because the emitted photon usually carries less energy and therefore has a longer wavelength than that of the excitation photon, the emitted fluorescence can be distinguished from the excitation light.

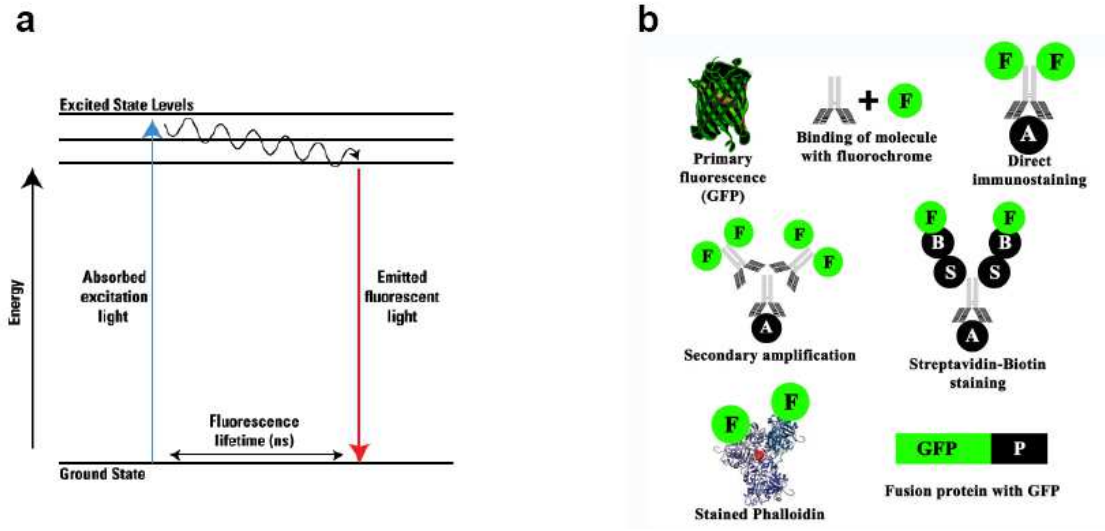

Figure 1. a) Jablonski energy diagram of fluorescence (adapted from Ref. [3]); b) Different ways of staining a target molecule with a fluorochrome. GFP means green fluorescent protein, A antigen, P protein of interest, F fluorochrome, S streptavidin and B is biotin.

BT.4

The excitation and photon emission from a fluorophore is cyclical, and until the fluorophore is irreversibly damaged (or photobleached), it can be repeatedly excited. Because of the fact that fluorophores can emit numerous photons through the cycle of excitation and emission, fluorescent molecules are used for a broad range of research applications. Both the excitation and emission wavelengths are specific characteristics of each fluorophore and they exhibit broad excitation and emission spectra. The spectra for fluorescent molecules are graphed on x,y plots that indicate the wavelengths which correspond to the maximum and minimum excitation and emission signal intensity for each fluorophore.

2.2.2. Fluorescence labelling of samples

There are two different types of fluorescence used to detect molecules of interest with light microscopy techniques. Primary fluorescence is the property of some substances of emitting fluorescence (autofluorescence). Secondary fluorescence is a fluorescence generated by staining the molecule of interest with a fluorescent molecule (fluorochrome) [1] [4].

There are different options to detect a molecule by fluorescence (see figure 1 and 3). A very common labelling method is immunostaining. It consists of detecting a molecule by an specific antibody directly labelled with fluorescence (direct immunoflurorescence) or using a first antibody against the molecule of interest and, afterwards, one or various secondary antibodies directed to the first one labelled with fluorescence (indirect immunofluorescence). Indirect immunofluorescence is commonly used as an amplification method due to the strong non-covalent interaction between streptavidin and biotin [5]. In this case, a primary antibody biotinilated and avidin complexed with the desired fluorochrome can be used.

Another detection method is the use of fluorescent (non immunological) dyes. These can be fluorescent-labelled molecules that bind specifically to the molecule of interest or locate in an specific compartment due to its physico-chemical properties.

Recently, the discovery of fluorescent proteins from different organisms and subsequent genetic engineering have made it possible to express, in living cells, the proteins of interest tagged with these genetically encoded fluorescent proteins [9] [10]. Numerous variants of fluorescent proteins have been developed for protein labelling or as reporters of specific conditions. This development has opened the field of *in vivo* microscopy, to follow many processes *in situ*.

2.3. Conventional fluorescence microscopy

Modern fluorescent microscopes universally use incident-light (epi-) illumination, where the excitation light comes through the objective. Objectives are therefore the condenser of the microscope.

Usually fluorescent microscopes use Mercury or Xenon lamps as light source, however, they are being progressively substituted by new metal-halide lamps that offer longer lifetime.

Another major component of a fluorescent microscope is the filter cube. It contains a set of three filters: an excitation filter, a dichroic mirror and a barrier filter. Traditional glass filters, such as excitation and barrier filters, absorb some wavelengths while passing others: longer (long-pass filters), shorter (short-pass filters) or of a specific band of wavelengths (band-pass filters). The dichroic mirror is an interference filter that acts as a chromatic beamsplitter, reflecting short wavelengths and transmitting long ones. In other words, the excitation filter permits only selected wavelengths from the illuminator to pass through on the way toward the specimen. Barrier filters are designed to block (absorb) the excitation wavelengths and permit only selected emission wavelengths to pass toward the eye or other detector. Dichroic mirrors are designed to efficiently reflect excitation wavelengths and pass emission wavelengths. All three filters have to be properly chosen to match the spectral excitation and emission characteristics of the fluorophore used to label the specimen. Multi-color images of multi-fluorophore staining must be composed by combining several single-color images acquired using different filter cubes. For this purpose, these different filter cubes are mounted in a filter wheel that can be turned manually or automatically.

2.4. Confocal laser scanning microscopy

Confocal laser scanning microscope (CLSM) uses a laser light source. Laser passes through a diaphragm (excitation pinhole) and is focused on a small point of the sample and it scans the sample point by point on the focal plane. Fluorescence or reflection light from the focal plane passes through an emission pinhole (rejecting out of focus light), and it is detected by a detector, generating optical sections. Finally, point by point information is compiled in a computer and a final image is composed (see figure 2a).

The main advantages of CLSM are: the ability to control the depth of field, elimination or reduction of background information away from the focal plane, serial production of thin and non-invasive optical sections (maximum axial resolution would be 0.5 micrometers) through fluorescent specimens that have a thickness ranging up to 50 micrometers or more (increasing axial resolution in “Z” dimension), improvement of lateral resolution until 0.2 micrometers or more (X-Y dimensions) and elimination of scatter light thanks to the point-by-point illumination (laser source). The mechanical improvements in confocal microscopy are: a powerful excitation light source (laser beam light versus mercury lamps), pinhole diaphragm, motorized “Z” stage and image detectors (new generation of photomultipliers versus CCD cameras) [2].

Modern CLSM instruments are equipped with 3-5 laser systems controlled by high-speed acousto-optic tunable filters (AOTFs), which allow a very precise regulation of wavelength and excitation intensity. Emission is detected by photomultipliers and some confocal systems can select freely the detection range [2] thus allowing versatile configuration and minimizing spectral crosstalk.

The non-invasive confocal optical sectioning technique enables the examination, with enhanced clarity, of both, living and fixed specimens, under a variety of conditions. With most confocal microscopy acquisition software packages, optical sections are not restricted to the perpendicular lateral (x-y) plane, but can also be collected and displayed in transverse planes (Fig. 2). Most of the software packages for image analysis, accompanying commercial confocal instruments, are capable of generating composite and multi-dimensional views of optical-section data acquired from stacks of optical section (often termed a z-series) (Fig. 2). The three-dimensional software packages can be employed to create either a single three-dimensional representation of the specimen or a video (movie) sequence compiled from different views of the specimen volume [11] [12].

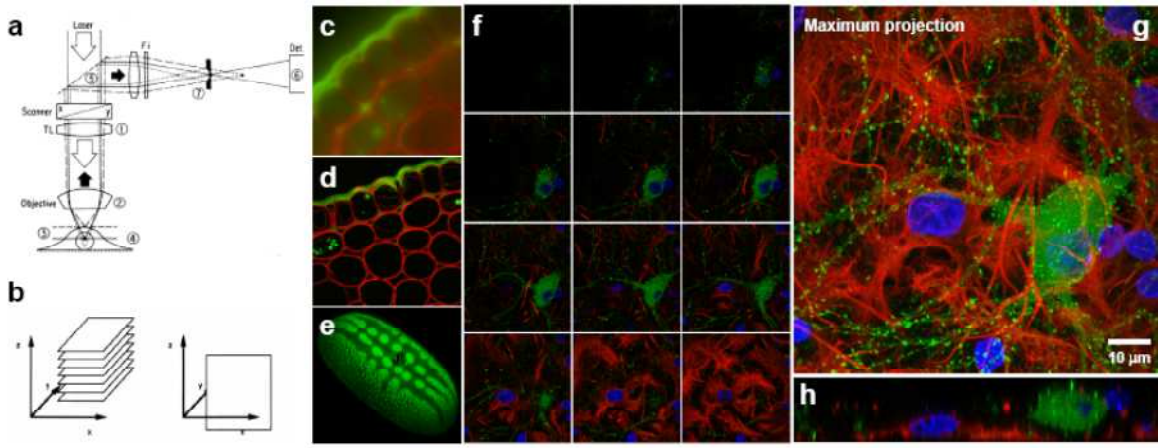

Figure 2 a) Depth discrimination in laser-scanning confocal fluorescent microscope. *1-Objective. 2-Objective lens. 3- Out of focus light emitted from the specimen. 4- In focus light emitted from the specimen. 5- Dicroic mirror. 6- Detector (photomultiplier) and 7- Pinhole diaphragm.* Figure adapted from *ref. 2. b) Optical sectioning: Stack of xy slices (left), xz slice (right);* Images of Convalaria obtained with widefield fluorescence microscopy (c) and CLSM (d) ; e) 3D reconstruction of a pollen grain obtained from optical sections (Image courtesy of Albert Lleal, CSIC); f, g an h) Triple fluorescence labelling of a culture of neurons and astrocytes. Green: GFP-Actin; Red: anti Glial fibrillary acidic protein; Blue: Hoechst; f) xy sections; g) Maximum projection; h) xz sections (Image courtesy of Miguel Morales,CIBIR-Rioja and University of Barcelona).

BT.4

CLSM is being used in a wide variety of very important and innovative biomedical applications such as: FRET (Fluorescence resonance energy transfer), photobleaching techniques, FISH (fluorescence *in situ* hybridization), *in vivo* imaging, ions imaging, 3D and nD digital reconstructions, colocalization of fluorophores, epitope tagging, morphometry and volumetry analisys, high-throughput screening, multicolor acquisition, profilometry, etc [2].

2.5. Nonlinear Microscopy

Nonlinear microscopy is based on the modification of the optical properties of matter by intense light, typically laser light [5] [6]. The nonlinear term refers to the response of matter to an applied optical field (light), which is not directly proportional to the stregth of the applied optical field. This response can result non linear in terms of intensity, as in two photon microscopy, or in the creation of radiation fields that propagate at new frequencies as in second harmonic generation or in new directions.

In contrast, single-photon excitation (conventional fluorescence) is directly proportional to the incident light, since each photon has an equal probability of exciting a molecule in the ground state.

2.5.1. Two-photon microscopy

Two-photon excitation is the process in which fluorescent molecules in the sample absorb two near infrared photons during the same quantum event. The probability of two-photon excitation is proportional to the square of the light intensity applied because it depends on the probability of one photon being there multiplied by the probability of another photon being there. The maximum probability of two-photon absorption is only achieved at the focal plane thus producing intrinsically optical sectioning. In this kind of microscopy, out of focus fluorescence is practically never generated, thus reducing the background from the acquired image and photobleaching and fototoxicity at out of focus planes.

The principal advantages of multiphoton microscopy for the study of biological samples are: optical sectioning, excitation at a single point of the sample in the focal plane, high penetration of the near infrared photons, low phototoxicity and photoextinction at out of focus planes.

The quantum-mechanical selection rules for two-photon excitation are very different from those for single photon excitation and result in very different absorption cross section from those for

single photon excitation [7]. The absorption cross sections of fluorophores are very different from the single photon cross sections and they commonly exhibit a broader two-photon excitation cross section. The emission characteristics of the excited fluorochrome are the same for the different absorption processes (single and two-photon processes).

Two photon microscope consists of a a laser scanning microscope with an ultrafast near infrared laser pumped by a solid-state laser, a high-numerical aperture lens and descanned or non-descanned detectors.

In order to have a high probability of two-photon excitation in the focal plane, a high density of photons is needed. This can be achieved by two factors. First of all, a pulsatile and powerful laser sends short peaks of photons of large intensity at high frequency. Secondly, a high collecting angle of the lens concentrates a big density of photons in the volume of the focal plane.

Detection can be performed by descanned and non-descanned detectors. In the descanned detection, pinholes are removed or completely open and the same optical pathway and scanning mirrors are used as in confocal laser scanning microscopy. Non-descanned detectors do not use pinholes, the emision is selected with dichroic mirrors and detected from the whole image without passing back through galvanometric scanning mirrors. One type of non-descanned detectors are those that are external, in which light does not pass back through the objective. These detectors are very efficient and suitable for light scattering samples because they detect the photons from the whole area.

The main applications of two-photon microscopy are: imaging of thick samples: intact tissue, animals (intravital microscopy, see fig. 3a) or tissue sections, live cell analysis during long periods of time due to less phototoxicity and photobleaching at the focal plane, excitation of ultraviolet fluorophores with near infrared laser (see fig. 3b), adaptability to new fluorescent probes (lipid probes), simultaneous excitation of various fluorophores (see fig. 3a), photoactivation, photolabelling, uncaging and photobleaching for molecular dynamic studies in living cells at a known volume, etc.

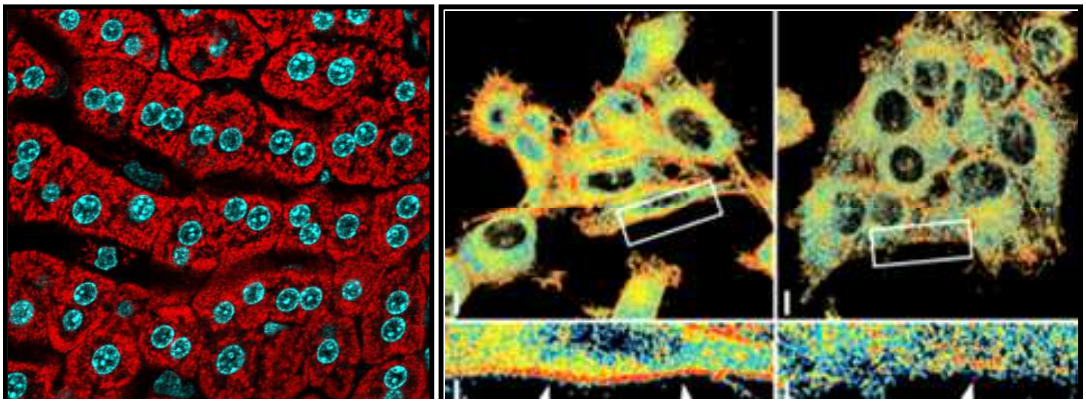

Figure 3. a) Two photon intravital microscopy of mouse liver. Image of liver of a mouse injected with Hoescht for DNA labelling (blue) and membrane potential sensitive probe TMRM (red) both excited at 800 nm (Figure adapted from ref. [17]). b) Two-photon imaging of an ultraviolet probe (Laurdan) to study lipid order in plasma membrane. General polarization (GP) images, of Laurdan-labeled wt (right) and mhtt (left) cells, were pseudo-colored, with blue to red representing fluid and ordered domains, respectively (Image courtesy of J. Alberch, University of Barcelona [8]).

2.5.2. Second Harmonic Generation

Non centrosymmetric molecules illuminated with a high-intensity light of a given frequency and wavelength have the capability to generate second harmonic, i. e. light with double frequency and half the wavelength of the fundamental light [5] [6].

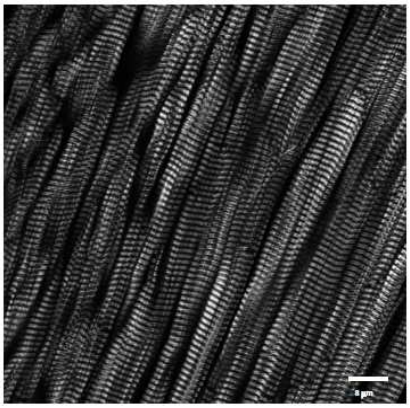

Second harmonic generation (SHG) is a nonlinear scattering process because its efficiency depends on the square of the incident light intensity. Therefore, second harmonic generation needs a very high intensity light that, in microscopy, it is only achieved at the focal plane by a powerful pulsing laser. As a result, SHG provides intrinsic optical sectioning. Another characteristic is that the generated wave propagates in the same direction as the incident light and in phase with it, although it has a different plane of polarization. As SHG and TPE imaging requirements are very similar, SHG imaging can also be performed, with some modifications, using a two-photon microscope.

Figure 4. Example of second harmonic generation application. Imaging of sarcomere distribution in cardiomyocites of left ventricle of mouse.

The main applications of SHG are the visualization, without staining, of structural proteins such as collagen, myosin and tubulin and the visualization of specific labellings with probes that generate second harmonics.

3. Applications of Light Microscopy in Biomedicine

3.1. Cell tracking

As its name suggests, particle or cell tracking, is the ability to follow the movements of cells or particles *in vivo* (during a time period), using light microscopy techniques such as transmitted light and fluorescence microscopy or other techniques. The idea is that one can follow tagged particles or cells by means of various detection methods over the time, in two or three dimensions. This kind of analysis can generate big amounts of data and a powerful image analysis is necessary. In order to optimize the process, image analysis automation should be incorporated (see 3.4 section below). Different processes can be analysed, for example: mitosis, apoptosis, cellular shape, direction and velocity of particles, organelles or cells, etc and they have many application in basic and clinical biomedical research.

In the following example, cell tracking with differential interference contrast imaging (DIC) and fluorescence (EGFP) showing that Hsp27 phosphorylation is required for BMP-2 induced cell migration was examined [4]. C2C12 cells were grown on 4-well coverslip-bottom plates, before being placed at 37ºC in a CO_2 incubation system. Images (typically 4 Z-stack sections) were recorded at 5-min intervals for 16 h using a LEICA TCS-SL confocal microscope. Individual cells were traced from the resulting time-lapse movies and analyzed using ImageJ software with manual cell tracking plug-in. Cell migration was analyzed by marking the position of the nucleus in individual cells in each frame to obtain the migration tracks. In this case, only the migration tracks are used for quantification of the total distance between time zero and the final time (Fig. 5). Also the velocity of the cells, directionality of the movement and quantification of mitosis, can be analyzed.

3.2. Fluorescence Resonance Energy Transfer

Fluorescence Resonance Energy Transfer (FRET) is a process where an excited fluorophore (donor) transfers energy to another fluorophore (acceptor). The resonance energy transfer is dependent on the distance, due to the dipole-dipole interaction from the donor and acceptor, and since it is non radiative, there is no photon emision. FRET technique can be used to report molecular associations and biochemical reactions. When it is combined with fluorescence microscopy, the FRET signal can be precisely located at the subcellular level where the process is taking place. This is very important because molecular associations and biochemical reactions

depend greatly on subcellular localization and on the differential and specific microenvironment conditions in that compartment or region.

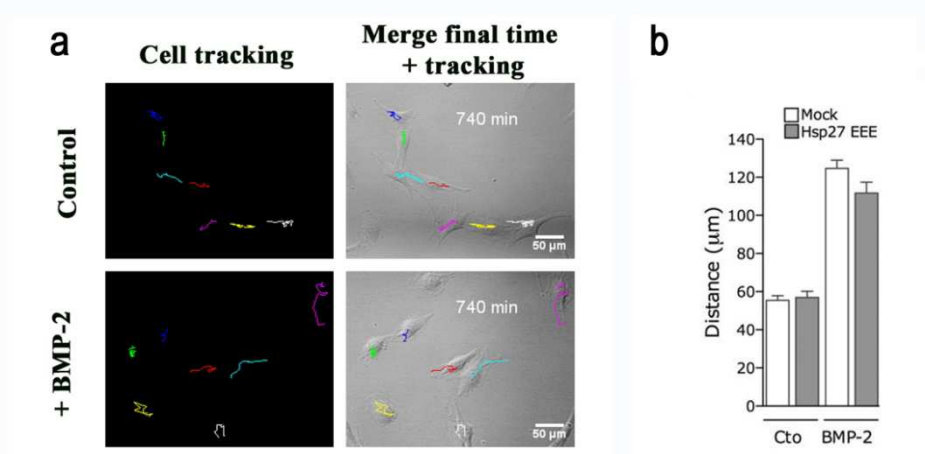

Figure 5. A) ImageJ analysis of cell tracking (total distance in microns) in presence or absence of BMP-2. B) Quantification of migration tracks. Histogram shows migration tracks obtained from at least 80 cells in each experimental condition from two independent experiments. Values correspond to the mean ± SEM. (Image courtesy of F. Ventura, University of Barcelona [4]).

There are different conditions for energy transfer to occur. First of all, donor and acceptor molecules have to be at a physical distance less than a specific radius- between 1- 10 nm. Secondly, the donor emision spectrum has to overlap with the acceptor absorption spectrum at least 30%. Finally, the orientation dipole transition of donor and acceptor molecules has to be approximately parallel. FRET pairs for fluorescence microscopy are couples of synthetic fluorophores. Each FRET pair is defined by a distance at which the efficiency of energy transfer is 50%. This distance is known as the Förster radius (R_0).The relation between FRET efficiency (E) and distance is defined by the equation

$$E = 1 / [1+(r / R_0)^6],$$

where r is the distance between donor and acceptor and R_0 is the Förster radius. It can be observed from Fig. 1 that FRET is very sensitive to distance and it decays very abruptly for an small increase of distance between donor and acceptor [14]. FRET has become a good tool to report changes in molecular proximity or biochemical reactions because of its sensitivity to changes in distance and the fact that the Förster radius of most of the FRET pairs are in the range of biomolecules size (1-10 nm).

Inter molecular proximity can be elucidated by measuring FRET between one molecule of interest labelled with donor and the other with acceptor fluorochrome. Intramolecular FRET can also be used as a reporter of biochemical reactions by designing molecules, with donor and acceptor in them, which change distance by changing conformation of aminoacids or proteins sensitive to the process of interest. The latter process reports a biochemical reaction such as phosphorilation, Ca2+ concentration, membrane microdomains.

3.2.1. Intensity-based FRET methods

Different methods exist for calculating FRET. During the energy transfer, a phenomenon of donor quenching (loss of emission signal) corresponding to an increase of acceptor intensity can be observed.

The different quantification FRET methods take advantage of the phenomena that occurr during the process. For example, acceptor photobleaching and sensitized emission are intensity-based methods that take advantage of donor loss of emission signal and of the increase in acceptor signal due to FRET, respectively. For instance, fluorescence lifetime measurement exploits the fact that donor fluorescence lifetime is reduced. Ratiometric methods are optimal for intramolecular FRET experiments.

Acceptor photobleaching is an intensity-based method that takes advantage of loss of donor signal due to FRET. It compares images of donor before and after photobleaching of the acceptor in a region of interest in the sample. If FRET occurs, donor will increase its emision signal after acceptor photobleaching (see example in fig. 6a). The efficiency is calculated as

$$E= (D2-D1)/D2,$$

where D2 is the donor intensity of the region of interest after acceptor photobleaching in that area and D1 is the donor intensity before photobleaching. For this method, fixed samples are necessary.

Sensitized emission method is another intensity-based method that takes advantage of the increase of acceptor signal under FRET conditions when illuminating specifically the donor . This method is based on the acquisition of an image called FRET channel that is the acceptor image under donor excitation light, together with the images of donor and acceptor (see fig. 6b). FRET image has to be corrected for i) the emission of acceptor directly excited with donor excitation light and ii) crosstalk of donor emision. The crossexcitation and crosstalk values are calculated from images of samples labelled only with either donor or acceptor. FRET corrected image can be normalized by the amount of donor or acceptor or both. FRET efficiency can be further calculated if the G factor is calculated. The latter factor is the ratio of increase of acceptor emission due to FRET to the quenched donor intensity due to FRET, for a particular fluorophore pair and instrument imaging settings.

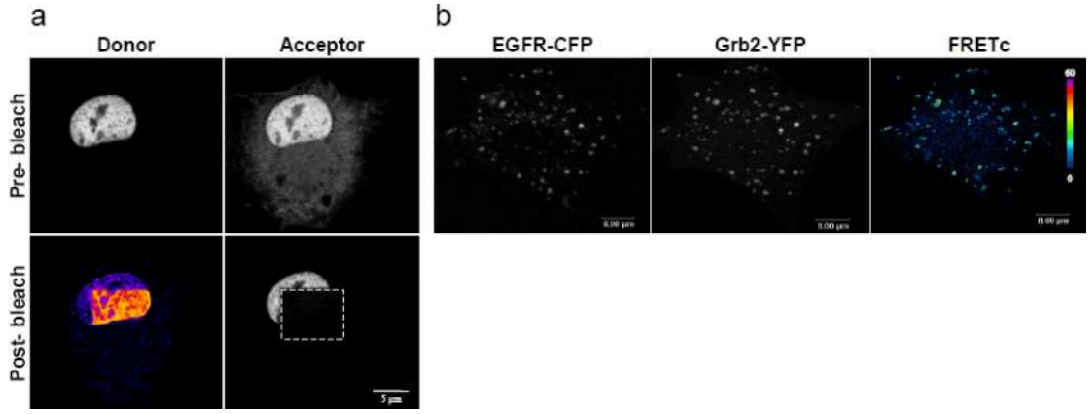

Figure 6.a) Acceptor photobleaching FRET experiment between cyan fluorescent protein (CFP), as donor, and yellow fluorescent protein (YFP), as acceptor, fused to two nuclear proteins. (Image courtesy of Anna Perearnau and Oriol Bachs, University of Barcelona); b) Sensitized emission FRET experiment between Epidermal growth factor receptor- CFP (EGFR-CFP), and Grb2-YFP. Maximum FRET signal is localized at endosomes. FRET corrected image is shown in pseudocolor in arbitrary linear units of fluorescence

3.3. Photobleaching techniques

Photobleaching is the irreversible loss of fluorescence after an exposure to high-intensity and continuous light. This phenomenon is used as a strategy to make evident the dynamics of molecules or the connection between compartments or cells in live cells, tissues or organisms. In a photobleaching experiment, under optimal conditions, fluorescence is irreversibly extinguished but the functionality of the tagged molecules is preserved. Molecules may be directly or indirectly labelled with fluorescent dyes or expressed as genetically-encoded fluorescent fusion proteins in live cells.

The l basis of these techniques is as follows. In unaltered cells, fluorescent molecules are in equilibrium. Photobleaching of molecules in a region of interest of the cell will disturb this equilibrium and redistribution of fluorescent and non fluorescent molecules along time will make evident the dynamics of the molecules. Photobleaching techniques are very flexible and can be adapted to resolve various biological problems [13].

The most straightforward photobleaching technique is fluorescence recovery after photobleaching (FRAP). In this technique, fluorescent molecules in a region of interest are bleached by a focused light (tipically a laser beam) and the fluorescence recovery in that region is

quantified and compared to the initial conditions. Fluorescence recovery into the bleached region is due to diffusion of surrounding non-bleached fluorescent molecules. Two parameters describe the molecular equilibration kinetics. The mobile fraction is the percentage of recovered fluorescence after photobleaching, compared to the initial conditions, and half time of recovery is the time at which half of the mobile fraction has recovered. Further analysis by kinetic modelling provides information on the molecular dynamics. This technique can provide information of mobile and immobile fraction, kinetics at different conditions, diffusion coefficient and association and dissociation kinetics (Fig. 7).

In Inverse FRAP experiments, all the fluorescent molecules in the cell, except for a small area, are bleached. The loss of fluorescence from the unbleached region in the postbleach images is then analysed. This technique allows to analyse dissociation parameters of molecules which are bound to an immobile structure (Fig. 7). FRAP can also be used as a contrast technique to visualize with a better signal-to-noise ratio the fluorescence structures dissociating from the region of interest.

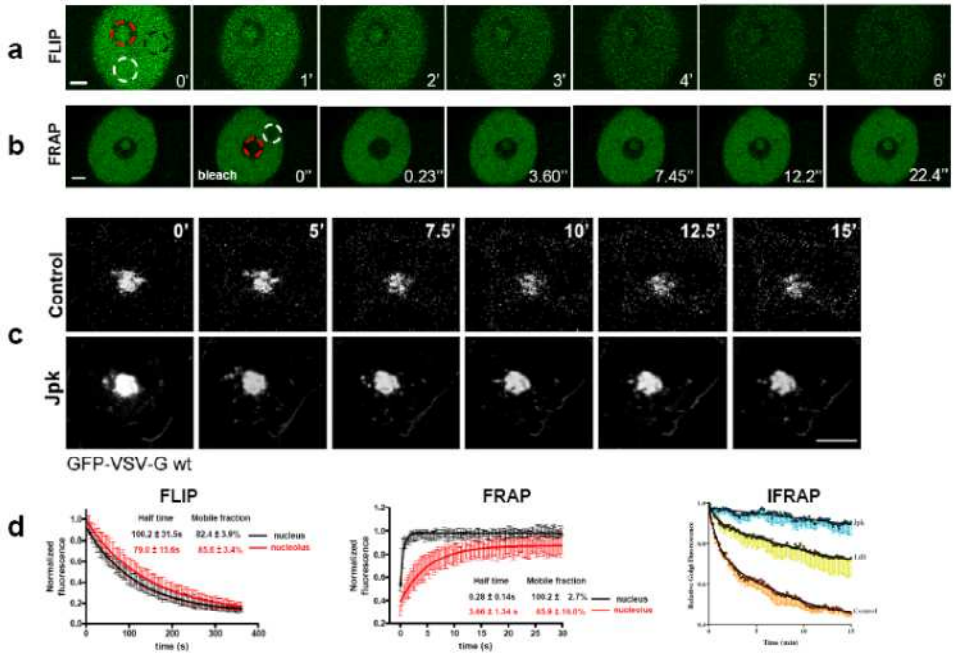

Figure 7. a) FLIP experiment of p21-GFP to evaluate connectivity between intranucleolar body (red) and nucleoplasm (white). Representative images at different timepoints; b) FRAP experiment to evaluate dynamics of p21- GFP in intranucleolar body (red) and nucleoplasm (white) under Adriamycine treatment.; c) Inverse FRAP experiment of GFP- vesicular stomatitis virus G wild type protein (GFP VSVG wt) in Golgi. Representative images at different timepoints of two different iFRAP experiments. d) Quantification of kinetic parameters of FLIP experiments in a); e) Quantification of kinetic parameters of FRAP experiments in b) f) Quantification of various iFRAP experiments under the effect of different actin disrupting reagents (jpk: jasplakinolide; LtB: LatrunculinB) (a, b, d and e adapted from Ref. [16]; c and f adapted from Ref. [15]).

Fluorescence Loss In Photobleaching (FLIP) experiments are different from FRAP experiments because a specified region of the cell is repetitively photobleached and the loss of fluorescence in non bleached parts of the cell is measured. These experiments are useful for studying connectivity between different regions and compartments of a cell and for studying fluxes between them (Fig. 7).

3.4. Extracting information from bioimaging: Image Analysis

Computer image analysis methods are available to help to observe the information in images, to minimize human bias, and to introduce rigor into the process of obtaining quantitative information.

Images have to be processed before any numerical data can be obtained. This image processing is performed in several steps. In a first step, images may be corrected to minimize defects of

acquisition (i.e, non-uniform illumination of the sample or high level of noise generated by the acquiring device). In a second step, differences in grey values (representing the brightness of the pixels) between the objects of interest and the background can be improved. Once objects or features to be measured are clearly identifiable, they can be easily segmented. Segmentation, the last step, will divide images into two domains, namely the objects and the rest. It generates, therefore, a two-level or binary image which can be used directly for quantification or can be applied over the original image as a mask, restricting those pixels in the original image that will be used for quantitative evaluation.

Image quantification can provide different types of information. The number of objects is one of the typical measurements that is obtained but many morphometric parameters can also be measured: area, shape, orientation, etc. Densitometric parameters (intensity, optical density) can also be obtained from image analysis. A common application derived from intensity measurements is for instance, the analysis of the degree of overlap between two different proteins, that is, the colocalization between them. Moreover, quantification can also be performed in multidimensional images. A stack or sequence of xyz images can be used, for instance, to make a 3D reconstruction to visualize the shape and appearance of real objects (Fig. 2e), or to measure 3D parameters such as the volume. The time dimension (xt, xyt, or xyzt images) allows the analysis of live biological processes. In this sense, the movement of cells (cell tracking, Fig. 5) or the concentration of ions (i.e. intracellular Ca^{2+}) after different treatments or in different biological conditions can be quantified. Moreover, as mentioned above, the loss and recovery of fluorescence (FLIP and FRAP respectively, Fig. 7) are also examples of intensity measurements over time.

Acknowledgements

The authors would like to acknowledge the invaluable contribution of Esther Castaño from her expertise in citometry. We would like to thank Elisenda Coll and Katarzyna Górka for their help in reviewing the manuscript and for image acquisition and processing.

References

[1] Pawley JB 2006 Handbook of biological confocal microscopy. New York: Plenum Press.
[2] Huang B, Babcock H, Zhuang X. 2010 Cell. 143(7):1047
[3] http://www.piercenet.com/browse.cfm?fldID=4DD9D52E-5056-8A76-4E6E 217FAD0D86B#brightness.
[4] Gamell C, Susperregui AG, Bernard O, Rosa JL, Ventura F. 2011 PLoS One 28
[5] Campagnola 2011 P.Anal Chem. 1;83(9):3224
[6] Cox G, Kable E. 2005 Methods in Molecular Biology 319
[7] Diaspro A, Chirico G, Collini M. 2005 Q Rev Biophys38(2):97
[8] Del Toro D, Xifró X, Pol A, Humbert S, Saudou F, Canals JM, Alberch J. 2010 J Neurochem. 115(1):153
[9] Prasher D, Eckenrode V, Ward W, Prendergast F, Cormier M 1992. Gene 111 (2): 229.
[10] Shaner N, Steinbach P, Tsien R. 2005. Nat Methods 2 (12): 905.
[11] Fellers TJ, Davidson MW 2007 Olympus Fluoview Resource Center. National High Magnetic Field Laboratory.
[12] Claxton N S, Fellers T J, Davidson M W 2008 Laser scanning confocal microscopy.
[13] Rabut, G., and J. Ellenberg. Live Cell Imaging: A Laboratory Manual. Vol. 1. R.D. Goldman and D.L. Spector, editors. Cold Spring Harbor Laboratory Press, Cold Spring Harbor. 101-127
[14] Stryer L, Haugland RP. Proc Natl Acad Sci U S A. 1967 58(2):719
[15] Lázaro-Diéguez F, Colonna C, Cortegano M, Calvo M, Martínez SE, Egea G. 2007 FEBS Lett. 7;581(20):3875
[16] Abella N, Brun S, Calvo M, Tapia O, Weber JD, Berciano MT, Lafarga M, Bachs O, Agell N. 2010
[17] Traffic 11(6):743
[18] Consejo General de Colegio Oficiales de Farmacéuticos. 2010. Biotecnología y Biofármacos (Módulo II).Plan Nacional de Formación Continuada. M-200075-2010- pp177

Bioinformatics: making large-scale science happen

Sergi Beltran

Unitat de Bioinformàtica, CCiTUB, Universitat de Barcelona. Parc Científic de Barcelona, Baldiri Reixach 10, 08028 Barcelona.

email: *beltran@ccit.ub.edu*

Abstract. Bionformatics is a rapidly evolving research field dedicated to analyzing and managing biological data with computational resources. This paper aims to overview some of the processes and applications currently implemented at CCiT-UB's Bioinformatics Unit, focusing mainly on the areas of Genomics, Transcriptomics and Proteomics.

1. Introduction

Bioinformatics is widely accepted to be the application of computational resources to the analysis and management of biological data. However, it was originally defined in 1970 by Ben Hesper and Paulien Hogeweg [1], as the "study of informatic processes in biotic systems" [2], and it was not until the rise of high throughput technologies in molecular biology that Bioinformatics, as is nowadays known, became an everyday word in science (Figure 1).

Computers and the Internet have allowed the current revolution in science, becoming essential to any field of study. On one hand, they provide communication services such as email, mailing lists, forums, papers or webinars. On the other, they are used to store and analyze data and provide online tools like databases, genome browsers, image banks or applications. Needless to say, the former services and tools have been possible through the development of programs, algorithms, statistical methods and even new programming languages, therefore generating knowledge by themselves.

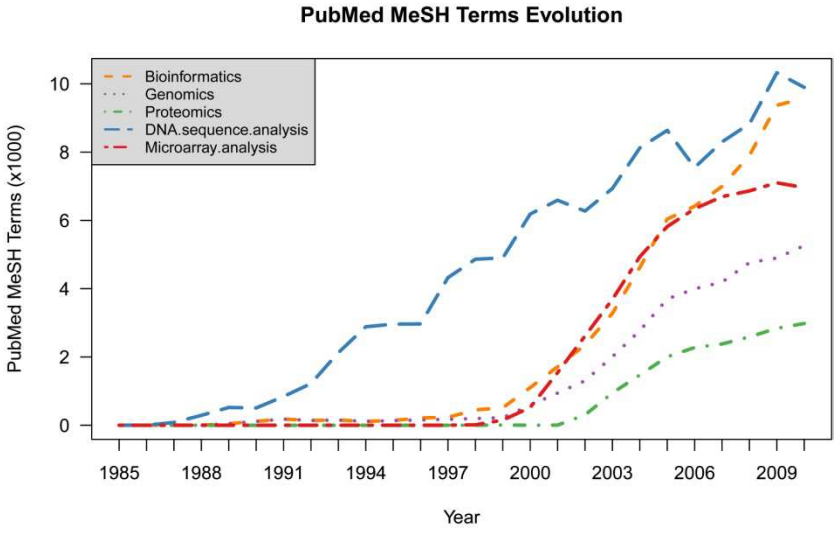

Figure 1. Number of articles by year classified by the following Medical Subject Headings (MeSH) terms from the Natio-nal Library of Medicine's con-trolled vocabulary: Bioinformatics, Genomics, Proteomics, DNA sequence analysis and Microarray analysis. Only data since 1985 are shown. Plot has been generated with R [3] and MEDSUM [4].

From a narrower point of view, Bioinformatics is associated with the analysis and management of massive amounts of data, be it DNA sequences, microarrays, in-situ hybridizations or microscope images. In that sense, Bioinformatics has been essential to the birth of Omics, fields that study the totality of a certain feature, and Systems Biology. To put it simple, the assembly and annotation of the Human genome [5, 6] or its proteome structure prediction [7] would have never been possible without Bioinformatics.

At CCiT-UB, the Bioinformatics Unit is mainly devoted to the areas of Genomics, Transcriptomics and Proteomics. It provides customized analyses, management, storage and visualization solutions to data from different sources such as next-generation *de novo* sequencing and re-sequencing, ChIP-on-chip, ChIPseq, DNA and protein microarrays, real time PCR or databases, amongst others. State of the art analyses are performed by using the latest software releases as well as developing and adapting programs to the researcher's needs.

2. Bioinformatics applied to Genomics, Transcriptomics and Proteomics

Next-generation sequencing (NGS, see the Genomics Unit paper in this issue) is a key achievement in molecular biology that is changing the way researchers work. While before it took years and endless resources to sequence a single genome, now it is possible to *de novo* sequence or re-sequence a small genome in a few hours and a complex one in just a few days. This new era has just begun, and in the near future it will be faster and cheaper to sequence a human genome, which might imply a big leap in personalized medicine [8]. Noteworthy, NGS has multiple applications

in fields such as metagenomics, where it can be used to decipher the microorganism's composition of samples like water, soil or feces [9, 10, 11].

However, obtaining the data is one thing, and making sense out of it is another and Bioinformatics must live up to this challenge; for example, algorithms and pieces of software that were originally designed to analyze small amounts of DNA must now be optimized and scaled up in order to deal with whole genomes, or even thousands of them [12, 13]. Moreover, all this data has to be stored in an accessible way, if possible with intuitive visualization tools, and usually has to be integrated or compared with other high-throughput data.

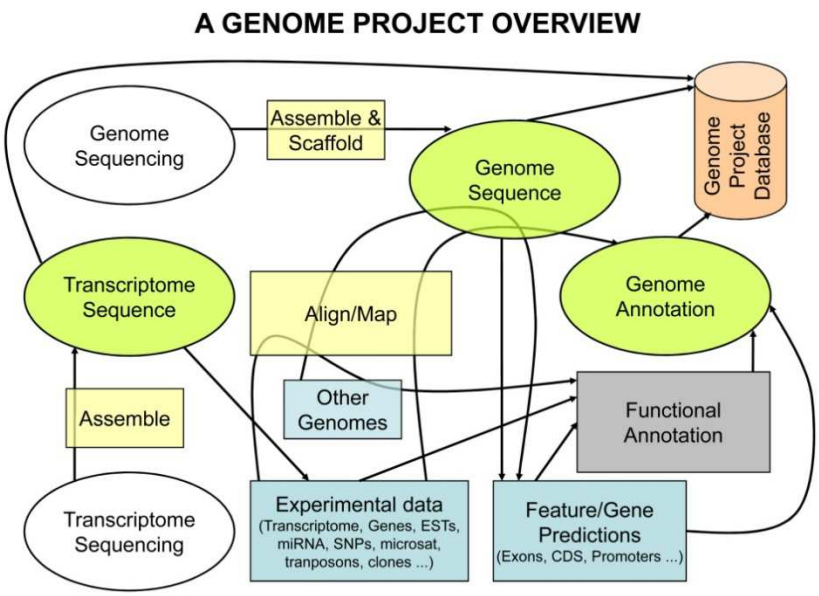

Figure 2. Non-exhaustive author's view of a genome project's workflow. Usually, a project will start by sequencing a genome or a transcriptome, which must be assembled into a consensus sequence. Annotation of this sequence can be done with *ab initio* predictions and/or using already available experimen-tal data from the same or other organisms. The relevant output from the project must be stored in the genome project's database. See main text for further discussion.

2.1. Genome-wide biology

A genome project (Figure 2) usually starts with *de novo* sequencing of the organism's DNA (genome sequencing). From the Bioinformatics point of view, it is a non-trivial step that starts by converting the experimental raw data (usually images) into usable sequences of DNA (reads). Quality control is an essential part since it must be ensured that only good quality reads are kept and primers, adapters and contaminants have been thoroughly detected and removed (Figure 3). With the aim of reconstructing the original sequence, those reads will be assembled (aligned and merged) into contigs which, if extra information like paired-end reads is available, will be sorted into scaffolds (Figures 2 and 4).

Once the genomic sequence is established, one or several annotation steps are usually performed (Figure 2). Annotation is the process of detecting and assigning features to the sequence. Amongst others, these features might be genes (Figure 4), open reading frames (ORFs), start and stop codons, transcriptions start sites (TSSs), splice donor and acceptor sites, regulatory regions, repeats, single-nucleotide polymorphisms (SNPs), miRNAs or protein motifs. Annotation can be achieved *in silico* using algorithms developed and trained to perform *ab initio* prediction of the features of interest. While some of these methods use the actual sequence as the only input, others compare it to other genomes by working under the assumption that biologically relevant strings of sequence are conserved throughout evolution. However, no matter how good the programs are, it is always desirable to have some experimental data to assess the predictions accuracy and adjust the algorithm's settings.

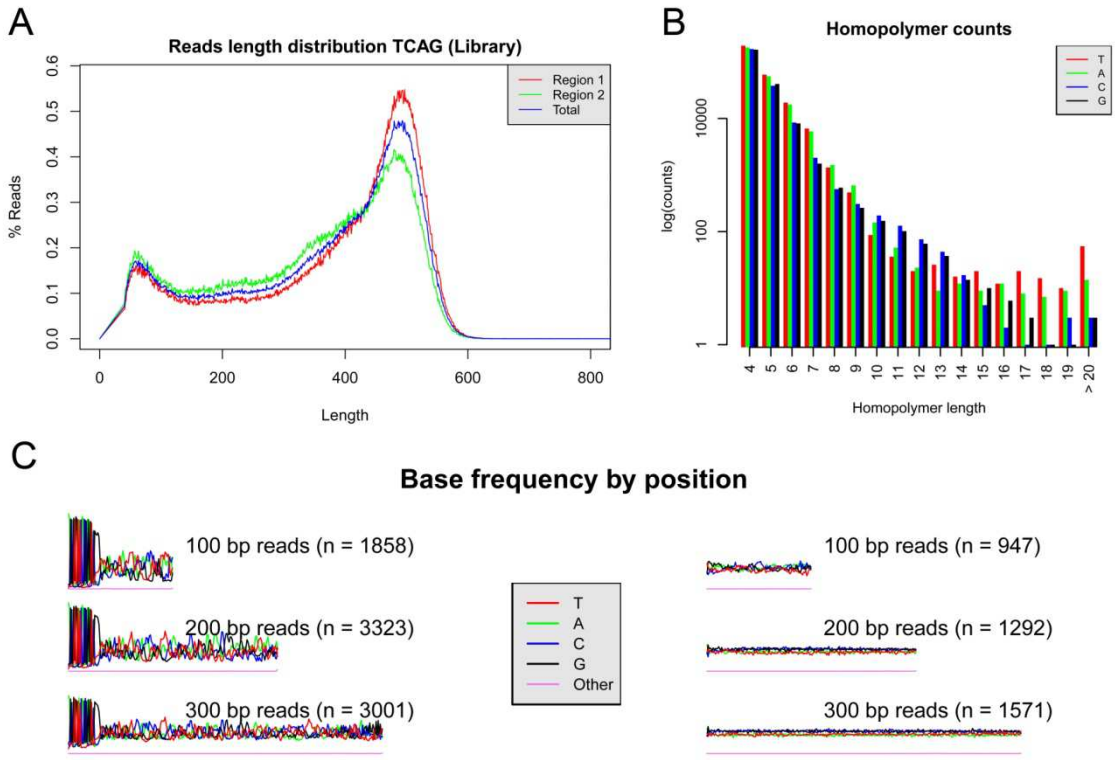

Figure 3. Some plots generated by our processing and quality control pipeline of Titanium FLX 454 sequencing runs performed at CCiT-UB's Genomics Unit. A) Percentage of reads from each length of the whole sequencing plate (blue), its first region (red) or its second region (green). B) Number of different size homopolymers from each base (see color legend). C) Percentage of each base (see legend) in each sequence position from 5' to 3' (left to right) in all reads with exactly 100bp, 200bp or 300bp. In comparison to the plot on the left, the one on the right had primers, adapters, polyA+, highly repetitive sequences and highly predominant sequences removed. All plots generated with R and Bioconductor packages [14, 15].

BT.5

High-throughput technologies enable whole genome annotation based on experimental evidence. For example, to find the binding sites of a certain protein, we can use the latter to perform chromatin immunoprecipitation, sequence the bound fragments and map them back to the genome, in a process known as ChIPseq. These results can also be used to predict putative binding site motifs (Figure 5A) that can be searched in the same or other related genomes. Or to elucidate the genes, and even their different transcripts, an organism's transcriptome can be sequenced and aligned to its corresponding genome (Figure 2).

Nevertheless, once a set of genes is described, functional annotation will provide them with a meaning by assigning names and functions (Figure 2). One of the most popular functional annotation methods is based on similarity comparison using BLAST [18] (Figure 4), in which the unknown nucleic and proteic sequences are queried against well annotated databases. The accuracy of the process increases as evolutionary distance between species decreases. Those results can then be used to group the genes/proteins into GeneOntology [19] categories or KEGG pathways [20] (Figure 6).

Finally, a decision has to be made on which data to store. Even with the actual continuous development of storage hardware, the rate at which new data are generated is posing a strain on storage facilities and, in many cases, only processed data can be kept. These data have to be organized in databases easily searchable by researchers and, if possible, accompanied with visualization tools like genome browsers (Figure 4).

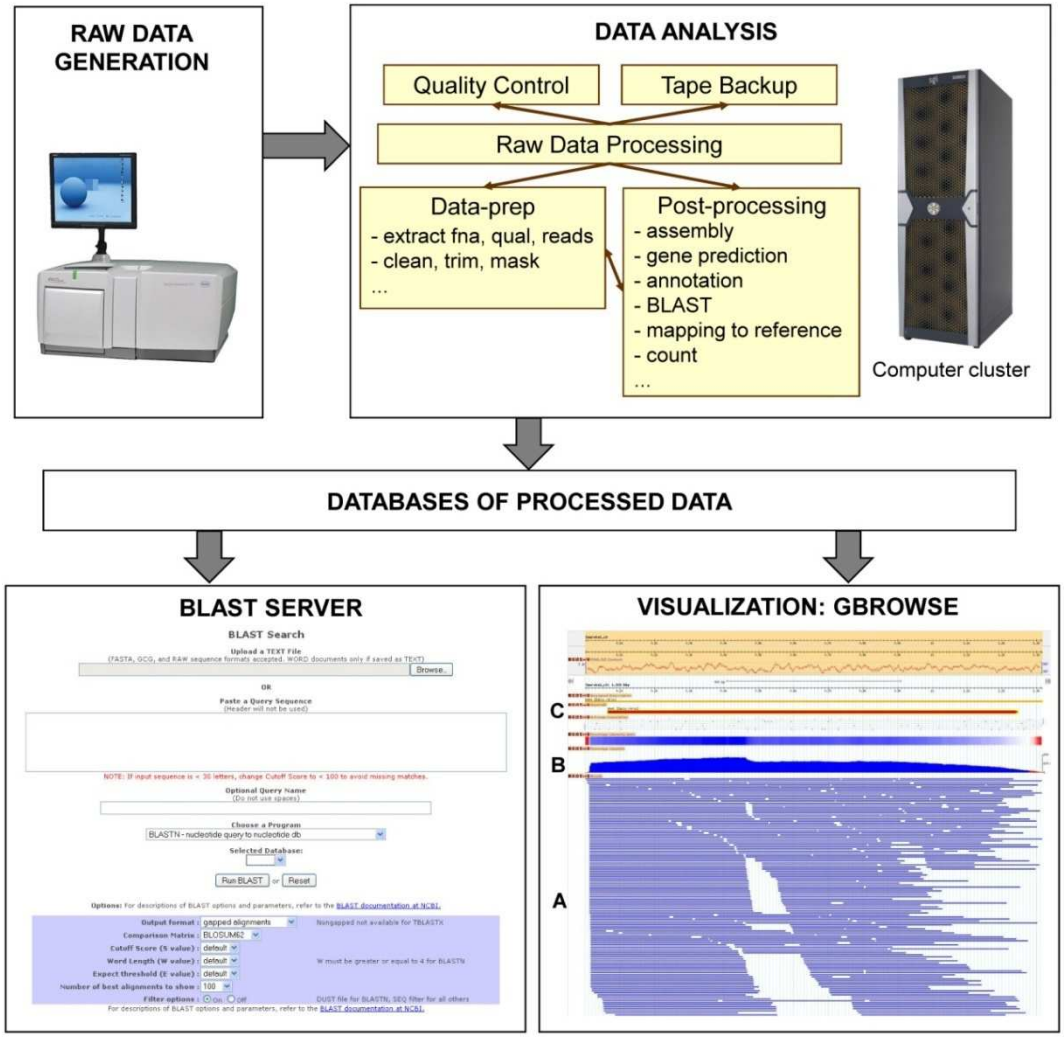

Figure 4. Bioinformatics Unit typical data workflow for a 454 sequencing project. Raw data generated by the Genomics Unit is transferred to our analysis cluster to conduct processing, quality control and backup. The nature of the experiment will determine the kind of data preparation and post-processing pipelines that must be applied. Processed data is then stored in databases that can be queried online to retrieve information in text format (not shown). In addition, results like assembled contigs can be blasted online (left) or visualized with GBrowse [16] (right). In this GBrowse example, some tracks from a contig are shown. In A), each horizontal blue line is one of the 454 reads that has been assembled to generate the contig. In B), the coverage of the contig is shown: y axis shows how many times each consensus base has been sequenced (this is, how many reads cover that base). In C), a putative gene (red box) inferred from similarity to another species. Preliminary data used in this example has been described in Martínez-Rodríguez et al. [17].

2.2. Biomedical applications

Bioinformatics are essential for the analysis of high-throughput experiments aimed to novel discovery, but can also be applied to the development and analysis of biomedical applications. For example, an annotated genome can be useful to design a DNA microarray aimed at classifying tumor types based on their gene expression profile, which might help to decide upon a treatment. In the same direction, *in silico* protein structural modeling can aid to find novel drug targets.

Whole genomes and transcriptomes from individuals sharing the same disease can be sequenced and compared in order to discover common variations amongst patients. If proofed, those variants become new treatment targets or, at least, candidates for developing a new molecular diagnostic kit based, for example, in nucleic acids hybridization or whole-gene sequencing. For that purpose, technologies like targeted sequence capture and molecular barcoding can help to bring costs down

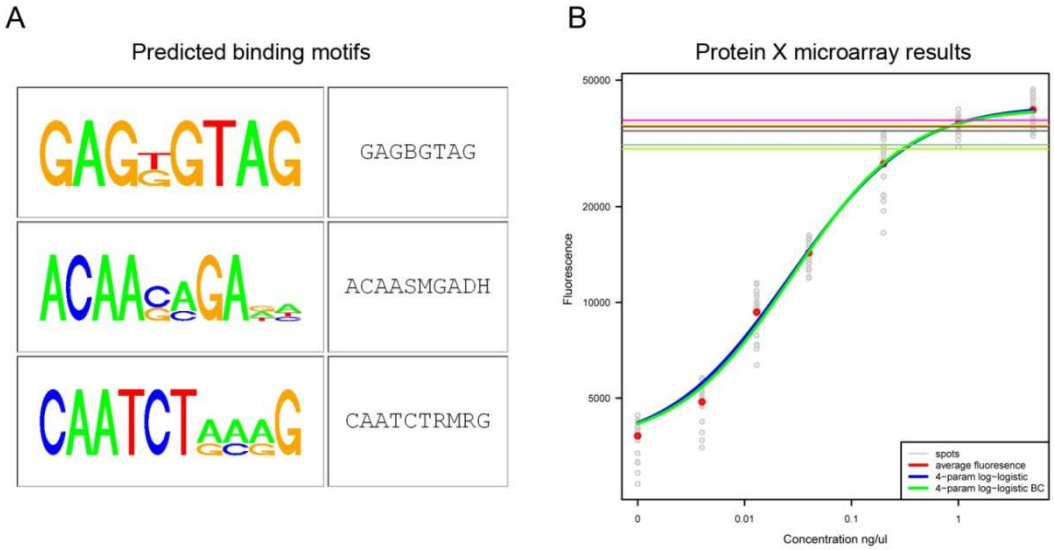

Figure 5. A) SeqLogos (left) and consensus sequence (right) of protein N putative binding sites predicted with BCRANK [21, 22]. B) Preliminary results from a protein microarray prototype produced at the PCB-UB Transcriptomics Platform by A. Sierra and L. Muixí from IDIBELL and L. Sevilla and J.I. Pons from PCB. Red circles show average normalized fluorescence at different concentrations from protein X replicates (in gray). Thick lines display the fitted 4 parameters log-logistic model with (green) or without (blue) Box-Cox transformation. Horizontal lines display observed fluorescence from different samples for which concentration of protein X wants to be assessed. Statistics and plots generated with R packages using scripts developed at CCiT-UB's Bioinformatics Unit.

BT.5

by restricting the area to sequence and allowing sample pooling, respectively. Alternatively, a protein microarray could be design to monitor the levels from relevant proteins in samples (Figure 5B).

What all these applications have in common is the need of Bioinformatics, first to analyze preliminary data, then to design it and, finally, to generate a method that ensures the standardized and correct analysis of the output.

2.3. Metagenomics

Metagenomics is a rapidly growing science that applies genomics to whole, usually microbial, communities, avoiding isolation and culture steps. Therefore, instead of trying to physically isolate and individually sequence all the organisms from a sample, its whole nucleotidic material, or certain common regions, can be sequenced at once and split afterwards by computational means.

There are endless potential applications derived from metagenomics analysis, ranging from health issues to earth matters and the bioinformatic pipelines must adapt accordingly. For example, without aiming to know what organisms they belong to, the sequences from a sample can be classified into evolutionary trees and quantity or proportions of the microbes, as well as diversity, can be computed. One application is to classify samples according to their microbial community composition, which might be useful to assess if a drug is working well in treating a gut disorder or if the soil is recovering from a certain contamination.

In addition, sequences can be compared to those from databases to elucidate which organisms, and in which quantity/proportion, are found in the community. In addition, the former can be

functionally classified. For example, certain organisms are only found in clean waters or are known to cause a disease, so quality control or preventive measures can be taken according to metagenomics results.

Last but not least, metagenomics can be applied to the discovery of new microbes and functions that might help develop novel biotechnological products directed towards pharmacy, food production, plague control, biofuel production or decontamination, just to mention a few. In fact, one of the most ambitious current science projects, the Global Ocean Sampling Expedition, is sailing around the globe taking samples to be sequenced and analyzed [23] in a worldwide enterprise benefitting from high-throughput sequencing and Bioinformatics.

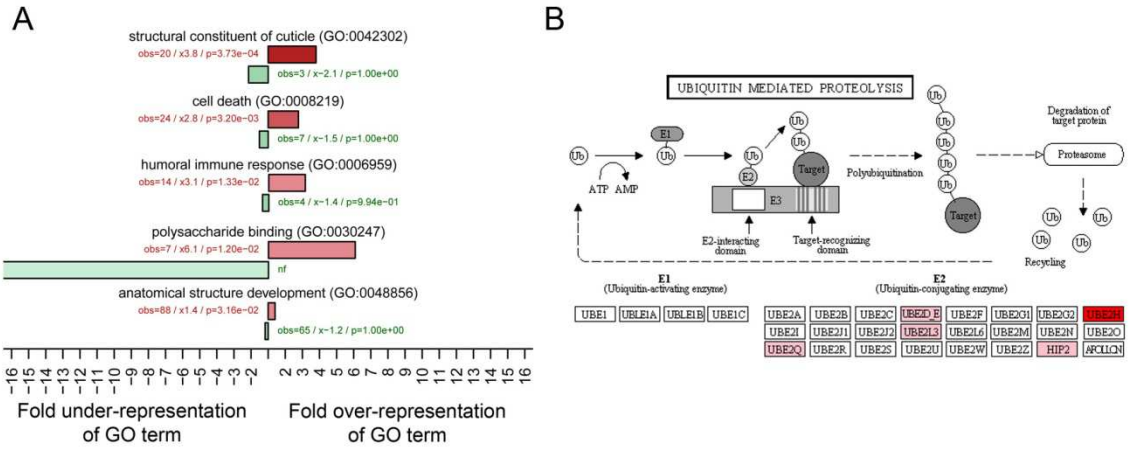

Figure 6. Examples of GeneOntology profiles and KEGG pathways visualization. A) GeneOntology barplots generated by Bioinformatics Unit on data processed with scripts adataped from [24] and [25]. Each bar's length shows that GO term fold under- (left) or over-representation (right) amongst down- (green) or up-regulated (red) genes from cut *D. melanogaster* wing discs at 24 hours compared to 0 hours [26]. obs = observed, x = fold enrichment or depletion (-), p = FDR adjusted p value, nf = not found. B) Upregulated genes (over 1.5x in pink and over 2.0x in red) from *D. melanogaster* dSAP18 mutants [27] shown in Ubiquitin mediated proteolysis KEGG pathways diagram. Only E1 and E2 are shown.

Acknowledgements

V. Gordo, P. Altube, C. Ligero and A. Godoy have implemented GBrowse, mySQL and BLAST server functionality, have developed scripts for automatic database updates and have scaled-up and improved our customized GeneOntology scripts. Thanks to B. Fusté and A. Arasanz (CCiTUB's Genomics Unit) for insightful discussions and help setting up the data processing and quality control pipeline for 454 sequencing data. Thanks also to Suport Informàtic for working towards adapting CCiTUB's resources to deal with big data loads.

References

1. Ben PH. Bioinformatica: een werkconcept. *Kameleon*. 1970;1(6):28-29.
2. Hogeweg P. The roots of bioinformatics in theoretical biology. *PLoS Comput Biol*. Mar 2011;7(3):e1002021.
3. Core. *R: A Language and Environment for Statistical Computing*. Vienna, Austria 2010.
4. Galsworthy M. MEDSUM: an online MEDLINE summary tool
5. Lander ES, Linton LM, Birren B, et al. Initial sequencing and analysis of the human genome. *Nature*. Feb 2001;409(6822):860-921.
6. Venter JC, Adams MD, Myers EW, et al. The sequence of the human genome. *Science*. Feb

2001;291(5507):1304-1351.

7. Bonneau R. The Human Proteome Folding Project
8. Mardis ER. The $1,000 genome, the $100,000 analysis? *Genome Med*. 2010;2(11):84.
9. Shi Y, Tyson GW, DeLong EF. Metatranscriptomics reveals unique microbial small RNAs in the ocean's water column. *Nature*. May 2009;459(7244):266-269.
10. Bell TH, Yergeau E, Martineau C, Juck D, Whyte LG, Greer CW. Identification of Nitrogen-Incorporating Bacteria in Petroleum-Contaminated Arctic Soils Using 15N DNA-SIP and Pyrosequencing. *Appl Environ Microbiol*. Apr 2011.
11. Reyes A, Haynes M, Hanson N, et al. Viruses in the faecal microbiota of monozygotic twins and their mothers. *Nature*. Jul 2010;466(7304):334-338.
12. Project 1G, Durbin RM, Abecasis GR, et al. A map of human genome variation from population-scale sequencing. *Nature*. Oct 2010;467(7319):1061-1073.
13. Genome IC, Hudson TJ, Anderson W, et al. International network of cancer genome projects. *Nature*. Apr 2010;464(7291):993-998.
14. Gentleman RC, Carey VJ, Bates DM,. Bioconductor: Open software development for computational biology and bioinformatics. *Genome Biology*. 2004;5:R80.
15. Pages H, Aboyoun P, Gentleman R, DebRoy S. *Biostrings: String objects representing biological sequences, and matching algorithms*.
16. Stein LD, Mungall C, Shu S, et al. The generic genome browser: a building block for a model organism system database. *Genome Res*. Oct 2002;12(10):1599-1610.
17. Martínez-Rodríguez G, Halm S, Planas J, Beltran S, Yúfera M. Transcriptomic analysis of gilthead seabream larvae by 454 pyrosequencing. Preliminary annotation results., 2010.
18. Altschul SF, Gish W, Miller W, Myers EW, Lipman DJ. Basic local alignment search tool. *J Mol Biol*. Oct 1990;215(3):403-410.
19. Ashburner M, Ball CA, Blake JA, et al. Gene ontology: tool for the unification of biology. The Gene Ontology Consortium. *Nat Genet*. May 2000;25(1):25-29.
20. Kanehisa M, Goto S. KEGG: kyoto encyclopedia of genes and genomes. *Nucleic Acids Res*. Jan 2000;28(1):27-30.
21. Ameur A. BCRANK: Predicting binding site consensus from ranked DNA sequences. 2010.
22. Bembom O. *seqLogo: Sequence logos for DNA sequence alignments*.º
23. Yooseph S, Sutton G, Rusch DB, et al. The Sorcerer II Global Ocean Sampling expedition: expanding the universe of protein families. *PLoS Biol*. Mar 2007;5(3):e16.
24. Beltran S, Blanco E, Serras F, et al. Transcriptional network controlled by the trithorax-group gene ash2 in Drosophila melanogaster. *Proc Natl Acad Sci U S A*. Mar 2003;100(6):3293-3298.
25. Beltran S, Angulo M, Pignatelli M, Serras F, Corominas M. Functional dissection of the ash2 and ash1 transcriptomes provides insights into the transcriptional basis of wing phenotypes and reveals conserved protein interactions. *Genome Biol*. 2007;8(4):R67.
26. Blanco E, Ruiz-Romero M, Beltran S, et al. Gene expression following induction of regeneration in Drosophila wing imaginal discs. Expression profile of regenerating wing discs. *BMC Dev Biol*. 2010;10:94.
27. Costa E, Beltran S, Espinàs ML. Drosophila melanogaster SAP18 protein is required for environmental stress responses. *FEBS Lett*. Jan 2011;585(2):275-280.

Genomics: more than genes

Ramon Seminago[1], Esther Castaño[2], and Amaya Amador[1]

1 Unitat Genòmica, CCiTUB, Universitat de Barcelona. Parc Científic de Barcelona. Baldiri Reixac, 10. 08028 Barcelona. Spain.

2 Unitat de Biologia (Bellvitge), CCiTUB, Universitat de Barcelona. Feixa llarga s/n. 08907 L'Hospitalet de Llobregat, Spain.

email: *ramons@ccit.ub.edu, ecastano@ccit.ub.edu, amaya@ccit.ub.edu*

Abstract. The fundamentals of Real-time Polymerase Chain Reaction, Automated capillary electrophoresis –Sanger sequencing and Fragment analysis– and "Next-generation" sequencing are reviewed. An overview of applications is presented using our own examples carried out in our facility.

1. Introduction

Genomics is the study of the nucleotide sequences – genes, regulatory sequences and non-coding regions – and their functions. The analysis of the pattern of expression and the regulation of the gene expression are also aims of this field. DNA sequencing was the origin and nowadays is the basis of genomics. Sanger sequencing technology has had an impressive influence in biology, and a revolution is occurring with the "Next-generation" Sequencing (NGS). However, other high-impact technologies in biology are closely related to Genomics as Real-time Polymerase Chain Reaction (Real-time PCR) (see Fig. 1). The three technologies presented in this chapter: Real-Time PCR, Automated Capillary Electrophoresis and NGS share some applications such as genotyping, species determination, and others. The best approach for a project is determined by many factors such as the number of samples, prior knowledge of the region or species, complexity of the samples and so forth. It should be highlighted that applications from these technologies reach other research areas since they provide useful genetic tools.

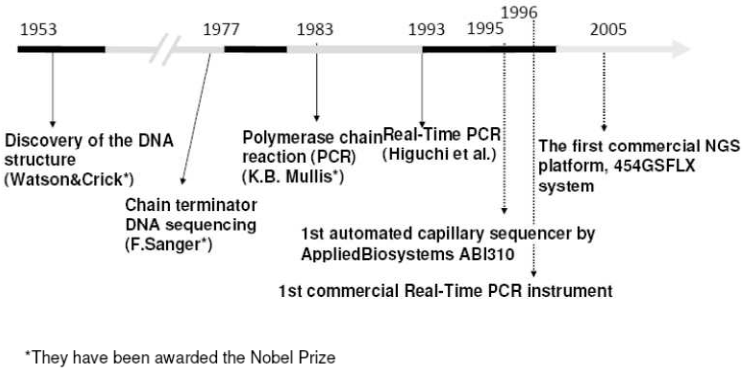

Figure 1: Chronology of technological advances in Genomics.

2. Real-Time PCR (qPCR)

2.1. Instruments of qPCR

The Genomic unit of the CCiTUB has five instruments of Real-Time PCR (qPCR), two SDS7700, two 7900HT and one LightCycler 480 II.

The LightCycler® 480 Real-Time PCR System (see Fig. 2) has an interchangeable 96 well and 384 well plate. The ABI PRISM 7700 has a unique sample block of 96 wells and the 7900HT instrument has an interchangeable 96 well, 384 well and TLDAs. The LightCycler® 480 and 7900HT, can analyze up to 384 samples simultaneously in 2 hours.

Figure 2: LigthCycler 480 II, Sequence Detector System 7900HT. ABI PRISM 7700

2.2. Methodology of qPCR

PCR was developed in 1983 by Kary Mullis[1]. It is a technique capable of generating large amounts of fragments of DNA from single or a few copies of this DNA. PCR, in brief, involves two oligonucleotide primers complementary to the ends of the sequence to be amplified and a heat-stable, Taq polymerase. The PCR consists in three repeated cycles: heat denaturation of DNA, annealing of primers to their complementary sequences of DNA template and a final step of

elongation of annealed primers with enzyme Taq Polymerase. The result is an exponential accumulation of the specific target of DNA, aproximately 2^n, where "n" is the number of cycles of amplification performed.

The quantitation and detection of this target of DNA is performed at endpoint analysis after the reaction has finished with an agarose gel electrophoresis. But this does not allow reliable quantification of the initial sample, probably because at the end point all samples have reached the same amount (plateau phase).

2.2.1. Real Time-PCR (qPCR)

This problem was solved in 1992 when Higuchi et al [2] described the Real-Time PCR (qPCR) with ethidium bromide. This system was an adapted thermal cycler used to irradiate the samples with ultraviolet light, and the detection of the fluorescence was performed with a computer-controlled cooled CCD camera. Amplification produces increasing amounts double-stranded DNA (dsDNA), which binds ethidium bromide, resulting in an increase of fluorescence detected by a CCD camera.

At present, we use other fluorescent molecules such as, TaqMan Probes, SyBr Green, LNA (Locked nucleic Acid), Molecular beacon Probes, Scorpions Primers, QuantiProbes, etc... Taqman Probes and SyBr green are the most widely used.

TaqMan® probe (see Fig. 3) is an oligonucleotide that is complementary to one of the strands of the amplicon and has a fluorescent reporter at the 5' end (FAM, VIC or NED..) and a quencher (TAMRA or Black Hole) at the 3' end. When Taq polymerase extends from the primer, it displaces the 5' end of the probe and it is degraded by 5'-3' exonuclease activitity of Taq polymerase. The reporter is separated from the quencher, and generates a fluorescent signal that increases with each cycle and is proportional to the amount of amplified product.

SyBr Green (see Fig. 4) is a dsDNA intercalating dye, that fluoresces once bound nonspecifically to the dsDNA. The fluorescence of SYBR Green I increases up to 1,000-fold when it binds dsDNA and this is proportional to the amount of dsDNA present.

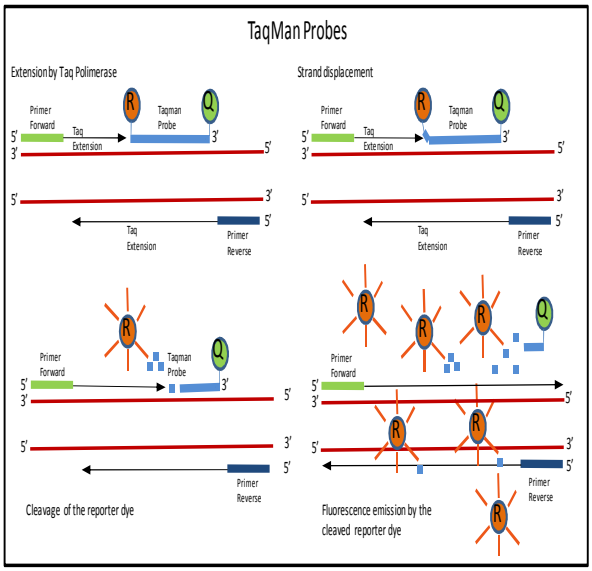

Figure 3: Taqman Probe Workflow

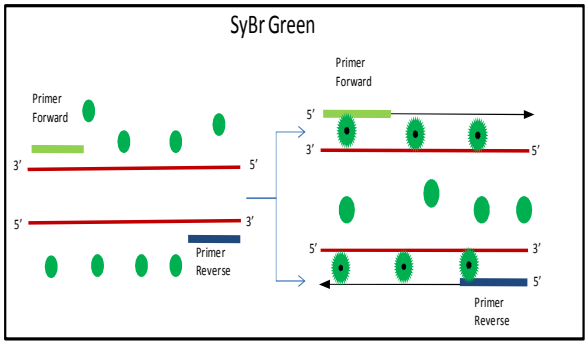

Figure 4: SyBr green workflow

The qPCR process can be divided in two phases; an exponential and a plateau phase (see Fig 5). At the beginning of PCR the fluorescence remains at background levels, there is amplification of DNA but the level of fluorescence is not detectable (cycles 1-15). In the exponential phase, there is enough amplified product to yield a detectable fluorescent signal. Finally, the PCR reaches the plateau phase where no fluorescence increases due to exhaustion of any reagents.

The threshold is the level of signal that reflects a statistically significant increase of fluorescence over the calculated baseline signal. The threshold cycle (Ct in Applied or Cp in Roche) is the intersection between an amplification curve and a threshold in the exponential phase. It is a relative measure of the concentration of target in the PCR reaction. The Ct value is inversely related to the amount of starting template. Therefore, small amounts of template have a high Ct and high amounts of template have a low Ct.

The most common method for relative quantitation is the Livak method [3] or $2^{-\Delta\Delta Ct}$ method, where:

$$\Delta C_{t(test)} = Ct(target) - Ct(endogenous) \qquad \Delta C_{t(control)} = Ct(target) - Ct(endogenous) \qquad \Delta\Delta C_t = \Delta C_{t(test)} - \Delta C_{t(control)}$$

This method relies on two assumptions. The first is that the reaction occurs with 100% efficiency (E = 10 [–1/slope]) and the second assumption is that there is an endogenous gene (or genes) that is expressed at a constant level between the samples.

When the efficiency is not 100% or there are differences between the genes, we use the Pfaffl method [4]:

$$Ratio = \frac{(E_{target\ gene})^{\Delta C_t \text{ target gene } (C_t \text{ Control- } C_t \text{ test})}}{(E_{endogenous\ gene})^{\Delta C_t \text{ endogenous gene}(C_t \text{ Control- } C_t \text{ test})}}$$

where E_{target} and $E_{endogenous}$ are the amplification efficiency of target gene and endogenous gene respectively. The result is the ratio of the target gene in the test sample to the calibrator sample, normalized to the expression of the reference gene.

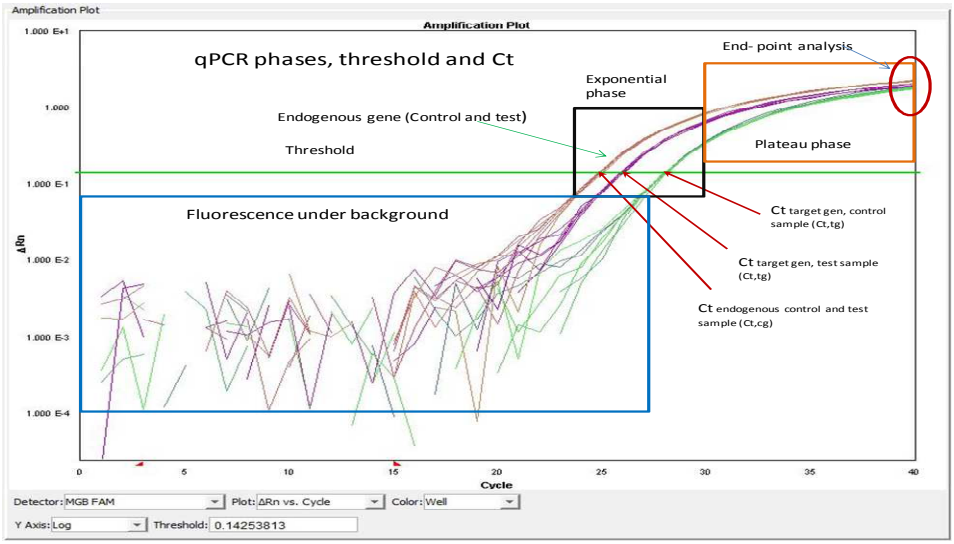

Figure 5: qPCR phases and concepts threshold and Ct

2.3. Applications of qPCR

qPCR systems can support different application or assay types. These assays can be divided into two categories (quantitative real-time PCR assays and endpoint assays) based on the time point during the assay at which data are being collected. Real time classical applications are absolute quantification or relative quantification.

2.3.1. Absolute Quantification

- *Microorganism quantification.* qPCR is considered as a method of choice for the detection and quantification of microorganisms. One of its major advantages is that is faster than conventional culture-based methods. It is also highly sensitive, specific and enables simultaneous detection of different microorganisms. For example, accurate quantification

is of prime importance for most food microbiology applications [5] or in correlating viral copy number with disease state.

- *Detection of genetically-modified organisms (GMO).* Several techniques have been developed for detection and quantification of GMO but qPCR is by far the most popular approach [6].

2.3.2. Relative Quantification

- *Gene expression.* In relative quantitation, changes in gene expression in a given sample relative to another reference sample (such as an untreated control sample) are analyzed. Because of the qPCR sensitivity and broad dynamic range, qPCR is frequently used to validate the results of microarray and next-generation sequencing-based gene expression profiling experiments [7].
- *MicroRNAs (miRNAs)* are a class of naturally-occurring noncoding RNAs that play a role in gene regulation. qPCR and microarray hybridization approaches as well as ultra high throughput sequencing of miRNAs (small RNA-seq) are popular and widely used profiling methods [8].
- *Copy-Number Variations (CNV).* Copy-number changes are known to be involved in numerous human genetic disorders. In this context, qPCR-based copy number screening may serve as the method of choice for targeted screening of the relevant disease genes and their surrounding regulatory landscapes [9].
- *Single cells.* Interest in single cell molecular analysis has risen dramatically over the last couple of years, chiefly because single cell molecular analysis is the only way to research genetic heterogeneity, i.e., differences in copy number or gene expression levels between individual cells, or genetically analyze very rare cells such as circulating tumor or fetal cells. Multiplex single-cell qPCR can be used to examine the expression of multiple genes within individual cells [10].

2.3.3. End-point detection

- *Allelic discrimination*: is a multiplexed end-point assay that detects variants of a single nucleic acid sequence. A common approach is to use hydrolysis (TaqMan) probes. The presence of two primer/probe pairs in each reaction allows genotyping of the two possible variants at the single-nucleic polymorphism (SNP) site in a target template sequence [11,12]. One fluorescent dye detector is a perfect match to the wild type (allele 1) and the other fluorescent dye detector is a perfect match to the mutation (allele 2).
- *High Resolution Melting (HRM)* analysis is a new, post-PCR analysis method used for identifying genetic variation in nucleic acid sequences (mutations, methylations, SNPs) in PCR amplicons. Simple and fast, HRM characterizes nucleic acid samples based on their disassociation (melting) behavior [13].

2.4. Examples of applications

2.4.1. Gene expression: Analysis of ubiquitin C-terminal hydrolase-1 expression levels in dementia with Lewy bodies

In the reported example [14], Real-Time PCR has been applied to test UCHL-1 gene expression in post-mortem frontal cortex of PD and DLB cases, compared with agematched controls. Parkinson disease and dementia with Lewy bodies are characterized by the accumulation of abnormal a-synuclein and ubiquitin in protein aggregates conforming Lewy bodies and Lewy neurites. Ubiquitin C-terminal hydrolase-1 (UCHL-1) disassembles polyubiquitin chains to increase the availability of free monomeric ubiquitin to the ubiquitin proteasome system (UPS) thus favoring protein degradation. TaqMan PCR assays demonstrated down-regulation of UCHL-1 mRNA in the cerebral cortex in DLB (either in pure forms, not associated with Alzheimer disease: AD, and in common forms, with accompanying AD changes), but not in PD, when compared with age-matched controls (Fig. 6).

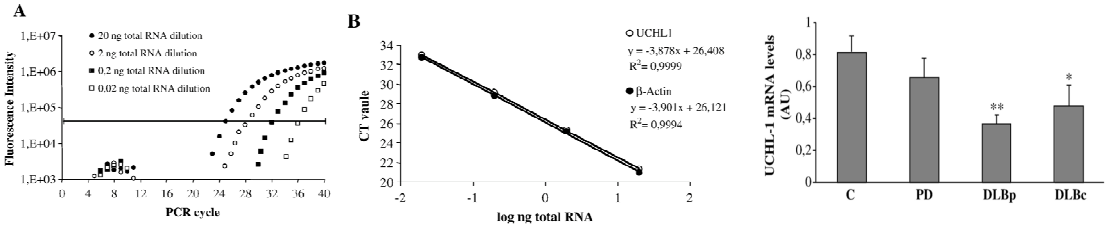

Figure 6: (A) Amplification plot of UCHL-1 using serial dilutions of control human brain RNA.The horizontal line represents the threshold line adjusted manually. (B) Representative standard curves for h-actin and UCHL-1 constructed from several concentrations of control human brain RNA. Ct values (y axis) vs. log of several RNA concentrations of control samples (x axis) show a reverse linear correlation. (C) Relative UCHL-1 gene expression in the frontal cortex of controls (C, n = 6), Parkinson's disease (PD, n = 6), Dementia with Lewy bodies, pure form (DLBp, n = 7) and common form (DLBc, n = 6). (C) UCHL-1 mRNA levels (mean T SEM) normalized with h-actin. *P < 0.05 and **P < 0.01 compared to control samples (ANOVA with post hoc LSD test).

2.4.1. Copy Number Variation and Allelic Discrimination: Lack of association between lipoprotein ((a) genetic markers and coronary heart disease in HIV-1-infected patients

BT.6

General population studies have shown associations between Copy Number Variation (CNV) of the LPA Kringle-IV type-2 (KIV-2) coding region, associated SNP and the CHD. The aim of the study was to confirm these associations in our HIV-1 cohort.

72 HIV patients were included. Genomic DNA was isolated from blood frozen at -20ºC. A multiplex qPCR was carried out using TaqMan technology for *LPA* KIV-2 and single-copy reference gene *RNaseP* in order to perform absolute quantifications. CopyCaller software (Applied Biosystems) was used for relative quantifications (See Fig 7). Allelic Discrimination was performed using TaqMan SNP Genotyping Assay (See Fig. 8). Fisher's exact test was used for comparisons.

No statistically significant differences were found between cases and controls in terms of CNV (p=0.66) neither in the SNP genotyping (p=0.58).

The clinical utility of these biomarkers to predict CHD in HIV population remains unclear.

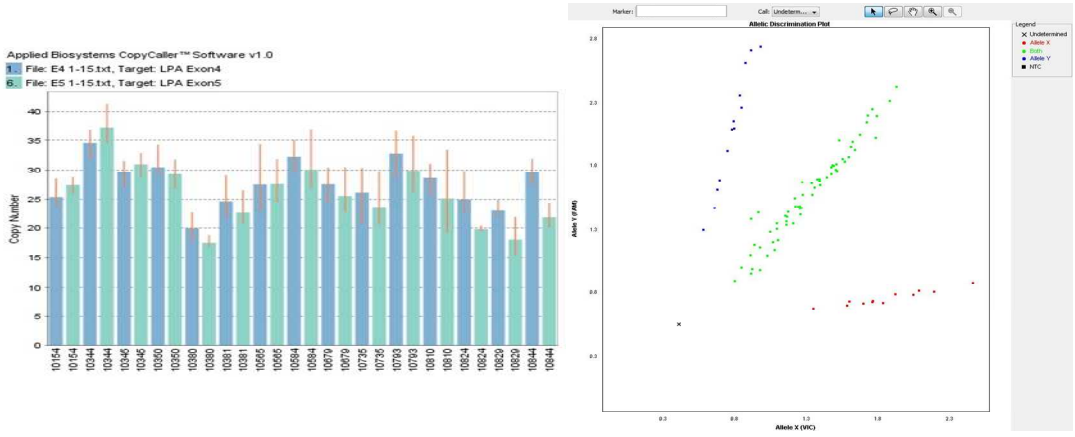

Figure 7: Copy Caller Software (Applied Biosystems) **Figure 8**: Plot of Allelic Discrimination

2.4.3. Quantitative detection of Lactarius deliciosus extraradical soil mycelium by real-time PCR and its application in the study of fungal persistence and interspecific competition

Real-Time PCR has been applied to quantify extraradical soil mycelium of edible ectomycorrhizal fungi [15,16,17,18]. Taqman probes and specific primers have been designed for the amplification of the ITSrDNA region of *Lactarius deliciosus*, *Boletus edulis* and *Tuber melanosporum*. The quantification of fungal mycelium allowed for undertaking studies on fungal persistence, seasonal

abundance of extraradical mycelium and interspecific competition. Basic protocols involved genomic DNA extraction to perform real-time PCR analysis. DNA extractions from soil mixed with known amounts of mycelium of the target fungus were used as standards. Significant correlations between mycorrhizas and ectomycorrhizal fungal mycelium were found whereas no relationship was observed between soil mycelium and fruit body production. Factors as soil type, soil depth and season influenced the amount of fungal mycelium recovered from soil.

Quantitative PCR is a powerful technique for extraradical mycelium quantification in studies aimed at evaluating the persistence of a target fungi in field plantations established with inoculated plants. Also, the positive relationship found between the vegetative phases of the symbiosis (mycorrhizas and extraradical mycelium) allowed to establish a non-destructive method for controlling fungal persistence in the field.

2.4.4. Identification of Variable Number Tandem Repeats (VNTRs) by High Resolution Melting (HRM)

The aim of this study is describe a screening method for the detection of both heterozygous and homozygous VNTR.

All samples were extracted with the same method from buccal swaps and were diluted to the same DNA concentrations. We test the optimum $MgCl_2$ with a dilution series, and the optimum is the lowest concentration resulting in high yield of target PCR products and no unspecific products. The HRM protocol was performed and monitored in a Light Cycler 480 II.

We show that it is possible to use HRM to distinguish heterozygous and homozygous VNTRs (See Fig. 9).

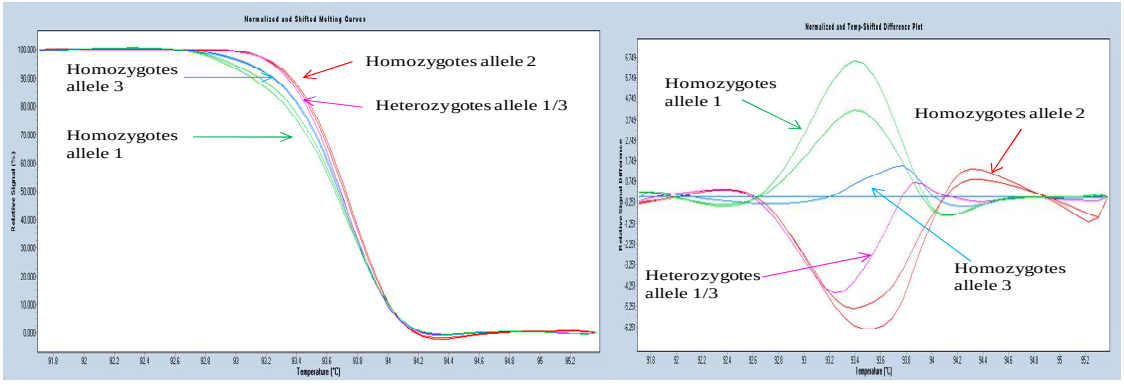

Figure 9: Plots of Normalized and shifted melting curve, and Normalized and Temp-Shifted Difference plot

3. Automated capillary electrophoresis (ACE)

Capillary electrophoresis and automated detection of fluorescently tagged DNA fragments (ACE) is the common instrumentation for DNA sequencing by Sanger chain terminator dideoxy method and Fragment analysis. Electrophoresis is a largely used technique in molecular biology. The application of an electric field produces the movement of the negatively charged DNA molecules through a polymer from the cathode to the anode and they are separated according to size. The smaller fragments run faster than the larger fragments. The DNA fragments have been previously labeled with fluorescent dyes so they are detected by the excitation of a laser beam at the end of the capillary (see Fig. 10). The Genomics Unit has two sequencers, a 48-capillary 3730 DNA Analyzer and a 96-capillary 3730*xl* DNA Analyzer (Fig. 11). The 3730*xl* can analyze up to 96 samples simultaneously in 2 hours (1152 samples/day, 980 Kbases with high quality 850 QV20 bases).

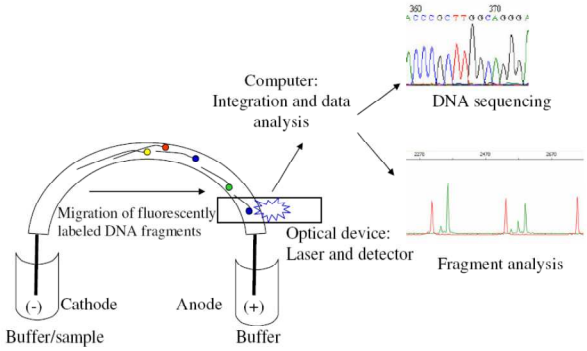

Figure 10: Scheme of the ACE and detection in automatic sequencers

Figure 11: 3730 and 3730*xl* DNA Analyzers at the CCiTUB.

3.1. Methodology and applications

3.1.1. Sanger dideoxy sequencing method

This method, also called the chain terminator method [19], is based on the synthesis of DNA in vitro with an optimized mix of deoxynucleotides (dNTPs) and modified nucleotides, dideoxynucleotides (ddNTPs). The incorporation of ddNTPs prevents the formation of the phosphodiester bridge with the previous dNTP so the DNA synthesis is stopped. Since there are billions of copies of the DNA template, the sequencing reaction results in a collection of DNA molecules of different length that differ in one nucleotide in size and terminate with a ddNTP. The electrophoresis separates the DNA molecules by size. DNA template can be PCR fragments, cDNA, gDNA or clone constructs.

The original method has been improved by the use of a thermally-stable DNA polymerase (PCR-like), the labelling with distinct fluorescent dyes and the ACE (see Fig. 12).

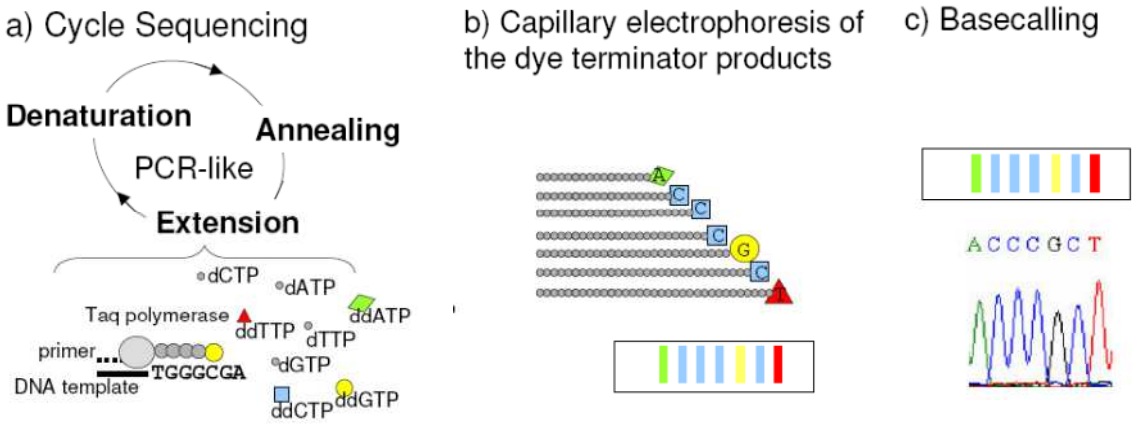

Figure 12: Schematic diagram of dye terminator cycle sequencing

3.1.2. Fragment analysis

Fragment analysis estimates the size for DNA fragments amplified by PCR with fluorescently labeled primers. The sample is pooled with a size standard of DNA fragments with known lengths, electrophoresed and detected together (see Fig.13).

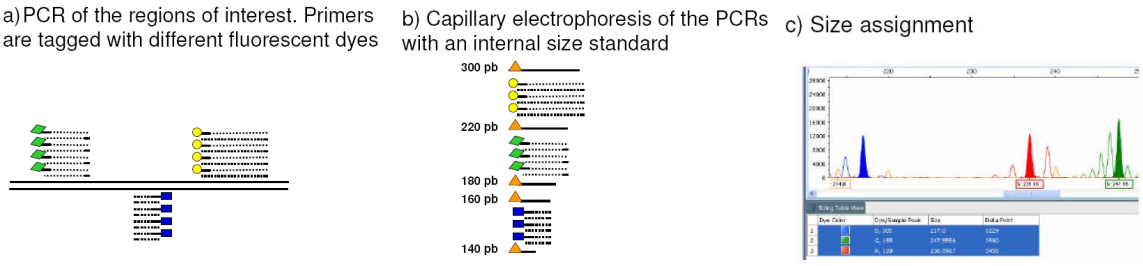

Figure 13: Schematic diagram of Fragment analysis

The Fragment analysis results are band patterns. The analysis of these profiles and their changes are used in a variety of applications as genotyping of individuals or strains, identification of species, linkage mapping studies, disease association studies, paternity testing and others (see Table 1).

Table 1: Main applications of ACE

	DNA sequencing	Fragment Analysis
	De novo sequencing of genomes Checking of clone constructs	
Genotyping and genetic variation	SNPs*, indels** and other structural variants	Microsatellites Analysis, Fragments Length Polimorphisms+
Gene Expression Analysis	mRNA sequencing: active genes, alternative splicing, ESTs§... Epigenetics :Methylation analysis	
Strains and Species identification	Resequencing	Microsatellites Analysis Fragments Length Polimorphisms
Linkage mapping and association studies	Resequencing	Microsatellites Analysis Fragments Length Polimorphisms

*SNPs (Single Nucleotides Polymorphisms) ** Indels (insertions-deletions), +Fragments Length Polimorphisms: AFLPs (Amplified fragment length polymorphisms), RFLPS (Restriction fragment length polymorphisms), MLPAs (Multiplex ligation-dependent probe amplifications), ESTs§ (Expression Sequences Tag).

3.2. Examples of applications

3.2.1. Nucleotide variation at the "Insuline-like" receptor (InR) gene in Drosophila

Population genetics studies the level and patterns of nucleotide variability. The major evolutionary processes are natural selection, genetic drift, mutation and migration. Most of the empirical data in this field comes from DNA sequencing. The *InR* gene is the first component of the highly conserved insulin-signaling pathway. It is known the influence of this pathway in processes as intermediary metabolism, reproduction, aging and growth. The variation of *Inr* might affect many phenotypic traits. The level and pattern of variation for the *InR* region has been analysed in *D. melanogaster*. PCR fragments of ~8-kb long (or alternatively two overlapping PCR fragments of ~5-kb long) that encompassed the *InR* gene were cycling sequenced and analysed by ACE [20] in eight lines of *D. melanogaster* and one line of *D. simulans* (see Fig. 14)

3.2.1. DNase I footprinting assay by ACE (DFACE)

This is an unusual application of ACE that combines Analysis of fragments and DNA Sequencing. DNase I Footprinting assay is used to study DNA protein interactions and identify the specific binding DNA sequence of the proteins. This technique is performed for analysis of the transcription factors in studies of regulation of gene expression. Briefly, a labelled probe of DNA (about 100-600 bp) that contains the region of interest is incubated with an extract of protein under test and followed by controlled digestion with DNase I. The enzyme only cuts the regions free of bounded protein. The digestion product is electrophoresed. The comparison of the DNase I digestion patterns with the protein extract, in the absence of protein and with a sequencing region of the DNA probe allows the identification of protected regions (seen as gaps in the footprint) due the interaction of the protein with the DNA.

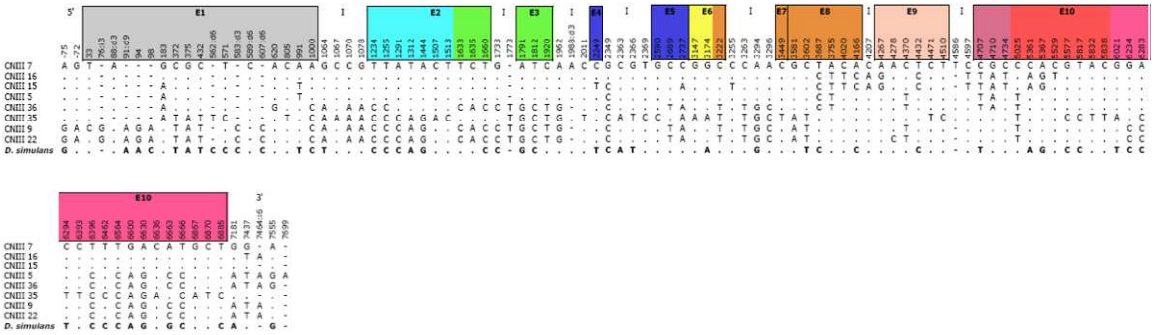

Figure 14: Nucleotide polymorphisms at the *InR* gene in .*D. melanogaster* and *D. simulans* Numbers at the top correspond to the position from the *InR* translation start codon. Dots indicate nucleotide variants identical to the first sequence. Dashes indicate gaps. For length polymorphisms, the position indicates the first affected site. d, deletion; i, insertion. E, exon; I, intron. Exons are denoted by numbers. Figure modified from [20].

In DFACE the classical radioactive label of the DNA probe and polyacrylamide gel electrophoresis is replaced by a fluorescent dye and ACE [21]. The analysis of the fragment pattern is performed with the Genemapper software. Figure 15 shows an example of validation of a DNAse I footprint assay of the transcription factor *Adf-1* of the *Adh* (Alcohol dehydrogenase) gene promoter in Drosophilidae [22].

BT.6

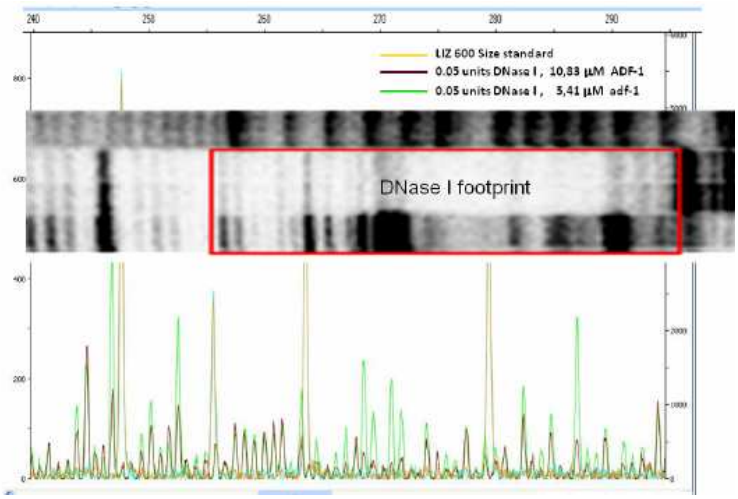

Figure 15: Comparison of DNase I footprinting of the transcription factor *Adf-1* of the *Adh* (Alcohol Dehydrogenase) gene promoter in Drosophilidae using a radioactive labeled probe and a polyacrylamide gel with the DNase I footprint obtained with the same FAM labeled probe and ACE in the 3730 DNA Analyzer. Figure is courtesy of E. Juan.

3.2.3. Microsatellites analysis in biodiversity and conservation studies

The use of molecular genetic techniques is common in other different fields of genomics and biomedicine. Fragment analysis is a useful tool for ecological studies. In particular microsatellites analysis are widely used in biodiversity and conservation studies. A microsatellite or short tandem repeat (STR) is a sequence of 2-7bp repeated tandemly distributed widely throughout the eukaryotic genomes. The number of repeats is highly variable.

The Genomics Unit has participated in the performance of a paternity determination of 12 microsatellites markers for 200 individuals, adults and chicks, from different locations of two subspecies of a game bird (see Fig. 16). Conclusions about mating choice, behavior, hybridization between wild and domesticated subspecies will arise from the post-analysis of these results (unpublished data). This kind of information is useful to game bird management.

4. Next-generation Sequencing

Sanger sequencing method has been preeminent in the last 30 years until the sudden appearance of the Next-generation sequencing (NGS). NGS, also called Massive Parallel Sequencing (MPS), are a group of diverse sequencing technologies that share two important features: no bacterial cloning in the preparation of the DNA template and a huge throughput of sequence data at a significantly decreased cost.

4.1. Instrumentation and chemistry

The Genomics Unit is equipped with the platform 454 Genome Sequencer FLX (Roche) (see Fig. 17). This platform is based in the miniaturization of pyrosequencing reactions [23] that occur simultaneously. One run produces 400Mb or more than 1 million high-quality reads of 400 bp of length. Each of the reads obtained comes from one molecule of DNA.

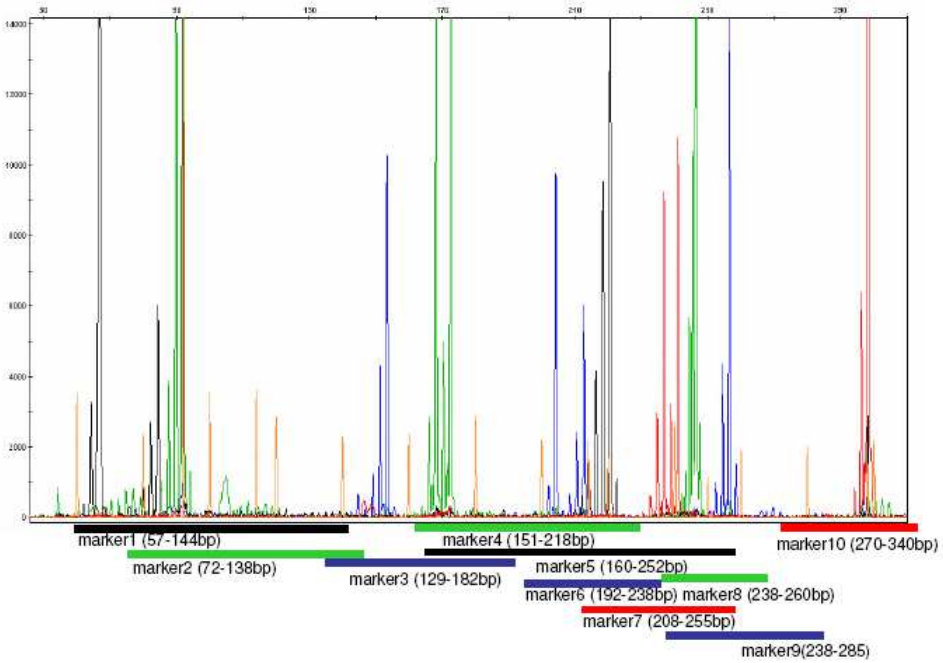

Figure 16. Plot of a multiplex PCR of 10 microsatellites markers of an individual. The colored bars below the peaks correspond to the size range of the microsatellites. Some ranges overlap but markers are distinguished by their fluorescent label.

Figure 17: 454 GS FLX (Roche)

The template preparation consists in the generation of a library of fragments with adaptors. Then they are bound to beads (one DNA molecule per bead) and clonally amplified by PCR into droplets of an oil-aqueous emulsion (emPCR). The adaptors contain the sequences needed to link to beads, to purify and enrich the amplified beads and to sequence them. After the emPCR, beads

carrying amplified DNA are purified and loaded into a special microwell plate (PTP, PicoTiterPlate), one bead per well. There 1 million of pyrosequencing reactions take place in parallel. The emissions of light from each well are recorded by a CCD camera, the image is processed and converted in flowgrams (see Fig. 18).

Bionformatics tools are needed in order to manage and analyse the overwhelming amount of obtained data.

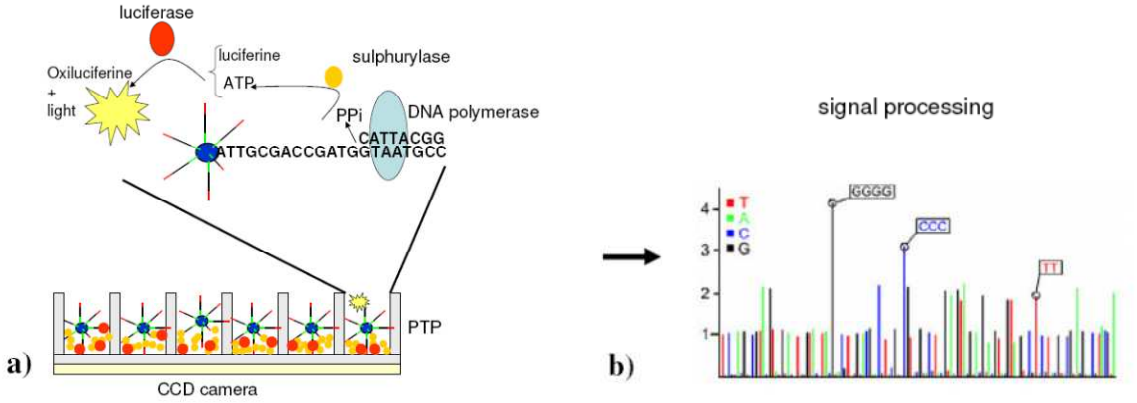

Figure 18: **a)** Schematics of the Pyrosequencing reaction. Cyclic flows of nucleotides are performed in a determined order. If the nucleotide flowed into the well is complementary to the synthesized DNA strand it is incorporated and a pyrophosphate (PPi) is released. An enzymatic cascade is coupled and generates a final emission of light whose intensity is directly proportional to the number of nucleotides incorporated in a single flow. Each bead contains millions of copies of a single fragment. **b)** The light signals are recorded and processed into flowgrams.

4.2. Applications

NGS technology has a broad range of applications in diverse fields of biology but the own special characteristics in read length, throughput and read accuracy of diverse platforms make some of them more suitable than others for particular applications. The greatest asset of 454 GS FLX is its long read length, about 450 bp up to 1000 bp with the latest improvements, so *de novo* genome and transcriptome sequencing are its main applications (see Table 2).

Table 2: Main applications of 454 GS FLX

De novo whole or partial genome
Resequencing
Ancient DNA and Paleobiology
Metagenomics: species identification and gene discovery
Transcriptome
Methylation/Epigenetics

Acknowledgments

The authors would like to thank Dr. Marta Barrachina, Dr. Isidre Ferrer, for allowing to use their gene expression results (Figure 6), Dr. Lander Egaña and Dr. Mireia Arnedo for their CNVs and SNPs unpublished results, Dr. Xavier Parlade for his absolute quantification results, Dr. M. Aguadé for her example of nucleotide variability, Dr. E. Juan for allowing to use her DFACE results and I. Sánchez Donoso for her collaboration in the example of microsatellites analysis.

References

[1] Mullis K. B; Faloona F. A; Scharf S; Saiki R. K; Horn G; Erlich H. A., 1986. Cold Spring Harbor Symposia on Quantitative Biology,
[2] Higuchi, R., Dollinger, G., Walsh, P. S., and Griffith, R. 1992. Biotechnology 10:413–417.
[3] Kenneth J. Livak and Thomas D. Schmittgenb Methods 2001 Vol 25, Issue 4,402-408
[4] Pfaffl MW 2001 RT-PCR. Nucl. Acids Res, 29: 2002-2007
[5] Postollec F., et al..2011. Food Microbiology 28: 343-861.
[6] Gasparic B., Tengs T, LaPaz JL., Holst-Jensen A., Pla M., Esteve T., Zel J., Gruden K. (2010). Anal Bioanal Chem 396:2023-9
[7] VanGuilderHD., Vrana KE., Freeman WM.2008. Biotechniques 44:619-26
[8] Benes V., Castoldi M. 2010.Methods 50:244-9.
[9] D'haene B, Vandesompele J, HellemanJ 2010 Methods 50 : 262–270
[10] Bengtsson M, Hemberg M, Rorsman P, Stahlberg A.2008 Mol Biol 9:63
[11] Afonina, I., Zivarts, M., Kutyavin, I., et al.1997. Nucleic Acids Res. 25:2657–2660.
[12] Kutyavin, I.V.et al.1997 Nucleic Acids Res. 25:3718–3723.
[13] Reed GH, Kent JO, and Wittwer CT (2007) Pharmacogenomics 8:597–608.
[14] M. Barrachina, E. Castaño, E. Dalfó, T. Maes, C. Buesa, and I. Ferrer 2006 Neurobiology of Disease 22 265 – 273 265 – 273.
[15] Parladé, J.; Hortal, S.; Pera, J.; Galipienso, L.. 2007. *Journal of Biotechnology* 128: 14-23
[16] Hortal, S.; Pera, J.; Parladé, J. 2008. *Mycorrhiza* 18: 69-77.
[17] Hortal, S.; Pera, J.; Parladé, J. 2009 *Mycorrhiza* 19:167–177.
[18] De la Varga, H.; Águeda, B.; Martínez-Peña, F.; Parladé, J.; Pera, J. 2011. Mycorrhiza DOI 10.1007/s00572-011-0382-2
[19] Sanger F., Nicklen S., Coulson, A. R. 1977 *Proc. Natl. Acad. Sci (USA)* 74: 5463-5467
[20] Guirao-Rico S and Aguadé M. 2009 Mol. Biol. Evol. 26(8)1723-1732.
[21] Zianni M. et al. 2006 . 17: 103-113.
[22] Lang M. and Juan E. 2010 *Nucleic Acids Res.*38(19):6404-6417.
[23] Hyman, E.D. 1988. Anal. *Biochem.* 174: 423–436.

"Next-generation" Sequencing (NGS): The new genomic revolution

Berta Fusté

Unitat Genòmica, CCiTUB, Universitat de Barcelona. Parc Científic de Barcelona. Baldiri Reixac, 10. 08028 Barcelona. Spain.

email: *bfuste@ccit.ub.edu*

Abstract. In the past 5 years "Next-generation" Sequencing (NGS) technologies have transformed genomics by delivering fast, inexpensive and accurate genome information changing the way we think about scientific approaches in basic, applied and clinical research. The inexpensive production of large volumes of sequence data is the main advantage over the automated Sanger method, making this new technology useful for many applications. In this chapter, a brief technical review of NGS technologies is given, along with the keys to NGS success and a broad range of applications for NGS technologies.

1. Introduction

Nearly three decades ago Fred Sanger [1] and Wally Gilbert [2] received the Nobel prize for chemistry sequencing technology (see Automated electrophoresis Technique in "Genomics: More than genes" in this issue). This technology known as "Sanger Sequencing" or "First-generation sequencing" has dominated the industry for almost two decades and led to a number of accomplishments, including the completion of the human genome sequence. In 2004, the International Human Genome Sequencing Consortium reported a genome sequence with high accuracy and nearly completed coverage of the human genome [3]. The approach consisted in "Sanger sequencing" more than 20.000 large bacterial artificial chromosome clones in which each one contained 100 kb fragments of the human genome. This project was performed during 10 years with multiple groups and companies participating. Although many technical improvements were achieved in this era, like automated capillary electrophoresis among others, new inventions were needed for sequencing large numbers of genomes. Recent efforts have been directed towards new methods known as "Next-generation" sequencing (NGS) technologies, which are capable to sequence a complete human genome in one week. In 2004, the 454 FLX Pyrosequencer from Roche was the first NGS sequencer to become commercially available [4]. The Solexa 1G Genetic Analyzer from Illumina was commercialized in 2006 [5]. The SOLiD System from Applied Biosystems was launched in 2007 [6]. Most recently, a "Third-generation" of sequencers has emerged. The HeliScope from Helicos BioSciences started shipping in early 2008 [7] and PacBIO RS from Pacific Biosciences in 2010 [8]. Although the first new technology appeared in 2004 more than 1000 next-generation sequencing-related manuscripts have appeared in the literature. NGS technology is not only changing our sequencing approaches and lowering the associated time and costs, it is also opening a wide variety of applications, types of biological samples, and new areas of biological inquiry.

2. Methodology

2.1. Principles of NGS technology

The principle of the NGS technologies can be summarized as the sequencing of a multiple-parallel array of DNA features using interactive cycles of enzymatic manipulation and imaging-based data collection [9]. Although the different platforms are quite diverse in sequencing biochemistry and generating the array, their work flow is conceptually similar. The first step consists in Library construction which is achieved by random fragmentation of DNA, followed by an *in vitro* ligation of common adaptor sequences. The second step implies the generation of clonally clustered amplicons to serve as sequencing templates. Polymerase Chain Reaction (PCR) amplicons derived from a single library molecule end up spatially clustered, either to a single location on a planar substrate (bridge PCR [10, 11], or to the surface of micron-scale beads, which can be recovered and arrayed (emulsion PCR [12]). Subsequently, the sequencing process itself consists of alternating cycles of enzyme-driven biochemistry and imaging-based data acquisition (Figure 1). Most of the platforms use sequencing by synthesis, that is, serial extension of primed templates, but the enzyme driving the synthesis can be either a polymerase [13] or a ligase [14]. Data are acquired by imaging of the full array at each cycle.

Besides their technical differences, other main concepts differ between platforms are: length of the generated sequences, production capacity that each platform can achieve per run, real-time DNA sequencing, and no need to amplify the sample before sequencing. These important points can lead to choosing one platform or other depending on the organism, application or expected result. Among the NGS platforms, the FLX-GS from Roche is the only one capable to generate long reads (average fragment length is around 400bp) but its sequencing capacity is low (350-400Mb). On the contrary, other platforms get their strength in their sequencing capacity. HighSeq 2000 from Illumina generates up 200Gb per run and 5050XL SOLiD system produces up to 20-30 Gb per day with the inconvenience that their fragment length is among 50-100bp. This is an important issue in order to determine which platform is optimal for your experiment. For example,

if a biological sample is an unknown genome, longer reads are needed to assemble it, but if your sample has a reference genome available and the study consists in variation discovery in individuals, high sequencing capacity plays a key role. On the other hand, creating great expectations, and already in the final experimental stage, are the "Third-generation" sequencers. This is the case of the new Real-time sequencing machine from Pacific BioSciences, which harnesses the natural activity of key enzymes involved in the synthesis and regulation of DNA, RNA or proteins. Also, there is the HelicoScope, which ADN amplification is not needed before sequencing, this being really interesting to avoid amplification bias, although in the present its fragment average-length is too short.

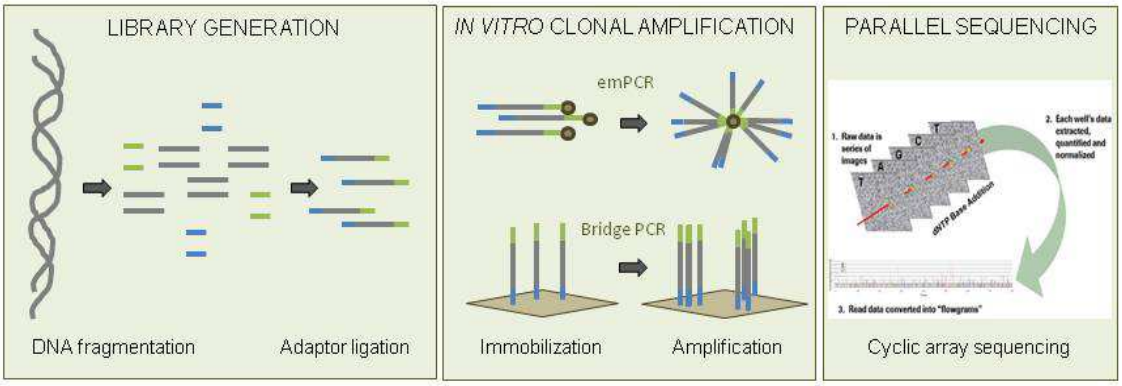

Figure 1: Work flow of Next Generation of DNA Sequencing.

2.2 Keys to NGS success: NGS vs. Sanger

Under standard conditions, Sanger sequencing results in a read length between 700-1000 bases. These are relatively long read lengths compared with NGS methods (400bp-Roche, 75bp-Solexa and 50bp-SOLiD). However, first generation sequencing is limited by the small amounts of data that can be processed per unit of time. The major advance offered by NGS is the ability to produce an enormous volume of data inexpensively [15]. In fact, the first version of the 454's instrument could easily generate a throughput equivalent to that, or more than 50 Applied Biosystem's 3730XL at about one-sixth of the cost [16]. The array based sequencing approach, where hundreds of millions of reads are obtained in parallel on a small area, lows the cost of DNA sequence production since the same reagent volume is used for all the sequences at once (Figure 2).

Another important point is the *in vitro* construction of a sequencing library, followed by *in vitro* clonal amplification to generate sequencing features, avoiding "*E. coli*" transformation and colony picking. Both steps are possible thanks to the common adaptors ligated in the library construction. These adaptors are also the responsible to extremely reduce the time, and consequently the cost of sequencing.

The accuracy, the degree to which a reconstructed sequence is free from errors, is one of the topics that can be considered as a disadvantage of NGS vs. Sanger sequencing although the greater output overcomes this challenge. NGS platforms can produce high number of reads providing greater depth and sequence confidence. Controversially, this great output from NGS technology comes with data management and analysis challenges. Significant computational infrastructure is required to process raw data generated by the sequencers and assemble or align them into contigs or scaffolds. But not only the computational infrastructure is a problem, a limited set of applications are covered with the instrument manufacturers software, and the need of specialized bioinformatitians is crucial for the success of this technology (see "Bioinformatics: making large-scale science happen" in this issue).

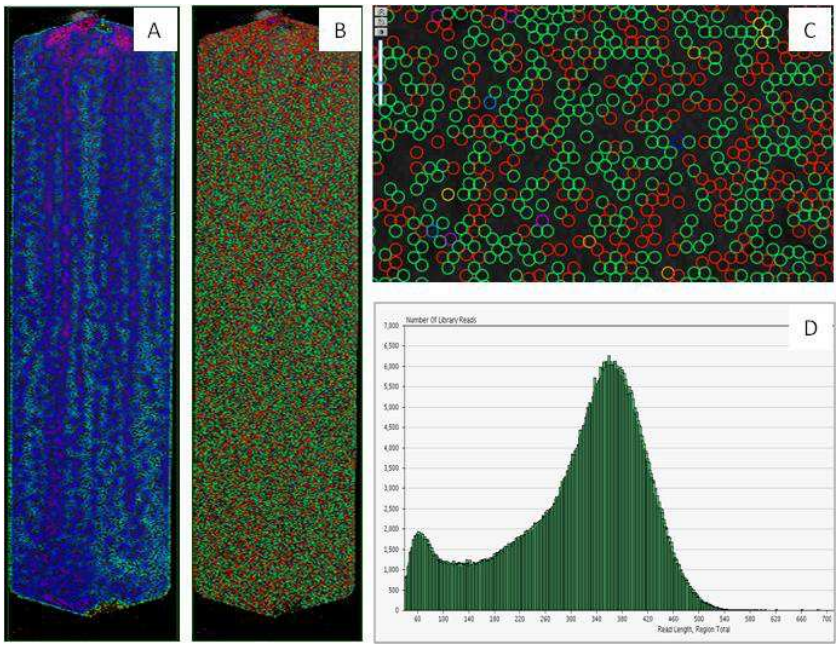

Figure 2. Results obtained from a run performed in a GS-FLX instrument from Roche at the Genomic Unit, CCiTUB. The fluidics subsystem ensures accurate reagent dispensing and flows the sequencing reagents across the wells of the PicoTiterPlate device. Panel A shows raw density of the beads load in a PicoTiterPlate. Panel B represents the quality control of all the reads sequenced in the same run. Panel C is an augmented area of a PicoTiterPlate: green circles represent pass filter wells, red circles are beads that contain the key pass (common adaptor) but the quality control considers that this reads are not good, blue and orange are control beads and purple represents empty beads, no common adaptor has been ligated. Chart D shows all the reads from a GS-FLX run and their distribution by length (bp).

3. Examples of applications

"Next-generation" DNA sequencing is accelerating biological and biomedical research, by enabling the comprehensive analysis of whole genomes, transcriptomes, and interactomes to become inexpensive, routine and wide spread [17]. Important applications include novel whole genomes and transcriptomes sequencing, full-genome resequencing or more targeted discovery of mutations or polymorphisms, mapping structural rearrangements, DNA-protein interactions through chromatin immunoprecipitation sequencing, gene expression, discovering noncoding RNAs, ancient genomes, metagenomics, and other applications that will appear over the next few years.

3.1. Novel whole genomes and transcriptomes sequencing

When we talk about genomic revolution, this is one of the applications that better shows the concept. During the last decade only researchers interested in human, rat, mouse and a few more had the genomic tools to develop their research since a reference genome and kits were available. NGS brings the opportunity to sequence what you want because no sequence knowledge is needed and it is relatively inexpensive and fast. For example, characterizing transcripts through sequences rather than through hybridization to a chip is advantageous in many ways, most importantly, because the sequencing approach does not require the knowledge of the genome sequence as a prerequisite and new transcripts can be described. From our experience in the Genomic Unit of the CCiTUB, a good strategy for a *de novo* transcriptome project consists in normalize the cDNA to generate full-length-enriched double stranded (ds) cDNA with equalized concentrations of different transcripts [18]. The cDNA normalization enhances the potential of the GS-FLX sequencing technology, since the equalized cDNA library can be sequenced without having an enormous

amount of repeated transcripts and obtaining a wide range of interested transcripts represented (Figure 3). Once this information is assembled and annotated, new genomic tools can easily be created (custom arrays, another NGS runs, Real-time PCR (see RT-PCR technology "Genomics: More than genes" in this issue)) to study gene expression under different conditions.

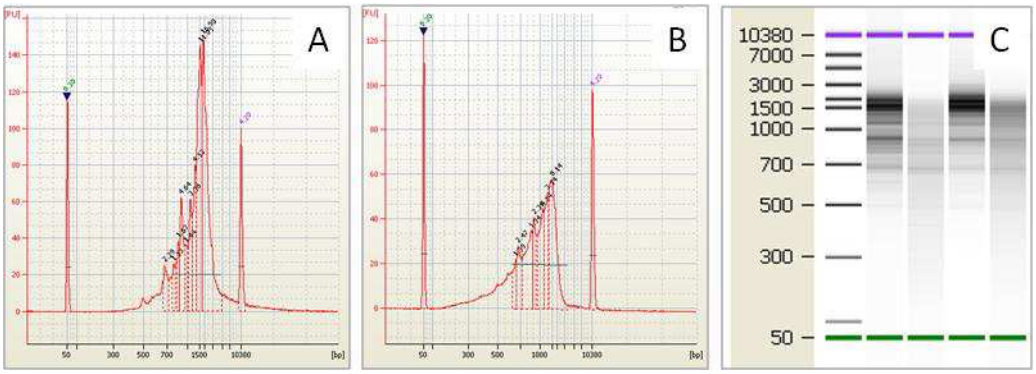

Figure 3: cDNA normalization results run in a Agilent 2100 Bioanalyzer at the Genomic Unit, CCiTUB. Panel A shows ds cDNA not normalized, panel B shows the same sample normalized and the panel C shows a gel where the most predominant transcripts have partially been enzymatic digested obtaining an equalized concentrations of all different transcripts.

3.2. Microsatellite discovery

Microsatellite discovery of non-model organism is another example where NGS are helping to open new areas of biological inquiry. Microsatellites are short segments of DNA that have a repeated sequence such as CACACACA, and they tend to occur in non-coding DNA. Over time, as animals in a population breed, they will recombine their microsatellites during sexual reproduction and the population will maintain a variety of microsatellites that is characteristic for that population and distinct from other populations which do not interbreed. NGS technologies are drastically reducing the time previously used by scientists to discover new markers to use in their research. Experiments performed in our lab showed that running 1/6 of a PicoTiterPlate in the GS-FLX system was able to generate over one hundred potential perfect microsatellites (di-, tri-, and tetranucleotides) with at least ten repeats ready to use by automated capillary electrophoresis (see Automated capillary electrophoresis "Genomics: More than genes" in this issue).

3.3. Targeted discovery of mutations or polymorphisms

For genomic resequencing, that is sequencing variation discovery in individuals of species for which a reference genome is available, a specific region of the genome across more individuals is frequently used in contrast to study the whole genome in fewer individuals. Some companies (NimbleGen, Qiagen, Fluidigm, RainDance) are developing different tools to target capture regions of the DNA. These strategies permit sequence specific genome regions to which a disease phenotype has been mapped, or exons of specific candidate genes belonging to disease, or the full complement of protein-coding DNA sequences.

Acknowledgements

I would like to thank Agustin Arasanz from Genomics Unit and Dr. Sergi Beltran from Bioinformatics Unit for their support in the optimization of the NGS technology at the CCiTUB, Dr. Josep Planas to promote the development of the experimental design for *de novo* Transcriptome sequencing projects, and Dr. Creu Palacín, Dr. Rocío Pérez and Dr. Marta Pascual for the opportunity to participate in their Microsatellite discovering projects.

References

[1] Sanger F et al 1977 Proc. Natl. Acad. *Sci. U.S.A.* **74** 5463.
[2] Maxam & Gilbert W 1977 Proc. Natl. Acad. Sci USA **74** 560
[3] International Human Genome Sequencing Consortium. 2004. Nature **409**, 860
[4] Margulies M, *et al.* 2005 Nature **437** 376.
[5] Jonhsons DS et al 2007 Science **316** 5830
[6] Picardi E 2010 Nucleic Acid Research **38** 14
[7] Harris, T.D *et al.* 2008 Science ***320,*** 106.
[8] Eid Jet al. 2009 Science **323**, 133
[9] Metzker M. 2009 Nature reviews **27** 150
[10] Adessi, C et al. 2000 Nucleic Acid Res. **28**, e87
[11] Fedurco, M et al. 2006 Nucleic Acid Res. **34**, e22
[12] Brenner, S et al. 2000 Nat. Biotechnol. **18**, 630
[13] Mitra RD & Church 2003. Anal Biochem **320** 55
[14] Mardis ER 2008. Annu Rev Genomics Hum Genet **9** 387
[15] Metzker M. 2010 Nat Rev Genet **11** 31
[16] Schuster SC 2008 Nature Methods **5** 16.
[17] Shendure J & Hanlee J 2008 Nature biotechnology **26**, 1135
[18] Shagin DA et al, 2002. Genome Res **12** 1935

Analyzing Peptides and Proteins by Mass Spectrometry: Principles and applications in Proteomics

Maria José Fidalgo[1], Eva Olmedo[1], Irene Fernández[2], and Josep Maria Estanyol[1]

[1] Unitat de Proteòmica, CCiTUB, Universitat de Barcelona. Casanova 143. 08036 Barcelona, Spain

[2] Unitat d'Espectrometria de Masses (Química), CCiTUB, Universitat de Barcelona. Facultat de Química. Martí i Franquès s/n. 08028 Barcelona, Spain.

email: *jmestanyol@ccit.ub.edu*

Abstract. The study of proteins has been a key element in biomedicine and biotechnology because of their important role in cell functions or enzymatic activity. Cells are the basic unit of living organisms, which are governed by a vast range of chemical reactions. These chemical reactions must be highly regulated in order to achieve homeostasis. Proteins are polymeric molecules that have taken on the evolutionary process the role, along with other factors, of control these chemical reactions. Learning how proteins interact and control their up and down regulations can teach us how living cells regulate their functions, as well as the cause of certain anomalies that occur in different diseases where proteins are involved. Mass spectrometry (MS) is an analytical widely used technique to study the protein content inside the cells as a biomarker point, which describes dysfunctions in diseases and increases knowledge of how proteins are working. All the methodologies involved in these descriptions are integrated in the field called Proteomics.

1. Introduction

Mass Spectrometry (MS) is an analytical technique that measures mass-to-charge ratios (m/z) of ionized molecules. Peptides and proteins can be analyzed by MS due to their capacity to ionize them under different conditions. Despite mass spectrometers were mainly used to determine the exact mass of low molecules in its first applications, the improvement of ionization methods and mass analyzers has enabled larger molecules such as polymers, peptides and proteins to be analyzed.

Before MS analysis of peptide and proteins started, EDMAN degradation had been used to identify the amino part of proteins through extrusion of aminoacids by chemical reactions. Due to the fact that the amino part of proteins are blocked in a high percentage of living cells, only highly abundant or purified proteins were able to be sequenced. Digestion of proteins by specific proteases and analysis of their peptides improved the methodology and solved this problem. However, the cost and slowness of this method were a handicap to perform high throughput analysis.

In the mid of 1960s preliminary studies for the determination of amino acid sequences in derivatizated peptides were published. The introduction of a matrix to ionize nonvolatile compounds was a significant progression in peptide analysis. In the early 80s, it was possible to determine the molecular mass of insulin and snake toxins with a molecular weight until 13 kDa. By the end of the decade, two new ionization systems were developed in the analysis of peptides and proteins, namely Matrix Assisted Laser Desorption Ionization (MALDI) and Electro Spray Ionization (ESI). These sources and the improvement of mass analyzers opened new perspectives for the analysis of higher molecular weight proteins.

Another important role in the high-throughput analysis of peptides and proteins was the whole genome sequencing of different species. Prior to this, the interpretation of spectra from MS analysis had to be done manually and this process was tedious and slow. After genomes were annotated, in silico comparison between spectra generated after MS analysis with those generated by software from databases, allowed to perform high-throughput analysis of complex samples.

2. Methodology and Applications

2.1. The mass spectrometer

A mass-spectrometer system consists of the following parts: an ionization source interface, where the sample is ionized; the analyzer, where compounds are measured as m/z ratio and the detector. Identification and characterization of peptides and proteins by MS is based on obtaining the exact mass of the molecule, as well as the exact mass of the derivatives of the molecule after a controlled breakdown in a collision cell. Proteins and peptides are polar non-volatile molecules that have to be introduced in gas phase to the MS. These types of analytes are normally soluble in aqueous solutions and specific methods of ionization to transfer them as gas phase into the mass spectrometer without extensive degradation have to be used. The typical ionization sources used in proteomics are MALDI and ESI.

2.2. Matrix Assisted Laser Desorption Ionization (MALDI)

The ionization source generates charged ions in gas phase from a solid-state sample aggregated with a matrix (usually alpha-cyano-4-hydroxycinnamic acid) into a plate. A laser provides the energy required to sublimate the sample and it allows charged ions enter in gas phase to the MS. A high voltage is applied at that moment and ionized molecules are accelerated at the same time inside a high vacuum tube where they fly depending on their mass. Light ions arrive faster than heavy ions to the detector. Most of the acquired ions are only single charge components despite they have more than one element that can be ionized. The resulting spectrum is a single charge spectrum for each molecule.

2.3. Elestrospray ionization (ESI)

The ionization source gets charged ions into gas phase from a liquid sample. This is achieved by

applying a voltage between the output of a capillary where the sample is being sprayed and the entrance of the mass spectrometer. This source produces a spray (micro drops) of sample and solvent. When the charge density at the droplet surface reaches a critical value, a so called Coulomb explosion occurs and several even smaller droplets are formed. The process of solvent evaporation, droplet contraction and Coulomb explosions is repeated until the sample is released from the final droplet. the sample is ready to be introduced into the mass spectrometer. While they go through within a heat capillary, the solvent is finally removed by evaporation. The analyte presents as many possible charges in the molecule as possible charged aminoacids may have in the sequence thus generating a multi charge sample. In this case, the spectrum for each molecule is more complex because each molecule could be present as different m/z spectra, depending on the various charges that each component has.

This ionization source is used in liquid samples before entering into the MS, and in most cases, especially in complex samples a High Performance Liquid Chromatography (HPLC) is coupled online, which introduces the sample sequentially. According to the flow used by the HPLC, we call ESI ionization source when the flow rate is about mL/min, microESI when the flow rate is about μL/min or nanoESI if the flow rate is about nL/min). The minor inner diameter of the columns, the small particle size used in the stationary phase of the chromatography and the decrease in HPLC flows, allows to increase the sensitivity in samples of low concentration of peptides or proteins.

The most common analyzers in the analysis of peptides and proteins are the following:

2.4. Time of Flight

The Time of Flight (TOF) analyzer is based on the time that ions take to fly from the ionization source to the detector, due to its kinetic energy acquired ($1/2\ mv^2$) by applying a voltage (approximately 20,000 volts) in the ionization source. These fast moving ions fly through a high vacuum tube, where peptides arrive first to the detector according to the m/z ratio. This analyzer allows a resolution of 15.000 to 40.000 and an accurate mass measurement of less than 10 ppm using internal calibration. Such analyzers are usually coupled to MALDI or ESI ionization sources.

2.5. Triple quadrupole

This mass analyzer consists of two quadrupoles separated by a collision cell. Ions must be moved from the source to the analyzer (different physical regions) where different functions take place. Ions with different m/z ratios have different stability when they are moved through an electromagnetic field. The first quadrupole (Q1) selects ions, the second (Q2) acts as a collision cell where backbone of the molecule is broken after colliding ions with a gas, and the third (Q3) acts as analyzer of m/z ratios. This type of analyzer allows at present *good* sensitivity, resolution and *accuracy*. It is useful in quantitative analysis for its resolution and sensitivity of small molecules. The most common ionization source used with this analyzer is the ESI.

2.6. Ion-Trap

The ion-trap analyzer is a special type of quadrupole analyzer, where ions are captured (trapped) into a three-dimensional region applying different voltages and magnetic fields. There are two different types, the 3D ion-traps and the linear ion-traps. In the 3D trap, ions produced in the ionization source are focused into the trap using an electrostatic lens system. An electrostatic ion gate pulses ions into the trap by pulses of voltages (V+ close, V- open) using an opening time that minimizes space-charge effects. A low-pressure of helium (1mTorr) is used in the trap to slow ions and improve resolution by concentrating them at the center of the trap using oscillating voltages. Changing amplitudes of voltage and radio frequency determines instability of ions, depending on a m/z ratio manner and, as a result, they can be detected. In that cycle, one single ion can be trapped, and after using different voltage frequencies, the collision of ions with the helium produces backbone fragmentation and structural information. Linear Ion Trap is a modified ion trap type where the trap is linear, improving ion capabilities and sensitivity. The mass resolution of these instruments varies from 3000 to 15.000.

2.7. Orbitrap

This analyzer is based on different resonances obtained from ions with different m/z ratio after they orbit in this analyzer. Ions are injected tangentially and oscillate inside in rings around a central electrode. Different m/z ratio generates different frequencies of oscillation and it is inversely proportional to a square root of m/z (Fig. 2). This analyzer allows at present resolution up to 200.000 (at m/z of 400) and accurate mass measurement of less than 1 ppm using internal calibration. Is the latest development in trapping devices.

Fourier Transform

Figure 1 LTQ VELOS ORBITRAP ETD high-resolution mass spectrometer at the CCiTUB (form Thermo Fisher Scientific).

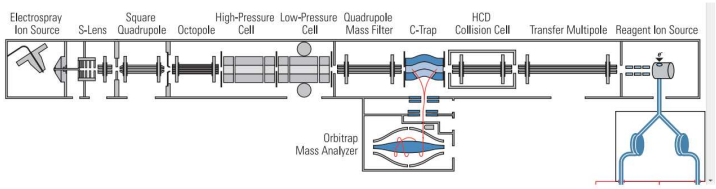

Figure 2 Cross section of a LTQ VELOS ORBITRAP-ETD high-resolution mass spectrometer (form Thermo Fisher Scientific).

BT.8

The Fourier Transform Ion Cyclotron Resonance (FT) is a m/z analyzer based on the cyclotron frequency of the ions under a fixed magnetic field. It gives the highest mass resolution used in proteomics (up to 750.000)

The instrumentation available at the CCiTUB to perform proteomic approaches is the following:

- MALDI TO VOYAGER DE (ABIsciex)
- MALDI TOF-TOF 4800 (ABIsciex)
- LCQ-DECA XP (Thermo)
- LTQ-VELOS-ORBITRAP-ETD (Thermo) (Fig. 1).
- Micro HPLC Surveyor (Thermo)
- Nano HPLC EASY (Proxeon)
- Nano LC-Ultra system (Eksigent)

3. Methodologies in Proteomics

Most of the mass spectrometer analyzers are not capable of analyzing beyond a m/z ratio of 4000 or 5000. This means that, in most cases, analysis of the sample is not performed with the intact protein due to its high molecular weight. Protein can be cut into small peptides using a controlled digestion (digestion in specific amino acids) by a specific proteases (trypsin, GluC, LysC, others) and the resulting peptides are analyzed by MS.

Due to the complexity of the sample (proteins digestion produces a considerable amount of peptides), prior to MS analysis, peptides have to be separated using chromatographic separation for instance HPLC (see section 3.1.1). Common chromatographic columns in peptide and protein separation are made of non-polar, highly hydrophobic stationary phases (mainly C18, or other) or ion exchange stationary phases (SCX, WAX or others).. The identification and characterization of peptides and proteins by MS relies on two basic concepts, namely obtaining the exact mass (both protein and peptides) and the possibility of breaking the molecule into different parts at the

backbone level in a controlled manner to identify the exact mass of the broken ions by tandem mass spectra.

3.1. Separation technologies

Protein MS identification is a technique highly dependent on separation of peptides and proteins to simplify samples previous to the analysis. There are different methods of separation of proteins or peptides; the gel based methods and the chromatographic methods.

3.1.1. High Performance Liquid Chromatography

HPLC is an analytical technique used to separate peptides and proteins according to their intrinsic properties. Usually Reverse Phase Liquid Chromatography (RPLC) is coupled on-line to ESI ionization sources to separate compounds using volatile mobile phase highly compatible with MS. During decades, efforts to improve peak capacity, sensitivity, reproducibility and speed in the analysis have been done. These efforts conduced to use long narrow capillary columns that improve sensitivity.

3.1.2. Multidimensional Liquid Chromatography

High complex samples containing thousands of proteins proteolytically digested by an enzyme are difficult to analyze after a single RPLC separation. Due to the extremely high number of analytes in the sample and the different dynamic range, a combination of different orthogonality chromatographic separation can be performed. Each dimension uses different molecular properties for the separation. One type of Multidimensional Liquid Chromatography (MudLC) is based on two types of chromatography. The first dimension is performed by a Strong Cation Exchange (SCX) resin followed by RPLC coupled on line to a MS. SCX resins are used due to their high capacity and good resolution. The high complex sample is loaded onto a SCX column and eluted in a series of increasing salt steps or salt gradients where each fraction is loaded onto a RP column coupled online to a MS. Other columns in the first dimension can be used such as hydrophilic stationary phase to separate peptides and proteins.

3.1.3. Affinity Chromatography

Another chromatographic technique useful for proteomic approaches is the affinity chromatography. A protein of interest to be studied is coupled to a resin and packed into a column. Proteins of cell lysates, from tissues, etc, flow through the column and proteins with affinity are bound. After eluting bound proteins, MS can identify them to perform functional proteomics approaches (see below). This technique can also be used for the enrichment of specific molecules as phosphates groups in peptides and proteins. This was very useful to enrich posttranslational modified (PTM) proteins and peptides.

3.1.4. Gel based separations

Gel-based approaches are techniques that separate proteins by their molecular weight (MW). Using ionic detergents such as SDS and a matrix of acrylamide, proteins move through to the acrylamide gels under an electric field depending on their molecular weight. Proteins can also be separated by charge under denatured conditions, without using ionic detergents, in a pH gradient. These two methods are the basis of separation of proteins by 2D-gels. With this methodology, we have a pattern in two dimensions where each spot in the gel is a protein, which can be sliced and digested in-gel by a proteinase. The resulting peptides can be analyzed by MS.

3.2. Proteomic approaches

Proteomic approaches for the identification of peptides and proteins means separation methodologies and MS analysis. The MS analysis can be performed after protein digestion and peptide separation where proteins are identified by sequencing peptides (The Bottom-Up Approach). Proteins can also be analyzed as intact molecules (Top-Down Methods) and the exact mass of the protein and their fragments measured after specific breakdown.

3.2.1. The Bottom-Up Approach

In this technique, proteins are digested into peptides prior to MS analysis. Exact mass of peptides and their broken components are determined to know structural information. These experiments require tandem data acquisition in which peptides are subjected to collision induced dissociation (CID). The tandem mass data collected are compared with in-silico-generated fragmentation using databases and a statistical algorithm from which a confidence number for the identification is given. There are different search methods for protein identification such as SEQUEST, MASCOT, XTANDEM, PHENYX. If a protein is pure enough (by chromatographic approaches or 2D gel separation) its identification can be done by peptide mass fingerprinting (PMF), where the protein is identified by listing the exact mass of peptides obtained by MS and compared to anotated proteins databases using specific algorithms.

3.2.2. Top-Down Methods

Top-Down Methods use the exact mass of the intact protein and their fragments for the identification.

Unlike the TOF analyzer that can analyze ranges greater than 100.000 uma without decreasing resolution, other mass analyzers work in a mass range from 2000 to 5000 m/z and the exact mass of a protein can be calculated by deconvolution of their multicharge spectra.

Different fragmentation reactions are needed to fragment intact proteins in this approach. Electron transfer dissociation (ETD) and Electron capture dissociation (ECD) are the most preferred. With these methods, we measure the intact protein directly, in contrast to the bottom-up approach that only measures peptides. This technique has limitations. Larger quantities of protein are required and high-mass accuracy instruments such as LTQ-ORBITRAP or FTMS are needed to resolve isotopic envelops of proteins.

3.3. Proteomic applications

3.3.1. Quantitative proteomics

Proteins can be quantified using MS, which represents one of the key components toward building a functional network. There are two types of MS-based quantitative proteomic methods: the relative quantitative proteomics which compare the relative amount of protein between samples, and the absolute quantitative proteomics which use a quantified standard to determine the exact amount of proteins in the sample.

There are different assays for quantitative MS. Samples can be labeled by isotope-labeling methods and the relative or absolute values between samples can be quantified. Other methods are label free methods, which have been used to quantify relatively protein content in different samples.

3.3.2. Isotope-labeling methods

Isotope-labeling methods bind different isotopic molecules to peptides to compare samples. They can be bound metabolically, chemically or enzymatically.

Metabolically isotope-labeling methods use stable isotopes of aminoacids (Arg, Lys) (^{15}N, ^{13}C for heavy labeling) to label peptides. For stable isotopic labeling aminoacids in cell culture approach (SILAC), cell media containing $^{13}C6$-Lys and $^{15}N4$-Lys are used. The relative abundance of proteins is calculated by measuring ratios of peptides experiment comparing heavy/light peptides pairs.

Chemical derivatization of peptides can also be used for protein quantification. Different aminoacids can by labeled chemically by different stable isotope tags to measure ratios between heavy/light labeled samples. Different aminoacids can be labeled for that purpose. Isotope-Coded Affinity Tags (ICAT) is used to label free cysteine and Isobaric Tags for Relative and Absolute Quantification (iTRAQ) is used for label free amines.

3.3.3. Label Free methods

Other strategies do not use label free active residues of aminoacids with different isotopes to perform relative quantification. In label-free quantitative methods, each sample is prepared, individually LC-MS/MS or LC/LC-MS/MS separated and analyzed. Protein quantification is performed by comparing measurements of ion intensity changes for the same peptides in different LC runs or on the spectral counting to calculate the total number of spectra of the proteins, also by comparing different LC runs.

3.4. Post translation modification proteomics

Proteins are molecules that can be modified enzymatically in specific aminoacids. This might control their activity, the partners that bind to them, the conformation of the protein, and other processes that regulate their function and also the quantity of the protein in the cell. Typical modifications are summarized in table 1.

3.4.1. Phosphoproteomics

Protein kinases are the major regulator of cell processes, and MS is the methodology of choice for identifying and also quantifying phosphorylation sites. This type of regulation has to be highly regulated, and the amount of phosphorytaled proteins present inside cells is not very high. For this reason, chromatographic strategies for enrichment of phosphoproteins or phosphopeptides have to be done prior to MS analysis.

Different affinity-based enrichments can be done for that purpose, immunoprecipitation using specific anti phospho-antibodies, metal oxide affinity chromatography (as TiO_2, Fe^{3+}, Ga^{3+}), cation exchange chromatography and also chemical derivatization of phosphate groups (Fig. 3).

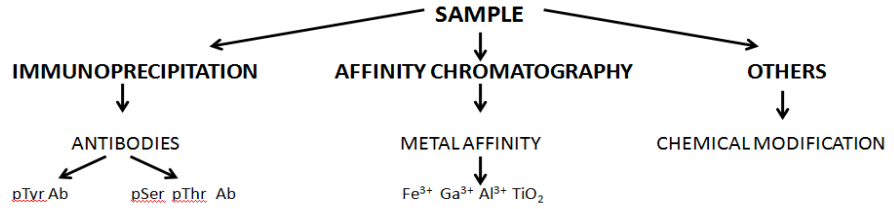

Figure 3
Schematic view of different approaches to enrich phosphorylated peptides and proteins

3.4.2. Glycoproteomics

Glycosylation is an important and abundant post-translational modification. Glycoproteins are involved in different roles as molecular and cellular recognition in development, cell growth, cellular communication and also in diseases as cancer progression and immune responses. Top down and bottom up approaches are used for the identification of glycosilated proteins. Performing MS/MS experiments, glycosilated peptids can be identified knowing also the glycosil groups added to the proteins.

3.4.3. Ubiquitin

Ubiquitin is a post-translational modification of proteins where a small peptide is attached to protein. This modification is very important in protein degradation and also for controlling protein levels in the cell. Using MS approaches, ubiquitin can be detected and the specific aminoacid where it is attached can be determined.

4. Examples of applications

The identification and sequencing of peptides and proteins by MS is nowadays the basis of high throughput proteomic analysis. Biomedicine and biotechnology are the major fields of interest, even that others are emerging, such as agriculture, veterinary, etc

4.1. MALDI-TOF/TOF Analysis of proteins: Peptide Mass Fingerprinting and Peptide Sequencing
In this example, proteins were extracted from their medium and separated by 2D-SDS-PAGE.The spot of interest was cut from the gel, washed and digested with trypsin. The tryptic peptides were eluted from the gel by washing, and analyzed by MALDI-TOF/TOF. The results are shown in Fig. 4.

Table 1. Typical modifications of proteins in specific aminoacids

MODIFICATION	INSERTED GROUP	DELTA MASS	SPECIFIC AMINOACIDS
Phosphorilation	H O(3) P	79.966331	S, T, Y
Acetylation	H(2) C(2) O	42.010565	K, NH2-terminal
Oxidation	O	15.994915	M, others
Glycositation	Sugars		
Ubiquitinization	H(6) C(4) N(2) O(2)	114.042927	K
Metylation	H(2) C	14.015650	

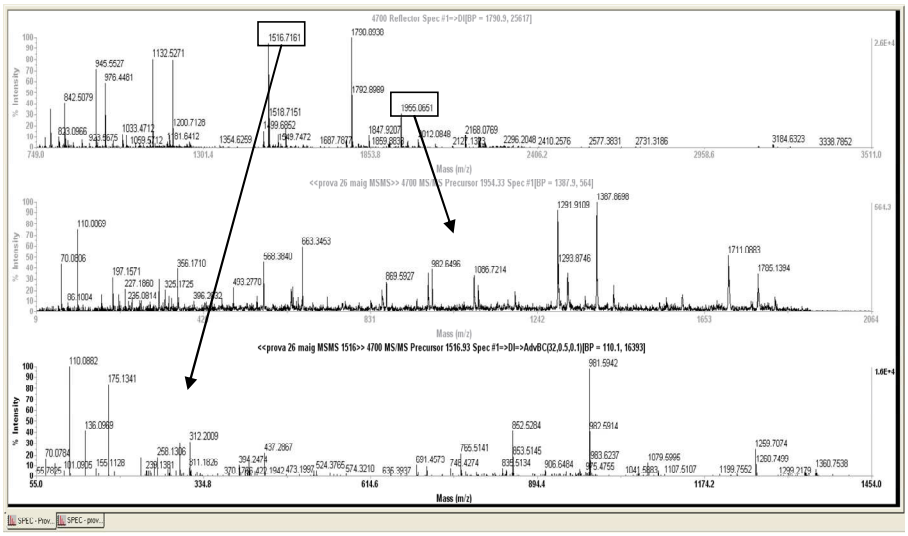

Figure.4 a) MALDIi TOF reflector spectrum of a tryptic digest (matrix: CHCA). Internal calibration with proteolitic fragments of Trypsin gives mass accuracy measurements for the peptides < 15ppm ensuring a good Peptide Mass Fingerprinting search. b) and c) MALDIi-TOF/TOF (MS/MS) spectra of the two tryptic peptides selected from the MS analysis. The good sensitivity and mass measurements ensure a good Peptide Sequence Analysis.

4.2. Quantitative proteomics
Quantification of proteins is an important differential analysis, such as in comparisons of samples from diseased and healthy states. In biomedicine is important to know which proteins are related to a disease. For these reason, proteomic analysis can be performed to quantify samples between controls to disease, and between different stages of a disease. To perform these experiments, samples can be compared using different approaches.

If isotopic tags are used as Isobaric tags for relative and absolute quantitation (iTRAQ) firstly proteins are digested and peptides labeled. The samples are mixed and separated by chromatography. The same peptides with different tag coelute from HPLC, and the mass spectrometer can analyze them. Specific software can quantify the relative amount of each tag and determine quantitation of the sample.

Label free methods perform an HPLC run for each sample. The total amount of spectra that identifies a protein is used to calculate the relative quantity of each protein by an algorithm. This technique is also useful in biomarker discovery in human disease.

4.3. Phosphorilation modifications.

Phosphorylation is the most highly studied and known post-translational modification for its relationship with cellular functions. To perform these experiments, firstly phosphorylated peptides must be enriched. For that purpose, different methods are used. If phosphoproteins want to be enriched, immunoprecipitation or metal affinity can be used. For peptides, after digestion proteins by a specific protease, phosphopeptides are enriched by metal affinity columns. The use of TiO_2 columns gives better results but others can be used (Fe^{3+}, Ga^{3+}..). An example of a phosphorilated peptide spectrum is shown below (fig. 5).

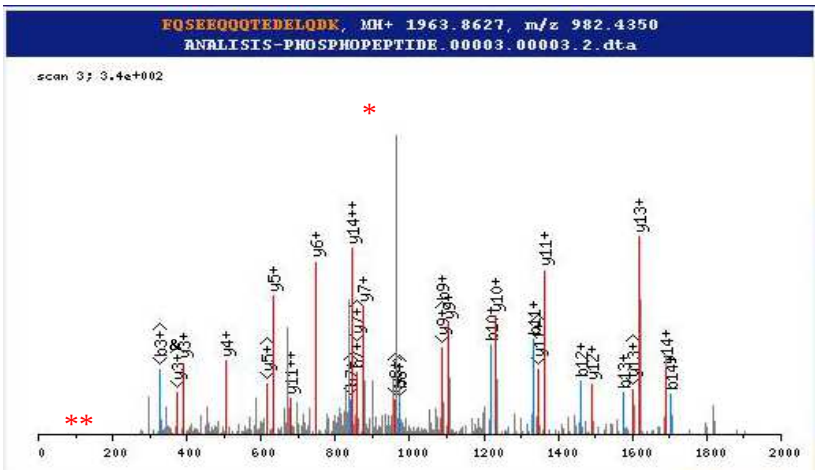

Figure. 5 Spectrum of EQsEEQQQQTEDELQDK phosphorilated peptide. * indicates non broken peptide. ** indicates phosphoserine

E Q s E E Q Q Q Q T E D E L Q D K

4.4. Functional proteomics

The study of protein-protein interactions by MS is an important field of analysis in the post-genomic era to understand protein function. A variety of MS–based approaches allows characterization of cellular protein-protein interactions and subsequent assignment of individual proteins to specific pathways and networks.

The idea is that proteins bind to other proteins to perform cell functions, by mean enzimatic activity or modulating this activity. There are different functional technology approaches that can be integrated together to have a global view of the functional biological systems. Proteomics based in affinity chromatography and MS can help us to find new functions of proteins unknown at that time.

To identify the proteins involved in biological processes and signaling pathways a proteomic approach consist of express a recombinant protein purification, immobilized it on a matrix and perform affinity chromatography using cell extracts or purified cell fractions, as nuclei, mitochondria, lysosomes, plasmatic membrane. After washing, the bound proteins obtained by these interactions are separated by a SDS.PAGE gel electrophoresis. Proteins are sliced from the gel, digested and identified by MS. Using this approach, hundreds of proteins can be identified, and the information obtained is processed using ontology databases in order to know all processes and pathways in which they are involved, as well as in which cellular compartment proteins they interact.

After sequencing proteins, all the information can be grouped in protein ontologies to understand the biological system.

4.5. Proteomics of promoters

Promoters of genes are the regions of DNA where regulator factors bind and regulate gene expression. Many of these regulators are proteins that bind directly to DNA or to other proteins that bind to DNA and regulate gene expression. There is an important field in biomedicine that studies how genes regulates their expression and how can be involved in diseases. MS can identify proteins

related to promoters by dsDNA affinity chromatography. For that purpose, dsDNA is coupled to a matrix in a column. Cell extracts are passed through the column and proteins with affinity to dsDNA will be kept in the column. After extensively washing, the proteins of interest are eluted from the column an identified by MS.

4.6. Analysis of intact proteins

High-resolution MS allows the characterization of intact proteins. An spectrum of an intact protein provides the exact mass of the molecule as well as the exact mass of all modified entities of it. For that analysis, it is essential to use high-resolution instruments such as Orbitraps or FT mass spectrometers. Both ionization methods, MALDI and ESI, can be used for that purpose, but MALDI mass spectrometers result in broad m/z peaks and low intensity for proteins above about 20 kDa. ESI ionization coupled to TOF analyzers or high-resolution instruments such as ORBITRAP or FTMS mass spectrometers can determine the exact molecular mass with a resolution of above of 120000 (see Figs. 6 and 7).

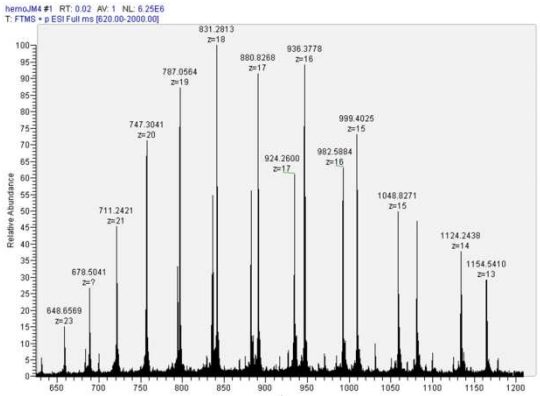

Figure 6 High-resolution spectrum of intact purified hemoglobin protein from blood.

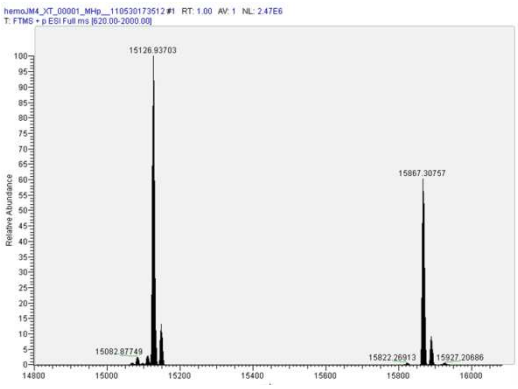

Figure 7 Exact mass of a hemoglobin protein after deconvoluted high resolution mass spectrum.

References

[1] Oliva R, de Mateo S, Estanyol JM. *Sperm cell proteomics.* Proteomics. 2009 Feb;9(4):1004-17. Review

[2] Vera J, Estanyol JM, Canela N, Llorens F, Agell N, Itarte E, Bachs O, Jaumot M. *Proteomic analysis of SET-binding proteins*. Proteomics. 2007 Feb;7(4):578-87.

[3] Estanyol, Josep M; Bachs, Oriol. *La proteómica como herramienta de diagnóstico y pronóstico: aplicación en el hepatocarcinoma*. GH Continuada. 2010;9:172-5.

[4] John R. Yates, Cristian I. Ruse,and Aleksey Nakorchevsky. *Proteomics by Mass Spectrometry: Approaches, Advances, and Applications*.. Annu. Rev. Biomed. Eng. 2009. 11:49–79

[5] Adam M. Hawkridge and David C. Muddiman. *Mass Spectrometry–Based Biomarker Discovery: Toward a Global Proteome*. Annu. Rev. Anal. Chem. 2009. 2:265–77

[6] Peter Roepstorff. Mass Spectrometry in the Analysis of Peptides and Proteins, Past and Present *Methods in Molecular Biology, Vol 61 Protein and Peptide Analysis by Mass Spectrometry*. J R Chapman Humana Press Inc , Totowa, NJ

Flow cytometry in the analysis of cellular populations

Esther Castaño[1] and Jaume Comas[2]

[1] Unitat de Biologia (Bellvitge), CCiTUB, Universitat de Barcelona. Feixa llarga s/n. 08907 L'Hospitalet de Llobregat, Spain.

[2] Unitat de Citometria. CCiTUB, Universitat de Barcelona. Parc Científic de Barcelona. Baldiric i Reixac, 10. 08028 Barcelona, Spain.

email: *jcomas@ccit.ub.edu, ecastano@ccit.ub.edu*

Abstract. Flow cytometry has become a valuable tool in cell biology. By analyzing large number of cells individually using light-scatter and fluorescence measurements, this technique reveals both cellular characteristics and the levels of cellular components. Flow cytometry has been developed to rapidly enumerate cells and to distinguish among different cell stages and structures using multiple staining. In addition to high-speed multiparametric data acquisition, analysis and cell sorting, which allow other characteristics of individual cells to be studied, have increased the interest of researchers in this technique. This chapter gives an overview of the principles of flow cytometry and examples of the application of the technique.

1. Introduction

Flow cytometry (FCM) is a technique used to rapidly detect and count microscopic particles such as cells, suspended in a stream of fluid. It allows simultaneous multiparametric analysis of the physical and/or chemical characteristics of up to thousands of particles per second. FCM is used in the diagnosis of health disorders, and has many applications in both research and clinical practice. Some instruments can physically sort particles based on their properties, so as to purify populations of interest. An impedance-based flow cytometry device was patented in 1953; the first fluorescence-based flow cytometry device was developed in the late 1960's [Shapiro, 2003].

1.1. Principle of flow cytometry

One or more beams of light (usually laser light) is directed onto a hydrodynamically- focused stream of fluid. A number of detectors are placed at the intersection of the stream with the light beam, to detect scattered light (forward scatter or FSC, in line with the light beam, and side scatter or SSC, perpendicular to it) and one or more fluorescent detectors. Each suspended particle -from 0.2 to 150 micrometers- passing through the beam scatters the light, and fluorescent chemicals found in the particle or attached to it may be excited, emitting light at a longer wavelength than the light source.

This combination of scattered and fluorescent light is recorded by the detectors and, by analyzing changes in brightness at each detector, information about the physical and chemical structure of each individual particle is obtained. FSC correlates with the cell volume and SSC depends on the inner complexity of the particle (shape of the nucleus, the amount and type of cytoplasmatic granules or the membrane roughness). Fluorescence detected is related to the presence of specific cellular structures (antigens, nucleic acid) or functions (viability, enzyme activity, membrane potential, intracellular ion concentration).

Modern flow cytometers are able to analyze several thousand particles every second, in "real time", and can actively isolate particles having specified properties. A flow cytometer is similar to a microscope, but instead of producing an image of the cell, flow cytometry offers "high-throughput" (for a large number of cells) automated quantification of set parameters. To analyze solid tissues, a single-cell suspension must first be prepared [Robinson, 1993; Darzynkiewicz, 1994.]

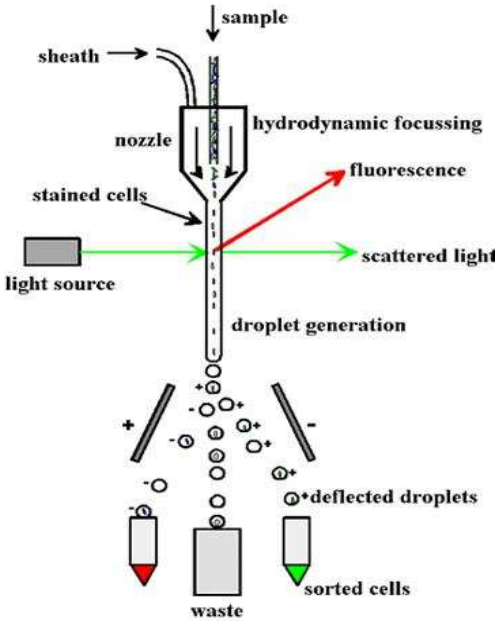

Figure 1. Schematics of a flow cytometer

2. Metodology

A flow cytometer has several components: 1) a flow cell - liquid stream (sheath fluid), which carries and aligns the cells so that they pass aligned through the light beam; 2) an optical system, with at least one light source (usually laser) and light collection devices (photodetectors or photomutiplier tubes); 3) an electronic system which generates and amplifies electrical signals from light. Acquisition and analysis of data is done by a computer connected to the flow cytometer. [Ormerod 1999, Ormerod 2000, Ormerod 2008].

Modern instruments usually have multiple lasers and fluorescence detectors. Increasing the number of lasers and detectors allows for multiple labelling. Certain instruments can even take digital images of individual cells, allowing for the analysis of fluorescent signal location.

Data generated by flow-cytometers can be plotted in a histogram, or in two-dimensional dot plots or even in three dimensions. The regions on these plots can be sequentially separated by creating a series of subset extractions ("gates"). Because different fluorescent dyes' emission spectra overlap, signals at the detectors have to be compensated. Data accumulated can be analyzed once the data are collected using appropriate software.

2.1. Fluorescence-activated cell sorting

Fluorescence-activated cell sorting (FACS) is a specialized type of flow cytometry. It provides a method for sorting a heterogeneous mixture of cells into two or more containers, one cell at a time, based upon the specific light scattering and fluorescent characteristics of each cell. It is a useful scientific instrument, as it provides fast, objective and quantitative recording of signals from individual cells as well as physical separation of cells of particular interest. The first cell sorter was invented in 1965 [Shapiro, 2003]

The cell suspension is entrained in the centre of a narrow stream of liquid. The flow is arranged so that there is a large separation between cells relative to their diameter; a vibrating mechanism causes the stream of cells to break into individual droplets. Just before the stream breaks into droplets, the flow passes through a fluorescence measuring station where the fluorescent character of interest of each cell is measured. Charge is applied directly to the stream, and the droplet retains charge of the same sign as the stream; the stream is then returned to neutral. The charged droplets then fall through an electrostatic deflection system that diverts droplets into containers based upon their charge [Shapiro, 2003; Longobardi, 2001].

2.2. Fluorescent labels

A wide range of fluorophores can be used as labels in flow cytometry, with a characteristic peak excitation and emission wavelength. Also, the emission spectra of the labels often overlap. Consequently, the combination of labels which can be used depends on the wavelength of the light used to excite the fluorochromes and the detectors available [Haugland, 2010].

Depending on the specificity of the fluorochromes detected, very different measurable parameters can be analyzed by flow cytometry: pigments content (chlorophyll, phycoerythrin…), total DNA or RNA content (cell cycle analysis, cell kinetics, proliferation, etc.), chromosome analysis and sorting (library construction, chromosome paint), protein expression and localization, phospho-proteins, transgenic products in vivo (particularly the green fluorescent protein (GFP) or related fluorescent cell surface antigens (Cluster of differentiation (CD) markers), intracellular antigens (various cytokines, secondary mediators, etc.), nuclear antigens, enzymatic activity, pH, intracellular ionized calcium, membrane potential, membrane fluidity, apoptosis (measurement of DNA degradation, mitochondrial membrane potential, permeability changes, caspase activity), cell viability, monitoring electro-permeabilization of cells, oxidative burst, multidrug resistance (MDR) in cancer cells. These parameters can be detected individually or combined, as far as fluorochromes used in detection can be spectrally resolved.

3. Applications

3.1. Clinical applications

3.1.1. Haematology

The distributed nature of the hematopoietic system makes it amenable to flow cytometric analysis. Applications in haematology include DNA content analysis, leukemia and lymphoma phenotyping, immunologic monitoring of HIV-infected individuals, and assessment of structural and functional properties of erythrocytes, leukocytes, and platelets. Antibodies against intracellular proteins such as myeloperoxidase and terminal deoxynucleotidyl transferase are also commercially available and permit the analysis of an increasing number of intracellular markers [Bollum, 1979].

- *Cluster of differentiation antigens on leukocytes*. Cell identification is involved in flow cytometry. In order to identify blood cells, it is necessary to define sets of cellular parameters, which include intrinsic (such as cell size, cytoplasmatic granularity…) and extrinsic parameters. The cluster of differentiation (CD) is a nomenclature used for the identification of cell surface molecules present on leukocyte cells. CD molecules can act in numerous ways, often acting as receptors or ligands. The International Workshop on Human Leukocyte Differentiation Human Cell Differentiation Molecules names and characterises CD molecules [Zola et al., 2006].

- *Reticulocytes.* The reticulocyte count reflects the erythropoietic activity of the bone marrow and is thus useful in both the diagnosis of anemias and in monitoring bone marrow response to therapy. Starting in the mid-1990s, automated flow-cytometric analysis has replaced traditional microscopic quantitation of reticulocytes. Reticulocyte analysis now includes measurements of the mRNA content and the maturity of reticulocytes, cell volume, hemoglobin concentration and content [Piva et al. 2010].

- *Hematopoietic stem cells*. The use of flow cytometry in stem cell research requires high levels of stringency and as ‘‘fool-proof’’ techniques as possible, because often the number of cell populations of interest are relatively small, compared to those in other fields of study. Because of these small numbers of cells, it is useful to take advantage of the benefits of contemporary instruments and multiple reagent combinations to learn the maximum possible about these populations. CD34, Hoeschst 33342, CD105, CD90, CD117, CD133, Sca-1, CD150 are some of the antigens and functional markers which have primarily been useful in the study of human and murine hematopoietic and other stem or progenitor cells [Preffer et al. 2009]. CD34 is a stage-specific antigen that is expressed on human hematopoietic stem and progenitor cells whose expression decreases with differentiation of the cell. Side population (SP) cells are stem and early progenitor cells identified as a subpopulation by their low Hoechst blue and red fluorescent emission signature. The characteristic Hoechst fluorescence SP ‘‘tail’’ [Goodell et al. 2005; Petriz 2006] is attributed to a highly active efflux of Hoechst 33342, via a p-glycoprotein multidrug/ATP binding cassette transporter Bcrp/ABCG2 protein.

3.1.2. Immunology

Characterization of lymphocyte subtypes and cytokine signalling is essential for understanding the complex nature of the immune system. Activation by antigens, suppression of normal immune activation, and disease states can affect the phenotypes of lymphocytes. Multiparametric phenotypic analysis by flow cytometry allows to distinguish one subpopulation of cells within a heterogeneous mixture, and thereby enables the study the dynamics of immune signalling in intact cells.

- *HIV infection*. Infection with the human immunodeficiency virus (HIV) and acquired immunodeficiency syndrome (AIDS) represent the most common clinical application of flow cytometric immunophenotyping of peripheral blood lymphocytes. CD4+ T cells are the main cellular targets of HIV infection; they are destroyed by several mechanisms and their number decreases with progression of disease. According to certain organizations, the clinical decision concerning initiation of antiviral therapy or prophylaxis of opportunistic infections are based on the numbers of CD4+ T cells, therefore, accuracy and precision in measuring lymphocyte subsets are crucial during the follow-up of these patients [Chattopadhyay et al., 2010].

- *Lymphocyte activation*. Lymphocyte response to mitogens is a habitually-used test in the evaluation of the immune system. The old usual method with [3H]thymidine yielded results which were difficult to interpret. The identification of cell surface structures

(e.g.,CD69), minimally expressed on resting PBMC and broadly expressed on activated lymphocytes very early following the addition of stimuli, enhances the potential for detection of low-frequency responses [Vernon et al. 1995]. CD69 is expressed on all activated lymphocytes, so it represents a generic marker to monitor individual subset responses to provocative stimuli. This assay allows the study of the activation at the level of specific T, B, and natural killer (NK) cells. CD69 expression is a good marker of cells capable of cytokine production, which itself is an indicator of activation.

To monitor an immune response, it is important to have procedures that can follow lymphocyte proliferation, both in vitro and in vivo. The intracellular fluorescent dye, CFSE, has been found to be particularly effective at monitoring lymphocyte division in many experimental situations. The method is based on the ability of CFSE to covalently label long-lived intracellular molecules. Following each cell division, the equal distribution of these fluorescent molecules to progeny cells results in halving of the fluorescence of daughter cells [Parish et al., 2001].

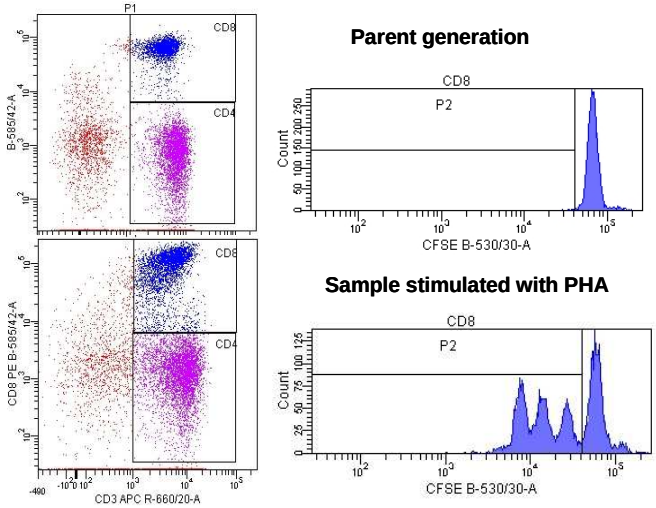

Figure 2. Cell proliferation indicated by dilution of CFSE in stimulated and unstimulated CD8 lymphocytes

3.1.3. Cancer biology and clinical oncology

In the last decade the main oncology application of cytometry has been the measurements of abnormalities of DNA content in tumor cells and with perturbation of the cell cycle by chemotherapeutic agents. By measurements with high resolution, the demonstration of abnormal cellular DNA content in several types of tumors can be of definite diagnostic value when combined with conventional diagnostic procedures.

Attempts to monitor cancer treatment by studying altered cell cycle distribution have not been successful, although some applications are of potential value. The main reasons for this are the complexity of tumor tissue as well as difficulties with interpretation of altered cell cycle distribution caused by drug combinations. For further progress in this field more emphasis on other cell constituents than DNA measured by flow cytometry is desirable, either as single or as multiparameter measurements. Interest remains in determination of drug sensitivity of tumor cells, or determinations of kinase activities in cells. The appreciation that various oncogenes are expressed in many human cancers has led to the development of cytometric techniques for detecting oncogenes by immunofluorescence.

3.2. Non-clinical applications

3.2.1. Flow cytometry of plant cells.

Flow cytometry on plant material is usually done on protoplast or cell suspensions. Chromosomes and plant subcellular organelles such chloroplasts and mitochondria have also been subjected to flow cytometric analysis.

The main area of application of flow cytometry is the measurement of DNA content for systematic, evolutionary or breeding purposes [Garcia et al., 2006; Torrel et al., 2001]. A reference standard of known DNA content is used (Fig. 3, Pisum sativum 'express long', where 2C=8.37 pg). Propidium iodide, which has no bias for AT or G-C-rich sequences within the genomes is commonly used as fluorescent stain. The measured fluorescence is directly proportional to DNA content. Using this procedure, up to 3.7% differences in DNA content has been resolved [Dolezel et al, 1995].

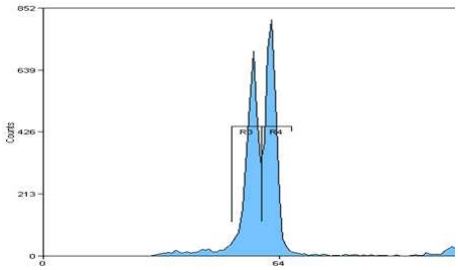

Figure 3: fluorescence distribution of propidium iodide stained nuclei fo standard (P. sativum, mode=57) compared to problem plant (mode= 62)

Measurements of the fluorescence of chlorophyll and other natural pigments as well as measurements of protein and nucleic acid content and specific antigens have been made in plant cells. Galbraith [Galbraith et al., 1995] has used GFP and its variants to study gene expression in plants.

3.2.2. Microbiology

Detection of microorganisms has been done from very different perspectives: biotechnology, environmental, clinical, food, sanitary or even military; the interest of a technique such as flow cytometry in microbial detection is clear since it allows the detection of microbes at a single-cell level.

DNA or protein content, membrane potential and immunofluorescence measurements of algae, bacteria, fungi and protozoa using flow cytometry had been reported in the literature by the mid-1980's, as had autofluorescence due to photosynthetic and other pigments. Differences in cell wall composition and in the outer membrane of bacteria, which are the basis of classical stains like the gram staining, can be detected by FCM. Commercial detection kits like the LIVE/ DEATH© BacLightTM bacterial counting and viability kit provides rapid and reliable assessment of bacterial viability in multiple applications [Haugland et al., 2010].

- *Environmental applications and marine biology*. Marine microorganisms detected by FCM include bacteria, phytoplankton, zooplankton and viruses. New species like *Prochlorococcus*, which is responsible almost of a third of the total bacterioplankton turnover of aminoacids, have been discovered using FCM (fig 4). DNA content and photosynthetic pigments are the most common parameters measured in oceanography. Specific organism (like the infective protozoa *Giardia* or *Microsporidium*) had been detected on water by flow using immunofluorescence techniques.

- *Clinical microbiology*. Blood, urine or spinal fluid have been used as clinical specimens when searching pathogens by flow. But FCM provides a tool not only for detection and identification of microbes, but measuring antimicrobial susceptibility testing, providing results in 2 to 7 hours, rather than in 15 to 24 hours, as it is the case when traditional culture methods are used. Bactericidal and the effect of bacteriostatic agents can be monitored by flow on cultures, measuring cell membrane permeability or membrane potential.

- *Food industry*. Food microbial analysis is routinely performed by colony counting. However, plate-culturing techniques are time consuming and they only reveal a small proportion (viable and cultivable) of the true microbial population. The application of FCM to foods is related to a correct setting of discriminator gates to select microbial counts from background particles. FCM has been applied on milk, brewing and oenology industries, and has been used for measurement of spoilage and pathogen microorganism contamination, starters and probiotics. [Comas and Rius, 2009]. Reported sensitivity of flow cytometry is ≤104 total bacteria/mL, and 103cells/mL for yeast.

3.2.3. Pharmacology and toxicology

Flow cytometric analysis of drug effects on cells in vivo has been considered as an alternative to animal testing. DNA content analysis has been used to determine effects of anticancer drugs on the cell cycle. In other cases, it is possible to study drug uptake directly, using fluorescent drugs such as anthracyclines or labeled analogs. Even when direct assessment of drug uptake on a cell-by-cell analysis is not possible, FCM can provide quantitative analyses of the effects of different drug doses on cell's metabolism over time courses. The measurement of apoptosis –the genetic controlled ablation of cells- is routinely done by flow cytometry using multiparametric approaches.

Standard tests of clastogenic agents such as bone marrow and blood erythrocyte micronucleus assays are performed by FCM detecting DNA-containing micronuclei in relative immature cells, and distinguishing them from immature erythrocytes which contain RNA [Derringuer et al., 1997].

3.2.4. Biotechnology

Industrial uses of flow cytometry include on-line monitoring of bioreactors or selection of yeast cells expressing antibodies. Flow cytometers without sorting capability are used for high-throughput screening; sample handling hardware has reduced the time needed to process a single sample to under two seconds. Sorters are used to isolate fractions from highly heterogeneous mixed populations, based on ligand binding and metabolic activity [Hewitt et al., 2001].

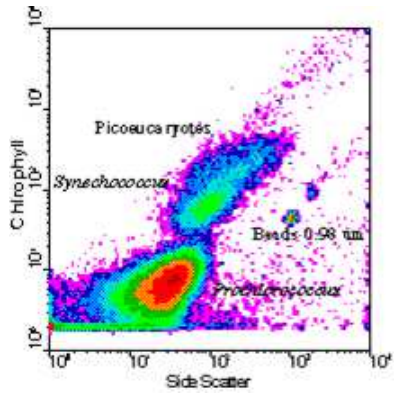

Figure 4. *Prochlorococcus:* FCM detection according to scatter and chlorophyll content. (D. Vaulot, CNRS).

4. Practical examples

4.1. Human Regulatory T-cell analysis.

Regulatory T cells (Tregs) play a critical role in maintaining immune modulation and are present in normal peripheral blood in low numbers. Cell cytometry can be used to evaluate the proportion of Tregs and memory T cells in peripheral blood. A description of the method used to identify and isolate these cells by flow cytometry is provided here.

Recipient peripheral heparinized blood samples were collected and PBMC were obtained by standard Ficoll density gradient centrifugation. Recipient PBMC were stained with the following monoclonal Abs: APC antiCD3, PerCP-Cy5.5 anti-CD8, FITC anti-CD4, APC anti-CD25, PerCP-Cy5.5 anti-CD127, PE anti-Foxp3, APC anti-CD45RA), all stains were carried out following the instructions of the manufacturer.

Flow cytometric experiments were carried out using a FACSCalibur (BD Bioscience). Excitation of the sample was done using a standard 488nm and 635nm laser. The instrument was set up with the standard configuration. FSC and SSC were used to gate lymphocytes cell population. As negative control, samples were incubated with corresponding isotype controls. A representative dot plot is shown in Fig. 5.

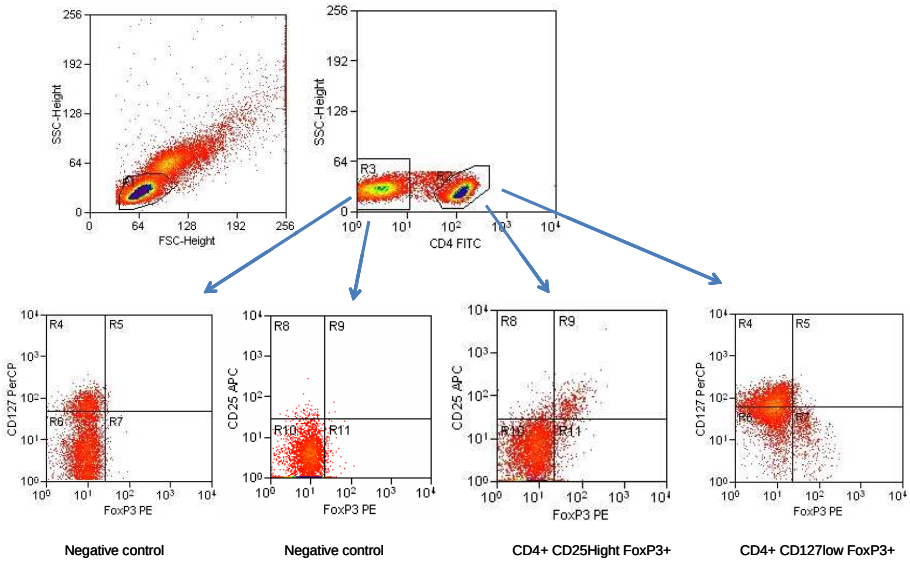

Figure 5. Representative dot plot used for the cytometric analysis of Foxp3+Tregs. Negative controls are also shown. Lymphocytes are identified using a routine scatter gate procedure. Events from the later gate are then transposed to the SSC vs. CD4 dot plot to obtain CD4+cells (R2) and CD4- cells (R3). CD4- (R3) cells were used as negative control. Finally, the cells from R2 or R3 gate are transposed to the CD127 vs. FoxP3 dot plot and the CD25 vs. FoxP3 dot plot.

BT.9

In conclusion, the evolution of memory/effector and regulatory T cells can be analyzed by cell cytometry in response to different treatments. It is possible identify and sort Tregs within a CD4+ lymphocyte population based upon high expression levels of CD25. As an alternative, CD127 can be used to identify Tregs as CD127low events within the CD4+CD25+ lymphocyte population. More details can be found elsewhere [Bestard 2011]

4.2. Detection of apoptosis induction in B-cell chronic lymphocytic leukemia cells without effect in T lymphocytes

B-cell chronic lymphocytic leukemia (B-CLL) is characterized by the accumulation of long-lived B lymphocytes. Most of the circulating cells appear to be nondividing and the clonal excess of B cells is mainly caused by defects that prevent programmed cell death rather than by alterations in cell cycle regulation. Glucocorticoids and other chemotherapeutic agents used clinically, including the nucleoside analogues 2-chloro-2-deoxyadenosine and fludarabine, induce apoptosis in B-CLL lymphocytes, suggesting that apoptosis is the mechanism of their therapeutic action. New apoptotic drugs can be alternative therapeutic option for CLL patients.

Experimental procedures: Seventy samples from patients with B-CLL who had not received treatment in the previous 6 months were studied. B-CLL was diagnosed according to standard clinical and laboratory criteria. Cells were obtained from the Hospital Clinic, Barcelona, Spain. Mononuclear cells from peripheral blood samples were isolated by centrifugation on a Ficoll-Hypaque (Seromed, Berlin, Germany) gradient and cryopreserved in liquid nitrogen in the presence of 10% dimethyl sulfoxide (DMSO).

Apoptosis was measured by annexin V binding. In apoptotic cells, the membrane phospholipid phosphatidylserine (PS) is translocated from the inner to the outer leaflet of the plasma membrane, thereby exposing PS to the external cellular environment. Annexin V is a 35-36 kDa Ca2+ dependent phospholipid-binding protein that has a high affinity for PS, and binds to cells with exposed PS. Annexin V staining precedes the loss of membrane integrity which accompanies the latest stages of cell death resulting from either apoptotic or necrotic processes. Therefore, staining with FITC Annexin V is used in conjunction with a vital dye such as propidiumiodide (PI) to identify early apoptotic cells (PI negative, FITC Annexin V positive). Viable cells with intact membranes exclude PI, wheras the membranes of dead and damaged cells are permeable to PI.

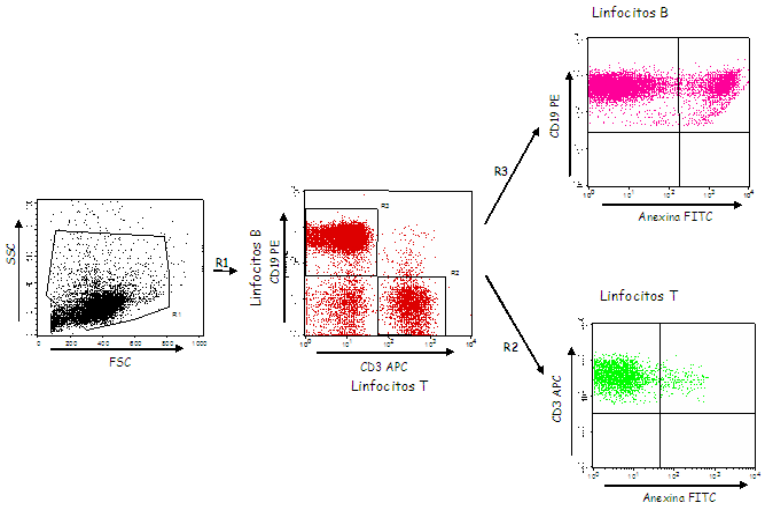

Figure 6: Representative dot plot used for the cytometric analysis of annexin-V+ in T (CD3+) and B (CD19+) cells. Lymphocytes are identified using a routine scatter gate procedure. Events from the later gate are then transposed to the CD19 vs. CD3 dot plot to obtain CD3+ CD19- cells (T lymphocytes) and CD3- CD19+ cells (B lymphocytes). Finally, the B or T cells are transposed to the CD19 or CD3 vs Annexin dot plot.

To analyze apoptosis in T cells from the samples, 500 000 cells were incubated for 24 hours with the indicated factors. Cells were then washed in PBS, and incubated in annexin-binding buffer with allophycocyanin (APC)–conjugated anti-CD3 and phycoerythrin (PE)– conjugated anti-CD19 for 10 minutes in the dark. Cells were then diluted with annexin-binding buffer and incubated with annexin V–FITC for 15 minutes in the dark. Then, annexin-binding buffer and PI were added just before flow cytometric analysis. Data were analyzed using Cell Quest software (Becton Dickinson, Mountain View, CA).

The precursor of nucleotide biosynthesis acadesine or 5-aminoimidazole-4-carboxamide (AICA) riboside has various effects in several types of eukaryotic cells. Because acadesine blocks glucocorticoid-induced apoptosis of quiescent thymocytes, it was examined whether glucocorticoid induced apoptosis in B-CLL cells was also blocked by acadesine. The effect of several doses of acadesine on the viability of B-CLL cells was analysed (data not shown). Unexpectedly, acadesine induced apoptosis. To determine whether the induction of apoptosis in B-CLL cells was selective to B population, the number of apoptotic Tcells (CD3_ cells) in CLL blood samples was analysed.

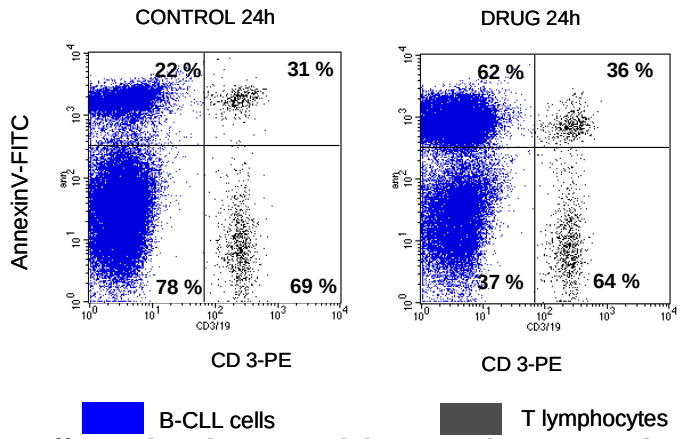

Figure 7: Acadesine effect on lymphocytes viability. Lymphocytes are identified using a routine scatter gate procedure (data not shown). Lymphocytes are then transposed to the CD3 vs AnnexinV dot plot to quantify apoptosis in B cells (CD3-) and in T cells (CD3+)

In conclusion, acadesine, 5-aminoimidazole-4-carbox-amide (AICA) riboside, induced apoptosis (62% in treated cells vs 22% in control) in B-cell chronic lymphocytic leukemia (B-CLL) cells, whereas T cells (CD3+) from these patients were not affected (31% in treated cells vs 36% in control). Flow cytometry is a practical and easy technique to analyse the induction of apoptosis in treated cells.

4.3. Flow cytometric detection of Plasmodium Falciparum in malaria-infected erythrocytes

Malaria is a parasitic disease caused by unicellular organisms of the genus Plasmodium. A large part of the life cycle of these parasites takes place in the blood circulation, where Plasmodium invade red-blood cells (RBC) in which they grow and multiply; this blood stage infection causes clinical symptoms and are targets for a number of drugs. The demonstration of the presence of parasites in the blood is used for diagnostics and treatment of the disease.

The analysis and detection of malaria infection by flow cytometry makes almost exclusive use of fluorescent dyes which are specific for nucleic acids. Since RBC do not contain DNA, DNA-specific fluorescence from infected RBC can only be due to the parasite DNA. In addition, since parasites multiply within the RBC, the fluorescence intensity of stained particles increases during the development of the parasites. As long as the DNA content of a parasite is 100-200 times less than the nucleated blood cells, they can be easily distinguished on the basis of their fluorescence intensity.

Most of the reported flow citometric studies on malaria parasites used A/T specific DNA dyes (Hoechst 33258, Hoechst 33342). Others non DNA-specific stains (Acridine orange, Propidium iodide) had also been successfully used. In the presented example, the Syto-11© fluorescent dye (Molecular Probes) has been used because 1) its high cell membrane permeability, that allows to stain samples without fixation or permeabilization procedures, 2) its high-intensity green fluorescence, which is strongly enhanced when bounded to DNA or RNA. Syto-11 is excited at 488nm, which is the most commonly light source found in the commercial flow cytometers.

BT.9

Cultures of *Plasmodium falciparum* 3D7 were grown in vitro in group B human RBCs (provided by the Banc de Sang i Teixits at the Vall d'Hebron Hospital in Barcelona) using previously described conditions. Briefly, parasites (thawed from glycerol stocks) were cultured in RPMI complete medium in a gas mixture of 94% N2, 5% CO2, and 3% O2. The cultures were contained in Petri dishes, and parasites were cultured at intervals of 2 days at ca. 3% hematocrit. For flow-cytometry analysis, non-infected RBCs and Plasmodium-infected RBCs samples were diluted to a final concentration of 1-10x106 cel/ml. The cell suspension is stained with 1 uL Syto 11 (0.5 mM in DMSO) to a final concentration of 0.5 µM. Samples were incubated from 5-10 minutes prior to flow cytometric analysis.

Flow cytometric experiments were carried out using an Epics XL flow cytometer (Coulter Corporation, Miami, Florida). Excitation of the sample was done using a standard 488nm air-cooled argon-ion laser at 15mW power. The instrument was set up with the standard configuration. FSC and SSC were used to gate red blood cell population. Green (525 nm) fluorescence for syto-11 was collected in a logarithmic scale. The single-cell population was selected on a forward-side scatter scattergram, and the green fluorescence from this population was analyzed.

Figure 8 shows the gating on RBC to exclude aggregates and cell debris (A), and how fluorescence of infected RBC can be detected in the gated population (B).

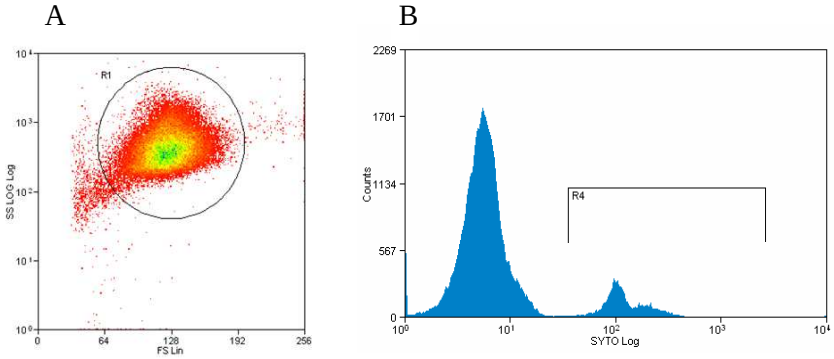

Figure 8. A: RBC population gated according to its scatter signal (horizontal, Forward Scatter; vertical: Side Scatter). B: Fluorescence histogram of Syto-11 obtained from an infected sample (horizontal axis: intensity of green fluorescence; vertical axis: frequency of cells). R4: region defined on Plasmodium infected cells.

In Fig. 9, a typical dotplot obtained combining FSC vs. green fluorescence can be seen; A has been obtained from a non-infected sample, while B has been obtained from an infected sample. Region R2 is used to quantify the percentage of *Plasmodium* infected cells. Its position is fixed according to the control (uninfected) sample, where R2 must be <0.1%.

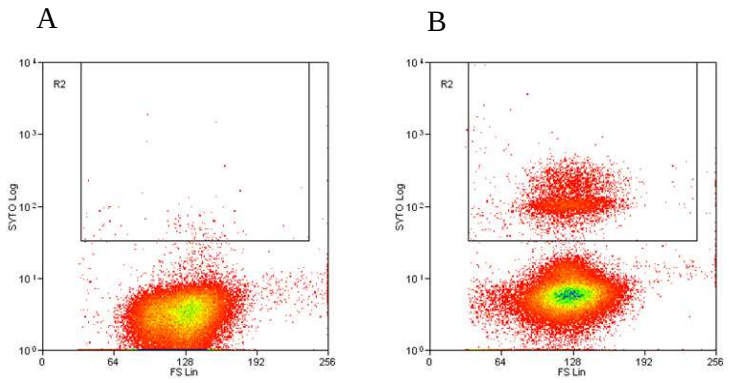

Figure 9: Comparison between a non-infected sample (a) (where false positive < 0.1%) vs. an infected (11% parasitemia) sample (b). (Horizontal axis: Forward Scatter; vertical axis: green fluorescence intensity). R2: infected cells.

In conclusion, detection of *Plasmodium falciparum* by flow cytometry using syto11 has proven to be a simple and fast procedure. As long as fixation and washing steps are not necessary when using this stain, the total time needed for staining and analyzing 50.000 RBC is less than 10 minutes. Flow cytometry has been a valuable tool especially for long batches of samples, where the alternative technique of microscopic counts is long and tedious. High correlation were found between microscopic and flow cytometry counts; minimum values of parasitemia detected by flow cytometry were about 0.5%

4.4. Stem cell identification and isolation on mouse intestine

Colorectal cancer (CRC) is the second cause of death by cancer; a frequent complication is regeneration of the tumour after therapy. There is an evidence that specific gene signature of intestinal stem cells (ISCs) predicts disease relapse in CRC patients. A description of the method used to identify and isolate these cells by flow cytometry is provided.

Small mouse intestine samples were disaggregated combi-ning enzymatic and mechanical methods; population of single, live cells were selected according to their scatter parameters and Propidium Iodide exclusion. A FacsARIA I SORP (Beckton Dickinsion, Ca, USA) was used for cytometric analysis and sorting. ISCs were identified by their high expression of the EphB2 receptor, which becomes gradually silenced as cells differenciate. Using EphB2 expression, mouse ISCs, crypt proliferative progenitors and differentiated cells were FACS-purified to define a gene program specific for normal ISCs. Epithelial cells (EpCAM+, CD45-, CD31-, CD 11b-) were sorted according to their different EphB2 surface expression; Paneth cells were removed using lectin marker (Fig. 10).

In conclusion, flow cytometry and sorting is a powerful technique to identify and purify intestinal stem cells and the stem-like cell population of the tumour, population which has been suggested to play a central role in colorectal cancer relapse.

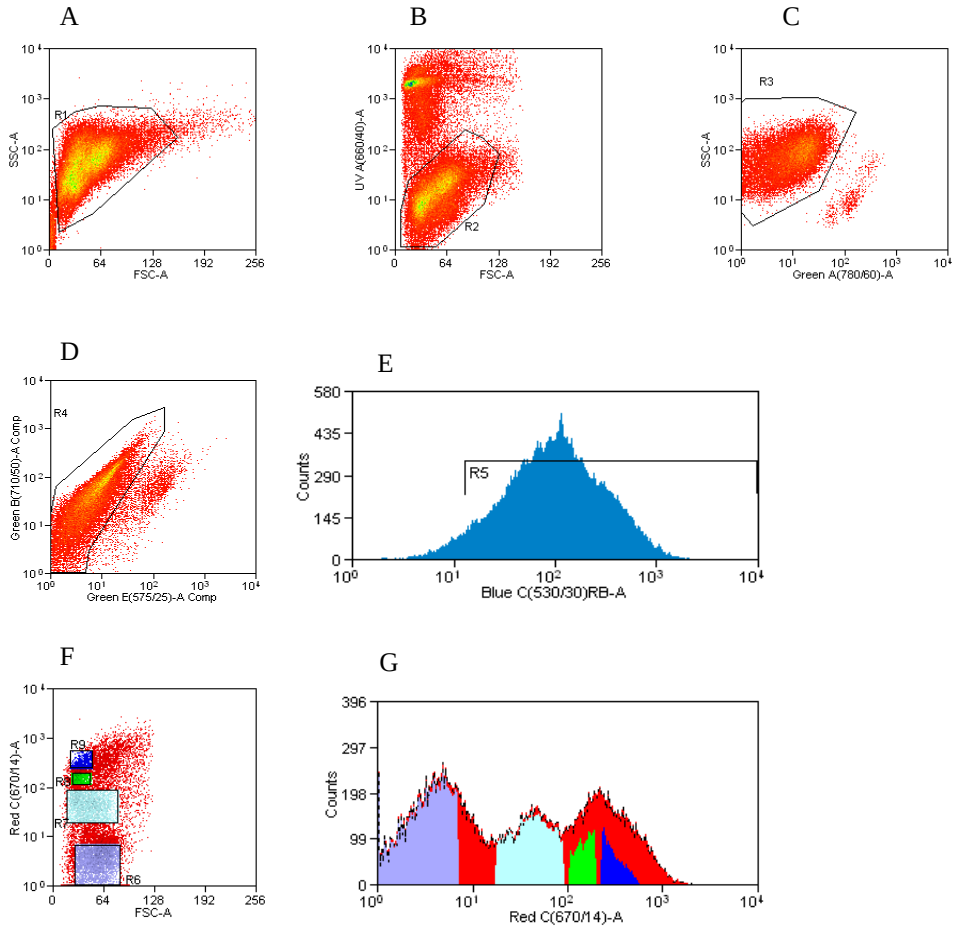

Figure 10: identification of intestinal stem cells by flow cytometry: live, single cells were identified combining scatter parameters (A) and viability by propidium iodide exclusion (B). Epithelial cells were then selected according to their pattern of antigen expression: exclusion of CD45+ CD11b+ CD31+ cells (C), and expression of EpCam (E); Paneth cells were also removed from the analysis (D). Remaining cells were then sorted according to their FSC and EphB2 expression (F); the profile of the sorted fractions according on their EphB2 expression can be seen on G. The profile of high EphB2, low FSC (dark blue color) corresponds to the stem cell population.

Acknowledgements

We would like to thank the authors and all the components of the Nephrology Department, Renal Transplant Unit, Bellvitge University Hospital, University of Barcelona for their kind permission and help in the publication of the example 4.1. The data provided in the example 4.2 is part of the work done by Joan Gil, from the Ciencies Fisiològiques II Department, University of Barcelona. We would like to acknowledge his help and support in the case presented. The data shown in the example 4.3 (Flow cytometric detection of *Plamodium*) is part of the work done by X. Fernàndez-Busquets and P. Urbán, from the Institut de Bioenginyeria de Catalunya (IBEC). We would like to acknowledge their help and support in the case presented. The work presented in example 4.4, "Stem cell identification and isolation on mouse intestine", is part of the work of E. Batlle's group. We would like to thank the authors, especially A. Merlos, and all the components of the Oncology program of the Institute for Research in Biomedicine (IRB) for their kind permission and help in the publication of this example.

References

Bollum, F. J. Terminal deoxynucleotidyl transferase as a hematopoietic cell marker. Blood. 54:1203–1215 (1979)

Bestard O, Cassis L, Cruzado JM, Torras J, Franquesa M, Gil-Vernet S, Lucia M, Grinyó JM.. Costimulatory blockade with mTor inhibition abrogates effector T-cell responses allowing regulatory T-cell survival in renal transplantation, Transpl Int 24:451-60 (2011).

Chattopadhyay P.K. , Roederer M Good cell, bad cell: Flow cytometry reveals T-cell subsets important in HIV disease CYTOMETRY Volume 77A, Issue 7, pages 614–622 (2010)

Comas, J, Rius, N. Flow cytometry applications in the food industry. J. Ind Microbiol Biotechnol) 36:999-1011 (2009)

Darzynkiewicz, Z., Robinson, J.P. & Crissman, H.A. (eds.): Cytometry. Second edition. Part B. Methods in Cell Biology, Volume 42, Academic Press, San Diego, USA, 1994. (ISBN 0-12-203052-4).

Derringer, SD, Torous, DK, Tometsko, KR. Simple and reliable enumeration of micronucleated erythrocytes with a single-laser flow cytometry. Mutat Res 390: 257-262 (1997)

Dolezel J. Ghode W.: sex determination in dioecious plants Melandrium album and M. rubum using high-resolution flow cytometry. Cytometry, 19:103-6, (1995).

Elisa Piva, Carlo Brugnara, Lino Chiandetti and Mario Plebani. Automated reticulocyte counting: state of the art and clinical applications in the evaluation of erythropoiesis. Clin Chem Lab Med;48:1369–1380 (2010)

Frederic Preffer and David Dombkowski Advances in Complex Multiparameter Flow Cytometry Technology: Applications in Stem Cell Research. Cytometry Part B (Clinical Cytometry) 76B:295–314 (2009).

Galbraith, DW, Lambert, GM, Grebenok, RJ, Sheen, J.: Flow cytometric analysis of transgene expression in higher plants: Green fluorescent protein. Methods Cell Biol 50:3-14 (1995).

Garcia, S, Garnatje, T, Twibell, J, Vallès, J. Genome size variation in the Artemisia arborescens complex (Asteraceae, Anthemideae) and its cultivars. Genome 49: 244-253 (2006)

Goodell MA. Stem cell identification and sorting using the Hoesch 33342 Side Population. Current Protocols in Cytometry Chapter 9: Unit 9.18 (2005) Wiley, New York (ISBN 0-471-16131-4)

Haugland, R.P The Molecular Probes® Handbook, 11th Edition—A Guide to Fluorescent Probes and Labeling. (2010)

Hewitt, CJ, Nebe-Von-Caron, G. An industrial application of multi-parameter flow cytometry: assessment of cell physiological state and its application to the study of microbial fermentations. Cytometry 44:179-187 (2001).

Longobardi Givan A. Flow Cytometry First Principles. 2nd edition (2001) Wiley-Liss (ISBN 0471382248)

Merlos-Suárez et al. “The intestinal Stem Cell Signature Identifies Colorectal Cancer Stem Cells and Predicts Disease Relapse”. Cell Stem Cell (2011), doi:10.1016 /j.stem.2011.02.020.

Ormerod, M.G. Flow Cytometry. 2nd edition. (1999) BIOS Scientific Publishers, Oxford. (ISBN 185996107X)

Ormerod, M.G. (ed.)) Flow Cytometry — A practical approach. 3rd edition. (2000 Oxford University Press, Oxford, UK. (ISBN 0199638241)

Ormerod M.G. Flow Cytometry — A basic introduction (2008). (ISBN 978-0955981203)

Parish, C.R. & Warren, H.S. Use of the intracellular fluorescent dye CFSE to monitor lymphocyte migration and proliferation. Curr. Protoc. Immunol. 4.9, 1–10 (2001)

Petriz J. Flow cytometry of the Side Population (SP) Current Protocols in Cytometry Supplement 39 Unit 9.23 (2006) Wiley, New York (ISBN 0-471-16131-4)

Robinson J.P editor. Handbook of Flow Cytometry Methods. (1993) Liss/Wiley, New York (ISBN 0471596345)

Robinson, J.P. et al. (eds.): Current Protocols in Cytometry. Wiley, New York (ISBN 0-471-

16131-4)
Shapiro H.M.: Practical Flow Cytometry (4 ed) (2003) Liss/Wiley, New York. (ISBN 0-471-41125-6)
Torrell, M, Vallès, J. Genome size in 21 Artemisia L. species (Asteraceae, Anthemideae): Systematic, evolutionary, and ecological implications. Genome 44: 231-238 (2001)
Vernon C. Maino, Maria A. Suni, and Joyce J. Ruitenberg Rapid Flow Cytometric Method for Measuring Lymphocyte Subset Activation Cytometry 20:127-153 (1995)
Zola H, Swart B, Banham A, Barry S, Beare A, Bensussan A, Boumsell L, D Buckley C, Bühring HJ, Clark G, Engel P, Fox D, Jin BQ, Macardle PJ, Malavasi F, Mason D, Stockinger H, Yang X. CD molecules 2006--human cell differentiation molecules. J Immunol Methods. 318 (1-2): 1–5. (2007).

Overview of molecular interactions using Biacore

Marta Taulés and Jaume Comas

Unitat de Citometria, CCiTUB, Universitat de Barcelona. Parc Científic de Barcelona. Baldiri i Reixac, 10. 08028 Barcelona. Spain.

email: *marta@ccit.ub.edu*

Abstract. Surface Plasmon Resonance (SPR) technology is a powerful tool for studying a wide range of different putative interactions. This kind of optical biosensors allow to obtain (in real time and without labelling) quantitative and qualitative information about the kinetics of the surface-binding process. The most critical points to keep in mind when using the technique are presented, as well as practical examples of applications.

1. Introduction

Putative molecular interactions demonstrated using different partners and different methods [1] is the best way to elucidate what is going on in a biological system. There are a wide range of methods available for detecting interactions (e.g., ELISA, pull downs, radio and fluorescence-ligand assays) useful for measuring high-affinity interactions. There are several label-free approaches for the detection of biomolecular interactions based on physical principles such as surface plasmon resonance (SPR), interferometry, diffraction and quartz microbalance. Those measurements are not possible using any other technology [2]. Among these, SPR based technology is the most widely used. In addition, SPR allows the analysis of weak interactions saving time and sample and having high throughput screening.

The analysis of molecular interactions using SPR is becoming the most used technique to study interactions between macromolecules without labeling and in real time. It helps us to answer different questions such as:

- How specific is an interaction?
- How strong is an interaction?
- How fast is an interaction (in terms of association and dissociation rates).
- What are thermodynamic parameters for an interaction?

As well mentioned in [3], when studying molecular interactions, the ligand is bound to a solid support, such as a sensor chip. After exposing the ligand to a potential binder (an analyte), the molecules can interact spontaneously. To be able to repeat the measurement in the same chip with different analyte concentrations, the surface of the chip needs to be regenerated. The regeneration agent should be selected by its ability for removing the analyte without significantly damaging the ligand. In addition, the nature of this regeneration agent gives us information about the kind of interaction.

Since the introduction of the first commercial SPR machine in 1990 by Pharmacia Biosensor AB, 25 suppliers of SPR instruments have appeared. Here we will discuss about the Biacore T100 instrument (General Electrics Healthcare), released in 2005 and recently upgraded to T200.

2. Methodology

2.1. Physical principles: What does Surface Plasmon Resonance (SPR) mean?

Total internal reflection (TIR) occurs when polarized light pass at a critical angle through a glass prism on a sensor chip. When a thin -about 50 nm- metal (usually gold) layer is added, photons become plasmons and a reduction (a dip) in the intensity of reflected light can be detected (Fig. 1a, 1b, 1c).

The angle at which the maximum loss of the reflected light intensity occurs is called resonance angle or SPR angle. The angle at which the minimum intensity is observed will shift from A to B. A change in the refractive index at the surface of the gold layer occurs as a result of binding of molecules to the gold layer side [4]. The refractive index in the side of the gold it is affected by the amount of mass bounded to the ligand. Fig. 2 shows a typical sensorgram:

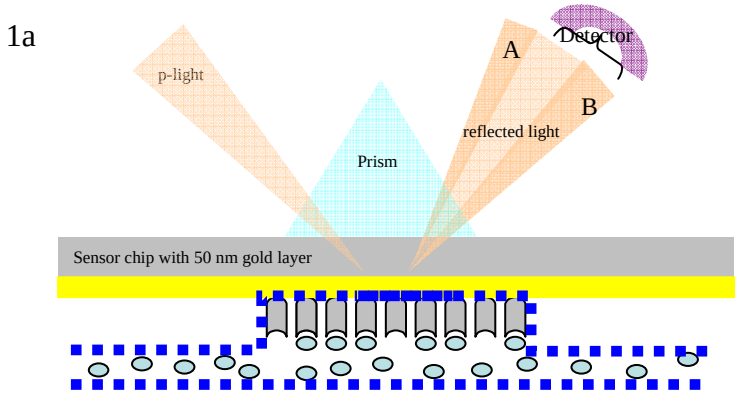

Figure 1a) The polarized light illuminates the sensor chip under conditions of total internal reflection. One binding partner (ligand) is immobilized on the chip, and the analyte is injected. Binding between the partners is increases the mass concentration at the surface of the chip resulting in an increase in the refractive index of the solution close to the surface and a shift in the position of the resonance angle (from A to B).

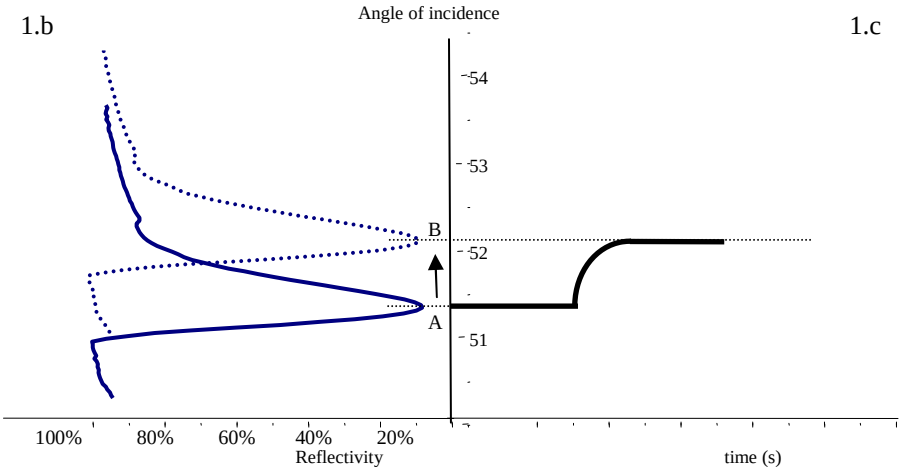

Figure 1b) Rotate SPR dips: reflected light versus incident angle. After the change in refractive index (binding), the angle changes and a shift of the SPR angle to position B appears. **Figure 1c)** Plot of the angle shift as a function of time (sensorgram).

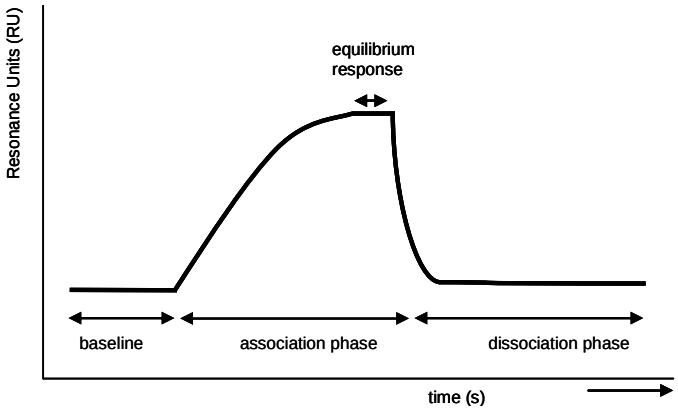

Figure 2) Sensorgram: the kinetics of the interaction can be studied in real time. The response increases during the association phase when the analyte pass across the flow cell and binds to the immobilized ligand. The end of the injection (association phase) might correspond to the equilibrium. After the injection stop (flow and time defined prior on the software) the running buffer is injected and the response decreases during the dissociation phase, where the analyte is spontaneously dissociating from the ligand.

2.2. Terminology

The terminology used in this area in listed in Table 1.

Table 1. Terminology used in Surface Plasmon technology

Resonance Units (RU)	1.000 RU (Resonance Units) correspond to a shift of 0.1º in the resonance angle, or a change in the refractive index of 10^{-3}. For CM5 chips (standard carboxy-methylation level of the dextran used for general purpose), 1.000 RU corresponds to a surface concentration of 1 ng/mm^2 for proteins. 150KDa corresponds to signals greater than 10.000RU (for CM5 chips).
Sensorgram	A plot illustrating the change of the signal on the surface of the sensor over time. The X-axis represents the time, and Y-axis represents resonances units (RU).
Ligand	The molecule immobilized on the surface of the sensor.
Analyte	The molecule in solution that interacts with the immobilized ligand.
Equilibrium dissociation constant (K_D) and affinity constant (K_A)	Constants representing the affinity between two molecules. They are a function of the concentrations of the complex AB ([AB]) and concentration free of A ([A]) and B ([B]) in the equilibrium state of the mixture of the two molecules A, B. The K_D is the reciprocal of the affinity constant K_A, where K_A=[AB]/[A][B]. Typical range of equilibrium association constants (K_A) is 10^5-10^{12} M^{-1}.
Association rate constant (k_a), dissociation rate constant (k_d)	k_a or k_{on} and k_d or k_{off} represent the rate at which the two molecules A and B associate and dissociate. $A+B \underset{k_d}{\overset{k_a}{\rightleftharpoons}} AB$ Association-rate constants, from 10^3 to 10^8 M^{-1} s^{-1}; and dissociation-range constants, from 10^{-6} to 1 s^{-1}.
Running buffer	Buffer used during the assay. The composition should be adapted according to the nature of the interaction.

BT.10

2.3. Commercial chips available

Several chips are available depending on the nature of its surface and binding capabilities: CM5 and CM7 are covered with carboxy-methylated dextran for immobilization via -NH_2, -SH, -CHO, -OH, or -COOH groups. They can attach proteins, nucleic acids, carbohydrates or small molecules. CM4 chips are used when the sample has a high positive charge. CM3 and C1 are indicated for very large analytes; C1 (carboxyl groups attached onto the gold) are recommended when the analyte has avidity for the dextran.

Other chips guarantee the orientation of the ligand: the NTA chip is used for immobilization of histidine-tagged molecules; SA or CAP kit for the immobilization of biotinylated peptides, proteins, nucleic acids, or carbohydates. The Sensor chip L1 is used to incorporate a molecule into a lipid bilayer; it is suitable for work with transmembrane proteins. In the HPA chip, liposomes are adsorbed spontaneously to the hydrophobic surface to form a supported lipid monolayer with the hydrophilic heads directed out toward the solution.

Finally, there are "naked" chips made of untreated gold surface (sensor chip AU) for its use with a wide variety of coating techniques. Customized surface chemistries using self-assembled monolayers (SAM) or other modifications can be designed.

2.4. Instrumentation

The T-100 is a fully-automated instrument (Fig. 3): robotic sampler loader, temperature regulation from 4 to 45 ºC (both for compartment containing the sample as well as the chip), buffer degasser and buffer selector (up to four buffers can be used).

Figure 3: The T-100 system

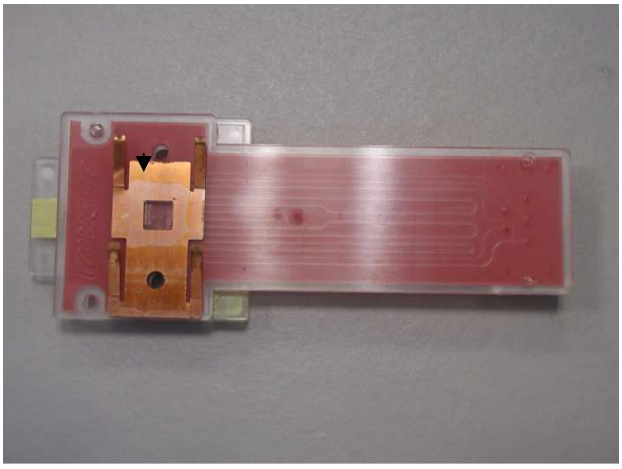

Figure 4: Integrated μ-Fluidic Cartridge (IFC), microfluidifics face.

The main parts of the system are:

- The SPR detection system or refractive index sensor. Biacore uses so-called Kretschmann configuration for the optical detection, with all components fixed. Reflected light intensity is monitored over a range of angles simultaneously; measures are dependent on surface concentrations and temperature.
- The Integrated μ-Fluidic Cartridge (IFC, Fig.4). The IFC is plugged vertically into the frontal part of the machine. The opposite face of the chip is matched with the optointerface (OI) and presented to the prism for optical detection of the signal.The small central square matches the chip and describes four flow cells (Fc). Those flow cells can work in single, pair wise or serial runs. Flow cell 1 can be used as reference cell when it connects to flow cell 2, 3 and 4; whereas Fc3 can be used as a reference for Fc4; these options are selected from the control software.
- Liquid handling system: it consists of two syringes and one peristaltic pump. The buffer selector valve is controlled from the software too (it can be use up to four different buffers); integrated buffer degasser: the running buffer do not need to be degassed prior to use

2.5. Experimental conditions and fitting of mathematical models:

The interpretation of the sensorgrams is not always obvious. The reason why some published data do not fit a simple bimolecular model (A+B=AB) could be the choice of a non recommended experimental design; the shape of the sensorgrams for those simple interactions should be a simple exponential. Square shapes correspond to very fast k_{on} and k_{off}. The deviations from these usual simple exponential shapes are usually caused by instruments artifacts, sample aggregation or other artifact not fully understood. In order to avoid pitfalls hindering these analysis data, it is imperative to be careful with a number of critical aspects: heterogeneity of the sample, mass transport, avidity,

non specific binding, mismatching between buffer running and sample or matrix effects. High flow rates or low density ligand immobilization contribute to minimize mass transport [5].

It is a common mistake to assume the purity of the ligand and analyte. Both of them must be monomeric in solution and form a 1:1 complex when mixed [6]. Basic proteins or sticky samples tend to bind to the dextran matrix; to avoid this problem you can couple the sample onto the surface or use CM4, CM3 or C1 sensor chips (which have a lower charge density) or add carboxymethyl-dextran to the running buffer and samples.

Another important point to consider is coupling, direct or indirect. Direct covalent coupling stabilizes the surface but usually the ligand is randomly oriented throught primaries amines (the heterogeneity onto the surface is raising). Capturing methods using antibodies (anti- GST, anti-Flag) contribute to create a homogeneous surface, but if the capturing step is not stable it may introduce a background surface decay which interferes with the analysis. Selecting the optimum immobilization method is a compromise between introducing surface heterogeneity or instability. It is recommended to use the surfaces at low density ligand, immobilizing an amount of ligand that gives Rmax in the range 20-500 RU (5-20 RU for low molecular weight compounds).

The binding capacity of the surface is a function of different parameters, where:

$$\mathbf{R_L = MW_L/MW_A \times R_{max}/s} \qquad \mathbf{R_{max} = MW_A/MW_L \times R_L \times s}$$

- R_{max} = Maximum binding capacity (in RU). Intensity of the response produced when the ligand is saturated.
- R_L = Response level (RU) of immobilized ligand.
- MW_A = Molecular weight of analyte
- MW_L = Molecular weight of ligand
- s = number of binding sites per ligand

The choice of a good reference surface [7] might correct the bulk refractive index changes, matrix effects, non specific binding, injection noise and baseline drift.

3. Applications

Cutting edge applications are summarized in [8]. There are very different fields where SPR biosensors can be used: drug discovery [9-11], characterization of nucleic acids [12, 13], proteins [14, 15], binding of ligand and receptor [16], determination of the domain of interaction between proteins using mutated proteins or peptides [17]. Biodetection in medicine [18], food and environment [19], development of biosensors of marine toxins using aptamers as a ligands or viral biosensors to detect human pathogens [20] haave been described. Development of vaccines [21], isotyping the immune response [22], or development of biosensor using olfactory receptors expressed in yeast (BOND Project) can also be found.

In the following section some examples of the use of the Biacore T100 in our institution are described:

3.1. Evaluation of dissociation rates after the injection of different peptides through liposomes

L1 chip (dextran with lipophilic substances alkyl chains) [23] was used for this purpose. The scanning electron microscopy (SEM) image of the chip after capturing liposomes is shown in fig.5.

3.2. Kinetics and affinity analysis of small molecule versus enzyme

A drug study on small molecules is presented using a well-known enzyme / inhibitor sytem.

The Biacore T-100 is one of the most sensitive SPR instruments available and can easily detect the binding of small molecules. The analysis can be performed on colored samples (e.g. furosemide) with no interference from absorption or scattering. In addition, when we use high-flow rate (>30 µl/min), we can achieve in less than 1 s the 100% of the sample concentration in the flow system. In this case, the detection and measurement was done in a short time. The methods used are summarized below in Table 2.

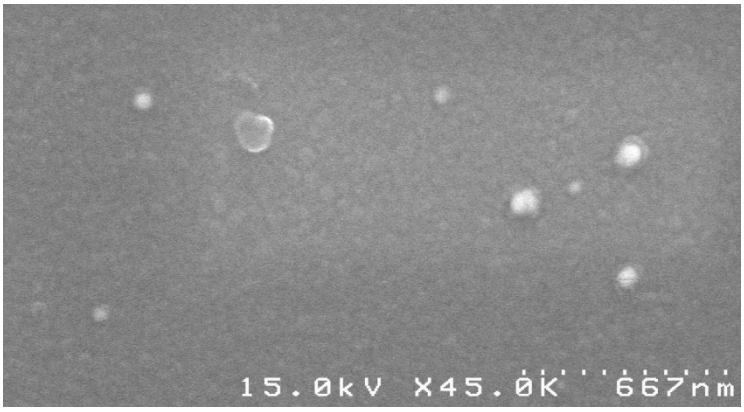

Figure 5. SEM micrograph of liposomes captured on the surface of a L1 chip. Liposomes (100nm) remain intact and circular after being attached to the surface.

Table 2. Methods used in a drug study

	Name	Molecular Weight	Reference
Ligand	human carbonic anhydrase II	30.000 Da	Sigma C# 2522
Analyte	Furosemide	331 Da	Sigma F# 4831
Buffer running	Phosphate buffer saline (PBS) from SIGMA # P4417 + 3% dimethyl sulfoxide (DMSO)		

3.2.1 Immobilization of CAII

The method used for the immobilization of CAII is shown in Table 3. In figure 6, the sensorgrams of immobilization are shown.

Table 3. Method used for the immobilization of CAII

AMINE COUPLING VIA REACTIVE ESTERS	
Before covalent bound: CM5 chip preconditioning: make contact with different pH range and kind of solutions (100mM HCl, 50mM NaOH, 0.1% SDS, water) one injection of each at 100 µl/min during 10s. Electrostatic preconcentration: The pH of the immobilization buffer (very low ionic strength) should be at least 0.5-1 < Isoelectrical point of the ligand to ensure a positive net charge. Elute the electrostatically bounded molecules from the chip surface with an injection of 50mM NaOH, 1M NaCl.	
Amine coupling via reactive esters: Carboiimides have been used to mediate the formation of amine bonds between a carboxylate group (present in the chip) and a primary or secondary amine (present in the ligand).	
EDC	0.4M 1-ethyl-3(3dimethylaminopropyl)-carboiimide in water
NHS	0.1M N-hydroxysuccinimide in water
Make up 1:1 (0.4M EDC/ 0.1M NHS for activating the chip surface) just before coupling. We have to reach 100-150 RU (for CM5 chips) when we have injected the mix during 7 min at 10 µl/min.	
Ethanolamine (deactivate excess reactive groups)	1M ethanolamine-HCl pH8.5. Inject the same time and flow such as an EDC/NHS mixture.
Ligand	20-100 µg/ml in immobilization buffer

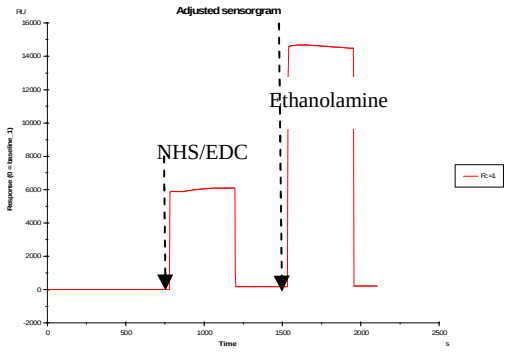

Figure 6a) Reference flow cell after injection of NHS/EDC and ethanolamine (for more detail see amine coupling via amine reactive esters).

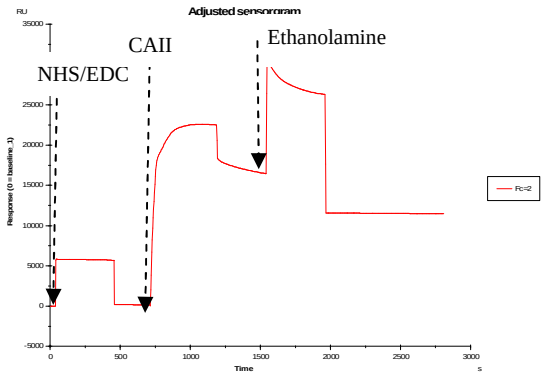

Figure 6b) Immobilization of CAII at 0.1mg/ml diluted in 10mM Sodium Acetat pH 4.9 during 15min at 5µl/min. The relative immobilization level of CAII is 11377 RU.

3.2.2 Steady-State Affinity and Kinetics analysis

As indicated in the formula described in section 2.5, the maximum binding capacity (Rmax) of this model should be: 331/30000*11377*1= 125 RU. However the observed Rmax was 15.4 RU (see Fig. 7). This can be interpreted as only 12% of the CAII being active; higher concentrations of CAII to reach the saturation of the ligand should be used.

BT.10

The matching results obtained by kinetics analysis and affinity analysis (Fig. 7a) must be considered. In affinity analysis, is required to reach the steady state (plateau) before the end of the analyte injection almost in one of the injections. It can be achieved by increasing the concentration of analyte injected or elongating the injection time. The affinity plot (Fig. 7b) is a simple isotherm (Y axis: Rmax, X axis: concentration), and K_D is calculated as half of the maximal response. In this example, the instrument, chip, buffer, enzyme immobilization and analyte were prepared as described in [24] using standard amine-coupling chemistry and blocked flow cell surface as a reference (see Fig 6a). Double referencing [6] was applied and the data evaluated using *BiaEval v 1.1 software*.

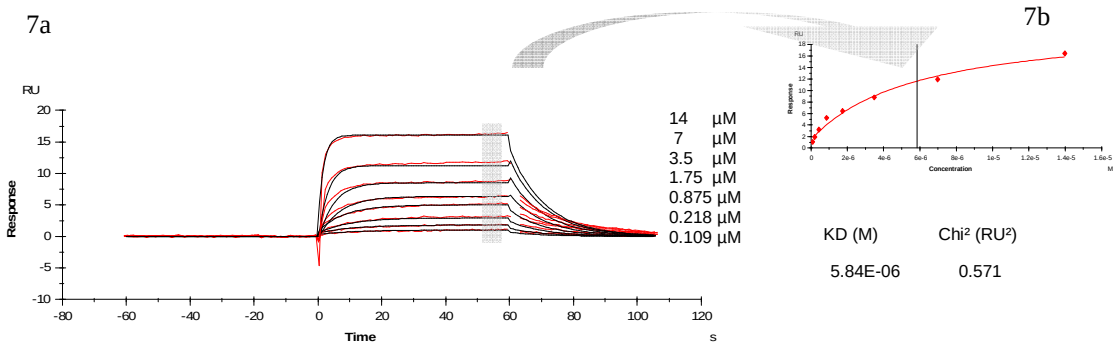

ka (1/Ms)	kd (1/s)	KD (M)	Rmax (RU)	Flow (µl/min)	Chi² (RU²)
3.54E+04	0.091	2.42E-06	15.4	50	0.23

Figure 7. Kinetics (a) and affinity (b) analysis using (CAII) as a ligand versus its inhibitor furosemide at 25ºC. Data sets were fit to a 1:1 model (black lines) by BiaEval 1.1.

Acknowledgements

We would like to thank Dr. M. A. Alsina, and M. Sánchez from Departament de Fisicoquímica (Facultat de Farmàcia, UB) and Dr. I. Haro and M. J. Gomara from "Grup d'Estudis Fisicoquímics de pèptids i proteïnes" (CSIC) for the liposomes-peptides applications; Dr. E. Prats and A. Domínguez (SEM Unit, CCiTUB) for Figure 5; Dr. J. Samitier, Dr. P. Iavicoli (Bond project), Dr. B. Prieto (toxins and aptamers field) from the Institute for Bioengineering of Catalonia (IBEC) and finally Dr. R. Álvarez (Citometry Unit, CCiTUB) for his Biacore knowledge transfer.

References

1. Jing, M. and M.T. Bowser, *Methods for measuring aptamer-protein equilibria: a review.* Anal Chim Acta. **686**(1-2): p. 9-18.
2. van der Merwe, P.A. and A.N. Barclay, *Analysis of cell-adhesion molecule interactions using surface plasmon resonance.* Curr Opin Immunol, 1996. **8**(2): p. 257-61.
3. Andersson, K., D. Areskoug, and E. Hardenborg, *Exploring buffer space for molecular interactions.* J Mol Recognit, 1999. **12**(5): p. 310-5.
4. Schasfoort RBM, T.A.e., *Handbook of Surface plasmon resonance. RSC Publishing Enschede: The Netherlands.* 2008.
5. Morton, T.A. and D.G. Myszka, *Kinetic analysis of macromolecular interactions using surface plasmon resonance biosensors.* Methods Enzymol, 1998. **295**: p. 268-94.
6. Myszka, D.G., *Improving biosensor analysis.* J Mol Recognit, 1999. **12**(5): p. 279-84.
7. Myszka, D.G., *Kinetic, equilibrium, and thermodynamic analysis of macromolecular interactions with BIACORE.* Methods Enzymol, 2000. **323**: p. 325-40.
8. Rich, R.L. and D.G. Myszka, *Survey of the year 2007 commercial optical biosensor literature.* J Mol Recognit, 2008. **21**(6): p. 355-400.
9. Sisquella, X., et al., *A single-molecule force spectroscopy nanosensor for the identification of new antibiotics and antimalarials.* FASEB J. **24**(11): p. 4203-17.
10. Neumann, T., et al., *SPR-based fragment screening: advantages and applications.* Curr Top Med Chem, 2007. **7**(16): p. 1630-42.
11. Shiau, A.K., M.E. Massari, and C.C. Ozbal, *Back to basics: label-free technologies for small molecule screening.* Comb Chem High Throughput Screen, 2008. **11**(3): p. 231-7.
12. Di Primo, C. and I. Lebars, *Determination of refractive index increment ratios for protein-nucleic acid complexes by surface plasmon resonance.* Anal Biochem, 2007. **368**(2): p. 148-55.
13. Misono, T.S. and P.K. Kumar, *Selection of RNA aptamers against human influenza virus hemagglutinin using surface plasmon resonance.* Anal Biochem, 2005. **342**(2): p. 312-7.
14. Alvarez-Moya, B., et al., *K-Ras4B phosphorylation at Ser181 is inhibited by calmodulin and modulates K-Ras activity and function.* Oncogene. **29**(44): p. 5911-22.
15. Nogami, K., et al., *Role of factor VIII C2 domain in factor VIII binding to factor Xa.* J Biol Chem, 1999. **274**(43): p. 31000-7.
16. Pattnaik, P., *Surface plasmon resonance: applications in understanding receptor-ligand interaction.* Appl Biochem Biotechnol, 2005. **126**(2): p. 79-92.
17. Lopez-Alcala, C., et al., *Identification of essential interacting elements in K-Ras/calmodulin binding and its role in K-Ras localization.* J Biol Chem, 2008. **283**(16): p. 10621-31.
18. Habauzit, D., J. Chopineau, and B. Roig, *SPR-based biosensors: a tool for biodetection of hormonal compounds.* Anal Bioanal Chem, 2007. **387**(4): p. 1215-23.
19. Homola, J., *Surface plasmon resonance sensors for detection of chemical and biological species.* Chem Rev, 2008. **108**(2): p. 462-93.
20. Caygill, R.L., G.E. Blair, and P.A. Millner, *A review on viral biosensors to detect human pathogens.* Anal Chim Acta. **681**(1-2): p. 8-15.

21. Varadarajan, R., et al., *Characterization of gp120 and its single-chain derivatives, gp120-CD4D12 and gp120-M9: implications for targeting the CD4i epitope in human immunodeficiency virus vaccine design.* J Virol, 2005. **79**(3): p. 1713-23.
22. Cooper, M.A. and W.M. Yokoyama, *Memory-like responses of natural killer cells.* Immunol Rev. **235**(1): p. 297-305.
23. Cooper, M.A., et al., *A vesicle capture sensor chip for kinetic analysis of interactions with membrane-bound receptors.* Anal Biochem, 2000. **277**(2): p. 196-205.
24. Papalia, G.A., et al., *Comparative analysis of 10 small molecules binding to carbonic anhydrase II by different investigators using Biacore technology.* Anal Biochem, 2006. **359**(1): p. 94-105.

Radiation Protection education and training in several ionising radiation applications

Immacula Rafecas

Unitat de Protecció Radiològica, CCiTUB, Universitat de Barcelona. Adolf Florensa 8, 08028 Barcelona. Spain.

email: *imma@ccit.ub.edu*

Abstract. Ionising radiation (IR) applications are quiet common among several areas of knowledge, medicine or industry. Medical X-rays, Nuclear Medicine, X-rays used in non-destructive testing or applications in research are a few examples. These radiations originate from radioactive materials or radiation emitting devices. Radiation Protection education and training (E&T) is of paramount importance to work safely in areas that imply the use of IR. The Technical Unit for Radiation Protection at the University of Barcelona has an extensive expertise in basic, initial and refresher training, in general or specific areas, as well as in courses validated by the Spanish Nuclear Safety Council or to satisfy specific needs with bespoke courses. These specific customer needs are evaluated and on-site courses can also be carried out.

1. Introduction

Ionising radiation (IR) applications are quiet common among several areas of knowledge, medicine or industry. The low intensity of some of them is counterbalanced by the huge number of people involved. Probably one of the most effective ways of keeping the risk at minimum is specific education and training (E&T) at different levels according to the area of application and responsibilities [1], thus spreading the radiation protection (RP) culture.

According to the International Radiation Protection Association (IRPA), the main objective of RP is to provide for the protection of man and his environment from hazards caused by radiation, and thereby to facilitate the safe use of medical, scientific, and industrial radiological practices for the benefit of mankind [2].

On the other hand, one of the pillars of RP is the ALARA concept. ALARA is the acronym for "As Low As Reasonably Achievable", the radiation protection optimisation principle, defined by the International Commission on Radiation Protection (ICPR) as follows [3]: "the likelihood of incurring exposures, the number of people exposed, and the magnitude of their individual doses should all be kept *as low as reasonably achievable***,** taking into account economic and societal factors." This goal can only be achieved by education and training programmes involving all stakeholders.

2. Ionising radiations nature and sources

2.1. Physical principles

It is said that "Radiation is a fact of life", because of its ubiquity. As radiation simply defines the process in which a body emits energy or particles that propagate through a medium, this can be found in different physical forms, commonly separated in two main groups: ionising and non-ionising radiations [4]. Non-ionising radiations include most of the electromagnetic spectrum (photons), from radio waves to ultraviolet light; and ionising radiations include X and gamma-rays, as well as particle emissions (e.g. alpha or beta particles) (Figure 1). Photons are emitted in many natural processes. For example, when a charge is accelerated it emits synchrotron radiation. During a molecular, atomic or nuclear transition to a lower energy level, photons of various energies will be emitted, from infrared light to gamma rays. A photon can also be emitted when a particle and its corresponding antiparticle are annihilated (e.g. electron-positron annihilation).

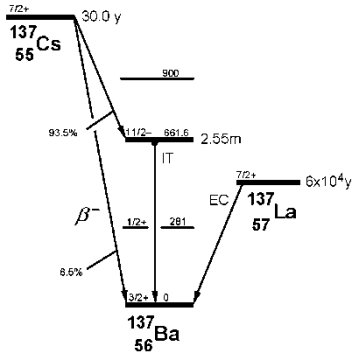

Gammas from ^{137}Cs (30.07 y)

Eγ (keV)	Iγ (%)	Decay mode
283.53 *4*	0.00058 *8*	β⁻
661.657 *3*	85.1 *2*	β⁻

Betas from ^{137}Cs (30.07 y)

Eβ endpoint (keV)	Iβ (%)	Decay mode
513.97	94.4 *2*	β⁻
892.22	0.00058 *8*	β⁻
1175.63	5.6 *2*	β⁻

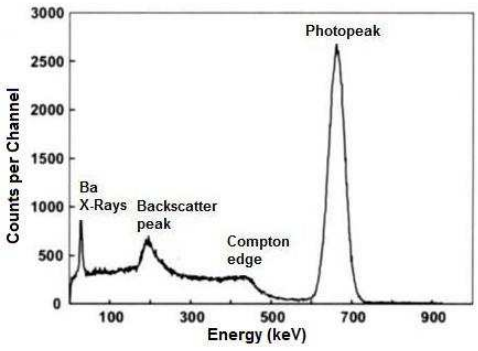

Figure 1: Decay scheme for Cesium-137 (^{137}Cs) (left); decay modes, energies and intensities (centre); and its corresponding Sodium iodide gamma spectrum (right).

The different kinds of electromagnetic radiation have different kinds of interactions with matter [5], and both ionising and non-ionising radiation can be harmful to organisms and can result in changes to the environment. But, non-ionising electromagnetic radiation has only sufficient energy

to change the rotational, vibrational or electronic valence configurations of molecules and atoms; meanwhile ionising radiation has sufficiently high energy to ionise atoms that means to strip an electron from an electron shell, which leaves the atom with a net positive charge (ion).

2.2. Natural sources of ionising radiations

Ionising radiation surrenders us in our direct environment, because it arises from natural processes, mainly from cosmic radiation, radioactivity in soils, minerals and in our body (^{40}K), inhalation of radon gas or radionuclides present in food and drink [6]. The impact of these natural sources can also be enhanced by human activities; such as flights, mining and other activities that led to the production of by-products known as NORM materials (Naturally Occurring Radioactive Materials) [7].

2.3. Artificial sources of ionising radiations

Artificial processes, such as medical X-rays, Nuclear Medicine, X-rays used in non-destructive testing, nuclear power production or applications in research are some examples. In general, these radiations originate from two different kinds of sources: radioactive materials or radiation emitting devices.

2.3.1. Radioactive materials

Radioactive materials are those materials that contain radioactive elements (radionuclides), which are unstable atoms that spontaneously emit radiations as they decay. Artificial radioactive materials can be found in two forms, known as sealed and non-sealed sources respectively. *Unsealed sources* consist of radioactive chemical compounds that are directly accessible and can be manipulated directly. For example, radioactively labelled dissolutions used as radiotracers in life science research, to study biochemical pathways. Nearly any chemical compound can be radiolabeled [8]: carbohydrates, lipids, amino acids, nucleic acids, hormones, drugs…

On the other hand, *sealed sources* usually consist of a sealed capsule (of non-radioactive material) that contains solid radioactive materials. They can form a part of a device, as in some radiotherapy equipment, or constitute individual items, such as the little sealed radioactive sources for educational purposes.

2.3.2. Radiation-emitting equipment. In contrast to radioactive materials, radiations emitted from this apparatus do not come from spontaneous decay but from an electric device (Figure 2), where radiation can only be generated and emitted as long as the device is switched on, so it depends on a power supply. Probably medical X-ray machines are the most widespread radiation emitting equipment [9], but devices such as electron microscopes and some type of cathode-ray tubes, generate ionising radiation as a by-product of some other function.

Particle accelerators also constitute radiation-emitting equipment. Linear accelerators (LINACs) are widely used in medicine, for radiotherapy and radiosurgery. Meanwhile circular accelerators can be used as synchrotrons to obtain synchrotron light or radiation (X-rays); or as cyclotrons, for proton therapy, or those used to produce the short-lived radionuclides for positron emission tomography (PET) in nuclear medicine imaging. Finally colliders, such as the Large Hadron Collider (LHC) at CERN are also sources of ionising radiation and particles [10].

3. Ionising radiations applications

3.1. Medical/Veterinary applications

Ionising radiation has two very different uses in medicine: for diagnosis and therapy. Both are intended to benefit the patients and, as with any use of radiation, the benefit must outweigh the risk.

Diagnostic X-ray examinations (Figure 3) are quite common and include a wide range of equipment variations. Simple X-rays are used in dental intraoral or panoramic examinations, traumatology, bone densitometry, mammography, etc. More specific equipment is needed in

Computed Tomography (CT) or in interventional radiology, which make use of C-arm apparatus in the operation theater [11].

Figure 2: Faxitron cabinet enclosed X-ray machine used in some X-ray UTPR-UB training courses

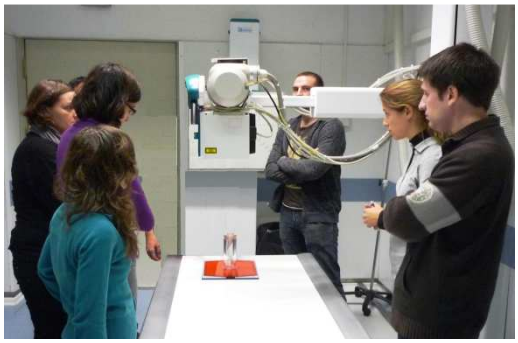

Figure 3: X-ray Quality control training session with UTPR-UB equipment

Some diagnostic procedures involve the administration of radionuclides as non-sealed sources to patients in Nuclear Medicine [12], as in bone gammagraphy (using special radionuclides as ^{99m}Tc) in the form of radiopharmaceuticals. Or in Positron Emission Tomography (PET), which makes use of short-lived radionuclides, at present mainly ^{18}F, with a half-live shorter than 2 minutes, in the form of ^{18}F-FDG (Fluor-deoxy-glucose).

On the other hand, the aim of radiotherapy is to cause damage to cancerous cells to stop its reproduction and the cancer progression. Radiations used are high-energy gamma rays from ^{60}Co sources or high-energy X-rays generated by linear accelerators. Small sealed radioactive sources can also be implanted in the patient's body in brachytherapy. Finally, in a few centers around the world accelerated proton beams are used for radiation therapy (Proton therapy) that can be precisely delivered in depth [13] due to the presence of the characteristic Bragg peak.

3.2. Industrial applications

Ionising radiations are powerful tools in industry, mainly in the so called non-destructive testing (NDT), where gamma sources or high-energy X-rays are used to obtain an image of the inner parts of pieces to verify the integrity of components or flaws [14]. Non-destructive testing can be applied as a part of the final product quality control assurance, or later in used components to localize cracks or worn pieces. It is fairly used in automotive, aeronautic or electronic industries, for instance. With a similar aim radioactive tracers may allow to find a hole in a tube or to measure wear in a motor.

X-ray inspection systems can be applied in different areas, from final product quality control for a wide range of packaged items to the well known baggage control security systems in airports and official buildings. In this sense food in cans, jars or packets are systematically scanned to find foreign materials (Figure 4), underfills and verify package contents in the food, beverage and drug packaging industries [15]. Furthermore, lately some countries are implementing the use of full body scanners [16] in airports and train stations to look for hidden objects; some of these devices are based on direct X-ray technology and others on backscatter X-rays.

Another industrial use of ionising radiations concerns gauges [17]. They can be used for example to control the level of replenishment in tanks of liquids or grainy substances, or even packed beverages. Or thickness gauges, useful to control the product thickness in continuous production, like that of paper, rubber, etc.

Figure 4: Different radiographic conditions in an experimental example designed by the UTPR-UB for a specific X-ray equipment course. It consists of a jar of food where two thin foreign objects have been detected by means of X-ray technology, showing different image qualities

In industrial irradiation facilities radiation is used for sterilization of mainly sanitary tools and equipment, among others; this includes different kind of products used in agriculture and flower-growing (soils, substrates, fertilizers, plastic flower pots and seeds). An advantage is that the object may be sealed in plastic before sterilization. An emerging use in food production is the sterilization of food using food irradiation [18]. Food irradiation seems to provide optimum results for inhibition treatment of tuber shoots, elimination of insects from fruits and seeds, delaying the maturing process of fruits and elimination of alterative microorganisms and pathogens in any type of food [19], helping to improve food-related health worldwide. Electron accelerators as well as gamma sealed sources (^{60}Co) are currently in use. At present, in the Spanish legislation food irradiation is only allowed for dried aromatic herbs, spices and vegetal condiments [20].

3.3. Scientific and biological Research applications

At the University of Barcelona (UB), as in all worldwide leader Research institutions, non-sealed radioactive sources are in use in low quantities as radioactive tracers, where radioactive atoms substitute its stable isotope in a molecule. Then as radioactive emissions from radioactive atoms can be relatively easily detected, this molecule can be followed in any physical, chemical or biological system (Figure 5). In biological systems radioactive tracers can be applied at the different study levels [21]: “in vivo” on different animal species, “in vitro” in cell culture systems, in nucleic acid or protein labeling techniques, Radioimmunoassay (RIA), as well as in subcelular localization of molecules, so in Molecular Biology; but also in drug discovery studies, Pharmacology, Biochemistry, Ecology and so on. A common and important aspect of most of these procedures is the detection technique, where Liquid Scintillation Counting (LSC) is a powerful technique [22] that is described elsewhere in this Handbook, as well as in the UTPR-UB training sessions (Figure 6).

A diagnostic-type X-ray machine or a cabinet enclosed X-ray machine may be used for imaging in research. For example at the UB’s Faculty of Biology Radioactive Facility it is currently in use with experimental animals (mouse, fish, squirrels, etc). X-ray techniques at UB facilities are also treated in depth elsewhere in this Handbook. The cabinet enclosed X-ray machine in Figure 2 is used in the corresponding UTPR-UB training courses.

3.4. Other uses

Many other applications of ionising radiations are in use, as ^{241}Am in ionic smoke detectors, measurement of humidity of soils in buildings and engineering technologies (nuclear gauges such as Troxler), precious stones irradiation to enhance its properties or for crosslinking of polymers. With a similar aim that ionising radiations are used in diagnostic imaging and NDT, they are applied to the study, conservation and restoration of art and cultural heritage [23].

In biology and agriculture, radiation is used to induce mutations to produce new or improved species. An interesting application in Biology/Agriculture is the “Sterile Insect Technique” to

control pests [24], where male insects are mostly sterilized with radiation and released in the fields, so that they have no offspring, thus reducing the next generation's population. This constitutes a method of biological control of pets for crops and insect vectors for sickness (Anopheles and Aedes mosquitoes, tsetse fly, etc).

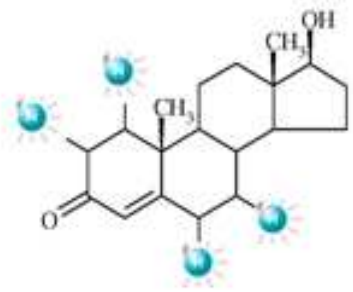

Figure 5: Example of tritium radiolabeled hormone *Testosterone, [1,2,6,7-^{3}H(N)]*

Figure 6: LSC sample preparation for its detection and quantification at a UB Radioactive Facility

People enrolled in all this and other applications involving the manipulation of materials or equipment that emits ionising radiations need to be trained according to their level of responsibility, magnitude of used sources and the application itself.

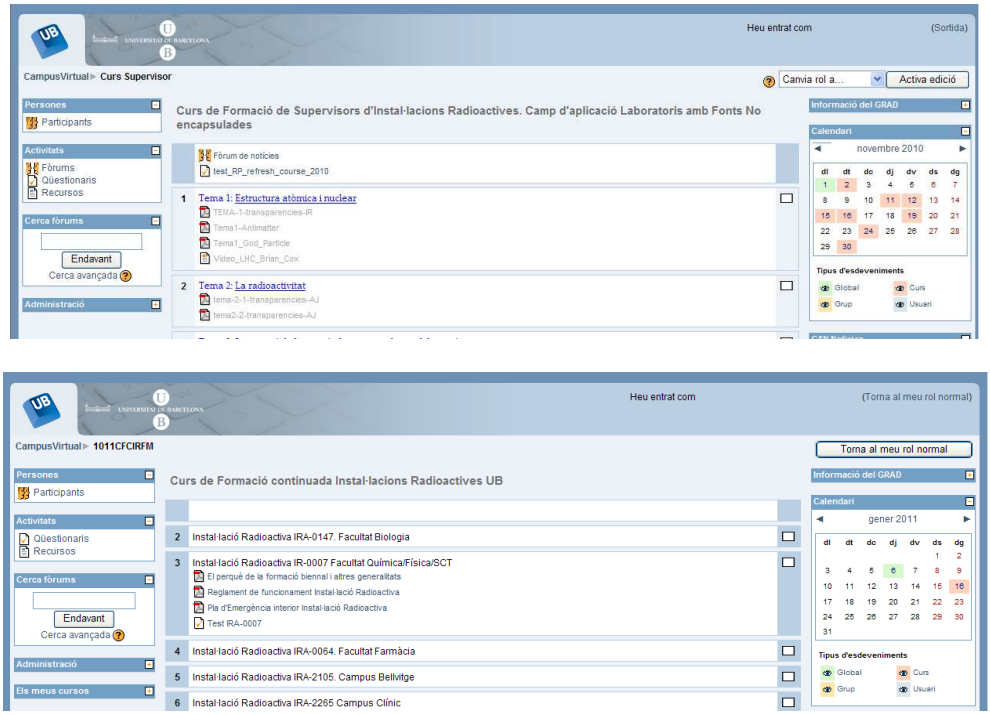

Figure 7: Two examples of web based UTPR-UB training courses implemented on the Moodle platform through the "UB Virtual Campus"

4. Methodology

4.1. Training levels

For practical reasons it is worth to distinguish between basic, initial and refresher training [25].

4.1.1. Basic training

It can be aimed at different collectives of non-exposed workers, for example:

- Workers who do not directly work with ionising radiations, but nevertheless work in the vicinity of radiation sources (including, for example, cleaning and maintenance staff) have to be trained in and informed of the potential hazards associated with radioactive sources and the basic protection and safety procedures.
- Personnel in management positions have responsibility to ensure that all workers, including contractors, receive adequate training in radiologic protection and safety.
- In this category information to stakeholders can also be included.

4.1.2. Initial training

This training is compulsory for any new exposed personnel:

- Students who are engaged in course work or research projects in which radioactive materials and radiation producing devices included in this category are used, and may need specific radiation safety training associated with their academic studies.
- Exposed workers with low level of responsibility need a training level similar to that mentioned above for students.
- Exposed workers with high level of responsibility in a lab or radioactive facility are required to have a licence by the regulatory body, usually as Operator or Supervisor. This is the case of the Spanish regulations [26], where these courses need to be validated previously by the Spanish Nuclear Safety Council (Consejo de Seguridad Nuclear, CSN).

4.1.3. Continuous training

In general the frequency of refresher training is determined by national regulations, but is quite common to establish an annual or biannual periodicity [27]. This can include or not, on the job training, as a means of training for a new practice or equipment.

4.2. Training methodology

Training methodology needs to fit the level and purpose of the training session or course, as well as its length and content. Presential courses or classroom based lectures are still one of the most effective methodology and face-to-face classes are irreplaceable for practicals. Therefore, in most cases, theoretical information is reinforced by the effective use of demonstrations, laboratory exercises, case studies, simulations and technical visits.

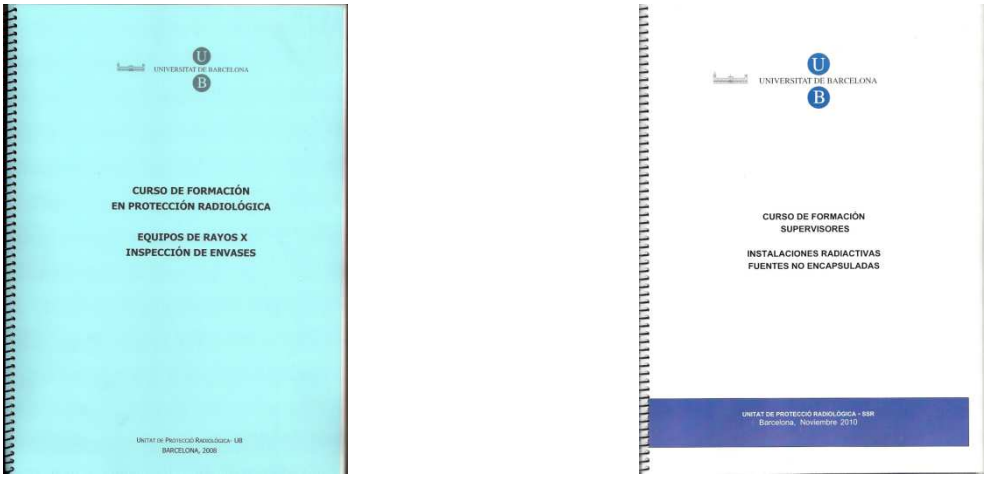

Figure 8: UTPR-UB Handbooks of several Radiation Protection training courses

But nowadays, web-based, on-line or e-learning (Figure 7) modalities have advantages in aspects such as minimizing timetable problems or time consuming trips to the formation centre. On the other hand, the availability of commercial platforms [28] and free, open-source platforms to implement these training modalities facilitates the widespread use of them.

4.3. Training in specific areas

Courses aimed at holding a validated license according to Spanish regulations, are divided in five specific areas [29]: 1) Radiotherapy, 2) Nuclear Medicine, 3) Labs holding non-sealed sources, 4) Industrial Radiography and 5) Processes control and analytical techniques. Furthermore, health professionals using X-ray equipment need to hold an official accreditation [30], to direct or to operate, an X-ray facility. But needs for training are constantly changing as at present health professionals on interventional radiology must undertake a more specific course (second level).

In spite of the improvement and specificity of the aforementioned areas, some cases are difficult to classify under one of the specific licences. For example, scientists in the Chemistry, Pharmacy or Biological applications very often need to hold a license under the specific area of "Labs holding non-sealed sources". But X-ray NDT on an art work needs to hold a licence on "Industrial Radiography".

Other professionals may need some kind of RP training and education [31]. This personnel can include staff of regulatory bodies, emergency response personnel, those involved in transport of radioactive materials, or dealing with the management of residual materials containing radioactive materials, technical staff from firms related to ionising emitting equipment, such as technical services from medical X-ray providing equipment, or X-ray inspection systems or staff operating a baggage control X-ray machine (EVAT firms).

It is worth mentioning that obviously members of a Radiation Protection Technical Unit (UTPR) must also undertake specific training, as Head of UTPR (official course in Spain exclusively organized at CIEMAT (Madrid)) or as RP expert (it can only be accredited by the UTPR Head). Their continuous training must be granted. On the other hand, at European level a wide diversity in the approaches of Member States as to the training and qualifications of radiation protection stakeholders has been described. This makes mutual recognition difficult between Member States and an improved level of harmonisation would be very useful [32].

Figure 9: UTPR-UB equipment used in RP training courses (radiation detectors and personal dosimeters)

5. UTPR-UB training expertise and capabilities

5.1. Training instrumentation and facilities at the UB

For practical exercises different kind of radiation detectors are available at the UTPR-UB (Figure 7), as well as several small calibration sources for demonstrating alpha, beta and gamma emissions, along with a set of absorbers. Also, samples of film badges, TLD dosimeter badges, and direct reading electronic personal dosimeters (Figure 9) are shown. Examples of personal shielding equipment such as Perspex screens and boxes, lead sheets and containers, or lead aprons are also on the spot.

Furthermore, the following big equipment can be used for more specific demonstrations: automatic liquid scintillation counters and spectrometers (LSC), NaI crystal spectrometers and counters, shielded X-ray cabinet (Figure 2) and automatic film processing equipment or electronic autoradiography plates and readers, just to mention some.

5.2. UTPR-UB training expertise and capabilities

Since 1988 training has been a central task of the UTPR-UB. Training ranges from initial training of new Radioactive Facility users (academic staff, researchers, technicians, students) to Supervisor courses validated by the CSN. Initial and refresh courses are of paramount importance in all contexts, especially in the research and university environment, where many people can be involved in low-level ionising radiation applications, but also where research personnel can have a high-turnover rate.

The first edition of a Supervisor accrediting training course at the UTPR-UB took place in 1990. Since then, more than three hundred people has been trained at this level in the application area of "Labs holding non-sealed sources" at their facilities.

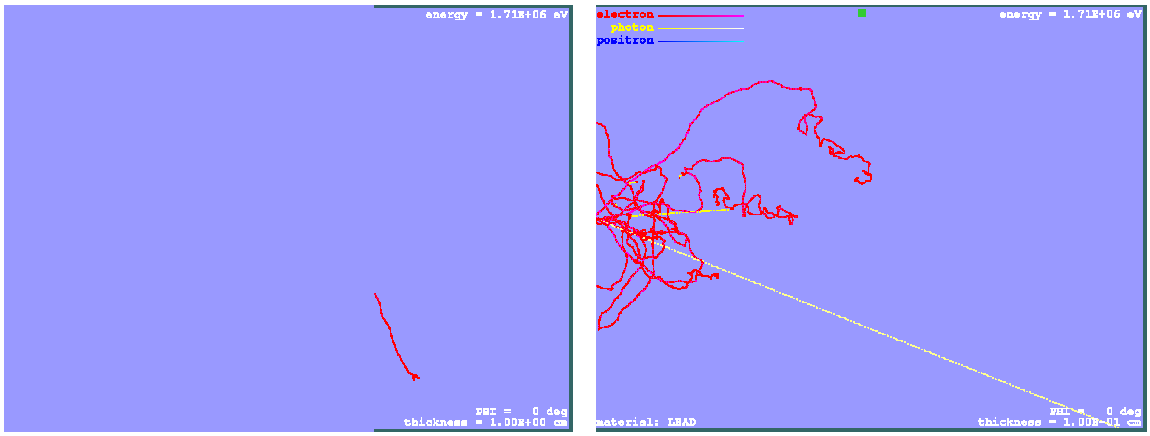

Figure 10: Images of Monte Carlo (PENLAYER) simulation used in RP training courses. In the example, 10 electrons with an energy equivalent to $E_{\beta max}$ of ^{32}P emissions interact with a 1-cm-thick slab of water (left) and a 1-mm-thick slab of lead (right). Notice Bremsstrahlung photon generation (yellow line) in the interaction of electrons with heavy materials.

Our training methodology is in constant evolution, and includes some simulation or web-based tools. For example, simple visual "electron-photon shower" simulation (e.g. the code PENLAYER from the general-purpose Monte Carlo program PENELOPE [33] developed at the UB) (Figure 10), or the use, as a complementary tool, of the Moodle platform by means of the "UB Virtual Campus" (Figure 7). Courses syllabus and contents are carefully revised prior to each edition, mainly to take into account the introduction of new Spanish/European legislation.

Furthermore, custom courses have also been developed on demand. For example, a specific course was organized for the technical staff from a supplier of enclosed cabinet X-Ray inspection systems for packed food. It included the development of a specific course handbook (Figure 8), attending classes, implementation of specific X-ray exercises, a final test and a satisfaction

questionnaire. Also, initial training sessions for staff of dental clinics using X-ray equipment have been developed.

References

[1] IAEA.2003 *Ocupational radiation protection: Protecting workers against exposure to ionizing radiation.* IAEA proceeding series

[2] IRPA. 2011 International Radiation Protection Association. www.irpa.net

[3] ICRP. 2006 *Annals of the ICPR. The optimisation of Radiological Protection. Broadening the process.* ICRP publication 101b. Ann. ICRP 36 3

[4] EPA. 2011 Environmental Protection Agency US. www.epa.gov

[5] Leroy C., Rancoita P-G.2009 *Principles of Radiation Interaction in Matter and Detection,* 2nd Edition. ISBN 978-981-281-827-0. Published by World Scientific Publishing Co.

[6] UNSCEAR. 1993 *Sources and effects of ionizing radiation.* UNSCEAR 1993 Report.

[7] IAEA. 2005 *Naturally occurring radioactive materials (NORM IV).* IAEA-TECDOC-1472

[8] Rennie M. 1999. *Proc Nutr Soc* **58** 4 935.

[9] HPA. 2011 Health Protection Agency UK. www.hpa.org.uk

[10] Blaizot J.P. et al. 2003 *Report of the LHC safety study group*. CERN-2003-001

[11] Kevles, Bettyann Holtzmann 1996 *Naked to the bone. Medical Imaging in the Twentieth Century*. Camden, NJ: Rutgers University Press. ISBN 0813523583

[12] Graham M.M., D.F. Matter 2007. *J Nucl Med* **48** 257

[13] Lewin W.P. et al. 2005. Proton beam therapy. *British Journal of Cancer* **93** 849

[14] Hellier C. 2003 *Handbook of Nondestructive testing Evaluation*. McGrawn Hill. ISBN 0-07-028121-1

[15] McFarlane N.J.B. et al. J. 2000 *Agr Eng Research* **75** 3 265

[16] ANSI 2002 Standard N43.17. *Radiation Safety for Personnel Security Screening Systems using X-rays.*

[17] IAEA. 2005. *Technical data on nucleonic gauges*. IAEA-TECDOC-1459

[18] FAO/IAEA.2009 *Irradiation to ensure the safety and quality of prepared meals*. ISBN 978-92-0-111108-1

[19] FAO. 1984 *General Standards for Irradiated Foods* and *Recommended International Code of Practice for the operation of radiation facilities used for treatment of food* CAC Vol.

[20] Real Decreto 348/2001, *Elaboración, comercialización e importación de productos alimenticios e ingredientes alimentarios tratados con radiaciones ionizantes*. BOE nº 82.

[21] Nielsen J.L., Nielsen. P.H. 2010 *Combined microautoradiography and fluorescence in situ hybridization (MAR-FISH) for the identification of metabollically active microorganisms. Handbook of Hydrocarbon and Lipid Microbiology* ISBN 978-3-540-77584-3

[22] Knoll G. 1999. *Radiation Detection and Measurement*. John Wiley and Sons. ISBN 0-471-07338-5

[23] Van Grieken R. 2002et al. *Non-destructive testing and microanalysis for the diagnostics and conservation of the cultural and environmental heritage.* Proceedings of Art 2002, Antwerp

[24] Collins S. R et al.2008. *J. Appl Entomology* **132** 5 398

[25] IAEA. 2001 Training in Radiation Protection and the Safe Use of Radiation Sources. Safety Report Series nº 20

[26] Real Decreto1439/2010 Modifica el Reglamento sobre Protección Sanitaria contra Radiaciones Ionizantes, aprobado por Real Decreto 783/2001.

[27] CSN. 2003 Instrucción IS-06 sobre formación en protección radiológica de los trabajadores de empresas externas. (BOE nº 132)

[28] Cole. J. 2005 Using Moddle: Teaching with the popular open source course management system. O'Reilly Community Press ISBN 0596008635

[29] CSN 1998 Guía de Seguridad del CSN 5.12 Homologación de cursos de formación de supervisores y operadores de instalaciones radiactivas

[30] CSN 2008 Nuclear Safety Council INSTRUCTION IS-17 *On the recognition of training courses and programmes for personnel that manage the operation of or operate equipment in X-ray facilities for medical diagnosis and the accreditation of the personnel of said facilities.*
[31] DOE US. 2007 *General employee radiological training handbook*. DOE-HDBK-1131-2007
[32] EUTERP. 2011 Harmonizing Europe's Radiation Protection Education & Training. www.euterp.eu
[33] Baró, J. Sempau, J. Fernández-Varea J.M., Salvat F. 1994 Nucl. *Instr. and Meth.* **B84** 465.

Liquid and solid scintillation: principles and applications

Carmen Benito[1], Andrés Jiménez[2], Cristina Sánchez[3], and Aurea Navarro-Sabaté[4]

Unitat de Protecció Radiològica, CCiTUB, Universitat de Barcelona.

[1] IRA Biologia. Diagonal 645. 08028 Barcelona, Spain.

[2] IRA Farmàcia. Joan XXIII s/n. 08028 Barcelona, Spain

[3] IRA Medicina. Casanovas 143. 08036 Barcelona, Spain.

[4] IRA Bellvitge. Feixa Llarga s/n. 08097 L'Hospitalet de Llobregat, Spain

email: *cbenito@ccit.ub.edu, andresjimenez@ccit.ub.edu, cristinasanchez@ccit.ub.edu, aureanavarro@ccit.ub.edu*

Abstract. Scintillation counting is one of the most important developments in the application of radioisotopes to procedures needed by scientists, physicians, engineers, and technicians from many diverse discipline for the detection and quantitative measurement of radioactivity. In fact, Scintillation is the most sensitive and versatile technique for the detection and quantification of radioactivity. Particularly, Solid and Liquid scintillation measurement are, nowadays, standard laboratory methods in the life-sciences for measuring radiation from gamma- and beta-emitting nuclides, respectively. This methodology is used routinely in the vast majority of diagnostic and/or research laboratories from those of biochemistry and biology to clinical departments.

1. Introduction

Radioactive isotopes of common elements are extremely useful in life science disciplines, among others, because radioactive atoms can be substituted for their non radioactive counterparts in chemical formulations. The resulting radioactive compound is easily detectable but still chemically identical to the original material.

Two different systems of detection and counting of radiolabeled compounds based on the scintillation technique have been developed: Solid Scintillation Counting (SSC) and Liquid Scintillation Counting (LSC) depending on the scintillator material used.

The most common scintillator materials are normally classified according to their nature. First, in SSC, the most used scintillator are crystals of inorganic material such as alkali halide crystals, mainly sodium iodide. The high atomic number and density of certain inorganic crystals make them suitable for gamma spectrometry with high-detection efficiencies. On the other hand, scintillators used in LSC tend to be either a liquid (organic solvents) or in solid form (plastics) and they are preferred for the detection of beta particles and neutrons.

In fact, the wide popularity of LSC is a consequence of numerous advantages, which are high efficiencies of detection, improvements in sample preparation techniques, automation including computer data processing, and the spectrometer capability of scintillation analyzers permitting the simultaneous assay of different nuclides.

Herein we summarize the basic principles of scintillation counting with examples of applications in biomedical and environmental sciences developed at the University of Barcelona with the support of Scientific and Technological Centers (CCiTUB) of this university.

2. Methodology

2.1. Physical principles of scintillation technique

Radioactive decay occurs with the emission of particles or electromagnetic radiation from an atom due to a change within its nucleus. Forms of radioactive emission include alpha particles (α), beta particles (β) and gamma rays (γ). Alpha & beta particles directly ionize the atoms with which they interact, adding or removing electrons. Gamma-rays cause secondary electron emissions, which then ionize other atoms. However, some irradiated atoms are not fully ionized by collision with emitted particles, but instead have electrons promoted to an excited state. Excited atoms can return to their ground state by releasing energy, in some cases as a photon of light. Such scintillation phenomena form the basis of a set of very sensitive radiation detection systems. To a first approximation this is a linear conversion of energy into photons and, therefore, the intensity of light in the scintillation is proportional to the initial energy deposited in the scintillator by ionizing radiation. This light emitted is taken as a measure of the amount of radioactivity in the sample [1].

2.2. Instrumentation. Scintillation counter apparatus

A scintillation counter measures ionizing radiation. A scintillation counter apparatus consists of a scintillator, a photo-multiplier tube (PMT), an amplifier, and a multichannel analyzer (Fig. 1).

A solid scintillation counter is aradiation detector which includes a scintillation crystal to detect radiation and produces light pulses while the liquid scintillation counter detect the scintillation produced in the scintillation cocktail by radiation.

The PMT is an electron tube that detects the blue light flashes from the scintillation and converts them into a flow of electrons and subsequently measured as an electric pulse. This consists of a photocathode (photoelectric emitter) that is connected to the negative terminal of a high tension battery. A number of electrodes called dynodes are arranged in the tube at increasing positive potential. When a scintillation photon strikes the photocathode of the PMT is released a photoelectron. Using a voltage potential, the electrons are attracted and strike the nearest dynode with enough energy to release additional electrons. The second-generation electrons are attracted and strike a second dynode, releasing more electrons. This amplification continues through 10 to 12 stages. More electrons are emitted and the chain continues, multiplying the effect of the first

charged particle. By the time the electrons reach the last dynode, enough have been released to send a voltage pulse across the external resistors. The magnitude of the resulting pulse height produced by the PMT is proportional to the photon intensity emitted by the scintillator (crystal NaI(Tl) in SSC or "cocktail scintillator" in LSC). This voltage pulse is amplified and recorded by a multichannel that classifies each voltage pulse. Pulses are collated into channels, and the counts per minute (CPM) in each channel is recorded. Each channel corresponds to a specific range of energies (channels are also known as counting windows), and counts with energies above or below set limits are excluded from a particular channel. When the counts have all been collated, the researcher knows the intensity of radiation, expressed as CPM, and its energy distribution, or spectrum. CPM is proportional to the amount of isotope in the sample, and the spectrum indicates the identity of the isotope.

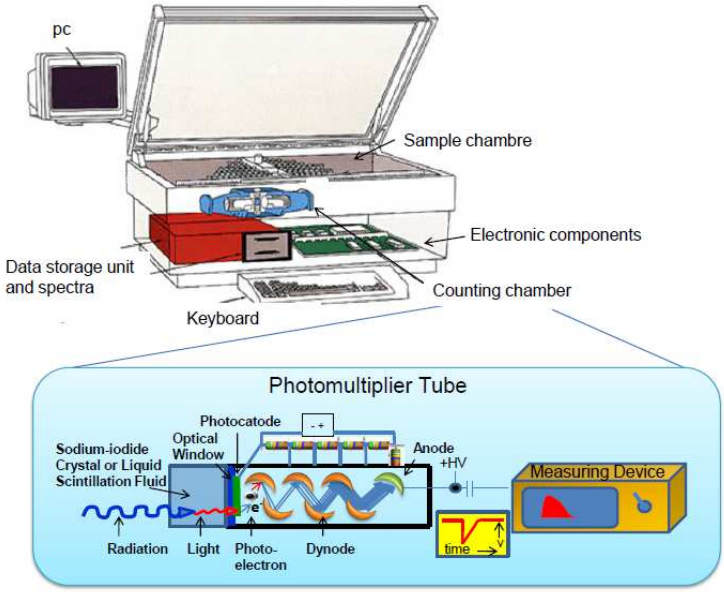

Figure 1. Illustration of a scintillation counter.

2.3. Mechanism of Solid and Liquid Scintillation Counting

In SSC, the transparent inorganic crystal, called scintillator, fluoresces when is irradiated by the sample (Figure 2 right). The most commonly used is Thallium-doped sodium iodide (NaI(Tl)). This detector is made of various sizes for different types of equipment. With this method, involves placing the sample containing the radioactivity into a glass or plastic container, called a scintillation vial that is deposited directly onto a solid scintillating material, dried, and counted in a scintillation counter also called Gamma counter [2].

Solid scintillation is excellent for γ radiation which is highly penetrating and interact with the NaI(Tl) detector by photoelectric, Compton and pair production mechanisms result in light or scintillations throughout a large crystal. An advantage of these techniques is that the same crystal is used for each sample, which enhances reproducibility. NaI(Tl) can be produced in large crystals, yielding good efficiency and producing intense bursts of light compared to other spectroscopic scintillators. Thus, NaI(Tl) is also suitable for use, making it popular for field applications such as the identification of unknown materials. However, because of the poor resolution of NaI-based detectors, they are not suitable for the identification of complicated mixtures of gamma ray-producing materials.

For α or β radiation counting, however, solid scintillation has severe limitations. The crystal must be protected from contamination by the sample, which means that the α and β particles must traverse a barrier prior to reaching the scintillator. In particular, α-radiation is severely attenuated by even 0.05 mm of aluminium or copper, and so cannot be expected to reach a scintillator crystal through even the thinnest shielding [1].

Crystal of zinc sulphide activated with silver, ZnS (Ag) is used in form of microcrystals pressed for the detection of heavy-charged particles (alpha, protons, fission products, etc.). In the case of alpha particles, the crystal mass thickness is about 5mg/cm^2, roughly equivalent to the scope of the alpha particles emitted by natural radionuclides. Because of its small thickness, this detector is very insensitive to beta particles or gamma radiation, property that is very useful when counting alpha particles in an intense background of beta particles or gamma photons.

In LSC, the samples are dissolved or suspended in a solution of organic liquid or cocktail scintillator (which is the sensor of the system) and the scintillation process takes place in a solution of scintillator rather than in a solid crystal. This allows close contact between the radioisotope atoms and the scintillator to assure efficient transfer of energy between the radioactive particles and the solution. Particularly, LSC is a standard laboratory method in the life-sciences for measuring radiation from beta-emitting nuclides [3].

Liquid scintillation cocktails absorb the energy emitted by beta particle and re-emit it as flashes of light (Figure 2 left) through two basic components, the aromatic solvent and small amounts of other additives known as fluors, i.e., scintillants or scintillators. In the first step, beta particles emitted from the sample transfer energy to the solvent molecules, which in turn transfer their energy to the fluors; the excited fluor molecules dissipate the energy by emitting photons of visible light (fluorescence). In this way, each beta emission (ideally) results in a pulse of light. The total number of photons from the excited fluor molecules constitutes the scintillation.

Some beta emitting isotopes (e.g. ^{32}P) can be analyzed on an LSC without using any cocktail, using a technique called Cherenkov counting. Cherenkov is based on charged particles passing through a transparent medium faster than the speed of light relative to the medium they are traversing (e.g., water, etc.). Cherenkov radiation (i.e., light), is produced being detected directly by the photomultiplier tubes.

In LSC, when a charged particle strikes the scintillator, a flash of light is produced, which may or may not be in the visible region of the spectrum, typically with low intensity in the ultraviolet region. Scintillation cocktails often contain additives that shift the wavelength of the emitted light to make it more easily detected. Many cocktails contain additional materials to extend their range of use to different sample compositions, but the solvent and the phosphor provide the scintillation of the mixture.

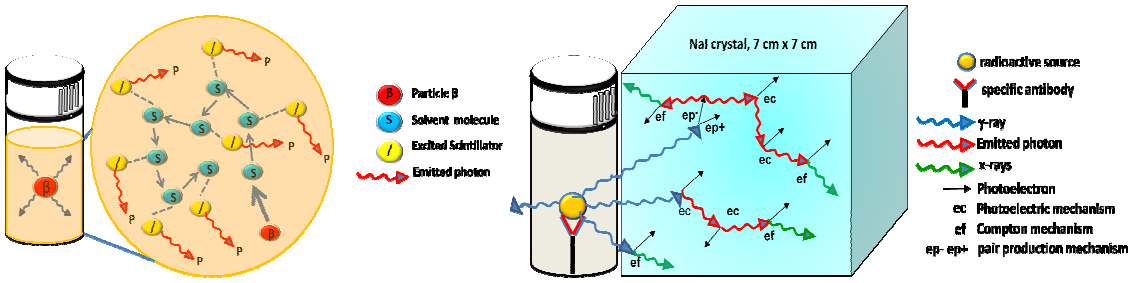

Figure 2. Left: Liquid Scintillation mechanism. Right: Solid Scintillation mechanism

2.4. Detection of interferences in solid and liquid scintillation counting

Solid scintillation gamma counting does not have the disadvantages of quenching normally associated with the liquid scintillation counting technique. This is because the sample is kept physically separated from the scintillator, which prevents any possible physical or chemical interference with the γ-energy transfer and scintillation processes.

In LSC there is a release of energy from the sample as photons, which is not due to the phenomenon of scintillation. This energy unduly increases the count or gives light pulses even in the absence of the radioactive sample producing interferences in the detection process. These must be eliminated from the sample or discriminated by the detection system. These interferences can be distinguished according to their origin:

- Chemiluminescence. It is the production of light as a result of a chemical reaction between components of the scintillation sample in the absence of radioactive material. This most typically occurs when samples of alkaline pH and/or samples containing peroxides are mixed with emulsifier-type scintillation cocktails, when alkaline tissue solubilizers are added to emulsifier type scintillation cocktails, or when oxidizing agents are present in the sample. Reactions are usually exothermic and result in the production of a large number of single photons. It has a slow decay time (from 0.5 hr to > 1 day, depending on the temperature) [4].
- Photoluminescence. Results in the excitation of the cocktail and/or vial by UV light (e.g., exposure to sunlight or UV lights laboratory). It decays more rapidly (usually < 0.1 hr).
- Quench. It is a reduction in system efficiency as a result of energy loss in the liquid scintillation solution. Because of quench, the energy spectrum detected from the radionuclide appears to shift toward a lower energy. The three major types of quench encountered are photon, chemical, and optical quench. Photon quenching occurs with the incomplete transfer of beta particle energy to solvent molecules. Chemical, sometimes called impurity, quenching causes energy losses in the transfer from solvent to solute. Optical or colour quenching causes the attenuation of photons produced in solute. This interference can be overcome through data correction or through careful sample preparation [4].

2.5. Quantitative analysis

In LSC, common nomenclature expresses the intensity of radiation emitted as disintegrations per minute (DPM, activity sample). The sample count rate depends on how efficiently nuclear decay events are converted to light flashes that are detected and quantified by the LSC [4].

Because the sample solution is always present, it can absorb nuclear decay energy thereby preventing this energy from being absorbed by the chemical fluorine molecules, or the solution can absorb photons of light that are emitted by the scintillation cocktail. This causes the phenomenon called quench defined as interference with the conversion of decay energy to photons emitted from the sample vial. In order to compensate for quench and determine the DPM (actual activity sample) from CPM (counts per minute measured), it is necessary to know the counting efficiency: % Eff = (cpm/dpm) x100

The lower the radiation energy of the radionuclide, the greater is the effect of quench on the counting efficiency of the sample. Techniques have been developed for applying these corrections, and a great deal of research has been carried out to improve the efficiency of counting, using various detection systems: internal standardization, sample spectrum quench correction, external standard quench correction, Direct DPM methods [5].

3. Applications

Solid and liquid scintillation techniques are used for the detection of radio labeled isotopes in areas as diverse as biomedicine, ecology and industry.

Scintillation counting capabilities include detection of alpha, beta and gamma emitters, in single, double and triple labelling, and also include the detection of these transmitters by counting in continuous flow (HPLC) and finally the scintillation proximity Assays (SPA)

Detecting and counting alpha emitting radionuclides are routine tasks in nuclear energy and environmental monitoring. Liquid scintillation counting of alpha particles provides high counting efficiency (near 100%). The accurate and sensitive measurement of alpha-emitting nuclides is essential in the nuclear fuel cycle, process control, radioactive waste management and environmental protection. However the energy resolution is quite poor, so they are not very useful for the identification of these radionuclides.

In detection of beta emitters, LSC is the most important application of scintillation counting, with the property that for high-energy beta emitters (^{89}Sr, ^{90}Y, ^{32}P) performance may be close to 100%, while for low energy is lower: 50-60% for ^{3}H, 95% for ^{14}C. However, it is often the

technique of choice for these weak beta emitters. LSC is extensively used, for in vivo and in vitro biomedicine research. The usefulness of radioisotopes in this research stems from their chemical identity with their non-radioactive counterparts. This allows their incorporation into "tracers", radiolabeled components which can be followed and detected through a series of reaction steps. Some of these studies include from carbohydrate [6, 7] and lipid [8, 9] metabolism assays, enzyme activity determination [10, 11], hormone studies [12, 13] to the amino acid [14] and nucleoside transport studies [15, 16, 17]. On the other hand, experimental procedures seek screening of peptide library with Radioligand binding assays [18]. Certain genetic and biochemical studies use high-energy beta emitters as in the case of ^{45}Ca, ^{32}P and ^{22}Na, which are used to quantify the LCS [19, 20, 21]. Other applications are radioactivity contaminant detections for environmental monitoring and ecology studies such as bacterial or microbial activity [22, 23].

Moreover, some beta-emitting isotopes can be analyzed on an LSC without using any cocktail or with only a little water, using a technique called Cherenkov counting [24].

Detection of gamma particles is of special interest in clinical and basic biomedical research. We noted several studies: Hormone determination in blood tests [12], analytical practice for hormone levels determination by radioimmunoanalisis techniques [25] and identification of different radionuclide contaminants in soil samples [26, 27, 28].

In this section we show some examples of applications of liquid and solid scintillations which briefly illustrate the capabilities of these techniques:

3.1. Cell Proliferation assays

Cell proliferation assays measure the incorporation of a radiolabeled DNA precursor, ^{3}H- or ^{14}C-Thymidine, into the replication strands of DNA produced during cell division. Cell proliferation studies based on the thymidine incorporation assay are employed frequently in immunological, cancer, stem cells, and pharmaceutical research to assess the ability of both, natural and synthetic compounds, to stimulate or inhibit cell proliferation.

Before a cell divides, its DNA is replicated and precursors are incorporated, thus if the cells are proliferating and [^{3}H]-Thymidine is added to the culture, it will be incorporated into the cells' DNA. The amount of [^{3}H]-Thymidine incorporated into the DNA is measured with a scintillation counter. The level of the radioactive signal depends on the proliferation rate.

Usually, an inhibitor of cell proliferation is added to the culture, in its presence the proliferation inhibition is calculated from the following expression: [%] of proliferation inhibition = [cpm (untreated) - cpm (treated)] / cpm (untreated)

The ^{3}H-Thymidine incorporation assay is commonly used to measure the effect of a pharmacological or drug treatment on proliferation of cultured cells [29], also to check an effect of cytotoxic drugs on tumor cells or carcinogenetic processes [30], to determine the cell cycle and its phases, to measure the rate of DNA synthesis or to detect antigen-specific T-cell proliferation in culture, among others.

3.2. Metabolites transport determination

The plasma membrane is a selectively permeable barrier between the cell and the extracellular environment. This permeability ensures that essential molecules such as glucose, amino acids, and lipids readily enter the cell, metabolic intermediates remain in the cell, and waste compounds leave the cell. In short, the selective permeability of the plasma membrane allows the cell to maintain a constant internal environment [31].

Transporters through conformational changes expose binding sites to their specific ligands that can join and be transported across the lipid bilayer of the cell membrane [32].

Different radiolabeled molecules are used in a wide range of metabolite transport applications from a simple study of its transport into the cell to more complete studies such as analysis of their metabolic pathways. Transport experiments can be carried out both in vivo(e.g. pumping substances through cell membranes, analyzing glycolysis pathways with ^{14}C-glucose) and in vitro(e.g. analysis, identification and / or quantification of enzyme activity).

Metabolite transport methodology in vitro is based on the incubation of cultured cells with a medium containing a radioactive substrate which will be incorporated to the cell. Briefly, after incubation cells are washed to eliminate the radioactive compound still present in the culture medium and then a cell lysate is obtained for each sample. Samples are mixed with the scintillation cocktail and counted in a LSC.

Herein we describe in detail three kinds of metabolite transport studies commonly assayed in our radioactive installation laboratories. These are: nucleoside transport, glucose transport and amino acid transport.

3.2.1. Nucleoside transport

The nucleotides are of great importance in cell physiology, since they constitute the structural elements of nucleic acids and are therefore essential for cell viability. Also, they intervene in energy homeostasis of the cell due to their involvement in many biochemical processes such as energy metabolism. The nucleosides can act as facilitators of a wide variety of specialized functions and play an important role in human physiology.

Different radiolabeled substrates can be used in nucleoside transport analysis such as the nucleosides: [^{3}H] Uridine, [^{3}H] Guanosine, [^{3}H] Cytidine and [^{3}H] Adenosine and nucleosides analogues: [^{3}H] Gemcitabine, and [^{3}H] Fludarabine [15, 33, 34, 35]. These are used in studies of drug resistance, cancer therapy and chemotherapy. Also, nucleoside reverse transcriptase inhibitors (eg. [^{3}H] MPP+(metformin), [^{3}H]3TC(lamivudine), [^{3}H]ABC(abacavir) and [^{3}H]AZT (azidothymidine)) can be used as radiolabeled substrates in "Short-Time" Uptake measurements, to determine their IC_{50} values [36].

Nucleoside transport methodology in monolayer cultured cells involves incubation of cells with a known concentration of cold substrate to study, to which an appropriate proportion of the radiolabeled substrate is added [37]. Once the cells have been incubated for the time required for testing, the uptake is stopped by washing and a cell lysate is obtained for each condition. Each sample is measured in a LSC in order to quantify the radioactivity retained which corresponds to the amount of substrate incorporated into the cell.

The nucleoside adenosine is among the most studied. Its interaction with membrane receptors maybe involved in the regulation of a variety of physiological processes among them, neurotransmission, cardiovascular activity, lipolysis or platelet aggregation (Figure 3A). In these processes, adenosine plays a role in cell protection (Figure 3B) [38].

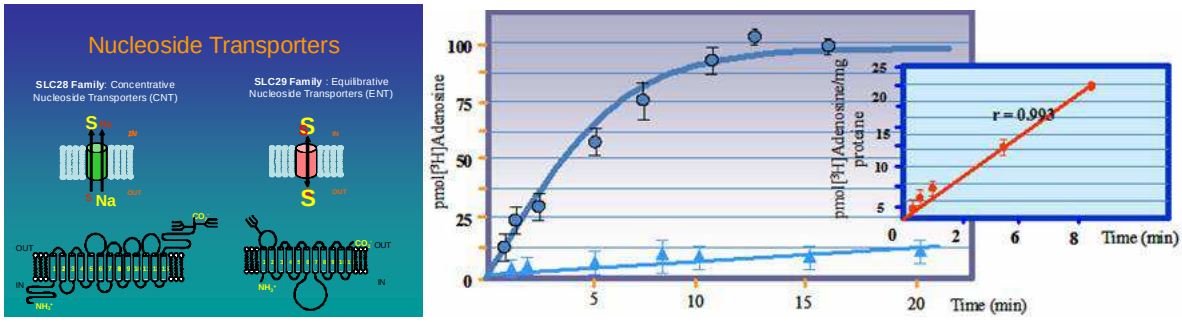

Figure 3: A) Image showing the two nucleoside transporter families. The nucleosides are relatively hydrophilic molecules, thus its internalization into cells is dependent on specific membrane transporters (Image courtesy of Dra I. Huber). B) [3H] Adenosine accumulation by rat testis mitochondria as a function of incubation time.

3.2.2. Glucose transport

Glucose uptake experiments are commonly used to measure cellular metabolic activity and glucose transport. Glucose uptake can be studied using radiolabeled glucose itself or radiolabeled glucose analogous such as 2-deoxy-D-glucose (2DG) or 3-O-methyl-D-glucose (OMG). The most common technique is the use of radiolabeled 2-deoxy-D-glucose, a glucose analog. Once 2-deoxy-D-glucose has been taken up by cells, it is phosphorylated and cannot be metabolized further. Labelled 2-

deoxy-D-glucose phosphate is trapped in the cell (unidirectional transport). By contrast, 3-O-methyl-D-glucose is not phosphorylated, and equilibrates across the cell membrane. Because equilibrium is usually reached rapidly, uptake is typically linear for only a short period of time. D-glucose itself (as opposed to glucose analogous such as 2-deoxy-D-glucose or 3-O-methyl-D-glucose) can be incorporated into lipids, providing a measurement of glucose transport.

As an example, we highlight a recent study carried out in a stable 3T3L1 cell line with a reduced expression of Caveolin-1 where the impact of this reduced expression on insulin action in adipose tissue is evaluated. In this study, the radiolabeled products used are the non-metabolizable glucose analogue 2-deoxy-^{3}H-glucose (to measure glucose uptake) and ^{14}C-Glucose (Glycolysis) [7].

Another interesting example is the comparison of glucose oxidation rates (realized using [U-^{14}C]-glucose) in cardiac cells that over express PGC-1α or silence it after being treated with TNF-α. The purpose of this study is to elucidate the specific mechanisms by which exposure to tumour necrosis factor-a (TNF-α) results in PGC-1α down-regulation in cardiac cells and, as a consequence, in metabolic dysregulation that underlies heart dysfunction and failure (Figure 4) [39]

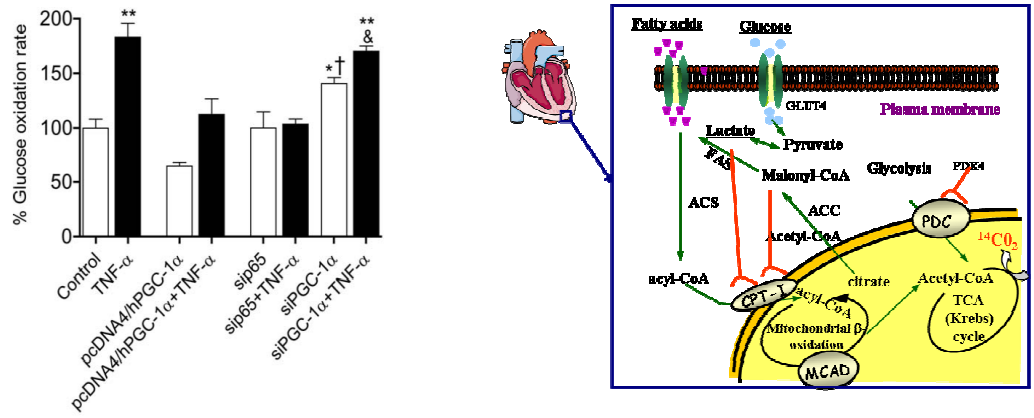

Figure 4 . The modulation of PGC-1α and p65 levels has a direct effect on glucose oxidation. The graph represents the [U-^{14}C]-glucose oxidation rates in control AC16 cells, and AC16 cells over expressing the human PGC-1α gene or with siRNA knock down of p65 or PGC-1α genes, and incubated with TNF-α. Thus, treatment with TNF-α induced the glucose oxidation rate up to 80% with regard to control cells and, as expected, down-regulation of PGC-1α expression with siPGC-1α increased the glucose oxidation rate up to 40%. The glucose oxidation rate was further increased when TNF-α was added to siPGC-1α compared with siPGC-1α alone (Adapted from [39]).

3.2.3. Amino acid transport

Amino acid transport across the plasma membrane mediates and regulates the flow of these ionic nutrients into cells and, therefore, participates in interorgan amino acid nutrition. In addition, for specific amino acids that act as neurotransmitters, synaptic modulators, or neurotransmitters precursors, transport across the plasma membrane ensures reuptake from the synaptic cleft, maintenance of a tonic level of their extracellular concentration, and supply of precursors in the central nervous system. Transfer of amino acids across the hydrophobic domain of the plasma membrane is mediated by proteins that recognize, bind, and transport these amino acids from the extracellular medium into the cell, or vice versa [40].

Functional studies based on saturability of transport, substrate specificy, kinetic behaviour, mode of energization, and mechanisms of regulation performed in perfused organs, isolated cells, and purified plasma membranes led to the identification of multiplicity agencies in the plasma membrane mammalian cells. In many of these studies, radiolabeled amino acids are used, as is the case of [^{3}H] Arginine [14, 41].

3.3. Radioimmunoassay

Radioimmunoassay (RIA) is a technique that allows the detection of very small quantities, of the order of nanograms, of biological or pharmacological substances, in blood or other fluid samples using antigen/antibody reactions. Among the most recent examples of RIA published by our researchers we emphasize those using ^{125}I-EGF [42], FGF21 [43] and 11-ketotestosterone and testosterone [13].

RIA is based on measuring the amount of radioactively-labelled antigen that is displaced from the specific antibody binding sites due to the arrival and subsequent unlabeled antigen competition (which is the unknown), knowing the amount of both, radioactively labelled antigen as unlabeled antigen in our sample. The measurement is made of the remaining free fraction before and after the addition of unlabeled antigen (Fig. 5).

The development of this technique offers several advantages over other detection methods. Sensitivity is the most important advantage as it is able to detect small amounts of substances as a result of the ability to measure very small amounts of radioactive tracers. A second advantage is the specificity, the ability of the technique to measure only the substance of interest in a sample that has a complex composition. The accuracy and reproducibility are others advantages since this technique allows to determine the effective amount of a substance and give highly reproducible measurements of concentrations in duplicate samples in a simple analysis.

The radioactivity of bound (cpm Bound) and unbound (cpm Free) components can be measured by standard techniques. The gamma counter is used in the case of those tracers that emit gamma rays, such as ^{125}I and ^{131}I. Due to the high specific activity of radiolabeled antigen or ligand, it is often easy to obtain high count values, allowing even greater statistical accuracy.

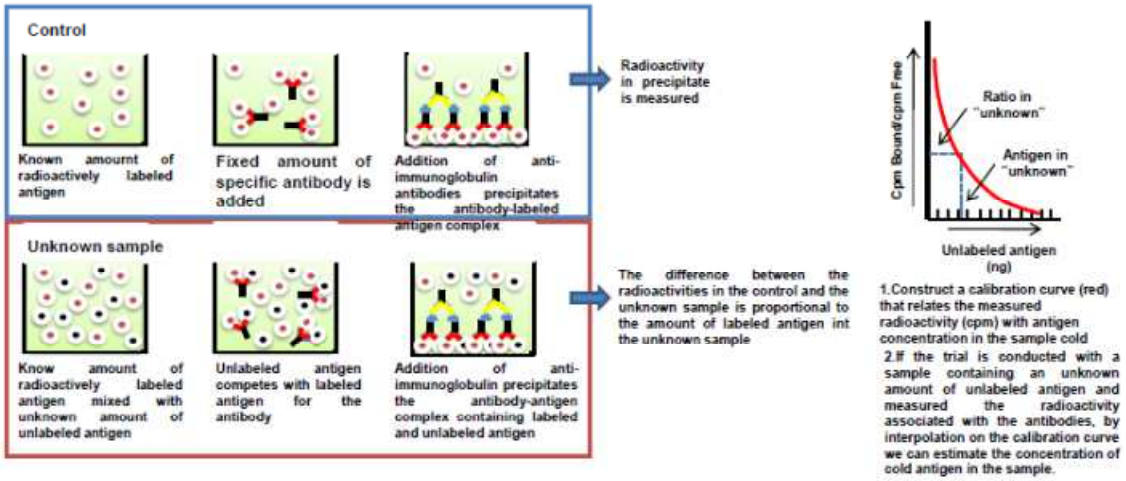

Figure 5. Experimental procedure of a Radioimmunoassay

3.4. Environmental liquid scintillation counting

Environmental liquid scintillation counting (LSC) is the measurement of both natural and anthropogenic radionuclides in the natural environment, but often radionuclide concentrations are low. Many radionuclides are routinely measured at natural environmental levels in a range of sample matrices including waters [44], sediments, soils, air, etc. These include isotopes of radium (Ra), uranium (U), thorium (Th), ^{210}Pb, ^{222}Rn, and ^{231}Pa. Monitoring the environment for radionuclide releases is associated with nuclear fuel cycle activities (fuel enrichment, fuel fabrication, power generation, and fuel reprocessing facilities). This would principally be the analysis of beta-emitting radionuclides without significant gamma emissions including ^{3}H, ^{14}C, ^{36}Cl, ^{89,90}Sr, ^{90}Y, ^{99}Tc, and ^{241}Pu but could also include analysis of alpha emitting radionuclides.

Studying the rates of processes in the environment would mainly be carried out using radionuclides of natural origins and would include ^{14}C dating, ground water movement and dating using ^{3}H, marine sediment mixing, productivity, and particle flux studies using ^{234}Th and ^{210}Pb/^{210}Bi/^{210}Po.

The photosynthetic activity of microorganisms in environmental samples can be determined by incubation with $NaH^{14}CO_3$ [22, 23].

3.4.1. Radiocarbon dating

The basis of radiocarbon dating technique is the relatively constant natural production rate of ^{14}C in the upper atmosphere, its uniform uptake as $^{14}CO_2$ into living plant material, conversion to plant carbohydrates, and subsequent transfer through the food chain. The end result of the food chain transfer is almost uniform labelling of all living organisms. ^{14}C dating is used in a wide range of scientific disciplines including geology, archaeological [45], mineral science, soil science, oceanography, climate reconstruction, etc. and LSC is commonly used for this measurements.

3.4.2. Food and additives studies

Petroleum derivatives are occasionally used to adulterate natural food and drink products without the buyer's knowledge. Because petroleum-based products are sufficiently old that they contain no ^{14}C, depletions in the natural ^{14}C content are normally indicative of adulteration.

Determination of $^{14}CO_2$ in biological samples, with the aim of quantifying total oxidation of oleic acid and glucose $^{14}CO_2$ is measured in different studies [8, 46].

Acknowledgements

We are very grateful to all the researchers using our radioactive facilities at the UB (IR-64, IR-147, IR-2105 and IR-2265) who have contributed to write and illustrate this chapter. We also thank I. Pinilla, I. Huber M. Camps and M. Vázquez for kindly providing images and for helpful comments that improved this contribution.

References

[1] Annunziata Michael F. 2003. The Montague Group, USA.

[2] Packard Instrument Company. 1999. Auto-Gamma Counting Systems. Reference manual. CobraII Series.

[3] Packard Instrument Company. 1995. Operation Manual. Tri-Carb Liquid Scintillation Analyzers. Models 2100TR/2300TR.

[4] Unitat de Protecció Radiològica- CCiTUB. 2010. Curso de Formación Supervisores. Instalaciones Radiactivas con Fuentes no encapsuladas.

[5] National Diagnostics Laboratory Staff. 2004. Principles and applications of liquid scintillation counting.

[6] Hondares E., Rosell M., Gonzalez F.J., Giralt M., Iglesias R., Villarroya F. *2010. Cell Metabolism 11, 206-212, March 3,.*

[7] González-Muñoz E., López-Iglesias C., Calvo M., Palacín M., Zorzano A., Camps M. *2009. Endocrinology Vol. 150, nº8, 3493-3502*

[8] Sánchez-Gurmaches J., Cruz-García L., Gutiérrez J., Navarro I. *2010. Am. J. Physiol. Regul. Integr. Comp. Physiol. 299(2): R562-72.*

[9] Guitart M. , Andreu A., García-Arumí E., Briones P., Quintana E., Gómez-Foix A., García-Martínez C. *2009. Mitochondrion 9, 266-272.*

[10] Egea, L.; Giménez, R.; Lúcia, D.; Modolell, I.; Badía, J.; Baldomà, L.; Aguilar, J. *2008. Biochim. Biophys. Acta-Molecular and Cell Biology of Lipids.1781: 270-276.*

[11] Montori-Grau M., Guitart M., Lerin C., Andreu A., Newgard Ch. B., García-Martínez C., Gómez-Foix A. 2007. *Biochem. J. 405, 107-113.*

[12] Vilà R., Cabot C., Villarreal I. , Monegal A., Ayet E., Romero M., Grasa M., Esteve M., Fernández-López J.A., Remesar X., Alemany M. 2011. *Journal of Steroid Biochemistry and Molecular Biology. 124, 99-111.*

[13] Marín-Juez R., Castellana B., Manchado M., Planas J.V. 2011. *General and Comparative Endocrinology. Vol. 172, 130-139.*

[14] Bartoccioni P., Rius M., Zorzano A., Palacín M., Chillarón J. 2008. *Human Molecular Genetic,. Vol. 17, Nº 12, 1845-1854.*
[15] Molina-Arcas M., Bellosillo B., Casado F.J., Montserrat E., Gil J., Colomer D., Pastor-Anglada M. 2003. *Blood. 101: 2328-2334.*
[16] Huber-Ruano (Huber-Ruano I. Current Drug Metabolism 2009)
[17] Fernández-Calotti P., Pastor-Anglada M. 2010. *Journal of Biological Chemistry.285,18:13589-13598.*
[18] Vendrell M., Soriano A., Casadó V., Díaz J.L., Lavilla R., Canela E.I., Lluís C., Franco R., Albericio F., Royo M. 2009. *ChemMedChem. 4, 1514-1522.*
[19] Leivar P., Antolín-Llovera M., Ferrero S., Closa M., Arró M., Ferrer A., Boronat A., Campos N. 2011. *The Plant Cell. Doi: 10.1105.*
[20] Lang M., Juan E. 2010. *Nucleic Acids Research. 38, 19: 6404-6417.*
[21] Larráyoz I. M., Casado F. J., Pastor-Anglada M., Lostao M.P. 2004. *Journal of Biological Chemistry Vol 279, 10:8999-9007.*
[22] Camarero, Ll.; Felip, M.; Ventura, M.; Bartumeus, F.; Catalan, J. 1999. *Journal of Limnology, 58(2), 203-212.*
[23] Felip, M.; Sattler, B.; Psenner, R.; Catalan, J. 1995. A*pplied and Environmental Microbiology. 61: 2394-2401.*
[24] Stamoulis K.C., Ioannides K.G., Karamanis D.T., Patiris D.C. 2007. *Journal of Environmental Radioactivity. 93:144-156.*
[25] García-Peláez B., Vilà R., Remesar X. 2008. *Obesity. 16, 2223-2231.*
[26] Gil-García C., Rigol A., Vidal M. 2009. *Journal of Environmental Radioactivity.* 100, 690-696.
[27] Vandenhove H., Gil-García C., Rigol A., Vidal M. 2009. *Journal of Environmental Radioactivity. 100, 697-703*
[28] Aldaba D., Fernández-Torrent R.,Rauret G., Vidal M., Rigol A. 2010. *Applied Radiation and Isotopes. 68:393-398.*
[29] Pacheco R., Oliva H., Martínez-Navío J.M., Climent N., Ciruela F., Gatell J.M., Gallart T., Mallol J., Lluis C., Franco R. 2006. *Journal of Immunology. 177:6695-6704.*
[30] Parra D., Manils J., Castellana B., Viña-Vilaseca A., Morán-Salvador E., Vázquez-Villoldo N., Tarancón G., Borràs M., Sancho S., Benito C., Ortega S., Soler C. 2009. *Cancer Res.; 69:6676-6684.*
[31] Darnell J., Lodish H, Baltimore D. *Molecular Cell Biology. 2th Edition. Scientific American Books.*
[32] Alberts B., Johnson A., Lewis J., Raff M., Roberts K., Walter P. Molecular Biology of the Cell. 5th Edition. Garland Science New York.
[33] García-Manteiga J., Molina-Arcas M., Casado F.J., Mazo A., Pastor-Anglada M. 2003. *Clinical Cancer Research. 9:5000-5008.*
[34] Fernández-Veledo S., Huber-Ruano I., Aymerich I., Duflot S., Casado F.J., Pastor-Anglada M. 2006. *Biochem. J. 337-344.*
[35] Molina-Arcas M., Marcé S., Villamor N., Huber-Ruano I., Casado FJ., Bellosillo B., Montserrat E., Gil J., Colomer D., Pastor-Anglada. 2005. *Leukemia. 19:64-68.*
[36] Minuesa G., Volk C., Molina-Arcas M., Gorboulev V., Erkizia I., Arndt P., Clotet B., Pastor-Anglada M., Koepsell H., Martínez-Picado J. 2009. *Journal of Pharmacology and Experimental Therapeutics. 329:252-261.*
[37] Ruiz-Montasell B., Casado J.F., Felipe A., Pastor-Anglada M. 1992. *J. Membr. Biol.128(3): 227-33.*
[38] Jiménez A., Pubill D., Pallàs M., Camins A., Lladó S., Camarasa J., Escubedo E. 2000. *European Journal of Pharmacology.398:31-39.*
[39] Alvarez-Guardia D., Palomer X., Coll T., Davidson M.M., Chan T.O., Feldman A.M., Laguna J.A., Vázquez-Carrera M. 2010. *Cardiovascular Research.87:449-458.*
[40] Palacín M., Estévez R., Bertran J., Zorzano A. 1998. *Physiological reviews. Vol.78. Nº 4:969-1054.*

[41] Yeramian A., Martin L., Serrat N., Arpa L., Soler C., Bertran J., McLeod C., Palacín M., Modolell M., Lloberas J., Celada A. 2006. Journal of Immunology. 176:5918-5924.
[42] Lladó A., Timpson P., Vilà de Muga S., Moretó J., Pol A., Grewal T., Daly R. J., Enrich C., Tebar F. 2008. *Molecular Biology of the Cell. Vol.19, 17-29.*
[43] Hondares E, Iglesias R, Giralt A, Gonzalez FJ, Giralt M, Mampel T, Villarroya F. 2011. *J. Biol. Chem. Vol.286, Nº15:12983-12990.*
[44] Zaata-García D., Llauradó M., Rauret G. 2009. *Applied Radiation and Isotopes. 67, 978–981*
[45] Mendoça M.L., Godoy J.M., Da Cruz R.P., Pérez R. A. 2006. Journal of Environmental Radioactivity. 88:205-214.
[46] Trocho C., Pardo R., Rafecas I., Virgili J., Remesar X., Fernández-López J.A., Alemany M. 1998. *Life Sciences. Vol.63, Nº5:337-349.*

X-Ray systems: Radiation protection program in basic research applications

Aurea Navarro-Sabaté[1] and Cristina Sánchez[2]

Unitat Tècnica de Protecció Radiològica, CCiTUB, Universitat de Barcelona.

[1] IRA Bellvitge. Feixa Llarga s/n. L'Hospitalet de Llobregat. 08907 Barcelona, Spain.

[2] IRA Medicina. Casanova, 143. 08036 Barcelona, Spain.

email: *aureanavarro@ccit.ub.edu, cristinasanchez@ccit.ub.edu*

Abstract. Although the radiation doses involved in basic research radiology are relatively small, the increasing number of radiological procedures makes risks becoming increasingly high. Quality control techniques in radiological practice have to ensure an adequate system of protection for people exposed to radiation. These techniques belong to a quality assurance program for X-ray machines and are designed to correct problems related to equipment and radiological practices, to obtain radiological images of high quality and to reduce the unnecessary exposures.

1. Introduction

X-Rays have come a long way from its origins in a small, dark German laboratory on 1895 when Roentgen discovered X-rays accidentally. In fact, he was doing some basic research in physics using a cathode ray tube (like in the back of your TV or computer monitor) to study electrical discharges in gas and discovered by chance that the device he was using produced X-rays. By doing basic scientific research with no specific practical goal, Roentgen discovered one of modern medicine's most useful diagnostic tools and won the first Nobel Prize in physics in 1901 [1]. By the time, scientists did not yet realize that X-rays were a form of electromagnetic radiation however the medical uses of X-rays were apparent.

X rays are short-wavelength electromagnetic radiations that can undergo various interactions with matter. Such interactions yield data which, when appropriately analyzed, can provide useful information on the materials irradiated. Machines, typically x-ray diffraction devices and x-ray spectrometers, have been designed to utilize very intense x-ray beams in order to facilitate microscopic examinations or elemental analyses of materials in industry, research laboratories and educational institutions.

One particularly useful property of X-rays is their ability to penetrate solid materials of considerable thickness and they can expose photographic films. Their short wavelength allows for high resolution imaging if appropriate optical components are available. However there are differences in penetration through different materials due to the differences in the material densities. X-rays have been used in a wide range of applications from medical science to industry because of their different properties.

The science of radiation protection grew out of the parallel discoveries of X-rays and radioactivity in the closing years of the 19th century. Radiation burns were recorded within a month of Roentgen's announcement of his discovery of X-rays. However, it was not until the death of Clarence Dally, Edison's chief assistant in the manufacture of X-ray apparatus, and the documentation of his struggle with burns and serial amputation of both arms to malignant ulceration and extensive lymph node involvement, that medical observers took seriously the notion that exposure to high doses of X-rays cause carcinogenic effects [2].

In recognition of the widespread applications of ionizing radiation to mankind worldwide and the potential adverse human health effects, it seems clear the necessity that norms for protection against radiation become legal requirements. These norms are developed from several government agencies in all countries worldwide. The International Commission on Radiological Protection (ICRP) and the specific European Union Council commission are the international regulatory bodies and the CSN (Consejo de Seguridad Nacional) is the national counterpart of the ICRP in Spain. The most important Spanish regulation on X-rays is the "Real Decreto 1085/2009, de 3 de julio, por el que se aprueba el Reglamento sobre instalación y utilización de aparatos de rayos X con fines de diagnóstico médico" [3]. These norms describe acceptance testing and Quality Assurance (QA) program, safe dose limits for radiation workers and for the general public, patient dose measurements, the checking of technical parameters from X-ray tubes, and the shielding required for the walls of an X-ray room among others.

This article summarizes the basic tasks of the Technical Unit for Radiation Protection of the University of Barcelona (UTPR-UB), which are carried out at various X-ray facilities, with examples of X-ray applications in research that show the scope of this technique.

2. Radiological Protection methodology

The new regulations require that each facility using X-ray equipment (including any medical diagnostic radiology unit, which can be dental or conventional, fluoroscopic, X-ray bone densitometry and computed tomography) establishes and carries out a quality assurance program. An ineffective quality assurance program can lead to poor quality images that can impair diagnosis or research, increase operating costs and contribute to unnecessary radiation exposure to staff and

mainly to patients, if it is the case of medical diagnostic radiology. Any extension of the basic quality assurance program is the responsibility of each X-ray facility.

The UTPR-UB is in charge to develop and implement a Radiological Protection Program also named QA program at any X-ray facility of UB or external institutions that handle their services. The QA program includes periodic Quality Control (QC) tests of the components in a diagnostic X-ray imaging system using equipment and test tools designed for that specific purpose, radiation levels checking, shielding studies, dosimetry and radiological protection administrative procedures. The latter procedures are aimed at verifying that QC testing is effective, i.e., the tests are performed regularly and correctly, the results evaluated promptly and accurately, and the necessary actions taken. They include recommendations regarding the responsibility for quality assurance action, staff training, equipment standards, and the selection of the appropriate equipment for each examination.

2.1. Quality control

It consists of a series of standardized tests developed to detect changes in X-ray equipment function from its original level of performance**.** The objective of such tests, when carried out routinely, allows prompt corrective actions to maintain X-ray machines in proper use and with an optimal image quality. Quality controls should be done at least annually or every time that an X-ray equipment has undergone a technical repair. Control test results must be within the tolerance allowed by law; otherwise the appropriate corrective actions must be issued.

2.1.1. *Quality of the radiation beam*

In X-ray equipments, three main indicators or variables express the essential characteristics as the quality of the X-ray beam, and the time for which they are produced. These are: a) Kilovoltage (kV) , which expresses the penetration power and the energy of the photon beam generated in the tube (a higher kV results in a higher energy and level of penetration of the beam); b) Milliamperage (mA), which expresses the "quantity" of photons generated in the tube (i.e. an increase in current causes an increase in the number of X-ray photons generated per unit area and time); c) Time (t), which expresses the time of issuance of the radiation beam (the longer the time, the higher the exposure).

The main control parameters checked in quality control tests are related to the quality of the radiation beam. Table 1 summarizes the main tests developed in the QC with their degree of tolerance allowed by law (data extracted from “Protocolo Español de Control de Calidad en Radiodiagnóstico [4])”.

2.1.2. Image quality

X-ray image quality directly affects the diagnostic results.The X-ray inspection programs concentrate on the measurement of X-ray machine parameters such as kVp and mAs, timer accuracy, collimation, etc. but image quality test enables objective measurement of background density, high-contrast resolution, density uniformity, low-contrast resolution, low-contrast detail, and film contrast. Image noise is the most important quality-limiting factor in radiological imaging, because it sets the limits of the detectability of details and also restricts possibilities to visualize the details by means of image enhancement (e.g., image sharpening and contrast increase). The image sharpness is often evaluated visually by the resolution seen in line-pair test object images and image noise by determining the threshold contrast. As an exemple, figure 1 shows a TOR CDR test image. The TOR CDR phantom is used, routinely, for conventional and non-subtractive digital radiography image quality tests [5]. It enables the following checks to be made: Sensitometric measurements (10 test point details, 5.6mm diameter), Resolution limit (0.5 to 14.3 LP/mm), Low-contrast large-detail detectability (17 details, 11mm diameter) and High-contrast small-detail detectability (17 details, 0.5mm diameter). In addition to checking the consistency of radiographic performance, the test object can be used to assess the relative performance of different screen-film combinations.

Table 1: QC tests and degree of tolerance

Parameter	Test	Tolerance allowed
Kilovoltage Calibration	Accuracy	<±10%
	Reproducibility	<10%
Radiation Wave form	Radiation Wave form	Ripple percentage indicated in manufacturer specifications
Exposure Time	Accuracy	Deviations <±10% for times >20ms Deviations specified by the manufacturer for times ≤ 20ms
	Reproducibility	<10%
Total filtration	HVL	<2.5mm Al for kV>70 <1.5mm Al for kV>70
Performance	Performance value	Orientative 30-65μGy/mAs at 1m for 80kV. (Or indicated in manufacturer specifications)
	Performance reproducibility	Variation rate <10%
	Variation of performance with current and charge	linearity coefficient <0.1 <15% for current changes <20% for charge changes
Geometric parameters	Film-focus distance	difference between measured and indicated 4%
	X-ray/Light Beam Alignment (Congruence of Collimators)	<±2% focus-phantom distance on each site of rectangle, being the sum of 4 sites less than <±3% Record field alignment <±1% focus-film distance
	Beam Orthogonality or perpendicularity	≤1.5º
Measurement of radiation leakage	Measurement of radiation leakage	< 1 mGy/h at 1m

Kilovoltage Calibration is one of the variables that determine the quality of a beam, a variation (relatively small) in the kVp generates an alteration in the contrast of the image and the transmitted intensity. Accuracy and reproducibility of kV are checked.

Accuracy sets the level of reliability of X-ray equipment examined. Test procedure: Perform at least 5 exposures with constant mA and ms (milliseconds) but with gradually increasing kVp or with constant mA and kVp but with gradually increasing ms.

Reproducibility test is important to assess the ability of the radiology team to reproduce always the same output values that define the radiation beam: voltage, time and dose. Test procedure: make repeated exposures a number of times on constant parameters to be recorded.

Radiation wave form: It shows the variation of x-ray intensity with time.

Exposure time: For the purposes of this test procedure, accuracy will mean the degree of agreement between the measured and indicated time values. Reproducibility will mean the degree of agreement between several measurements of the exposure time at the same indicated time on the x-ray control panel.

Half Value Layer (HVL) is defined as the thickness of material needed, brought in the beam, to reduce beam intensity by half. From the HVL, it can be checked if the beam total filtration is in correspondence with the minimum requirements. Test procedure: Place an ionisation chamber 1 m from the focal spot. Make repeated exposures adding increasing thicknesses of 1 mm aluminium plates every two exposures and record them until the recorded exposure is less than half the exposure without additional filtration.

Total Filtration (TF) is assessed by measuring the HVL of the X-ray beam at a known kV, followed by an estimation process based on calculations.

Performance: corresponds to the value of the dose rate in air per charge unit: μGy/mAs

Performance reproducibility: Is the coefficient of variation of different performance measures under the same conditions.

Variation of performance with current and charge: Check the consistency of performance with the variation of the charge and current. It is calculated with the coefficient of linearity between two consecutive measurements.
Film-focus distance: The distance between the focal spot of the x-ray tube, or the radiation source, and the film.
***X*-ray/Light Beam Alignment** (Coincidence): The alignment between the light field and the radiation field permits the technologist to position the field to expose only the anatomy of interest. Misalignment may result in unnecessary or repeat exposure. Test procedure: Adjust the collimator so that the light beam covers exactly one of the inner patterns of the test tool (i.e. 15x15 square of Visi X test tool), perform an exposure and compare with the irradiated fluorescence square appeared. Record its difference in mm.
Beam Orthogonality or perpendicularity. This parameter includes both the possible deviations in angulation (between the central beam radiation and perpendicular to the receiver input image) and displacement.
Radiation leakage: The tube housing is made of lead in order to absorb all radiation, which is not directed at the patient. The amount of radiation, which has "leaked" from the housing should be minimal. Test procedure: Close the X-ray tube diaphragm, Surround the X-ray tube with a lead apron or equivalent shielding and take radiation exposures measurements at different points.

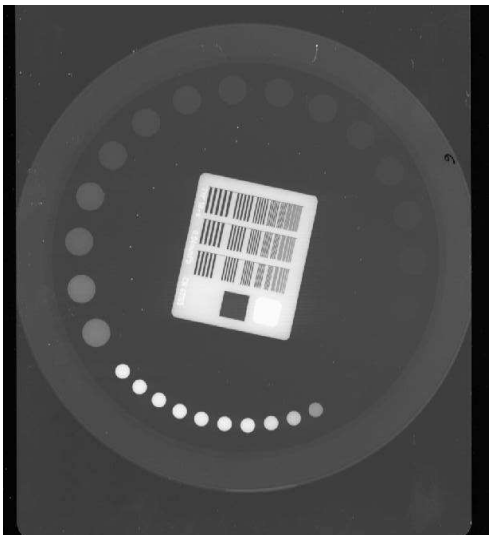

Figure 1. Radiography of a test object model TOR CDR (Leeds test objects Ltd.). This TOR CDR test image shows different test patterns such as low and high contrast objects, test point details for sensitometric measurements, spatial resolution bar phantom, and gray-scale objects. After an initial grey-scale check, image quality is measured simply by counting the number of details detected and the number of bar-patterns resolved in the image (image taken with a TOR CDR radiographic test object from the UTPR-UB).

2.1.3. Radiation levels

In the planning of any X-ray facility the main priority is to ensure that persons in the vicinity of the facility are not exposed to levels of radiations which surpass the current regulatory exposure limits (this means that radiation levels in controlled areas that are occupied routinely by radiation workers must be such that: first, no radiation worker is occupationally exposed to more than 20 mSv per year; and second, non-public person receives more than 1mSv per year). The system of radiation dose limits in use in Spain (and in most other countries) is based on the recommendations of the ICRP. In order to meet these requirements, radiation levels should be monitored in the vicinity of an X-ray unit and if necessary, appropriate actions must be taken to ensure adequate shielding. In general, attention to the basic principles of distance, time and shielding are required to determine shielding needs. In general, the radiation exposure to individuals depends primarily on the amount of radiation produced by the source, the distance between the exposed person and the source of the radiation, the amount of time that an individual spends in the irradiated area, and the amount of protective shielding between the individual and the radiation source.

Quantification of the scatter radiation levels prevalent at X-ray facilities of research areas is necessary to delineate the level of occupational exposure of radiation to which the technician-operators are exposed and to facilitate radiation protection measures. Those areas occupied by any other individual such as visitors or employees who do not work routinely with or around radiation sources are of special attention and cannot exceed 1mSv per year. The measurement of scattering radiation in the vicinity of X-ray offices must be reported annually and recommendations for improving the security level must be suggested if necessary.

In a medical diagnostic radiology unit, the same considerations with regard to working staff and general public must be taken into account but also a special interest in the actions is necessary to ensure that the patient receives doses as low as possible in any diagnostic exposure.

2.2. Shielding study

Shielding requirements are usually specified following the calculation concept of the ICRP. The methodology proposed calculates the exposure levels of primary, scatter and leakage radiation emitted from an X-ray source (figure 2), following the ALARA (as low as reasonably achievable) principle. Each x-ray installation must be assessed for shielding requirements based on the: dimensions of the room, positions of the x-ray control, vertical bucky and operator, proposed construction materials (protective screens, walls, floors, doors), areas adjacent to x-ray room (occupancy, future use), x-ray workload. According to the characteristics of the x-ray room or x-ray equipment, protection may be required for structural materials as lead covered walls or doors. Structural protection plans must be supplied to the UTPR prior to construction or for existing buildings prior to use of the x-ray equipment in the room. In other X-ray facilities will be sufficient to provide a barrier shielding with a mobile x-ray lead barrier and to make available personal protective accessories including: lead aprons, collars, gloves and lead-coated glass products when needed.

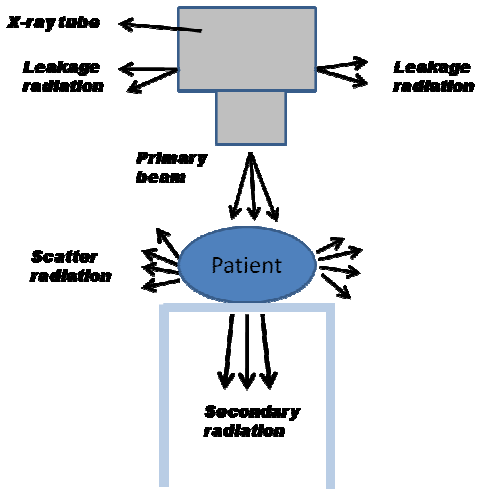

Figure 2: X-ray unit and radiation types

2.3. Dosimetry

Personal dosimeters are intended to monitor occupational doses thereby providing a mechanism for restricting future radiation exposures to an individual, so that the recommended maximum permissible limits are not exceeded. Area dosimetry can be used in some cases so that the dose of exposed personnel shall be estimated from these data using an appropriate protocol. Depending on the analytical X-ray system design, monitoring the extremity doses could be necessary. The dosimeter readings are kept as records for every staff for the purpose of evaluating their radiation history and possible risks involved.

2.4. Staff training

The QA program should include the means to provide appropriate training for all personnel with QA responsibilities and especially those directly involved with QC testing. A continuing education program is necessary to keep personnel up-to-date. UTPR-UB has the qualified personnel to perform adequate QA program in radiology facilities. It also undertakes training courses for personnel involved in handling x-ray equipment.

3. Examples of applications

X-ray imaging is a key technique for medical imaging, non-destructive testing, and basic research applications. Medicine and dentistry remains the most common use of X-rays being employed routinely at doctor offices and hospitals. However, X-rays are also widely used in other applications from airport security to industrial inspection and quality control systems, or in art restoration studies, among others. Researchers use X-ray systems in many different applications

ranging from pneumology and cardiology studies using pigs and dogs X-ray images to radiographs of small animals (such as mouse, rats, fishes and coral radiographies in biomedicine or marine biology department studies respectively), molecular structure determination by X-ray crystallography (the most famous example along these lines is the double helix structure of the DNA molecule, as determined by Franklin, Crick and Watson) to grain and seed inspection in agriculture department studies.

Although radiographic units exist in a wide variety of configurations we have focused on cabinet X-ray systems and conventional X-ray systems (in the latter case by selecting examples of applications of fluorography, dental and conventional X-ray machines). Herein we report some specific examples of X-ray application developed at the UB.

3.1. Cabinet X-Ray imaging system

The term "cabinet X-ray system" refers to an X-ray system with the X-ray tube installed in an enclosed, interlocked cabinet. The main advantage of the system is that no additional shielding must be added to the facility where the X-ray machine is installed as the cabinet provides the necessary shielding. The cabinet X-Ray unit located at IR-147 (at the Biology Faculty of the UB) is a Faxitron model [6] with maximum operating conditions of 130 kV and 3 mA (figure 3a). This imaging system has very different possibilities for research applications.

First, this unit is used in biomedical and basic research projects, for example to produce highly detailed radiographs of small animals. Radiographic images like that shown in figure 3b allowed to record both shape and meristic characters of axial skeleton and vertical fins of zoarcid fish specimens from the Southern Ocean which provided the necessary information to identified a new species *Santelmoa carmenae* [7].

Second, the non-destructive nature of X-rays generated at selected excitation voltages, may be used to reveal internal details of any items, from thin low density objects such as documents (those made of paper or cardboard can be viewed through soft X-rays), to more dense objects such as those made of heavy metals. This may be useful to reveal latent fingerprints from difficult surfaces and to inspect overwritten watermarks, obliterated serial numbers and other markings or ink components such as transition metals in the context, for example, of detecting differences between a counterfeit banknote and a genuine one as shown in figure 3c. Moreover, numerous examples illustrate the usefulness of a simple and compact cabinet X-ray system in forensic laboratories, particularly when preservation of evidence is important and because X-ray analysis is used to screen objects non-invasively. It allows doing radiography of excised organs to determine cause of death, and spatter patterns on clothing to determine firing distance.

Third, radiography, in general, and cabinet X-ray systems, in particular, have their applications in industry where they are valuable for non destructive testing of products for defects. Because the industry attaches great importance to the quality assurance, X-ray imaging is used in the research and development, as well as in the production departments. A very good application is to check, for example, electrical components by digital X-ray inspection on completeness and a correct assembly of the single components. Electronic components are becoming increasingly miniaturized. Only high-resolution and high-magnification X-ray technology provides the necessary means to inspect such components. Cabinet X-ray systems offer manufacturers and industrial service providers a tool to investigate, in a non-destructive manner, objects and object properties that cannot be inspected optically. Typical inspection tasks includes: Inspection of bond wires and bonding areas, void analysis of conductive and non-conductive die bonds, inspection of flip-chip solder joints in processor cases and analysis of discrete components such as capacitors and inductors (figure 3d).

Also, X-ray inspection in industry offers the capability to confirm the integrity of a product and so ensure compliance with quality standards. X-ray images can reveal contaminants (such as metals, bone, glass, plastics, ceramic, cement, etc) and product defects (such as missing, cracked or broken parts) that can not be seen with the naked eye. I.e.: In quality control of the food industry, thanks to the use of X-rays, metal contaminants can be seen such as a screw in a glass container containing prepared food for infants that may, otherwise, go unnoticed (figure 3e).

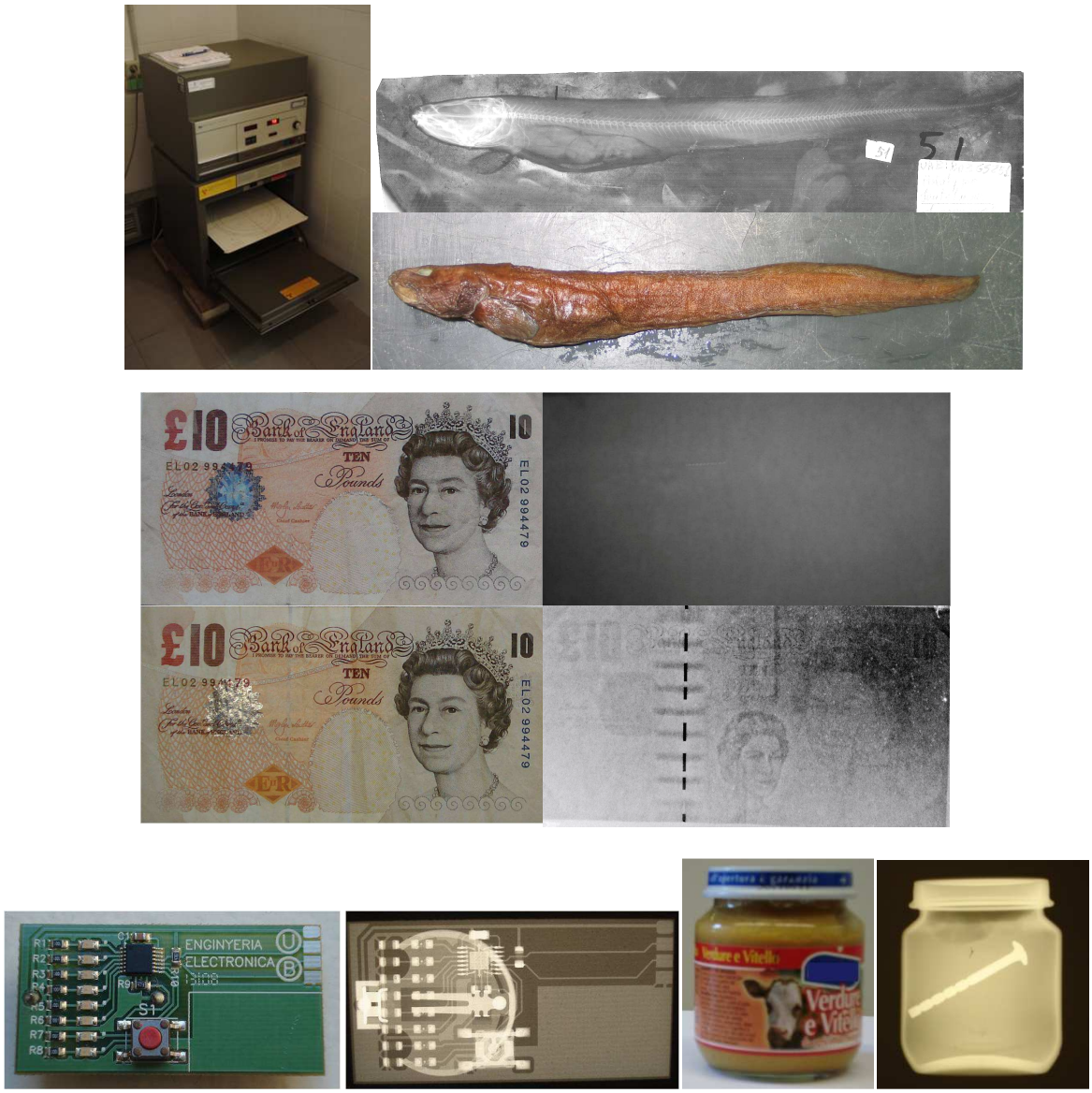

Figure 3: Applications with Faxitron cabinet X-ray system. A) Faxitron cabinet X-ray system at IR-147 facilities of UB. B) radiographic and photografic image of Santelmoa carmenae [7] . Holotype, UAB: B03GSZ51, male, 264 mm SL, from Gerlache Strait, Southern Ocean (Images kindly provided by Jesus Matallanas) C) Left: counterfeit (top) and genuine (bottom) £10 notes. Right: soft X-radiographs that have been scanned and inverted to enhance contrast. Radiographic image for original and counterfeit banknote was obtained with 12Kv during 40sec radiation and using Kodak film. The major difference between the two notes is the absence of the strip of metal, Queen's head, and the rest of the script on a £10. **D)** Electronic microchip and its radiography. With X-ray inspection systems, weld and solder joint quality can be easily and quickly inspected. **E)** Radiography of a glass container containing prepared food for infants with a screw inside.

The X-ray baggage inspection system similar to the Faxitron cabinet X-ray system is a particular example used to examine luggage at airports and people baggage at some official building control access for possible weapons, contraband and bombs detection.

Finally, once again for its simplicity and for being compact and shielded, the cabinet X-ray system can be used as an alternative to a conventional X-ray unit for applications in agriculture and Ecology studies (e.g.. radiography inspection of grain and seeds with radiographic images provides information about viability, infestation, damage or contamination, radiography of wood rings is used to evaluate seasonal growth characteristics), in Archaeology studies (i.e. to visualize

archaeological artefacts to aid in the preparation and cleaning of rare and often delicate structures) or in Art restoration (for works of art in small format to reveal previous works and changes that have been painted over).

3.2. Conventional X-Ray systems

Conventional X-ray systems offer many possibilities of applications being the medical diagnostic the most common used. However, here we have focused our attention on research applications developed at different departments of the UB. We present three examples of X-ray applications in research projects with three different X-ray units: a mobile conventional X-ray unit, a dental intraoral X-ray and a C-arm fluoroscopy unit.

3.2.1. Conventional X-ray applications in Art Restoration

The Department of conservation and restoration at the Fine Arts School (UB) uses a mobile conventional X-rays, located at IR-2376 which operating from 40 kV to 80 kV has revealed some interesting discoveries hidden in works of art.

Thus, the most commonly used method of holistic art conservation and art restoration science is X-ray radiography. The latter technique is useful for inspection in maintenance and preservation of works of art, their protection from future damage, deterioration, or neglect, and repair or renovation of works that have deteriorated or been damaged. For example, in the past, historical paintings have sometimes been painted over by other artists. But also, old paintings have often been painted over in order to manufacture fakes on chronological authentic canvas. The goal of the modern conservator is to determine in a non-invasive way, like X-ray radiography, the remaining original portions of the painting and to gain an understanding of how the painting had been treated over the years or to find out whether there is an older painting behind the visible one (as the examples shown in figure 4 and figure 5).

Figure 4: One of the most remarkable finds by the Department of conservation and restoration of the Fine Arts School (UB), was an image of Sta. Barbara observed, thanks to the X-rays, beneath a completely different painting in which were men playing cards. (Images kindly provided by Anna Nualart from the Department of conservation and restoration of the Fine Arts School (UB))

3.2.2. Dental X-Ray machine applications in preclinical practices and research

Dental X-ray units are a basic technique for pre-clinical practices at the Faculty of Dentistry. Undergraduate students learn the technique of intraoral radiography practicing isolated teeth. This enables them to become familiar with the dental diagnosis and started in the early invasive practices to rebuild a tooth or eliminate a cavity (figure 6a).

Figure 5: **Christ photographic and radiographic images.** In polychrome wood carvings, it can be basically seen the number of pieces of wood that comprises the support (most sizes are not made of one piece of wood) between the type of lace pieces and anchors (especially metal pins). In the case of Christ, we see several layers of overlapping colors, with numerous losses of pictorial material. Notice that there is a radiological contrast of pigments in the area of the cloth, with less contrast than the skin. This is due to the presence of metallic pigments in pictorial layers of the skin of Christ, which consists of, very likely, lead white. The overlap of paint layers (different thicknesses) and the fact that the obverse and reverse of the piece remain on the same plane make the resulting X-ray image both spectacular and difficult to understand without having the original side. (Images kindly provided by Anna Nualart from the Department of conservation and restoration of the Fine Arts School (UB)).

Dental X-ray units have also a wide range of applications in clinical research studies. For example, the X-ray image is crucial for the monitoring of dental implant techniques. The dental implant's surfaces, shapes and sizes are usually submitted to animal experimental assays (usually in dogs) in order to assess their characteristics: osteointegration, resistence, tisular adaptation, etc. (figure 6b).

A) 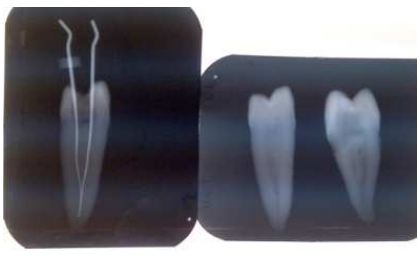

B) 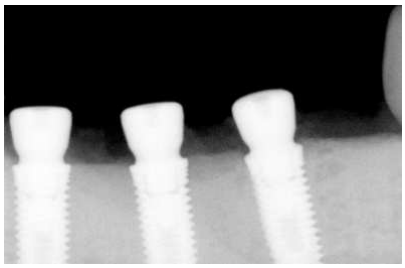

Figure 6. A) Left image: radiography to visualize the opening cameral of a lower premolar. Right image**:** Diagnostic imaging to check the anatomy of the tooth and see the number of lines of this molar pieces as their pulp chamber. **B)** Intra oral radiography. Intra-operative radiography from implants, 3 months post-operative control in a dog. (Image kindly provided by the Human Anatomy and Embryology Unit Laboratory, Faculty of Dentistry, UB)

3.2.3. Studies of experimental animal models with a C-arm fluoroscopy unit

The C-arm fluoroscopy unit installed at RX/30639 in the animal facilities of the Medicine College is an Arcadis Avantic model from Siemens with a maximum operating conditions of 120 kV and 15,2 mA (figure 7a). It is a surgical mobile X-ray unit that can produce images continuously. In continuous fluoroscopy, X-rays are continuously applied to the patient (a pig in this case of angiographic studies) to produce dynamic clinical images that may be recorded on videotape.

X-ray animal imaging has been recognized as an important tool in preclinical research and the development of novel diagnostic probes and imaging tools for a disease specific diagnosis and therapy monitoring. Most of this therapeutic and diagnosis studies have to be assayed in animal models before to achieve clinical trials in humans. In this context, nowadays, one of the main focus is on the investigation of angiogenesis related processes using pigs as experimental animal models [8]

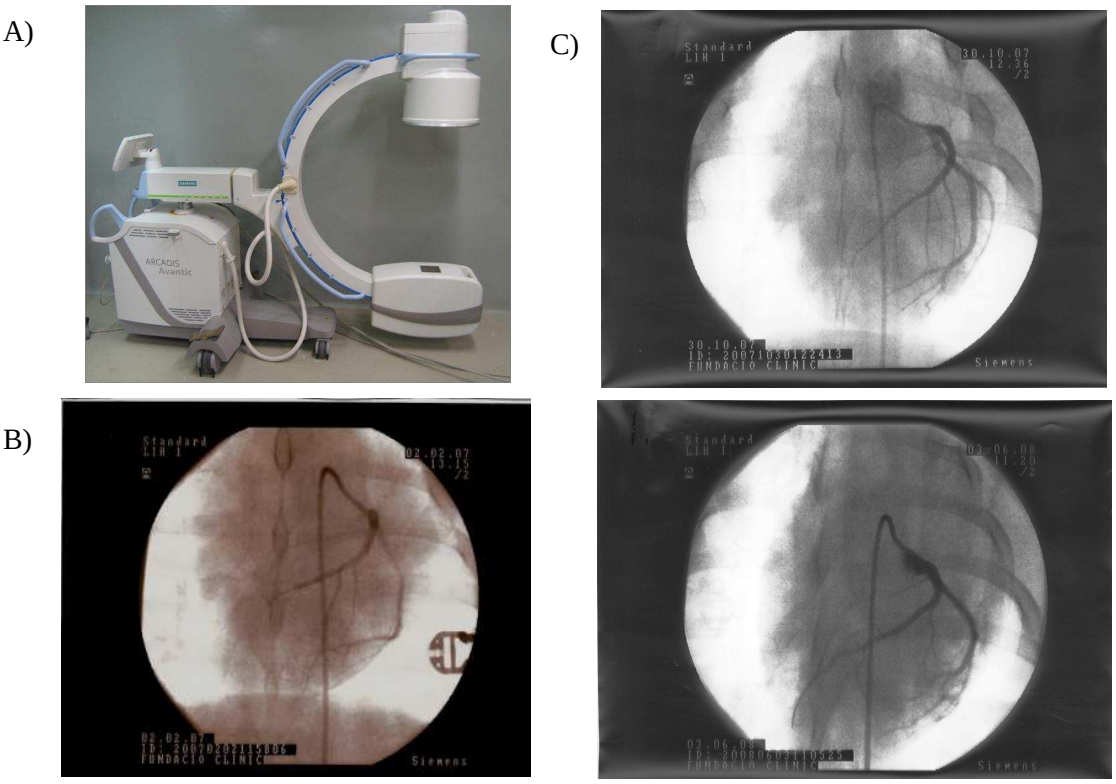

Figure 7: **C-arm fluoroscopy applications** A) C-arm fluoroscopy unit installed at RX/30639 in animal facilities of the medicine college. B) Angiography showing a myocardial infarction in pig, induced by placing an angioplasty catheter into the middle segment of the left anterior descending (LAD) artery and inflating it for 90 minutes, to later study therapeutic strategies. In this image a iodine contrast media has been injected into blood vessels or the chambers of the heart to produce the angiogram. (Image kindly provided by M. Rigol and N. Solanes). C) Injection of radio-opaque contrast substance of the entire tree to draw blood from the pig's coronary arteries. Contrast compounds containing iodine, which are radiopaque are injected in the artery or veins to highlight these vessels. The contrast compounds consist of highatomic number elements that largely attenuate X-rays and hence the hollow vessel can be more readily observed. (Image kindly provided by M. Rigol and N. Solanes)

Acknowledgements

We thank our colleagues Imma Rafecas for technical procedures information and Carmen Benito for technical support and helpful discussions with the faxitron cabinet X-ray system. We are especially grateful to all those researchers who have provided us with images for this contribution: Jesus Matallanas, from the Faculty of Bio Sciences at the Universitat Autónoma de Barcelona; Anna Nualart Torroja from the Department of conservation and restoration of the Fine Arts School (UB); Núria Solanes and Montserrat Rigol from IDIBAPS institute; preclinical practices professors of the Faculty of dentistry (UB); Cristina Manzanares, from the Human Anatomy and Embryology Unit Laboratory of the Faculty of Dentistry (UB). We also thank the Electronics department of the Faculty of Physics (UB) for providing the electronic microchip.

References

[1] http://nobelprize.org/nobel_prizes/physics/laureates/1901/rontgen-bio.html
[2] Clarence Dally: An American Pioneer. Raymon A. Gagliardi. American Journal of Roentgenology (1991) 157:922.
[3] http://www.boe.es/boe/dias/2009/07/18/pdfs/BOE-A-2009-11932.pdf
[4] http://www.sepr.es/html/recursos/descargables/Prot_CCRD_2010%20_Borr.pdf
[5] http://www.leedstestobjects.com/
[6] http://www.faxitron.com/
[7] Jesús Matallanas (2010). Description of two new genera, Santelmoa and Bentartia and two new species of Zoarcidae (Teleostei, Perciformes) from the Southern Ocean.". Polar Biology 33: 659-672.
[8] Rigol M, Solanes N, Farré J, Roura S, Roqué M, Berruezo A, Bellera N, Novensà L, Tamborero D, Prat-Vidal C, Huzman MA, Batlle M, Hoefsloot M, Sitges M, Ramírez J, Dantas AP, Merino A, Sanz G, Brugada J, Bayés-Genís A, Heras M (2010). Effects of adipose tissue-derived stem cell therapy after myocardial infarction: impact of the route of administration. J Card Fail. 16(4): 357-66.